

EDITORIAL BOARD

Jiri Cizek (Waterloo, Canada)
David P. Craig (Canberra, Australia)
Raymond Daudel (Paris, France)
Ernest R. Davidson (Bloomington, Indiana)
George G. Hall (Nottingham, England)
Jan Linderberg (Aarhus, Denmark)
Frederick A. Matsen (Austin, Texas)
Roy McWeeney (Pisa, Italy)
William H. Miller (Berkeley, California)
Keiji Morokuma (Atlanta, Georgia)
Joseph Paldus (Waterloo, Canada)
Ruben Pauncz (Haifa, Israel)
Siegfried Peyerimhoff (Bonn, Germany)
John A. Pople (Evanston, Illinois)
Alberte Pullman (Paris, France)
Pekka Pyykkö (Helsinki, Finland)
Leo Radom (Canberra, Australia)
Klaus Ruedenberg (Ames, Iowa)
Henry F. Schaefer III (Athens, Georgia)
Isaiah Shavitt (Columbus, Ohio)
Per Siegbahn (Stockholm, Sweden)
Au-Chin Tang (Kirin, Changchun, China)
Rudolf Zahradnik (Prague, Czech Republic)

ADVISORY EDITORIAL BOARD

David M. Bishop (Ottawa, Canada)
Giuseppe del Re (Naples, Italy)
Fritz Grein (Fredericton, Canada)
Mu Shik Jhon (Seoul, Korea)
Mel Levy (New Orleans, Louisiana)
Jens Oddershede (Odense, Denmark)
Mark Ratner (Evanston, Illinois)
Dennis R. Salahub (Montreal, Canada)
Harel Weinstein (New York, New York)
Robert E. Wyatt (Austin, Texas)
Tokio Yamabe (Kyoto, Japan)

ADVANCES IN QUANTUM CHEMISTRY

**FROM ELECTRONIC STRUCTURE TO TIME-DEPENDENT PROCESSES:
A VOLUME IN HONOR OF GIUSEPPE DEL RE**

EDITOR-IN-CHIEF

PER-OLOV LÖWDIN

PROFESSOR EMERITUS

DEPARTMENT OF QUANTUM CHEMISTRY
UPPSALA UNIVERSITY
UPPSALA, SWEDEN

AND QUANTUM THEORY PROJECT
UNIVERSITY OF FLORIDA
GAINESVILLE, FLORIDA

EDITORS

**JOHN R. SABIN
MICHAEL C. ZERNER**

QUANTUM THEORY PROJECT
UNIVERSITY OF FLORIDA
GAINESVILLE, FLORIDA

ERKKI BRÄNDAS

DEPARTMENT OF QUANTUM CHEMISTRY
UPPSALA UNIVERSITY
UPPSALA, SWEDEN

GUEST EDITORS

ALESSANDRO LAMI

ISTITUTO DI CHIMICA QUANTISTICA ED
ENERGETICA MOLECOLARE DEL CNR
PISA, ITALY

VINCENZO BARONE

DIPARTIMENTO DI CHIMICA
UNIVERSITÀ DI NAPOLI FEDERICO II
NAPLES, ITALY

VOLUME 36



ACADEMIC PRESS

San Diego London Boston New York Sydney Tokyo Toronto

This book is printed on acid-free paper. (∞)

Copyright © 2000 by ACADEMIC PRESS

All Rights Reserved.

No part of this publication may be reproduced or transmitted in any form or by any means, electronic or mechanical, including photocopy, recording, or any information storage and retrieval system, without permission in writing from the Publisher.

The appearance of the code at the bottom of the first page of a chapter in this book indicates the Publisher's consent that copies of the chapter may be made for personal or internal use of specific clients. This consent is given on the condition, however, that the copier pay the stated per copy fee through the Copyright Clearance Center, Inc. (222 Rosewood Drive, Danvers, Massachusetts 01923), for copying beyond that permitted by Sections 107 or 108 of the U.S. Copyright Law. This consent does not extend to other kinds of copying, such as copying for general distribution, for advertising or promotional purposes, for creating new collective works, or for resale. Copy fees for pre-2000 chapters are as shown on the title pages. If no fee code appears on the title page, the copy fee is the same as for current chapters. 0065-3276/00 \$30.00

Explicit permission from Academic Press is not required to reproduce a maximum of two figures or tables from an Academic Press chapter in another scientific or research publication provided that the material has not been credited to another source and that full credit to the Academic Press chapter is given.

Academic Press

A Harcourt Science and Technology Company

525 B Street, Suite 1900, San Diego, California 92101-4495, USA

<http://www.apnet.com>

Academic Press

24-28 Oval Road, London NW1 7DX, UK

<http://www.hbuk.co.uk/ap/>

International Standard Book Number: 0-12-034836-5

PRINTED IN THE UNITED STATES OF AMERICA

99 00 01 02 03 04 BB 9 8 7 6 5 4 3 2 1

Contributors

Numbers in parentheses indicate the pages on which the authors' contributions begin.

Carlo Adamo (45), Dipartimento di Chimica, Università di Napoli Federico II, Naples I-80134, Italy

Mirko Sarzi Amadè (151), Dipartimento di Chimica Organica, Università di Pavia, Pavia 27100, Italy

Celestino Angeli (271), Dipartimento di Chimica, Università di Ferrara, Ferrara I-44100, Italy

Vincenzo Aquilanti (341), Dipartimento di Chimica, Università di Perugia, Perugia I-06123, Italy

I. Baraldi (121), Dipartimento di Chimica, Università di Modena, Modena, I-41100, Italy

C. Barbier (1), UFR de Chimie-Biochimie, Université Claude Bernard Lyon 1, F 69622 Villeurbanne, France

Vincenzo Barone (27, 45), Dipartimento di Chimica, Università di Napoli Federico II, Naples I-80134, Italy

Gaston Berthier (1), Laboratoire d'Etude Théorique des Milieux Extrêmes, Ecole Normale Supérieure, F 75231 Paris cedex 05, France

Raffaele Borrelli (301), Cattedra di Chimica Teorica, Università di Napoli, Federico II, Naples I-80134, Italy

Mario Bossa (169), Dipartimento di Chimica, Università "La Sapienza," Rome I-00185, Italy

Meziane Brahimi (301), Cattedra di Chimica Teorica, Università di Napoli, Federico II, Naples I-80134, Italy

Gabriella Capecchi (341), Dipartimento di Chimica, Università di Perugia, Perugia I-06123, Italy

Amedeo Capobianco (301), Cattedra di Chimica Teorica, Università di Napoli, Federico II, Naples I-80134, Italy

Simonetta Cavalli (341), Dipartimento di Chimica, Università di Perugia, Perugia I-06123, Italy

Frank De Proft (77), Department of Chemistry and Biochemistry, University of North Carolina, Chapel Hill, North Carolina 27599

Mariangela Di Donato (301), Cattedra di Chimica Teorica, Università di Napoli, Federico II, Naples I-80134, Italy

- Andrea di Matteo** (45), Dipartimento di Chimica, Università di Napoli Federico II, Naples I-80134, Italy
- Alessandro Ferretti** (283), Istituto di Chimica Quantistica ed Energetica Molecolare del CNR, Pisa 56126, Italy
- Sándor Fliszár** (27), Département de Chimie, Université de Montréal, Montréal, Québec, Canada H3C 3J7
- Remo Gandolfi** (151), Dipartimento di Chimica Organica, Università di Pavia, Pavia 27100, Italy
- Ireneusz Grabowski** (231), Institute of Physics, Nicholas Copernicus University, Toruń 87-100, Poland
- Roberto Improta** (301), Cattedra di Chimica Teorica, Università di Napoli, Federico II, Naples I-80134, Italy
- Karol Jankowski** (231), Institute of Physics, Nicholas Copernicus University Toruń 87-100, Poland
- Werner Kutzelnigg** (185), Lehrstuhl für Theoretische Chemie, Ruhr-Universität Bochum, Bochum D-44780, Germany
- Alessandro Lami** (283), Istituto di Chimica Quantistica ed Energetica Molecolare del CNR, Pisa 56126, Italy
- Xiangzhu Li** (231), Department of Applied Mathematics, University of Waterloo, Ontario, Canada N2L 3G1
- Shubin Liu** (77), Department of Chemistry and Biochemistry, University of North Carolina, Chapel Hill, North Carolina 27599
- T. Marino** (93), Dipartimento di Chimica, Università della Calabria, I-87030 Arcavacata di Rende (CS), Italy
- Roy McWeeny** (365), Dipartimento di Chimica e Chimica Industriale, Università di Pisa, Pisa 56126, Italy
- T. Mineva** (93), Institute of Catalysis, Bulgarian Academy of Sciences, 1113 Sofia, Bulgaria
- Fabio Momicchioli** (121), Dipartimento di Chimica, Università di Modena, Modena I-41100, Italy
- Guglielmo Monaco** (301), Cattedra di Chimica Teorica, Università di Napoli, Federico II, Naples I-80134, Italy
- Giorgio O. Morpurgo** (169), Dipartimento di Chimica, Università "La Sapienza," Rome I-00185, Italy
- Simone Morpurgo** (169), Dipartimento di Chimica, Università "La Sapienza," Rome I-00185, Italy
- Agnes Nagy** (77), Department of Chemistry and Biochemistry, University of North Carolina, Chapel Hill, North Carolina 27599
- Josef Paldus** (231), Department of Applied Mathematics, University of Waterloo, Ontario, Canada N2L 3G1
- Robert G. Parr** (77), Department of Chemistry and Biochemistry, University of North Carolina, Chapel Hill, North Carolina 27599
- Andrea Peluso** (301), Cattedra di Chimica Teorica, Università di Napoli, Federico II, Naples I-80134, Italy

- Carlo Petrongolo** (323), Dipartimento di Chimica, Università di Siena, Siena I-53100, Italy
- G. Ponterini** (121), Dipartimento di Chimica, Università di Modena, Modena I-41100, Italy
- Augusto Rastelli** (151), Dipartimento di Chimica, Università di Modena, Modena I-41100, Italy
- Christian Rolando** (271), Département de Chimie, Ecole Normale Supérieure F 75231 Paris cedex 05, France
- N. Russo** (93), Dipartimento di Chimica, Università della Calabria, I-87030 Arcavacata di Rende (CS), Italy
- Fabrizio Santoro** (323), Dipartimento di Chimica, Università di Siena, Siena I-53100, Italy
- E. Sicilia** (93), Dipartimento di Chimica, Università della Calabria, I-87030 Arcavacata di Rende (CS), Italy
- Yves G. Smeyers** (253), Instituto de Estructura de la Materia, CSIC, Madrid E-28006, Spain
- Michèle Suard** (271), Département de Chimie, Ecole Normale Supérieure, F 75231 Paris cedex 05, France
- M. Toscano** (93), Dipartimento di Chimica, Università della Calabria, I-87030 Arcavacata di Rende (CS), Italy
- D. Vanossi** (121), Dipartimento di Chimica, Università di Modena, Modena I-41100, Italy
- Edouard C. Vauthier** (27), Institut de Topologie et de Dynamique des Systèmes, Paris, France
- Giovanni Villani** (283), Istituto di Chimica Quantistica ed Energetica, Molecolare del CNR, Pisa 56126, Italy
- Pasquale von Herigonte** (185), Lehrstuhl für Theoretische Chemie, Ruhr-Universität Bochum, Bochum D-44780, Germany



Giuseppe Del Re (third from the left) in a photograph taken on the occasion of a meeting of the “Académie de Philosophie de Sciences” of Bruxelles, held in Vico Equense, in the Bay of Naples, in the year 1986. The other people are (from left to right): E. Scheibe, the eminent physicist J. A. Wheeler, and C. Dillworth.

Preface

Giuseppe Del Re was one of the early pioneers of quantum chemistry in Italy. We, the guest editors of this volume, were among his many students and still retain a vivid and happy memory of his lectures on the subject: he took the greatest care in clarifying the meaning of all the key concepts and always insisted that the ultimate goal of the beautiful theory he was unraveling before our eyes was, quite simply, to provide a useful tool for interpreting complex chemical phenomena. He made it clear to us that even if the Schrödinger equation provides, in principle, the means of calculating all molecular properties, it can never provide an "explanation" of anything. It has to be considered simply as a starting point for deriving, through a series of approximations, simplified models from which one could form concepts and interpretive schemes better adapted to the task of explaining, for example, trends in behavior of molecules in a given class and why they differ from those of molecules in another class. Giuseppe Del Re came from a classical and humanistic tradition and this may partly account for his continuing interest in philosophy and epistemology, meaning and interpretation, rather than the technicalities of calculation. His lectures were punctuated by excursions into literature and philosophy and helped us to appreciate the unity of all scientific and cultural endeavor.

In his own research, Del Re belongs firmly to the old school: he is a strenuous defender of the interpretive role that theory should have in chemistry, an attitude that is particularly appreciated by those of us who (growing up in the computer age) have sometimes been tempted to identify progress in quantum chemistry with progress in computer science.

The guest editors of this volume, along with many of his past and present students and collaborators, felt that Giuseppe Del Re deserved special recognition and that a special issue of *Advances in Quantum Chemistry* in his honor would be a fitting celebration of his 65th birthday. The idea was warmly encouraged by the Editors, Per-Olov Löwdin (with whom Giuseppe began his work in the field in the 1950s), Michael Zerner, and Erkki Brändas, and enthusiastically received by the contributors to this volume.

The contents of this special issue, with their many references to the scientific work of Giuseppe Del Re, provide an eloquent testimony to his influence. It remains only for us to draw attention to a few main themes in his activity and to indicate some of the points at which his contributions have proved, in our opinion, most original and fruitful.

First, it should be remarked that Giuseppe's capacity for debate was legendary. There are many anecdotes about his "round table" discussions (a very popular means of information exchange in Italy), where he would bring together a few eminent scientists from leading quantum chemistry groups in Europe (usually in remote and beautiful surroundings, e.g., on an island in the Bay of Naples) for a few days of almost unbroken discussion and argument about our discipline, where it was going, and what we were trying to do. The debates were hardly ever made public, but their impact on the participants was enormous. In those debates, a recurrent theme was the latent antithesis between the quantitative and qualitative approaches to quantum chemistry, fueled by the impressive development of computer technology and computational methods. Del Re's standpoint, supported by his many reminders about the necessity for compromise between accuracy and understanding, was that all *bona fide* methods, whether containing empirical parameters or not, could contribute to our understanding of observed facts provided they were based on "good physics." Among the ideas that he transmitted to his students and young collaborators was a belief that a qualitative rule with a vast field of applicability is far better than a quantitatively accurate result that gives no hint about general trends. In a certain sense, the density functional approach illustrates such ideas: it is a direct descendant from the free-electron gas and other one-electron models containing orbitals and empirical parameters within a sophisticated mathematical framework, and it appears to give reliable results of wide generality.

One of the earliest and best known contributions of Giuseppe Del Re also illustrates his quest for simplicity combined with generality: it concerns the implementation of Roothaan's SCF approach, in a very approximate form, by a "multi-local" treatment of each atom in the presence of its nearest neighbors. The procedure is "cyclic," involving one atom at a time, and applicable to very large molecules. Consequently it has been, and continues to be, widely used in "quantum biology." The use of localized orbitals, including in particular hybrid orbitals, is one of his continuing activities: apart from its historical interest, the concept of hybridization lies at the root of most textbook descriptions of molecular bonding in organic molecules, in inorganic compounds, and in the solid state. Del Re's commitment to localized-orbital descriptions, wherever possible, together with his *a priori* procedures for the construction of "optimum" hybrids, paves the way for the development of linear scaling procedures for the treatment of large molecules at both semi-empirical and *ab initio* levels. It is noteworthy that recent developments in *ab initio* valence bond theory add considerable support to the immense value of the hybridization concept and its use in all such applications.

Another seminal paper by Del Re and his collaborators was in the field of polymers and solids; again it concerned the implementation of the Roothaan SCF method, this time to systems with a periodic structure. This important area has developed enormously during the past 30 years, with many applications in new-materials technology and polymer science, but the contribution by Del Re *et al.* was among the very first in the field. Other relevant papers deal with the problem of surface states and chemisorption, including the definition of electro-negativity for a species absorbed on a metallic surface.

Already by the end of the 1960s, Del Re had convinced himself that quantum chemists should not confine their attention to structural and the more traditional spectroscopic aspects of chemistry, but should take account of the time evolution of systems prepared in nonstationary states, thus moving from the study of the time-independent Schrödinger equation to that involving time. With this prescience he no doubt anticipated the development of laser sources, with shorter and shorter pulses (down to a few femtoseconds) and of time-resolved spectroscopic techniques that were to furnish results that would provide challenges for new generations of theoreticians. His own contributions were mainly to the time-dependent approach to chemical reactions, to nonadiabatic coupling and non-radiative transitions, to intramolecular energy redistribution, and to electron and proton transfer reactions.

In recent years, intellectual curiosity coupled with his broad cultural background, has prompted Giuseppe Del Re to explore areas across the boundaries between pure science and the humanistic disciplines, leading him into the history of chemistry, epistemology, the problems of complexity, and the mind-body relationship.

We hope that this brief presentation will convey some idea of his scientific and nonscientific interests and of the depth of his influence on others; as a teacher, his aim has always been not simply to “inform,” but rather to form the minds of his students. It is therefore a particular pleasure for both of us, and for all the other authors, to have contributed to his special volume of *Advances in Quantum Chemistry*.

ALESSANDRO LAMI
VINCENZO BARONE

Biographic Notes

Giuseppe Del Re was born in Naples, April 4, 1932. He is a full professor of theoretical chemistry at the University of Naples and a full member of the International Academy for the Philosophy of Science (Brussels) and of the European Academy for Environmental Problems. He is a founding member of the International Academy for Transdisciplinary Research and Studies (Paris).

Del Re's main achievements in his primary research field are marked by the well-known "Del Re method" for the determination of charges in molecules and by the introduction of "maximum localization hybrids" in the molecular orbital method. Both procedures have been used by researchers throughout the world.

Del Re has published over 170 scientific papers in internationally recognized journals and authored a book on electronic states of molecules. He has been an invited professor in Canada, Germany, and France.

Selected List of Giuseppe Del Re's publications (number from the whole list in parentheses)

1. (8) G. Del Re: A Simple MO-LCAO Method for the Calculation of Charge Distribution in Saturated Organic Molecules. *J. Chem. Soc. (London)* 4031 (1958).
2. (13) G. Del Re: An Application of the Semi-empirical MO-LCAO Method to Indoxazene and Anthranil. *Tetrahedron* 10, 81 (1960).
3. (14) G. Del Re: On the Non-orthogonality Problem in the Semi-empirical MO-LCAO Method. *Il Nuovo Cimento* 17, 644 (1960).
4. (17) G. Del Re and R. Parr: Toward an Improved pi-Electron Theory. *Rev. Modern Phys.* 35, 604 (1963).
5. (18) G. Del Re: Hybridization and Localization in the Tight-Binding Approximation. *Theoret. Chim. Acta (Berl.)* 1, 188 (1963).
6. (25) G. Berthier, A. Veillard, and G. Del Re: Proton Splitting Constants and Hybridization in Aromatic Free Radicals. *Phys. Lett.* 8, 313 (1964).

7. (28) G. Del Re, U. Esposito, and M. Carpentieri: Bent Bonds, Hybridization, and the Maximum Localization Criterion. *Theoret. Chim. Acta (Berl.)* 6, 36 (1966).
8. (34) M. Suard, G. Berthier, and G. Del Re: Nova methodus adhibendi approximationem molecularium orbitalium ad plures iuxtapositas unitates. *Theoret. Chim. Acta (Berl.)* 7, 236 (1967).
9. (35) G. Del Re: On the Choice and Definition of Atomic-Orbital Bases. I. General Considerations; Promotion and Hybridization; Electric Dipole Moments. *Int. J. Quantum Chem. I*, 239 (1967).
10. (36) G. Del Re, J. Ladik, and G. Biczó: Self-Consistent-Field Tight-Binding Treatment of Polymers. I. Infinite Three-Dimensional Case. *Phys. Rev.* 155, 997 (1967).
11. (38) W. Kutzelnigg, G. Del Re, and G. Berthier: Correlation Coefficients for Electronic Wavefunctions. *Phys. Rev.* 172, 49 (1968).
12. (39) G. Del Re, J. Ladik, and M. Carpentieri: On the Effect of the Inclusion of Overlap in Tight-Binding Band Calculations of Solids. *Acta Phys. Hung.* 24, 391 (1968).
13. (40) R. McWeeny and G. Del Re: Criteria for Bond Orbitals and Optimum Hybrids. *Theoret. Chim. Acta (Berl.)* 10, 13 (1968).
14. (53) B. Nelander and G. Del Re: Chemical Bonds and Ab-Initio Molecular Calculations. *J. Chem. Phys.* 52, 5225 (1970).
15. (58) G. Del Re: Bond Energies in MO-LCAO Treatments of Saturated Molecules. *Gazz. Chim. It.* 102, 929 (1972).
16. (61) G. Del Re: Bond Properties from a Localized MO-LCAO Approach. *Int. J. Quantum Chem.* 7S, 193 (1973).
17. (64) G. Del Re: Current Problems and Perspectives in the MO-LCAO Theory of Molecules. *Adv. Quantum Chem.* 8, 95–136 (1974).
18. (65) A. Lami and G. Del Re: Decadimento degli stati molecolari eccitati. *La Chimica e l'Industria* 56, 365 (1974).
19. (69) G. Del Re: Localization, Bonds, and Physical Models of Molecular Reality. In "Localization and Delocalization in Quantum Chemistry" (O. Chelvet *et al.*, eds.), pp. 153–174. Dordrecht: Reidel (1976).
20. (70) G. Del Re: The Non-orthogonality Problem and Orthogonalization Procedures. In "Quantum Science, Methods, and Structure" (Calais *et al.*, eds.), pp. 53–74. New York: Plenum Press (1976).
21. (72) G. Del Re and A. Lami: Aspects of the Quantum Theory of Chemical Reactions. *Bull. Soc. Chim. Belg.* 85, 995 (1976).
22. (83) G. Del Re, G. Berthier, and J. Serre: Electronic States of Molecules and Atom Clusters. *Lecture Notes in Chemistry*, Vol. 13, pp. 1–177. Berlin: Springer (1978).
23. (87) G. Del Re, V. Barone, N. Montella, and A. Julg: On the Shapes of Weakly Adsorbed Two-Dimensional Clusters. *Surf. Sci.* 97, 537–552 (1980).

24. (89) G. Del Re and J. Ladik: Adsorption of Molecules on Polymers. I. A General Analysis in Terms of the Green-Matrix Version of the Local-Impurity SCF Approach. *Chem. Physics* 49, 321–332 (1980).
25. (94) G. Del Re: Ground-State Charge Transfer and Electronegativity Equalization. *J. Chem. Soc. (Far. Trans. II)* 77, 2067–2076 (1981).
26. (95) G. Del Re: Analyse théorique de la Chimisorption en tant que Phénomène Local. In “Les Agrégats” (Cyrot-Lackmann, ed.), pp. 365–401. Paris: Editions de Physique (1981).
27. (107) G. Del Re: H-Bond Charge-Relay Chains in Multi-Heme Cytochromes and Other Biomolecules. In “Spectroscopy of Biological Molecules” (C. Sandorfy and T. Theophanides, eds.), pp. 15–37. Dordrecht: Reidel (1984).
28. (108) G. Del Re: Frequency and Probability in the Natural Sciences. *Epistemologia* 7, spec. issue p. 75 (1984).
29. (115) G. Del Re, S. Fliszar, M. Comeau, and C. Mijoule: Net Charges and Valence AO's in the Methylamines: The Hydrogen Basis Set and the Properties of Nitrogen. *Can. J. Chem.* 63, 1487–1491 (1985).
30. (116) G. Del Re, A. Peluso, and C. Minichino: H-Bridges and Electron Transfer in Biomolecules. Study of a Possible Mechanism on a Model Charge-Recombination System. *Can. J. Chem.* 63, 1850–1856 (1985).
31. (118) G. Del Re, M. Kolar, and F. Cyrot-Lackmann: Iterative LCAO Treatment with Overlap and Band Occupation in the Iron-Group Metals. *J. Phys.* 46, 927–932 (1985).
32. (129) G. Del Re: The Historical Perspective and the Specificity of Chemistry. *Epistemologia* 10, 231–240 (1987).
33. (130) M. C. Barreto, P. Ciambelli, G. Del Re, and A. Peluso: A Theoretical Study of Ion Selectivity of Zeolites. *J. Phys. Chem. Solids* 40, 1–12 (1987).
34. (132) C. Liegener and G. Del Re: Chemistry vs. Physics, the Reduction Myth, and the Unity of Science. *Z. f. Allg. Wissenschaftstheorie* 18, 165–174 (1987).
35. (139) G. Del Re: Cause, Chance, and the State-Space Approach. In “Probability in the Sciences” (E. Agazzi, ed.), pp. 89–101. Dordrecht: Kluwer (1988).
36. (142) G. Del Re, C. Barbier, and G. Villani: Toward a Description of Reactions of CO and H₂ and Fe Surfaces Based on SCF Hybrid AOs and Electronegativity Equalization. *Nuovo Cimento* 12, 103–115 (1990).
37. (147) G. Del Re, W. Foerner, D. Hofmann, and J. Ladik: Discrete State Approach to the Time Dependence of Molecular Phenomena. *Chem. Phys.* 139, 265–281 (1989).
38. (151) G. Del Re and C. Adamo: Oximine Form of the Peptide Bond as a Transient Modification in Enzyme Redox Reactions. *J. Phys. Chem.* 95, 4231–4238 (1991).

39. (160) G. Del Re: Reactivity Indices. Remarks on Present State and Prospects. *Theoret. Chim. Acta* 85, 109–119 (1993).
40. (165) C. Angeli, G. Del Re, and M. Persico: Quasi-bond Orbitals from Maximum-Localization Hybrids for ab Initio CI Calculations. *Chem. Phys. Lett.* 233, 102–110 (1995).
41. (170) A. Peluso and G. Del Re: On the Occurrence of a CT Step in Aromatic Nitration. *J. Phys. Chem.* 100, 5303–5309, (1996).
42. (179) G. Del Re: “The Ontological Status of Molecular Structure,” in press, Hyle: Karlsruhe (1999).

HALF A CENTURY OF HYBRIDIZATION[‡]

by C. Barbier* and G. Berthier**

(*) U.F.R. de Chimie-Biochimie, Université Claude Bernard Lyon 1
43 Boulevard du 11 Novembre 1918, F 69622 Villeurbanne cedex

(**) Laboratoire d'Etude Théorique des Milieux Extrêmes
Ecole Normale Supérieure, 24 rue Lhomond, F 75231 Paris cedex 05

Vidisne aliquando Clitumnus fontem? Si nondum vide...
(*Plin. Secund., Epist. VIII, 8*)

CONTENTS

1. Introduction : A perennial concept
 - 1.1 The first period
 - 1.2 Valence state theory
 - 1.3 The present status of hybridization
 2. Theoretical determination methods of hybrid orbitals
 - 2.1 Geometrical constructions
 - 2.2 Maximum overlap criteria : The Del Re method
 - 2.2.1 Building procedure for maximum localization hybrids
 - 2.2.2 The lone-pair problem
 - 2.2.3 Extensions to large basis sets
 3. Conclusion : A multiple-purpose instrument
 - 3.1 Miscellaneous structural applications
 - 3.2 Quantum-chemical flashback
- References

[‡] dedicated to Professor G. Del Re

1. Introduction : A perennial concept

Through its ups and downs, the concept of orbital hybridization is most significative for the perspectives opened out by Quantum Chemistry from about 1930. Let us only mention all the disputes in which it was involved during almost one century with regard to tricky questions of molecular structure (*i.e.*, the supremacy of valence-bond pictures over molecular orbitals or *vice-versa*, the physical content of the resonance theory, the localization *versus* delocalization dilemma and so on...). Furthermore, its study gives us a good example of the specificity of the scientific explanation among chemists (*i.e.*, the rejection of reductionism to Physics [1]).

1.1 The first period

The algebraic manipulation of atomic orbitals to which the name of hybridization has been attached was initiated by Pauling [2]. Merging together the idea of shared electron pairs of the classical valence theory of Lewis and the quantum mechanical treatment newly presented by Heitler and London for the hydrogen molecule [3], he offered a somewhat intuitive description of the chemical bond in complex molecules by using "hybrid orbitals of maximum bond-forming power" [4]. More concretely, the four valences of the carbon atom in the methane molecule were assigned to four sp^3 orbitals whose axes of maximum electron density were arranged in conformity with the dictum [5] "There is a large amount of experimental evidence suggesting that the carbon atom has four valencies radiating from the centre to the corners of a regular tetrahedron".

In subsequent independent papers, Pauling [4] and Slater [6] generalized the valence-bond treatment made for the H_2 molecule to polyatomic systems as H_2O , NH_3 , CH_4 *etc* ... where an atom of the first period (the second row) is linked to hydrogens by several two-electron bonds ; they described the valence orbitals coming from the central atom by appropriate s and p combinations known later as hybrid orbitals. At the same time Hund [7] and Mulliken [8] presented another quantum theory of valence, the molecular orbital method in LCAO form, using the spectroscopic concept of molecular configuration built from s, p, d ...pure atomic orbitals. The actual status of the hybridization process was clarified by Van Vleck [9], who showed that the various approximations

introduced in the quantum mechanical treatment of valence were responsible for many differences of interpretation rather than the content of the methods themselves. For instance, hybridization involved in the perfect pairing of localized electron-pairs and resonance limited to chemically significant bond functions amount the same thing [10,11] This culminates in the final equivalence of methods starting from common sets of -pure or mixed- atomic orbitals (*i.e.*, valence bond or molecular orbital treatments including all the possible distributions of electrons in the wave function) first proved for very simple systems [12,13] and later generalized [14,15].

1.2 Valence state theory

From the point of view of Natural Philosophy, the concept of atomic valence states, developed by Van Vleck, Mulliken and others [9,16,17,18] in close connection with hybridization, is a major achievement, for it gives a microscopic picture of the atom *in situ* taking into account the level of complexity to be preserved in the theoretical analysis of chemical facts [1]. The basic ingredient of the theory consists in a formal decoupling of some paired electrons for the atom considered in accordance with its valence in molecules : To do that, two steps may be necessary : first, promoting one electron of a 2s filled subshell, if necessary, into the adjacent p shell (case of carbon s^2p^2 versus $s^1p^1p^1$) or d shell (case of transition metals s^2d^{n-2} versus s^1d^{n-1}) ; second, randomizing the spins of the valence electrons with respect to each other (*i.e.*, by means of the value $1/2 K_{jj}$ assigned to the exchange term corresponding to the valence orbitals of the atoms in question [16]).

The valence state definition above is just operative, for it generates energy terms calculable from spectroscopic data in the frame of the Slater model of atoms in their neutral and adjacent ionized states. The valence orbitals can be defined in pure or hybrid forms, corresponding to familiar s,p tetrahedral (te), trigonal (tr) and digonal (di) sets for light atoms, or to the huge variety of s,p,d combinations for heavier atoms [19,20]. To conclude by a fairly common remark on the valence states, we will add the fact that their building-up process from atomic experimental data, the F_k and G_k Slater parameters [21], implies that they do not be thought as physical observables, but rather to a linear combination of genuine spectroscopic states [22]. Without going into details of

chemistry, the energy loss due to the contribution of atomic excited states in this mixture is said to be largely paid by the formation of bonds.

1.3 The present status of hybridization

Nowadays, the concept of hybridization remains the basis of the most popular description of the molecular bonding, namely that of σ , π - and δ - chemical bonds between atoms in organic [23] as well as inorganic compounds and solids [24]. The terminology of hybridization gives us a simple way to characterize "atoms in molecules" [25] by their valence states, which in the same time precises the type of geometry of the atomic site considered. We can use hybridization not only to sketch the spatial distribution of the binding electron pairs, but also according to Pauling to describe lone pairs with privileged directions depending on their percentage of s and p characters [26,27]. If, finally, we pass over the questions connected to its theoretical origin, hybridization can be considered as a simple way for describing, both in speaking and in writing, the so-called molecular observables in terms of atomic components.

Another reason for the success of such interpretations lies in the fact that hybridization becomes a flexible model applicable to systems of arbitrary shape when it is equipped with the maximum overlapping principle establishing a link between bond strengths and overlap integrals of hybrid orbitals centered on neighbouring atoms [28,29]. As it will be shown in the next section, this is the guiding idea of Murrell [30], Coulson [31] and Del Re [32] for *a priori* calculations of hybrids in a molecule. In the seventies, however, hybridization has been fiercely criticized by people pretexting that its use supposes a preliminary knowledge of the molecular structure to be predicted and preferring the VSEPR orbital-free model of Gillespie instead [33]. In so far as a qualitative picture of the molecular structure is requested, it would be better to say that both models are basically isomorphous, mimicking molecules by a set of initially equivalent sites whose interaction is afterwards governed by an energy criterion (*i.e.*, the maximum overlapping principle of hybridization, or the hierarchy of electron-pair repulsions in the VSEPR model [34]). By no means, the quantum-chemical applications of the hybridization concept are really concerned in this quarrel ignoring the fact it is first of all a procedure intended to prepare atoms in a molecule to bonding. To end the matter, suffice it to speak in measured terms

of hybridization : i) it is a way for constructing "chemical orbitals" , that is to say wave functions which preserve the concept of bond properties [35,36] and in the same time gives us good starting points for the developpement of various semi-empirical or *ab initio* treatments-. ii) it is not an experimentally observable phenomenon, but according to Coulson merely "a feature of a theoretical description".

2. Theoretical determination methods of hybrid orbitals

2.1 Geometrical constructions

To avoid possible problems of linear dependence , it is generally assumed that the hybrid orbitals h_{Ai} centered on a given atomic site A are orthonormal :

$$\langle h_{Ai} | h_{Aj} \rangle = \delta_{ij} \quad (1)$$

If so, the direction and form of hybrids starting from the central atom A of a highly symmetrical system, as methane or complexes of transition metals, for instance $[\text{Co}(\text{NH}_3)_6]^{3-}$, are defined by the geometry of the molecule, independently of the nature of the nearest neighbours B. In such cases, hybridization of orbitals on atom A gives us a convenient basis for describing the set of equivalent bonds A-B by combination with the orbitals of atoms B ; hybrids of A adapted to the symmetry of the molecule (*i.e.*, to its directed valences) are easily determined by projecting a set of central-field orbitals s,p,d ... of atom A into the irreducible representations of the point group to which the molecule belongs [19]. Lists of all the possible types of s,p,d hybrids for highly symmetrical molecules and a number of s, p, d, f combinations are given in the literature [37,38]. Hybrids for some compounds of lower symmetry have been also reported [39,40].

More generally, hybrids pointing in any direction around an atomic site A can be obtained by straightforward geometrical constructions [41] provided the form of the molecule is already known (*i.e.*, by another theoretical or experimental way). The vectorial character of the p_x , p_y , p_z orbitals transforming as the axes of a cartesian coordinate system ensures the success

of such calculations, except if the valence angles become smaller than 90° : A well known example is cyclopropane, a three-membered ring with bond angles of 60° to be described according to Coulson and Moffitt [42] by a model of hybridized "banana bonds" explaining its conjugation properties as a substituent on aromatic nuclei. A somewhat similar situation occurs with four-membered rings, as cyclobutane [43]. It has been suggested [44] that the difficulties leading to bent banana bonds in small rings could be circumvented by accepting combinations with complex coefficients as solutions for hybrids. The difficulties due to the occurrence of broken symmetry solutions with respect to time reversibility when using complex wave functions can be solved by separating real and imaginary parts in variational calculations [45]. However, bent bonds formed from real orbitals are a little more convenient [46].

If we limit ourselves to s and p combinations, we can state without any doubt that the bonds formed between an atom A and its neighbours B using appropriate geometrical hybrids verify the principle of "maximum overlapping of atomic orbitals" (M.O.A.O. criterion) even if the atoms B linked to A are different. Clearly, the integrated product $h_A h_B$ of a pair of σ hybrid orbitals giving the best bond energy E_{AB} will be as large as possible if the directions of h_A and h_B in space coincide, the overlap between h_A and h_B being maximum. However, hybridization of d (and f) put some problems to theoreticians, for instance the preservation of the cylindrical symmetry properties of s p d hybrids [47] and the unicity of possible solutions [48], but they are not serious according to Pauling [49]. The alternative suggested by Daudel and Bucher [50] was relaxing the orthogonality constraints.

2.2 Maximum overlap criteria : The Del Re method

Methods for *a priori* determination of atomic hybrids using the principle of maximum overlapping have been implemented towards the sixties, either in global form or in a more local form. The procedures used by Murrell for quasi centro-symmetrical molecules [30] and by Coulson and Goodwin [31] consist in simply maximizing the sum of all overlap integrals between σ paired orbitals. More or less different techniques have been suggested later [51,52] The method developed by Del Re from 1963 [32] is a more refined multi-local treatment involving each atom and its next neighbours in turn. Taking the likeness of the eigenvectors of the overlap and effective Hamiltonian matrices for granted as a

consequence of the possibility of evaluating off-diagonal terms approximately by means of the Mulliken proportionality rule to overlap (see [53,54]), this procedure is based on a principle of "maximum localization of hybrid orbitals" (M.L.H.O. criterion). The best hybrids are the ones which lead to a localization of the overlap matrix of the whole molecule, under the condition that the set of orbitals assigned in this manner to each atom be orthonormal. Here, the word "localization" means that the resulting Hamiltonian is -to a certain degree of approximation- factorized in 2x2 blocks corresponding to the various pairs of bonded atoms, except if the presence of several large off-diagonal elements suggests the idea of many-center bonds. Such a definition gives us a unique set of hybridized functions for each atom of a molecule consistent with the maximum overlapping criterion and in the same time an efficient computational procedure for any system. The equations of the Del Re hybridization method have been written out first in the case of single-zeta s, p valence orbitals of first-row atoms and generalized later to more complicated basis sets, as it will be discussed below.

2.2.1 Building procedure of maximum localization hybrid orbitals

Consider a system composed of atoms A, B, C *etc* ... and let χ_A, χ_B, χ_C be their respective 2s, 2p_x, 2p_y, 2p_z valence orbitals defined in a single coordinate system. The basis set of the whole molecule can be represented by the row vector $\chi = (\chi_A, \chi_B, \chi_C \text{ etc } \dots)$ collecting all these basis functions :

$$\chi = (2s_A \quad 2p_{xA} \quad 2p_{yA} \quad 2p_{zA} \quad 2s_B \quad 2p_{xB} \quad 2p_{yB} \quad 2p_{zB} \dots) \quad (2)$$

The overlap matrix $S = (\chi^\dagger, \chi)$ formed of diagonal elements AA, BB all equal to the 4x4 unit matrix **I** and of off-diagonal blocks AB, AC *etc* ... such as $S_{AB} = (\chi^\dagger_A, \chi_B)$ can be written as follows :

$$S = \begin{array}{cccc} & \mathbf{I} & \mathbf{S}_{AB} & \mathbf{S}_{AC} & \dots \\ \mathbf{S} = & \dots & \mathbf{I} & \mathbf{S}_{BC} & \dots \\ & \dots & \dots & \mathbf{I} & \dots \end{array} \quad (3)$$

where S_{AB} , S_{AC} etc ... are the overlap matrices between pure atomic orbitals of A, B, C etc ...

$$\begin{array}{rcccl}
 & & \langle 2s_A | 2s_B \rangle & \langle 2s_A | 2p_{xB} \rangle & \dots \\
 S_{AB} = & & \langle 2p_{xA} | 2s_B \rangle & \langle 2p_{xA} | 2p_{xB} \rangle & \dots \\
 & & \dots & \dots & \dots
 \end{array} \quad (4)$$

We have to find a unitary transformation U changing the χ basis into a new one χ' such as U only mixes the orbitals belonging to a same atom without mixing them with those of other atoms. Then the χ' basis is changed into

$$\chi = (\chi_A U_A \quad \chi_B U_B \quad \chi_C U_C \quad \text{etc} \quad \dots) \quad (5)$$

and S_{AB} and S into

$$S'_{AB} = U^\dagger_A S_{AB} U_B \quad (6)$$

$$\begin{array}{rcccl}
 & \mathbf{I} & U^\dagger_A S_{AB} U_B & U^\dagger_A S_{AC} U_C & \dots \\
 S' = U^\dagger S U = & \dots & \mathbf{I} & U^\dagger_B S_{BC} U_C & \dots \\
 & \dots & \dots & \mathbf{I} & \dots
 \end{array} \quad (7)$$

The localization would be perfect if each of the off-diagonal blocks S'_{AB} , S'_{AC} ... contains only one non-zero element on its diagonal, say λ_{AB} λ_{AC} ... , for a given hybrid of atom A should form a bond with only one hybrid belonging to each of its neighbouring atoms B, C ... Therefore, the U transformation has to keep the diagonal blocks of S unchanged and to transform the remaining part of the S matrix in order to have only one element in each row and column. It is always possible to arrange the hybrid orbitals of any (polyatomic) molecule in such a way that the overlaps $\langle h_{AB} | h_{BA} \rangle$, $\langle h_{AC} | h_{CA} \rangle$ etc ... are on the

diagonal of their S'_{AB} S'_{AC} *etc...* respective blocks. The maximum overlap condition will be practically satisfied if all the S'_{XY} blocks are as close as possible to diagonal matrices, that is to say if the S' whole matrix has the following form :

$$S' = \begin{pmatrix} 1 & 0 & 0 & 0 & \lambda_{AB} & \dots & \dots & \dots & \dots \\ 0 & 1 & 0 & 0 & \dots & \dots & \dots & \dots & \dots \\ 0 & 0 & 1 & 0 & \dots & \dots & \dots & \dots & \dots \\ 0 & 0 & 0 & 1 & \dots & \dots & \dots & \dots & \dots \\ \lambda_{BA} & \dots & \dots & \dots & 1 & 0 & 0 & 0 & \dots \\ \dots & \dots & \dots & \dots & 0 & 1 & 0 & 0 & \dots \\ \dots & \dots & \dots & \dots & 0 & 0 & 1 & 0 & \dots \\ \dots & \dots & \dots & \dots & 0 & 0 & 0 & 1 & \dots \\ \dots & \dots & \dots & \dots & \dots & \dots & \dots & \dots & \dots \end{pmatrix} \quad (8)$$

where the terms of the off-diagonal blocks explicitly written are those having the largest absolute values for bond-hybrid overlaps. For instance, we have:

$$\begin{aligned} (U^\dagger_A S_{AB} U_B)_{11} &= \lambda_{AB} && \text{for the AB block} \\ (U^\dagger_B S^\dagger_{AB} U_A)_{11} &= \lambda_{BA} && \text{for the BA block} \end{aligned} \quad (9)$$

with $\lambda_{BA} = \lambda_{AB}$. Putting U^\dagger_{A1} and U^\dagger_{B1} for the first rows of U^\dagger_A and U^\dagger_B , that is to say :

$$U^\dagger_{A1} S_{AB} U_B = (\lambda_{AB}) \times (1, 0, 0, 0) \quad (10)$$

$$U^\dagger_{B1} S^\dagger_{AB} U_A = (\lambda_{AB}) \times (1, 0, 0, 0) \quad (11)$$

and multiplying Eqs (10) and (11) on the right by U^\dagger_B and U^\dagger_A respectively, we get

$$U^\dagger_{A1} S_{AB} = \lambda_{AB} U^\dagger_{B1} \quad (12a)$$

$$U^\dagger_{B1} S^\dagger_{AB} = \lambda_{AB} U^\dagger_{A1} \quad (12b)$$

or after multiplying Eq. (12a) by S^\dagger_{AB} , substituting Eq. (12b) and transposing :

$$\mathbf{S}_{AB}\mathbf{S}_{AB}^{\dagger}\mathbf{U}_{A1} = \lambda_{AB}^2 \mathbf{U}_{A1} \quad (13)$$

Similarly,

$$\mathbf{S}_{AB}^{\dagger}\mathbf{S}_{AB}\mathbf{U}_{B1} = \lambda_{AB}^2 \mathbf{U}_{B1}$$

Thus, \mathbf{U}_{A1} and \mathbf{U}_{B1} are the eigenvectors associated with the largest eigenvalues of $\mathbf{S}_{AB}\mathbf{S}_{AB}^{\dagger}$ and $\mathbf{S}_{AB}^{\dagger}\mathbf{S}_{AB}$ respectively. If we now pass to the pair of atoms A C, we can apply the same treatment to the \mathbf{S}'_{AC} block matrices, so that we have a new pair of equations defining \mathbf{U}_{A2} and \mathbf{U}_{C1} and so on ... This process has been repeated for each atom, giving a number of conditions depending on its number of valence orbitals and next-neighbours (here, four).

The eigenvectors computed from the largest eigenvalues of Eq. (13), say $\hat{\mathbf{U}}_{A1}$, $\hat{\mathbf{U}}_{A2}$, $\hat{\mathbf{U}}_{A3}$, $\hat{\mathbf{U}}_{A4}$, $\hat{\mathbf{U}}_{B1}$, $\hat{\mathbf{U}}_{B2}$, $\hat{\mathbf{U}}_{B3}$, $\hat{\mathbf{U}}_{B4}$ etc ..., give only a first approximation $\hat{\mathbf{U}}$ of the unitary transformation \mathbf{U} we wanted. It is due to the fact that the local transformations $\hat{\mathbf{U}}_A$, $\hat{\mathbf{U}}_B$ defined in this way for the various atoms A, B etc...are not unitary because the overlap matrices connecting each of them with its neighbours do not generally commute. This deficiency can be cured by substituting unitary transformations \mathbf{U}_A , \mathbf{U}_B for $\hat{\mathbf{U}}_A$, $\hat{\mathbf{U}}_B$ etc ... as close as possible from the latter (*i.e.*, by requiring that the scalar product of the $\hat{\mathbf{U}}_A$ and \mathbf{U}_A vectors is maximum) Using Eq. (13), the corresponding variational problem writes:

$$\delta\{\sum_i [\lambda_{Ai}^2 (\hat{\mathbf{U}}_{Ai}^{\dagger}\mathbf{U}_{Ai} + \mathbf{U}_{Ai}^{\dagger}\hat{\mathbf{U}}_{Ai}) - \sum_j \mathbf{M}_{ij} \mathbf{U}_{Ai}^{\dagger} \mathbf{U}_{Aj}]\} = 0 \quad (14)$$

with a symmetrical set \mathbf{M}_A of Lagrange multipliers \mathbf{M}_{ij} preserving the unitary character of the \mathbf{U}_A transformations. Differentiating Eq. (14), we get a couple of transposed equations such as:

$$\hat{\mathbf{U}}_A \Lambda_A^2 = \mathbf{M}_A \mathbf{U}_A \quad (15)$$

where Λ_A^2 is a diagonal matrix of elements

$$\lambda_{A1}^2 = \lambda_{AB}^2, \lambda_{A2}^2 = \lambda_{AC}^2, \text{ etc ...} \quad (16)$$

We can solve them by assuming that the \mathbf{U}_A blocks forming the \mathbf{U} unknown transformation are the products of two new unitary matrices \mathbf{V}_A and \mathbf{W}_A^\dagger , the first one permitting by the same token to reduce \mathbf{M}_A to its diagonal form \mathbf{m}_A :

$$\mathbf{U}_A = \mathbf{V}_A \mathbf{W}_A^\dagger \quad (17a)$$

$$\mathbf{M}_A = \mathbf{V}_A \mathbf{m}_A \mathbf{V}_A^\dagger \quad (17b)$$

Then, Eq.(15) and its transpose are replaced by

$$\hat{\mathbf{U}}_A \Lambda_A^2 = \mathbf{V}_A \mathbf{m}_A \mathbf{W}_A^\dagger \quad (18a)$$

$$\Lambda_A^2 \hat{\mathbf{U}}_A^\dagger = \mathbf{W}_A \mathbf{m}_A \mathbf{V}_A^\dagger \quad (18b)$$

equivalent to $\hat{\mathbf{U}}_A \Lambda_A^2 \mathbf{W}_A = \mathbf{V}_A \mathbf{m}_A \quad (19a)$

$$\Lambda_A^2 \hat{\mathbf{U}}_A^\dagger \mathbf{V}_A = \mathbf{W}_A \mathbf{m}_A \quad (19b)$$

Multiplying Eq. (18b) by Eq. (19a) and Eq. (18a) by Eq. (19b) on each side, we obtain two eigenvalue equations, namely :

$$\Lambda_A^2 \hat{\mathbf{U}}_A^\dagger \hat{\mathbf{U}}_A \Lambda_A^2 \mathbf{W}_A = \mathbf{W}_A \mathbf{m}_A^2 \quad (20a)$$

$$\hat{\mathbf{U}}_A \Lambda_A^4 \hat{\mathbf{U}}_A^\dagger \mathbf{V}_A = \mathbf{V}_A \mathbf{m}_A^2 \quad (20b)$$

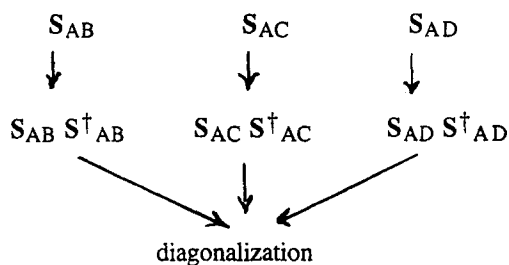
the resolution of which gives \mathbf{W}_A and \mathbf{V}_A , that is to say the hybridization matrix $\mathbf{U}_A = \mathbf{V}_A \mathbf{W}_A^\dagger$ for each atom A we were looking for. However, it is necessary to make sure that the elements of the \mathbf{m}_A matrix as calculated from Eq. (19a) have non-negative values, a condition which may be always ensured by changing signs in the columns of \mathbf{W}_A initially computed from Eq.(19b) [32].

In Fig.1, we give the flow chart of the computer program to be implemented in order to determine the best possible hybridization matrix U for a molecule satisfying the criterion of maximum overlap according to Del Re. The successive steps of the calculation for a given atom, say A , are :

1. Construct the overlap matrices S_{AB} , S_{AC} ...
2. Compute $S_{AB} S_{AB}^\dagger$ and $S_{AB}^\dagger S_{AB}$, $S_{AC} S_{AC}^\dagger$ and $S_{AC}^\dagger S_{AC}$ etc ...
3. Evaluate the eigenvalues λ^2 of the couples of AB , AC etc ... product matrices
4. Select the highest eigenvalues $(\lambda^2_{AB})_{\max}$, $(\lambda^2_{AC})_{\max}$,... and the corresponding eigenvectors and form the \hat{U}_A blocks, the columns of which are the eigenvectors associated with $(\lambda^2_{AB})_{\max}$, $(\lambda^2_{AC})_{\max}$ etc ...
5. Form the diagonal matrix Λ from the λ squared precedent values
6. Calculate and diagonalize the $\Lambda^2_A \hat{U}_A^\dagger \hat{U}_A \Lambda^2_A$ product, the eigenvectors of which are the columns of the new matrix W_A and the eigenvalues are the elements m_{Ai}^2 .
7. Calculate and diagonalize the $\hat{U}_A \Lambda^4_A \hat{U}_A$ product, the eigenvectors of which are the columns of the new matrix V_A .
8. Form the product $V_A W_A^\dagger = U_A$ giving the hybridization matrix of the orbital centered on atom A (and the angles between resulting hybrids from their s and p percentages)
9. Repeat for the next atom B and so on ...

Fig.1 - Résumé of the hybridization algorithm for atom A linked to atoms B, C, D

$$\chi = (s_A p_{xA} p_{yA} p_{zA} \quad s_B p_{xB} p_{yB} p_{zB} \quad s_C p_{xC} p_{yC} p_{zC} \quad s_D p_{xD} p_{yD} p_{zD})$$



$$\lambda^2_{Ai} = \lambda^2_{AB}, \lambda^2_{AC}, \lambda^2_{AD}$$

$$\hat{U}_{Ai} = \hat{U}_{AB}, \hat{U}_{AC}, \hat{U}_{AD}$$

Λ^2 : diagonal matrix formed
by the elements λ^2_{Ai}

\hat{U}_A : square matrix formed
by the eigenvectors \hat{U}_{Ai}

$$\Lambda^2_A \hat{U}_A^\dagger \hat{U}_A \Lambda^2_A$$

$$\hat{U}_A \Lambda^4_A \hat{U}_A^\dagger$$

diagonalization

diagonalization

$$m^2_A \text{ and } W_A$$

$$m^2_A \text{ and } V_A$$

$$V_A W_A^\dagger = U_A$$

The algorithm of Fig.1 works satisfactorily as soon as atom A is able to use all its valence orbitals to form as many bond hybrids with its partners B, because a well-defined non-zero λ_{Ai}^2 value is effectively found for each hybrid. In the case of an insufficient number of partners B as in Fig.1, the zero input-values assigned to orthogonal orbitals corresponding to absent links have to be treated in different ways according to the structure of the molecule considered :

- i) A belongs to a conjugated system ; $\lambda_{Ai}^2=0$ corresponds to a $(2)p\pi$ pure atomic orbital
- ii) A is a heteroatom bearing a σ lone-pair, as nitrogen in amines or oxygen in carbonyls ; $\lambda_{Ai}^2 = 0$ has to be substituted by an appropriate non-zero value in order to have a set of hybrids correctly directed [55], as will be described in Section 2.2.2
- iii) A is a radicalic center, as in trivalent carbon compound ; $\lambda_{Ai}^2 = 0$ is retained or substituted by another value, according as the species in question is a π or a σ free radical

In passing, we will note that the algorithm first developed for hybridization can be adapted to the problem of the localization of the normal vibration modes given by the GF Wilson method [56].

2.2.2 The lone-pair problem

The sole maximum localization criterion is unable to give physically significant results for the σ lone pair of a heteroatom because the not-overlapping hybrid corresponding to it is completely determined by the orthogonalization condition with the bond hybrids. As a result, the 2s valence orbital is ill-balanced between the components of the whole set of resulting hybridized functions, and so the angles between them is in poor agreement with the experimental bond angles ; for instance, the bonding hybrids of water appear to have a high s-character, so that they form a too large angle (138° *versus* 105° for the experimental bond angle). In such cases the maximum localization criterion strictly limited to bond overlaps (*i.e.*, without any restriction on non-bonding hybrids, except for the orthogonalisation condition) yields undesirable bent bonds.

The situation is drastically changed by introducing new conditions on non-bonding electrons, for instance on energetical reasons. According to considerations going back to Pauling, the fact that non-shared electrons of an

atom have the propensity of occupying lower energy levels and, consequently, hybrid orbitals whose s-character is more important than that of the bonding ones, can be envisaged. This was, in fact, the origin of the hierarchy of the electron-pair repulsion terms in the Gillespie-Nyholm model [33].

The solution retained by Del Re *et al.* was to treat the question in a heuristic suitable way. The non-bonding orbitals of A are determined as if they were overlapping with a non-specified orbital belonging to a phantom partner B' in addition to its real neighbours B₁, B₂, ... The corresponding λ^2_{Anb} value between, say 0 and 0.5, was adjusted by plotting the angle of the resulting hybrids, to be associated to the bonds between A and B₁, B₂, ... *versus* the experimental angle B₁AB₂ in reference molecules. Using ordinary Slater orbitals for the overlap integrals requested by the Del Re method, it is found that the value $\lambda^2_{\text{nb}} = 0.25$ give bond hybrids practically equal to the experimental bond angles in water and ammonia, whereas they are slightly smaller than their experimental counterparts in some methyl derivatives.

In computer programs using hybridization routines, an automatic procedure for evaluating the weights λ^2_{Anb} assigned to the σ lone-pair hybrids of atom A has been devised, namely the arithmetic mean of the weights λ^2_{AB} corresponding to the set of bond hybrids from A divided by a scale factor κ . Different values have been suggested for κ , 1.45 [57] or 1.30 [58] according to the method in which hybridization has been implemented. For generality's sake, λ^2_{Anb} is finally multiplied by the number of electron pairs occupying the non-bonding hybrids: 0 for a vacant hybrid, 0.5 for a σ hybrid with a single non-paired electron (σ free radicals), 1.0 for a doubly occupied hybrid (σ lone pairs).

A non-empirical alternative supporting a value λ^2_{Anb} close to 0.2 which has been adopted for lone-pair weights in the preceding treatment was presented later [59], using the concept of eccentric functions to enlarge the valence basis set of heteroatoms by means of lone-pair functions (LPF). The NH₃ molecule was studied as a test without and with a LPF in the vicinity of nitrogen. A reference calculation with Slater orbitals of exponents $\zeta_{2s}^{\text{N}} = \zeta_{2p}^{\text{N}} = 1.90$, $\zeta_{1s} = 1.24$ for valence orbitals gives bond hybrids reproducing the experimental bond angle HNH provided a weight $\lambda^2_{\text{Nnb}} = 0.21$ is assigned to the lone-pair hybrid. If a 1s hydrogenic function of exponent ζ_{LP} is located on the C₃ symmetry axis at a non-zero distance R_{LP} from the nitrogen atom, the standard hybridization procedure gives a complete set of non-zero eigenvalues λ^2_{Ai} , hence the possibility of having correct bond hybrids by adjusting the parameters

ζ_{LP} and R_{LP} properly. The best result, obtained with a semi-diffuse LPF ($\zeta_{LP} = 0.3$) close to nitrogen ($R_{LP} = 0.1$ a.u.), compares fairly well with the primitive empirical procedure.

2.2.3 Extensions to enlarged basis sets

The hybridization procedure described in Section 2.2.1 is fulfilled by a sequence of block transformations starting with overlap matrices S_{AB} generated, for convenience, by minimal sets of s and p orbitals. This particularity, however, does not create serious difficulties for possible extensions to more general basis sets. The 4x4 dimensions of the block matrices originally considered have to be only increased in conformity with the size of the bases in question.

The addition of five d orbitals to an s and p set, either as extra orbitals in the second period (the third row) from silicon to chlorine, or as valence orbitals for transition metal complexes is taken into account straightforwardly by raising the dimensions of the block matrices up to nine [60]. However, mixing the d functions added to the valence orbitals of non-metals, for instance sulphur, or keeping them in their primitive form, has not a great importance, because they play just a role of polarization functions in molecular structure calculations using hybridization [61].

The case of atoms described by extended basis sets with several s and p functions *per* shell is a little more complicated [62]. For instance, let us consider the split-valence sets built in double-zeta form from Slater or contracted Gaussian orbitals, which are commonly used for ab-initio calculations of organic compounds. An example is the very popular 3-21 G and 6-31 G sets of Pople implemented in current computer programs of Quantum Chemistry. For each atom, this description involves an inner group of rather concentrated functions 2s and 2p and an outer group of more diffuse functions 2s' and 2p' (large exponents and small exponents, respectively). First of all, it is necessary to begin the procedure by orthogonalizing the inner and outer functions 2s and 2s', 2p and 2p' centered on a same atom A, for the generally important one-center overlap between the inner and the outer sets should destroy the meaning of any hybridization method based on the values of two-center overlap integrals. The choice of a definite orthogonalization transformation for this purpose, *e.g.* those of Schmidt or Löwdin, is immaterial.

It is then possible to perform all the transformations sketched in Section 2.2.2 after doubling the 4x4 size of the various block-matrices indicated on the chart of Fig.1. The eigenvectors corresponding to the lowest eigenvalue λ^2_i give hybridized double-zeta orbitals, to be assigned to bonds and lone pairs as usual, whereas the existence of a second set of hybridized orbitals corresponding to the next eigenvalue λ^2_i suggests other possible applications, for example in genuine double-zeta valence bond calculations.

Other hybridization procedures for double-zeta basis sets may be imagined, for instance by using projection techniques [63] : Starting with a set of hybrids obtained from a parent minimal basis (*e.g.*, STO 3G *versus* 6-31 G) we can project the latter hybrids into the space spanned either by the inner subset or the outer subset of the original split-valence basis. The extension of the Del Re algorithm for hybridization to multiple-zeta sets does not raise any major difficulty, which illustrates both the flexibility of the method and the perennality of the concept.

3. Conclusions : A multiple-purpose instrument

3.1 Miscellaneous structural applications

For a long time, and still nowadays, hybridization has been used as a starting point for, so to say, a "linnean classification" of molecular observables ; it enables us to rationalize a large body of experimental data : Internuclear distances, bond angles, vibration frequencies and even chemical reactivity [64,65], or their theoretical counterparts coming from quantum-mechanical calculations in terms of standard s, p, d ... atomic contributions. We are not willing to go back to this matter in its entirety, because it is presented in textbooks for most of these properties ; as little less standard topics, we have preferred to turn us to those properties which are known by the generic name of spin coupling constants in magnetic resonance spectroscopy.

The quantum-mechanical picture of hyperfine structures presented by the spin-spin nuclear magnetic resonance (NMR) and electron-spin resonance (ESR) spectra involves a variety of spin Hamiltonian parameters of molecular origin whose magnitude determines that of the coupling constants. In such an analysis, the most characteristic term arises from the Fermi -or contact - operator :

$$H_{\text{Fermi}} \propto \sum_{\text{elec}} \sum_{\text{nuc}} \delta(r_{\text{elec}} - r_{\text{nuc}}) S_{\text{elec}} I_{\text{nuc}} \quad (21)$$

(see *e.g.* [66]), the importance of which is connected with the values of electron densities (in NMR) or spin densities (in ESR) on the nuclei experimentally tested. The specific form of Fermi operators implies that the magnitude of the contact terms is determined by the *s* local character of the molecular wave function on some nuclei, *i.e.*, by the relative importance of its *s* atomic components in these points. Let us add that other spin operators involved in magnetic resonance spectroscopy, such as the electron-spin and spin-spin dipole operators give, for their part, contributions determined by the *p* character of the wave function. In this matter, hybridization is of paramount importance for the understanding of spin coupling constants in terms of electronic structure.

The $^1J_{XY}$ coupling constants between two chemically bonded nuclei X and Y in NMR give a striking example of the explanatory power of the hybridization concept, especially for the $^{13}\text{C} - \text{H}$ and $^{13}\text{C} - ^{13}\text{C}$ couplings, where the Fermi contact term is known to be dominant over all the other types of magnetic interactions. Their experimental values can be rationalized by formulas of the form:

$$^1J_{XY} = k s_X s_Y + \ell \quad \text{with } s_H = 1 \quad (22)$$

k and ℓ being parameters determined from spectroscopic data by least-square fittings in appropriate series of chemical compounds, and *s* the *s*-percentage of the atomic hybrids forming the X - Y bond. Actually, this relationship works well for the couplings across the CH and CC bonds of acetylene, ethylene and ethane, where the *s* fractional character of the *sp*, *sp*² and *sp*³ standard hybrids varies from 0.50 to 0.33 and 0.25. Of course, explicite hybridization calculations are needed for hydrocarbons having particular structures (for instance three- or four-membered cycles [67])). The *k* proportionality factor is much greater than the ℓ constant, so that the latter may be ascribed to small perturbation effects not included in the Fermi contact term.

In ESR spectroscopy, the large quantity of data gathered between 1960 and 1980 has been interpreted in terms of σ and π spin densities, according to the orbital description of the unpaired electron in an independent-particle model. Within this picture, a σ radical has a singly occupied orbital belonging to the

same subset as the hybridized bond and lone-pair σ orbitals, while a π radical uses an orbital built from atomic functions perpendicular to the planar or locally planar σ framework [68,69]. So it is easy to understand by symmetry reasons why the electron-spin coupling constants of the σ free radicals are dominated by the direct contribution of the contact term, the magnitude of which depends on the s character of the singly occupied orbital, whereas the couplings of the π radicals have indirect contributions due to σ - π spin-polarisation mechanisms only [70,71].

Still, the concept of hybridization is relevant even for electron-proton couplings a_i^H because their values are practically determined by the spin density ρ_i located on the next-neighbour atom i of the proton considered, for instance the unsaturated carbon C to which H is attached. These couplings are governed by relationships of the form

$$a_i^H = Q \rho_i \quad (23)$$

where Q is a proportionality factor possibly depending on other characteristics of carbon C_i . If the spin densities are known, it is possible to derive an empirical value Q_{exp} for this factor using experimental data. The variation of Q_{exp} inside a series of related molecules enables us, by comparison with the bond angles, to see whether the usual hypothesis of atomic hybrids directed to each other has to mitigate in some cases.

To illustrate the last point, we will consider the ESR spectra coming from an unpaired electron in π electron systems of unsaturated monocycles C_nH_n . Using $1/n$ as spin densities ρ_i^π for carbon C_i , the ratio $Q_{\text{exp}} = a_i^H / \rho_i^\pi$ computed from the experimental data does not change appreciably, in spite of apex angles CCC deviating very much from the 120° standard value for $n = 6$. This fact is easily understood in the frame of the hybridization theory by assuming that Q_{exp} is not determined by the values of the cyclic bond angles, but by the less sensitive values predicted by the Del Re hybridization theory [72]; in other words, the straight bond hypothesis has to be relaxed for strongly strained systems.

Let add that similar considerations cannot be developed without caution in the case of long-range spin parameters of NMR and ESR spectroscopies, because these couplings result from a delicate balance of many effects (see [73]). Their study (including possible vibrational contributions) requires much

sophistication in the application of quantum mechanical methods to the evaluation of spin-hamiltonian parameters by perturbation theories at the semi-empirical level (see *e.g.* [74]) as well as at the non-empirical one. A striking example in ESR spectroscopy is the calculation of the electron-proton spin coupling constants for vinyl, the prototype of σ free radicals [75].

3.3 Quantum-chemical flashback

Beside its various applications to structural purposes in Chemistry, the concept of hybridization has a long story in Theoretical Chemistry as an intermediate tool in the construction of realistic molecular wave functions. In the old days of Quantum Mechanics, it was confidently used to determine bond and lone-pair functions for molecular orbital and valence-bond treatments, especially in the frame of the perfect pairing approximation (see *e.g.* [5]). Later, this approach was revived in order to start with convenient building blocks for writing a total wave function where electronic interaction can be introduced either in a perturbative way, as in the PCILO method [76], or in a variational way passing through quasi-localized orbitals at various approximation levels of the VB and MO theories. (for a recent example see [77]). Presently, SCF-CI treatments using delocalized molecular orbitals seem to be still preferred, but it may be interesting for many reasons including Chemistry to have the possibility of replacing a set of pure s,p,d *etc...* functions by its equivalent in terms of hybrids adapted to the structure of the molecule in question. This is the aim of hybridization procedures, like the Del Re method. Both points of view have been exploited in the CS-INDO-CI semi-empirical method [78,79], where the basic core parameters responsible for the agreement with experiment as concerns conformations and spectra are determined on a set of hybrid orbitals, but the CI computation of the electronic spectrum itself uses pure atomic orbitals, just for convenience's sake.

To conclude this review, we should like emphasize the fact that no serious argument can be presented for an exclusive use of pure atomic orbitals in quantum-chemical calculations, except that of the separation of the radial and angular parts of the wave function in the Hartree-Fock picture of the atoms themselves [80]. To the defenders of the traditional s, p, d ... orbitals, we wish to reply that there are four coordinate systems for which the Schrödinger equation of the hydrogenic atom can be solved [81], instead of eleven for a wave

equation without any potential term (see *e.g.* [82,83]), and that one of them, the parabolic system, gives rise to sp hybrids directly [84]. Taking this argument *stricto sensu*, we could be tempted to connect the origin of hybridization to the degeneracy of the s and p levels in hydrogen-like atoms; and so its importance should gradually decrease from carbon where the 2s and 2p levels have very close orbital energies to nitrogen and oxygen atoms, in conformity with the primitive ideas of Pauling. However, we can also state that the formation of a chemical bond creates an internal electric field suggesting by its analogy to a Stark effect that the polar-coordinates picture is not really adequate for atoms in molecules. More generally, hybridization can be considered as a way to prepare a local set of orbitals belonging to some irreducible representations of a certain point group [19], in other words to break the isotropy of the atom and to raise the organization level of matter in this way[85].

References

- [1] G. Del Re, *Epistemologia*, **10**, 231 (1987).
- [2] L. Pauling, *Proc. Nat. Acad. Sci.*, **14**, 359 (1928).
- [3] W. Heitler and F. London, *Zeits. f. Physik*, **44**, 455 (1927).
- [4] L. Pauling, *J. Amer. Chem. Soc.*, **53**, 1367 (1931).
- [5] W. G. Penney, "The Quantum Theory of Valence", chap.1, Methuen and Co, London (1935)
- [6] J.C. Slater, *Phys. Rev.* **38**, 1109 (1931).
- [7] F. Hund, *Zeits. f. Physik* **73**, 1 (1931).
- [8] R. S. Mulliken, *Phys. Rev.* **40**, 55 (1932)
- [9] J. H. Van Vleck *J. Chem. Phys.*, **1**, 177 and 219 (1933).
- [10] J. Guy, *Compt. Rend. Acad. Sci.*, **223**, 670 (1946).
- [11] C. A. Coulson, *J. Chim. Phys.*, **46**, 198 (1949).
- [12] J. C. Slater, *Phys. Rev.*, **41**, 255 (1932).
- [13] H. C. Longuet-Higgins, *Proc. Roy. Soc.*, **60**, 270 (1948)
- [14] W. Moffitt, *Proc. Roy. Soc.*, **A 218**, 486 (1953)
- [15] M. Sender and G. Berthier, *J. Chim. Phys.*, **56**, 946 (1959)
- [16] R.S. Mulliken, *J. Chem. Phys.*, **2**, 782 (1934)
- [17] W. Moffitt, *Proc. Roy. Soc.*, **A202**, 534 and 548 (1950)

- [18] J. Hinze and H.H. Jaffé, J. Amer. Chem. Soc., **84**, 540 (1962).
- [19] G. E. Kimball, J. Chem.phys., **8**, 188 (1940)
- [20] J. Hinze and H.H. Jaffé, Can. J. Chem., **41**, 1315 (1963)
- [21] J. Hinze and H.H. Jaffé, J. Chem. Phys., **38**, 1834, (1963)
- [22] H. H. Voge, J. Chem. Phys., **4**, 581 (1936).
- [23] W. Kutzelnigg, G. Del Re and G. Berthier, Fortsch. Chem. Fortsch., n°22, Springer-Verlag, Heidelberg (1971)
- [24] G. Del Re, G. Berthier and J. Serre, Lect. Note Chem., n°13, Springer-Verlag, Berlin (1980)
- [25] W. Moffitt, Rep. Prog. Phys., **17**, 173 (1954).
- [26] L. Pauling, The Nature of the Chemical Bond, Chap. 4, Cornell Univ. Press, Ithaca, New-York (1960)
- [27] A.D. Walsh, J. Chem. Soc. pp 2260-2331 (1953) (10 articles)
- [28] A. Maccoll, Trans.Far.Soc., **46**, 369 (1950)
- [29] R.S. Mulliken, J. Phys. Chem., **56**, 295 (1952)
- [30] J.N. Murrell, J. Chem. Phys.,**32**, 767 (1960)
- [31] C.A. Coulson and T.H. Goodwin, J. Chem. Soc. p.2851 (1962)
ibid., p.3161 (1963)
- [32] G. Del Re, Theor. Chim. Acta, **1**, 188 (1963)
- [33] R.J. Gillespie and R.S. Nyholm, Quart. Rev. London, **11**, 339 (1957)
- [34] G. Berthier and J. Serre, L'Actualité Chimique, p. 46 (1973)
- [35] R. McWeeny and G. Del Re, Theor. Chim. Acta, **10**, 13 (1968)
- [36] G. Del Re, Int. J. Quan. Chem. Symp., **7**, 193 (1973)
- [37] F.A. Cotton, Chemical Applications of Group Theory, Chap. 8, J. Wiley, New-York (1963)
- [38] A. Julg, Lect. Note Chem.,n°9, Springer-Verlag, Berlin (1978)
- [39] M.J.S. Dewar, H. Kollmar and W.K. Li, J. Chem. Educ., **52**, 305 (1975)
- [40] G. Gilli and V. Bertolasi, J. Chem. Educ., **60**, 638 (1983)
- [41] A. Julg, Chimie Théorique, Chap.3, Dunod, Paris (1964)
- [42] C.A. Coulson and W. Moffitt, Phil. Mag., **40**, 1 (1949)
- [43] A. Julg, Annales de la Faculté des Sciences de Marseille, **30**, 565 (1960)
- [44] O. Martensson and Y. Öhrn, Theor. Chim. Acta, **9**, 133 (1967)
- [45] E. Brandas and O. Martensson, Chem. Phys. Lett., **3**, 315 (1969)
- [46] C.A. Coulson and R.J. White, Mol. Phys.,**18**, 577 (1970)
- [47] R. Hultgren, Phys. Rev. , **40**, 891 (1932)
- [48] R.E. Powell, J. Chem. Educ., **45**, 45 (1968)

- [49] L. Pauling and V. McClure, *J. Chem. Educ.*, **47**, 15 (1970)
L. Pauling, *Proc. Natl. Acad. Sci.*, **72**, 4200 (1975) -
ibid., **73**, 274 and 1403 (1976)
- [50] R. Daudel and A. Bucher, *J. Chim. Phys.*, **42**, 6 (1945)
- [51] M. Randic and Z. Maksic, *Theor. Chim. Acta* **3**, 59 (1965) -
ibid. Chem. Rev. **72**, 43 (1972)
- [52] I. Hubac, V. Laurinc and V. Kvasnicka, *Chem. Phys. Lett.* **13**, 357 (1972)
- [53] P.G. Lykos and H.H. Schmeising, *J. Chem. Phys.*, **35**, 288 (1961)
- [54] G. Berthier, G. Del Re and A. Veillard, *Nuovo Cim.* **44**, 315 (1966)
- [55] G. Del Re, U. Esposito and M. Carpentieri
Theor. Chim. Acta, **6**, 36 (1966)
- [56] M. Bagatti, *Tesi di Laurea, Universita di Modena* (1990)
private communication of Prof. A. Rastelli
- [57] S.A. Pozzoli, A. Rastelli and M. Tedeschi,
J. Chem. Soc. Far. Trans. II, **69**, 256 (1973)
- [58] V. Barone, J. Douady, Y. Ellinger and R. Subra,
J. Chem. Soc. Far. Trans II, **75**, 1597 (1979)
- [59] C. Barbier, G. Berthier, D. Piazzola and G. Del Re,
J. Molec. Struct. (THEOCHEM), **259**, 59 (1992)
- [60] G. Del Re and C. Barbier, *Croat. Chim. Acta*, **57**, 787 (1984)
- [61] A. Carnevali, *Tesi di Dottorato, Universita di Modena* (1993),
private communication of Prof. F. Momicchioli
- [62] V. Barone, G. Del Re, C. Barbier and G. Villani,
Gazz. Chim. Ital., **118**, 347 (1988)
- [63] M. Bagatti, *Tesi di Dottorato, Universita di Modena* (1994)
private communication of Prof. A. Rastelli
- [64] G. Del Re and F. Zuccarello, *Croat. Chim. Acta*, **64**, 449 (1991)
- [65] F. Zuccarello and G. Del Re, *J. Molec. Struct. (THEOCHEM)*,
260, 249 (1992)
- [66] R. McWeeny, *J. Chem. Phys.*, **42**, 1717 (1965)
- [67] A. Veillard and G. Del Re, *Theor. Chim. Acta*, **2**, 55 (1964)
- [68] M.C.R. Symons, *J. Chem. Soc.*, p.2276 (1965)
- [69] G. Berthier, H. Lemaire, A. Rassat and A. Veillard,
Theor. Chim. Acta **3**, 213 (1965)
- [70] H.M. McConnell, *J. Chem. Phys.*, **24**, 764 (1956)
- [71] S.I. Weissman, *J. Chem. Phys.*, **25**, 890 (1956)

- [72] G. Berthier, A. Veillard and G. Del Re, *Phys. Lett.*, **8**, 313 (1964)
- [73] Y. Ellinger, B. Lévy, Ph. Millié and R. Subra,
in "Localization and Delocalization in Quantum Chemistry" ,
O. Chalvet *et al.* (eds), Vol.I, pp 283-326, D. Reidel, Dordrecht (1975)
- [74] C. Barbier, G. Berthier, I. Baraldi and F. Momicchioli,
J. Molec. Struct. (THEOCHEM), **000**, 000 (1999)
- [75] C. Angeli, A. Di Matteo and V. Barone,
Chem. Phys. **000**, 000 (1999)
- [76] S. Diner, J.P. Malrieu and P. Claverie, *Theor. Chim. Acta*, **13**, 1 (1968) ;
ibid., **13**, 18 (1968)
- [77] C. Angeli, G. Del Re and M. Persico, *Chem. Phys. Lett.*, **223**, 102 (1995)
- [78] F. Momicchioli, I. Baraldi and M.C. Bruni, *Chem. Phys.*, **70**, 161 (1982)
ibid., **82**, 22 (1983)
- [79] I. Baraldi, F. Momicchioli and G. Ponterini,
J. Molec. Struct.(THEOCHEM), **110**, 187 (1984)
- [80] M. Delbrück, *Proc. Roy. Soc.*, **A 129**, 689 (1930)
- [81] P.M. Morse and H. Feshbach, *Methods of Theoretical Physics*,
Part I, Chap; 5, McGraw-Hill, New-York (1953)
- [82] L.P. Eisenhart, *Phys. Rev.*, **74**, 87 (1948)
- [83] E.G. Kalnins, W. Miller and P. Winternitz,
SIAM J. Appl. Math., **30**, 630 (1976)
- [84] D.B. Cook and P.W. Fowler, *Amer. J. Phys.*, **49**, 857 (1981)
- [85] A. Laforgue, *Acta Biotheor.*, **40**, 221 (1992)

The authors are indebted to their colleagues of the Ecole Normale Supérieure de Paris and of the Universities of Modena, Pisa and Napoli for their help at various stages of this work.

Summary

The hybridization principle of atomic orbitals used from the thirties up to the present days as a prelude to the formation of chemical bonds is surveyed. The exposé is centered on the *ab-initio* procedure of overlap-matrix localization suggested by G. Del Re in 1963 (*Theoretica Chimica Acta* **1**, pp 188-197), and its successive extensions and various applications in Quantum Chemistry are described. Some conceptual aspects of hybridization are discussed.

Keywords : valence states, hybridization, localization, magnetic resonance

Core and valence electrons in atom-by-atom descriptions of molecules

Sándor Fliszár¹, Edouard C. Vauthier², Vincenzo Barone³

¹*Département de Chimie, Université de Montréal, CP 6128 Succ. Centre-ville, Montréal, Québec, H3C 3J7 Canada.* ²*Institut de Topologie et de Dynamique des Systèmes, 1, rue de la Brosse, Paris, France.* ³*Dipartimento di Chimica, Università di Napoli 'Federico II', via Mezzocannone 4, Napoli, Italia I-80134*

Abstract

The core-valence electron partitioning in molecules is adequately described by the energy formulas $E_k^v = (V_k - V_{ne,k}^c + V_k^{cv})/\gamma_k^v$ for the valence region of atom k in a molecule and $E_k^{ion} = (V_{ne,k}^c - V_k^{cv})/\gamma_k^c$ for the k th ionic core left after removal of the valence electronic charge, where V_k and $V_{ne,k}^c$ are, respectively, the total potential energy involving center k and the core nuclear-electronic potential energy of its N_k^c core electrons. V_k^{cv} denotes the interaction between N_k^c and the electronic and nuclear charges found outside the core region k . Properly selected γ_k^v and γ_k^c parameters, treated as constants, lead to valence-region energies in good agreement with those deduced from the total molecular energies E and the equation $E^v = E - \sum_k E_k^{ion}$. The point-charge-potential model for V_k^{cv} , embodied in $V_k^{cv} = -N_k^c[(V_k - V_{ne,k}^c)/Z_k]$, improves the accuracy of the results. These formulas are best suited for atom-by-atom (or bond-by-bond) descriptions of molecules because E_k^v is expressed solely in terms of the appropriate electrostatic potentials at the individual nuclei and does not depend on any particular mode of partitioning a molecule into atomic subunits.

Contents

- 1 Introduction
- 2 Working formulas
- 3 Results
 - 3.1 Ground-state atoms A and their ions A⁺ and A⁻
 - 3.2 Molecules
- 4 Conclusions and Prospects
- Glossary
- References

1 Introduction

Two popular concepts of chemistry are tackled in this paper, namely *i*) the partitioning of the electronic charge of ground-state atoms, ions and molecules into core and valence parts and *ii*) the mental decomposition of molecules into ‘atomic subunits’. The familiar core–valence separation, of course, translates the old idea that chemical properties are largely governed by the outer (or *valence*) atomic regions, while the subdivision into ‘atomic’ subunits acknowledges the fact that atoms-in-the-molecule – such as those defined by Bader [1], for example – are convenient model building blocks for the interpretation of molecular properties. Both concepts are intuitively appealing but neither is cast in formal theory and the way they overlap certainly merits attention.

Let us first comment on the theoretical partitioning of a molecule into atomic subunits. The total energy, E , of that molecule in its ground state is most appropriately expressed as a sum of atomic-like terms E_k , with no extra contributions, i.e., $E = \sum_k E_k$. (Incidentally, note that this atom-by-atom decomposition of a molecule easily transforms into an equivalent bond-by-bond description of the same [2, 3]: the concept of a molecule viewed as a collection of chemical bonds is just another facet of the atoms-in-a-molecule description.) Now, little needs be added in that matter because – as we shall see – our results do not depend on the way the virtual boundaries of the atomic-like subunits in that molecule are defined. What does matter, however, is that such a partitioning is consistently made in *real space*.

Turning now to the core–valence separation of electronic charge, theory is relatively straightforward in the familiar *orbital space* where the energy is partitioned from the outset into orbital energies $\varepsilon_i = \varepsilon_{1s}, \varepsilon_{2s}$, etc. Things are somewhat more involved in real space, however, if we abandon the orbital-by-orbital electron partitioning in favor of a description based on the stationary ground-state electron density $\rho(\mathbf{r})$ [3]–[6]. Sure, our real-space and the orbital-space core–valence separations appear for what they are: two facets of the same reality, but the real-space approach is clearly preferred in the present context because atom-by-atom (or bond-by-bond) descriptions are by their very nature treated in real space.

In real space, our core–valence separation is valid only for discrete solutions, namely for $N^c = 2$ core electrons for the first-row elements or $N^c = 2$ and 10 e for the second row. For ground-state atoms, ions and molecules we get [3]–[6]:

$$E^v = \frac{1}{3}(T^v + 2V^v) \quad (1)$$

$$E_k^{\text{ion}} = \frac{1}{3} \left[T_k^c + 2(V_{ne,k}^c + V_{ee,k}^{cc}) \right] \quad (2)$$

$$E = E^v + \sum_k E_k^{\text{ion}} \quad (3)$$

(1) for the valence-region energy E^v , (2) for the energy E_k^{ion} of the k th ionic core – i.e., the ion left behind after removal of the valence-region electrons – and (3) for the total energy, E , of the entire system, atom, ion or molecule. Equations (1)–(3) were successfully tested for atoms and ions, both near the Hartree–Fock limit [4] and with SDCI wave functions [5]. Numerous examples were also given for molecules [6], using SCF Gaussian-type basis sets.

Yet, these formulas are not congenial with our atom-by-atom descriptions. This is primarily due to a host of two-electron Coulomb and exchange terms – such as valence-other-valence and core-other-valence multi-center integrals – which, besides being intrinsically complex, require beforehand specification of the boundaries delimiting the individual ‘atoms’ in a molecule. Hence the idea of bypassing this sort of problem in favor of a considerably simplified approach, one that highlights the rôle of the electrostatic potentials.

The total (electronic and nuclear) potential energy involving nucleus Z_k ,

$$V_k = -Z_k \int_0^\infty \frac{\rho(\mathbf{r})}{|\mathbf{r} - \mathbf{R}_k|} d\mathbf{r} + Z_k \sum_{l \neq k} \frac{Z_l}{R_{kl}}, \quad (4)$$

plays a prominent part in the formulas developed earlier [3, 4, 6], such as

$$E_{\text{atom } k}^v = \frac{1}{\gamma_k^v} (V_k - V_{\text{ne},k}^c + V_k^{\text{cv}}) \quad (5)$$

$$E_k^{\text{ion}} = \frac{1}{\gamma_k^c} (V_{\text{ne},k}^c - V_k^{\text{cv}}) \quad (6)$$

where γ_k^v and γ_k^c are valence and core parameters, respectively, of atom k . (These equations apply both to isolated atoms and to atoms in a molecule.) At first, it does not seem relevant to inquire into these γ_k^v and γ_k^c parameters. Indeed, if $1/\gamma^v$ denotes the appropriate average (in a molecule) of all the individual $(1/\gamma_k^v)$ ’s weighted by the $(V_k - V_{\text{ne},k}^c + V_k^{\text{cv}})$ terms of Eq. (5), one can show that [3, 6]

$$(3 - \gamma^v) E^v = \sum_i \int^{\text{val}} \nu_i \phi_i^* \hat{F} \phi_i d\tau \quad (7)$$

where $\int^{\text{val}} \dots d\tau$ means: integration over the valence space, \hat{F} and ϕ_i being the familiar Hartree–Fock operator and the i th eigenfunction with occupancy ν_i , respectively. Combining this result with the formula $E^v = \sum_k E_{\text{atom } k}^v$ using Eq. (5), one eliminates γ^v and gets Eq. (1). We proceed in a similar manner to get rid of the γ_k^c parameters and end up with Eq. (2). Briefly, the γ parameters are not an issue in our final energy formulas (1)–(3). In the present instance, however, we find it useful to examine the γ_k^v and γ_k^c parameters and their merits in energy calculations featuring the total electrostatic potentials at the nuclei. In this perspective, remembering the definition of $V_{\text{ne},k}^c$,

$$V_{\text{ne},k}^c = -Z_k \int_0^{r_{\text{b},k}} \frac{\rho(\mathbf{r})}{|\mathbf{r} - \mathbf{R}_k|} d\mathbf{r}, \quad (8)$$

we obtain our basic working formula from Eqs. (4)–(6), namely [6]

$$E = \sum_k \frac{1}{\gamma_k^v} \left[-Z_k \int_{r_{b,k}}^{\infty} \frac{\rho(r)}{|\mathbf{r} - \mathbf{R}_k|} d\mathbf{r} + Z_k \sum_{l \neq k} \frac{Z_l}{R_{kl}} + V_k^{cv} \right] + \sum_k \frac{1}{\gamma_k^c} (V_{ne,k}^c - V_k^{cv}) . \quad (9)$$

Equation (9) is a form of (3). The first right-hand-side term is E^v . Note that it is given as a sum of atomic-like terms, thus achieving a ‘natural’ atom-by-atom partitioning with no reference to any particular definition of atomic regions in the molecule.

2 Working formulas

The form of E^v represented in Eq. (9) is not convenient because it contains V_k^{cv} . This quantity is presently difficult to evaluate, although an approximation has been offered for it [6], but we can simplify things as follows. In the right-hand side of (9) we add and subtract the quantity

$$\sum_k \frac{1}{\gamma_k^v} (V_{ne,k}^c - V_k^{cv})$$

and write the last term of (9) using Eq. (6). Thus we get E^v from (3), namely

$$E^v = \sum_k \frac{1}{\gamma_k^v} \left[-Z_k \int_0^{\infty} \frac{\rho(r)}{|\mathbf{r} - \mathbf{R}_k|} d\mathbf{r} + Z_k \sum_{l \neq k} \frac{Z_l}{R_{kl}} \right] - \sum_k \frac{\gamma_k^c}{\gamma_k^v} E_k^{\text{ion}} . \quad (10)$$

Now, the most obvious merit of this equation is that it expresses valence-region energies in terms of the *total* (electronic and nuclear) potential energies of the individual nuclei Z_k . Contrasting with Eq. (9), V_k^{cv} is not any longer required. Applying Eq. (4), we can reformulate (10) in a more compact manner:

$$E^v = \sum_k \frac{1}{\gamma_k^v} (V_k - \gamma_k^c E_k^{\text{ion}}) \quad (11)$$

$$E^v = \sum_k \left(\frac{V_k}{\gamma_k} - E_k^{\text{ion}} \right) \quad (12)$$

with

$$\frac{1}{\gamma_k} = \left[\frac{1}{\gamma_k^v} (V_k - V_{ne,k}^c + V_k^{cv}) + \frac{1}{\gamma_k^c} (V_{ne,k}^c - V_k^{cv}) \right] \times \frac{1}{V_k} .$$

It is thus clear that γ_k^v , γ_k^c and γ_k cannot all be treated as constants. It is our task to sort out the better approximation: a constant γ_k for each chemical species k or at least approximately constant γ_k^v and γ_k^c parameters instead.

The pertinent numerical γ_k parameters can be obtained from the appropriate potentials [7]–[9] by applying Eq. (12) in its form $E^\nu + \sum_k E_k^{\text{ion}} = \sum_k V_k/\gamma_k$. To get the γ_k^ν parameters, on the other hand, we use Eq. (11).

In doing so, we can tentatively associate a constant γ_k^ν companion with each atom concerned. This is an approximation, of course, implying that $V_{\text{ne},k}^c - V_k^{\text{cv}}$ is treated as a constant for every atom k , as revealed by Eq. (6). We shall now lift this constraint and use an approximation for V_k^{cv} instead, namely [6]

$$\begin{aligned} V_k^{\text{cv}} &= N_k^c \int_{r_{b,k}}^{\infty} \frac{\rho(\mathbf{r})}{|\mathbf{r} - \mathbf{R}_k|} d\mathbf{r} - N_k^c \sum_{l \neq k} \frac{Z_l}{R_{kl}} \\ &= -\frac{N_k^c}{Z_k} (V_k - V_{\text{ne},k}^c). \end{aligned}$$

(This approximation is similar to the point-charge-potential simplifications introduced [10] for core-other-core and core-other-nucleus interactions, showing that the net effect of the core interaction energy is to shield the nuclear charges in the internuclear repulsion energy.) Hence the E^ν of Eq. (9) becomes

$$E^\nu = \sum_k \frac{1}{\gamma_k^\nu} \left[\frac{Z_k - N_k^c}{Z_k} (V_k - V_{\text{ne},k}^c) \right] \quad (13)$$

and conveys the instructive picture of an atomic-like valence-region energy E_k^ν determined by the potential, $(V_k - V_{\text{ne},k}^c)/Z_k$, of the whole of the charge exterior to the core k , in the field of a nucleus with ‘effective’ charge $Z_k^{\text{eff}} = Z_k - N_k^c$. $N_k^c = 2$ electron for the first-row atoms. In principle, one should compute $V_{\text{ne},k}^c$ *in situ*, i.e., for the core k with 2 electrons as it stands in the actual molecule. In practice, we approximate this term by taking its free-atom value. This should not be too poor, however, because these V_{ne}^c energies are rather insensitive to changes taking place outside the core, as exemplified by the study of ions [5, 6], at least as regards charge variations, but we are less firm about hybridization changes that could eventually affect $V_{\text{ne},k}^c$.

3 Results

3.1 Ground-state atoms A and their ions A^+ and A^-

The γ^ν parameters are easily obtained from Eq. (5) or (7) and the E^ν given by (1). A few examples (Table 1), worked out at a near-Hartree-Fock level, using Slater orbital bases optimized by Clementi and Roetti [11], illustrate this point. SDCI calculations [5] of E^ν , V_{ne}^ν , V_{ne}^c and $V_{\text{ee}}^{\text{cv}}$, on the other hand, give the results offered in Table (2) for γ^ν and γ^c , from (5) and (6), respectively, and for the corresponding average γ parameter, i.e., $\gamma = (V_{\text{ne}}^\nu + V_{\text{ne}}^c)/E$.

Table 1: Calculation of γ^v using Eq. (1) and either (5) or (7)^a: selected SCF results (au) assuming $N^c = 2$ electron for the first-row atoms and $N^c = 10$ electron otherwise

Atom	E^v	V_{ne}^v	V_{ee}^{cv}	$\sum_i \int_{r_b}^{\infty} \nu_i \phi_i^* \hat{F} \phi_i d\tau$	γ^v
C	-5.29213	-17.93001	5.73185	-3.67875	2.30491
N	-9.67722	-31.68660	8.66992	-6.01506	2.37844
O	-15.76258	-50.63349	12.12703	-8.77867	2.44299
Ne	-34.90915	-109.15785	20.93432	-16.50036	2.52728
Si	-3.41577	-25.80118	18.15187	-2.59824	2.23938
Ar	-18.76438	-102.66606	56.33979	-9.96330	2.46894
Ti	-52.51967	-238.18801	106.92894	-26.29829	2.49925
Cr	-79.78837	-345.31702	142.03989	-36.08587	2.54772
Fe	-114.95163	-478.88367	181.76337	-47.75977	2.58463

^aThe results indicated for γ^v are the averages of those obtained from (5) and (7). The scatter about each γ^v , one-half the difference between the two estimates, is approximately 0.00002 (N, Ti, Cr), 0.00005 (C, Ne, Si) and 0.00010 (O, Ar, Fe).

Table 2: Ground-state atoms. Calculation^a of γ^v , Eq. (5), γ^c , Eq. (6), and of their average value, $\gamma = (V_{ne}^v + V_{ne}^c)/E$

Atom	γ^v	γ^c	γ
Be	1.959049	2.323379	2.299300
B	2.152885	2.330617	2.312081
C	2.271768	2.341700	2.331715
N	2.352893	2.352991	2.352973
O	2.417977	2.361730	2.373685
F	2.468382	2.370470	2.394329
Ne	2.508181	2.378835	2.414150
Mg	1.901697	2.399881	2.397877
Si	2.217002	2.387883	2.385824
S	2.366828	2.381580	2.381240
Ar	2.453850	2.378879	2.381571

^aSDCI results using van Duijneveldt's (13s 8p) basis [12] enriched by two *d* and one *f* functions from [13] for Be-Ne, with $N^c = 2$ electron. The second-row atoms were calculated with the 6-311G* basis of [14], with $N^c = 10$ e.

The verification submitted in Table 1 is relevant because of the pivotal rôle played by the $\int_{r_b}^{\infty} \nu_i \phi_i^* \hat{F} \phi_i d\tau$ integrals. They represent the link between orbital theory and our real-space model [4]: it is the identity, for isolated atoms,

$$\sum_i \int_{r_b}^{\infty} \nu_i \phi_i^* \hat{F} \phi_i d\tau = T^v + V_{ne}^v + V_{ee}^{cv} + 2V_{ee}^{vv}$$

(and a similar expression for molecules [6]) that takes us from Eqs.(5) and (7) to Eq.(1). This sum of integrals also equals $\sum_i N_i^v \varepsilon_i$, where $N_i^v = \int_{r_b}^{\infty} \nu_i \phi_i^* \phi_i d\tau$ is the number of valence electrons of orbital ε_i , a result duplicating that given by direct evaluations of T^v , V_{ne}^v , V_{ee}^{cv} and V_{ee}^{vv} and corroborating those of Table 1. Now, considering the little we know about the γ^v parameters, it may seem a good idea to conceal them by using Eq.(7), but we look for more and better, of course, in view of anticipated applications of Eqs.(11)–(13).

Selected ions A^+ and A^- , as well as their corresponding neutral ground-state atoms A , were probed with the help of SDCI computations using Atomic Natural Orbital (ANO) bases [5], namely ANO[7s6p3d] [15]. The γ^v results for carbon are 2.0367 (C^+), 2.2755 (C) and 2.5120 (C^-). For nitrogen we get 2.1585 (N^+), 2.3571 (N) and 2.5451 (N^-). The results for oxygen are $\gamma^v = 2.2482$ (O^+), 2.4231 (O) and 2.5851 (O^-). Finally, fluorine gives 2.3229 (F^+), 2.4730 (F) and 2.6140 (F^-). Addition and withdrawal of one e provoke roughly similar absolute changes of γ^v . Using the finite-difference approximation, we can thus offer rough estimates for $\partial\gamma^v/\partial N$, namely: 0.238 ± 0.001 (C), 0.193 ± 0.005 (N), 0.168 ± 0.006 (O) and 0.146 ± 0.005 for F . The average $\gamma = (V_{ne}^v + V_{ee}^c)/(E^v + E^{ion})$ parameters, on the other hand, change less rapidly than the corresponding γ^v 's. For carbon we get γ values of 2.2700 (C^+), 2.3316 (C) and 2.3844 (C^-). The results for nitrogen are 2.2949 (N^+), 2.3529 (N) and 2.4000 (N^-) and for oxygen we get 2.3191 (O^+), 2.3735 (O) and 2.4200 (O^-). The corresponding $\partial\gamma/\partial N$ derivatives are, in our approximation, 0.057 ± 0.004 (C), 0.053 ± 0.005 (N) and 0.050 ± 0.004 for oxygen. The relevance of these estimates is in the fact that they may suggest that possible differences between the γ 's (or γ^v 's) of like atoms in a molecule cannot be ruled out a priori, although they are anticipated to be minor for small differences in electron populations, ΔN , between these atoms. This point is relevant in the study of molecules.

As concerns the core γ^c parameters in the ion-atom series A^+ , A and A^- , inspection of Eq.(6) reveals relatively small changes, owing to the relatively small variations suffered by $V_{ne}^c - V_{ee}^{cv}$. For example, in ANO[7s6p3d] calculations, one finds γ^c values of 2.3050 (C^+), 2.3417 (C) and 2.3629 (C^-) or $\gamma^c = 2.3490$, 2.3688 and 2.3828 for F^+ , F and F^- , respectively. Generally speaking, the γ^c parameters of the ground-state ions and atoms vary less rapidly than the corresponding valence parameters, γ^v , but, of course, this does not imply that the γ^c 's could be treated as constants.

Table 3: Core parameters of selected atoms^a, au

Parameter	C	N	O
V_{ne}^c	-70.198495	-96.664711	-127.435155
V_{ee}^{cc}	3.925284	4.735331	5.566473
V_{ee}^{cv}	5.732918	8.672469	12.127447
T^c	35.384361	49.651339	66.607747
E^{ion}	-32.387354	-44.735807	-59.043206
γ^c	2.344477	2.354650	2.363737

^aSCF results in the $[5s\ 3p]$ basis, for $N^c = 2$ electron.

3.2 Molecules

A substantial part of the results presented here was obtained with Dunning's contracted GTO($9s\ 5p|6s$) \rightarrow $[5s\ 3p|3s]$ basis [16]. A few results were deduced with an enlarged GTO($9s\ 5p\ 2d|6s\ 2p$) \rightarrow $[5s\ 3p\ 1d|3s\ 1p]$ basis [8]. Finally, we also discuss some post-Hartree-Fock density functional (DFT) results, using namely the B3LYP functional [9, 17] with Pople's 6-311G($2df, 2p$) basis [13, 14] and the $vD(2df, 2pd)$ set obtained from van Duijneveldt's ($13s\ 8p\ 2d|8s\ 2p$) basis [12] enriched by f functions on C and d functions on H taken from Ref. [13]. We close with a wealth of B3LYP/6-311G(d, p) tests of our energy formulas.

Let us now start with the results obtained by means of the $[5s\ 3p|3s]$ basis. The required potentials at the nuclei, $\sum_k V_k/Z_k$, summed for the individual atoms $k = H, C, N$, etc., are taken from Ref. [8], along with the corresponding conventional total energies, E . Table 3 collects additional pertinent parameters for use in conjunction with these Hartree-Fock SCF calculations. Table 4 presents applications of our formulas (11) and (12). The latter, identified as 'Approximation A', uses one single γ_k for each individual atom C, N, etc. The results under the heading 'Approx. A' are obtained with $\gamma_H = 2.208281$, $\gamma_C = 2.326420$, $\gamma_N = 2.346751$ and $\gamma_O = 2.371427$: they compare reasonably well with the valence-region energies E^v deduced from Eq. (1). The root-mean-square (RMS) deviation between the two sets of results, i.e., Approx. A and Eq. (1), is 0.1162 au. We should not attach too much importance to the value found for γ_H , however, at least not to the present one obtained from a fit with SCF potentials. Tests made for the same collection of molecules assuming $\gamma_H = 2$ gave γ_k values of 2.332084 (C), 2.347693 (N) and 2.371472 (O) and a RMS error of 0.1563 au. These parameters unfortunately elude very accurate definitive determinations, particularly as concerns hydrogen.

The application of Eq. (11), 'Approximation B', considers constant core and valence parameters, γ_C^c , γ_N^c , etc., and γ_C^v , γ_N^v , etc., respectively. The data analysis using the potentials of Ref. [8] and the parameters of Table 3 led to the

Table 4: SCF calculations of valence-region energies using the contracted GTO(9s 5p|6s) \rightarrow [5s 3p|3s] basis

Molecule	E^v , atomic units ^a			
	Approx. A	Approx. B	Approx. C	Eq. (1)
C ₂	-10.7091	-10.5107	-10.6742	-10.6015
CH ₄	-7.6857	-7.8058	-7.7852	-7.8120
C ₂ H ₆	-14.3253	-14.4611	-14.4396	-14.4380
C ₃ H ₈	-20.9759	-21.1271	-21.0978	-21.0765
<i>i</i> -C ₄ H ₁₀	-27.6310	-27.7981	-27.7565	-27.7250
<i>c</i> -C ₃ H ₆	-19.8357	-19.8750	-19.8760	-19.8867
C ₂ H ₄	-13.2204	-13.2443	-13.2366	-13.2626
C ₃ H ₆	-19.8466	-19.8849	-19.8759	-19.8869
<i>i</i> -C ₄ H ₈	-26.4897	-26.5426	-26.5266	-26.5311
C ₃ H ₄	-18.7100	-18.6373	-18.6609	-18.7106
C ₂ H ₂	-12.0856	-11.9967	-12.0119	-12.0114
C ₆ H ₆	-36.4762	-36.2313	-36.2731	-36.3221
N ₂	-19.3385	-19.2954	-19.3333	-19.3456
NH ₃	-11.4667	-11.5976	-11.5084	-11.4116
<i>cis</i> -N ₂ H ₂	-20.6064	-20.6631	-20.6004	-20.5070
N ₂ H ₄	-21.8288	-21.9906	-21.8590	-21.6286
HCN	-15.8321	-15.7632	-15.7525	-15.7104
CH ₂ N ₂	-25.6958	-25.6558	-25.7570	-25.9382
NH ₂ CN	-26.1254	-26.0828	-26.0444	-26.0586
CH ₃ CN	-22.3470	-22.2862	-22.3063	-22.3400
O ₂	-31.4699	-31.4847	-31.4765	-31.4155
H ₂ O	-17.1864	-17.2790	-17.1370	-16.9789
CO	-21.2441	-21.1483	-21.1932	-21.2472
CO ₂	-36.9046	-36.8036	-36.8898	-37.1025
HCHO	-22.4878	-22.4880	-22.4615	-22.3908
H ₂ CCO	-27.7562	-27.6611	-27.7275	-27.8637
CH ₃ OH	-23.7362	-23.8430	-23.7407	-23.5925
(CH ₃) ₂ O	-30.2651	-30.3869	-30.3258	-30.2148
(C ₂ H ₅) ₂ O	-43.6220	-43.7761	-43.6884	-43.5350
N ₂ O	-34.7434	-34.6955	-34.8352	-34.9742
HCNO	-31.5344	-31.4531	-31.4750	-31.4924

^aApprox. A: from Eq. (12). Approx. B: from Eq. (11) using $\gamma_H = 2$ and the appropriate γ_k^v 's for C, N and O. Approx. C: from Eq. (13), assuming $\gamma_H = 2$ and the γ_k^v parameters ($k = \text{C, N, O}$) indicated in the text.

Table 5: DFT tests of Eq. (12) for E^ν , using the B3LYP functional, and comparison with experimental results (atomic units)

Molecule	E^ν , 6-311G(2df, 2p) ^a		E^ν , vD(2df, 2pd) ^b		Exptl. ^c
	Approx. A	Eq. (3)	Approx. A	Eq. (3)	
CH ₄	-8.1189	-8.1203	-8.1133	-8.1179	-8.1079
C ₂ H ₂	-12.5468	-12.5271	-12.5409	-12.5227	-12.5239
C ₂ H ₄	-13.8071	-13.7865	-13.7920	-13.7821	-13.7754
C ₂ H ₆	-15.0354	-15.0285	-15.0317	-15.0233	-15.0119
c-C ₃ H ₆	-20.6682	-20.6887	-20.6685	-20.6810	-20.6756
C ₆ H ₆	-37.8201	-37.8252	-37.8035	-37.8089	-37.8165

^aApprox. A: calculated with $\gamma_H = 1.921351$ and $\gamma_C = 2.324862$. The root-mean-square (RMS) deviation relative to the results given by Eq. (3) is 0.0148 atomic units. In Eq. (3) we have used $E_C^{\text{ion}} = -32.4164$ au.

^bApprox. A: calculated with $\gamma_H = 1.939924$ and $\gamma_C = 2.322853$. The RMS deviation relative to the results deduced from Eq. (3) is 0.0109 au. E_C^{ion} was taken at -32.4236 atomic units in applications of Eq. (3).

^cUsing $E_C^{\text{ion}} = -32.416$ and $E_C^{\text{atom}} = -37.8558$ atomic units, from the appropriate sums of ionization potentials [18], and the experimental data reported in Refs. [3] and [9].

following γ_k^ν values: $\gamma_H = 2.219194$, $\gamma_C = 2.219904$, $\gamma_N = 2.309741$ and $\gamma_O = 2.398473$. The RMS deviation between the results given by this approximation and those of Eq. (1) is 0.1168 au, i.e., practically the same as that found for Approximation A. Brute-force tests were also made assuming $\gamma_H = 2$. In this manner we get $\gamma_C^\nu = 2.259024$, $\gamma_N^\nu = 2.315356$ and $\gamma_O^\nu = 2.399152$. Again, the RMS error, 0.1588 au, is practically the same as before.

Now we come to Eq. (13). Tests conducted with $N^c = 2$ e for C, N and O and the V_{ne}^c parameters of Table 3 lead to $\gamma_H = 2.106044$, $\gamma_C^\nu = 2.179528$, $\gamma_N^\nu = 2.288607$ and $\gamma_O^\nu = 2.377505$, which reproduce the pertinent E^ν energies with a RMS deviation of 0.0814 au. With $\gamma_H = 2$, on the other hand, the same data show that $\gamma_C^\nu = 2.199068$, $\gamma_N^\nu = 2.291413$ and $\gamma_O^\nu = 2.377765$ and the RMS deviation is now 0.0983 au (Table 4, ‘Approximation C’).

All these γ parameters were obtained from squared-error minimizations. The data analysis reveals that the best fits for hydrogen follow a very shallow ‘minimum valley’, so that the reported γ_H parameters obtained from these fits should be taken with a grain of salt. The value $\gamma_H = 2$ which was tested here is consistent with – and loosely justified by – the virial ratio for H, $V_{ne}/E = 2$. A reasonable explanation for possible distortions of the γ_H value is perhaps linked to the basis used for hydrogen. This point is briefly examined with the help of DFT results (Table 5) and SCF computations using enriched bases.

Calculations made with the GTO(9s 5p 2d|6s 2p) \rightarrow [5s 3p 1d|3s 1p] basis set for C₂, CH₄, C₂H₆, cyclo-C₃H₆, C₂H₄ and C₂H₂ lead to $\gamma_H = 2.030123$ and $\gamma_C = 2.331540$. The enriched 6-311G(2df, 2p) and vD(2df, 2pd) basis sets and implementation of the B3LYP functional further lower γ_H , which is now ~ 1.940 , with $\gamma_C \sim 2.323$ (Table 5). Under the circumstances, we may consider $\gamma_H = 2$ as an acceptable simple approximation in applications of Eq. (12).

As a rule, all the pertinent parameters occurring in Eqs. (11)–(13) ideally follow from genuine direct calculations in the basis selected for the molecules. For use with the reported B3LYP DFT computations, however, we resort to large basis set SDCl results [5] – which are our best estimates – namely E_k^{ion} energies of -32.42360 (C), -44.75357 (N) and -59.07876 au (O), $\gamma_k^c E_k^{\text{ion}}$ values of -75.92636 (C), -105.30473 (N) and -139.52809 au (O), as well as $V_{\text{ne},k}^c$ core energies of -70.19056 , -96.65147 and -127.43866 au for C, N and O, respectively. (No effort was made to ‘adjust’ any of these parameters to achieve better fittings or a better agreement between theory and experiment.)

In this fashion, applying here Eq. (11), the vD(2df, 2pd) basis set and the B3LYP functional give $\gamma_H = 1.942245$ and $\gamma_C^v = 2.215875$, which reproduce the expected valence energies of Table 5 with a RMS deviation of 0.0115 au. The results obtained with Chipman’s so-called TZ2P’f basis [9, 19] and the B3LYP functional are similar to those given by the vD(2df, 2pd) basis, namely $\gamma_H \sim 1.94$, $\gamma_C \sim 2.322$ and $\gamma_C^v \sim 2.21$, with RMS deviations of ~ 0.01 au. Finally, using the vD(2df, 2pd)/B3LYP potentials in Eq. (13), we get for the hydrocarbons of Table 5 that $\gamma_H = 1.926485$ and $\gamma_C^v = 2.146586$, and the RMS deviation now drops to 0.008 au with the use of this approximation.

Additional tests were carried out with the popular 6-311G(d, p) basis [14]: 70 molecules were studied at the HF level and 50 with the B3LYP functional. Our three approximations, Eqs. (11), (12) and (13), yield Hartree–Fock results similar to those given by [5s 3p|3s] calculations, with RMS errors of 0.159, 0.161 and 0.106 au, respectively, for $\gamma_H = 2$ and slightly better results – with RMS errors of 0.114, 0.115 and 0.079 au for Approximations A, B and C, respectively – when the constraint $\gamma_H = 2$ is lifted. DFT calculations in the same basis, using the B3LYP functional, are reported in Table 6 for $\gamma_H = 2$. Approximation A makes use of Eq. (12) with $\gamma_C = 2.322864$, $\gamma_N = 2.343435$ and $\gamma_O = 2.365145$. From Eq. (11) – Approximation B – one gets the valence parameters $\gamma_C^v = 2.216425$, $\gamma_N^v = 2.300834$, and $\gamma_O^v = 2.376273$. Approximation C, Eq. (13), gives $\gamma_C^v = 2.141722$, $\gamma_N^v = 2.258417$ and $\gamma_O^v = 2.345518$. The RMS errors, 0.098, 0.101 and 0.066 au for Approximations A, B and C, respectively, illustrate the merits of our simple formulation of atomic-like valence-region energies and of letting $\gamma_H = 2$. Though systematic, the improvements achieved by lifting the latter constraint are not truly significant, as indicated by the corresponding RMS deviations of 0.092, 0.094 and 0.066 au, respectively.

Table 6: Valence-region energies deduced from DFT potentials at the nuclei, using the 6-311G(*d,p*) basis and the B3LYP functional ($\gamma_{\text{H}} = 2$)

Molecule	E^v , atomic units ^a				
	Approx. A	Approx. B	Approx. C	Eq. (3)	Exptl. ^b
CH ₂	-6.7729	-6.7711	-6.7896	-6.7409	-6.7439
CH ₃ ·	-7.4098	-7.4104	-7.4126	-7.4302	-7.4305
CH \equiv C·	-11.8518	-11.8453	-11.9016	-11.7823	-11.8401
CH ₂ CH·	-13.0918	-13.0913	-13.1072	-13.0798	-13.0974
C ₂ H ₅ ·	-14.3136	-14.3154	-14.3156	-14.3363	-14.3401
CH ₄	-8.0373	-8.0397	-8.0294	-8.1102	-8.1079
C ₂ H ₆	-14.9432	-14.9465	-14.9364	-15.0091	-15.0119
C ₃ H ₈	-21.8473	-21.8521	-21.8386	-21.9099	-21.9195
C ₄ H ₁₀	-28.7527	-28.7588	-28.7419	-28.8105	-28.8279
<i>i</i> -C ₄ H ₁₀	-28.7464	-28.7528	-28.7348	-28.8115	-28.8304
<i>c</i> -C ₃ H ₆	-20.6049	-20.6058	-20.6180	-20.6592	-20.6756
C ₂ H ₄	-13.7466	-13.7483	-13.7459	-13.7668	-13.7754
C ₃ H ₆	-20.6468	-20.6505	-20.6441	-20.6732	-20.6877
1,3-C ₄ H ₆	-26.3215	-26.3234	-26.3348	-26.3441	-26.3689
Isoprene	-33.2186	-33.2219	-33.2302	-33.2483	-33.2814
CH ₂ =C=CH ₂	-19.3940	-19.3936	-19.4142	-19.4223	-19.4369
C ₂ H ₂	-12.5644	-12.5667	-12.5630	-12.5075	-12.5239
C ₆ H ₆	-37.8125	-37.8151	-37.8351	-37.7670	-37.8165
N ₂	-19.9979	-19.9964	-20.0251	-20.0488	-19.9844
NH ₃	-11.9257	-11.9309	-11.8569	-11.8225	-11.7839
N ₂ H ₄	-22.6071	-22.6141	-22.5157	-22.3944	-22.3160
CH ₃ NH ₂	-18.7846	-18.7880	-18.7345	-18.7113	-18.6757
<i>i</i> -C ₃ H ₇ NH ₂	-32.5677	-32.5736	-32.5152	-32.5200	-32.4979
CH ₃ NHNH ₂	-29.4137	-29.4181	-29.3480	-29.2915	-29.2162
(CH ₃) ₂ NNH ₂	-36.2467	-36.2496	-36.2015	-36.1880	-36.1200
<i>cis</i> -HNNH	-21.2106	-21.2123	-21.1925	-21.1563	-21.0858
CH ₃ NNCH ₃	-34.9682	-34.9674	-34.9659	-34.9730	-34.8971
Pyrrole	-35.8537	-35.8593	-35.8428	-35.7781	-35.7735
Pyrrolidine	-38.3004	-38.3039	-38.2697	-38.1878	-38.1840
Pyridazine	-45.0084	-44.9933	-45.0943	-45.1502	-45.1097
Pyrazine	-45.0311	-45.0141	-45.1176	-45.1799	-45.1408
HCN	-16.3470	-16.3459	-16.3372	-16.2749	-16.2463
CH ₃ CN	-23.1603	-23.1554	-23.1667	-23.1926	-23.1645
NH ₂ CN	-26.9281	-26.9270	-26.9094	-26.8985	
O ₂	-32.3421	-32.3604	-32.3200	-32.2073	-32.0239
H ₂ O	-17.6779	-17.6847	-17.5468	-17.3687	-17.2864
CO	-21.8222	-21.8215	-21.8449	-21.8439	-21.7687
CO ₂	-37.9904	-37.9856	-38.0111	-38.0600	-37.8921

Table 6: B3LYP/6-311G(*d,p*) valence-region energies (continued)

Molecule	E^v , atomic units ^a				
	Approx. A	Approx. B	Approx. C	Eq. (3)	Exptl. ^b
HCHO	-23.1610	-23.1572	-23.1232	-23.0340	-22.9508
CH ₃ CHO	-30.0416	-30.0369	-30.0003	-29.9489	-29.8726
<i>n</i> -C ₃ H ₇ CHO	-43.8096	-43.8057	-43.7751	-43.7530	-43.6877
(CH ₃) ₂ CO	-36.9447	-36.9404	-36.8959	-36.8633	-36.7916
H ₂ CCO	-28.6521	-28.6464	-28.6776	-28.7218	-28.6473
(CH ₃) ₂ O	-31.2550	-31.2525	-31.2029	-31.1459	-31.0660
(C ₂ H ₅) ₂ O	-45.0731	-45.0732	-45.0155	-44.9587	-44.8903
HCNO	-32.3024	-32.2970	-32.3433	-32.3667	
NO ₂	-42.0831	-42.0911	-42.1446	-42.2216	-42.0049
CH ₃ NO	-33.5659	-33.5620	-33.5723	-33.4795	-33.4686
CH ₃ NO ₂	-49.6731	-49.6700	-49.6835	-49.7469	-49.5390
NH=CH-NO ₂	-58.8654	-58.8577	-58.9487	-59.1303	-58.8913

^aThe E_k^{ion} , $\gamma_k^c E_k^{\text{ion}} = V_{\text{ne},k}^c - V_k^{c,v}$ and $V_{\text{ne},k}^c$ parameters used in Eqs. (11)–(13) are SDCI results in the $\text{vD}(13s\,8p\,2d\,1f)$ basis, taken from Ref. [5].

^bDeduced with $E_C^{\text{ion}} = -32.416$, $E_N^{\text{ion}} = -44.802$, $E_O^{\text{ion}} = -59.194$, $E_C^{\text{atom}} = -37.8558$, $E_N^{\text{atom}} = -54.6121$ and $E_O^{\text{atom}} = -75.1102$ au (from the appropriate sums of ionization potentials [18]) and the thermochemical data found in [20].

4 Conclusions and Prospects

Perhaps the first question that comes to mind when subdividing a molecule into atomic-like parts is about the boundaries of the so-called ‘atoms-in-the-molecule’; then one may proceed with the identification and calculation of all the relevant energy components, namely the electronic kinetic energy of each individual ‘atom’ k , l , etc, the potential energy of the electronic charge of each ‘atom’ k in the field of its own nucleus Z_k and the two-electron integrals involving exclusively the same charge, plus all the interactions between the nucleus and electrons of one ‘atom’ with the nuclei and electrons of the other ‘atoms’ found in a molecule. All this is feasible and rests on a partitioning in real space. This approach also implicates a postulate, however, regarding the distribution of the two-center terms, say, those involving ‘atoms’ k and l , among the partners involved. The usual $\frac{1}{2}$ and $\frac{1}{2}$ assignment may be criticized, perhaps not on grounds of fairness, but on scientific merit. Yet, we shall assume that all these problems are adequately solved and contemplate a core-valence separation on top of the atom-by-atom partitioning. Briefly, here we look for atomic-like valence-region energies.

This endeavour clearly requires the use of a core-valence separation that is described in real space. This is possible in principle because the equation exists, $E^v = \frac{1}{3}(T^v + 2V^v)$, but we still face, with added complications, the problems met with the above 'atoms-in-the-molecule' model. Future considerations will perhaps encourage direct use of this equation for E^v , but at this point in time we find it instructive to achieve that goal by means of simple approximations.

The very simplest one is rooted in Politzer's formula $E_k = V_k/\gamma_k$ connecting E_k , the energy of atom k , to V_k/Z_k , the total potential at its nucleus with charge Z_k . The γ_k parameters are treated as constants for each type $k = \text{H, C, etc}$ and their proper selection is known to give reasonably accurate results. The valence energy $E_k^v = E_k - E_k^{\text{ion}}$ calculated on this basis (approximation A) for atom k is *not* a direct product of, but is consistent with, our core-valence separation in real space.

When this separation is taken into account, E_k^v depends parametrically on the potential of the sole electronic and nuclear charges found *outside* its core, in the field of both the nuclear charge Z_k and the charge of its N_k^c core electrons. This picture is translated by the equation $E_k^v = (V_k - V_{\text{ne},k}^c + V_k^{\text{cv}})/\gamma_k^v$ where $V_{\text{ne},k}^c$ and V_k^{cv} are, respectively, the core nuclear-electronic potential energy of its N_k^c core electrons and the interaction of N_k^c with the exterior of that core. As before, V_k denotes the customary total potential energy involving Z_k . The k th ionic core left after removal of the valence electronic charge is described by the equation $E_k^{\text{ion}} = (V_{\text{ne},k}^c - V_k^{\text{cv}})/\gamma_k^c$. Two approximations were considered by reference to these expressions for E_k^v and E_k^{ion} . The first one, approximation B, assumes that γ_k^v and γ_k^c can be treated as constants for each type of atom while the second, approximation C, rests on a simple approximation for V_k^{cv} .

Approximation B lends itself to very convenient tests if we rewrite our basic formula as follows: $E_k^v = V_k/\gamma_k^v - (\gamma_k^c/\gamma_k^v)E_k^{\text{ion}}$. Its accuracy turns out to be virtually the same as that of approximation A. This can be understood because the latter obeys to practically the same formula, namely $E_k^v = V_k/\gamma_k - E_k^{\text{ion}}$. Still the fact remains that we cannot justify *both* our approximations, A and B, because their parameters, γ_k , γ_k^v and γ_k^c , cannot be simultaneously constant. This is so because $1/\gamma_k$ is the weighted average of $1/\gamma_k^v$ and $1/\gamma_k^c$ (Section 2) and V_k , at least, is certainly not to be treated as a constant. This criticism illustrates the pitfalls of these formulas when used with approximate constant γ_k parameters, notwithstanding the acceptable numerical results. On the other hand, this definition of the average $1/\gamma_k$ pin-points the place of Politzer's formula in the framework of core-valence theory in real space as a simple form of the basic relationship $E_k = E_k^v + E_k^{\text{ion}}$.

Our third approximation, C, describes V_k^{cv} in the point-charge-potential model. Again, E_k^v depends solely on the charges found outside the core region k , but in the field of an expanded 'effective nuclear charge', $Z_k^{\text{eff}} = Z_k - N_k^c$.

Numerical tests, using large basis sets such as the $(9s\,5p|6s) \rightarrow [5s\,3p|3s]$, the 6-311G(d, p) and the van Duijneveldt $(13s\,8p)$ set enriched by 2 d and 1 f functions, for example, conducted for representative collections of molecules, consistently indicate, both at the Hartree-Fock level and in post-Hartree-Fock B3LYP DFT calculations, that our approximation C is more accurate than the other two, A and B. The constraint of a constant γ_k^c included in B means indeed that $V_{ne,k}^c - V_k^{cv}$ is treated as if it were constant. Now, $V_{ne,k}^c$ itself is reasonably close to being a constant, but not V_k^{cv} , as suggested by the approximation $V_k^{cv} = -N_k^c[(V_k - V_{ne,k}^c)/Z_k]$ used in C. This may help to explain why our third approach outperforms the other two. Future studies could perhaps enhance accuracy by using $V_{ne,k}^c$ terms *as they are* in the actual molecules instead of their free-atom values (as done in this work), but only on a minor scale.

Let us now go back to the more basic concepts depicted in our equations. In a molecule, each nucleus Z_k surrounded by the train of its N_k^c core electrons is considered (in turn) in the field of all the other (electronic and nuclear) charges of that molecule. This description carries important corollaries. It is atomic-like to begin with. What this means is that we need not worry about the boundaries of 'atoms-in-the-molecule' to get atomic-like valence energies, in sharp contrast with the situation that would prevail in applications of the formula $E^v = \frac{1}{3}(T^v + 2V^v)$. The calculation of E_k^v only requires the knowledge of the conventional *total* potential at the nucleus k , which is easy to compute. Finally, as a direct consequence of the latter requirement, it is possible to gain access to E_k^v by means of density functional methods.

In Kohn-Sham theory, Pauli and Coulomb correlation, as well as the correlation contribution to the kinetic energy, are incorporated in the exchange-correlation functional $E_{xc}^{KS}[\rho]$. No problem arises with straight sums of kinetic plus potential energies, but the calculation of the kinetic energy plus *twice* the potential energy would require special consideration. Now, no such difficulty exists in our present use of DFT results, based on the potentials at the nuclei.

Our extensive numerical analyses have surely benefited from the precision added by the use of DFT methods. The 6-311G(d, p) basis set and the B3LYP functional have proven most adequate at a level approaching experimental accuracy. It is thus welcome that introduction of the point-charge-potential approximation not only reveals its soundness in our present applications but also improves the utilization of the formula for E_k^v by adding to its precision. It is fair to conclude that we are now in a position to associate a reasonably accurate valence energy with each individual atom in a molecule or, perhaps more vividly, an equally accurate difference $\Delta E_k^v = E_k^v - E_{k(\text{atom})}^v$ with respect to the free-atom valence-region energy. The latter information, which is a measure of the binding of an atom in a molecule, may find its way in future atom-by-atom (or bond-by-bond) descriptions of molecular properties.

Glossary

In our real-space core-valence separation, $r_{b,k}$ defines the boundary of the region around nucleus k that contains the N_k^c core electrons associated with it. The pertinent energy components are:

- T^v , the kinetic energy of the valence electrons.
- T_k^c , the kinetic energy of the N_k^c core electrons of the k th ionic core.
- $V_{ne,k}^c$, the attraction between the N_k^c core electrons and the nucleus with charge Z_k belonging to the k th core.
- $V_{ne}^v = V_{ne} - \sum_k V_{ne,k}^c$, the nuclear-electronic attraction of the valence electron, V_{ne} being the *total* nuclear-electronic potential energy of the system (atom or molecule).
- V_{ee}^{vv} , the repulsion involving exclusively valence electrons.
- $V_{ee,k}^{cc}$, the interelectronic repulsion between the N_k^c electrons of core k .
- $V_{ee}^v = V_{ee} - \sum_k V_{ee,k}^{cc}$, where
- V_{ee} is the total interelectronic repulsion of the system (atom or molecule).
- V_{nn} , the internuclear repulsion energy.
- $V^v = V_{ne}^v + V_{ee}^v + V_{nn}$, the ‘valence’ potential energy for use in Eq. (1).

A particularly important potential-energy component is

- V_k^{cv} = interaction energy between the N_k^c core electrons and the electronic and nuclear charges found outside the k th core region containing Z_k and N_k^c . For isolated atoms, V_k^{cv} reduces to V_{ee}^{cv} , the repulsion between core- and valence-region electrons.

Dedication and Acknowledgements

It is our pleasure to dedicate this work to Professor Giuseppe Del Re as a heartfelt token of esteem and gratitude for the many things we learned from him over the years, cementing a friendship in science and Life.

Őszinte barátsággal, avec nos sentiments respectueux e sincera gratitude.

S. F., E. C. V. and V. B.

References

- [1] R. F. W. Bader, *'Atoms in Molecules, a Quantum Theory'*, Clarendon, Oxford, 1990.
- [2] S. Fliszár, *J. Amer. Chem. Soc.* **102**, 6946 (1980).
- [3] S. Fliszár, *'Atoms, Chemical Bonds and Bond Dissociation Energies'* (Lecture Notes in Chemistry **63**), Springer-Verlag, Heidelberg, Berlin, 1994.
- [4] S. Fliszár, N. Desmarais, G. Dancausse, *Can. J. Chem.* **70**, 537 (1992); N. Desmarais, G. Dancausse, S. Fliszár, *Can. J. Chem.* **71**, 175 (1993).
- [5] N. Desmarais, S. Fliszár, *Theor. Chim. Acta* **94**, 187 (1996).
- [6] S. Fliszár, *Theor. Chem. Acc.* **96**, 122 (1997).
- [7] P. Politzer, *J. Chem. Phys.* **64**, 4239 (1976); P. Politzer, *J. Chem. Phys.* **69**, 491 (1978).
- [8] S. Fliszár, M. Foucrault, M.-T. Béraldin, J. Bridet, *Can. J. Chem.* **59**, 1074 (1981).
- [9] V. Barone, S. Fliszár, *J. Mol. Struct. (Theochem)* **369**, 29 (1996).
- [10] L. R. Kahn, P. Baybutt, D. G. Truhlar, *J. Chem. Phys.* **65**, 3826 (1976).
- [11] E. Clementi, C. Roetti, *At. Data Nucl. Data Tables* **14**, 179 (1974).
- [12] F. B. van Duijneveldt, Technical Report RJ 945. IBM Research Laboratories, San Jose, CA (1971).
- [13] M. J. Frisch, J. A. Pople, J. S. Binkley, *J. Chem. Phys.* **80**, 3265 (1984).
- [14] R. Krishnan, J. S. Binkley, R. Seeger, J. A. Pople, *J. Chem. Phys.* **72**, 650 (1980).
- [15] K. Pierloot, B. Dumez, P.-O. Widmark, B. O. Roos, *Theor. Chim. Acta* **90**, 87 (1995).
- [16] T. H. Dunning, *J. Chem. Phys.* **53**, 2823 (1970).
- [17] V. Barone, *Chem. Phys. Lett.* **226**, 392 (1994); *J. Chem. Phys.* **101**, 6834 (1994); *J. Chem. Phys.* **101**, 10666 (1994); V. Barone, C. Adamo, *Chem. Phys. Lett.* **224**, 432 (1994); V. Barone, *Theor. Chim. Acta* **91**, 111 (1995).

- [18] C. E. Moore, *Natl. Stand. Ref. Data Ser.*, (US Natl. Bur. Stand.) **34** (1970).
- [19] D. M. Chipman, *Theor. Chim. Acta* **76**, 73 (1989); *J. Chem. Phys.* **91**, 5455 (1989).
- [20] E. C. Vauthier, M. Blain, S. Odier, V. Barone, M. Comeau, S. Fliszár, *J. Mol. Struct. (Theochem)* **340**, 63 (1995); J. D. Cox, G. Pilcher, '*Thermochemistry of Organic and Organometallic Compounds*', Academic Press, London, 1970; G. Herzberg, '*Molecular Spectra and Molecular Structure III. Electronic Spectra and Electronic Structure of Polyatomic Molecules*', van Nostrand Reinhold Co., New York. Toronto, 1966; M. J. S. Dewar, G. P. Ford, *J. Amer. Chem. Soc.* **99**, 1685 (1977).

From Classical Density Functionals to Adiabatic Connection Methods. The State of the Art.

Carlo Adamo, Andrea di Matteo and Vincenzo Barone

Dipartimento di Chimica, Università Federico II
via Mezzocannone 4, I-80134 Napoli, Italy

Abstract

This contribution is devoted to the impact of density functional (DF) theory in the field of computational chemistry. After a short discussion of the theoretical background, the attention is focussed on the role played by exchange and correlation functionals in determining the overall performances of DF methods. The theoretical behavior of the most common exchange functionals, like those proposed by Becke in 1988 and by Perdew and Wang in 1991, will be compared with that of more recent proposals. A particular attention will be devoted to high-gradient low density regions, which dominate weak non covalent interactions. An analysis of the most common correlation functionals, e.g. those introduced by Lee, Yang and Parr and by Perdew and Wang in 1991, will be also carried out. Next, the most recent development of DF theory, namely the adiabatic connection methods (ACMs), will be treated. The numerical performances of the most recent ACM approaches will be examined in detail, with special reference to the development of new parameter-free ACMs. Finally, some results obtained on a standard molecular data set and on some "delicate" chemical systems will be discussed.

Contents

1. *Introduction*
2. *Theoretical background*
 - 2.1 The Kohn-Sham approach
 - 2.2 The generalized SCF model
 - 2.3 Density functionals
 - 2.4 Adiabatic connection methods
3. *Applications*
 - 3.1 Covalent interactions
 - 3.2 Non covalent interactions
 - 3.3 Reactivity
 - 3.4 Molecular properties
 - 3.5 Excited electronic states
4. *Conclusion*

1. INTRODUCTION

The quantum mechanical approach to chemistry has two long standing goals. The first one is the *a-priori* prediction of the structure, properties and reactivity of molecules formed by atoms of the whole periodic table. The second, and not less ambitious, objective is the interpretation of the above results in terms of chemical concepts, such as bond energies, inductive effects and electronegativity, for example. Thanks to the impressive development of computer power and to the implementation of very efficient algorithms, the most sophisticated post Hartree-Fock (HF) methods (like multireference configuration interaction and coupled clusters) [1-6] are nowadays able to provide, when coupled to large basis sets [7-9], data of chemical accuracy for geometrical structures, binding energies and physico-chemical properties. However, their scaling with the number of active electrons is so heavy (at the 7th or 8th power) that applications to chemically significant systems remain prohibitive. Furthermore, interpretation of the results in terms of chemical concepts is very complicated. Less sophisticated conventional methods, like HF or low-order many-body techniques (e.g. MP2 [10]), work well essentially for the ground electronic states of closed-shell molecules formed by main group atoms [10,11].

Methods rooted in the density functional (DF) theory [12] are more promising, since they are able to include a large amount of correlation energy in a formalism that requires in essence the same resources as the HF method. In particular the Kohn-Sham (KS) approach [13] has led to DF implementations strongly resembling the corresponding HF algorithms [14-20]. As a consequence, most popular ab-initio programs now include DF capability, and specialized DF packages are well established. In the following we will make explicit reference to the Gaussian implementation [21] concerning both algorithms and computations.

The development of GGA (generalized gradient approximation) and beyond GGA functionals in the last years [22-43] has significantly improved the results provided by the so called local density approximation (LDA) [44-46]. Together with the reasonable scaling with the number of electrons, the major strength of these DF methods is their consistent accuracy both for closed- and open-shell systems along the whole periodic table. As a rule of thumb, it can be said that current functionals including gradient corrections provide for any molecular system results of the same quality as the MP2 method for organic molecules. It must be pointed out also that, from a chemist's point of view, all the KS methods are particularly interesting, since they retain the ease of interpretation of single determinant methods.

Furthermore, recent work has shown that the approaches rooted in the adiabatic connection method (ACM), in which a fraction of HF exchange is mixed together with DF exchange, provide even better results [47-59]. Some questions are open about the empirical parameters which rule the ratio between HF and DF

contributions. In fact, a possible drawback of ACM approaches is that the percentage of HF and DF exchange terms could depend on the particular kind of atom, interaction, and/or property investigated. Although systematic analyses are still lacking, an increasing number of studies suggest that the same set of parameters provide reliable results for the strength of standard covalent bonds, electron deficient interactions, harmonic and anharmonic frequencies, and one-electron properties. At the same time, some limitations of the current ACMs have been recently rectified, especially concerning non-covalent interactions, like those found in van der Waals and charge transfer complexes, or the activation energies governing some organic reactions, like proton transfer and the Walden S_N2 inversion. Next the reduction or the complete removal of optimized parameters in ACMs has brought some significant enhancement in the field of hybrid HF/DF methods.

The aim of the present contribution is to illustrate the state of the art in this complex scenario and to better define the field of application of classical DF and less-conventional adiabatic connection approaches. To this end, after a short introduction about the foundation of DF theory, we discuss in some detail the physical behavior of the exchange and correlation functionals. The ACMs are next introduced devoting particular attention to the most recent developments. Finally a number of examples, covering different chemical situations, are illustrated.

2. THEORETICAL BACKGROUND

2.1 The Kohn-Sham approach

Density functional (DF) theory rests on the two theorems of Hohenberg-Kohn (HK) [13]. The first of these states that for systems with a nondegenerate ground state and a given electron-electron interaction there is a one-to-one mapping between the external (local) potential and the ground state wave function as well as the diagonal one-electron density. Therefore the wave function is uniquely determined by the one-electron density, i.e. it is a functional of the density, and so are all properties, being ground state expectation values of the associated operators. In particular also the total energy and its components, such as the kinetic energy, are functionals of the density. The second HK theorem defines a density functional for the energy, $E_v[r]$, for a system with given external potential v . This energy functional will have a minimum for the exact ground state density associated with that external potential.

It has not proven possible to find sufficiently accurate approximations for $E_v[r]$, so that a single Euler-Lagrange equation for the density would yield an accurate density and energy. In particular, it is very difficult to find a good density functional for the kinetic energy. Therefore applications of DF theory in chemistry invariably use the one-electron model of Kohn and Sham (KS). They

introduced an auxiliary system of noninteracting electrons moving in a local potential called $v_s(r)$. This potential has the property that the occupied KS orbitals give the exact (correlated) electron density of the system. It has been proven that, under certain conditions, such a potential exists, and by HK theorems applied to noninteracting electrons, it must be unique. The important quantities in KS theory may be now defined. Suppose the KS potential $v_s(r)$ is known, then the KS equations

$$h_{KS}\phi_i(r) = \varepsilon_i\phi_i(r) \quad (1)$$

with

$$h_{KS} = \left[-\frac{1}{2} \nabla^2 + v_s(r) \right] \quad (2)$$

give the exact density as

$$\rho(r) = \sum_i^N |\phi_i(r)|^2 \quad (3)$$

Since the KS potential is uniquely determined by the density, the same applies to the solutions of the KS equations. Therefore, the kinetic energy of the electrons described by the KS orbitals is a functional of the density:

$$T_s[\rho] = \sum_i^N \langle \phi_i^*[\rho(r)] | -\frac{1}{2} \nabla^2 | \phi_i[\rho(r)] \rangle \quad (4)$$

From these equations, we get the exact total energy of the system:

$$E = T_s[\rho] + \int \rho(r_1) v(r_1) dr_1 + \frac{1}{2} \int \frac{\rho(r_1)\rho(r_2)}{r_{12}} dr_1 dr_2 + E_{xc} \quad (5)$$

Here v is the external potential of the system, in our case always the nuclear potential

$$v(r_1) = V_N(r_1) = \sum_A \frac{-Z_A}{|R_A - r_1|} \quad (6)$$

The only unknown quantity in eqn (5) is the exchange-correlation energy E_{xc} , which is therefore defined by this equation. This quantity plays a crucial role in DF theory. It is, after a KS calculation, the only quantity for which a reliable estimate is needed to obtain a good total energy.

Moreover, it determines also the KS potential itself. It is possible to prove that the KS potential is given by:

$$v_s(r) = v(r) + \int \frac{\rho(r')}{|r - r'|} dr' + v_{xc}[\rho(r)] \quad (7)$$

where v_{xc} is the functional derivative of E_{xc}

$$v_{xc}[\rho(r)] = \frac{\delta E_{xc}}{\delta \rho(r)} \quad (8)$$

So the KS equations have the final form:

$$h_{KS}\phi_i(\mathbf{r}) = \left[-\frac{1}{2}\nabla^2 + V_N + V_C + v_{xc}(r) \right] \phi_i(r) = \varepsilon_i \phi_i(\mathbf{r}) \quad (9)$$

where the Coulomb potential is given by

$$V_C(r) = \int \frac{\rho(r')}{|r - r'|} dr' \quad (10)$$

2.2 The generalized SCF model

The solution of the KS problem, expressed by eqn. (9), is similar to the procedure utilized for the HF model, both methods resting on a self consistent field (SCF) solution for the evaluation of the total energy. The SCF equations are built by expanding the ϕ_i in a set of one-electron basis functions:

$$\phi_i(r) = \sum_{\mu=1}^m C_{i\mu} \chi_{\mu}(r) \quad (11)$$

so that the electron density can be described in terms of these functions and of the corresponding one-body density matrix \mathbf{P}

$$\rho(r) = \sum_{\mu\nu} P_{\mu\nu} \chi_{\mu}(r) \chi_{\nu}(r) \quad (12)$$

The total SCF energy is:

$$E_{SCF} = \sum_{\mu\nu} P_{\mu\nu} H_{\mu\nu} + \frac{1}{2} \sum_{\mu\nu\lambda\sigma} P_{\mu\nu} P_{\lambda\sigma} (\mu\nu|\lambda\sigma) + E_{xc} \quad (13)$$

where the $H_{\mu\nu}$ are the matrix elements of the one-electron operator

$$H^{core} = -\frac{1}{2}\nabla^2 + V_N \quad (13a)$$

In a spin unrestricted formalism

$$\rho(r) = \rho^{\alpha}(r) + \rho^{\beta}(r); P(r) = P^{\alpha}(r) + P^{\beta}(r) \quad (14)$$

and the KS equation (9) is transformed into a secular equation from which the eigenvalues and eigenfunctions are obtained:

$$F^{\sigma} C^{\sigma} = S C^{\sigma} \varepsilon^{\sigma} \quad (15)$$

with the orthonormality conditions

$$(C^{\sigma})^{\dagger} S C^{\sigma} = I \quad (16)$$

where σ refers to either α or β spin. The F^{σ} are Fock-like matrices, whose elements are

$$F_{\mu\nu}^{\sigma} = \frac{\partial E_{SCF}}{\partial P_{\mu\nu}^{\sigma}} \quad (17)$$

C^{σ} are the matrices of the molecular orbital coefficients, S is the atomic overlap matrix and ε^{σ} are diagonal matrices of the KS orbital eigenvalues. Now the difference between HF and KS approaches resides in the term E_{xc} , which is

$$E_{xc}^{HF} = -\frac{1}{2} \left(\sum_{\mu\nu\lambda\tau} P_{\mu\nu}^{\alpha} P_{\lambda\tau}^{\alpha} + P_{\mu\nu}^{\beta} P_{\lambda\tau}^{\beta} \right) (\mu\lambda|\nu\tau) \quad (18)$$

in HF theory, and

$$E_{xc}^{KS} = \int f(\rho^{\alpha} \rho^{\beta}) dr \quad (19)$$

in KS theory. In most cases the integral (19) cannot be computed analytically and must be obtained by numerical quadrature. This introduces a number of technical problems, which, although reasonably well under control in the most recent packages [60-64], suggest the development of grid-free methods [65,66]. Furthermore, many current KS implementations employ various auxiliary fitting or projection techniques to aid in the evaluation of the Coulomb and/or exchange-correlation potential [14,15,19,20]. Although fitting can reduce the computational effort for small systems, this is no longer the case for large molecules. In some particularly efficient procedures, the integrands of eqn (19) can be obtained without evaluation of the Hessians of the densities, even though these appear in eqn (8). As a consequence, the cost of the exchange-correlation part of the electronic calculation scales linearly with the size of the atomic basis set used in the expansion of the molecular orbitals. Of course, the evaluation of the Hessians cannot be avoided when computing analytical gradients, or second derivatives. This task is, however, performed only once in each optimization step.

2.3 Density functionals

The key-problem in KS theory is to determine an analytical form for the E_{xc} term. The knowledge of the exact expression of the E_{xc} term leads, through eqn (5), to the exact total energy. Unfortunately, this expression is unknown, and approximations must be used. The most common approach to the problem of the representation of E_{xc} is to separate the correlation contribution from the exchange counterpart. This distinction is somewhat artificial in the context of DF theory, but the separation between these two terms considerably simplifies the discussion. Let us start with the simplest DF approach to the problem of exchange functional, i.e. the local spin density approximation (LSD), in which the functional for the uniform electron gas of density ρ is integrated over the whole space:

$$E_x^{LSD} = A_x \sum_{\sigma} \int \rho_{\sigma}(r)^{4/3} dr \quad (20)$$

where

$$A_x = -\frac{3}{2} \left(\frac{3}{4\pi} \right)^{1/3} \quad (21)$$

Such an approach underestimates the exchange energy by about 10%. Starting from eqn (20) several corrections for the nonuniformity of atomic and molecular densities have been proposed. In particular, those based on density gradients have received considerable attention, due to their simplicity. These corrections,

collectively referred to as generalized gradient approximation (GGA), are usually expressed in terms of an enhancement factor over the exchange energy of the uniform electron gas, so that the total exchange energy takes the form:

$$E_X^{\text{GGA}} = E_X^{\text{LSD}} - \sum_{\sigma} \int F[x] \rho_{\sigma}(r)^{4/3} dr \quad (22)$$

where x is the dimensionless reduced gradient:

$$x = \frac{|\nabla \rho_{\sigma}|}{(\rho_{\sigma})^{4/3}} \quad (23)$$

A number of semiempirical GGA exchange functionals, which contain parameters obtained by fitting the exchange atomic energies have been proposed. Roughly speaking, these functionals can be divided in two main classes. In the first one, we may group those which can be considered as modifications of the functional proposed by Becke in 1988 [25] (hereafter referred to as B), whose enhancement factor can be expressed as

$$F^B[x] = \frac{bx^2}{1 + 6bx \sinh^{-1}} \quad (24)$$

where b is a constant. In this class we include the functional developed by Perdew and Wang in 1991 (hereafter PW) [46], the so-called CAM family of functionals [17], and the exchange functional of Chermette and co-workers [29].

The other class contains all the functionals which can be expressed as polynomial function of the reduced density gradient. Among them, we can mention those introduced by Becke in 1986 (B86) [22,23], by Perdew and Wang in 1986 (P) [24], by Lacks and Gordon in 1993 (LG) [27] and the very recent functional of Gill (G) [30], either in its original form or in the modified form proposed by Handy. For instance, the enhancement factor of the P functional is:

$$F^P = [1 + a_2 s^2 + a_4 s^4 + a_6 s^6]^{1/15} \quad (25)$$

where

$$s = \frac{1}{2(3\pi^2)^{1/3}} x \quad (26)$$

and a_2 , a_4 , and a_6 are constants

It is possible to have a rough idea about the performances of the different exchange functionals by computing the total exchange atomic energies for the first and second rows of the periodic table. Standard exchange functionals usually give total atomic exchange energy within 1% of the HF exchange energies, as is well evidenced by the data reported in table I.

All the above mentioned functionals generally provide atomic or molecular properties with a reasonable precision, so that conventional DF methods are claimed to deliver results comparable to those obtained by second-order many body perturbation approaches (MP2). From a purely formal point of view, the reasons for such good performances are not yet evident.

In particular, a number of physical conditions that must be satisfied by an exchange functional have been established, but only few of the current exchange functionals obey to them.

Table I. Magnitude of the exact exchange energy (Hartrees) and difference between exact exchange energy and various density functional for the exchange energy, for neutral atoms. All calculations employ Hartree-Fock densities for the computed ground-state configuration and term and the aug-cc-pVQZ basis set (unless explicitly noted)

atom	HF	Δ LSD	Δ PW	Δ B	Δ G	Δ LG
H	-0.313	+0.045	+0.006	+0.003	+0.002	+0.003
He	-1.026	+0.142	+0.009	+0.001	-0.003	-0.002
Li	-1.781	+0.243	+0.018	+0.006	+0.003	+0.001
Be	-2.666	+0.354	+0.001	+0.009	+0.010	-0.002
B	-3.770	+0.474	+0.015	+0.010	-0.016	-0.007
C	-5.077	+0.590	+0.027	+0.009	-0.022	-0.010
N	-6.607	+0.706	+0.030	+0.011	-0.022	-0.010
O	-8.219	+0.835	+0.016	-0.005	-0.050	-0.033
F	-10.045	+0.956	+0.002	-0.019	-0.066	+0.051
Ne	-12.110	+1.076	+0.006	-0.029	-0.034	+0.057
Na	-14.018	+1.234	+0.013	-0.010	-0.010	+0.038
Mg	-15.992	+1.383	+0.016	-0.006	-0.011	+0.039
Al	-18.091	+1.541	+0.026	+0.003	-0.024	+0.029
Si	-20.304	+1.696	+0.036	+0.012	-0.023	+0.017
P	-22.642	+1.849	+0.046	+0.020	+0.002	+0.001
S	-25.035	+2.012	+0.053	+0.024	-0.030	+0.007
Cl	-27.545	+2.168	+0.057	+0.029	-0.033	+0.018
Ar	-30.185	+2.322	+0.061	+0.031	-0.004	+0.031
abs. aver. error		1.090	0.025	0.013	0.019	0.019
max error		2.322	0.061	0.031	0.066	0.057

Among others, three conditions are of particular importance. The first constraint is related to the behavior in the small x region, where the GGA exchange functional should reduce to E_x^{LSD} in order to recover the correct uniform gas limit. The second condition was defined by Levy, who showed that some scaling properties can be satisfied if the asymptotic form of the functional for large x is $x^{-\alpha}$, where $\alpha \geq 1/2$ [68,69]. The last condition is the so called "Lieb-Oxford bound" [70], which states that:

$$E_x \geq E_{xc} \geq -1.679 A_x \int \rho(r)^{4/3} dr \quad (27)$$

The behavior of some of the most common functionals with respect to these three constraints is reported in table II. The B functional does not obey neither the Levy condition nor the Lieb-Oxford bound, but its numerical performances are better than those provided by the PW functional, which respects all the above mentioned constraints.

This situation is, of course, quite disturbing and some efforts have been done to design an exchange functional which couples a rigorous theoretical formalism with good numerical performances. For instance, we have recently found that some modifications of the PW exchange functional (hereafter referred to as mPW) induce significant improvements of its numerical results, while retaining the same parameters and correct physical behavior of the original model. Furthermore, the correct asymptotic conditions are less important in the high density (which corresponds to covalent bonds), than in low-density region. This point is of particular importance, since these latter regions are responsible for non-covalent interactions, such as H-bond, van der Waals (vdW) and charge transfer(CT) [39].

Table II. A set of minimal physical requirements for the exchange functional

requirement	B	PW	B86	LG	G
correct uniform gas limit	Yes	Yes	Yes	Yes	Yes
Levy condition	No	Yes	No	Yes	No
Lieb-Oxford bound	No	Yes	No	Yes	No
good fitting of atomic exchange energies	Yes	Yes	Yes	Yes	Yes

The situation is well evidenced by computing the HF and DF differential exchange energy for the He dimers, i.e; the exchange energy of the atom pair minus the exchange energy of the two free atoms. In figure I are reported the DF errors, computed with respect to the HF differential exchange energy, for the He pairs. This plot evidences the significant error obtained in the long-range region ($d > 2.0$ Å) by using conventional exchange functionals. In contrast, an improved behavior is obtained by properly designed functionals, like the mPW or the LG one.

Many approximate functionals have been proposed for the remaining part of the total energy, i.e. the correlation energy. The development of an improved local form of this functional is of special interest for large systems because the complexity of the system will be significantly reduced. Recently, a new form of $E_c[\rho]$ based on the functional expansion and the adiabatic connection formulation of DF has been advanced which is a sum of integrals of various powers of the density [37]:

$$E_c = C_1 N + C_2 \int \rho^{2/3}(r) dr + C_3 \int \rho^{1/3}(r) dr \quad (28)$$

where C_n are constants to be determined and N is the number of electrons in the system. In spite of its accuracy, this functional, called the Liu-Parr (LP) correlation functional, has the fundamental deficiency, that the corresponding correlation potential approaches infinity for all densities that fall to zero at large values of r . This fact rules out the possibility of applying the LP functional, without truncation, in a KS-SCF procedure.

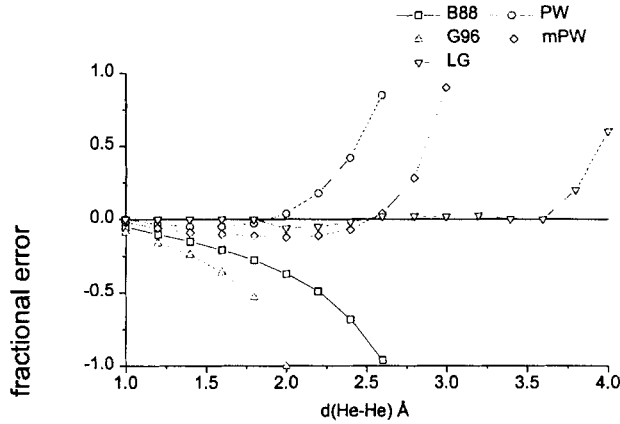


Figure 1. Computed DF fractional error for the exchange energy in the He-He interaction.

Starting from eqn (28) and applying the Padé summation approximation, it is possible to define a family of correlation functionals, which has the general form:

$$E_c^{[m,n]} = \int \rho(r) \frac{p_m(\zeta)}{q_n(\zeta)} dr \quad (29)$$

Here, $\zeta = \rho^{-1/3}$, the superscripts label the order of the Padé approximant employed, and p_m and q_n are polynomials of order m and n , respectively. The lowest expansions of eqn (29) are:

$$E_c^{[0,1]} = \int \rho(r) \frac{a_0}{b_0 + b_1 \zeta} dr \quad (30)$$

$$E_c^{[1,2]} = \int \rho(r) \left(\frac{a_0 + a_1 \zeta}{b_0 + b_1 \zeta + b_2 \zeta^2} \right) dr \quad (31)$$

Equation (30) is the form proposed by Wigner over sixty years ago [70].

A different approach to the problem of the correlation representation starts from the definition of a local correlation functional with the correct asymptotic behaviour, which i.e. correctly reproduces the correct uniform gas limit. The most common functional with this characteristic is the Vosko-Wilk-Nuisar (VWN) parametrization of the Monte Carlo results of Ceperly and Alder [45]]. More recently Perdew and Wang proposed an improved local correlation functional [46]:

$$E_c^{\text{LDA}} = -2a\rho(1 + \alpha_1 r_s) \log \left[1 + \frac{1}{2a(\beta_1 r_s^{1/2} + \beta_2 r_s + \beta_3 r_s^3 + \beta_4 r_s^4)} \right] \quad (32)$$

where a , α_1 , β_1 , β_2 , β_3 , and β_4 are constants, and

$$r_s = \left(\frac{3}{4\pi\rho} \right)^{1/3} \quad (33)$$

As for the exchange functionals, local correlation functionals reproduce only in part the total correlation energy and GGA corrections are in order. In particular the correlation functional proposed by Lee, Yang and Parr (LYP) [71] embodies a Wigner-like functional (eqn 30) as the local contribution. The analytical expression of the LYP functional is:

$$\begin{aligned} E_c^{\text{LYP}} = & -\frac{4a}{1+d\rho^{-1/3}} \frac{\rho_\alpha \rho_\beta}{\rho} - 2^{11/3} \frac{3}{10} (3\pi^2)^{2/3} ab\omega(\rho) \rho_\alpha \rho_\beta (\rho_\alpha^{8/3} + \rho_\beta^{8/3}) \\ & + \frac{\partial E_c^{\text{LYP}}}{\partial \rho_\alpha \nabla \rho_\alpha} \nabla \rho_\alpha \nabla \rho_\alpha + \frac{\partial E_c^{\text{LYP}}}{\partial \rho_\alpha \nabla \rho_\beta} \nabla \rho_\alpha \nabla \rho_\beta + \frac{\partial E_c^{\text{LYP}}}{\partial \rho_\beta \nabla \rho_\beta} \nabla \rho_\beta \nabla \rho_\beta \end{aligned} \quad (34)$$

where

$$\begin{aligned} \frac{\partial E_c^{\text{LYP}}}{\partial \rho_\alpha \nabla \rho_\alpha} &= -ab\omega(\rho) \left[\frac{1}{9} \rho_\alpha \rho_\beta \left\{ 1 - 3\delta(\rho) - [\delta(\rho) - 11] \frac{\rho_\alpha}{\rho} \right\} - \rho_\beta^2 \right] \\ \frac{\partial E_c^{\text{LYP}}}{\partial \rho_\alpha \nabla \rho_\beta} &= -ab\omega(\rho) \left\{ \frac{1}{9} \rho_\alpha \rho_\beta [47 - 7\delta(\rho)] - \frac{4}{3} \rho^2 \right\} \\ \frac{\partial E_c^{\text{LYP}}}{\partial \nabla \rho_\beta \nabla \rho_\beta} &= -ab\omega(\rho) \left[\frac{1}{9} \rho_\alpha \rho_\beta \left\{ 1 - 3\delta(\rho) - [\delta(\rho) - 11] \frac{\rho_\beta}{\rho} \right\} - \rho_\alpha^2 \right] \\ \omega(\rho) &= \frac{e^{-c\rho^{-1/3}}}{1+d\rho\rho^{-1/3}} \rho^{-11/3} \\ \delta(\rho) &= c\rho^{-1/3} \frac{d\rho^{-1/3}}{1+d\rho\rho^{-1/3}} \end{aligned} \quad (35)$$

and a, b, c, d are constants.

In a similar way, the local PW correlation functional of eqn (32) can be significantly improved by adding a gradient correction. The resulting GGA correlation functional is:

$$E_c^{PW91} = E_c^{LDA} + \rho H \quad (36)$$

where

$$H = \frac{\beta^2}{2\alpha} \log \left[1 + \frac{2\alpha}{\beta} \frac{t^2 + At^4}{1 + At^2 + A^2t^4} \right] + C_{c0} [C_c - C_{c1}] t^2 e^{-100s^2}; \quad (37)$$

$$A = \frac{2\alpha}{\beta} \left[e^{-2\alpha\epsilon_c/\beta^2} - 1 \right]^{-1}; \quad (38)$$

$$C_c = C_1 + \frac{C_2 + C_3 r_s + C_4 r_s^2}{1 + C_5 r_s + C_6 r_s^2 + C_7 r_s^3}; \quad (39)$$

$$t = \frac{|\nabla \rho|}{2 \left[\frac{4}{\pi} (3\pi^2 \rho)^{1/3} \right]^{1/2}} \quad (40)$$

$$\epsilon_c = \rho E_c^{LDA} \quad (41)$$

and $\alpha, \beta, C_{c0}, C_{c1}, C_1, C_2, C_3, C_4, C_5, C_6$ and C_7 are constants.

As for the exchange functionals, a set of "minimal" requirements has been established (see table III). In this connection it must be mentioned that the LYP functional does not reach the exact uniform electron gas limit and does not allow for a distinct treatment of parallel and antiparallel spin correlation, but gives vanishing correlation for one-electron systems

Table III. A set of minimal physical requirements for the correlation functional

Requirements	PW91	LYP
exact uniform gas limit	Yes	No
parallel and anti-parallel spin treatment	Yes	No
vanishing correlation for one-electron system	No	Yes
good fitting of atomic correlation energies	Yes	Yes

Despite its theoretical weakness, the LYP functional is one of the best forms of the correlation functional currently available, generally performing better than the PW functional, especially for molecules containing first-row atoms.

In table IV are reported the total correlation energies for the atoms belonging to the first two rows of the periodic table.

Table IV. Exact correlation energy and errors of some density functionals (in a.u.) for neutral atoms. All calculations employ Hartree-Fock densities for the computed ground-state configuration and term.

atom	Exact	PW	LYP
H	0.000	-0.006	0.000
He	-0.042	-0.003	-0.002
Li	-0.046	-0.011	-0.007
Be	-0.094	0.000	-0.001
B	-0.125	+0.001	-0.003
C	-0.157	+0.001	-0.010
N	-0.189	-0.007	-0.005
O	-0.258	+0.003	-0.007
F	-0.322	+0.006	-0.004
Ne	-0.390	+0.014	+0.007
Na	-0.398	-0.005	-0.010
Mg	-0.444	-0.004	-0.015
Al	-0.479	-0.008	-0.017
Si	-0.520	-0.010	-0.011
P	-0.553	-0.018	-0.013
S	-0.634	-0.004	-0.001
Cl	-0.714	+0.012	+0.040
Ar	-0.787	+0.019	+0.036
abs. aver. error		0.007	0.010
max error		0.019	0.036

2.4 Adiabatic connection methods

The adiabatic connection formula is at the root of the ACMs. This formula is usually expressed in the form:

$$E_{xc} = \int_0^1 U_{xc,\lambda} d\lambda \quad (42)$$

with

$$U_{xc,\lambda} = \langle \Psi_\lambda | V_{ee} | \Psi_\lambda \rangle - \frac{e^2}{2} \iint \frac{\rho(r)\rho(r')}{|r-r'|} dr dr' \quad (43)$$

here λ is an electronic coupling strength parameter that *switches on* the Coulomb repulsion between electrons and $U_{xc,\lambda}$ is the corresponding potential energy of exchange and correlation for electron-electron interaction at intermediate coupling strength λ . The integrand of eqn (42) refers explicitly to the potential energy only, the kinetic part of the exchange correlation energy being generated, by the λ integration. This formula connects the noninteracting KS reference system ($\lambda=0$) to the fully interacting real system ($\lambda=1$), through a continuum of partially interacting systems ($0 \leq \lambda \leq 1$), all sharing a common density ρ . Becke showed that the simplest approximation to eqn (42) can be expressed by a two-point formula [48]:

$$E_{xc}^{ACM} = \frac{1}{2} (E_{xc, \lambda=0} + E_{xc, \lambda=1}) \quad (44)$$

An application of eqn (44) is the so called half-and-half (h&h) ACM approach, which is obtained if $E_{xc, \lambda=0} = E_x^{HF}$, the HF exchange, and $E_{xc, \lambda=1} = E_x^{LSD}$, the LSD approximation to exchange, are used. Variants of the h&h method, including GGAs, are defective in several respects and cannot be considered significant improvements over standard functionals, even if they provide good results for some difficult systems. A more valuable approach has been next obtained by Becke using a three parameter equation [47]:

$$E_{xc}^{ACM} = a_{x0} E_x^{LSD} + (1 - a_{x0}) E_x^{HF} + a_{x1} \Delta E_x^{GGA} + E_c^{LSD} + a_c \Delta E_c^{GGA} \quad (45)$$

where ΔE_x^{GGA} and ΔE_c^{GGA} are the generalized gradient contributions to the exchange and correlation contribution, and E_x^{LSD} and E_c^{LSD} their LSD counterparts. The three semiempirical parameters, a_{x0} , a_{x1} and a_c , have been determined by fitting the heats of formation of a standard set of molecules. Even if the original work uses the Perdew-Wang (PW) correlation functional, the most popular implementation is the so-called B3LYP method, which uses (in a self-consistent way) the B exchange functional together with the LYP correlation functional:

$$E_{xc}^{B3LYP} = a_{x0} E_x^{LSD} + (1 - a_{x0}) E_x^{HF} + a_{x1} \Delta E_x^B + E_c^{VWN} + a_c \Delta E_c^{LYP} \quad (46)$$

where the LSD contribution to the exchange energy is that of a uniform spin-polarized electron gas and the local correlation component is represented by the VWN parametrization. Since the local (Wigner) part of the LYP correlation functional is not too different from the correlation energy of the uniform electron gas, the last term is usually replaced by:

$$\Delta E_c^{LYP} = E_c^{LYP} - E_c^{VWN} \quad (47)$$

This protocol is nowadays considered as the most powerful among all the ACM approaches, providing, at a fraction of the computational costs, numerical results close to those obtained by the most refined post-HF methods. On the basis of such an experience, Becke has recently proposed a single-parameter version of his ACM approach [49]:

$$E_{xc}^{ACM} = a_0 E_x^{HF} + (1 - a_0) (E_x^{LSD} + \Delta E_x^{GGA}) + E_c^{LSD} + \Delta E_c^{GGA} = a_0 (E_x^{HF} - E_x^{GGA}) + E_{xc}^{GGA} \quad (48)$$

where a_0 ranges between 0.28 and 0.16, depending on the choice of the GGA correlation functional. This parameter is, once again, chosen to obtain the best fitting to the experimental data of a standard set of molecules.

Very recently, several authors focused their attention on the theoretical evaluation of the exact mixing coefficients in ACM approaches. In particular, Perdew and co-workers argue that the optimum integer value ruling the HF/DF exchange ratio can be determined by the lowest order of the Gorling-Levy perturbation theory

which provides an accurate description of the dependence of $E_{xc,\lambda}$ upon the coupling constant λ . They showed that the $E_{xc,\lambda}$ term has a correct dependence, i.e. it has the correct value, slope and second derivative at $\lambda = 1$, only for $a_0 = 1/4$ [53].

Following these works, we have introduced a parameter-free version of the B3LYP approach, in which only the HF and the DF exchange contributions are mixed together in the ratio 1/4, while the correlation part is entirely included at the DF level [54]. Starting from eqn (48), we have defined the B1LYP protocol, which uses the Becke exchange and LYP correlation functionals as:

$$E_{xc}^{B1LYP} = \frac{1}{4} E_x^{HF} + (1 - \frac{1}{4})(E_x^{LSD} + \Delta E_x^B) + E_c^{VWN} + \Delta E_c^{LYP} = \frac{1}{4} E_x^{HF} + \frac{3}{4}(E_x^{LSD} + \Delta E_x^B) + E_c^{LYP} \quad (49)$$

Note that, while slightly different B3LYP functionals are obtained choosing different fittings for the correlation energy of the free electron gas, this problem completely disappears in the B1LYP model. As is the case for the popular B3LYP protocol, the B1LYP approach has been used in a fully self-consistent way, that is the iterative determination of the KS orbitals is performed by the whole functional including contributions from GGA and HF exchange.

3 APPLICATIONS

3.1 Covalent interactions

The so called G2 set of molecules is nowadays considered a standard for the validation of new quantum chemical approaches [72]. Table V collects an error statistic for several quantum mechanical approaches concerning the geometric and thermodynamic parameters of 32 molecules belonging to the G2 set, together with dipole moments and harmonic vibrational frequencies.

From these data, it is clear that all the GGA methods provide geometric parameters with comparable accuracies, the error ranging between 0.012 and 0.014 Å. In contrast, a variety of results are obtained for the atomization energies, the BLYP protocol being the less accurate (9.6 kcal/mol) and the mPWPW the most accurate (6.7 kcal/mol) one. In particular, it is remarkable that protocols including exchange functionals with the correct asymptotic behaviour (i.e. LG and mPW) provide thermochemical parameters with a greater precision than those obtained by more conventional exchange functionals (i.e. B and PW).

As concerns the correlation part, the PW functional seems to outperform the LYP functional, the results obtained at the BPW level being better than those provided by the BLYP protocol. The inclusion of some HF exchange induces a significant improvement of the performances. In particular, the mPW3PW protocol performs at least as well as the B3LYP version and should be preferred in view of its

improved asymptotic behaviour. In the same vein, a comparison between B1LYP and mPW1PW approaches shows that both models give results close to those provided by 3-parameter ACM methods, thus offering a significant improvement over the underlying GGA functionals (BLYP and mPWPW) without adding any additional parameter. Furthermore, all the ACM methods approach the accuracy of the most refined post-HF methods, such as CCSD[T]. Note, however, that the comparisons offered in table V are quite unfair for some post-HF methods, which would require larger basis sets to give converged results.

Table V. Mean absolute deviations obtained by different methods for some properties of 32 molecules of the G2 data set. Bond lengths, bond angles and harmonic frequencies are computed using the 6-311G(d,p) basis, set while atomization energies and dipole moments are evaluated by the 6-311++G(3df,3pd) extended basis set.

Method	Bond lengths (Å)	D ₀ (kcal/mol)	Dipole moments (D)	Harm. freq. (cm ⁻¹)
<i>HF and post-HF</i>				
HF	0.022	82.0	0.29	144
MP2	0.014	23.7	0.28	99
CCSD[T]	0.005	11.5	0.10	31
<i>local and GGA</i>				
LSD	0.017	43.5	0.25	75
BPW	0.014	6.0	0.11	69
BLYP	0.014	9.6	0.10	59
LGLYP	0.013	7.2	0.10	60
PWPW	0.012	8.6	0.12	66
mPWPW	0.012	6.7	0.11	65
<i>three-parameter ACM</i>				
B3LYP	0.004	2.4	0.08	31
B3PW	0.008	4.8	0.08	45
mPW3PW	0.008	2.6	0.08	37
<i>parameter-free ACM</i>				
B1LYP	0.005	3.1	0.08	33
B1PW	0.010	5.4	0.10	48
LG1LYP	0.005	4.0	0.10	45
mPW1PW	0.010	3.5	0.10	39

The results reported above give some indications about the performances of the different DF protocols. It must be remarked, anyway, that the geometries and harmonic frequencies of the G2 set of molecules are relatively well described by all the most common quantum mechanical methods. There are, however, well known molecular systems which are much more demanding, some of which are considered in the following.

As a first test, we have selected cis-FONO, which has been recently investigated in detail by several other methods [73]. The results collected in table VI

unambiguously show that the B1LYP protocol outperforms the MP2 method concerning both geometries and harmonic vibrational frequencies. In particular, both the average and maximum error on frequencies are nearly half the corresponding B3LYP values. Furthermore, contrary to HF and post-HF computations, at the B1LYP level even the relatively modest 6-311+G(d,p) basis set provides satisfactory results, thus significantly enlarging the dimensions of difficult systems amenable to quantitative studies.

Table VI. Geometrical parameters(Å and degrees) and harmonic frequencies (cm^{-1}) computed for cis FONO by different methods, using the TZ2Pf basis set.

	CCSD[T]	MP2	LSD	BLYP	B3LYP	B1LYP	B1LYP ^a
F-O	1.433	1.414	1.704	1.779	1.441	1.428	1.438
O-N	1.445	1.488	1.182	1.205	1.397	1.421	1.424
N-O	1.116	1.155	1.168	1.187	1.158	1.153	1.155
FON	110.4	108.4	114.6	177.0	113.2	112.4	112.8
ONO	115.8	114.6	137.4	137.4	118.1	117.1	117.2
$\omega_1(\text{a}')$	1747	1744	1871	1695	1756	1803	1816
$\omega_2(\text{a}')$	933	977	1284	1170	925	954	932
$\omega_3(\text{a}')$	787	799	578	704	802	823	804
$\omega_4(\text{a}')$	441	329	500	455	341	394	359
$\omega_5(\text{a}')$	277	267	185	171	174	263	247
$\omega_6(\text{a}'')$	381	366	741	536	449	407	405
avg.abs. err.		33	199	107	51	33	37
Max error		112	360	237	103	56	82

The structures and the hyperfine splittings (hfs) of organic free radicals provide another severe challenge to theoretical chemistry, since they are related to subtle details of the ground state electronic wave function. Here we analyze the dihydronitrosyl radical for which both experimental and refined theoretical results are available in the literature [56-59]. The most relevant physico-chemical observables obtained by different methods for H_2NO are shown in table VII. From these data, it is quite apparent that the B1LYP approach provides results very close to the B3LYP one, concerning both geometric and magnetic parameters. Taking the UQCISD[T] results as a reference rather than experimental values (which involve significant vibrational averaging), both the B1LYP and B3LYP models provide reliable results. The only departure from the reference values concerns a slight underestimation of the isotropic hfs of nitrogen, for which the B1LYP approach offers even some improvement over the B3LYP method (8.3 vs. 7.6 G). As has been already reported in literature, the PW correlation functional provides quite poor isotropic hfs for non-hydrogen atoms and the situation is only slightly improved by adding some HF exchange.

Table VII. Geometrical parameters (Å and degrees) and isotropic hyperfine splittings (hfs, G) for H₂NO, computed by different methods.

Parameter	QCISD[T] a	BLYP	BPW	B3PW	B3LYP	B1LYP	exp
d(NO)	1.278	1.294	1.282	1.296	1.277	1.276	1.280
d(NH)	1.016	1.024	1.023	1.014	1.015	1.013	1.010
HNH	119.0	118.5	118.2	119.0	119.0	119.0	122.7
τ^b	16.9	16.6	16.4	16.0	16.6	16.7	
hfs (¹⁴ N)	10.1	6.5	5.3	6.0	7.6	8.3	9.7
hfs (H)	-11.0	-9.5	-9.6	-12.0	-10.9	-11.2	-10.5

a) TZ2P basis set; b) out-of-plane angle.

3.2 Non covalent interactions

Van der Waals complexes, such as the dimers of rare-gas atoms, are very difficult to handle in the framework of DF methods. In particular, standard methods, including some ACM approaches, significantly underestimate the stabilities of these complexes. The structural and energetic characteristics of the energy minima of He and Ne dimers, computed by a number of DF methods, are collected in table VIII.

Table VIII Bond lengths and dissociation energies for He₂ and Ne₂. All values are computed using the 6-311++G(3df,3pd) basis set.

Dimer	method	d (Å)	D _e (eV)
He ₂	BPW, BLYP, B1LYP, B3LYP		unbound
	PWPW	2.61	0.010
	mPWPW	3.06	0.003
	mPW1PW	3.07	0.002
	exact	2.97	0.001
Ne ₂	BPW, BLYP, B1LYP, B3LYP		unbound
	PWPW	2.85	0.020
	mPWPW	3.20	0.008
	mPW1PW	3.18	0.007
	exact	3.09	0.004

Two limiting situations are evidenced by these data. From the one hand, all the protocols using the B exchange functional predict a vanishing interaction between He atoms, while, from the other hand, a strong interaction is found at the PWPW level. Between these two extremes, the mPWPW conventional DF approach gives much improved results and an even better agreement with the exact values is obtained at the mPW1PW level.

The results are better evidenced in the graphs of figure 2, which represent the potential energy profiles for the He-He interaction, computed by several DF

methods. All the plots are comprised between the BPW repulsive curve and the strong attractive curve of the PWPW functional. In the middle, and close to the exact profile, lie both the mPWPW and the mPW1PW plots.

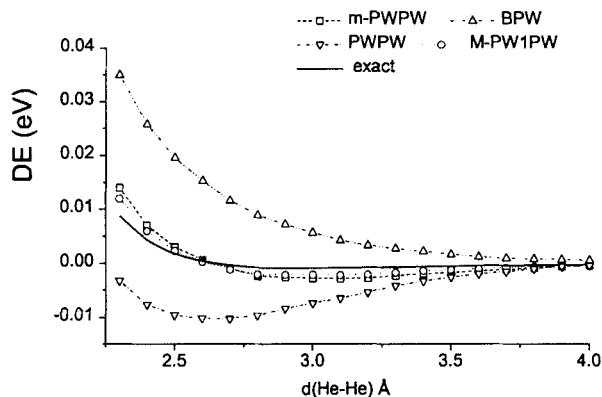


Figure 2. Potential energy curves for the interaction of two He atoms

A similar behaviour is obtained for the Ne dimer, where a variety of situations is predicted by standard pure DF approaches, while a good agreement with the "exact" data is found for all the models which include the mPW functional (see table VIII).

An even more stringent test is represented by CT complexes, and in particular those arising from a π - σ type interaction, such as that of ethylene with a halogen molecule. These systems are very difficult to describe either at the post-HF and DF levels. Among the well characterized CT systems, we have focussed our attention on the simple ethylene-chlorine complex. Furthermore, even if several possible molecular arrangements are possible, the axial-perpendicular structure is the most stable one. So we have limited our attention only to this molecular arrangement, whose main molecular parameters are reported in table IX.

The most striking features in the calculations with the different methods are the chlorine-ethylene distances, which are directly related to the interaction strengths. In this connection, all the GGA methods provide very short intermolecular distances, even if the LGLYP result can be considered a significant improvement over the other GGA values.

Table IX Some relevant geometrical parameters (Å), harmonic stretching Cl-Cl frequencies (cm^{-1}) and complexation energies (kcal/mol) for the $\text{Cl}_2\text{-C}_2\text{H}_4$ complex. The energies are computed at the 6-311++G(3df,3pd) level, using 6-311G(d,p) geometries and are corrected for BSSE and ZPE

	MP2	mPWPW	BLYP	LGLYP	mPW1P W	B1LYP	LG1LYP	exp
d(Cl-plane)	3.003	2.627	2.707	2.728	2.834	2.901	2.887	3.128
d(Cl-Cl)	2.044	2.149	2.183	2.203	2.062	2.093	2.104	
$\omega(\text{Cl-Cl})$	506	379	359	362	467	447	460	
ΔE_{comp}	-1.6	-3.2	-2.6	-2.9	-1.4	-1.1	-1.3	-1.7/ -2.7

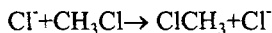
The inclusion of some HF exchange increases the distance up to 2.83 Å for the mPW1PW model. This last value is equal to the B3LYP estimate (2.84 Å), but it is not accurate enough to describe this parameter properly. The best agreement with the reference MP2 value (3.00 Å) is found at the B1LYP level (2.901 Å). In contrast, it must be remarked that all the methods provide geometries for the free molecules (not reported in table IX) which are in good agreement with experimental results.

The trend in the geometrical parameters is reflected in the harmonic frequencies and, in particular, in the stretching of the Cl-Cl bond. In this complex, the intermolecular distance is directly related to the $\sigma\text{-}\pi$ electron donation from chlorine to ethylene, which weakens the Cl-Cl bond. As a consequence an overestimation of this interaction induces a very low Cl-Cl stretching frequency. This is the case for the conventional DF approaches, which predict harmonic wave numbers significantly lower than the experimental estimate. In contrast, a better agreement is found at the mPW1PW level, whose value is close to the MP2 prediction (467 vs. 506 cm^{-1} , respectively).

In the same table are reported the interaction energies, corrected for both zero point energy (ZPE) and basis set superposition error (BSSE) effects [74]. As expected, these energies show a strong correlation with the intermolecular distances. For instance, the BPW model predicts a strong $\text{Cl}_2\text{-C}_2\text{H}_4$ interaction (-3.6 kcal/mol), which is reduced to -1.4 kcal/mol at the mPW1PW level. This last value is only slightly lower than the MP2 estimate (-1.6 kcal/mol) or the experimental findings (between -1.7 and -2.7 kcal/mol).

3.3 Reactivity

As a first test of kinetic predictions we have chosen the $\text{S}_{\text{N}}2$ reaction, whose importance in organic chemistry is well evidenced by the accumulation of a large body of experimental and theoretical data [75-80]. From a theoretical point of view, several studies have shown these reactions to be extremely sensitive to the theoretical model used [77,78]. Already the simple Walden inversion:



is difficult to describe by quantum mechanical methods. This reaction is characterized, in the gas-phase, by a double-well energetic profile, with two minima corresponding to the formation of a pre- and post- reaction ion-molecule complex ($\text{Cl}^- \cdots \text{CH}_3\text{Cl}$) and with a saddle point (SP) of D_{3h} symmetry (ClCH_3Cl^-). The most significant quantities are the complexation energy of the ion-molecule complex (ΔE_{comp}), the activation energy, i.e. the relative energy of the D_{3h} saddle point with respect to the ion-molecule complex (ΔE^\ddagger), and the overall barrier (ΔE_{ovr}), defined as the difference between these two energies. The geometrical parameters of the ion-molecule complex and of the SP are collected in table X.

The key parameter differentiating the various functionals is the distance between the chloride anion and the carbon of the methyl chloride. Once again, the MP2 results can be considered as the reference data, the distance being 3.270 Å and 2.317 Å for the ionic-complex and for the SP, respectively. All the GGA models lead to a too short distance for the ion-molecule complex and a too long bond length for the Cl-Cl bond in the SP. The inclusion of some HF exchange significantly improves the performances, even if the computed values are still far from the MP2 results.

Table X. Main geometrical parameters of the ion-complex $\text{Cl}^- \cdots \text{CH}_3\text{Cl}$ and of the corresponding saddle point for the Walden inversion. All values are computed at the 6-311+G(d,p) level.

Parameter	MP2	BPW	mPWPW	LGLYP	mPW1PW	LG1LYP	B1LYP
ion-complex							
d(C...Cl)	3.270	3.133	3.108	3.113	3.157	3.168	3.189
d(CCl)	1.810	1.870	1.870	1.922	1.828	1.862	1.857
d(CH)	1.085	1.090	1.089	1.088	1.083	1.082	1.081
a(ClCH)	108.8	107.9	107.9	106.9	108.5	107.8	107.9
saddle point							
d(CCl)	2.317	2.366	2.362	2.444	2.328	2.395	2.373
d(CH)	1.073	1.079	1.079	1.078	1.072	1.071	1.071

These geometrical trends are reflected in the computed energetical parameters (see table XI). In particular, an increasing of the Cl-C distance induces a significant stabilization of the SP structure with respect to the minimum. The effect may be so relevant to induce a negative value for ΔE_{ovr} . This is true for all the conventional DF methods considered in the present paper, as well as all the ACMS which embody the LYP correlation functional. In particular, the B1LYP method predicts an overall barrier of -0.8 kcal/mol. In contrast, the mPW1PW approach predicts a positive, albeit small, value for ΔE_{ovr} , thus restoring the right trend.

Table XI. Complexation energy of the ion-molecules complex (ΔE_{comp}), activation energy (ΔE^\ddagger), and overall activation energy relative to reactants (ΔE_{ov}) for the Walen inversion. All the values are in kcal/mol.

	G2+(MP2)	BPW	mPWPW	LGLYP	mPW1PW	LG1LYP	B1LYP	exp
ΔE_{comp}	10.6	9.4	10.5	11.6	10.0	10.7	9.8	12.2 ± 2.0
ΔE^\ddagger	13.0	6.4	6.3	10.6	10.4	8.9	8.9	13.3 ± 2.0
ΔE_{ov}	2.6	-3.0	-4.2	-1.0	0.4	-1.8	-0.9	1.0 \pm 1.0

As concerns the other energetical quantities, we found that complexation energies are relatively well reproduced by all the DF methods. A greater sensitivity to the functional used in computations is found, instead, for ΔE^\ddagger , whose estimates range between 6.3 (mPWPW) and 10.6 (LGLYP) kcal/mol.

Table XII. Energy barriers (Ea), activation energies at 0 K (Ea(0)) and reaction energies (Er) for addition to trans-butadiene according to different methods using the SVP basis set. B3LYP geometries have been used in all the computations and all data are expressed in kcal/mol.

dienophile	parameter	HF	MP2	CAS(6,6)	QCISD(T)	G2M	B3LYP
C ₂ H ₄	Ea	45.0	17.9	43.8	25.0	20.8	22.4
	Ea(0)	47.5	19.4	46.3	27.5	23.3	24.9
	Er	-42.8	-52.5		-46.5	-41.3	-43.1
H ₂ CO	Ea	45.9	20.8	50.0	26.5	23.3	21.7
	Ea(0)	48.9	23.8	53.0	29.5	26.3	24.7
	Er	-26.0	-31.6		-28.3	-24.7	-27.4
H ₂ CS	Ea	26.4	4.5	26.4	11.1	4.8	6.7
	Ea(0)	28.8	6.9	28.8	13.5	7.2	9.1
	Er	-40.6	-48.1		-42.4	-39.1	-40.2

The mechanism of the Diels-Alder (DA) reaction has attracted interest and stimulated debate since its discovery [81]. Both experimental data and quantum-mechanical calculations indicate that the reaction occurs through a concerted mechanism, although, in some cases, stepwise mechanisms involving diradical intermediates are only slightly less favourable [82,83]. In particular, for the reaction between ethylene and butadiene thermochemical estimates indicate that the activation energy for the formation of the biradical intermediate is only slightly higher (by 2.7 kcal/mol) than the barrier governing the concerted mechanism [82,84]. While the QCISD(T) approach reproduces quantitatively this trend, the CAS method overstabilizes biradical species leading to a preference for

the stepwise mechanism [85]. Since the effect of dynamical correlation (not taken into account in the CAS model) should be even larger for the addition of H_2CO and H_2CS due to the presence of lone pairs, we will take QCISD(T) results as our references. Then UQCISD(T)/SVP results indicate that the stepwise mechanism is even less likely for H_2CO and H_2CS than for C_2H_4 . As a consequence we have concentrated our attention on the concerted mechanism. The experimental activation energy for addition of ethylene to trans-butadiene is 27.5 kcal/mol , which gives an estimated value at 0K of $25.1 \pm 2 \text{ kcal/mol}$. Adding the zero point correction to bare energy barriers, only QCISD[T], G2 and B3LYP results fall within the error bar of the experimental estimate (see table XII).

The energy barriers and reaction energies for the three prototypical DA reactions are compared in table XII. The most striking aspect of this table is the non negligible effect of basis set extension in post-HF methods and the remarkable agreement between G2 and B3LYP approaches. On the other hand, the HF and MP2 methods are not sufficiently reliable, whereas MP4 results are quite close to QCISD[T] ones. This would allow to avoid the lengthy iterative computations involved in all the variants of the coupled cluster approach, but the huge basis set needed to obtain G2-like results is prohibitive for larger systems.

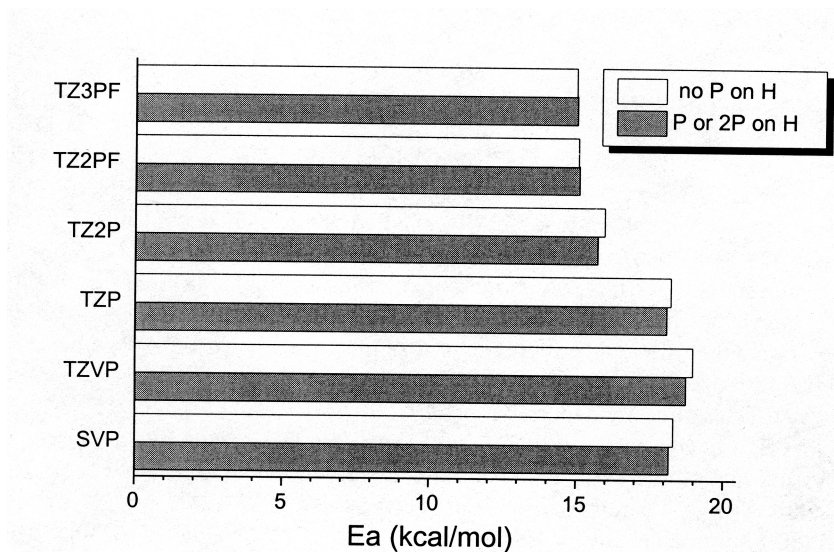


Figure 5. Effect of the basis set on the MP2 activation energy of the DA reaction between ethylene and butadiene.

A better analysis of basis set saturation can be performed by a progressive refinement of the starting SVP basis set. The results obtained for the energy barrier governing addition of H_2CO are shown in figure 5. Very similar trends have been found for addition of C_2H_4 and H_2CS . It is quite apparent that polarization functions on hydrogen atoms are playing a negligible role, whereas the balanced description of π bonds in different stages of formation requires a triple- ζ valence space coupled to double sets of polarization functions on non-hydrogen atoms. The role of f functions, although not completely negligible, is comparatively less important, whereas addition of a third set of polarization functions is essentially useless.

In summary, the smallest basis set suggested for quantitative studies of DA reactions by post-HF methods is of TZ2P quality, possibly with a single set of polarization functions on hydrogen atom. However, coupling these basis set requirements with the need of a refined treatment of correlation (at least MP4) produces a computational model which becomes prohibitive for all, but the smallest prototypical reactions.

The situation is even worse considering that comparison between concerted and stepwise mechanisms requires the use of the even more expensive coupled cluster approaches. In such circumstances we think that a much more viable route is offered by the B3LYP/SVP model, which provides quite reliable results for all the aspects considered in this paragraph [85].

3.5 Molecular properties: NMR chemical shifts

A number of approaches have been proposed for the computation of NMR properties in the framework of DF approaches [86-91]. Here we will make explicit reference to the GIAO model, which appears particularly effective [92,93]. It has been recently pointed out that the MP2 method predicts chemical shifts which are closer to experiment than those obtained using DF approaches, including the B3LYP model [93]. It is so natural to include, as a stringent test, the computation of chemical shieldings. In particular, we have selected some examples in order to investigate the different possible hybridizations of carbon atoms. We have next added the ozone molecule, which is a particularly difficult test for NMR properties [90,92]. The results are collected in table XIII.

Let us first analyze the results for ^{13}C . From the data reported in the table, it is apparent that all the computational methods provide reliable results for chemical shieldings of sp^3 carbons. For instance the mPW1PW value for the methylic carbon of formaldehyde is 154 ppm, whereas the MP2 value is 163 ppm, both values being close to the experimental finding (153 ppm). In going to sp^2 carbon atoms, like the carboxylic one in the same molecule, a dramatic change is observed. In particular both MP2 and B3LYP methods fail in predicting the shielding constants, the computed values being 1 and -27 ppm, respectively. In

contrast, the mPW1PW approach gives results close to the experimental value. Finally, the chemical shifts of the sp carbon, in CH_2CO , is well reproduced by the mPW1PW model (-10 ppm), which gives values close to MP2 (-11 ppm) and to experiment (-8 ppm). In contrast a dramatic difference is observed for the B3LYP value (-38 ppm).

It must be noted that for chemical shifts of first-row nuclei, and carbon in particular, the inclusion of HF exchange has a small effect. For instance GIAO-BLYP and GIAO-B3LYP chemical shifts have been shown to differ by few ppm [91,93]. So the differences found in the present study can be attributed to the improved asymptotic properties of the underlying GGA functional.

Table XIII. Absolute isotropic NMR shieldings (ppm) computed by the 6-311+G(2d,2p) basis set at 6-31G(d) geometries.

molecule	atom	HF	MP2	B3LYP	mPW1PW	exp.
O_3	O central	-2767	2875	-10110	-1046	-724
	O terminal	-2861	1248	-1426	-1459	-1290
CH_3CHO	C(CH_3)	162	163	148	154	153
	C(CHO)	-15	1	-27	-14	-14
CH_2CO	C(CH_2)	177	190	174	189	188
	C(CO)	-38	-11	-38	-10	-8
$\text{CH}_3\text{CH}_2\text{OH}$	C(CH_3)	174	178	164	170	170
	C(CH_2)	136	134	118	127	132

A more demanding test is represented by ozone, since correlation effects play a huge role both on the structure and on the NMR properties of this molecule. The results obtained by the mPW1PW model are compared in table XIII to those obtained by HF and MP2 methods [141]. The most striking feature of these data is the poor performance of the MP2 approach in predicting the shielding constants of both oxygens, concerning absolute values and even signs. In contrast, all the ACM methods, including the mPW1PW one, give the right trend, even if the absolute values are significantly underestimated with respect to the experimental data. It must be emphasized, anyway, that quantitative accuracy cannot be expected from single-determinant calculations in this situation, where the use of multiconfigurational approaches is mandatory [92]. Furthermore, the role played in this case by the neglected current dependency of the exchange correlation functional [86] could be particularly significant.

3.6 Electronic excitation energies

Time-dependent DF theory (TD-DF) provides a formally rigorous extension of Hohenberg-Kohn-Sham DF theory, which is time independent, to the situation where a system, initially in its ground stationary state, is subject to a time-dependent perturbation modifying its external potential, v [95]. A stationary action principle may be derived, analogous to the minimum energy principle of Hohenberg-Kohn theory, and this can be used to derive the time-dependent KS equations [95]. Since the dynamic polarizability describes the response of the dipole moment to a time-dependent electric field, it may be calculated from the response of the charge density obtained from TD-DF. This allows the determination of the electronic excitation spectrum in the usual dipole approximation, because the poles of the dynamic polarizability determine the excitation energies [96]. Here we adopt the implementation of the TD-DF model introduced by Scuseria and co-workers [97] using, on the basis of previous studies [97,98], the 6-31+G(d) basis set of Foresman *et al.* [99].

There is a growing interest in the application of TD-DF to the calculation of adiabatic excitation energies [96-98,100,101]. The results obtained for low excitation energies are usually superior to the those obtained by HF-based methods, like the Random Phase Approximation (RPA) [102], or the Configuration Interaction with Single excitations (CIS) [98,100,103]. In addition, given that the time dependent HF (TDHF) scheme can be derived along the same lines as TD-DF, Bauernschmitt and Ahlrichs [98] have also included the ACM model in the calculation of energies, showing that the B3LYP functional represents a further improvement over conventional DF methods. In this connection, it has been suggested that the numerical performances of the different functionals strongly depend on their ability to predict reliable molecular ionization potentials (IP) [96]. This points out that, like in ground-state computations, the domain of applicability of TD-DF rests on the development and validation of suitable functionals. We expect that the mPW1PW functional gives results at least comparable with those provided by other ACM approaches, because it provides comparable IP's, but has an improved long range behavior.

In table XIV are collected our mPW1PW results together with HF-based and experimental data from ref. 98. The chosen molecular set, even if limited, is in our opinion quite representative, since it includes $\pi \rightarrow \pi^*$, $\sigma \rightarrow \pi^*$ and $n \rightarrow \pi^*$ transitions.

The table shows that reliable results are obtained also in this case by the mPW1PW model, which provides data slightly closer to the experiment than their B3LYP counterparts. An even larger improvement is found with respect to RPA and CIS values. It is interesting to note also that the largest deviation is found for C_2H_4 , whose IP is one of the less accurately predicted by the mPW1PW model.

Table XIV. Vertical excitation energies (eV) computed at different theoretical levels using the 6-31+G(d,p) basis set at 6-31G(d) geometries.

molecule	transition	CIS	RPA	TD/B3LYP	TD/mPW1PW	exp.
N ₂	$\sigma_g \rightarrow \pi_g$	10.0	9.8	9.4	9.3	9.3
H ₂ CO	$n \rightarrow \pi^*$	4.6	4.4	4.1	4.1	4.1
C ₂ H ₄	$\pi \rightarrow \pi^*$	7.7	7.8	8.5	8.5	8.0
C ₅ H ₅ N	$\pi \rightarrow \pi^*$	6.1	5.9	5.1	5.2	5.0
	$n \rightarrow \pi^*$	6.8	6.8	5.3	5.4	5.4

4. Conclusion

The present contribution explores the reliability of current density functionals concerning a number of structural, thermodynamic, kinetic and spectroscopic properties. Together with local and gradient corrected functionals, hybrid models including some Hartree-Fock exchange have been also considered.

A very important point is that, contrary to methods based on a Hartree-Fock zero-order wave function, those rooted in the Kohn-Sham approach appear equally reliable for closed- and open-shell systems across the periodic table. Coupling the reliability of the results with the speed of computations and the availability of analytical first and second derivatives paves the route for the characterization of the most significant parts of complex potential energy surfaces retaining the cleanness and ease of interpretation of a single determinant formalism. This is at the heart of more dynamically based models of physico-chemical properties and reactivity.

Very recently the time dependent DF approach has given access also to excited electronic states via a theoretically sound and computationally effective model. Also in this case the first results are very promising and open the doors of the realm of photophysical processes. Finally, coupling of these models with effective treatments of polarizable continua and of translational periodicity starts to allow the study of chemical processes in condensed phases.

Despite these remarkable features, it remains still true that the exact density functional is unknown, and approximations must be introduced. Like in the early days of semiempirical methods, current density functionals are based on some combination of two limiting strategies, namely 1) fitting of some set of experimental data and 2) fulfillment of a number of well known physical constraints. Although most existing functionals combine both approaches, attention is being shifted to the first aspect even at the expense of introducing a

huge number of parameters, of overemphasizing the thermochemistry of organic molecules, and of abandoning even the most fundamental physical constraints (e.g. the free electron gas limit). On the other side, a new ACM method has been recently introduced in which all the parameters (other than those in its local spin density, LSD, component) are fundamental constants. Furthermore, the first numerical tests show that this model is competitive with current highly parametrized functionals. Thus it should allow the analysis of general trends along classes of molecules and, hopefully, the derivation of new thumb rules. This is exactly in the spirit of one of the most constant remarks of professor Del Re, namely that "one should always select the method which gives the *greatest insight* into one's physical or chemical problem, keeping in mind that a qualitative rule covering many data is far better than a very good quantitative result which gives no hint as to general trends".

References

- [1] L.A.Curtiss, K.Raghavachari, G.W.Trucks and J.A.Pople, *J. Chem. Phys.* 94, 7221 (1991).
- [2] J.M.L.Martin, *J.Chem.Phys.* 97,5007 (1992).
- [3] J.A.Montgomery, Jr., J.W.Ochterski and G.A.Peterson, *J.Chem.Phys.* 101,5900 (1994).
- [4] R.Poul-Amerigo, M.Merchan, I.Nebot-Gill, M.Malmqvist and B.O.Roos, *J.Chem.Phys.* 101,4893 (1994).
- [5] M.R.A. Blomberg, P.E.M.Siegbahn and M.Svensson, *J.Phys.Chem.* 98,2062 (1994).
- [6] H.Partridge and C.W.Bauschlicher, *J.Phys.Chem.* 98,2301 (1994).
- [7] T.H.Dunning, Jr. *J.Chem.Phys.* 90,1007 (1989).
- [8] P.O.Widmark, P.A.Malmquist and B.O.Roos, *Theor.Chim.Acta* 77,291 (1990).
- [9] J.Almlöf and P.R.Taylor, *Adv.Quantum Chem.* 22,301 (1991).
- [10] J.A.Pople, J.S.Binkley and R.Seeger, *Int.J.Quantum Chem.* S10,1 (1976).
- [11] R.Krishnan, M.J.Frisch and J.A.Pople, *J.Chem.Phys.* 72,4244 (1980).
- [12] R.G. Parr and W. Yang, "Density Functional Theory of Atoms and Molecules" (Oxford University Press, New York, 1989).
- [13] P.Hohenberg and W.Kohn, *Phys.Rev.B* 136,864 (1964); W.Kohn and L.J.Sham, *Phys.Rev.A* 140,1133 (1965).
- [14] T.Ziegler, *Chem.Rev.* 91,651 (1991).
- [15] J.Andzelm and E.Wimmer, *J.Chem.Phys.* 96,1280 (1992).
- [16] B.G.Johnson, P.M.W.Gill and J.A.Pople, *J.Chem.Phys.* 98,5612 (1993); B.G.Johnson, *J.Chem.Phys.* 101,9202 (1994) (E).
- [17] G.J.Laming, V.Termath and N.C.Handy, *J.Chem.Phys.* 99,8765 (1993).
- [18] N.Oliphant and R.J.Bartlett, *J.Chem.Phys.* 100, 6550 (1994).

- [19] J. Baker, J. Adzelm, A. Scheiner and B. Deley, *J. Chem. Phys.* 101, 8894 (1994).
- [20] A. St-Amant and D. R. Salahub, *Chem. Phys. Lett.* 169, 387 (1990).
- [21] M. J. Frisch, G. W. Trucks, H. B. Schlegel, G. E. Scuseria, M. A. Robb, J. R. Cheeseman, V. G. Zakrzewski, J. A. Montgomery, Jr., R. E. Stratmann, J. C. Burant, S. Dapprich, J. M. Millam, A. D. Daniels, K. N. Kudin, M. C. Strain, O. Farkas, J. Tomasi, V. Barone, M. Cossi, R. Cammi, B. Mennucci, C. Pomelli, C. Adamo, S. Clifford, J. Ochterski, G. A. Petersson, P. Y. Ayala, Q. Cui, K. Morokuma, D. K. Malick, A. D. Rabuck, K. Raghavachari, J. B. Foresman, J. Cioslowski, J. V. Ortiz, B. B. Stefanov, G. Liu, A. Liashenko, P. Piskorz, I. Komaromi, R. Gomperts, R. L. Martin, D. J. Fox, T. Keith, M. A. Al-Laham, C. Y. Peng, A. Nanayakkara, C. Gonzalez, M. Challacombe, P. M. W. Gill, B. Johnson, W. Chen, M. W. Wong, J. L. Andres, C. Gonzalez, M. Head-Gordon, E. S. Replogle, and J. A. Pople, *Gaussian 98 (Revision A.2)*, Gaussian Inc.: Pittsburgh PA, 1998.
- [22] A. D. Becke, *J. Chem. Phys.* 84, 4524 (1986).
- [23] A. D. Becke, *J. Chem. Phys.* 85, 7184 (1986).
- [24] J. P. Perdew and Y. Wang, *Phys. Rev. B* 33, 8800 (1986).
- [25] A. D. Becke, *Phys. Rev. A* 38, 3098 (1988).
- [26] J. P. Perdew, in "Proceeding of the 21st Annual International Symposium on the Electronic Structure of Solids", (Eds. P. Ziesche and H. Eschrig, Akademie Verlag, Berlin 1991)
- [27] D. J. Lacks and R. G. Gordon, *Phys. Rev. A* 47, 4681 (1993).
- [28] P. M. W. Gill and J. A. Pople *Phys. Rev. A* 47, 2383 (1993).
- [29] A. Lembarki, F. Rogemond and H. Chermette, *Phys. Rev. A* 52, 3704 (1995).
- [30] P. M. W. Gill, *Mol. Phys.* 89, 433 (1996).
- [31] R. Neumann, R. H. Nobes and N. C. Handy, *Mol. Phys.* 87, 1 (1996).
- [32] J. P. Perdew, K. Burke and M. Ernzerhof, *Phys. Rev. Lett.* 77, 3865 (1996), *ibid* 78, 1396 (1997) (E).
- [33] T. van Voorhis and G. E. Scuseria, *Mol. Phys.* 92, 601 (1997).
- [34] R. Neumann and N. C. Handy, *Chem. Phys. Lett.* 266, 16 (1997).
- [35] A. D. Becke, *J. Chem. Phys.* 107, 8554 (1997).
- [36] M. Filatov and W. Thiel, *Mol. Phys.* 91, 847 (1997).
- [37] S. Liu and R. G. Parr, *Phys. Rev. A* 55, 1791 (1997).
- [38] R. D. Adamson, P. M. W. Gill and J. A. Pople, *Chem. Phys. Lett.* 284, 6 (1998).
- [39] C. Adamo and V. Barone, *J. Chem. Phys.* 108, 664 (1998).
- [40] N. C. Handy and D. J. Trozer, *J. Chem. Phys.* 108, 2545 (1998).
- [41] H. L. Schmider and A. D. Becke, *J. Chem. Phys.* 108, 9624 (1998).
- [42] T. van Voorhis and G. E. Scuseria, *J. Chem. Phys.* 109, 400 (1998).
- [43] E. I. Proynov and D. R. Salahub, *Phys. Rev. B* 49, 7874 (1994); E. I. Proynov, S. Sirois and D. R. Salahub, *Int. J. Quantum Chem.* 64, 427 (1997).
- [44] P. A. M. Dirac, *Proc. Cambridge Phil. Soc.* 26, 376 (1930).
- [45] S. H. Vosko, L. Wilk and M. Nuisar, *Can. J. Phys.* 58, 1200 (1980).

- [46] J.P. Perdew and Y. Wang, *Phys. Rev. B* 45, 13244 (1992).
- [47] A.D. Becke, *J. Chem. Phys.* 98, 5648 (1993).
- [48] A.D. Becke, *J. Chem. Phys.* 98, 1372 (1993).
- [49] A.D. Becke, *J. Chem. Phys.* 104, 1040 (1996).
- [50] K. Burke, M. Ernzerhof and J.P. Perdew, *Chem. Phys. Lett.* 265, 155 (1997).
- [51] O. Gritsenko, R. van Leeuwen and E.J. Baerends, *Int. J. Quantum Chem.* 30, 163 (1997).
- [52] M. Ernzerhof, *Chem. Phys. Lett.* 263, 499 (1996).
- [53] M. Ernzerhof in "Density Functionals: Theory and Applications", vol.500 of *Lecture Notes in Physics*, (Eds. D.P.Joubert, Springer Verlag, Berlin, 1998).
- [54] J.P. Perdew and M. Ernzerhof, *J. Chem. Phys.* 105, 9982 (1996).
- [55] C. Adamo and V. Barone, *Chem. Phys. Lett.* 274, 242 (1997).
- [56] V. Barone, in "Recent Advances in Density Functional Methods", part I, (Ed. D.P. Chong, World Scientific Press, Singapore 1996), pp.287-334.
- [57] N.Regà, M.Cossi, V.Barone, *J.Chem.Phys.* 105,11060 (1996).
- [58] N.Regà, M.Cossi, V.Barone, *J.Am.Chem.Soc.* 120,5723 (1998).
- [59] C.Adamo, R.Subra, A.di Matteo, V.Barone, *J.Chem.Phys.*, in press.
- [60] A.D.Becke, *J.Chem.Phys.* 88,2547 (1988).
- [61] C.W.Murray, N.C.Handy and J.Laming, *Mol.Phys.* 78, 997 (1993).
- [62] P.M.W.Gill, B.G.Johnson and J.A.Pople, *Chem.Phys.Lett.* 209,506 (1993).
- [63] B.I.Dunlap, J.W.D.Connolly and J.R.Sabin, *J.Chem.Phys.* 71,3396 (1979).
- [64] R.E.Stratmann, J.C.Burant, G.E.Scuseria and M.J.Frisch, *J.Chem.Phys.* 106,10175 (1997).
- [65] Y.C.Zheng and J.E.Almlöf, *Chem.Phys.Lett.* 214,397 (1993).
- [66] J.E.Almlöf and Y.C.Zheng in "Recent Advances in Density Functional Methods" part II (Ed. by D.P. Chong, World Scientific Press, Singapore 1997), pp.15-40.
- [67] M. Levy and J.P. Perdew, *Phys. Rev. A* 32, 2010 (1985).
- [68] M. Levy and J.P. Perdew, *Phys. Rev. B* 48, 11638 (1993).
- [69] E.H. Lieb and S. Oxford, *Int. J Quantum Chem.* 19, 427 (1981).
- [70] E. Wigner, *Phys.Rev.* 40,749 (1932).
- [71] C.Lee, W. Yang and R.G.Parr, *Phys.Rev.B* 37,785 (1988).
- [72] B.G. Johnson, P.M.W. Gill and J.A. Pople, *J. Chem. Phys.* 98, 8765 (1993).
- [73] T.J. Lee, C.W. Baushlicher, C.E. Dateo and J.E. Rice, *Chem. Phys. Lett.* 228, 583 (1994).
- [74] S. F. Boys and F. Bernardi, *Mol. Phys.* 19, 553 (1970).
- [75] S.S. Shaik, H.B. Schlegel and S. Wolfe "Theoretical aspects of physical organic chemistry. The SN_2 mechanism" (Wiley, New York, 1992).
- [76] T.N. Truong and E.V. Stefanovich, *J. Phys. Chem.* 99, 14700 (1995).
- [77] M.N. Glukhovtsev, A. Pross and L. Radom, *J. Am. Chem. Soc.* 117, 2024 (1995).

- [78] M.N. Glukhovtsev, R.D. Bach, A. Pross and L. Radom, *Chem. Phys. Lett.* 260, 558 (1996).
- [79] J.W. Larson and T.B. McMahon, *J. Am. Chem. Soc.* 106, 517 (1984).
- [80] S.E. Barlow, J.M. van Doren and V.M. Bierbaum, *J. Am. Chem. Soc.* 116, 10645 (1994)
- [81] K.N.Houk, J.Gonzalez and Y.Li, *Acc.Chem.Res.* 28,81 (1995).
- [82] W.V.E.Doering, W.R.Roth, R.Breuckman, L.Figge, H.W. Lennartz, W.D. Fessner and H.Prinzbach, *Chem.Ber.* 121,1 (1988) and refs. therein.
- [83] Y.Li and K.N.Houk, *J.Am.Chem.Soc.* 115,7478 (1993).
- [84] H.M.Frey and R.Pottinger, *J.Chem.Soc.Far.Trans.* 7,1827 (1977).
- [85] V.Barone and R.Arnaud, *J.Chem.Phys.* 106, 8727 (1997).
- [86] V.G. Malkin, O.L. Malkina, M.E. Casida and D.R. Salahub, *J. Am. Chem. Soc.* 116, 5898 (1994).
- [87] G. Schreckenbach and T.Ziegler, *J. Chem. Phys.* 99, 606 (1995).
- [88] A.M. Lee, N.C. Handy and S.M. Colwell, *J. Chem. Phys.* 103, 10095 (1995)
- [89] G. Rauhut, S. Puyear, K. Wolinski and P.Pulay, *J. Phys. Chem.* 100, 6130 (1996).
- [90] M. Kaupp, O.L. Malkina and V.G. Malkin, *J. Chem. Phys.* 106, 9201 (1997).
- [91] M. Bühl, *Chem. Phys. Lett.* 267, 251 (1997).
- [92] K. Wolinski, J.F. Hinton and P. Pulay, *J. Am. Chem. Soc.* 112, 8251 (1990).
- [93] J.R. Cheeseman, G.W. Trucks, T.A. Keith and M.J. Frisch, *J. Chem. Phys.* 104, 5497 (1998).
- [94] J. Gauss, J.F. Stanton, *J. Chem. Phys.* 104, 2574 (1996).
- [95] E.K.U. Gross and W. Kohn, *Adv. Quantum Chem.* 21, 255 (1990).
- [96] M.K. Casida, C. Jamorski, K.C. Casida and D.R. Salahub, *J. Chem. Phys.* 108, 4439 (1998).
- [97] R.E. Stratmann, G.E. Scuseria and M.J. Frisch, *J. Chem. Phys.*, in press.
- [98] R. Bauernschmitt and R. Ahlrichs, *Chem. Phys. Lett.* 256, 454 (1996).
- [99] J.B.Foresman, M. Head-Gordon, J.A.Pople and M.J.Frisch, *J. Phys. Chem.* 96, 135 (1992).
- [100] C. Jamorski, M.E. Casida and D.R. Salahub, *J. Chem. Phys.* 104, 5134 (1996).
- [101] M. Petersilka and E.K.U. Gross, *Int. J. Quantum Chem. Symp.* 30, 181 (1996).
- [102] T.H. Dunning and V. McKoy, *J. Chem. Phys.* 47, 1735 (1967).
- [103] J.B. Foresman, H. Head-Gordon, J.A. Pople and M.J. Frisch, *J. Phys. Chem.* 96, 135 (1992).

Exchange-Energy Density Functionals as Linear Combinations of Homogeneous Functionals of Density

Shubin Liu ^{a,b}, Frank De Proft ^c, Agnes Nagy ^d, and Robert G. Parr ^a

^a Department of Chemistry, and ^b Department of Biochemistry and Biophysics,
University of North Carolina, Chapel Hill, North Carolina 27599-3290

^c Eenheid Algemene Chemie, Vrije Universiteit Brussel, Faculteit Wetenschappen,
Pleinlaan 2, 1050 Brussels, Belgium

^d Institute of Theoretical Physics, Kossuth Lajos University
H-4010 Debrecen, Hungary

Abstract

In a recent publication [R.G. Parr and S. Liu, *Chem. Phys. Lett.* **267**, 164(1997)], it has been argued that the total electron-electron repulsion energy density functional $V_{ee}[\rho]$ can be expressed as a sum of functionals homogeneous of degrees one and two, with respect to density scaling. In this paper, starting from the Levy-Perdew virial relation, we demonstrate that one of the components of $V_{ee}[\rho]$, the exchange energy density functional $E_x[\rho]$, can be expressed reasonably well in this way in a simple form. Namely, $E_x[\rho]$ can be expressed as a linear combination of the classical electron-electron repulsion $J[\rho]$ and the various electrostatic potentials at nuclei due to the electrons. Numerical tests are made for atoms, ions, and a few molecules. Good agreement between the accurate and the estimated exchange energies is observed.

Table of Contents

- I. Introduction
- II. Theory: Exchange-Energy Density Functional
- III. Computational Methods
- IV. Results and Discussion
- V. Summary

I. Introduction

Density functional theory (DFT) [1,2] provides a convenient approach for investigating electronic structures of atoms, molecules, and solids. It is theoretically simple, conceptually meaningful, and computationally effective. Much effort has been devoted to its development in recent decades [3,4]. According to the Hohenberg-Kohn theorems [5], every atomic or molecular ground-state property is a functional of the electron density. Working with the density ρ instead of the wave function Ψ , DFT is capable of much reducing calculation because ρ is a function of only three spatial variables while Ψ is a function of $4N$ variables, with N the number of electrons. In the Kohn-Sham DFT scheme [6], in which the concept of orbital is still retained, the results of DFT are in principle exact, even though calculations employ a single Slater determinant wave function, just as in Hartree-Fock theory.

The central problem in DFT is to find the exact, or at least good approximate functional form for the universal energy density functional $F[\rho]$, which is the sum of the kinetic energy functional $T_s[\rho]$, the nuclear-electron attraction $V_{ne}[\rho]$, the classical Coulomb inter-electron repulsion $J[\rho]$, and the exchange-correlation energy functional $E_{xc}[\rho]$. In the Kohn-Sham scheme, only $E_{xc}[\rho]$ is unknown. The oldest model is the local density approximation (LDA) proposed by Thomas [7], Fermi [8], and Dirac [9] long ago, in which $T_s[\rho]$ and $E_x[\rho]$ are homogeneous functionals of degree $5/3$ and $4/3$ in $\rho(\mathbf{r})$, respectively. LDA is exact for the homogeneous electron gas. It has been recently proved [10] that in the LDA approximation for inhomogeneous systems these same homogeneities of $T_s[\rho]$ and $E_x[\rho]$ hold.

LDA, however, is too crude an approximation to be quantitatively useful for atoms and molecules. A relative energy error of around 15% is typical. An immediate improvement for $F[\rho]$ is to include contributions from the density gradient, giving the gradient expansion approximation (GEA) and the generalized gradient approximation (GGA) [11,12]. These approximations are exact when the density gradient $|\nabla\rho(\mathbf{r})|$ is everywhere very small, i.e., the density of the system is slowly varying. Good results from these approaches are found, especially in energetics, geometry prediction, rotation-vibrational spectroscopy, etc. A relative error of less than 5% is routinely obtained.

On the other hand, energy functionals based on the GEA/GGA and their Padé approximations are much less satisfactory in determining functional derivatives [13] as well as in some other applications, such as in describing London dispersion forces [14], spin resonance phenomena [15], transition states of chemical reactions [16, 17], and structures of some molecules [18, 19]. The main failures of these functionals are three: (i) failure to give the correct asymptotic behavior [13,20] of their functional derivatives; (ii) failure to reproduce the behavior of the potential near the nuclear cusp; and (iii) failure to treat the regions where a large gradient of density is present [21]. In atoms and molecules, gradients are not everywhere small.

In our own recent efforts to develop new theoretical means to approximate the universal functional $F[\rho]$, the functional expansion viewpoint has been featured [10,22-33]. For a finite electronic system, it has been shown that for any well-behaved functional

$Q[\rho]$ there exists an infinite functional expansion in terms of functional derivatives [20,24]:

$$\begin{aligned}
 Q[\rho] = & C + \int \rho(\mathbf{r}) \frac{\delta Q[\rho]}{\delta \rho(\mathbf{r})} d^3r \\
 & - \frac{1}{2} \iint \rho(\mathbf{r}_1) \rho(\mathbf{r}_2) \frac{\delta^2 Q[\rho]}{\delta \rho(\mathbf{r}_1) \delta \rho(\mathbf{r}_2)} d^3r_1 d^3r_2 \\
 & + \frac{1}{3!} \iiint \rho(\mathbf{r}_1) \rho(\mathbf{r}_2) \rho(\mathbf{r}_3) \frac{\delta^3 Q[\rho]}{\delta \rho(\mathbf{r}_1) \delta \rho(\mathbf{r}_2) \delta \rho(\mathbf{r}_3)} d^3r_1 d^3r_2 d^3r_3 \\
 & \dots,
 \end{aligned} \tag{1}$$

This functional expansion series can be reexpressed [24] as the sum of functionals homogeneous of degree 0, 1, 2, ..., respectively, with respect to the density scaling [22]:

$$Q[\rho] = \sum_{j=0}^{\infty} H_j[\rho], \tag{2}$$

where $H_j[\rho]$ is a density-homogeneous functional of degree j , that is [22,24],

$$\int \rho(\mathbf{r}) \frac{\delta H_j[\rho]}{\delta \rho(\mathbf{r})} d\mathbf{r} = j H_j[\rho] \tag{3}$$

Applications have been carried out for the correlation energy density functional $E_c[\rho]$ [22,28,31,32], the kinetic and exchange energy functionals [24], the kinetic component of the correlation energy [32,33], the current-density functional theory [29], the second-order density matrix [30], and the total energy of atoms and molecules [23].

Very recently, it has been argued that for some special energy density functionals, such as the electron-electron repulsion $V_{ee}[\rho]$ [25], the kinetic energy density functional $T_s[\rho]$ [26], and thus the universal functional $F[\rho]$ [27], the functional expansion series may take a simplified form. For example, for $V_{ee}[\rho]$, the series truncates at the second order, and for $T_s[\rho]$, the series truncates at the first order. This suggests that the electron-electron repulsion can be expressed as the sum of functionals homogeneous of degree 1 and 2, respectively, with respect to the density scaling [25], and the kinetic energy density functional can be taken to be homogeneous of degree 1 in density [26]. In the present paper, starting from the Levy-Perdew virial relation [34], we construct an approximation along this line for the exchange energy density functional $E_x[\rho]$. Applications are made for atoms, ions, and simple molecules. Atomic units are used throughout.

II. Theory: Exchange-Energy Density Functional

For any well-behaved density functional $Q[\rho]$ whose homogeneity in coordinate scaling is degree k , one has the identity [35]:

$$Q[\rho] = -\frac{1}{k} \int \rho(\mathbf{r}) \mathbf{r} \cdot \nabla \frac{\delta Q[\rho]}{\delta \rho(\mathbf{r})}(\mathbf{r}) d\mathbf{r}. \quad (4)$$

The exchange functional $E_x[\rho]$ is well known to be homogeneous of degree one in coordinate scaling [1,2], that is, the Levy-Perdew relation [34],

$$E_x[\rho] = - \int \rho(\mathbf{r}) \mathbf{r} \cdot \nabla v_x(\mathbf{r}) d\mathbf{r}, \quad (5)$$

where $v_x(\mathbf{r})$, defined as

$$v_x(\mathbf{r}) = \frac{\delta E_x[\rho]}{\delta \rho(\mathbf{r})}, \quad (6)$$

is the exchange potential.

Now, taking functional derivative of the two sides of Eq. (5) with respect to the density, one obtains

$$v_x(\mathbf{r}) = -\mathbf{r} \cdot \nabla v_x(\mathbf{r}) - \int \rho(\mathbf{r}') \mathbf{r}' \cdot \nabla \frac{\delta v_x(\mathbf{r}')}{\delta \rho(\mathbf{r})} d\mathbf{r}'. \quad (7)$$

If the second-order functional derivative term is neglected, Eq. (7) becomes

$$v_x(\mathbf{r}) = -\mathbf{r} \cdot \nabla v_x(\mathbf{r}), \quad (8)$$

whose simplest solution is

$$v_x(\mathbf{r}) = \frac{c_1}{r}, \quad (9)$$

where c_1 is a constant to be determined. Hence, the approximate exchange energy density functional up to the first order takes the following form

$$E_x^1[\rho] = c_1 \int \frac{\rho(\mathbf{r})}{r} d\mathbf{r}. \quad (10)$$

Equation (10), however, does not satisfy the translation invariance condition, proposed by Leeuwen and Baerends [36],

$$\int \rho(\mathbf{r}) \mathbf{R} \cdot \nabla v_x(\mathbf{r}) d\mathbf{r} = 0, \quad (11)$$

where \mathbf{R} is an arbitrary translation vector. Combining Eq. (11) with Eq. (5), one has

$$E_x[\rho] = - \int \rho(\mathbf{r}) (\mathbf{r} - \mathbf{R}) \cdot \nabla v_x(\mathbf{r}) d\mathbf{r}. \quad (12)$$

Repeating the procedure from Eqs. (7) to (10), one obtains the following formula for the exchange energy density functional to the first order,

$$E_x^1[\rho] = c_1 \int \frac{\rho(\mathbf{r})}{|\mathbf{r} - \mathbf{R}|} d\mathbf{r}. \quad (13)$$

For atomic systems, with the obvious choice $\mathbf{R} = \mathbf{0}$, Eq. (13) reduces to Eq. (10). For molecular systems, it is convenient to choose \mathbf{R} as the coordinates for some nucleus.

Taking the functional derivative with respect to the density again in Eq. (7), and neglecting the third-order term, one gets

$$v'_x(\mathbf{r}, \mathbf{r}') = -\mathbf{r} \cdot \nabla_{\mathbf{r}'} v'_x(\mathbf{r}, \mathbf{r}') - \mathbf{r}' \cdot \nabla_{\mathbf{r}} v'_x(\mathbf{r}, \mathbf{r}'), \quad (14)$$

where

$$v'_x(\mathbf{r}, \mathbf{r}') = \frac{\delta^2 E_x[\rho]}{\delta \rho(\mathbf{r}) \delta \rho(\mathbf{r}')} = \frac{\delta v_x(\mathbf{r})}{\delta \rho(\mathbf{r}')}. \quad (15)$$

One simple solution of Eq. (14) is

$$v'_x(\mathbf{r}, \mathbf{r}') = \frac{c_2}{|\mathbf{r} - \mathbf{r}'|}, \quad (16)$$

where c_2 is another constant to be determined, giving

$$E_x^2[\rho] = c_2 \iint \frac{\rho(\mathbf{r})\rho(\mathbf{r}')}{|\mathbf{r} - \mathbf{r}'|} d\mathbf{r} d\mathbf{r}'. \quad (17)$$

Therefore,

$$E_x[\rho] = E_x^1 + E_x^2 + \dots = \sum_i c_i \int \frac{\rho(\mathbf{r})}{|\mathbf{r} - \mathbf{R}_i|} d\mathbf{r} + c_2 \iint \frac{\rho(\mathbf{r})\rho(\mathbf{r}')}{|\mathbf{r} - \mathbf{r}'|} d\mathbf{r} d\mathbf{r}' + \dots. \quad (18)$$

Notice that in Eq. (18), the first term at the right-hand side is a linear combination of the electrostatic potentials due to the electrons at the various nuclei \mathbf{R}_i . These quantities have been of interest in many theoretical works that estimate the total energy and binding energy [37,38], etc. For atoms, the first term is just $-V_{ne}/Z$, where V_{ne} is the nuclear-electron attraction energy and Z is the nuclear charge. The second term in Eq. (18) is just the classical electron-electron Coulomb repulsion energy. One then can rewrite Eq. (18) for atoms as

$$E_x[\rho] = E_x^1 + E_x^2 + \dots = -c_1 \frac{V_{ne}}{Z} + 2c_2 J + \dots. \quad (19)$$

From the density scaling point of view, the first term in Eq. (18) is homogeneous of degree one, and the second term is homogeneous of degree two. This formula is consistent with our general description that any well-behaved functional can be expanded in terms of functionals homogeneous of degree 1, 2, ... [24]. In addition, if one takes just the first two terms in Eq. (18) we see that $E_x[\rho]$ thereby has been expressed as the sum of functionals homogeneous of degrees one and two.

From the theoretical point of view, Eq. (18) belongs to the regime of the weighted-density approximation (WDA) [39,40], in which an energy density is expressed as a function of \mathbf{r} and $\rho(\mathbf{r})$, i.e.,

$$E_x[\rho] = \int e_x(\mathbf{r}, \rho(\mathbf{r})) d\mathbf{r}. \quad (20)$$

The approximations most often employed in atomic and molecular studies are the local density approximation (LDA), in which the energy density is a function of the density only, and its extension, the gradient expansion approximation and/or generalized gradient approximation (GEA/GGA), where besides the local density, the nonlocal density gradient is included in the energy density function formulation; that is,

$$E_x[\rho] = \int e_x(\rho(\mathbf{r}), |\nabla\rho(\mathbf{r})|) d\mathbf{r}. \quad (21)$$

Elsewhere [41], two of the present authors, have shown that even for the simplest hydrogen-like systems, a proper description for both the energy functional and its potential must go beyond WDA and GEA/GGA frameworks. The approximation needed takes the form

$$E_x[\rho] = \int e_x(\mathbf{r}, \rho(\mathbf{r}), |\nabla\rho(\mathbf{r})|) d\mathbf{r}. \quad (22)$$

We thus anticipate that because of the rather different form Eq. (18) takes, its capability to reproduce accurate exchange energy results for many-electron atoms and molecules may be limited. Also, the exchange potential stemming from Eq. (18) is divergent at a nuclear cusp, and it does not in general decay as $-\frac{1}{r}$ when r is very large. These flaws, however, do not detract from its interest as an example of constructing new approximate functionals from homogeneous functionals.

III. Computational Methods

Neutral, positive, and negative atomic systems from H to Xe, and the Be iso-electronic series from B^+ to Cr^{+20} and Ne series ions from Ne^{+1} to Ne^{+9} are investigated. A few first-row monohydrides from LiH to HF are examined as an example of the application to molecules. The restricted Hartree-Fock wavefunctions of Koga et al. [42] have been used for atomic systems. For molecules, calculations are performed at the B3PW91/6-311++G(3d, 2p) level.

Neutral atom results are used as data sets for least-square fits to determine the two constants c_1 and c_2 . Since it is expected that Eq. (18) is not generally applicable because of its simple form, we fit the constants for every period. After the constants are determined, predictions are made for cations and anions, as well as other ionic series, the Be iso-electron series and the Ne ion series. For the molecules studied, the sum of the electrostatic potentials at the two nuclei is used, and a separate least-square fit is made.

IV. Results and Discussion

Table 1 shows the exact and fitted exchange values for neutral atoms up to $Z=54$. The fitted constants for each period are listed in the bottom of the table. From the table, one finds that except for the hydrogen atom, the overall relative deviation is around 1-2% for the first row, with the error becoming smaller for later rows. For example, for the fourth period, $Z = 37 \sim 54$, the average error is 0.06%. The relative magnitude of E_x^1 and E_x^2 for large atomic number atoms vary little as Z varies. For $Z = 10, 18, 36$, and 54 , for example, E_x^1 is 72, 74, 69, and 70% of the total. For $Z = 2$, E_x^1 is 92% of the total.

The large error found in the hydrogen atom case presumably results from the discrepancy between Eq. (18) and the correct formalism for the hydrogen-like system [41]. For the one-electron atomic system, the classical interelectron repulsion should cancel the total exchange energy [43,44], i.e.,

$$E_x = -J, \quad (23)$$

so that there is no net two-electron interaction energy. This requirement is not satisfied in Eq. (18), in which E_x depends on both V_{ne}/Z and J for atoms.

In Tables 2 and 3, predictions are made of exchange energies for the first positive and negative ions of atoms, respectively. Good agreement with the accurate values is found. The general tendency and the average error percentage of these predictions are about the same as those of Table 1 on which the least square fits were made. The fourth row of elements generates the best data. The average error of this row in Table 3 is just 0.09%, and in Table 2, 0.13%.

Another example showing that Eq. (18) produces good results for heavy atoms is exhibited in Table 4, where accurate and predicted exchange energies for the Be iso-electron series are given. The estimated results are calculated by using the constants of the first-row fit. One sees that as the atomic charges Z increases from B^+ , the error percentage decreases from 1.11% to 0.13%. The larger the atomic number, the more accurate the estimated result.

Table 5 shows the accurate and predicted exchange energy results for the Ne positive ions series. Except for the one-electron Ne^{+9} cation, one finds the relative error is less than 2% for each species, falling in the same range of error as the first-row species in Table 1.

To test the more general applicability of Eq. (18), we have investigated a few molecular species. Table 6 shows the ab initio and estimated results for the first-row mono hydrides. Ab initio results are obtained at the B3PW91/6-311++G(3d, 2p) level with the optimized geometry. The quantities computed include the classical Coulomb repulsion energy J , the electrostatic potential at each nucleus V_{ne1} and V_{ne2} , and the exchange energy from the B3PW91 functional. Then, a least-square fit is performed to determine the constants c_1 and c_2 in Eq. (18) for this set of molecules. The absolute error of the fitted results is less than 0.02 a.u., the relative error around 1% or less. Equation (18) is a good approximation for molecular systems.

Table 1. The accurate and fitted exchange energies for the first 54 neutral atoms (a.u.)

Atom	Accurate	Fitted	Error%	Atom	Accurate	Fitted	Error%
1	-0.3125	-0.2929	-6.27	28	-61.624	-61.559	-0.10
2	-1.026	-1.042	1.56	29	-65.793	-65.750	-0.07
3	-1.781	-1.796	0.86	30	-69.640	-69.577	-0.09
4	-2.667	-2.706	1.46	31	-73.517	-73.407	-0.15
5	-3.744	-3.764	0.53	32	-77.444	-77.345	-0.13
6	-5.045	-5.009	-0.72	33	-81.432	-81.365	-0.08
7	-6.596	-6.457	-2.11	34	-85.493	-85.488	-0.01
8	-8.174	-8.108	-0.80	35	-89.635	-89.717	0.09
9	-10.000	-9.997	-0.03	36	-93.852	-94.055	0.22
10	-12.110	-12.140	0.24	37	-97.895	-98.049	0.16
11	-14.020	-14.058	0.27	38	-101.953	-102.066	0.11
12	-15.990	-16.035	0.28	39	-106.185	-106.270	0.08
13	-18.070	-18.082	0.07	40	-110.542	-110.586	0.04
14	-20.280	-20.254	-0.13	41	-115.122	-115.137	0.01
15	-22.640	-22.553	-0.39	42	-119.690	-119.676	-0.01
16	-25.000	-24.974	-0.11	43	-124.169	-124.148	-0.02
17	-27.510	-27.530	0.07	44	-129.123	-129.059	-0.05
18	-30.19	-30.229	0.13	45	-133.989	-133.904	-0.06
19	-32.677	-32.745	0.21	46	-139.142	-139.060	-0.06
20	-35.212	-35.294	0.23	47	-144.040	-143.910	-0.09
21	-38.031	-38.096	0.17	48	-148.916	-148.814	-0.07
22	-40.993	-41.039	0.11	49	-153.826	-153.713	-0.07
23	-44.089	-44.116	0.06	50	-158.780	-158.689	-0.06
24	-47.489	-47.505	0.03	51	-163.766	-163.738	-0.02
25	-50.686	-50.681	-0.01	52	-168.825	-168.862	0.02
26	-54.190	-54.162	-0.05	53	-173.924	-174.062	0.08
27	-57.835	-57.790	-0.08	54	-179.092	-179.337	0.14

The fitted parameters for $E_x[\rho] = c_1 \int \frac{\rho(\mathbf{r})}{|\mathbf{r} - \mathbf{R}|} d\mathbf{r} + 2c_2 \iint \frac{\rho(\mathbf{r})\rho(\mathbf{r}')}{|\mathbf{r} - \mathbf{r}'|} d\mathbf{r}d\mathbf{r}'$,

- (i). $C_1 = -0.27615$ and $C_2 = -0.053636$ for $Z = 1 - 10$;
- (ii). $C_1 = -0.31864$ and $C_2 = -0.034591$ for $Z = 11 - 18$;
- (iii). $C_1 = -0.34814$ and $C_2 = -0.02593$ for $Z = 19 - 36$;
- (iv). $C_1 = -0.39475$ and $C_2 = -0.01870$ for $Z = 37 - 54$.

Table 2. Predicted exchange energies for the first cation of the first 54 elements (a.u.).

Cation	Accurate	Predict	Error%	Cation	Accurate	Predict	Error%
2	-0.625	-0.5858	-6.27	29	-65.063	-64.816	-0.38
3	-1.652	-1.662	0.57	30	-69.511	-69.197	-0.45
4	-2.507	-2.515	0.31	31	-73.344	-73.065	-0.38
5	-3.492	-3.531	1.11	32	-77.242	-76.952	-0.36
6	-4.712	-4.710	-0.03	33	-81.201	-80.936	-0.33
7	-6.124	-6.083	-0.67	34	-85.227	-85.022	-0.24
8	-7.739	-7.665	-0.96	35	-89.332	-89.208	-0.14
9	-9.566	-9.474	-0.96	36	-93.109	-93.504	0.43
10	-11.617	-11.527	-0.77	37	-97.812	-97.832	0.02
11	-13.902	-13.866	-0.26	38	-101.86	-101.820	-0.04
12	-15.863	-15.804	-0.37	39	-105.93	-105.878	-0.05
13	-17.893	-17.855	-0.21	40	-110.25	-110.164	-0.08
14	-20.045	-19.982	-0.31	41	-114.67	-114.552	-0.10
15	-22.307	-22.232	-0.34	42	-119.42	-119.227	-0.16
16	-24.687	-24.610	-0.31	43	-124.06	-123.834	-0.18
17	-27.075	-27.121	0.17	44	-128.53	-128.329	-0.16
18	-29.820	-29.766	-0.18	45	-133.65	-133.356	-0.22
19	-32.294	-32.565	0.84	46	-138.58	-138.274	-0.22
20	-35.108	-35.086	-0.06	47	-143.95	-143.548	-0.28
21	-37.673	-37.685	0.03	48	-148.78	-148.426	-0.24
22	-40.621	-40.596	-0.06	49	-153.66	-153.363	-0.19
23	-43.703	-43.639	-0.15	50	-158.59	-158.307	-0.18
24	-46.917	-46.816	-0.21	51	-163.56	-163.324	-0.14
25	-50.572	-50.377	-0.38	52	-168.58	-168.416	-0.10
26	-53.752	-53.584	-0.31	53	-173.66	-173.582	-0.04
27	-57.379	-57.181	-0.34	54	-178.81	-178.825	0.01
28	-61.149	-60.924	-0.37	55	-184.02	-184.147	0.07

Parameter values from Table 1.

Table 3. Predicted exchange energies for the first anion of the first 54 elements (a.u.).

Anion	Accurate	Predict	Error%	Anion	Accurate	Predict	Error%
1	-0.3955	-0.421	6.48	28	-61.899	-62.007	0.17
3	-1.827	-1.867	2.17	29	-65.846	-65.964	0.18
5	-3.843	-3.899	1.46	31	-73.595	-73.614	0.03
6	-5.150	-5.205	1.06	32	-77.564	-77.610	0.06
7	-6.648	-6.712	0.97	33	-81.587	-81.689	0.12
8	-8.352	-8.443	1.08	34	-86.200	-85.864	-0.39
9	-10.274	-10.412	1.35	35	-89.852	-90.143	0.32
11	-14.062	-14.162	0.71	37	-97.925	-98.171	0.25
13	-18.150	-18.221	0.39	39	-106.32	-106.517	0.19
14	-20.373	-20.444	0.35	40	-110.71	-110.871	0.15
15	-22.711	-22.788	0.34	41	-115.17	-115.322	0.13
16	-25.168	-25.262	0.37	42	-119.74	-119.870	0.12
17	-27.749	-27.871	0.44	43	-124.38	-124.520	0.11
19	-32.715	-32.846	0.40	44	-129.17	-129.271	0.08
21	-38.203	-38.347	0.38	45	-134.00	-134.123	0.09
22	-41.173	-41.310	0.33	46	-139.01	-139.080	0.05
23	-44.283	-44.414	0.29	47	-144.09	-144.143	0.04
24	-47.535	-47.650	0.24	49	-153.91	-153.942	0.02
25	-50.917	-51.025	0.21	50	-158.89	-158.974	0.05
26	-54.436	-54.539	0.19	51	-163.92	-164.068	0.09
27	-58.095	-58.200	0.18	52	-168.99	-169.232	0.14
				53	-174.13	-174.469	0.19

Parameter values from Table 1.

Table 4. Predicted exchange energies for the Be-isoelectronic series from B to Cr (a.u.).

	Accurate	Predict	Error%
B ⁺	-3.492	-3.531	1.11
C ⁺²	-4.314	-4.352	0.88
N ⁺³	-5.135	-5.172	0.72
O ⁺⁴	-5.956	-5.992	0.61
F ⁺⁵	-6.776	-6.811	0.52
Ne ⁺⁶	-7.596	-7.630	0.45
Na ⁺⁷	-8.415	-8.449	0.41
Mg ⁺⁸	-9.235	-9.268	0.36
Al ⁺⁹	-10.054	-10.09	0.33
Si ⁺¹⁰	-10.874	-10.906	0.29
P ⁺¹¹	-11.693	-11.725	0.27
S ⁺¹²	-12.513	-12.543	0.24
Cl ⁺¹³	-13.332	-13.362	0.23
Ar ⁺¹⁴	-14.152	-14.182	0.20
K ⁺¹⁵	-14.971	-14.999	0.19
Ca ⁺¹⁶	-15.79	-15.818	0.18
Sc ⁺¹⁷	-16.61	-16.637	0.16
Ti ⁺¹⁸	-17.429	-17.455	0.15
V ⁺¹⁹	-18.248	-18.275	0.15
Cr ⁺²⁰	-19.068	-19.093	0.13

Evaluated using $c_1 = -0.27615$ and $c_2 = -0.0053626$. See Table 1 and text.

Table 5. The accurate and predicted exchange energies for the Ne cation series (a.u.).

	Accurate	Predict	Error%
Ne ⁺⁹	-3.125	-2.929	-6.27
Ne ⁺⁸	-6.028	-5.997	-0.52
Ne ⁺⁷	-6.843	-6.808	-0.52
Ne ⁺⁶	-7.596	-7.630	0.45
Ne ⁺⁵	-8.552	-8.467	-0.99
Ne ⁺⁴	-9.446	-9.290	-1.65
Ne ⁺³	-10.265	-10.084	-1.77
Ne ⁺²	-10.994	-10.835	-1.44
Ne ⁺¹	-11.617	-11.527	-0.77

Table 6. The approximated density functional and fitted exchange energies for a few first-row monohydrides. The calculated data were obtained at the B3PW91/6-311++G (3df, 2p) level. See text.

Mols.	J	V_{ne1}^*	V_{ne2}^*	E_x	
				DFT	Fitted (Error %) **
LiH	5.192	2.235	6.073	-1.685	-1.704 (1.10)
BeH	8.544	2.741	8.807	-2.421	-2.428 (0.30)
BH	13.284	3.269	11.830	-3.260	-3.271 (0.33)
CH	19.917	3.894	15.191	-4.290	-4.276 (-0.32)
NH	28.664	4.582	18.864	-5.454	-5.444 (-0.18)
OH	39.872	5.324	22.885	-6.814	-6.795 (-0.28)
FH	53.834	6.112	27.216	-8.315	-8.334 (0.22)

* V_{ne1} is defined as the electrostatic potential $\int \frac{\rho(\mathbf{r})}{|\mathbf{r} - \mathbf{R}_H|} d\mathbf{r}$ at the hydrogen nucleus, and

V_{ne2} is defined as the electrostatic potential $\int \frac{\rho(\mathbf{r})}{|\mathbf{r} - \mathbf{R}_X|} d\mathbf{r}$ at the other atom.

** The fitted formula for this series of molecules is:

$$E_x[\rho] = -0.17665 \sum_{i=1}^2 \int \frac{\rho(\mathbf{r})}{|\mathbf{r} - \mathbf{R}_i|} d\mathbf{r} - 0.09088 \iint \frac{\rho(\mathbf{r})\rho(\mathbf{r}')}{|\mathbf{r} - \mathbf{r}'|} d\mathbf{r} d\mathbf{r}',$$

V. Summary

To illustrate the argument that any well-behaved functional can be expressed as the sum of density-homogeneous functionals, starting from the Levy-Perdew relation, we have shown that the exchange energy density functional can be written, at least approximately, as the sum of functionals homogeneous of degree one and two, respectively, with respect to the density scaling. This formula is consistent with the recent suggestion that the functional $V_{ee}[\rho]$, of which $E_x[\rho]$ is a part, has a truncated functional expansion and can be expressed as a combination of density homogeneous functionals of degrees one and two. Though an approximation, the formulation gives good estimation of the exchange energy for both atoms and ions, especially for large systems. Extension to simple molecules, the first-row monohydrides, also gives good fits.

Acknowledgment

This work has been supported by National Science Foundation, the Petroleum Research Fund of the American Chemical Society, the North Carolina Supercomputing Center, and the Hungarian-U.S. Science and Technology Joint Fund. SBL thanks Professor Jan Hermans for partial support from a Research Resource project in computational structural biology (NIH grant RR08102). FDP is a postdoctoral fellow of the Fund for Scientific Research-Flanders (Belgium) and also has been supported by Fulbright and NATO travel grants enabling a stay at the University of North Carolina. RGP acknowledges with pleasure the steady friendship, over many years, both professional and personal, of Giuseppe Del Re. Professor Del Re is a theoretical chemist with firm conviction, often eloquently expressed, that the understanding of molecular electronic structure demands careful mathematical analysis as well as computation, and both deep and earnest thought.

Reference

- [1]. R.G. Parr and W. Yang, *Density Functional Theory of Atoms and Molecules* (Oxford University Press, Oxford 1989).
- [2]. N.H. March, *Electron Density Theory of Atoms and Molecules* (Academic Press, London 1992); R.M. Dreizler and E.K.U. Gross, "Density Functional Theory - an Approach to the Quantum Many-Body Problem" (Spring-Verlag, 1990).
- [3]. Parr, R.G.; Yang, W. *Annu. Rev. Phys. Chem.* **1995**, 46, 701.
- [4]. Kohn, W.; Becke, A.D.; Parr, R.G. *J. Phys. Chem.* **1996**, 100, 12974.
- [5]. P. Hohenberg and W. Kohn, *Phys. Rev. B* **136**, 864(1964).
- [6]. W. Kohn and L.J. Sham, *Phys. Rev. A* **140**, 1133(1965).
- [7]. L.H. Thomas, *Proc. Camb. Phil. Soc.* **23**, 542(1927).
- [8]. E. Fermi, *Z. Phys.* **48**, 73(1928).

- [9]. P.A.M. Dirac, *Proc. Cam. Phil. Soc.* **26**, 376(1930).
- [10]. R.G. Parr, S. Liu, A. Kugler and A. Nagy, *Phys. Rev. A* **52**, 969(1995).
- [11]. D.L. Langreth and M.J. Mehl, *Phys. Rev. B* **28** 1809(1983).
- [12]. J.P. Perdew and Y. Wang, *Phys. Rev. B* **33** 8800(1986).
- [13]. C.J. Umrigar and X. Gonez, *Phys. Rev. A* **50**, 3827(1994).
- [14]. S. Kristyan and P. Pulay, *Chem. Phys. Lett.* **229**, 175(1994).
- [15]. H.U. Suter, V. Pleß, M. Ernzerhof and B. Engels, *Chem. Phys. Lett.* **230**, 398(1994).
- [16]. B.G. Johnson, C.A. Gonales, P.M.W. Gill, and J.A. Pople, *Chem. Phys. Lett.* **221**, 100(1994).
- [17]. S. Gronert, G.L. Merrill, and S.R. Kass, *J. Org. Chem.* **60**, 488(1995).
- [18]. D.A. Plattner and K.N. Houk, *J. Am. Chem. Soc.* **117**, 4405(1995).
- [19]. H.M. Sulzbach, H.F. Schaefer III, W. Klopper, and H.P. Luthi, *J. Am. Chem. Soc.* **118**, 3519(1996).
- [20]. S. Liu, R.G. Parr, and A. Nagy., *Phys. Rev. A* **52**, 2645(1995).
- [21]. D.J. Lacks and R.G. Gordon, *J. Chem. Phys.* **100**, 4446(1994).
- [22]. S. Liu and R.G. Parr, *Phys. Rev. A* **53**, 2211(1996).
- [23]. S. Liu and R.G. Parr, *J. Chem. Phys.* **106**, 5578(1997).
- [24]. S. Liu and R.G. Parr, *Phys. Rev. A* **55**, 1792(1997).
- [25]. R.G. Parr and S. Liu, *Chem. Phys. Lett.* **276**, 164(1997).
- [26]. R.G. Parr and S. Liu, *Chem. Phys. Lett.* **280**, 159(1997).
- [27]. S. Liu and R.G. Parr, *Chem. Phys. Lett.* **278**, 341(1997).
- [28]. S. Liu, P. Sule, R. Lopez-Boada, and A. Nagy, *Chem. Phys. Lett.* **257**, 68(1996).
- [29]. S. Liu, *Phys. Rev. A* **56**, 1328(1996).
- [30]. S. Liu, *Phys. Rev. A* **54**, 4863(1996).
- [31]. Y.A. Wang, S. Liu, and R.G. Parr, *Chem. Phys. Lett.* **267**, 14(1997).
- [32]. R. Lopez-Boada, V. Karasiev, and S. Liu, *Chem. Phys. Lett.* **270**, 443(1997).
- [33]. S. Liu, V. Karasiev, R. Lopez-Boada, and F. De Proft, *Int. J. Quantum Chem.* **69**, 513(1998).
- [34]. M. Levy and J.P. Perdew, *Phys. Rev. A* **32**, 2010(1985).
- [35]. S.K. Ghosh and R.G. Parr, *J. Chem. Phys.* **82**, 3307(1985).
- [36]. R. van Leeuwen and E.J. Baerends, *Phys. Rev. A* **49**, 2421(1994).
- [37]. P. Politzer and R.G. Parr, *J. Chem. Phys.* **61**, 4258(1974).
- [38]. S. Fliszar, *Charge, Distributions, and Chemical Effects* (Spring-Verlag, Neew York, 1983).
- [39]. J.A. Alonso and L.A. Girlfalco, *Phys. Rev. B* **17**, 3735(1978).
- [40]. O.V. Gritsenko, N.A. Cordero, A. Rubio, L.C. Balbas and J.A. Alonso, *Phys. Rev. A* **48**, 4197(1993).
- [41]. S. Liu and R.G. Parr, *J. Comp. Chem.* **22**, 2(1999).
- [42]. Koga, T.; Tatewaki, H.; Thakkar, A. J. *Phys. Rev. A* **47**, 4510(1993).
- [43]. D. Tozer, *Phys. Rev. A* **56**, 2726(1997).
- [44]. P.M.W. Gill and J.A. Pople, *Phys. Rev. A* **47**, 2383(1993).

Density functional computations and mass spectrometric measurements. Can this coupling enlarge the knowledge of gas-phase chemistry ?

T. Marino, N. Russo, E. Sicilia and M. Toscano
Dipartimento di Chimica, Universita' della Calabria,
I-87030 Arcavacata di Rende (CS), Italy

and

T. Mineva
Institute of Catalysis, Bulgarian Academy of Sciences, 1113 Sofia, Bulgaria

Abstract

A series of gas-phase properties of the systems has been investigated by using different exchange-correlation potentials and basis sets of increasing size in the framework of Density Functional theory with the aim to determine a strategy able to give reliable results with reasonable computational efforts.

Contents

1. Introduction

2. Theory

- 2.1 Kohn-Sham method
- 2.2 Reactivity indices
- 2.3 Thermochemical properties
- 2.3 Computational details

3. Results and discussion

- 3.1 Ions geometries
- 3.2 Preferred attach sites
- 3.3 Proton affinity and gas-phase basicity
- 3.4 Gas-phase acidity
- 3.5 Metal ion affinity
- 3.6 Potential energy surfaces

4. Conclusions

References

1. Introduction

The last decade has known an extraordinary and unexpected increase of the use of Density Functional Theory (DFT) in a wide variety of chemical fields ranging from material science to homogeneous and heterogeneous catalysis, to organic, organometallic and inorganic chemistry, to biochemical and pharmacological problems [1-10]. This occurred when the traditional computational techniques (Coupled-Cluster, Multireference Configuration-Interaction, and Generalized Valence Bond approaches) resulted in great advances in their accuracy. The appeal of DFT stays in the fact that it accounts for electron correlation with a computational effort of the same order as the simplest Hartree-Fock (HF) methods.

The main characteristic of DFT is to consider the electron density as the principal variable rather than the wave function. The reliability of this theory depends on the goodness of the functionals used to describe the exchange-correlation energy.

The availability of many exchange-correlation functionals derived by different approximations (gradient-corrected, adiabatic connection), together with the possibility to express the derivatives analytically, allows to DFT to reach an high accuracy in the description of electronic and spectroscopic features of the molecular systems. This is well documented in a series of recent reviews and books [1-9].

As suggested by Kohn, Becke and Parr [11], the use of DFT is preferable (over the traditional methods) for systems with more than 5-10 atoms for which a lower accuracy is acceptable. This does not mean that for system with a less number of atoms the DFT is not reliable. With regard to this fact we mention the recent work of Seminario [6], in which, the DF atomization energy of water, obtained with different exchange-correlation functionals, is well reproduced: the results are closer to the experiment than that obtained at CCDS(T) high level of theory which is often chosen as reference when the experimental data are not available.

Despite the large number of DFT applications, relatively few works have been devoted to the reproduction or prediction of many gas-phase thermochemical properties [12-23] that are currently obtained with the modern mass-spectrometric techniques.

In this work we will show the potentiality of DFT in obtaining gas-phase chemical properties such as the proton affinity (PA), the gas-phase basicity (GPB) and acidity (GPA) and the metal ion affinity (MIA).

In addition we will consider the possibility to obtain reliable theoretical information on the preferred attach sites for proton and metal cations and on the potential energy surfaces (PES) that cannot be determined experimentally even with the most modern and sophisticated mass-spectrometric instruments [22,23]. Furthermore, we will propose the way to rationalize some of chemical properties by using the concepts of hardness, softness and other reactivity indices (Fukui functions) for which an exact definition exists only in the framework of DFT [11]. These last fascinating tools can contribute to increase furthermore the DFT use going in the "core" of molecules to predict and explain basic chemical concepts.

2. Theoretical background

The implementation of density functional theory is based on solving the non-relativistic Kohn-Sham one-electron equations [24] which differ from the Hartree-Fock ones by the inclusion of the exchange-correlation potential $v_{xc}(r)$, and must be solved self-consistently:

$$\left(-\frac{1}{2}\nabla^2 + v(r) + \int \frac{\rho(r')}{|r-r'|} dr' + v_{xc}(r) - \epsilon_j \right) \phi_j(r) = 0 \quad (1)$$

$$\rho(r) = \sum_{j=1}^N |\phi_j(r)|^2 \quad (2)$$

$$v_{xc}(r) = \frac{\delta E_{xc}[\rho(r)]}{\delta \rho(r)} \quad (3)$$

The ground state energy is given by

$$E = \sum_j \epsilon_j - \frac{1}{2} \int \frac{\rho(r)\rho(r')}{|r-r'|} dr dr' - \int v_{xc}(r)\rho(r)dr + E_{xc}[\rho(r)] \quad (4)$$

where ϵ_j and ρ are the self consistent quantities and $E_{xc}[\rho]$ is the exchange-correlation energy functional which is unknown. So, for the practical use of this theory, a good approximation for $E_{xc}[\rho]$ is necessary. The most widely used exchange-correlation functional employs the so-called local density approximation (LDA) [25]. In the LDA the exchange-correlation energy is given by

$$E_{xc}^{LDA}[\rho(r)] \equiv \int \epsilon_{xc}(\rho(r))\rho(r)dr \quad (5)$$

LDA or its local spin density (LSD) formulation [26] reproduces well the geometries of many-particle systems, but fails in the description of their energetic features.

The introduction of the generalized gradient approximation (GGA) [27], improves considerably the reliability of the method also for the computation of the energetic parameters. In the GGA the exchange-correlation energy functional is:

$$E_{xc}^{GGA} = \int f(\rho(r)|\nabla\rho(r)|)dr \quad (6)$$

where $f(\rho, |\nabla\rho|)$ is a function of the density and of its gradient at a given position. Several gradient corrected exchange [28-30] and correlation [31-34] functionals have been proposed. In our study we use different combinations of those of Becke [28] and Perdew and Wang [30] for the exchange and the functionals proposed by Perdew [31] and Proynov [34] for the correlation. Recently, Becke [29] has introduced the so-called hybrid functional that is based on the "adiabatic connection" formula [35]. Because of its reliability, largely validated in the literature [36-38], we employ in our work also the B3LYP functional which uses the Becke gradient

correction to the exchange [29] (B3) and the Lee-Yang-Parr [32] (LYP) one to the correlation part. The explicit formula of this potential is:

$$E_{xc}^{B3LYP} = (1 - A)E_x^{Slater} + AE_x^{HF} + BE_x^{Becke} + CE_c^{LYP} + (1 - C)E_c^{VWN} \quad (7)$$

where the E_x exchange terms are that of Slater [39], that calculated by the Hartree Fock method and that proposed by Becke [29] and the E_c terms are the correlation functionals of Lee-Yang-Parr [32] and Vosko-Wilk- Nusair [40], respectively.

2.1 Reactivity Indices

The reactivity and stability of a system can be studied applying the concept of chemical hardness. Incorporation of the concepts of hardness and softness into DFT has led to the mathematical identification of η as the second derivative of the total energy with respect to the number of electrons N [41,42]:

$$\eta = \left[\frac{\partial^2 E}{\partial N^2} \right]_{v(r)} \quad (8)$$

or, equivalently:

$$\eta = \left[\frac{\partial \mu}{\partial N} \right]_{v(r)} \quad (9)$$

where the chemical potential, μ , is the first derivative of the total energy relative to the electron number. Derivatives are taken at constant external potential $v(r)$.

Softness is defined as the inverse of hardness:

$$S = \frac{1}{\eta} \quad (10)$$

Conventionally, the hardness is obtained from the values of the ionization potential (I) and the electron affinity (A), $\eta = (I - A)/2$, through the finite difference method. While the chemical potential is constant everywhere within the molecule, the hardness, and then the softness, is a function of the position. Thus, in addition to the global definition of η and S , the local hardness [43] and local softness [44] have been introduced.

The ab-initio SCF and DFT computations [45-52] of η are generally performed using the simple molecular orbital theory that allows one to compute the hardness as the energy difference between the highest occupied orbital (HOMO) and the lowest unoccupied orbital (LUMO) [53]:

$$\eta_{HL} = \frac{\epsilon_{LUMO} - \epsilon_{HOMO}}{2} \quad (11)$$

This approximation fails if the HOMO-LUMO energy difference is close to zero. Moreover, for a more accurate computation of η , the contribution to the hardness of various orbitals should be taken into account. Recently, different approaches, accounting for the orbital hardness values, have been proposed [54-56].

The computations, presented here, are based on an approach that uses the fractional occupation number concept [57-58]. The original idea to exploit fractional occupation numbers in the framework of DFT is due to Janak [59] who generalized the earlier work of Slater [60], using the $X\alpha$ approach.

The validity of the Janak theorem in DFT, for N - and v -representable densities, has been discussed by many authors [61-66].

In this approach, when the principle of the electronegativity equalization [67] is satisfied, the hardness matrix elements can be defined [68,69] as the first derivative of the Kohn-Sham orbital eigenvalues (ϵ_i) with respect to the orbital occupation numbers (n_j):

$$\eta_{ij} = \frac{\partial \epsilon_i}{\partial n_j} \quad (12)$$

This expression takes into account the response of the i -th orbital to the change of the occupation number of the j -th orbital.

Applying the Pearson's principle [70], that states the more localized system is less reactive, the orbital hardness can be interpreted as a measure of the degree of electron localization of a given orbital [71]. Moreover, in such a manner, the two particle interelectronic interaction, that is the most significant contribution in the hardness evaluation, is considered [69].

Numerically, the hardness matrix elements are calculated by the finite difference method [57]

$$\eta_{ij} = \frac{\epsilon_i(n_j - \Delta n_j) - \epsilon_i(n_j)}{\Delta n_j} \quad (13)$$

The reciprocal of hardness matrix is the softness one [68] $\{s_{ij}\} = \{\eta_{ij}\}^{-1}$. Then, the absolute hardness is calculated by:

$$\eta = \frac{1}{\sum_{ij} s_{ij}} \quad (14)$$

The η value is directly related to the electron localization (system stability) and the softness is associated to the reactivity indices [68,71]. The hard (soft) systems correspond to a high (low) stability.

The formalism of DFT allows one to introduce another important local variable, the Fukui function $f(\mathbf{r})$, originally defined by Parr and Yang [68] as the first derivative of the electronic chemical potential μ with respect to the external potential $v(\mathbf{r})$:

$$f(\mathbf{r}) = \left[\frac{\delta\mu}{\delta v(\mathbf{r})} \right]_N = \left[\frac{\partial \rho(\mathbf{r})}{\partial N} \right]_v \quad (15)$$

The Fukui function measures how sensitive a system's chemical potential is to an external perturbation at a particular point. In the approach used by us, the Fukui indices are approximated by the equation:

$$f_i = \frac{\partial n_i}{\partial N} = \frac{\Delta n_i}{\Delta N} = \left(\frac{\partial n_i}{\partial \mu} \right) \left(\frac{\partial \mu}{\partial N} \right) = \eta \sum_j s_{ij} \quad (16)$$

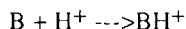
with $\sum_i f_i = 1$.

Following this formalism, the chemical potential can be computed from the orbital softness values through the use of the orbital Fukui index.

$$\mu = \frac{\partial E}{\partial N} = \sum_i \frac{\partial E}{\partial n_i} \left(\frac{\Delta n_i}{\Delta N} \right) = \sum_i \epsilon_i f_i \quad (17)$$

2.2 Thermochemical properties

Gas-phase proton affinity (PA) is defined as the negative of the enthalpy for the process:



and can be calculated as follows:

$$PA = -\Delta H = -[E_{cl}(BH^+) - E_{cl}(B) + (E_{vib}(BH^+) - E_{vib}(B))] + 5/2 RT \quad (18)$$

The E_{cl} terms are obtained from the calculations and E_{vib} includes the zero point energy and temperature corrections to the vibrational enthalpy derived by computed harmonic vibrational frequencies. The corrections due to translation, vibration and rotation are treated classically, using the equipartition theorem. The consideration that BH^+ and B rotational contributions are quite similar, that the proton has only translational degrees of freedom and that the eventually different populations of the vibrational states that originate bringing the system from zero degrees to room temperature, are practically cancelled in the calculation of PA, yield us to consider

only a further contribution of $3/2RT$. Thus $5/2RT$ represents the translational energy of proton and the $\Delta(PV)=RT$ term necessary to convert the energy in enthalpy.

The absolute gas-phase basicity (GPB) is calculated as the negative of the standard free energy ΔG :

$$\Delta G = \Delta H - T\Delta S \quad (19)$$

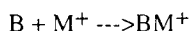
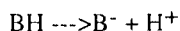
The entropy contribution is given by

$$-T\Delta S = -T [S(\text{BH}^+) - S(\text{B}) - S(\text{H}^+)] \quad (20)$$

where, at 298 K, the $TS(\text{H}^+)$ term has a value of 7.76 kcal/mol [72].

In the case of gradient corrected calculations the BH^+ and B entropies have been obtained by a simple procedure that uses the theoretical harmonic frequencies and the equilibrium geometries.

Two different processes must be considered to calculate the gas-phase acidity (GPA) and the metal ion affinity (MIA), respectively:



The way to obtain the GPA is the same as in the case of GPB, whilst, the computations of MIA follows the criteria used for PA determination.

2.3 Computational details

Gaussian 94 [73], DeMon [74] and DGauss [75] packages have been employed for the calculations.

Full geometry optimizations without symmetry constraints have been executed in all cases. Vibrational analyses have been performed in the framework of internal procedures implemented in the used codes.

The five functionals employed are:

- B3LYP (Becke exchange + Lee, Yang and Parr correlation) [29,32]
- BP (Becke exchange +Perdew correlation) [28,31]
- PWP (Perdew and Wang exchange + Perdew correlation) [30,31]
- BLAP3 (Becke exchange + Proynov correlation) [28,34]
- PLAP3 (Perdew exchange + Proynov correlation) [30,34]

The first three have been chosen because they represent the currently most popular functionals for applications to molecular systems, while the latter two because they have been used, until now, in few cases.

The basis sets selected consist of:

- The Gaussian 94 internal 6-31G** [76] to which polarization and/or diffuse functions, as specified in the Tables, have been added .
- Valence triple- ζ basis set (TZVP) of Godbout et al. [77]
- cc-pVT(Q)Z and AUG-cc-pVT(Q)T triple- and quadruple- ζ basis set of Dunning et al. [78]

For Se, Te and Ni heavy atoms the Huzinaga type-model core potentials have been used that treat explicitly the $3d^{10} 4s^2 4p^4$, $5s^2 5p^4$ and $3p^6 3d^9 4s^1$ electrons, respectively.

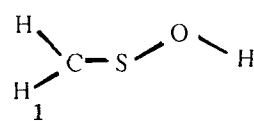
3. Results and discussion

3.1 Ion geometries

The performance of DF methods in the reproduction of reliable geometrical parameters for neutral molecules has been largely confirmed [1-10]. Usually errors of about 0.02 Å and few degrees with respect to the experimental data, are found for bond lengths and valence angles, respectively. Less data exist, in the literature, for the charged species probably because of a minor experimental information. The few density functional works [12-19] demonstrate a reasonable reliability also in this case.

We report here the structures of some cationic systems in order to contribute to the validation of DF methods.

In Figures 1 and 2, the geometrical parameters of CH_2SOH^+ and O_3H^+ , obtained at PWP/TZVP, BP/TZVP and B3LYP/6-31G** levels, are reported together with other theoretical results [79,80]. The data of protonated cytosine reported in figure 3 are obtained at BP/TZVP level and compared to the experimental ones [81,82].



Parameters	PWP	B3LYP	BP	MP2
C-H	1.099	1.085	1.096	1.085
C-S	1.621	1.597	1.614	1.597
S-O	1.645	1.604	1.629	1.610
O-H	0.995	0.975	0.987	0.977
H-C-S	122.2	123.1	122.6	121.7
H1-C-S	116.1	115.6	115.7	116.2
C-S-O	102.9	103.8	103.3	102.8
S-O-H	109.8	111.0	110.1	110.7

Figure 1. Protonated sulfine geometry. Distances are in Å and angles in degrees.

As is shown the DF gradient corrected structures are characterized by bond lengths which are sometime longer than the corresponding distances obtained by B3LYP/6-31G**, MP2/6-31G** [79] and CCSD/DZ+P [80] computations.

In the case of O_3H^+ , MP2/6-31G** method is unable to distinguish between the two O-O lengths. Valence angles are, instead, of the same order in all the calculations.

Parameters	PWP	B3LYP	BP	CCSD	MP2
O1-O2	1.187	1.169	1.189	1.200	1.265
O2-O3	1.529	1.408	1.490	1.342	1.274
O3-H	1.008	0.995	1.006	0.994	0.996
O1-O2-O3	114.5	114.3	114.1	112.8	114.4
O2-O3-H	100.4	102.1	100.4	101.2	104.3

Figure 2. O₃H⁺ geometry. Distances are in Å and angles in degrees.

parameters	BP	EXPa	EXPb
C4-C5	1.407	1.413	1.413
C5-C6	1.359	1.341	1.346
C6-N1	1.345	1.362	1.365
N1-C2	1.387	1.381	1.381
C2-N3	1.401	1.387	1.384
N3-C4	1.351	1.352	1.353
N4-C4	1.324	1.313	1.315
C2-O2	1.204	1.211	1.212
C4-C5-C6	118.1	118.5	118.4
C5-C6-N1	121.9	122.5	122.2
C6-N1-C2	123.6	121.5	121.7
N1-C2-N3	112.7	114.9	114.7
C2-N3-C4	125.9	125.1	125.3
N3-C4-N4	119.9	119.5	119.5
N1-C2-O2	124.5	123.5	123.4

Figure 3. Protonated cytosine geometry. Distances are in Å and angles in degrees. a) from ref. 81; b) from ref. 82.

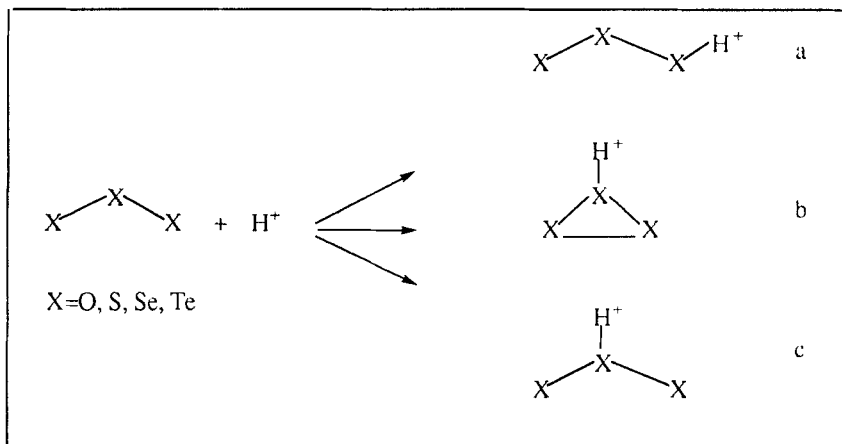
For protonated cytosine (see Figure 3) it is possible to compare our BP/TZVP results with those coming from two sets of experimental determinations [81,82]. The agreement, now, is very good. A similar concordance was found for protonated adenine [19] nucleic acid base.

3.2 Preferred attach sites

It is well known that experimental gas-phase studies are often unable to predict the preferred attach site of the proton or metal cations on a molecular system, but, this information is of fundamental importance for understanding the chemical reactivity of a given species. Thus, theoretical investigations can represent a very useful alternative to solve this problem. Reliable predictions on this matter are possible only if high level theoretical methods are employed. There are already evidences [14,17,19] that the DF methods are powerful tools for this type of determination.

In the schemes 1-3 three different protonation processes, that we have studied, are depicted and Table 1 collects the relative results obtained using different functionals.

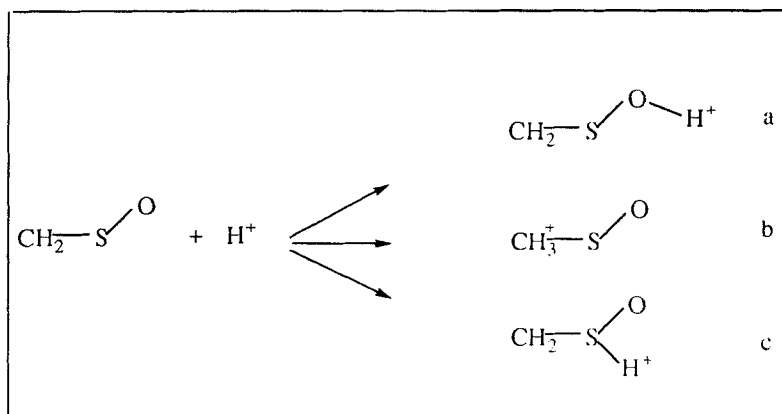
The protonation of X_3 ($X=O, S, Se, Te$) species can give rise to the **a**, **b** and **c** isomers (see scheme 1).



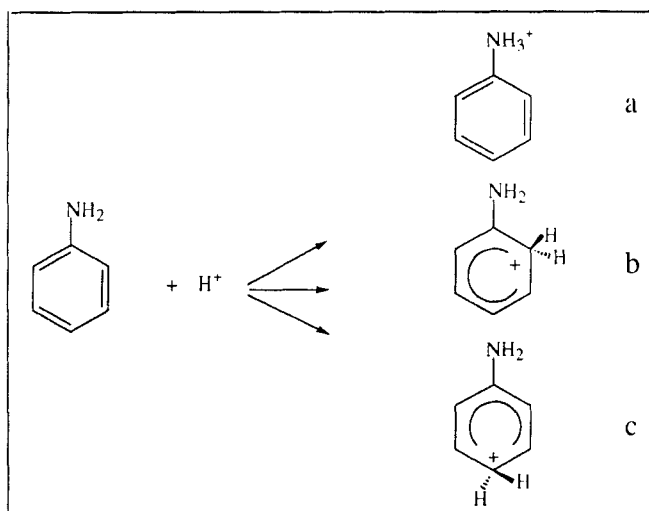
Scheme 1

Our study shows that the trans form **a** is favoured over the other two in the case of oxygen, sulphur and selenium but not for tellurium for which the cyclic form **b** is the most stable one. The energy difference between the absolute and the relative minimum **b** decreases significantly in going from O_3 to Se_3 systems and becomes negative in the Te_3 one. For O_3H^+ and S_3H^+ species the comparison is possible with previous ab-initio QCISD calculations [79,83]. The stability order of isomers is the same and the energy differences quite similar.

In the sulfine (CH_2SO) molecule proton can attach, in principle, the carbon as well as the oxygen and the sulphur atoms (see Scheme 2) for obtaining three cationic forms. Our study, performed employing the PWP gradient corrected and B3LYP hybrid functionals, shows that the structure **a** (in which H^+ binds oxygen atom) is the most stable one followed by **b** (proton on carbon) and **c** (proton on sulphur) forms with the latter at about 50 kcal/mol above the global minimum (see Table 1).



Scheme 2



Scheme 3

The PWP and B3LYP results confirm the experimental hypothesis that indicates the **a** isomer as the most abundant and quantify the energy difference between the three

stable minima.

The protonation process has been rationalized computing the orbital Fukui indices of neutral sulfine.

Following the procedure previously described and briefly reported in the method section, we found (at PWP level) that the Fukui index associated with orbital lone pair of oxygen in sulfine, has the value of 0.04 eV, while those associated with carbon and sulphur, are 0.19 and 0.21 eV, respectively. Speaking in terms of hard-soft theory of Pearson, we can indicate the orbital with the lowest Fukui index as the most reactive in the electrophilic reaction with H^+ .

The protonation of aniline is the object of our next example (see Scheme 3). Notwithstanding different experimental gas-phase studies [84-86] the question regarding the preferred protonation site on this molecule remains matter of controversy. The situation in solution is instead well defined. As it is shown in Table 1, both PWP and B3LYP calculations indicate that the protonation on the para-carbon is slightly favoured over that on nitrogen atom.

Table 1. Relative energies (in kcal/mol) at 0 K for the minima of the protonation processes depicted in the schemes 1-3.

Species	Isomer	PWP/TZVP	B3LYP/6-311++G**	Previous works
O ₃	a	0.0	0.0	0.0 ^a
	b	56.2	55.5	47.1 ^a
	c	58.1	58.7	58.9 ^a
S ₃	a	0.0	0.0	0.0 ^b
	b	17.3	15.1	16.6 ^b
	c	33.6	36.3	35.1 ^b
Se ₃	a	0.0	0.0	/
	b	7.6	11.0	/
	c	35.2	41.9	/
Te ₃	a	0.0	/	/
	b	-1.5	/	/
	c	31.5	/	/
CH ₂ SO	a	0.0	0.0	0.0 ^c
	b	19.2	22.8	19.9 ^c
	c	48.7	50.2	52.0 ^c
C ₆ H ₅ NH ₂	a	2.8	1.9	/
	b	5.8	4.2	/
	c	0.0	0.0	/

a) from ref.80; b) from ref.17; c) from ref.79

A recent mass-spectrometry study [86] concludes that the processes that yield **c** and **a** isomers are favoured respectively by thermodynamic and kinetics factors. Because of the small energy difference between the two minima (see Table 1), it is difficult to discriminate exactly what of the two processes is the most probable, but, the possibility that both isomers can be populated in gas-phase is reasonable.

An alternative indication can come, also in this case, from the computation of orbital Fukui indices of neutral aniline. We found a value of 0.19 and 0.06 eV for the orbitals mainly associated with nitrogen and para-carbon, respectively. So, the

electrophilic attack of the proton seems to occur preferentially on the para-carbon because of its lower Fukui index value.

3.3 Proton affinity and gas-phase basicity

The determination of the proton affinity has a long history both from experimental and theoretical views. In the 1984 Lias et al. [87] compiled a comprehensive list of relative PA for a number of compounds and assigned absolute values on the basis of the best data available at that time. Subsequently the scale was considerably modified with data coming from new mass-spectrometry equilibrium and kinetic experiments [88-91].

Smith and Radom [92-94] showed that the G2(MP2) theoretical procedure is able to estimate proton affinity within a target accuracy of about 2 kcal/mol. The compounds studied by these authors are of small size (containing from 1 to 4 first row atoms) because of the relatively great computational efforts required by the method. Recently, the possibility to use the DF methods in the PA evaluation has been tested by different authors [12,14,17,19] with encouraging results. From these studies it emerges that DF prediction of PA has almost the same accuracy of G2(MP2) one, but in a fraction of computer time.

In this work, the reliability of DF methods in the PA evaluation will be demonstrated firstly for small molecules and subsequently for larger systems, as amino-acids and nucleic acid bases.

Tables 2 collects the PA values for NH_3 obtained employing different basis sets and exchange-correlation functionals.

Table 2. PA and GPB (in kcal/mol) at 298 K for ammonia.

Method	PA (298 K)	Δ PA	GPB (298 K)	Ref.
B3LYP/6-31G**	210.4	6.8	202.0	this work
B3LYP/6-311++G**	203.8	0.2	194.9	this work
B3LYP/cc-pVTZ	205.7	2.1	196.8	this work
B3LYP/AUG-cc-pVTZ	203.2	-0.4	194.3	this work
B3LYP/TZVP	204.1	0.8	195.3	this work
B3LYP/cc-pVQZ	204.2	0.9	195.4	this work
B3LYP/AUG-cc-pVQZ	203.2	-0.4	194.4	this work
PWP/TZVP	202.4	-0.9	194.1	this work
BP/TZVP	202.7	-0.6	194.4	this work
BLAP3/TZVP	205.7	2.4	197.4	this work
PLAP3/TZVP	209.1	5.8	200.8	this work
G2	204.2	0.6	/	92
G2(MP2)	204.2	0.6	/	94
G2(MP2,SVP)	204.0	0.4	/	94
EXP	203.6	0.0	/	89

In the case of B3LYP computations the convergence of the results, as a function of the basis set dimension, has been tested using basis sets of increasing size starting from the double zeta (6-31G**) to arrive to quadruple zeta (AUG-cc-pVQZ) quality. As it is shown in Table 2, the 6-31G** basis set does not give reliable results. The introduction of the diffusion functions (6-311++G**) improves strongly the values of PA. The deviation, with respect to the experimental data, is of only 0.2 kcal/mol.

From the values obtained by the larger basis sets (AUG-cc-pVTZ, AUG-cc-pVTQZ), it is evident that the convergence is reached already at 6-311++G** level. The use of TZVP valence basis set gives also results in excellent agreement with experimental evidences (the deviation is of 0.4 kcal/mol). On the basis of these results this same set TZVP has been used in connection with other exchange-correlation functionals.

PWP and BP results are close to the B3LYP one, while BLAP3 and PLAP3 computations overestimate the PA by 2.4 and 5.8 kcal/mol, respectively (the experimental value is 203.6 kcal/mol). Our best estimations well agree with high level theoretical data obtained with the G2 procedures [92].

The benchmark indicates that the PA of ammonia is very well reproduced employing the 6-311++G** or the TZVP basis sets coupled with B3LYP, PWP and BP exchange-correlation potentials. For this reason, the PA and GPB of other further compounds reported in Tables 3-5 are calculated at these levels of theory.

Due to their great importance in chemistry, we have firstly considered the amine series (see Table 3).

Table 3. PA at 298 K (in kcal/mol) for amine series.

System	PA _{PWP/TZVP}	PA _{B3LYP/6-31++G**}	PA _{EXP} ^a	PA _{EXP} ^b	PA _{EXP} ^c
NH ₃	202.4	203.8	203.3	204.0	204.8
CH ₃ NH ₂	213.0	214.7	215.3	214.1	216.1
(CH ₃) ₂ NH	219.3	221.5	222.5	220.6	224.1
(CH ₃) ₃ N	226.4	226.7	/	225.1	229.1

a) from ref. 90; b) from ref. 95; c) from ref. 89

The different experimental scales propose the same trend of basicity for these compounds but differ in the absolute values evaluation.

Both the PWP and B3LYP PA_s follow the experimental trends. In particular B3LYP results are very similar to those obtained by Lias *et al.* [95] and the agreement between all other data is sufficiently satisfactory.

Table 4 collects the absolute gas-phase basicity (GPB) and the global hardness (η) values obtained at PWP and B3LYP levels of theory for ammonia and some aliphatic amines.

Table 4. GPB at 298 K (in kcal/mol) and η (in eV) values for amine series.

System	GPB _{PWP/TZVP}	GPB _{B3LYP/6-311++G**}	η
NH ₃	194.1	195.7	7.16
CH ₃ NH ₂	205.2	206.7	5.24
(CH ₃) ₂ NH	211.6	213.5	4.28
(CH ₃) ₃ N	218.6	218.8	3.76

In Figure 4 the PWP profile of GPB is reported together with the η one.

The GPB increases going from NH₃ to Me₃N species. Thus ammonia must have the largest proton affinity as indicated by the largest η value of 7.16 eV.

In the Figure 4 the good correlation between GPB and η behaviours is evident.

In Tables 5 and 6 we have reported our PA and GPB results for a number of compounds for which other previous theoretical [14,80,96,97] and experimental [98-102] data are available.

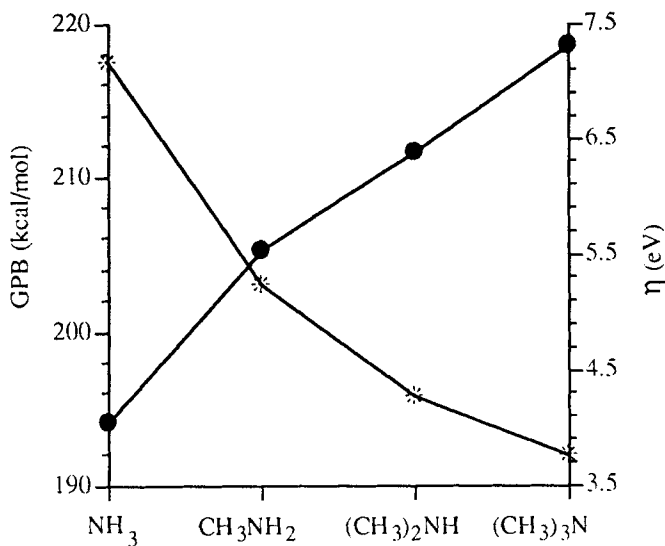


Figure 4. Gas-phase basicity and global hardness profiles for some aliphatic amines.

Table 5. PA (kcal/mol) for ozone, sulfine, glycine, alanine, cytosine, thymine, adenine and guanine.

Species	PWP/TZVP	BP/TZVP	B3LYP/6-311++G**	OTHER	EXP
O ₃	149.4	146.8	143.4	149.5 ^a	148.0 ± 3
CH ₂ SO	188.4	207.8	193.8	188.3 ^b	188.0 ^g
Glycine	214.2	213.8	211.5	213.6 ^c	213.6 ^h
Alanine	216.0	215.5	215.5	216.7 ^d	215.8 ⁱ
Cytosine	/	229.1	/	227.0 ^d	225.9 ^l
Thymine	/	208.8	/	/	209.0 ^l
Adenine	/	225.8	/	/	224.2 ^l
Guanine	/	230.3	/	225.8 ^c	227.4 ^l

a) from ref. 80; b) from ref. 96; c) from ref. 14; d) from ref. 14; e) from ref. 97; f) from ref. 98; g) from ref. 99; h) from ref. 100; i) from ref 101; l) from ref. 102.

For glycine and alanine amino acids, all the employed functionals and basis sets are able to reproduce correctly the experimental PA and GPB values. A very good agreement between theoretical and experimental determinations is found also in the

case of the nucleic acid bases at BP level. The maximum deviation from experiment is of 3.2 kcal/mol (about 1.5%) and occurs for cytosine.

For O₃ and CH₂SO the BP values of PA appear to be the less accurate, but the examples concerning the protonation reactions on oxygen atom and the relative PA determinations are too limited to decide about the performance of density functional methods in this case.

Table 6. GPB (kcal/mol) for ozone, sulfine, glycine and alanine, and cytosine, thymine, adenine and guanine.

Species	PWP/TZVP	BP/TZVP	B3LYP/6-311++G**	OTHER	EXP
O ₃	142.3	139.7	135.6	/	/
CH ₂ SO	179.8	199.8	185.3	/	181.3 ^b
Glycine	206.2	205.8	203.8	206.7 ^a	206.2 ^c
Alanine	208.1	207.6	207.7	208.7 ^a	207.4 ^d
Cytosine	/	221.3	/	/	/
Thymine	/	201.3	/	/	//
Adenine	/	217.9	/	/	/
Guanine	/	222.7	/	/	/

a) from ref. 14; b) from ref. 99; c) from ref. 100; d) from ref. 101

In Figure 5 the theoretical PA values of several nitrogen containing compounds are compared with those proposed by experimental studies.

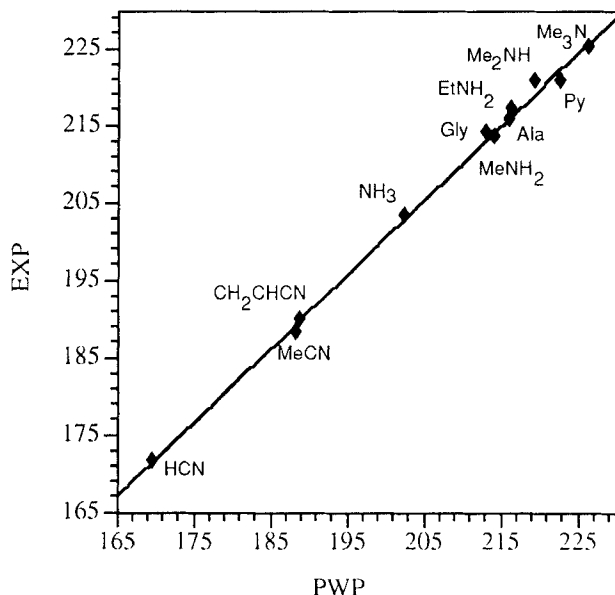


Figure 5. Theoretical proton affinity versus experimental values. Data are in kcal/mol. ($R^2 = 0.997$).

The fitting procedure shows that, for these compounds, in which the protonation occurs on nitrogen atom, the values of PA obtained at PWP/TZVP level can be treated with confidence.

3.3 Gas-phase acidity

In Table 7 we have reported ΔH^{acid} (the enthalpy variation for the deprotonation process) and the gas-phase acidity (GPA) at 298 K for the formic acid obtained at different levels of theory.

The use of B3LYP functional with the 6-31G** basis set is, as it is evident, insufficient to give reliable results of acidity: the error with respect to experimental value [103] is of 13.8 kcal/mol. A significant reduction of the discrepancy is obtained, gradually, improving the basis sets: the B3LYP/6-311++G**, /AUG-cc-pVTZ and /AUG-cc-pVQZ computations are affected by errors of about 4.0, 3.0 and 0.8 kcal/mol, respectively.

If the TZVP basis set is used in connection with hybrid potentials, the ΔH^{acid} value becomes 344.7 kcal/mol. The BP/TZVP and PWP/TZVP gradient corrected computations give ΔH^{acid} of 345.0 and 343.0 kcal/mol, respectively. BLAP3/TZVP and PLAP3/TZVP ΔH^{acid} deviate from experimental values by 3.4 and 1.2 kcal/mol. Considering that the experimental uncertainty is of ± 2 kcal/mol, almost all our results seem to be reliable as well as those obtained with GVB [104] and G2 [16] procedures. A good convergence is reached already with the TZVP basis set. The importance of this result lies in the possibility to compute GPA for larger system with acceptable computer efforts.

Table 7. GPA (in kcal/mol) at 298 K for formic acid.

Method	ΔH^{acid}	GPA	Ref.
B3LYP/6-31G**	358.8	351.0	this work
B3LYP/6-311++G**	341.0	333.3	this work
B3LYP/AUG-cc-pVTZ	342.0	334.2	this work
B3LYP/AUG-cc-pVQZ	345.8	338.1	this work
B3LYP/TZVP	344.7	337.0	this work
PWP/TZVP	343.0	335.2	this work
BP/TZVP	345.0	337.3	this work
BLAP3/TZVP	348.4	340.7	this work
PLAP3/TZVP	346.2	338.5	this work
GVB+CI	346.3	/	104
G2	343.8	/	16
G2(MP2)	344.2	/	16
G2(MP2,SVP)	344.1	/	16
EXP	345 \pm 2	/	103

The calculations performed for acetic and propanoic acids (see Table 8) confirm the opportunity to use the medium-sized TZVP basis set to obtain good results. On the other hand the lack of other theoretical data regarding the propanoic acid reflects the difficulty to treat, with expensive procedures, such a kind of system.

The relationship between total hardness and gas-phase acidity has been investigated in the case of the aliphatic alcohol series. Data are reported in Table 9 and depicted in Figure 6.

Table 8. GPA at 298 K (in kcal/mol) for acetic and propanoic acids.

Method	ΔH_{acid}	GPA	ΔH_{acid}	GPA
	CH ₃ COOH		CH ₃ CH ₂ COOH	
B3LYP/6-311++G**	345.0	337.2	345.2	337.5
B3LYP/TZVP	347.5	339.7	347.5	339.7
PWP/TZVP	346.5	338.7	345.9	338.1
BP/TZVP	348.5	340.8	350.9	343.2
GVB+CI	352.1 ^a	/	/	/
MP2	347.0 ^b	/	/	/
G2(MP2)	346.1 ^b	/	/	/
EXP	348. \pm 3 ^c	/	/	340.3 \pm 2 ^c

a) from ref. 104; b) from ref. 16; c) from ref. 95

Table 9. GPA at 298 K (in kcal/mol) and global hardness (in eV) values for alcohol series.

System	GPA _{B3LYP/6-311++G**}	GPA _{EXP}	η
MeOH	371.6	375.0 ^a	7.60
EtOH	368.3	370.7 ^a	6.25
n-PrOH	367.8	368.1 ^b	5.67
n-BuOH	367.4	367.1 ^b	5.11
n-PeOH	367.1	366.3 ^b	4.48

a) from ref. 95; b) from ref. 105

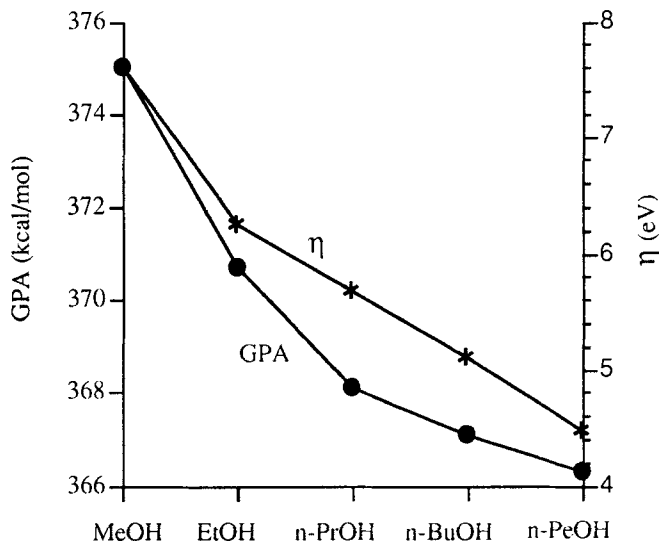


Figure 6. Experimental gas-phase acidity and global hardness profiles for some aliphatic alcohols.

It is possible to note that:

- theoretical and experimental values are in good agreement;
- the absolute GPA values decrease in going from MeOH to n-PeOH, consequently the acidity of the ROH increases;
- global hardness decreases underlying a lower affinity for the proton in the series.

Finally we have computed the GPA for glycine and alanine amino-acids. The results are collected in Table 10 together with the available experimental data. Single point calculations on the optimized MP2/6-31G* geometry have been performed at MP2 and MP4 levels with different basis sets (see Table 10).

Taking as reference the measured value [106] of 342.3 kcal/mol for glycine and 341.5 kcal/mol for alanine, and considering that experimental ΔG were obtained by assuming a fixed T ΔS (6.9 kcal/mol) that is lower than all other calculated values for both molecules, all our theoretical values can be defined quite good. In particular the G2 procedure gives a difference of -1.1 kcal/mol between the experimental and theoretical values in the case of glycine and -0.7 kcal/mol for alanine [107]. MP4/6-311+G** computations give errors of 1.0 (glycine) and 1.4 (alanine) kcal/mol.

At the MP2/6-311+G(d,p) level, ΔG deviations of -3.0 and -2.7 kcal/mol for glycine and alanine are found, respectively.

The deviations resulting from the B3LYP/6-311+G** (6-311++G**) computations are: -2.4 (-3.5) kcal/mol for glycine and -2.0 (-2.9) kcal/mol for alanine.

The gradient-corrected PWP/TZVP functional gives differences of -3.3 kcal/mol for both glycine and alanine. Finally the BP/TZVP ΔG values deviate from the experimental ones by 2.1 kcal/mol for glycine 0.1 kcal/mol for alanine.

Table 10. GPA (in kcal/mol) at 298 K for glycine and alanine amino-acids.

Method	ΔH^{acid}	GPA	ΔH^{acid}	GPA
	Glycine		Alanine	
MP2/6-311+G(3df,2p)	340.2	332.4	339.6	331.8 ^a
MP4/6-311+G**	344.2	336.4	343.7	335.9 ^a
B3LYP/6-311+G**	340.8	333.0	340.3	332.5
B3LYP/6-311++G**	338.7	331.9	339.1	331.6
PWP-TZVP	339.8	332.1	339.0	331.2
BP-TZVP	345.3	337.5	342.3	334.6
G2	342.1	334.3	341.5	333.8 ^a
EXP	342.3	335.4	341.5	334.5 ^b

a) from ref. 107; b) from ref. 106

3.4 Metal ion affinity

The determination of the metal ions affinity for the organic bases is important to elucidate the acid-base reaction mechanism as well as to obtain information about fundamental biochemical processes (i.e. synthesis, replication structural integrity and cleavage of DNA and RNA) [108].

Because of the presence of the metal, theoretical investigation is often difficult and requires an appropriate treatment of electron correlation and the use of opportune basis sets.

Recently Del Bene [109] has investigated the basis set and the correlation energy effect on lithium ion affinities for a series of first- and second- row neutral bases employing the Hartree-Fock and the Moller-Plesset perturbation methods.

We have performed similar calculations, in the framework of density functional theory, with the aim to define the basis set convergence limit and the influence of the exchange-correlation potential on the interaction of lithium cation with ammonia.

Data are reported in Table 11 together with previous theoretical [109] and experimental [110] results.

The B3LYP computations are strongly influenced by the basis set quality. In fact, as in other cases, the 6-31G** set does not describe well the interaction. Our data, together with those reported in literature and included in Table 11, provide further evidences about the importance of the inclusion of diffuse functions on non-hydrogen atoms in order to obtain better agreement with experiment. From the Table it is clear that, good accuracy, can be reached employing medium sized basis sets. Using the same TZVP bases, we have tested the role of the exchange-correlation functionals in the determination of Li^+ affinity for NH_3 . Comparison with measured value reveals that B3LYP/TZVP gives the better MIA (37.4 vs 39.1 kcal/mol) followed by PWP/TZVP (36.6 kcal/mol) and BP/TZVP (28.3 kcal/mol). Both the calculations performed by the LAP3 functional do not differ significantly with respect to those executed at PWP and BP levels, respectively. In other words, this fact, could mean that the choice of the exchange functional is important.

Table 11. MIA at 298 K (in kcal/mol) of Li^+ for NH_3

Method	MIA	Ref.
B3LYP/6-31G**	45.6	this work
B3LYP/6-311++G**	40.1	this work
B3LYP/cc-pVTZ	41.4	this work
B3LYP/AUG-cc-pVTZ	39.1	this work
B3LYP/TZVP	37.4	this work
B3LYP/cc-pVQZ	40.1	this work
B3LYP/AUG-cc-pVQZ	39.3	this work
PWP/TZVP	36.6	this work
BP/TZVP	28.3	this work
BLAP3/TZVP	29.9	this work
PLAP3/TZVP	36.5	this work
MP2/cc-pVDZ	45.8	109
MP2/cc-pVTZ	41.2	109
MP2/cc-pVQZ	39.8	109
MP2/AUG'-cc-pVDZ	38.6	109
MP2/AUG'-cc-pVTZ	38.7	109
MP2/AUG'-cc-pVQZ	38.9	109
MP4/cc-pVDZ	45.4	109
MP4/cc-pVTZ	41.1	109
MP4/AUG'-cc-pVDZ	38.4	109
MP4/AUG'-cc-pVTZ(-df)	39.1	109
MP4/AUG'-cc-pVTZ	38.6	109
HF/AUG'-cc-pVTZ	39.8	109
CCSD(T)/AUG'-cc-pVTZ	38.7	109
EXP	39.1	110

On the basis of the performed benchmark on ammonia, we have extended the study to the first terms of aliphatic amine series, using only the B3LYP/6-311++G** computational procedure. The results are collected in Table 12. The theoretical values follow strictly the experimental trend.

Taking into account that experimental absolute lithium affinities are accurate to ± 2 kcal/mol [110], and that the values referred to the different amines are very close, we can attribute to the used method a good reliability in the reproduction of these parameters.

Table 12. Absolute Li^+ affinities (MIA) at 298 K (in kcal/mol).

System	$\text{MIA}_{\text{B3LYP/6-311++G**}}$	$\text{MIA}_{\text{EXP}}^{\text{a}}$
NH_3	40.1	39.1
CH_3NH_2	41.5	41.1
$(\text{CH}_3)_2\text{NH}$	42.3	42.2
$(\text{CH}_3)_3\text{N}$	41.7	42.1

a) from ref. 110

The next example regards the determination of Li^+ and Na^+ ions affinity for glycine and cytosine. Because our aim is also that to establish what functional can have general reliability for all kind of systems, we have used, in this case, the PWP/TZVP combination. On the other hand this choice is easily justified by the similar MIA values of Table 11.

Table 13 resumes the results obtained. We can note that for glycine our values are quite similar to the measured ones. In the case of cytosine the MIA,s are overestimated by about 10 kcal/mol. This fact can be explained considering that Li^+ and Na^+ cations form a bridge bond with the N1 and O2 atoms of the ring, determining a redistribution of the net charges and consequently a bond order variation that, neither PWP/TZVP nor B3LYP/6-311++G** calculations are able to take into account.

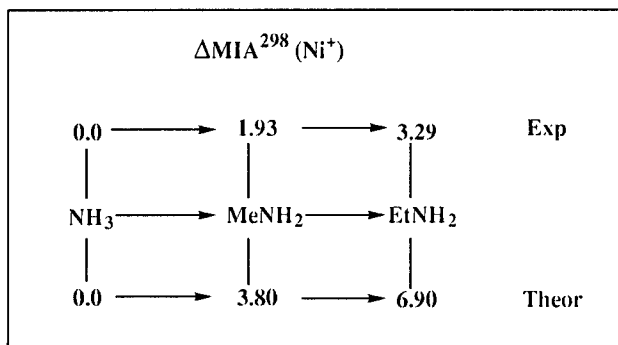
Table 13. Li^+ and Na^+ MIA (kcal/mol) at 298 K for glycine and cytosine.

System	$\text{MIA}_{\text{PWP/TZVP}}$	MIA_{EXP}
Gly- Li^+	54.2	51.0 ^a , 51.9 ^b
Gly- Na^+	42.1	39.4 ^a , 38.0 ^b
Cyt- Li^+	62.5	55.5 ^a
Cyt- Na^+	53.2	42.3 ^a

a) from ref. 111; b) from ref. 112

Finally we have performed some calculations in order to verify the performance of density functional methods in the prediction of MIA when transition metals are involved. Because of the availability of the experimental information [113], we have chosen to investigate the interaction of Ni^+ cation with ammonia, methyl- and ethyl-ammonia. The relative metal ion affinity (ΔMIA) values are shown in the Scheme 4 and compared with experimental counterparts. The dissociation limit for Ni^+ -amine

systems is represented by the metal ion in the its ground state (2D) and the free amines. As it is evident B3LYP/6-311++G** computation reproduces only the trend proposed by the experiment, but the absolute values are strongly overestimated. The same behaviour has been obtained with the PWP functional. The overestimation is related to the well known fact that density functional methods fail in the description of electronic states of transition metal isolated atoms [7-9]. For this reason, present results must be considered as qualitative rather than quantitative indications.

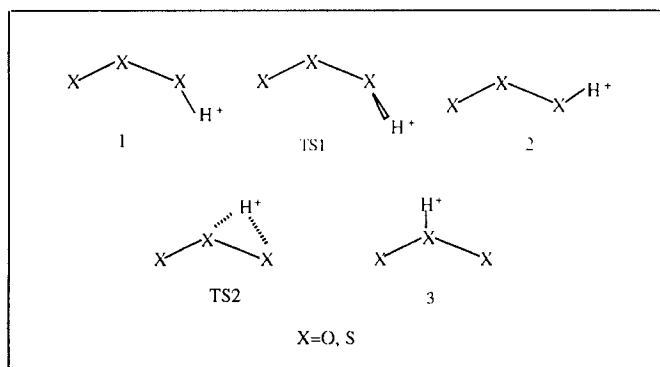


Scheme 4

3.6 Potential energy surfaces

The study of reaction paths, in DFT, is not a new [114,115]. Thus we have chosen to explore the potential energy surfaces (PES) introducing the possibility to rationalize the results through the computations of the global hardnesses along the whole reaction path, with the aim to verify if, for the studied processes, the maximum hardness principle (MHP) [53] is satisfied.

In the scheme 5 are depicted the stationary points of O₃ and S₃ protonation paths studied at PWP/TZVP level.



Scheme 5

Energetic and hardness profiles are drawn in Figures 7 and 8, respectively.

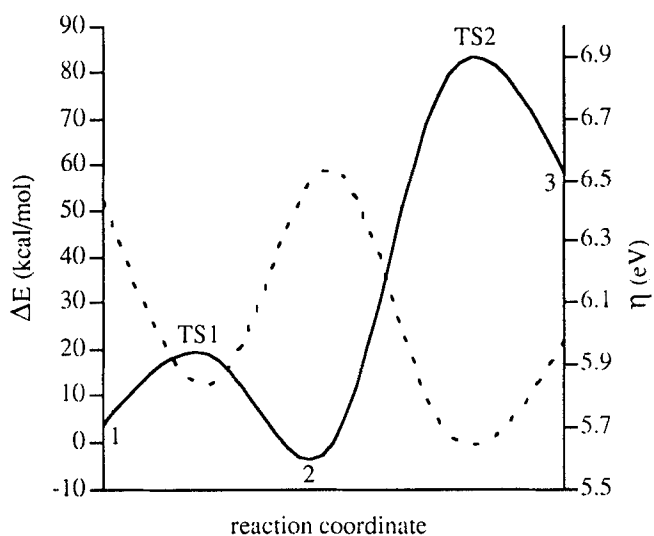


Figure 7. Relative energies and global hardness profiles for the protonation reaction of O_3 .

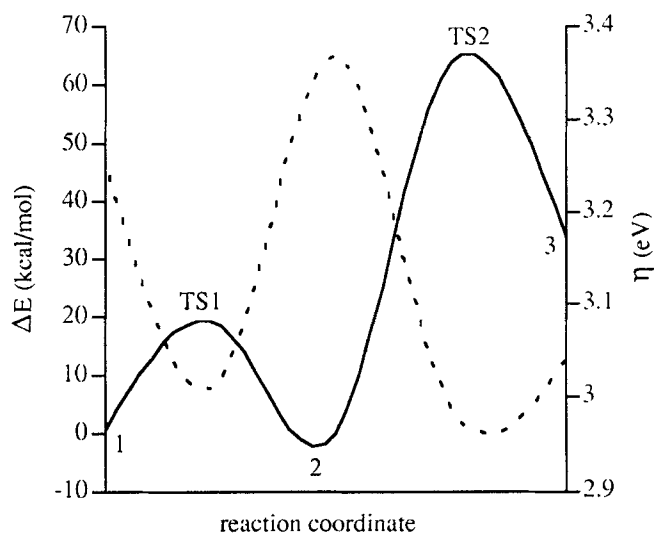


Figure 8. Relative energies and global hardness profiles for the protonation reaction of S_3 .

From the energetic point of view the trans isomer 2 is the global minimum in the PES of both processes followed by 1 and 3 structures. Two transition states connect the 1-2 (TS1) and 2-3 (TS2) isomers.

Following the MHP principle, we must expect that the energetic and hardness curves, as a function of the reaction coordinate, be specular, if the chemical potential does not change significantly along the reaction paths. As is evident from Figure 7 and 8, this circumstance is verified for both the studied processes.

In particular the maximum hardness value is found for the absolute minimum and decreases in correspondence of relative minima and transition states following the stability order.

4. Conclusions

From the results presented above, we make the following conclusions:

- In the determination of ions geometries, the comparison with experimental data, underlines, in some case, the importance of the employed functional in determining reliable structures.

- Accurate information on preferred attack sites and potential energy surfaces can be obtained with computational costs lower than those required by HF methods including configuration interaction.

- Thermochemical properties are well reproduced even with medium-sized basis sets such as the 6-311++G** and TZVP.

- Metal ions affinities, for transition metal containing systems, can be defined good from a qualitative point of view, but, the absolute values are not so accurate and require improvements in the computation of atomic energy.

- DFT based descriptors of reactivity are powerful tools for the explanation of all examined processes.

Acknowledgements

We are grateful to the Italian MURST and CNR and Bulgarian National Scientific Foundation for financial support.

References

- [1] Salahub, D. R. and Zerner, M. C.(eds.), 1989, "*The Challenge of d and f electrons*", Am. Chem. Soc., ACS Symp. Ser. n. 394, Washington.
- [2] Labanowski, J. and Andzelm, J. (eds.), 1991, "*Density Functional Methods in Chemistry* ", Springer Verlag, New York.
- [3] Chong, D. P. (ed.), 1995, "*Recent Advances in Density Functional Methods.*", World Scientific, Singapore, Vol 1.
- [4] Chong, D. P. (ed.), 1997, "*Recent Advances in Density Functional Methods.*", World Scientific, Singapore, Vol 2.
- [5] Seminario, J. M. and Politzer, P. (eds.), 1995, "*Density Functional Theory: a Tool for Chemistry* ", Elsevier, New York.
- [6] Seminario, P. (ed.), 1996, "*Recent Developments and Applications of Modern Density Functional Theory.*", Elsevier, New York.
- [7] Salahub, D. R. and Russo, N. (eds.), 1992, "*Metal Ligand Interaction. From Atoms, to Clusters, to Surfaces* ", Kluwer, Dordrecht.

- [8] Salahub, D. R. and Russo, N. (eds.), 1996, ""*Metal-Ligand Interactions: Structure and Reactivity*", Kluwer, Dordrecht.
- [9] Ziegler, T., *Chem. Rev.*, **91**, (1990) 651.
- [10] Johnson, B. G., Gill, P. M. W. and Pople, J. A., *J. Chem. Phys.*, **98**, 5612 (1993).
- [11] Kohn, W., Parr, R.G. and Becke, A.D., *J. Phys. Chem.*, **100**, 12974 (1996).
- [12] Chandra, A. K. and Goursot, A., *J. Phys. Chem.*, **100**, 11596 (1996).
- [13] Marino, T., Russo, N., Sicilia, E. and Toscano, M., in "*Selected Topics in Mass Spectrometry in the Biomolecular Sciences*", Caprioli, R. M., Malorni, A., Sindona, G. (eds.), 1997, Kluwer, Dordrecht, 163.
- [14] Topol, I.A., Burt, S. K., Toscano, M. and Russo, N., *J. Mol. Struct. (Theochem)*, **430**, 41 (1998).
- [15] Merril, G. N. and Kass, S. R., *J. Phys. Chem.*, **100**, 17465 (1996).
- [16] Smith, B. J. and Radom, L., *Chem. Phys. Lett.*, **254**, 123 (1995).
- [17] Mineva, T., Russo, N., Sicilia, E. and Toscano, M., *JCS Faraday Trans.*, **93**, 3309 (1997).
- [18] Pointet, K., Milliet, A., Hoyau, S. and Renou-Gonnord, M. F., *J. Computat. Chem.*, **18**, 629 (1997).
- [19] Russo, N., Toscano, M., Grand, A. and Jolibois, F., *J. Computat. Chem.*, **19**, 989 (1998).
- [20] De Proft, F., Amine, S., Choho, K. and Geerlings, P., *J. Phys. Chem.*, **98**, 5227 (1994).
- [21] Remko, M., Liedl, K. R. and Rode, B. M., *JCS Perkin Trans. 2*, 1743 (1996).
- [22] Cooks, R. G. and Kruger, T. L., *J. Am. Chem. Soc.*, **99**, 1279 (1977).
- [23] Kebarle, P., *Ann. Rev. Chem. Phys.*, **28**, 445 (1979).
- [24] Kohn, W. and Sham, L.J., *Phys. Rev.*, **A140**, 1133 (1965).
- [25] Gunnarsson, O., Johnson, M. and Lundquist, I., *Phys. Rev.*, **B20**, 3136 (1979).
- [26] Salahub, D. R., *Adv. Chem. Phys.*, **69**, 447 (1987).
- [27] Becke, A.D., *Phys. Rev.*, **A38**, 3098 (1988).
- [28] Becke, A.D., *J. Chem. Phys.*, **88**, 2547 (1988).
- [29] Becke, A. D., *J. Chem. Phys.*, **98**, 5648 (1993).
- [30] Perdew, J.P., Wang, Y., *Phys. Rev.*, **B33**, 8800 (1986).
- [31] Perdew, J.P., *Phys. Rev.*, **B33**, 8822 (1986).
- [32] Lee, C., Yang, W. and Parr, R. G., *Phys. Rev.*, **B37**, 785 (1988).
- [33] Perdew, J. P., *Phys. Rev.*, **B45**, (1992) 13244; *ibid.* **B44**, 13298 (1991).
- [33] Perdew, J. P., *Physica*, **B172**, 1 (1991).
- [34] Proynov, E. and Salahub, D. R., *Phys. Rev.*, **B49**, 7874 (1994).
- [35] Harris, J., *Phys. Rev.* **A29**, 1648 (1984).
- [36] Stevens, P. J., Devlin, F. J. Chabrowski, C. F. and Frisch, M. J., *J. Chem. Phys.*, **98**, 11623 (1994).
- [37] Baker, J., Andzelm, J., Muir, M. and Taylor, P. R., *Chem. Phys. Lett.*, **236**, 53 (1995).
- [38] Bauschlicher, C. W. and Partridge, H., *J. Chem. Phys.*, **103**, 1788 (1995).
- [39] Slater, J. C., *Phys. Rev.*, **81**, 385 (1951).
- [40] Vosko, S.H., Wilk, L. and Nusair, M., *Can. J. Phys.*, **58**, 1200 (1980).
- [41] Parr, R.G. and Pearson, R.G., *J. Am. Chem. Soc.*, **105**, 7512 (1983).

- [42] Gazquez, J. L., *Struct. and Bond.*, **80**, **27** (1993). Note that the definition of the hardness, given in the text differs from the original one by a conventional factor of 2.
- [43] Berkowitz, M. and Parr, R.G., *J. Chem. Phys.*, **88**, 2554 (1988).
- [44] Yang, W. and Parr, R. G., *Proc. Natl. Acad. Sci. USA*, **82**, 6723 (1985).
- [45] Chattaraj, P. K., Liu, G. H. and Parr, R. G., *J. Phys. Chem.*, **237**, 171 (1995).
- [46] Pearson, R. G. and Palke, W. E., *J. Phys. Chem.*, **96**, 3283 (1992).
- [47] Datta, D. *J. Phys. Chem.*, **96**, 2409 (1992).
- [48] Pal, N.; Vaval, N. and Roy, S. *J. Phys. Chem.*, **97**, 4404 (1993).
- [49] Chattaraj, P. K.; Nath, S. and Sannigrahi, A. B. *Chem. Phys. Letters*, **212**, 223, (1993).
- [50] Chattaraj, P. K.; Nath, S. and Sannigrahi, A. B. *J. Phys. Chem.*, **98**, 9143 (1994).
- [51] Kar, T. and Scheiner, S. *J. Phys. Chem.*, **99**, 8121 (1995).
- [52] Ghanty, T. K. and Ghosh, S. K. *J. Phys. Chem.*, **100**, 12295 (1996).
- [53] Pearson, R.G., *J. Chem. Educ.*, **64**, 561 (1987).
- [54] Galvan, M., Dal Pino, A. Jr. and Joannopoulos, *Phys. Rev. Letters*, **70**, 21 (1993).
- [55] Liu, G., H., *J. Chem. Phys.*, **106**, 165 (1997).
- [56] Grigorov, M., Weber, J., Chermette, H. and Tronchet, J.M.J., *Int. J. Quantum Chem.*, **61**, 551 (1997).
- [57] Mineva, T., Russo, N. and Sicilia, E., *J. Am. Chem. Soc.*, **120**, 9053 (1998).
- [58] Mineva, T., Neshev, N., Russo, N., Sicilia, E. and Toscano, M., *Adv. Quantum. Chem.*, in press.
- [59] Janak J.F., *Phys. Rev.*, **B18**, 7165 (1978).
- [60] Slater, J.C., 1974, "*The Self Consistent Field for Molecules and Solids*", McGraw-Hill, New York, v. 4.
- [61] Perdew, J.P. and Zunger, A. *Phys. Rev.*, **B23**, 5048 (1981).
- [62] Harris, J., *Int. J. Quantum Chem.*, **13**, 189 (1979).
- [63] Harris, J., *Phys. Rev.*, **A 29**, 1648 (1984).
- [64] Englisch, H. and Englisch, R., *Phys. Stat. Sol.*, **123**, 711 (1984); *ibidem*, **124**, 373 (1984).
- [65] Valiev, M.M. and Fernando, G.W., *Phys. Rev.*, **B 52**, 10697 (1995).
- [66] Gopinathan, M., S. and Withehead, M. A., *Israel J. Chem.*, **19**, 209 (1980).
- [67] Sanderson, R. T., 1976, in "*Chemical Bonds and Bond Energy*", Academic, New York, 2nd edn.
- [68] Parr, R.G and Yang, W., 1989, "*Density-Functional Theory of Atoms and Molecules*", Oxford University Press, New York.
- [69] Neshev, N. and Mineva T., in "*Metal-Ligand Interactions: Structure and Reactivity*", Russo, N. and Salahub, D. R., 1996, Kluwer, Dordrecht, 361.
- [70] Pearson, R. G., *Coord. Chem. Rev.*, **100**, 403 (1990).
- [71] Cohen, M. H., Ganduglia-Pirovano, M. V. and Kudrnovsky, J., *J. Chem. Phys.*, **101**, 8988 (1994); *ibidem* **103**, 3543 (1995).
- [72] Benson, S.W., 1976, "*Thermochemical Kinetics*", John Wiley & Sons, New York.
- [73] Frisch, M. J., Trucks, G. W., Schlegel, H. B., Gill, P. M. W., Johnson, B. G., Robb, M. A., Cheeseman, J. R., Keith, T. A., Petersson, G. A., Montgomery, J. A., Raghavachari, K., Al-Laham, M. A., Zakrzewski, V. G.,

- Ortiz, J. V., Foresman, J. B., Cioslowski, J., Stefanov, B. B., Nanayakkara, A., Challacombe, M., Peng, C. Y., Ayala, P. Y., Chen, W., Wong, M. W., Andreas, J. L., Replogle, E. S., Gomperts, R., Martin, R. L., Fox, D. J., Binkley, J. S., Defrees, D. J., Baker, J., Stewart, J. P., Head-Gordon, M., Gonzales, C., Pople, J. A., 1995, Gaussian Inc Pittsburg, PA.
- [74] St Amant, A., PhD Thesis, Universite de Montreal, Canada (1992).
- [75] UNICHEM 3.0 Cray Research Inc. 2360 Pilot Knob Road, Mendota Heights, MN 55, (1994).
- [76] Hariharan, P. C. and Pople, J. A., *Theor. Chim. Acta*, **28**, 213 (1973).
- [77] Godbout, N., Salahub, D. R., Andzelm, J. and Wimmer, E., *Can. J. Chem.*, **70**, 560 (1992).
- [78] Woon, D. E. and Dunning, T. H., *J. Chem. Phys.*, **98**, 1358 (1993).
- [79] Gozzo, F. C., and Eberlin, M. N., *J. Mass. Spectrom.*, **30**, 1553 (1995).
- [80] Meredith, C., Quelch, G. E. and Shaefer III, H. F., *J. Am. Chem. Soc.*, **113**, 1187 (1991).
- [81] Stewart, E. L., Foley, C. K., Allinger, N. L., and Bowen, J. P., *J. Am. Chem. Soc.*, **116**, 7282 (1994).
- [82] Clowney, L., Shri, S. C., Srinivasan, A. R., Westbrook, J., Olson, W. K. and Berman, H. M., *J. Am. Chem. Soc.*, **118**, 509 (1996).
- [83] Rubio, J., Russo, N. and Sicilia, E., *Int. J. Quantum Chem.*, **61**, 415 (1997).
- [84] Smith, R. L., Chyall, L. J., Beasley, B. J. and Kanttamaa, *J. Am. Chem. Soc.*, **117**, 7971 (1995).
- [85] Pollack, S. K., Devlin III, J. L., Summerhays, K. D., Taft, R. W. and Hehre, W. J., *J. Am. Chem. Soc.*, **99**, 4583 (1977).
- [86] Nold, M. J. and Wesdemiotis, C., *J. Mass. Spectrom.*, **31**, 1169 (1996).
- [87] Lias, S. G., Liebman, J. F. and Levine, R.D., *J. Phys. Chem. Ref. Data*, **13**, 695 (1984).
- [88] Adams, N. G., Smith, D., Tichy, M., Javaheryt, G., Twiddy, N. D. and Ferguson, E. E., *J. Chem. Phys.*, **91**, 4037 (1989).
- [89] Meot-Ner, M. and Sieck, W., *J. Am. Chem. Soc.*, **113**, 4448 (1991).
- [90] Szulejko, J.E. and McMahon, T.B., *J. Am. Chem. Soc.*, **115**, 7839 (1993).
- [91] Bisling, P. G. E., Ruhl, E., Brutschy, B. and Baumgartel, H., *J. Phys. Chem.*, **91**, 4310 (1987).
- [92] Smith, B. J. and Radom, L., *J. Am. Chem. Soc.*, **115**, 4885 (1993).
- [93] Smith, B. J. and Radom, L., *Chem. Phys. Lett.*, **231**, 345 (1994).
- [94] Smith, B. J. and Radom, L., *J. Phys. Chem.*, **99**, 6468 (1995).
- [95] Lias, S. G., Bartmess, J. E., Liebman, J. F., Holmes, J. L., Levin, R. D. and Mollard, W. G., *J. Phys. Chem. Ref. Data suppl.*, **1**, 17 (1988).
- [96] Ruttink, P. J. A., Francis, J. T., Burges, P. C. and Terlouw, J. K., *J. Phys. Chem.*, **100**, 9694 (1996).
- [97] Colominas, C., Luque, F. J. and Orozco, M., *J. Am. Chem. Soc.*, **118**, 6811 (1996).
- [98] Cacace, F. and Speranza, M., *Science*, **265**, 208 (1994).
- [99] Bouchoux, G. and Salpin, J. Y., *J. Am. Chem. Soc.*, **118**, 6516 (1996).
- [100] Zhang, K.; Zimmerman, D.M.; Chung-Phillips, A.; Cassidy, C.J., *J. Am. Chem. Soc.*, **115**, 10812 (1993).
- [101] Locke, M.J. and McIver, R.T., *J. Am. Chem. Soc.*, **105**, 4226 (1983).
- [102] Greco, F., Liguori, A., Sindona, G., Uccella, N., *J. Am. Chem. Soc.*, **112**, 9092 (1990).

- [103] Bartmess, J. E. and McGiver R. T., in "*Gas Phase Ion Chemistry*" Bowers, M. T., 1992, Academic Press, New York, Vol. 2.
- [104] da Motta Neto, J. and Nascimento, M. A. C., *J. Phys. Chem.*, **100**, 15105 (1996).
- [105] Boand, G., Houriet, R. and Gaumann, T., *J. Am. Chem. Soc.*, **105**, 2203 (1983).
- [106] O'Hair, R. A. J., Bowie, J. H. and Gronert, S., *Int. J. Mass Spectrom. Ion Processes*, **117**, 23 (1992).
- [107] Topol, I. A., Burt, S. K., Toscano, M. and Russo, N., *J. Am. Chem. Soc. Mass Spectrom.*, in press.
- [108] Lippard, S. A. and Berg, J. M., 1994, "*Principles of Bioinorganic Chemistry*", University Science Books, Mill Valley, CA.
- [109] Del Bene, J. E., *J. Phys. Chem.*, **100**, 6284 (1996).
- [110] Woodin, R. L. and Beauchamp, J. L., *J. Am. Chem. Soc.*, **100**, 501 (1978).
- [111] Cerda, B. A. and Wesdemiotis, C., *J. Am. Chem. Soc.*, **118**, 11884 (1996).
- [112] Bojesen, G., Breindhal, T. and Andersen, U., *Org. Mass Spectrom.*, **28** 1448 (1993).
- [113] Chen, L-Z. and Miller, J. M., *J. Organomet. Chem.*, **448**, 225 (1993).
- [114] Abashkin, Y., Russo, N. and Toscano, M., *Theoretica Chimica Acta*, **91**, 169 (1995).
- [115] Abashkin, Y., Burt, S. K. and Russo, N., *J. Phys. Chem.*, **101**, 8085 (1997).

A Recent Development of the CS INDO Model. Treatment of Solvent Effects on Structures and Optical Properties of Organic Dyes[‡]

by I. Baraldi, F. Momicchioli¹, G. Ponterini and D. Vanossi

Dipartimento di Chimica, Università di Modena, Via Campi 183, I41100 Modena, Italy

Abstract

A CS INDO scheme incorporating solvent polarity effects according to Klopman's model is applied to examine geometric modification and solvatochromism of merocyanine dyes exhibiting peculiar behaviours. Qualitatively speaking, the model reproduces quite well the most important effects. The advantages of the CS INDO-solvaton approach with respect to other semiempirical procedures including solvation are discussed.

Contents

1. Introduction

- 1.1 The CS INDO hamiltonian and its previous applications
- 1.2 Theoretical models of solvent
- 1.3 Merocyanines: the most suitable test systems

2. Electrostatic solvent effects within the CS INDO scheme

- 2.1 SCF solvaton model
- 2.2 Solvent effects on spectra
- 2.3 Computational details

3. Results and discussion

- 3.1 Detailed test calculations on merocyanine M1
- 3.2 Geometrical distortion and solvatochromism of merocyanines M2 and M3

4. Conclusions

[‡]dedicated to Professor G. Del Re

¹momicchioli@imoax1.unimo.it

1. Introduction

1.1 The CS INDO hamiltonian and its previous applications

The CS INDO model hamiltonian [1] was conceived as a practical tool for dealing with photophysical and photochemical properties of large conjugated systems such as laser dyes, natural pigments, etc. CS INDO has two main features: i) it is free from the most striking limitations of the current NDO-type techniques concerning ground state potential surfaces (conformations, rotational barriers, etc.), ii) it is capable of correctly describing both ground and excited state properties within one and the same approximation scheme and parametrization. The essential point of the modified INDO scheme was to replace the usual set of pure s, p, d etc. atomic orbitals with a corresponding set of hybridized orbitals reflecting the molecular structure. The advantages deriving from the use of orbital hybridization within a delocalized MO-SCF treatment have been recently reviewed with reference to the CS INDO method [2] and are clarified by Barbier and Berthier in this issue from a more general point of view [3]. A common question of these approaches is the hybridization procedure. Initially we used hybrid orbitals adapted to the geometry of the molecule (i.e. directed along the bonds) [1], but the current CS INDO version adopts the automatic hybridization procedure formulated by Del Re in 1963 for s, p orbital sets [4] and later adapted for the treatment of lone pairs [5,6] and s, p, d basis sets [7]. However, apart from the implemented procedure, in the CS INDO method the orbital hybridization is above all a way of preparing a set of "chemical orbitals" [3] (σ , π , n) enabling an effective parametrization of the different core interactions to be found with reference to their "chemical" character (σ - σ , σ - π , π - π , etc.). For a full description of the CS INDO method we refer to previous work [1,2,8]. Here, we simply recall that after an exhaustive test on conformations and electronic spectra of conjugated non-rigid hydrocarbons (e.g. diarylethylenes [9] and biaryls [10]) during the last decade the CS INDO hamiltonian has been successfully adapted to the study of ground and excited state properties of quite a few more systems, including cyanine dyes [2,11], donor-acceptor-type stilbene derivatives [12], sulphur compounds [8] and carbenes [13]. Recently, the CS INDO method has proved to be a very suitable frame for working out a new quantum-mechanical CIPSI-type approach to the properties of electronically excited states of very large molecular and supramolecular systems [14]. The latest application of CS INDO concerned the calculation of spin-spin nuclear coupling constants of conjugated polyenes and cyanines by a second-order double perturbation treatment [15].

1.2 Theoretical models of solvent

Going on with the developing strategy of our method, lately we have faced the problem of the solvent effects in the CS INDO frame. In previous papers [2,11d,11e,12] we had limited ourselves to evaluating the solvation energy of a solute molecule within the solvaton model [16,17] using the atomic charges derived from a CS INDO SCF CI treatment of the isolated molecule. Although such procedure can provide qualitatively reasonable predictions about the effects of the solvent polarity on the electronic transitions [18] and the potential energy surfaces [2,11d,11e,12], it disregards the effects of the solvent on the electronic structure of the solute molecules. The latter effects are generally accounted for according to two different approaches [19]: the so-called supermolecule approach, in which the solvent molecules surrounding a solute molecule are explicitly included in the quantum-mechanical calculation, and the continuum approach in which the operator of the solute-solvent interaction is approximated representing the solvent as a polarizable continuous medium. In the present paper, we report a CS INDO SCF CI study for solvated molecules falling within the continuum theories [20] and based, in particular, on the classic solvaton model [16] which is known to be very suitable for semiempirical methods [21-23]. An alternative simple model, often implemented at the semiempirical level, is the self-consistent reaction field (SCRF) model [24] based on the Onsager dipolar approximation. This technique, however, has two main drawbacks: i) it fails to deal with those solute structures where significant local charge densities result in vanishing dipole moments, and ii) it suffers from a certain arbitrariness involved in the choice of size and shape of the solute cavity. The solvaton model is formally free from both these limitations. In particular Klopman's model, where the polarized solvent is represented by a set of fictive charges reflecting the local charge distribution of the solute, may in principle account for "microscopic" details and, hence, may be an effective tool for describing solvent polarization effects. In principle, these procedures, like all continuum approaches, can only treat dielectric solvent effects. However, specific solvent effects can be described, too, within such schemes by extending the quantum mechanical calculation to include the solute molecule and some strongly interacting solvent molecules (semi continuum approach [19]).

1.3 Merocyanines: the most suitable test systems

To test the effectiveness of the new CS INDO-based procedure we searched for compounds exhibiting large solvent effects on their structural and optical properties. From this point of view merocyanine dyes are most suitable in view of the dramatic dependence of their UV/vis spectra on the solvent polarity [25,26]. The current interpretation of this behaviour is based on the fact that merocyanines are formed by an amino group (electron donor) and a carbonyl

group (electron acceptor) linked by a conjugated system so that their π -electronic structure can be qualitatively described in terms of resonance between a neutral form and a charge-separated form as shown in Fig.1 for three selected chromophores (M1, M2, M3). Thus, the structural and spectral changes observed with merocyanines on changing the polarity of the solvent can be regarded as the result of a solvent-induced change in the relative stability of the two predominant mesomeric structures. Following up a concise report of the results concerning M1 and M3 [27], in this work we present an exhaustive study on the three chromophores of Fig.1.

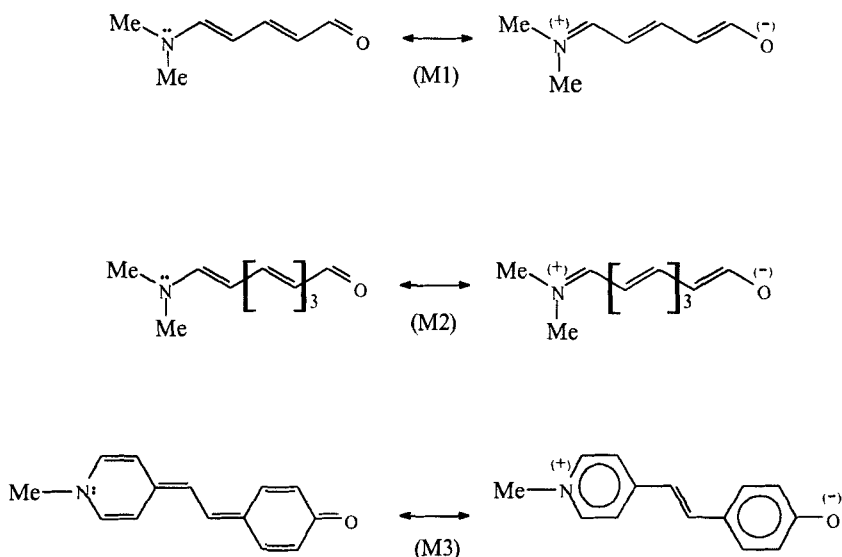


Figure 1: Neutral and charge-separated resonance structures of two vinylogue merocyanine dyes (M1, M2) and a conjugated betaine dye (stilbazolium betaine) (M3).

The proposed calculation procedure will be first tested by analysing in detail the effects of the solvent polarity on the structure and electronic spectra of the simple merocyanine M1. Afterwards, the selected calculation procedure will be applied to the more complex dyes M2 and M3, characterized by equal length of the conjugated path connecting the donor and acceptor group, but exhibiting opposite solvatochromic effects. To be precise, the acyclic merocyanine M2 shows, like the simpler chromophore M1, positive solvatochromism [25] (i.e. bathochromic shift of the first absorption band on increasing solvent polarity),

while M3 (the widely studied stilbazolium betaine [28-31]) provides a typical example of negative solvatochromism [25] (i.e. hypsochromic spectral shift on increasing solvent polarity). It will be shown that the CS INDO method, incorporating the SCF treatment of the solute-solvent interaction according to the solvaton model, is capable of correctly describing the main modifications, both geometrical and spectral, of merocyanine dyes accompanying a change of the solvent polarity. Moreover, we notice that the interpretative success of the valence bond formulation of Fig.1 suggests that the polarization of the solvent surrounding the solute should primarily reflect the π -electron charge distribution. This problem will be thoroughly analysed in section 3, where we will show that, within the solvaton model, the observed behaviours of π -conjugated donor-acceptor chromophores can generally be well described using the net π -electron charges.

2. Electrostatic solvent effects within the CS INDO scheme

2.1 SCF solvaton model

As said in section 1, the electrostatic solute-solvent interaction was incorporated in the CS INDO SCF equations according to Klopman's formulation [16] of the virtual charge model. Briefly, the physical model consists in associating with each atom of the molecule, with net charge Q , an imaginary particle (solvaton) with charge $-Q$, simulating the local reaction field generated by the orientated solvent distribution and interacting with all molecular charges according to Born's law [32]. This model leads to generalized Born equations for the solvation energy like that proposed by Hoijtink et al. as early as 1956 [33] and afterwards put by Heidrich et al. [17] in the form

$$E_{sol} = k(\epsilon) \left[\sum_A^N \frac{Q_A Q_{A'}}{r_A^{eff}} + \sum_A^N \sum_{B'(\neq A')}^N \frac{Q_A Q_{B'}}{r_{AB} + r_B^{eff}} \right] \quad (1)$$

where $k(\epsilon) = \frac{\epsilon - 1}{2\epsilon}$, ϵ being the dielectric constant of the solvent, Q_A is the net atomic charge on atom A , $Q_{A'} = -Q_A$ is the charge of the solvaton associated with atom A , r_{AB} is the distance between atoms A and B , and $r_{A(B)}^{eff}$ (the effective radius of atom $A(B)$) is used as a parameter to correctly balance the interactions of a solvaton with the atomic centre to which it is attached and with adjacent atomic centres. Eq. (1) using the net atomic charges of the unsolvated molecule, can provide a reasonable evaluation of the electrostatic solvent effects on the molecular energy in the ground and the excited states [2,11d,11e,12], but in order

to describe the effects of the polarized solvent on the molecular charge distribution, solvation has to be explicitly included in the SCF MO calculation. Germer [21] was the first to incorporate the solvent effects into an SCF treatment using the solvaton model within an all-valence-electron Mulliken type SCF MO method [34]. Afterwards, the solvaton model was applied by Miertus and Kysel [22,23] in the framework of neglect of differential overlap (NDO) methods of the PPP and CNDO type. In this work, we implemented the same model within the CS INDO method. In short, seeing that the solvent is represented as a set of point charges (solvatons), the electronic hamiltonian of a solute molecule may be written as

$$\hat{H}_{el}^s = \hat{H}_{el}^0 - k(\varepsilon) \left[\sum_i^M \sum_{B'}^N \frac{Q_{B'}}{r_{iB'}} - \sum_A^N \sum_{B'}^N \frac{Z_A Q_{B'}}{r_{AB'}} \right] \quad (2)$$

where \hat{H}_{el}^0 is the usual gas-phase hamiltonian and the second term represents the solute-solvent interaction. In eq. (2) indexes i , A and B' refer to electrons, nuclei and solvatons, respectively, Z_A is the core charge of atom A , $r_{iB'}$ is the electron-solvaton distance and $r_{AB'}$ is the nucleus-solvaton distance, other symbols having the same meaning as in eq. (1). As is evident, \hat{H}_{el}^s depends on the molecular charge distribution, so the Schroedinger equation $\hat{H}_{el}^s \Psi = E \Psi$ turns out to be non-linear in the function Ψ . Sanhueza et al. [35] have shown that in these cases the solutions of the Schroedinger equation cannot be obtained from the direct variation of the functional $\langle \Psi | \hat{H}_{el}^s | \Psi \rangle / \langle \Psi | \Psi \rangle$. In order to overcome this difficulty one has to choose between two strategies: 1) to formulate a modified SCF procedure based on an appropriate variational functional [35] or 2) to solve the problem iteratively by carrying out a sequence of standard SCF calculations with fixed solvaton charges [20]. According to the second approach, which was adopted in the present study, the Fock operator (electron i) including the solvent interaction and the corresponding Fock matrix element $F_{\mu\nu}^s$ take the simple forms

$$\hat{F}^s(i) = \hat{F}^0(i) - k(\varepsilon) \sum_{B'}^N \frac{Q_{B'}}{r_{iB'}} \quad (3)$$

and

$$F_{\mu\nu}^s = F_{\mu\nu}^0 + V_{\mu\nu} = F_{\mu\nu}^0 - k(\varepsilon) \sum_{B'}^N \left\langle \chi_\mu(i) \left| \frac{Q_{B'}}{r_{iB'}} \right| \chi_\nu(i) \right\rangle \quad (4)$$

The integrals appearing in the second term of eq. (4), that may have attractive or repulsive character according to the sign of the solvaton charge $Q_{B'}$, should be evaluated as consistently as possible with the assumptions of the adopted all-valence-electron method. This point deserves some attention since at times the solvent interaction matrix elements have been evaluated using approximations different from those peculiar to the calculation of $F_{\mu\nu}^0$ [36,37]. To be more precise, the electron-solvaton interaction integrals of eq. (4) are assimilable to electron-core attraction integrals $\left\langle \chi_\mu(i) \left| \frac{-Z_B}{r_{iB}} \right| \chi_\nu(i) \right\rangle$ and hence should be treated in an equivalent manner. In particular, if all the INDO assumptions are used [38] the Fock matrix element, eq. (4), reduces to the following form,

$$F_{\mu\mu}^s = F_{\mu\mu}^0 - k(\varepsilon) \sum_{B'}^N Q_{B'} \gamma_{AB'} \quad (\mu \in A) \quad (5)$$

$$F_{\mu\nu}^s = F_{\mu\nu}^0$$

where the only non-vanishing elements of the solvent interaction matrix are the diagonal ones, $\left\langle \chi_\mu(i) \left| \frac{Q_{B'}}{r_{iB'}} \right| \chi_\mu(i) \right\rangle$, expressed in terms of solvaton charges $Q_{B'}$ and electron repulsion integrals $\gamma_{AB'}$. It should be noted that use of the CNDO assumptions yields the same matrix elements as far as the solvent interaction is concerned [22,23]. On the other hand, the same approximation has been also adopted within NDDO type schemes [37], where the non-diagonal matrix elements $\left\langle \chi_\mu(i) \left| \frac{Q_{B'}}{r_{iB'}} \right| \chi_\nu(i) \right\rangle$, $\mu, \nu \in A$, should in principle be retained [38]. We also notice that within this scheme the CS INDO based approach differs from other NDO-type procedures only for the calculation of the \hat{F}^0 matrix elements. Moreover, in keeping with eq. (1) $\gamma_{AA'}$ and $\gamma_{AB'}$ entering the electron-solvaton interaction terms should be calculated using $r_{AA'} = r_A^{\text{eff}}$ and $r_{AB'} = r_{AB} + r_B^{\text{eff}}$ respectively. This choice, implying $\gamma_{AA'} < \gamma_{AA}$ and $\gamma_{AB'} < \gamma_{AB}$, is expected to guarantee a qualitatively correct ratio between "monocentric" and "bicentric" electron-solvaton interactions. However, as already found by Miertus and Kysel [22], the results are not significantly influenced by taking $\gamma_{AA'} = \gamma_{AA}$ and

$\gamma_{AB'} = \gamma_{AB}$. Thus, for the sake of simplicity, we used the set of γ_{AB} integrals for both electron-electron and electron-solvaton interactions.

The virtual charge model was reappraised from a more general point of view by Costanciel and Tapia [39]. They referred to the total electrostatic energy of the charge system, including the self-energy of the solvaton system neglected in Klopman's model [16], and found that, in order to recover the Born formula for the solvation energy, the $k(\epsilon)$ factor of the solute-solvent interaction term had to be taken equal to $\frac{\sqrt{\epsilon}-1}{\sqrt{\epsilon}}$ rather than to $\frac{\epsilon-1}{2\epsilon}$. However, as has already been pointed out [23,29,40,41], such modification has little practical importance since, owing to the qualitative character of the model, $k(\epsilon)$ should be considered as a parameter related to the medium polarity. Moreover, following the approach proposed by Jano [42,43], Costanciel and Tapia split up the solvaton system into a set of point virtual charges $k(\epsilon)Z_{B'}$, corresponding to the charges of the atomic cores Z_B , and a virtual charge distribution $k(\epsilon)\rho'$, corresponding to the electron charge distribution ρ , and thereby got for the solvent interaction matrix element the form

$$V_{\mu\nu} = -k(\epsilon) \left[\sum_B^N \left\langle \chi_\mu(i) \left| \frac{Z_{B'}}{r_{iB'}} \right| \chi_\nu(i) \right\rangle + 2 \sum_j^{occ} \left\langle \chi_\mu(i) \left| \hat{J}_j \right| \chi_\nu(i) \right\rangle \right] \quad (6)$$

where the second sum is over the occupied molecular orbitals. As is evident, this expression of $V_{\mu\nu}$ is quite different from the one of eq. (4) derived according to Klopman's model. However, both expressions yield the Fock matrix elements given in eq.s (5) when CNDO or INDO approximations are applied. The two treatments become non-equivalent only going beyond the INDO level of approximation (NDDO, *ab initio*). That said, the Klopman model, describing the solvent surrounding the solute molecule as a set of point charges Q_A , seemed to us to be preferable for its simplicity.

Once the closed-shell Hartree-Fock equations including electrostatic solute-solvent interaction have been solved, the total energy of the solvated molecule at the SCF level is obtained by the expression

$$E^s = \frac{1}{2} \sum_\mu \sum_\nu P_{\mu\nu}^s (h_{\mu\nu}^s + F_{\mu\nu}^s) + E^{CR} + k(\epsilon) \left[\sum_A^N \sum_{B'}^N Z_A Q_{B'} \gamma_{AB'} \right] \quad (7)$$

where the first term represents the electronic energy of the solute molecule in the field of the solvaton, E^{CR} is the core-core repulsion energy and the last term is the core-solvaton interaction energy. In principle, the geometry of the ground state molecule in a given solvent, i.e. at a fixed value of $k(\epsilon)$, has to be determined by minimizing E^s with respect to the structural parameters. Such a direct approach to the solvent-induced geometry distortions is unfeasible through the current NDO procedures adopting spectroscopic parametrizations (CNDO/S, INDO/S) because of the overall imbalances between attractive and repulsive interactions characterizing these hamiltonians. As a matter of fact, previous CNDO/S type studies using the virtual charge model evaluated the geometry changes by resorting to empirical relationships between bond lengths and bond population indexes [29,40,41]. On the other hand, thanks to the correct force balance peculiar to the CS INDO hamiltonian, we were able to perform direct geometry optimizations with qualitatively good results.

2.2 Solvent effects on spectra

The optimized ground state geometry and the corresponding SCF molecular orbitals were the starting data for investigating solvent-induced shifts of the absorption spectra by a proper CI treatment. Details of the adopted procedures will be given in the next paragraph. Here, we will simply outline the general aspect of the approach. Briefly, we have to do with the calculation of the electronic transition of a solvated molecule from the equilibrium ground state to a Franck-Condon excited state. Such a transition occurs in a time too small to allow the oriented solvent cage to rearrange appreciably, so the solvaton charges experienced by the Franck-Condon excited state are practically those suitable to the ground state (Q_{B^*})¹. This condition is automatically satisfied by the calculation since the excited configurations are developed on the SCF MOs optimized for the ground configuration of the solvated molecule. In other words, the CI calculation will provide directly the properties of the “vertical” absorption transition.

It is worth noting that the so-obtained spectral shift, i.e. the difference in transition energy between solvated and gas phase molecules, can be seen as made up of two contributions: 1) a polarization contribution ΔE_{pol} reflecting the effects of the polarized solvent on the electronic structure of the solute, and 2) an

¹ This description disregards instantaneous effects due to solvent polarization induced by the change in charge density associated with the electronic transition [19]. In principle such effects may be appreciable [24], but we will shortly show (section 3) that the solvatochromic behaviours of merocyanines can be correctly predicted in terms of the only effects related to the dielectric constant of the solvent.

electrostatic contribution ΔE_{sol} related to Coulomb interactions between atomic and solvaton charges. This decomposition is obtainable considering that the molecular orbital energies in the presence of the solvent can be expressed as:

$$\varepsilon_j^s = \langle \phi_j^s(1) | \hat{F}^s(1) | \phi_j^s(1) \rangle = \varepsilon_j^p - k(\varepsilon) \sum_A \sum_{\mu \in A} \sum_{B'} c_{\mu j}^2 Q_{B'} \gamma_{AB'} \quad (8)$$

where ε_j^p is the energy of the j^{th} molecular orbital in the absence of the solvent, yet including polarization effects, and the second term represents the electrostatic interaction between electron 1, formally assigned to orbital j , and the solvatons. Using eq. (8) the energy of the transition from the ground to an excited configuration can be expressed as the sum of a contribution for the isolated solvent-polarized molecule and an electrostatic contribution. For a mono-excited singlet configuration, e.g. the H \rightarrow L one (H=HOMO, L=LUMO) characterizing the intense long wavelength transition of the molecules under study, the transition energy can be written as

$$\begin{aligned} E_{HL} &= \varepsilon_L^p - \varepsilon_H^p + 2K_{HL} - J_{HL} + k(\varepsilon) \sum_A \sum_{\mu \in A} \sum_{B'} Q_{B'} \gamma_{AB'} (c_{\mu H}^2 - c_{\mu L}^2) \\ &= E_{HL}^p + k(\varepsilon) \sum_A \sum_{B'} \Delta Q_A Q_{B'} \gamma_{AB'} \end{aligned} \quad (9)$$

where the first term provides the polarization contribution through the relationship $\Delta E_{pol} = E_{HL}^p - E_{HL}^0$, and the second term is nothing but ΔE_{sol} , i.e. the analogue of the classic solvation effect obtainable by eq. (1). In the case of a multiconfigurational S-CI description of the excited state, the decomposition $\Delta E = \Delta E_{pol} + \Delta E_{solv}$ can be made as well by deriving $\Delta Q_A = Q_A^* - Q_A$ from the CI calculation for the isolated solvent-polarized molecule, but the result will be slightly different from that of the direct CI calculation for the polarized molecule in the presence of the solvent.

The main points of the above discussion concerning the absorption spectra hold also for the solvent polarity effects on the position of the fluorescence bands, provided that the time for the excited state equilibration (involving geometrical relaxation of the solute and solvent reorganization) is shorter than its lifetime. In this case, usually occurring in liquid solutions, the emission takes place from the equilibrium excited state to a Franck-Condon ground state, so in principle the fluorescence transition should be calculated using geometry and solvaton charges optimized for the excited state. The solution of this non-trivial problem is not

included in the present study which is specifically concerned with the solvation shifts of the absorption spectra.

2.3 Computational details

The CS INDO program [1,2], modified by the incorporation of the solute-solvent interaction as described in section 2.1, was used to calculate molecular geometries, charge distributions and electronic absorption spectra of the merocyanines M1-M3 (Fig.1) as a function of the solvent polarity index $k(\varepsilon)$.

The parametrization adopted in this work was the same as that discussed in detail in previous papers [1,11d,2]. Here, we will simply recall the following points:

1) The CS INDO screening constants $k_{\mu\nu}$, defined with reference to the set of hybrid AOs ($\mu, \nu = \sigma, \pi, n$) set up according to the Del Re method [4-7], were given the values: $k_{\sigma\sigma} = 1$, $k_{\pi\pi} = 0.55$, $k_{\sigma\pi} = 0.68$, $k_{n\pi} = 0.64$, $k_{n\sigma} = 0.74$, $k_{nn} = 0.71$.

2) The two centre repulsion integrals γ_{AB} were calculated according to Ohno-Klopman [44].

3) For the calculation of the core repulsion energy $E^{CR} = \sum_A \sum_{B>A} E_{AB}^{CR}$ [1], the atomic pair parameter α_{CO} was taken equal to 1.25 a.u. on the basis of C-O bond length optimizations in some test molecules. All other pair parameters α_{AB} were kept equal to 1.50 a.u. as in previous CS INDO applications.

For each of the three chromophores the geometry was first optimized at $k(\varepsilon) = 0$ starting from idealized structures near neutral forms (Fig.1)². In the optimization processes only the C-C, C-N, C-O and N-Me bond lengths were allowed to vary. The rings of M3 were assumed to be planar and have local C_2 symmetry. Moreover, the small length difference between d and f bonds of M3 (Fig.4) was *a priori* disregarded. The same procedure was then repeated for a set of increasing $k(\varepsilon)$ values starting each time from the optimized bond lengths of the preceding calculation. At every value of $k(\varepsilon)$ we first optimized the geometry using the net charges obtained for the isolated molecule ($k(\varepsilon) = 0$) as the solvaton charges. Lastly, all calculations were refined performing an iterative procedure, at fixed geometry, until convergence of the solvaton charges. All calculations of this phase, providing solvent-induced variations of ground-state geometries and charge distributions, were carried out at the simple SCF level.

² In the case of vinylogue merocyanine dyes such as M1 and M2, the neutral forms are often called "polyene like", while the names "quinonoid" and "benzenoid" are currently used to indicate the neutral and charge-separated form, respectively, of M3.

The solvent shift effects on the electronic absorption spectra were calculated within a standard S-CI approach, which is especially suitable for (mero)cyanines dyes considering the dominant role of the singly-excited (HOMO-LUMO) configuration in their longest wavelength absorption band [11]. In view of the qualitative character of the present study, minor effects due to polyexcited configurations were left out *a priori*. The MO active spaces were chosen each time to include all π , n and π^* molecular orbitals. Within this scheme, we calculated the energy of the first $\pi \rightarrow \pi^*$ transition, the associated oscillator strength and the excited state charge distribution and dipole moment as a function of $k(\epsilon)$. In principle, lone pairs of electrons on the oxygen atom might give rise to $n \rightarrow \pi^*$ transitions of rather low energies. On the other hand, $n \rightarrow \pi^*$ transitions were found by our calculations above the first $\pi \rightarrow \pi^*$ -essentially HOMO-LUMO- transition, except for the case of chromophore M1 at $k(\epsilon) = 0$ where the first excited singlet state was predicted to be of the $n\pi^*$ type. The presence of these states is of no consequence with regard to the pronounced solvatochromism of the first intense $\pi \rightarrow \pi^*$ absorption band of merocyanines, so we shall not discuss them in this study. Any analysis of the $n\pi^*$ excited states is therefore put off till future work concerning photophysical and photochemical properties of merocyanines.

Lastly, it is to be pointed out that the solvaton charges must be carefully selected in order to produce correct polarization effects. In particular, for merocyanine dyes virtual net π -electron charges appeared to be more suitable than total net atomic charges. This crucial point will be discussed in detail in section 3.1.

3. Results and discussion

3.1 Detailed test calculations on merocyanine M1

First, we will show that the field generated by the polarized solvent has to be conveniently modelled.

In fact, the inclusion of solute-solvent interaction in the SCF calculations allows the solvent effects on the electronic structure of the solute to be taken into account, but type and size of such effects are strongly dependent on the adopted solvent model. Within Klopman's model, where solvatons represent local fields generated by the solvent orientation, solvent effects follow a very simple mechanism first described by Germer [21]. Briefly, this consists in the tendency to an increase of electronic charge at a negative centre due to the positive charge of the solvaton associated with it (of course, the opposite tendency will occur at a positive centre). Now, according to the resonance theory picture of merocyanines (Fig.1), an increase in solvent polarity is expected to enhance the stability of the charge-separated form and, hence, to cause a drift of electrons from the amino

group to the carbonyl group. Thus, the solvaton charges must have rather definite characteristics in order that polarization effects may be correctly reproduced by calculations. In the case of a merocyanine dye, this requires a positive solvaton at the oxygen atom and a negative solvaton at the nitrogen atom to be simultaneously present. This way the electrons of the conjugated chain will experience an attractive force in the region of the acceptor group and, at the same time, a repulsive force in the region of the donor group. In general, however, MO SCF calculations do not meet this requirement since they lead to negative net charges, (i.e. positive solvatons) at both the oxygen and the nitrogen atomic centres. This is shown by Tab.1, which reports the net atomic charges of merocyanine M1 derived from CS INDO, INDO and AM1 [45] SCF calculations. As is evident, all SCF procedures yield similar results for the atoms of the conjugated system and assign oxygen and nitrogen atoms negative net charges. The net charges, both total and π type, associated with methyl groups as well as the net charges of the hydrogen atoms have minor importance in relation to the solvent polarity effects [27] and, accordingly, are disregarded in this discussion.

Table 1

Net total and π -electron charges on the atoms of the conjugated path as obtained for merocyanine M1 by CS INDO, INDO and AM1 MO SCF calculations. The calculated dipole moments and their components are also reported (last four rows).

	CS INDO		INDO		AM1	
	Total	π	Total	π	Total	π
N ₁	-.1260	.2306	-.1265	.2387	-.3095	.2343
C ₂	.1994	.0785	.1613	.0646	.0430	.0816
C ₃	-.1258	-.1499	-.0969	-.1379	-.3103	-.1994
C ₄	.1470	.1274	.1074	.0997	-.0259	.0925
C ₅	-.1240	-.1065	-.0904	-.0892	-.2886	-.1034
C ₆	.5818	.3934	.3145	.1847	.2071	.2775
O ₇	-.6137	-.5101	-.3263	-.2746	-.3111	-.3408
μ	8.3099		5.9293		6.3672	
μ_x^a	-8.0015		-5.7796		-6.2113	
μ_y^a	2.2430		1.3243		1.4001	
μ_z^a	0.		0.		0.	

^(a)For the orientation of the axes see Fig.2

The results of Tab.1 and the foregoing considerations on the polarization determining forces question the effectiveness of a solvaton field set up using directly the total net atomic charges. As a matter of fact, a series of detailed CS INDO calculations using the complete set of solvatons corresponding to the total net atomic charges led to unsatisfactory results for both solvent-induced geometrical distortions and spectral shifts of M1. To be more precise, charge distribution, bond lengths and HOMO-LUMO transition energy turned out to be scarcely sensitive to a change in polarity of the solvent in contrast with experimental evidence [18,25].

To overcome this impasse, the only thing to do is to adopt a solvaton set reflecting a right mixture of neutral and charge-separated resonance structures. From Tab.1 it emerges that a solvaton set of such a type is the one corresponding to the subset of the net π -electron charges that are not very dependent on the approximations of the method.

Concerning the use of the reduced solvaton set, two points are to be noticed. First of all this choice proved compulsory for merocyanines like M1 and M2, where the π -electronic structure in nonpolar solvent is better represented by the neutral form, while it is less important in merocyanines like M3 where the initial structure is characterized by almost equal contributions of the neutral and charge-separated forms. According to Griffiths [26] these two types of merocyanines can be classified as weakly polar (M1,M2) and moderately polar (M3), respectively. However, the use of the net π -electron charges is suitable for all donor-acceptor dyes, as it agrees with the resonance theory formulation, but generalization of this choice to chromophores of different types requires specific analyses. The second consideration is suggested by the calculated ground state dipole moments reported in Tab.1. The component analysis points out that all calculations predict the dipole moment to point roughly from the oxygen atom to the nitrogen atom. This means that SCRF techniques, where the solvent effects are introduced by the Onsager dipolar term [24,31], are less influenced by the local charge distribution and should at least be capable of correctly predicting the direction of effects. However, compared to this advantage, the SCRF approaches have the drawback of a dramatic dependence of the calculated solvent effects on the choice of the cavity size [31].

In the course of this paragraph we will present and discuss the result obtained on ground and first $^1(\pi\pi^*)$ excited state of M1 using a set of solvatons corresponding to the net π -electron charges. Figure 3 shows how the bond lengths within the conjugated chain are predicted to evolve on increasing the polarity factor $k(\epsilon)$. Clearly, on passing from $k(\epsilon)=0$ to $k(\epsilon)=0.9$ the C-C bond lengths evolve from an appreciable alternation, with b and d shorter than c and e (for labelling see Fig.2), towards equalization.

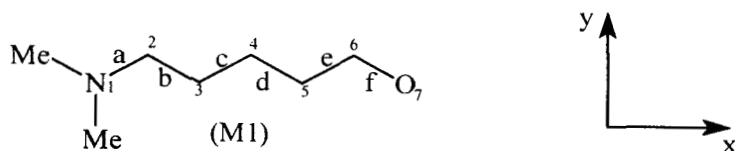


Figure 2: Numbering of atoms and labelling of bonds in chromophore M1. The axes orientation is also reported.

The effect can be quantified in terms of the bond length alternation (BLA) parameter, defined as the difference between the average length of “single” bonds and that of the “double” bonds [31]. Now, BLA changes from 0.048 at $k(\epsilon) = 0$ to 0.028 at $k(\epsilon) = 0.9$ (see Fig.3). With reference to the resonance theory picture of M1 (Fig.1), these BLA values mean that: i) in vacuum the neutral form is favoured, ii) on increasing the polarity of the solvent the weight of the ionic form augments but the cyanine-like structure (BLA=0) is not reached even in extremely polar media ($k(\epsilon) = 0.9$). Such behaviour is in keeping with the observed positive solvatochromism of chromophore M1 [25] since the cyanine-like structure (BLA=0) is expected to correspond to a maximum in the wavelength of the first absorption band. This will be shortly confirmed by CS INDO S-CI calculations of the excited state properties.

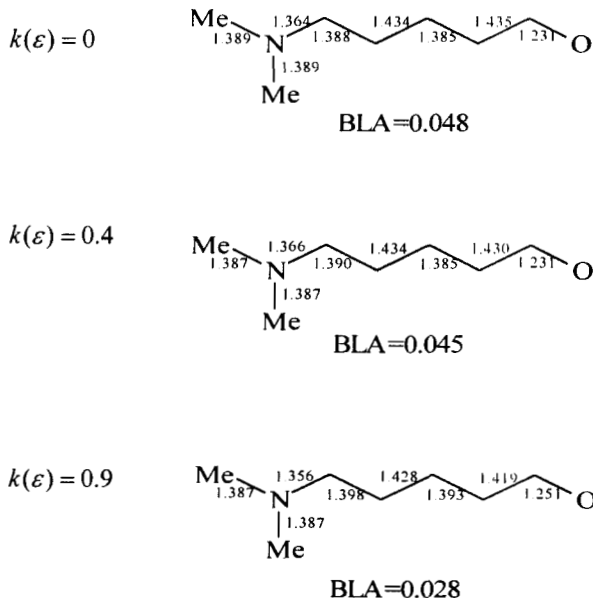


Figure 3: Ground state bond lengths and bond-length-alternation (BLA) parameters in (Å) of merocyanine M1 at three different values of the polarity factor $k(\epsilon)$. Bonds b-e (for labelling see Fig.2) were used to calculate BLA parameter.

The solvent induced changes of charge distribution and dipole moment are illustrated by Tab.2 (part A), where net charges of atoms other than nitrogen and oxygen have been disregarded for the sake of simplicity. Table 2 emphasizes the drift of electrons from the donor to the acceptor group, as well as the consequent dipole moment increase, accompanying an increase of the solvent polarity. Part B of Tab.2 shows that more marked effects are obtained after iterative refinement of the solvaton charges.

Table 2

Ground state net charges on nitrogen (Q_N) and oxygen (Q_O) atoms and dipole moments of M1 at six different values of $k(\epsilon)$, as obtained before (A) and after (B) iterative adjustment of the solvaton charges.

$k(\epsilon)$	A			B		
	Q_N	Q_O	μ/D	Q_N	Q_O	μ/D
0	-.1260	-.6137	8.310	-.1260	-.6137	8.310
0.2	-.0980	-.6838	9.480	-.0951	-.6918	9.656
0.4	-.0677	-.7494	10.629	-.0520	-.7813	11.462
0.6	-.0318	-.8167	12.040	.0263	-.8888	14.366
0.8	.0033	-.8807	13.384	.1313	-.9998	18.072
0.9	.0211	-.9122	14.071	.2147	-1.0542	20.333

Table 3

Properties of the first $^1(\pi\pi^*)$ excited state of M1 obtained at S-CI level before (A) and after (B) iterative adjustment of the solvaton charges: excitation energy (E), oscillator strength (f) and net charges on nitrogen (Q_N^*) and oxygen (Q_O^*) atoms at six different values of $k(\epsilon)$.

$k(\epsilon)$	A				B			
	E/eV	f	Q_N^*	Q_O^*	E/eV	f	Q_N^*	Q_O^*
0	4.349	1.310	.1392	-.6283	4.349	1.310	.1392	-.6283
0.2	4.283	1.294	.1700	-.6952	4.277	1.292	.1726	-.7029
0.4	4.223	1.282	.1991	-.7580	4.197	1.277	.2150	-.7882
0.6	4.150	1.292	.2213	-.8203	4.102	1.279	.2606	-.8883
0.8	4.099	1.296	.2488	-.8805	4.067	1.285	.3391	-.9940
0.9	4.079	1.297	.2604	-.9098	4.077	1.309	.4034	-1.0470

The analysis of the excited state properties of M1 as a function of the polarity factor $k(\epsilon)$, was performed with the geometry optimized for the ground state and adopting, for the sake of comparison, both the solvaton set corresponding to the net charges of the unsolvated molecule (calc. A) and the self-

consistent solvation set (calc. B). The results are summarized in Tab.3. Calculation A predicts a red shift of about 2200 cm^{-1} of the first $\pi \rightarrow \pi^*$ (essentially HOMO-LUMO) transition in the whole range of polarity considered (from $\sim 4.35\text{ eV}$ at $k(\epsilon) = 0$ to $\sim 4.08\text{ eV}$ at $k(\epsilon) = 0.9$). This prediction is in qualitative good agreement with an observed red shift of $\sim 4000\text{ cm}^{-1}$ of the long wavelength $\pi \rightarrow \pi^*$ absorption maximum of M1 on passing from n-hexane to water solution [25]. From a quantitative point of view, the solvent shift appears to be underestimated by the calculation, but for an accurate comparison one should state at what extent the observed shift in water may be affected by specific effects [46] disregarded by the theoretical model. Moreover, our prediction may be more or less appreciably affected by the neglect of the contribution due to instantaneous electron polarization of the solvent associated with the $S_0 \rightarrow S_1$ excitation. As a matter of fact, the SCRF-INDO/S study of Karelson and Zerner [24] including such contribution predicted a more marked red shift of the first $\pi \rightarrow \pi^*$ transition of M1. The oscillator strength is predicted to be little affected by a change of solvent polarity: it retains a value of about 1.3 in the entire range of $k(\epsilon)$, with a small drop at intermediate polarities. To our knowledge, no experimental data concerning solvent effects on the intensity of the long-wavelength band of M1 have been reported till now, so the quality of this prediction cannot be established at present. The comparison between the values of Q_N^* and Q_O^* with those of Q_N and Q_O of Tab.2 points out that the $S_0 \rightarrow S_1(\pi\pi^*)$ transition results in a charge-transfer between donor and acceptor group and, hence, in a dipole moment increase (see later). However, accurate comparative analysis of Tabs 2 and 3 reveals that the size of such charge transfer drops smoothly on going from $k(\epsilon) = 0$ to $k(\epsilon) = 0.9$. The results of calculation B are very similar apart from the following two aspects: i) the transition energy presents a minimum at $k(\epsilon) = 0.8$ (corresponding to a red shift of $\sim 2300\text{ cm}^{-1}$) that would involve the occurrence of a small blue shift (negative solvatochromism) at very high solvent polarity; ii) the decrease in charge-transfer character of the $S_0 \rightarrow S_1$ transition with increasing the solvent polarity is a little more pronounced than that found with calculation A. The small negative solvatochromism at $k(\epsilon) > 0.8$ has never been observed. On the other hand, given the indeterminate relationship between $k(\epsilon)$ and the dielectric constant of the solvent, we cannot attach a clear meaning to the results obtained at values of $k(\epsilon)$ as high as 0.8-0.9.

The above trends of the ground and excited state charge distributions obtained by calculations A and B indicate that: i) $S_0 \rightarrow S_1$ transition brings about a dipole moment increase, the size of which decreases with an increase in solvent polarity, and ii) at all $k(\epsilon) > 0$ the dipole moment increase predicted by calculation B is smaller than that found by calculation A. This is clearly

confirmed by Fig.4 where are reported the ground and excited-state dipole moments of M1 calculated by A and B procedures at six different values of $k(\epsilon)$. Among other things, the results of Fig.4 are consistent with the current interpretation of the observed solvatochromic effect in terms of dipole moment variations associated with the electronic transition.

Finally, we will briefly discuss the splitting up of the π - π^* shift in a polarization (ΔE_{pol}) and an electrostatic (ΔE_{solv}) contribution. Table 4 reports the results obtained by both A and B procedures using eq.9 valid for the single-configuration (HOMO-LUMO) description of S_1 . With both procedures ΔE_{pol} and ΔE_{solv} have in general the same sign but their relative contribution changes markedly with a change in $k(\epsilon)$.

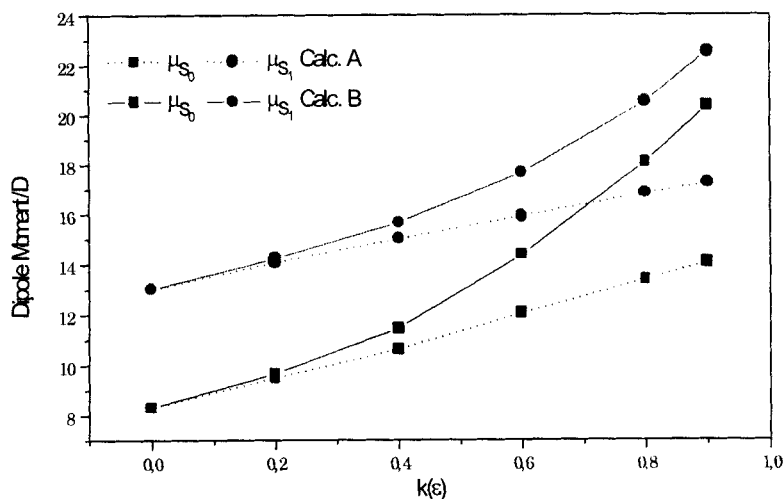


Figure 4: Dipole moments (in D) of the ground state (S_0) and the first $^1(\pi\pi^*)$ excited state (S_1) of chromophore M1 as a function of the polarity factor $k(\epsilon)$. Excited state dipole moments were calculated at the S-CI level.

In particular, the polarization contribution, which dominates at low polarity, decreases with increasing $k(\epsilon)$ becoming comparable (calc. A) or smaller (calc. B) than the electrostatic one. However, ΔE_{pol} contributes significantly even at high values of $k(\epsilon)$. This may explain at least partly why in a previous CS

INDO CI calculation on a M1-like compound [18], introducing only electrostatic effects through eq.1, the solvent shift of the long wavelength $\pi\text{-}\pi^*$ transition had been underestimated.

Table 4

Analysis of the solvent shift of the $\pi\text{-}\pi^*$ (HOMO-LUMO) transition of M1 in terms of polarization (ΔE_{HL}^{pol}) and electrostatic (ΔE_{HL}^{solv}) contributions calculated according to eq.9. Calculation B included iterative adjustment of the solvaton charges.

$k(\epsilon)$	A				B			
	E_{HL}	ΔE_{HL}	ΔE_{HL}^{pol}	ΔE_{HL}^{solv}	E_{HL}	ΔE_{HL}	ΔE_{HL}^{pol}	ΔE_{HL}^{solv}
0	4.603	—	—	—	4.603	—	—	—
0.2	4.549	.054	.055	-.001	4.545	.058	.061	-.003
0.4	4.499	.104	.096	.008	4.480	.123	.111	.012
0.6	4.430	.173	.131	.042	4.401	.202	.107	.095
0.8	4.384	.219	.134	.085	4.391	.212	.034	.178
0.9	4.366	.237	.122	.114	4.415	.188	.057	.131

3.2 Geometrical distortion and solvatochromism of merocyanines M2 and M3

On the basis of the results discussed in section 3.1, concerning solvation effects on structure and electronic spectrum of chromophore M1, we decided to carry out a corresponding study for merocyanines M2 and M3 (Fig.5) constituted by π -conjugated chromophores of the same "length", yet characterized by opposite solvatochromic behaviours.

The geometries were first optimized at various values of $k(\epsilon)$ by CS INDO SCF treatments with fixed solvaton charges corresponding to the net π -electron charges of the unsolvated molecules. Then, calculations of solvent effects on charge distributions and dipole moments of S_0 and first $^1(\pi\pi^*)$ excited state S_1 , as well as on the S_0 - S_1 transition energy were carried out by procedure B (i.e. including iterative refinement of the solvaton set) which is expected to stress the peculiarities of the two systems. Figures 6 and 7 report the optimized bond lengths of M2 and M3, respectively, and the corresponding BLA parameter at $k(\epsilon)=0.0, 0.4, 0.9$. Not surprisingly, the results concerning M2 (Fig.6) are similar to those presented in previous section for M1 in that the initial structure presents a marked bond length alternation (BLA=0.052) which weakens in

solvents of increasing polarity (BLA=0.040 at $k(\epsilon)=0.9$). In this case, however, the extent of bond equalization is a little smaller than that found for M1.

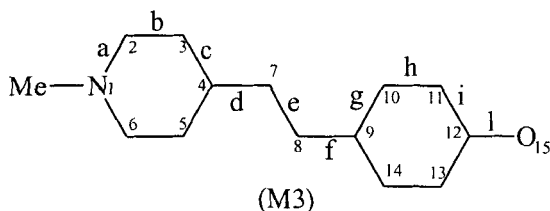
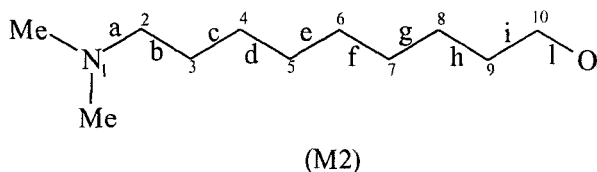


Figure 5: Numbering of atoms and labelling of bonds in merocyanines M2 and M3.

In other words, on increasing the solvent polarity the resonance hybrid (Fig.1) undergoes an enrichment in the ionic form, even if the neutral form remains the leading one. As we have said above for M1, such a BLA pattern is consistent with a positive solvatochromism in the entire range of $k(\epsilon)$. The solvent induced geometrical distortion of M3 shows a completely different trend (Fig.7) which can be most conveniently analyzed with respect to bonds d, e, f belonging to the central polymethinic fragment. Contrary to what is found with M2, in this case the initial structure is characterized by almost equalized bond lengths (BLA=0.016), with a very slight prevalence of the neutral (quinonoid) form. Increasing $k(\epsilon)$, BLA becomes negative at about $k(\epsilon)=0.4$ and drops to -0.021 at $k(\epsilon)=0.9$ reflecting an increasing relative weight of the charge-separated (benzenoid) form. The results of Figs 6,7 can be compared with those obtained by Albert *et al.* [31] using the SCRF model within the INDO method. The present work and ref. [31] are in good agreement as far as the general trends of the bond lengths are concerned.

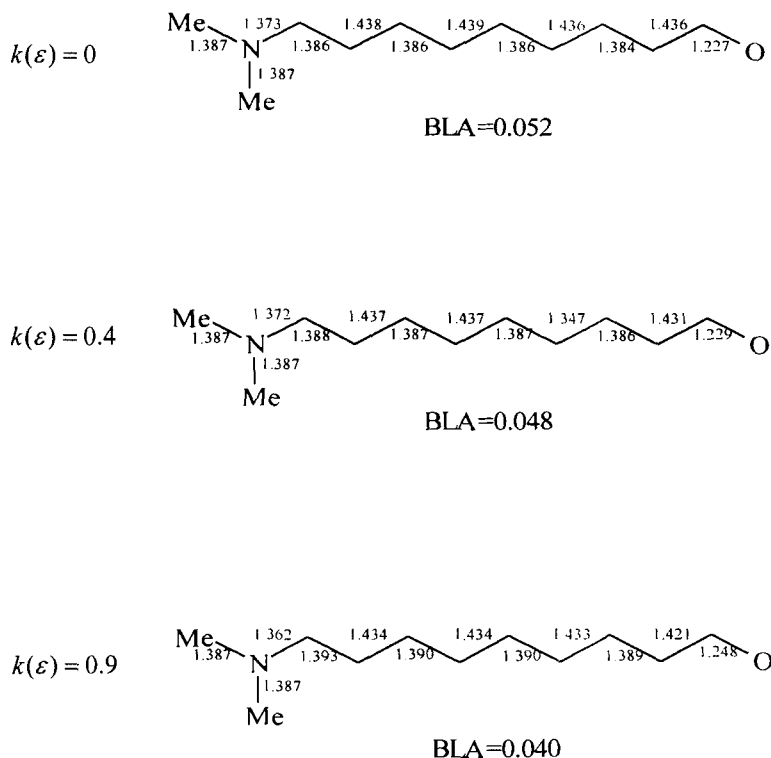


Figure 6: Ground state bond length and bond-length-alternation (BLA) parameter (in Å) of merocyanine M2 at three different values of the polarity factor $k(\epsilon)$. Bonds h-i were used to calculate BLA parameter. For labelling of the bonds see Fig. 5.

We simply note that the SCRf-INDO approach favours, more than ours, the neutral forms in non-polar media (BLA=0.086 and 0.038 for M1 and M3, respectively, at $\epsilon=1$) and finds a little higher variations of BLA on going from apolar to very polar solvents (BLA=0.073 and -0.026 for M2 and M3, respectively, at $\epsilon=78.5$). As for M3, even more pronounced BLA variations were found by Benson and Murrell within a simple PPP scheme [28] and by Botrel et al. [29] using the virtual charge model of Costanciel and Tapia [39] within the CNDO/S method (ref. [28]: 0.03 to -0.09, ref. [29]: 0.077 to -0.076). Direct comparison with ref.s [28,29], however, is not very significant since in both cases solvent-induced geometrical distortions were evaluated using empirical relationships between bond lengths and bond indexes.

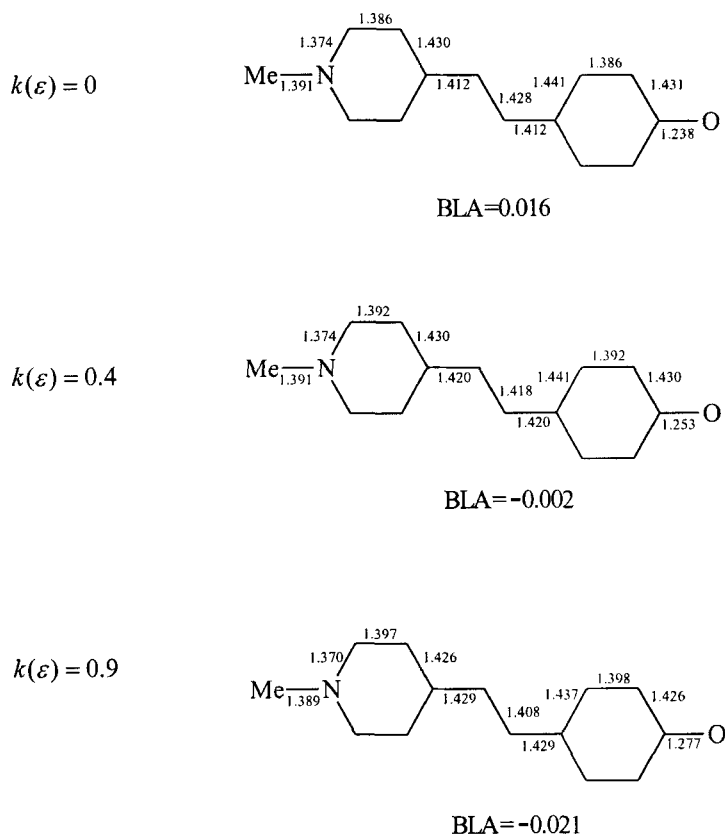


Figure 7: Ground state bond length and bond-length-alternation (BLA) parameter (in Å) of merocyanine M3 at three different values of polarity factor $k(\varepsilon)$. Bonds d, e and f were used to calculate BLA parameter. For labelling of the bonds see Fig.5.

The response of the charge distributions of M2 and M3 to an increase in solvent polarity is illustrated by Tab.5, where net charges on nitrogen and oxygen atoms and dipole moments are reported for six different values by $k(\varepsilon)$. In both M2 and M3 the electron population on the oxygen atom augments by about half an electron on going from $k(\varepsilon)=0$ to $k(\varepsilon)=0.9$, but the starting charge distributions are rather different. This is emphasized by the calculated dipole moments that amount to ≈ 9.9 D and ≈ 17.6 D for M2 and M3 at $k(\varepsilon)=0$ and undergo considerable increases of comparable size when the polarity factor passes from 0.0 to 0.9.

Table 5

Ground state net charges on nitrogen (Q_N) and oxygen (Q_O) atoms and dipole moments of chromophores M2 and M3 at six different values of $k(\epsilon)$, as obtained using the iteratively adjusted solvaton charges.

$k(\epsilon)$	M2			M3		
	Q_N	Q_O	μ/D	Q_N	Q_O	μ/D
0	-.1366	-.6085	9.892	-.0263	-.6919	17.630
0.2	-.1091	-.6836	11.552	.0384	-.7892	22.227
0.4	-.0723	-.7739	14.061	.1334	-.9070	28.826
0.6	-.0115	-.8811	18.230	.2655	-1.0179	35.788
0.8	.0836	-.9907	24.135	.4276	-1.1126	41.952
0.9	.1482	-1.0432	27.465	.5331	-1.1558	45.318

Now let us examine solvent effects on the properties of the first $^1(\pi\pi^*)$ excited state. Table 6 provides a summary of the calculation results and emphasizes the different behaviours of the two dyes. Like M1, chromophore M2 is predicted to undergo a positive solvatochromic effect of $\approx 2770 \text{ cm}^{-1}$ (0.34 eV) within the considered range of polarity. On the other hand, in M3 the $S_0 \rightarrow S_1$ transition undergoes first a slight bathochromic shift (between $k(\epsilon)=0$ and 0.2) and then a large hypsochromic shift resulting in a global negative solvatochromic effect of $\approx 6030 \text{ cm}^{-1}$ (0.75 eV).

Table 6

Properties of the first $^1(\pi\pi^*)$ excited state of chromophores M2 and M3 at the S-CI level: excitation energy (E), oscillator strength (f) and net charges on nitrogen (Q_N^*) and oxygen (Q_O^*) atoms at six different values of $k(\epsilon)$. Calculations used the iteratively adjusted solvaton charges.

$k(\epsilon)$	M2				M3			
	E/eV	f	Q_N^*	Q_O^*	E/eV	f	Q_N^*	Q_O^*
0	3.546	2.235	-.0200	-.6186	2.944	2.270	.0155	-.6709
0.2	3.495	2.207	.0124	-.6927	2.912	2.089	.0647	-.7613
0.4	3.414	2.174	.0510	-.7811	2.955	1.806	.1406	-.8762
0.6	2.293	2.132	.1065	-.8848	3.193	1.497	.2583	-.9913
0.8	3.212	2.063	.1912	-.9912	3.526	1.320	.4256	-1.0882
0.9	3.203	2.034	.2511	-1.0426	3.692	1.243	.5399	-1.1370

All these predictions are in very good agreement with experimental data. In fact, for chromophore M2 Albert *et al.* [31] reported a 2533 cm^{-1} red shift of the main absorption band ($\tilde{\nu}_{\text{max}}/\text{cm}^{-1}=23810$ in *n*-hexane and 21277 in dimethylformamide) while stilbazolium betaine (M3) is very well known for its considerable negative solvatochromism ($\tilde{\nu}_{\text{max}}/\text{cm}^{-1}=16130$ [25] or 16142 [46] in chloroform and 22520 [25] or 22624 [46] in water). Moreover, the existence of an inverted solvatochromism of M3 at low polarity, already predicted by other semiempirical calculations including solvation [28,29], has been experimentally confirmed [46]. Table 6 shows that quite different solvent effects are also predicted for M2 and M3 as far as the intensity of the main absorption band is concerned. Such effects are negligible for M2, where the oscillator strength undergoes just a slight drop of 0.2 on going from $k(\epsilon)=0$ to $k(\epsilon)=0.9$, while they are very pronounced in the case of M3 where f falls from 2.27 at $k(\epsilon)=0$ to 1.24 at $k(\epsilon)=0.9$. Unfortunately, no clear experimental data regarding solvation effects on f have been reported, so for now the latter predictions cannot be validated.

Quite encouraging indications on the effectiveness of our CS INDO-solvaton approach come from a comparison with the previous theoretical studies [28,29,31]. A significant comparison is possible, in particular, with ref. [31] where dyes M2 and M3 were both studied within the SCRF model starting from INDO-SCRF optimized geometries and using an INDO/S type parametrization to calculate solvent dependent optical properties. The results of ref. [31] confirm the difficulties of the SCRF model related to the choice of size and shape of the cavity including the solvent molecule. As a matter of fact, no choice of the cavity radius (spherical cavities were assumed) proved able to give reasonable predictions for the opposite solvatochromism of M2 and M3. Realistic cavity radii, related to actual molecular sizes, led to overestimation of the positive solvatochromic effect of M2 ($\sim 5200\text{ cm}^{-1}$ instead of 2533 cm^{-1}) and predicted a slight positive solvatochromism for M3, too, in contrast with experimental evidence. On the other hand, the use of smaller radii evaluated in terms of the solute density led to an acceptable trend of the transition energy for stilbazolium betaine (M3) but produced at the same time a huge positive solvatochromic effect for M2 ($\sim 24000\text{ cm}^{-1}$). From these results, it seems to us that the SCRF model is inadequate to account for different solvatochromic behaviours, unless it resorts to *ad hoc* choices of the cavity size. Our CS INDO-solvaton model is free from this type of inadequacy since, as we have clearly shown, one and the same modelling of the solvaton set was able to correctly describe all the observed variations of the transition energy of M2 and M3 with solvation.

The comparison with refs [28,29] is less significant since they treated only the case of chromophore M3. Our work is in qualitatively good agreement with both of them as regards the pronounced negative solvatochromism of M3 as well

as the turn-up of the transition energy at low solvent polarity. We notice, however, that those papers largely overestimated the global solvation effect (ref. [28]: $\sim 10500\text{ cm}^{-1}$; ref. [29]: $\sim 9700\text{ cm}^{-1}$; this work: $\sim 6030\text{ cm}^{-1}$; expt.: 6390 cm^{-1} [25], 6480 cm^{-1} [46]). This is related to the fact that, as we said above, ref.s [28,29] predicted a very large variation of BLA reflecting a big imbalance of the resonance hybrid towards the charge-separated (benzenoid) form on going from non-polar to very polar solvents.

Finally, we shall discuss the solvent polarity effects on excited state charge distributions and dipole moments (Tab.6 and Figs 8,9). As already found for M1 (calc. B), in chromophore M2 $S_0 \rightarrow S_1$ excitation induces an appreciable charge transfer from donor to acceptor group, the size of which drops slightly with increasing the solvent polarity. Such a trend, which emerges comparing in detail Tab.5 and Tab.6, implies that: i) $S_0 \rightarrow S_1$ excitation brings on an increase in dipolar moment at all values of $k(\epsilon)$, and ii) $\Delta\mu(S_1 - S_0)$ decreases smoothly on increasing the polarity of the solvent. This is emphasized by Fig.8 which enables the above discussed solvatochromic behaviour to be interpreted in terms of dipole moment variations [25]. Of course, things are quite different for chromophore M3. Comparison between Q_N^*, Q_O^* (Tab.6) and Q_N, Q_O (Tab.5) shows that at all values of $k(\epsilon)$, except for $k(\epsilon) = 0$, $S_0 \rightarrow S_1$ excitation causes a slight enrichment of the resonance hybrid in the quinonoid form. As a direct consequence, the excited-state dipole moment is lower than that of the ground state (Fig.9) consistently with the negative solvatochromism of chromophore M3.

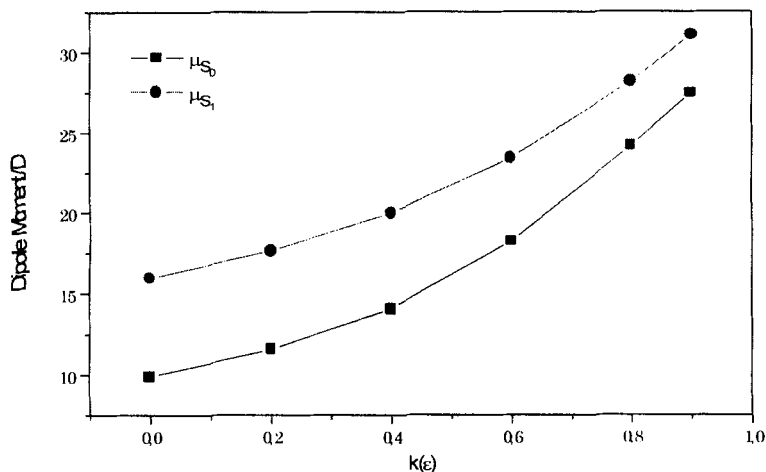


Figure 8: Dipole moments (in D) of the ground state (S_0) and the first $^1(\pi\pi^*)$ excited state (S_1) of chromophore M2 as a function of the polarity factor $k(\epsilon)$. Excited state dipole moments were calculated at the S-CI level.

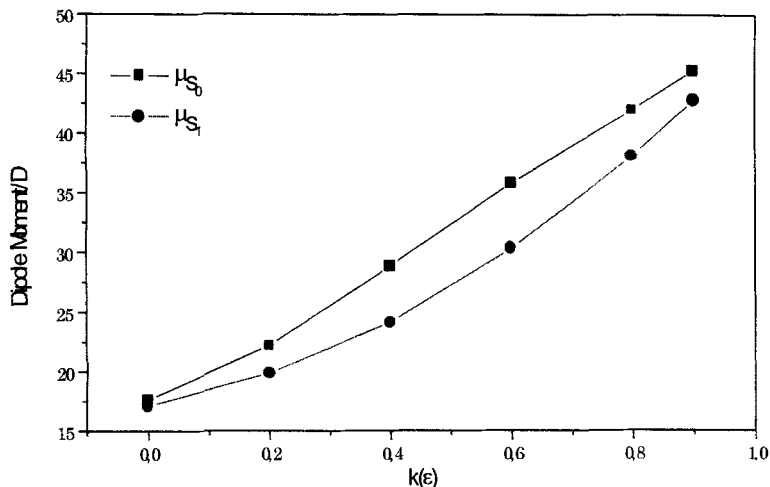


Figure 9: Dipole moments (in D) of the ground state (S_0) and the first $^1(\pi\pi^*)$ excited state (S_1) of chromophore M3 as a function of the polarity factor $k(\epsilon)$. Excited state dipole moments were calculated at the S-CI level.

The small positive solvatochromism of M3 at low polarity is reflected by the different behaviour at $k(\epsilon) = 0$ where charge distribution and dipole moment were found to be almost unaffected by $S_0 \rightarrow S_1$ excitation.

4. Conclusions

Molecules with extended π -conjugation are receiving an increasing attention for a number of applications involving in general their electronic excited states. In particular, donor-acceptor organic chromophores (e.g. donor-acceptor stilbene derivatives, push-pull polyenes, merocyanines, etc.) have recently attracted great interest with reference to their peculiar emission as well as linear and non-linear optical properties. The theoretical treatment of these problems calls for a pragmatic quantum-chemical procedure combining simplicity and adaptability to the study of the above mentioned systems in different contexts. The CS INDO model, set up according to a pseudo-potential type criterion using hybridized atomic orbitals, has proved to be a quite useful tool in this field. Aiming at further improving the method, lately we have faced the problem of introducing the solvent interaction in the CS INDO SCF scheme. As a first step we disregarded specific interactions and limited ourselves to treating electrostatic interactions in the frame of the continuum model. In keeping with the aims of the

method we adopted the classic solvation model which assures the maximum simplicity and does not require additional parameters as do, for instance, approaches based on the reaction field model. To probe the effectiveness of the CS INDO-solvation scheme we addressed merocyanine dyes for their well known sensitiveness to the solvent polarity and we concentrated, in particular, on the positive solvatochromism of two vinylogue merocyanine dyes (M1, M2) as opposite to the large negative solvatochromism of stilbazolium betaine (M3). The detailed results reported here are quite satisfactory for both the geometrical distortions and the spectral shifts induced by changes in the medium polarity. We stress, particularly, the success of the simple CS INDO-solvation approach in predicting both direction and order of magnitude of solvatochromic effects. This was achieved without especial devices apart from the use of solvation sets reflecting the net π -electron charges, a model consistent with the current interpretation of the solvatochromism of donor-acceptor dyes in terms of the relative weights of a neutral and a charge-separated structure. As a logical development, now we might introduce specific interactions by treating the "solute" as a supermolecule, formed by a solute molecule and some strongly hydrogen bonded solvent molecules, embedded in the dielectric continuum. Similarly, a supermolecule approach might be used to study dielectric solvent effects on the optical properties of aggregates of dye molecules.

Lastly, we want to point out that the CS INDO based procedure reported here is capable of correctly describing solvent effects on both ground- and excited-state properties by one and the same hamiltonian. This represents a methodological improvement with respect to all other semiempirical approaches that are forced to use different model hamiltonians (e.g. INDO, INDO/S) for geometry optimization and electronic structure calculation, or to bypass the problem of a direct geometry optimization resorting to empirical relationships between bond lengths and bond indexes.

Acknowledgements

The authors wish to express their gratitude to Prof. G. Berthier for many stimulating discussions and assistance in the course of this work and to Profs. C. Barbier and A. Rastelli for their help with the hybridization procedures. Thanks are also due to Università di Modena and Consiglio Nazionale delle Ricerche (Roma) for financial support.

References

- [1] F. Momicchioli, I. Baraldi and M.C. Bruni, *Chem.Phys.* **70**,161 (1982); *ibid.*, **82**, 22 (1983).
- [2] F. Momicchioli, I. Baraldi, A. Carnevali and G. Ponterini, in: *Strategies and applications in quantum chemistry*, Y. Ellinger, M. DeFranceschi Eds., Kluwer Acad.Pub., p379, Dordrecht, The Netherlands (1996).
- [3] C. Barbier and G. Berthier, *Adv. Quantum Chem.* ,this issue.
- [4] G. Del Re, *Theor. Chim Acta* **1**, 188 (1963).
- [5] G. Del Re, U. Esposito and M. Carpentieri, *Theor. Chim. Acta* **6**, 36 (1966).
- [6] S. A. Pozzoli, A. Rastelli, and M. Tedeschi, *J. Chem. Soc. Faraday II* **69**, 256 (1973).
- [7] G. Del Re and C. Barbier, *Croat. Chim. Acta* **57**, 787 (1984).
- [8] A. Carnevali, Doctorate Thesis in Chemical Sciences, University of Modena, (1993).
- [9] I. Baraldi, F Momicchioli and G. Ponterini, *J. Mol. Struct. (THEOCHEM)* **110**, 187 (1984); G. Bartocci, F. Masetti, U. Mazzucato, A. Spalletti, I. Baraldi and F. Momicchioli, *J.Phys.Chem.* **91**, 4733 (1987); F. Momicchioli, I. Baraldi and E. Fischer, *J.Photochem. Photobiol. A. Chem.* **48**, 95 (1989); U. Mazzucato and F. Momicchioli, *Chem.Rev.* **91**, 1679 (1991).
- [10] I. Baraldi, G. Ponterini, and F. Momicchioli, *J. Chem. Soc. Faraday II* **83**, 213 (1987); I. Baraldi, M.C. Bruni, M. Caselli and G. Ponterini, *J. Chem. Soc. Faraday II* **85**, 65 (1989).
- [11] (a) F. Momicchioli, I. Baraldi and G. Berthier, *Chem.Phys.* **123**, 103 (1988); (b) F. Momicchioli, I. Baraldi, G. Ponterini and G. Berthier, *Spectrochim.Acta* **46A**, 775 (1990); (c) I. Baraldi, A. Carnevali, F. Momicchioli and G. Ponterini, *Spectrochim.Acta* **49A**, 471 (1993); (d) I. Baraldi, A. Carnevali, M. Caselli, F. Momicchioli, G. Ponterini, G. Berthier, *J.Mol.Struct.(Theochem)* **330**, 403 (1995); (e) I. Baraldi, A. Carnevali, F. Momicchioli, G. Ponterini nd G. Berthier, *Gazz.Chim.It.* **126**, 211 (1996).
- [12] S. Marguet, J.C. Mialocq, P. Millie, G. Berthier and F. Momicchioli, *Chem. Phys.* **160**, 265 (1992); F. Momicchioli, I. Baraldi, A. Carnevali, M. Caselli and G. Ponterini, *Coord.Chem.Rev.* **125**, 301 (1993).
- [13] A. Despres, V. Lejeune, E. Migirdicyan, A. Admasu, M.S. Platz, G. Berthier, O. Parisel, J.P. Flament, I. Baraldi and F. Momicchioli, *J.Phys.Chem.* **97**, 13358 (1993); G. Parisel, G. Berthier and E. Migirdicyan, *Can.J.Chem.* **73**, 1869 (1995).
- [14] A. Germain, Doctorate Thesis, University of Paris Sud, 1996; S. Marguet, A. Germain and P. Millié, *Chem.Phys.* **208**, 351 (1996).
- [15] C. Barbier, G. Berthier, I. Baraldi and F. Momicchioli, *J.Mol.Struct. (THEOCHEM)* **433**, 231 (1998).

- [16] G. Klopman, *Chem. Phys. Letters* **1**, 200 (1967).
- [17] D. Heidrich, U. Göring, W. Förster and C. Weiss, *Tetrahedron* **35**, 651 (1979).
- [18] I. Baraldi, S. Ghelli, Z.A. Krasnaya, F. Momicchioli, A.S. Tatikolov, D. Vanossi and G. Ponterini, *J.Photochem.Photobiol. A:Chem*, **105**, 297 (1997).
- [19] L. Salem, *Electrons in chemical reactions: first principles*, Chapter 8, Wiley, New York, 1982.
- [20] For a comprehensive review of the continuum theories of solvation, see J. Tomasi and M. Persico, *Chem.Rev.* **94**, 3027 (1994).
- [21] H.A. Germer, *Theoret.Chim.Acta* **34**, 145 (1974); *ibid.* **35**, 273 (1974).
- [22] S. Miertus and O. Kysel, *Chem.Phys.* **21**, 27 (1977).
- [23] S. Miertus and O. Kysel, *Chem.Phys.Letters* **65**, 395 (1979).
- [24] M. T. Karelson and M. C. Zerner, *J. Phys. Chem.* **96**, 6949 (1992).
- [25] C. Reichardt, *Solvent effects in organic chemistry*, Verlag Chemie, Weinheim (1979).
- [26] J. Griffiths, *Colour and constitution of organic molecules*, Academic Press, London (1976).
- [27] I. Baraldi, F. Momicchioli, G. Ponterini and D. Vanossi, *Chem. Phys.* **238**, 353 (1998).
- [28] H.G. Benson and J. Murrell, *J. Chem. Soc., Faraday Trans 2* **68**, 137 (1972).
- [29] A. Botrel, A. Le Beuze, P. Jacques and H. Straub, *J.C.S. Faraday II* **80**, 1235 (1984).
- [30] J. O. Morley, *J. Mol. Structure(Theochem)* **304**, 191 (1994).
- [31] I. D. L. Albert, T.J. Marks and M.A. Ratner, *J.Phys.Chem.* **100**, 9714 (1996).
- [32] M. Born, *Z.Phys.* **1**, 45 (1920).
- [33] G. J. Hoijtink, E. de Boer, P.H. van der Meij and W.P. Weijland, *Rev.Trav.Chim.* **75**, 487 (1956).
- [34] R.S. Mulliken, *J.Chim.Phys. Physicochem.Biol.* **46**, 497 (1949); *ibid.* **46**, 675 (1946).
- [35] J.E. Sanhueza, O. Tapia, W.G. Laidlaw and M. Trsic, *J.Chem.Phys.* **70**, 3096 (1979).
- [36] M. Kondo, S. Watanabe and I. Ando, *Mol.Phys.* **37**, 1521 (1979).
- [37] C.J. Cramer and D.G. Truhlar, *J.Am.Chem.Soc.* **113**, 8305 (1991).
- [38] J. Sadley, *Semiempirical methods of quantum chemistry*, Ellis Horwood Ltd., 1985.
- [39] R. Costanciel and O. Tapia, *Theoret.Chim.Acta* **48**, 383 (1978).
- [40] A. Botrel, F. Corre and A. Le Beuze, *Chem.Phys.* **74**, 383 (1983).
- [41] A. Botrel, B. Aboad, F. Corre and F. Tonnard, *Chem.Phys.* **194**, 101 (1995).
- [42] I. Jano, *Compt.Rend.Acad.Sci. (Paris)* **261**, 103 (1965).

- [43] I. Jano, *Chem. Phys. Letters* **106**(1984)60.
- [44] K. Ohno, *Theoret. Chim. Acta* **2**(1964)219; G. Klopman, *J. Am. Chem. Soc.* **86**, 4550 (1964).
- [45] M. J. S. Dewar, E. G. Zoebisch, E. F. Healy and J. P. Stewart, *J. Am. Chem. Soc.* **107**, 3902 (1985).
- [46] P. Jacques, *J. Phys. Chem.* **90**, 5535 (1986).

Regioselectivity and Diastereoselectivity in the 1,3-Dipolar Cycloadditions of Nitrones with Acrylonitrile and Maleonitrile. The Origin of ENDO/EXO Selectivity*

Augusto Rastelli*, Remo Gandolfi** and Mirko Sarzi Amadè**

(*) Dipartimento di Chimica, Università di Modena, 183 Via Campi, 41100 Modena, Italy.

(**) Dipartimento di Chimica Organica, Università di Pavia, 10 V.le Taramelli, 27100 Pavia, Italy

Contents

1. Introduction
2. Experimental Results
3. Computational Methods
4. Transition Structures and Activation Parameters
5. Solvent Effects
6. Comparison with the Experimental Results
7. Origin of Endo/Exo Selectivity: Analysis of TS structures
8. Origin of Endo/Exo Selectivity: Analysis of Activation Barriers
9. Conclusions
10. References

1. Introduction

The nitron functionality is a 4- π -electron system capable of undergoing reactions with other multiply bonded systems in a process, the 1,3-dipolar cycloaddition, not unlike the Diels-Alder reaction. The foreseen potentiality of nitron cycloadditions¹ has been largely confirmed in the last thirty years so that such reactions are now of primary importance in organic synthesis.² A serious problem with nitron cycloadditions is that, in principle and often in practice, two regioisomeric adducts and two diastereoisomeric adducts can emerge from such reactions, a feature that can limit their efficiency. Moreover, the factors influencing the product selectivity are still insufficiently understood. Actually, in spite of the large amount of experimental data, only a few qualitative remarks have been advanced about the origin of endo/exo selectivity³ whereas regioselectivity, traditionally interpreted with the use of Frontier Orbital Theory (FOT),⁴ has been recently shown⁵ to obtain frequent incorrect qualitative predictions as a consequence of the incorrect predictions obtained with the monodeterminantal MO calculations on which FOT procedure is based. In particular, a complete inversion of the prediction is caused by the inclusion of electron correlation in the cycloadditions of nitrile oxides and nitrones.

In the last decade the Department of Organic Chemistry of the University of Pavia has made an intensive work on this subject and an interesting collection of new experimental results is now available for theoretical consideration.

* Dedicated to Professor G. Del Re

In the present paper we show that the experimental behaviour can be well reproduced by standard theoretical calculations limited to the reactions of the prototype nitron (H-nitron), provided that a fairly high level of electron correlation be introduced, either with the Moeller-Plesset perturbation technique or with the use of the Density Functional procedures.

Afterwards, the relative activation energies of the diastereoisomeric transition structures are split into contributions able to represent the factors the organic chemist is used to invoke in the attempt to "understand" the variety of the reaction outcome, *i.e.* steric and electrostatic repulsions, deformation energy of reactants, incipient bond energies, trough-space delocalisations and their subsets often called secondary interactions. The analysis of delocalisation energies rests on the use of hybrid basis sets derived from Del Re's Maximum Localisation Criterion.⁶

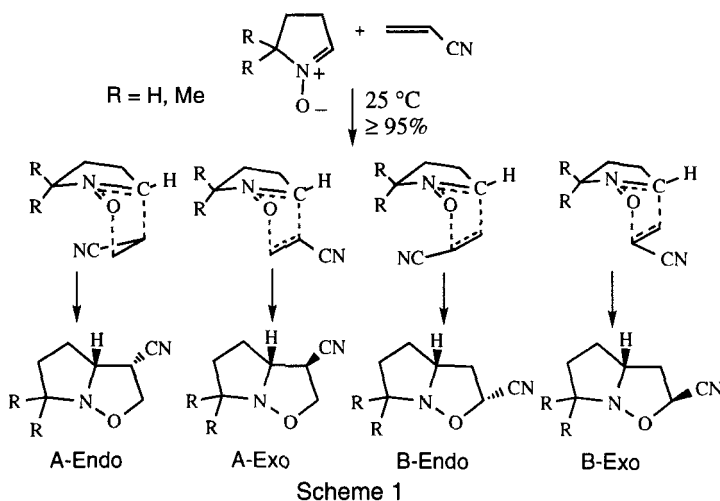


Table 1. Reaction rate constants ($\text{L mol}^{-1}\text{s}^{-1}$), activation free enthalpies (kcal mol^{-1}) and adduct relative yields (%) of the reaction of 1-pyrroline-1-oxides with acrylonitrile in different solvents at 298 K.

Solvent	$k (\times 10^4)$	$\Delta^\ddagger G$	Aendo	Aexo	Bendo	Bexo
$R = H$						
Cyclohexane ^a	62.4	20.45	60.0	6.0	13.0	21.0
Benzene ^b			36.0	5.0	19.0	40.0
Dichloromethane ^c	2.09	22.47	29.0	5.5	20.0	45.5
Acetonitrile ^d	4.44	22.03	17.0	4.0	21.5	57.5
$R = Me$						
Cyclohexane	7.40	21.71	25.5	4.5	20.0	50.0
Benzene			9.0	2.5	24.5	64.0
Dichloromethane	0.77	23.05	6.5	2.5	24.0	67.0
Acetonitrile	1.51	22.65	3.5	1.5	23.5	71.5

^a ϵ (dielectric constant) = 2.02, ^b ϵ = 2.27, ^c ϵ = 8.93, ^d ϵ = 35.94

2. Experimental results

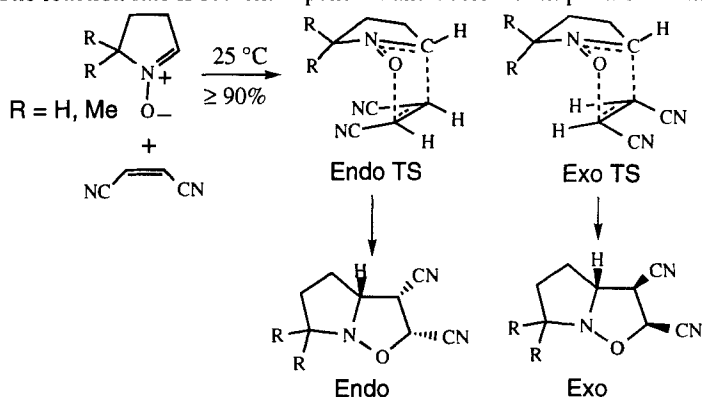
Let us report here the results of the reactions of 1-pyrroline-1-oxide and 5,5-dimethyl-1-pyrroline-1-oxide with acrylonitrile (Scheme 1 and Table 1) and maleonitrile (Scheme 2 and Table 2). In our regiochemical notation, A-adducts involve the α -carbon atom of the alkene in the new forming C...C bond, whereas B-adducts involve the β -carbon atom; endo/exo notation, as usual, defines the diastereoisomeric relation of the C-N-O nitron-group with respect to the substituent(s). The isomer definition is made clearer in the transition structures which are taken to be "concerted" according to the extant literature.⁷ One can see that all the adducts allowed are present in the reaction mixture with variable, but non negligible fractions. The same is true for the reactions of 3,4-dihydro-isoquinoline-N-oxide and C-phenyl-N-methylnitrone,^{3d} whereas the reactions of N-H-nitrone (H-nitrone),⁸ N-Me-nitrone⁹ and N-(t-Bu)-nitrone^{3b,c} lead to a single adduct, which, in our notation, is the B-regioadduct (Scheme 3). The experimental trends extracted from Tables 1-2 and from the cited literature can be summarised as follows:

i) In general, all the four adducts are present in the reaction mixture; we should expect that the activation free energies of the various isomers are confined in a range of less than 3 kcal mol⁻¹.

ii) The exo-diastereoisomeric forms and the B-regioisomeric forms enhance their percentage in polar solvents.

iii) The reactions of simple nitrones like H-nitrone, N-Me-nitrone and N-t-Bu-nitrone give only one B-adduct, whereas diastereoselectivity is absent due to inter conversion of endo/exo adducts.

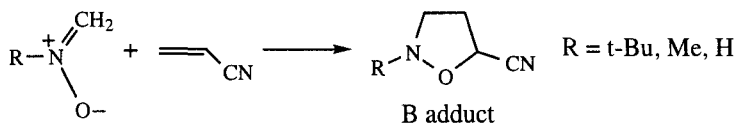
iv) The reaction rate is solvent dependent and decreases in polar solvents.¹⁰



Scheme 2

Table 2. Adduct relative yields (%) of the reaction of 1-pyrroline-1-oxides with maleonitrile in different solvents at 298 K.

Solvent	endo	exo	endo	exo
	R = H		R = Me	
Benzene	77.0	23.0	48.0	52.0
Dichloromethane	72.0	28.0		
Acetonitrile	61.0	39.0	37.0	63.0



Scheme 3

3. Computational Methods

Geometries for all the structures were obtained both at the HF/6-31(d)¹¹ and at the B3LYP/6-31G(d)¹² levels of theory, utilising gradient geometry optimisation and default threshold for convergence.¹³ The searches were limited to concerted transition structures; critical points were fully characterised as minima or first order saddle points by diagonalizing the Hessian matrices of the optimised structures; transition structures (TS) were found to have only one negative eigenvalue, the corresponding eigenvector involving the expected formation of the two new bonds. Electron correlation was included *via* Moeller-Plesset perturbation theory up to the fourth order (MP4(SDQ)/6-31G(d)). Vibration frequencies, in the harmonic approximation, were calculated for all the optimised structures and used to compute zero-point energies, their thermal corrections, vibrational entropies, and their contributions to activation enthalpies, entropies and free enthalpy. For sake of comparison a few calculations were done with the use of a DZVP basis set DFT-optimised¹⁴ with the pure Becke's exchange functional¹⁵ and the LYP correlation functional¹⁶ (BLYP).

Solvent effects were evaluated by different self consistent reaction field (SCRF) procedures: i) the parametrisation AM1-SM4 for cyclohexane and AM1-SM2.1 for water, implemented on the AMSOL-V suite of programs,¹⁷ ii) the *ab initio* Pisa model (interlocking spheres)¹⁸ implemented in the Gamess (Rev.97) package and, with different options, in the Gaussian 94 package.

The analysis of activation barriers was conducted with the use of a procedure recently proposed by our group and explored in a number of problems concerning the origin of rotational barriers^{19a,c-d} and some specific stereochemical aspects of the reactivity of medium-size organic molecules.^{19b,e-f} In short, it amounts to projecting the energy matrix into a basis set of symmetrically orthogonalised hybrid atomic orbitals (HOA); the hybrid basis is obtained by a unitary transformation of the AO basis set according to the Maximum Localisation Criterion^{6,20}. The basis functions 'assigned' to chemically meaningful molecular subsystems (bonds, π -systems, lone pairs, inner shells, molecular fragments) define diagonal blocks of the energy matrix suited to represent the localised subsystems, whereas off-diagonal blocks introduce electron delocalisation between subsystems. Removing selected groups of interactions from the energy matrix in the SCF procedure causes changes in wavefunction and total energy which define the effects of those interactions. In the present paper a minimal basis set (STO-3G) and the uncorrelated HF approximation were adopted, but we have shown that the procedure can be extended to the use of redundant basis sets^{19d} and to post-SCF methods.²¹ For this analysis, Link 501 of the Gaussian 92 package has been modified to deal with hybridisation and with the options for the suppression of selected interactions.

4. Transition Structures and Activation Parameters

Table 3 collects activation energies, kinetic nuclear contributions and thermodynamic activation parameters, together with the predicted isomer distributions of TSs.

The uncorrelated HF calculation and the MP2//HF calculation furnish the highest and the lowest energy barriers, respectively, and the complete inversion of regioselectivity of the reaction with acrylonitrile (A-regiospecificity in the former case, B-regiospecificity in the latter). The preference assigned to endo adducts, on the contrary, is insensitive to the level of calculation and it is confirmed by the results of the reaction of H-nitrone with maleonitrile. The activation energy barriers obtained with the density functional B3LYP/6-31G(d) method are quite similar to those obtained with the MP4(SDTQ) post-SCF method; the regiochemical predictions, however, are qualitatively different, the former being 50% of A-regioadducts, the latter 3%. The use of the B3LYP/6-311+G(2d,p)//B3LYP/6-31G(d) model leads to a systematic increase of energy barriers (about 4 kcal mol⁻¹) and to a larger content of A-adducts in the reaction mixture (69%). Energy barriers and TS distribution, while depending on the model used for energy calculations, do not vary significantly with the choice of the optimised structures; so, the results of MP4 single-point calculations done on HF-optimised TSs and on B3LYP-optimised ones are very similar and so are the kinetic contributions on the two kinds of TSs (Table 3, second section); moreover, kinetic contributions do not introduce significant differences among the various isomers so that selectivity is essentially determined by the relative activation energies. The third section of Table 3 reports the thermodynamic activation properties (gas phase) in the approximations MP4/HF and B3LYP (in italics) and their selectivity predictions.

Table 3. Activation parameters and product distributions of the cycloadditions of Acrylonitrile and Maleonitrile with H-Nitrone.^a

ACRYLONITRILE+H-NITRONE								
Structure	Aendo	%	Aexo	%	Bendo	%	Bexo	%
HF/6-31G(d)	21.28	78	22.6	21	27.04	0	28.10	0
MP2/6-31G(d)//HF	5.59	0	6.88	0	1.69	86	2.78	13
MP3/6-31G(d)//HF	11.36	21	12.43	3	10.68	65	11.78	10
MP4SDTQ/6-31G(d)//HF	8.52	3	9.71	0	6.56	81	7.53	16
B3LYP/6-31G(d)	8.41	41	9.29	9	8.42	40	9.32	8
B3LYP/6-311+G(2d,p)	12.75	58	13.73	11	13.33	22	13.90	8
MP4SDTQ/6-31G(d)//B3LYP	7.90	4	9.16	1	6.13	78	7.03	17
BLYP/DZVP ^b	11.86	14	12.92	2	11.06	54	11.42	29
	HF	DFT	HF	DFT	HF	DFT	HF	DFT
$\delta^{\#}\text{ZPE}$	2.16	2.06	2.18	2.09	2.11	1.99	2.08	1.93
$\delta^{\#}\text{H}$	1.71	1.66	1.72	1.68	1.58	1.63	1.56	1.58
$\delta^{\#}\text{G}$	11.86	11.68	11.92	11.76	11.93	11.56	11.89	11.46
$\Delta^{\#}\text{H}$	10.23	10.07	11.43	10.97	8.14	10.05	9.09	10.90
$-\Delta^{\#}\text{S}$	34.01	33.64	34.17	33.84	34.68	33.28	34.64	33.15
$\Delta^{\#}\text{G}$	20.37	20.09	21.63	21.05	18.48	19.95	19.42	20.78
MALEONITRILE+H-NITRONE								
Structure	Endo	%	Exo	%				
HF/6-31G(d)	21.68	96	23.50	4				
MP2/6-31G(d)//HF	2.13	97	4.16	3				
MP3/6-31G(d)//HF	9.62	96	11.54	4				
MP4SDTQ/6-31G(d)//HF	5.66	96	7.50	4				
B3LYP/6-31G(d)	7.65	96	9.49	4				
B3LYP/6-311+G(2d,p)	12.83	93	14.37	7				
	HF	DFT	HF	DFT				
$\delta^{\#}\text{ZPE}$	1.78	1.67	1.78	1.67				
$\delta^{\#}\text{H}$	1.48	1.48	1.49	1.49				
$\delta^{\#}\text{G}$	11.49	11.22	11.53	11.26				
$\Delta^{\#}\text{H}$	7.14	9.13	8.99	10.98				
$-\Delta^{\#}\text{S}$	33.56	32.67	33.67	32.77				
$\Delta^{\#}\text{G}$	17.15	18.87	19.03	20.75				

^aEnergy in kcal mol⁻¹, entropy in eu, standard state of the molar concentration at 298K. First section: single-point electronic activation energies at the levels of calculation shown in the first column for the structures optimised at the HF/6-31G(d) and B3LYP/6-31G(d) levels; in italics the percent isomer distribution; ^bDZVP basis set of ref. 14 (full structure optimisations). Second section: $\delta^{\#}\text{H}$, $\delta^{\#}\text{G}$ are the nuclear kinetic contributions to the activation enthalpy and free enthalpy (to be added to the electronic activation energy); $\delta^{\#}\text{ZPE}$ is the contribution of zero point energy. $\delta^{\#}\text{G}$ includes the reaction statistical factors. Third section: activation thermodynamic parameters using activation energies from MP4(SDTQ)/6-31G(d)//HF-6-31G(d) and DFT-B3LYP/6-31G(d) (in italics).

5. Solvent effects

The contributions of solvent effects on the activation free enthalpies of the reactions under study are reported in Tables 4 and 5 where also a comparison can be done among the different procedures. These effects are given by the differences between the solvent effects on the TSs and those on the reactants. The total solvent effect (TOT for reactants and TOT[#] for the activation free enthalpy) consists of two contributions, labelled CDS(CDS[#]) for "cavitation+dispersion+structural" and ENP(ENP[#]) for "electronic+nuclear+polarisation" in the AMSOL procedure, CDR(CDR[#]) for "cavitation+dispersion+repulsion" and ELEC(ELEC[#]) for "electrostatic" in the Tomasi procedure.

Table 4. Solvent effects.^a

		AMSOL/SM4 Cyclohexane ($\epsilon=2.02$)			AMSOL/SM2.1 Water ($\epsilon=78.4$)			TOMASI/GAMESS97 Water ($\epsilon=78.4$)		
	Reactants	CDS	ENP	TOT	CDS	ENP	TOT	CDR	ELEC	TOT
(1)	H-nitrone	-0.14	-4.64	-4.78	-3.72	-9.05	-12.77	4.39	-12.66	-8.28
(2)	acrylonitrile	-0.93	-1.99	-2.91	-2.03	-1.94	-3.97	6.26	-6.41	-0.15
(3)	maleonitrile	-1.00	-3.88	-4.88	-4.61	-3.12	-7.73	6.70	-9.86	-3.16
TSs	structure	CDS [#]	ENP [#]	TOT [#]	CDS [#]	ENP [#]	TOT [#]	CDR [#]	ELEC [#]	TOT [#]
(1)+(2)	Aendo	-0.59	1.83	1.24	0.87	4.98	5.85	-1.64	4.99	3.36
	Aexo	-0.60	1.19	0.59	0.53	3.82	4.35	-1.85	4.20	2.36
	Bendo	-0.48	2.14	1.66	1.03	5.26	6.29	-1.79	5.87	4.08
	Bexo	-0.50	1.40	0.90	0.75	4.21	4.96	-1.86	4.36	2.51
(1)+(3)	Endo	-0.44	2.08	1.64	1.56	4.98	6.54	-1.46	4.10	2.65
	Exo	-0.44	0.92	0.48	1.15	2.92	4.06	-1.58	2.66	1.09

^aEnergies in kcal mol⁻¹; unrelaxed HF/6-31G(d) geometries; the total contribution (TOT[#]) to the activation free enthalpy is due to the cavitation+solute/solvent dispersion+solvent structural rearrangement term (CDS[#]) and to the electronic+nuclear+polarization term (ENP[#]) in the AMSOL model; in the Tomasi model CDR[#] is the cavitation+dispersion+repulsion term and ELEC[#] is the electrostatic contribution; ab initio calculations are standard HF/6-31G(d).

Table 5. Effect of electron correlation on the evaluation of the electrostatic contribution to the solvent effect.^a

	Dichloromethane $\epsilon = 8.9$		Cyclohexane $\epsilon = 2.02$	
	HF	B3LYP	HF	B3LYP
Aendo	3.91	2.41	1.80	1.07
Aexo	3.44	1.86	1.65	0.83
Bendo	5.11	1.70	2.46	0.89
Bexo	4.17	0.87	2.12	0.55
Endo	3.19	0.63 ^b	2.89	0.53
Exo	2.70	0.39	2.69	0.33

^aEnergies in kcal mol⁻¹. ^bConvergence failed; interpolated value

In all the evaluations of Table 4, the solvent effects on the activation free enthalpies are positive, increase with increasing solvent dielectric constants and tend to be larger for the endo than for the exo adducts. This behaviour, in accord with the experimental trend, is due to the electrostatic contribution; the CDS[#] and CDR[#] contributions, in fact, are rather independent of the isomeric reaction considered and, moreover, appear to obtain comparable values in every 1,3-dipolar cycloaddition. For the Tomasi parametrisation in water, for example, the CDR[#] contribution for the cycloadditions of diazomethane and nitrile oxides to substituted alkenes^{5b} amounts to -1.85 ± 0.14 kcal mol⁻¹. This finding can be traced back to the view that the CDR term is approximately proportional to the solvent accessible surface area (the cavity area) of solutes and to the feature of TSs of having very alike structures of the new forming pentatomic ring so that the changes of the cavity areas from reactants to TSs are similar.

At variance with the endo/exo selectivity, the solvent effects of Table 4 do not explain the observed increase of the B-regioadducts due to the increased solvent polarity. We show in Table 5 that the inclusion of electron correlation in the evaluation of the solvent effect succeeds in reproducing the experimental trend of reaction rates, of endo/exo selectivities and of regioselectivities as a function of the increasing dielectric constant of the solvent.

6. Comparison with the experimental results

The final results summarised in Table 6 show that the two calculations (MP4(SDTQ)/HF/6-31G(d) or B3LYP/6-31G(d) for activation energies plus HF/6-31G(d) or B3LYP/6-31G(d) for zero-point energies, thermal effects and entropies, plus solvent effects, limited to the electrostatic contributions, evaluated according to the Tomasi model at the B3LYP/6-31G(d) level, lead to similar results.

Table 6. Isomeric distribution (%) and apparent activation free enthalpy ($\Delta^\#G_{app}$ in kcal·mol⁻¹) of the cycloadditions of Acrylonitrile and Maleonitrile with H-Nitrone.^a

ACRYLONITRILE+H-NITRONE									
Structure %	Aendo		Aexo		Bendo		Bexo		$\Delta^\#G_{app}$
Gas-phase	3	36	0	7	80	45	16	12	18.35 19.48
Cyclohexane	2	26	0	8	71	46	26	20	19.17 20.37
Dichloromethane	1	10	0	5	54	42	45	42	19.82 21.14

MALEONITRILE+H-NITRONE						
Structure %	Endo		Exo		$\Delta^\#G_{app}$	
Gas-phase	96	96	4	4	17.13	18.85
Cyclohexane	94	94	6	6	17.65	19.37
Dichloromethane	94	94	6	6	17.74	19.46

^aActivation energies (kcal mol⁻¹) from MP4(SDTQ)/6-31G(d)/HF/6-31G(d), nuclear contribution from HF/6-31G(d) and, in italics, from B3LYP/6-31G(d), nuclear contributions from B3LYP/6-31G(d). Solvent effects from Table 5 (Tomasi model in B3LYP/6-31G(d)). $\Delta^\#G_{app}$ is the activation free enthalpy of the overall reaction yielding the plurality of TSs. $\Delta^\#H_{app}$ and $\Delta^\#S_{app}$, in the gas-phase, are 8.39 (10.22) kcal·mol⁻¹ and -33.40 (-31.06) eu for the reaction of acrylonitrile, 7.21 (9.20) kcal·mol⁻¹ and -33.25 (-32.35) eu for the reaction of maleonitrile.

The only interesting difference is that the B3LYP electronic activation energies overestimates the presence of A-adducts, both with respect to the MP4 calculations and the experiment; moreover, it has been noted in the discussion of Table 3 that this shortcoming cannot be recovered by the use of a larger basis set for B3LYP energy calculations and that the regioselectivity is strictly dependent on the way and extent the electron correlation is introduced.

Other than giving a very good account of the experimental qualitative behaviour, the above results probably offer a reasonable quantitative evaluation of the reaction parameters. The apparent activation free enthalpy of the reaction of 1-pyrroline-1-oxide and 5,5-dimethyl-1-pyrroline-1-oxide with acrylonitrile have been measured²² in cyclohexane (20.4 ± 0.4 and 21.7 ± 0.4 kcal mol⁻¹, respectively) and in dichloromethane (22.4 ± 0.2 and 23.0 ± 0.8 kcal mol⁻¹) at 298K; the rate constants for the reactions of H-nitrone have not been measured, but it can be stressed that N-monosubstituted nitron, *e.g.* t-Bu-nitrone, exhibits a high reactivity in 1,3-dipolar cycloadditions, which is similar to that of 1-pyrroline-1-oxide so that the evaluations of Table 6 emerge to be surprisingly good. Moreover, the activation entropy of the reaction of 5,5-dimethyl-1-pyrroline-1-oxide with acrylonitrile in cyclohexane has been estimated²² -31.9 eu, a value which is well reproduced by our calculations in the gas-phase (-33.4, -31.1, footnote of Table 6).

7. Origin of Endo/Exo Selectivity: Analysis of TS Structures

Since the discovery of the very remarkable 100% endo selectivity of the reactions of nitronic esters with dimethyl maleate, maleic anhydride and maleimides^{23a} secondary orbital interactions involving the nitrogen atom of the 1,3-dipole and the substituents on the dipolarophile have been postulated as strong endo-orienting factors, able to overwhelm the contrasting steric factors (Figure 1).

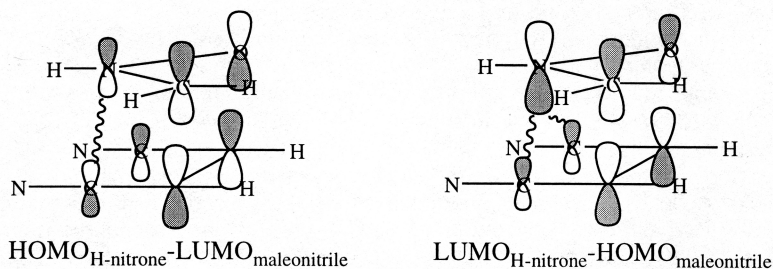


Figure 1. Schematic representation of FO interactions in the endo TS. Secondary orbital interactions between the nitron nitrogen atom and the carbon atoms of the cyano groups are indicated.

Since then researchers in the field of nitron cycloaddition seem to have more or less tacitly assumed that secondary interactions play an important role in determining endo/exo selectivity also in the case of N-alkyl and N-arylnitron cycloadditions.^{2a,23} However, our experimental endo/exo selectivity studies²⁴ for the reactions of cyclic and open-chain nitrones with *Z*-disubstituted dipolarophiles revealed a clear-cut dominance (77% in benzene) of the endo mode only in one case: the reaction of 1-pyrroline-1-oxide with maleonitrile, a reaction where the steric effects

contrasting the endo-orientation are at their minimum and also, owing to the high dipole moment of maleonitrile and to the feature that the alignment of the two dipoles is favourable to the endo-orientation,²⁵ the electrostatic effects should assist endo-selectivity. This experiment and the whole of the experimental data²⁴ cast serious doubt on the role of secondary interactions as important endo-orienting factors in nitron cycloadditions. In this connection it should be stressed that also for the Diels-Alder reaction the assumed role of secondary interactions as major endo-orienting factors has been questioned²⁶, although a more recent paper seems to offer theoretical evidence for their determining effect.²⁷

The theoretical prediction (endo 96%, Table 6) for the reaction of H-nitrone with maleonitrile, where the steric hindrance to endo-orientation is possibly further reduced with respect to the reaction of 1-pyrroline-1-oxide, is very reasonable. The optimised transition structures reported in Figure 2 give evidence of a well concerted mechanism and offer some qualitative insight on the interactions between the reaction partners.

i) The dihedral angle between the CNO plane of the nitron fragment and the average plane of the new forming bonds is 125 degrees (126 degrees for DFT structure) in the endo orientation and 126 degrees (127 degrees for DFT structure) in the exo orientation; the finding that these angles are much larger than 90 degrees and nearly the same in endo and exo orientations reveals that both steric hindrance and secondary orbital interactions in the endo orientation should be much less important than it could be supposed from Figure 1.

ii) The pyramidalisation of the nitron nitrogen shows the uplifting of this atom on passing from reactants to transition structure, which eventually results in the development of the nitrogen lone-pair on the opposite side with respect to the direction of approach of the dipolarophile. This pyramidalisation, taken as the height (in Å) of the pyramid with the nitrogen atom at the apex and the three atoms connected to it at the base, is very similar in the endo (0.187 Å and 0.199 Å for HF and DFT structures, respectively) and in the exo (0.182 Å and 0.194 Å) transition structures and does not support the view of a significantly different involvement of this group in the two orientations.

iii) In general, the structural differences between endo and exo modes are small but they appear to suggest that the endo mode is slightly *earlier* than the exo one. For example, a) the length of the new forming C...C (C...O) bond is only slightly shorter (longer) in the exo than in the endo mode, but their sum is slightly shorter in the exo mode; b) the average pyramidalisations of the reactive centres are slightly more advanced in the exo orientation; c) the C-C bond of the maleonitrile fragment (the C=C bond of the reactant) is longer in the exo mode, all these trends being more evident in the DFT structures than in the HF ones. A slightly earlier TS for the endo than for the exo mode suggests that the endo mode is not disfavoured by larger steric and electrostatic factors, the former being only slightly larger, the latter being more favourable to the endo orientation (Figure 3). These remarks strongly reduce the need of further endo-orienting factors.

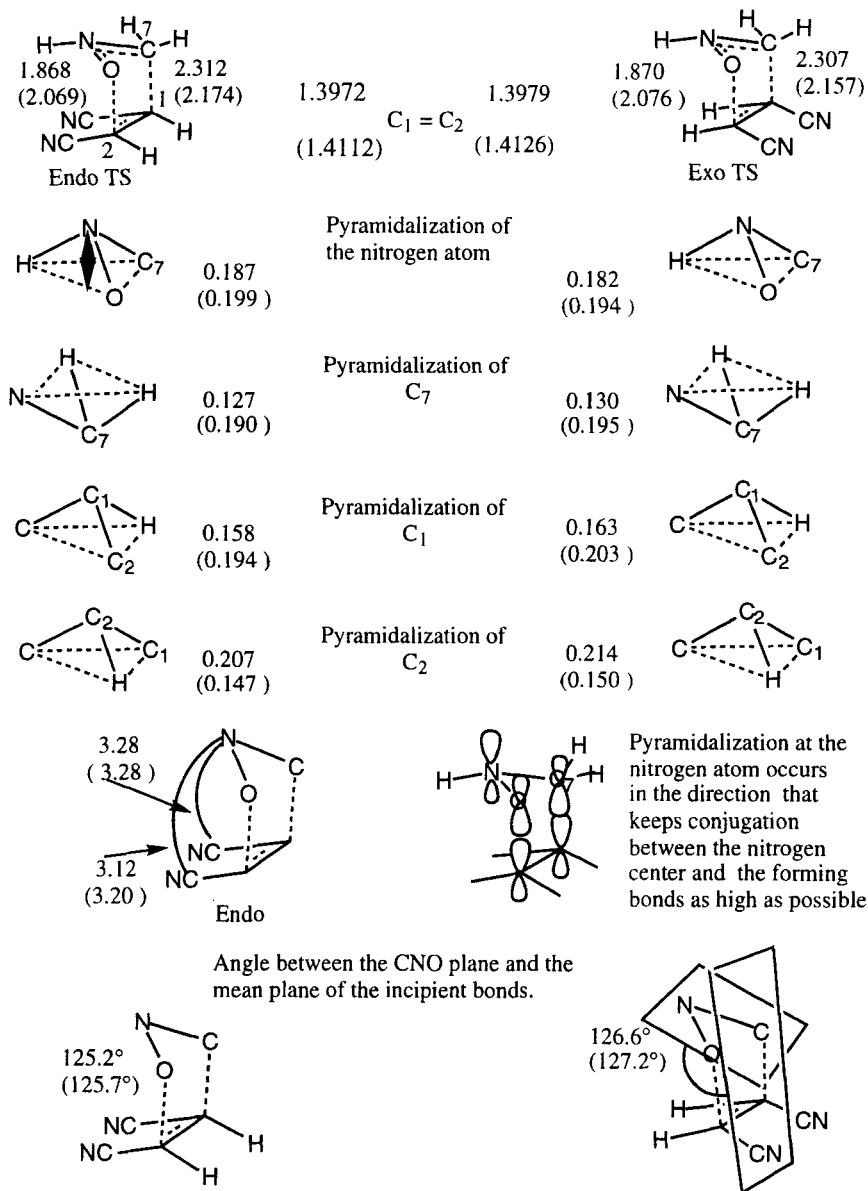


Fig.2 Geometry details of Endo and Exo HF/6-31G* (B3LYP/6-31G*) transition structures (TS). Distances in Å, angles in degrees.

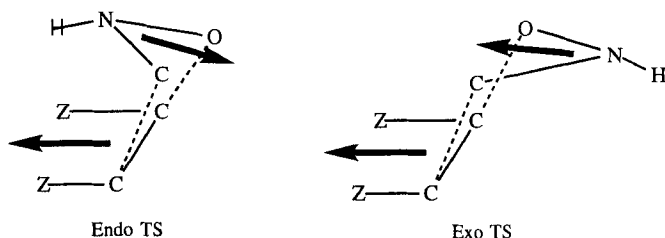


Figure 3. Dipole moment orientations.

8. Origin of Endo/Exo Selectivity: Analysis of Activation Barriers

The activation energy can be resolved into a number of contributions corresponding to the conceptual steps of the structural changes undergone by the chemical system from the reactant to the transition state. Isolated reactants are deformed to the geometries they assume in the TS (model state of separated deformed reactants) and *deformation energy* is obtained by difference. Then the deformed reactants are driven, facing each other, into the overall geometry of the TS, avoiding any electron delocalisation between them and, in particular, preventing the formation of the new bonds and any through-space delocalisation (model state of localised reaction partners in the TS); this is obtained by suppressing the off-diagonal block representing the electronic coupling between the deformed reactants in the TS energy matrix (the density matrix is accordingly block-factorised); the energy difference between the two models is taken to represent the *classical* (nuclear plus electrostatic) *interactions* between the fragments in the TS. *Delocalization energy* is the difference between the energy of the TS and the energy of the model state of localised partners in the TS.

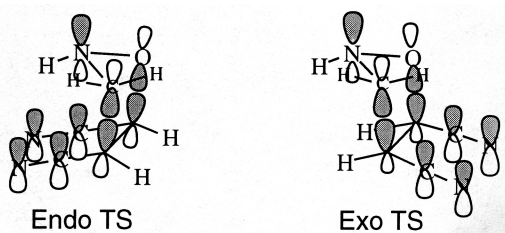


Figure 4. Hybrid atomic orbital basis set for the forming bonds, p "lone pair" on the nitrene nitrogen atom (Nlp) and CN π bond conjugated with the forming bonds in the endo and exo TSs.

The delocalisation energy between the two fragments can be resolved into various contributions; as a first step we choose to evaluate the energy contributions due to the forming bonds, to the valence through-space interactions, to the core interactions and to the residual terms. The unitary transformation of the atomic minimal basis set of the TS into the basis set of symmetrically orthogonalised hybrids^{6,19,20} assigns four hybrids to the subsystem of the two new forming bonds, two hybrids to every σ -bond, one hybrid to every lone-pair, one 1s orbital to every core and the suitable orbitals to π -systems (Figure 4). Although preserving invariance of the fi-

nal results, the density matrix shows a fairly good localisation of the subsystems and also gives insight to the largest interactions between them. The interactions between the fragments of the TS (fragment 1 is H-nitrone, fragment 2 is maleonitrile) are collected in groups representing the interactions of the core orbitals between the fragments (*Core*), the interactions of the hybrids of the forming bonds (*Bond*), the interactions of all the remaining hybrids of fragment 1 with all the remaining hybrids of fragment 2 (*Trough-Space*), and the cross interactions between the hybrids of the three groups (*Residual*).

Then calculations are done where a) all the three groups of interactions are removed from the energy matrix; b) each of the three groups is removed while leaving active all other groups and c) each group is left alone while suppressing all the other groups. The energy differences between the full calculation (where all the interactions are active) and calculations b) and between calculations c) and calculation a) provide two evaluations of the stabilisation introduced by each group; the average value is taken as the delocalisation effect of the group.

It is interesting to underline that the average delocalisation effects of the different groups are additive under the assumption that the total effect is represented as the sum of all single and of all distinct pairs of interactions.^{19c} Actually, in many examples^{19c-f} they have been found to be almost perfectly additive.

Table 7. Contributions to the difference of endo/exo activation energies for the cycloaddition of H-Nitrone to Maleonitrile.^a

Structure of TSs	MALEONITRILE+H-NITRONE					
	HF/6-31G(d)			B3LYP/6-31G(d)		
	ENDO	EXO	Δ	ENDO	EXO	Δ
ΔE_{att} (ENDO-EXO)			-1.73			-1.49
1) Deformation	24.88	25.24	-0.37	26.80	27.40	-0.60
a-H-nitrone	9.47	9.04	0.43	12.20	11.91	0.29
b-Dipolarophile	15.41	16.20	-0.80	14.60	15.49	-0.90
2) Class.Rep	126.43	127.95	-1.51	101.59	104.59	-3.00
3) Delocalisation	-143.04	-143.20	0.16	-119.73	-121.84	2.12
1 +2 +3=E_{att}	8.27	9.99	-1.73	8.66	10.15	-1.49
Analysis of Delocalisation Energy 3)						
4) Bond	-139.44	-139.87	0.43	-116.63	-118.87	2.24
5) Trough-Space	-3.45	-3.12	-0.32	-2.48	-2.19	-0.29
6) Core	-0.01	-0.01	-0.00	-0.01	-0.01	-0.00
7) Residual	-0.16	-0.20	0.05	-0.61	-0.78	0.17
check 4+5+6+7=3	-143.04	-143.20	0.16	-119.73	-121.84	2.12
Analysis of Trough-Space Delocalisation Energy 5)						
8) N-H,Nlp // frag2	-0.40	-0.33	-0.06	-0.49	-0.38	-0.11
9) Other // frag2	-3.05	-2.79	-0.26	-2.00	-1.81	-0.19
check 8+9=5	-3.45	-3.12	-0.32	-2.50	-2.19	-0.30
10) N-H,Nlp // subst.	-0.28	-0.37	0.09	-0.29	-0.45	0.15
11) Other // frag2	-3.16	-2.76	-0.40	-2.18	-1.74	-0.45
check 10+11=5	-3.44	-3.13	-0.31	-2.48	-2.18	-0.29
12) NH // subst.	-0.08	-0.01	-0.07	-0.06	-0.01	-0.04
13) Nlp // subst.	-0.19	-0.36	0.16	-0.23	-0.43	0.20
check 12+13=10	-0.28	-0.37	0.09	-0.29	-0.45	0.15

^aSingle-point HF/STO-3G calculations using HF/6-31G(d) and B3LYP/6-31G(d) optimized structures. Energies in kcal mol⁻¹.

A full analysis, at the HF/STO-3G level, of the contributions to the difference of endo/exo activation energies is reported in Table 7. First of all it can be noted that the relative energies of the endo TSs are negative also when they are calculated at the HF/STO-3G level with the HF/6-31G(d) and B3LYP/6-31G(d) optimised TSs.

Deformation energies appear to be, on the whole, lower for the endo than for the exo orientation, in coherence with the finding that the endo mode has an earlier TS. The lower deformation energy of the maleonitrile fragment in the endo TSs can be faced to the lower pyramidalizations of the C1 and C2 reaction centres and the shorter (less deformed) C1-C2 bonds in the endo than in the exo TS (Figure 2), while the slightly higher energy deformation of the endo-nitrone fragment is coherent with the higher pyramidalization of the nitrogen atom in the endo than in the exo structures.

Still in accord with the remarks on the structural differences of endo and exo TSs, classical repulsions confer a significant preference to the endo mode. This preference can be also attributed to the fact that classical repulsions, other than including the steric effects of non-bonded groups in the TSs and the electrostatic interactions, include the strong repulsions between the reacting centres which are, on the whole, closer in exo than in endo structures; this last contribution to classical repulsions will be counteracted by the stabilisation introduced by the new forming bonds, which should be higher in the exo (than in the endo orientation), where the sum of the bond lengths of the new forming bonds appears to be lower. As a matter of fact, the delocalisation energy is large, favours the exo orientation and succeeds in recovering part of the disadvantage of the exo TS due to classical repulsions. Deformation energy, classical repulsions and total delocalisation energy are additive by definition and their sum amounts to the activation barrier. According to the discussed results the preference for the endo TS appears to be due to the lower reactant deformation in the TS and to the lower classical repulsions, partly counteracted by a lower delocalisation.

The values obtained for bond energies (Bond) represent almost the whole of the stabilisation due to electron delocalisation (97%) and their changes follow the trend already discussed for the whole delocalisation energy and for the classical repulsions with respect to the lengths of forming bonds. It must be added that bond energy cannot be taken as the energy of the localised forming σ -bonds but, more properly according to the definition, to the stabilisation induced by the new bond formation in a rather delocalised system, extended to the substituents of the dipolarophile fragment and to the N-lone pair of the nitrone fragment.

Through-space interactions are stabilising, small and give a modest preference to the endo orientation; core interactions are not significant, residual interactions are very small and poorly selective. Let us note that the four components of delocalisation energy are additive in the limits of the reported decimals.

It is already evident that, in this reaction, through-space interactions (secondary interactions in other models) *do not include* the supposedly strong endo-orienting factor and that bond delocalisation (primary overlaps in other languages²⁸) is a significant exo-orienting factor.

However, let us complete our analysis by calculating the effects of the interaction of the (N-H,N-lone pair) fragment of the nitrone moiety with fragment 2 (maleonitrile) and with only the CN substituents of fragment 2. The first interaction (NH,Nlp//frag2) represents only the 10-20% of the through-space stabilisation and it is unselective, whereas the modest endo orienting effect of all through-space interactions is given by other interactions including, with a dominant weight, the *vicinal* (with respect to the forming bonds) interactions, *i.e.* the non-bonded interac-

tions between the bonds of the reacting C centres of maleonitrile and the bonds (and lone pairs) of the reacting C and O reacting centres of H-nitrone. The vicinal effect can be strongly changed by suitable substituents on the reacting centres and, with the due account of the changed steric and electrostatic effects, it could explain the variable endo/exo selectivity of the reactions of substituted nitrones and alkenes²³ and, in particular, the unexpectedly high endo selectivity (100%) of the reactions of nitronic esters with dimethyl maleate, maleic anhydride and maleimides.^{23a,29}

Coherently, the subset of (N-H,Nlp//subst.) interactions are small and unselective; after further resolution into the component interactions (N-H//subst.) and (Nlp//subst.) one can see that the former interaction is negligible and that the latter interaction other than being small and poorly selective tends to be exo-orienting. Let us recall that this last interaction had been postulated (Figure 1) as the strong endo-orienting factor able to counteract the unfavourable steric effects.

9. Conclusions

Density Functional methods and highly correlated Hartree-Fock methods were used to study the concerted reactions of nitrone with acrylonitrile and maleonitrile with the aim of elucidating their regioselectivity and diastereoselectivity. Activation thermodynamic parameters were calculated in the gas-phase and the solvent effect on activation free enthalpy was evaluated with the Pisa model. A new set of pertinent experimental data was produced. The theoretical results showed a very good agreement with the experimental data available for this class of reactions; the account of regioselectivity required highly correlated calculations (MP4/6-31G(d)//HF/6-31G(d)) for the energy barriers and correlated calculations (MP2 or B3LYP/6-31G(d)) for solvent effects; endo/exo selectivity and its trend with the increasing solvent polarity were well accounted for at any level of calculation.

The debated problem of finding the electronic endo-orienting factor able to counteract the steric effects inherent to the endo mode of reaction was then approached with a detailed analysis of the geometry of the transition states and a quantitative evaluation of the interactions between the reaction partners and between selected groups of them. The interactions were defined and calculated with the use of orthogonalised basis sets of hybrids obtained with the Del Re's maximum localisation criterion.

Our conclusions were that in the reaction of maleonitrile with H-nitrone i) the only strong endo-orienting factor is the long-range electrostatic one, included in classical repulsions. ii) Through-space interactions are only modestly endo-orienting in the reaction of maleonitrile with H-nitrone, iii) the effect being assigned due to the contribution of vicinal interactions, while iv) the subset of through-space interactions involving the (NH,Nlp) moiety is very small and unselective. v) The most popular candidate to the role of strong endo-orienting effect, *i.e.* the interaction of the nitrone N-lone pair with the substituents on the reacting centres of maleonitrile, (Nlp//subst.), was found to be ineffective.

In the competing endo/exo orientations, the reaction can reach the exo TS at the cost of an increased repulsion between the reacting centres and a slightly increased deformation of the maleonitrile fragment; this cost is partly recovered by new bond formation. Since vicinal interactions are more favourable to the endo than to the exo mode, the endo mode emerges to be favoured also in the absence of further endo-orienting effects.

Acknowledgement. Financial support from MURST and CNR is gratefully acknowledged.

References

- 1) J.J. Tufariello, *Acc. Chem. Res.* **12**, 396 (1979).
- 2) (a) J.J. Tufariello, *Nitrones in 1,3-Dipolar cycloaddition Chemistry*, A. Padwa Ed. (Wiley-Interscience, New York, 1984), Vol 2, p. 396-403. (b) K.G.B. Torsell, *Nitrile Oxides, Nitrones and Nitronates in Organic Synthesis* (VCH Publishers, New York, 1987). (c) E. Breuer, H.G. Aurich and A. Nielsen, *Nitrones, Nitronates and Nitroxides* (John Wiley and Sons, New York, 1989). (d) P.N. Confalone and E.M. Huil, *The (3+2) Nitron Olefin Cycloaddition Reaction in Organic Reactions* (John Wiley and Sons, New York, 1988, Vol. 36, p 1-173). (e) P. Grunanger and P. Vita-Finzi, *Isoxazoles* (Wiley-Interscience, New York, 1991, Part 1, Chapter 3).
- 3) (a) R. Huisgen, *Introduction, Survey and Mechanism in 1,3-Dipolar Cycloaddition*, A. Padwa Ed. (Wiley-Interscience, New York, 1984), Vol 1, p. 1-176. (b) J. Sims and K.N. Houk, *J. Am. Chem. Soc.* **95**, 5798 (1973). (c) K.N. Houk, A. Bimanand, D. Mukheyel, J. Sims, J.-M. Chang, O.C. Kaufman and L.N. Domelsmith, *Heterocycles* **7**, 293 (1977). (d) R. Gandolfi, unpublished results.
- 4) (a) K.N. Houk, J. Sims, R.E. Duke Jr., R.W. Strozier and J.K. George, *J. Am. Chem. Soc.* **95**, 7287 (1973). (b) K.N. Houk, J. Sims, C.R. Watts and L.J. Luskus, *J. Am. Chem. Soc.* **95**, 7301 (1973).
- 5) (a) A. Rastelli, M. Bagatti and R. Gandolfi, *J. Am. Chem. Soc.* **117**, 4965 (1995). (b) A. Rastelli, R. Gandolfi and Mirko Sarzi Amadè, in the press in the *J. Org. Chem.*
- 6) G. Del Re, *Theor. Chim. Acta* **1**, 188 (1963).
- 7) (a) R. Huisgen, *J. Org. Chem.* **41**, 403 (1976). (b) J.J.W. McDouall, M.A. Robb, U. Niazi, F. Bernardi, and H.B. Schlegel, *J. Am. Chem. Soc.* **109**, 4642 (1987). (c) R. Sustmann, W. Sicking and R. Huisgen, *J. Am. Chem. Soc.* **117**, 9679 (1995). (d) C. Sosa, J. Andzelm, C. Lee, J.F. Flake, B.L. Chenard and T.W. Butler, *Int. J. Quantum Chemistry* **49**, 511 (1994).
- 8) M. Ochiai, M. Oboyashi and K. Morita, *Tetrahedron* **23**, 2641 (1967). N.K.A. Dalgard, K.E. Larsen and K.B.G. Torsell, *Acta Chem. Scand. B* **38**, 423 (1984).
- 9) E.J. Farnefeld and A.J. Pike, *J. Org. Chem.* **44**, 835 (1977).
- 10) However, in acetonitrile ($\epsilon=35.94$) the reaction rate is higher than in dichloromethane ($\epsilon=8.93$). The measures in acetonitrile will be given further consideration.
- 11) W.J. Hehre, R. Ditchfield and J.A. Pople, *J. Chem. Phys.* **56**, 2257 (1972). J.D. Dill and J.A. Pople, *J. Chem. Phys.* **62**, 292 (1975). J.S. Binkley and J.A. Pople, *J. Chem. Phys.* **66**, 879 (1977). W.J. Hehre, L. Radom, P.v.R. Schleyer and J.A. Pople, *Ab Initio Molecular Orbital Theory* (Wiley, New York, 1986).
- 12) A.D. Becke, *J. Chem. Phys.* **98**, 1372 (1993).
- 13) M.J. Frisch, G.W. Trucks, H.B. Schlegel, P.M.W. Gill, B.G. Johnson, M.A. Robb, J.R. Cheeseman, T.A. Keith, G.A. Petersson, J.A. Montgomery, K. Raghavachari, M.A. Al-Laham, V.G. Zakrzewski, J.V. Ortiz, J.B. Foresman, J. Cioslowski, B.B. Stefanov, A. Nanayakkara, M. Challocombe, C.Y. Peng, P.Y. Ayala, W. Chen, M.W. Wong, J.L. Andres, E.S. Replogle, R. Gomperts, R.L. Martin, D.J. Fox, J.S. Binkley, D.J. Defrees, J. Baker, J.P. Stewart, M. Head-Gordon, C. Gonzales and J.A. Pople, *Gaussian 94* (Revision A.1); Gaussian, Inc.: Pittsburg, PA, 1995.

- 14) F. Sim, D.R. Salahub, S. Chin and M. Dupuis, *J. Chem. Phys.* **95**, 4317 (1991). F. Sim, A. St-Amant, I. Papai and D.R. Salahub, *J. Am. Chem. Soc.* **114**, 4391 (1992).
- 15) A.D. Becke, *J. Chem. Phys.* **88**, 2547 (1988).
- 16) C. Lee, W. Yang, R.G. Parr, *Phys. Rev. B* **37**, 785 (1988).
- 17) D.J. Giesen, C.J. Cramer and D.G. Truhlar, *J. Phys. Chem.* **99**, 7137 (1995). C.J. Cramer, G.D. Hawkins, G.C. Lynch, D.J. Giesen, I. Rossi, J.W. Storer, D.G. Truhlar and D.A. Liotard, *AMSOL-version 5.0*, **1995**.
- 18) S. Miertus and J. Tomasi, *Chem. Phys.* **65**, 239 (1982). S. Miertus, E. Scrocco, and J. Tomasi *Chem. Phys.* **55**, 117 (1981). E.L. Coitino, J. Tomasi and O.N. Ventura, *J. Chem. Soc. Faraday Trans.* **90**, 1745 (1994).
- 19) (a) A. Rastelli, M. Cocchi and E. Schiatti, *J. Chem. Soc. Faraday Trans.* **86**, 777 (1990). (b) A. Rastelli, M. Cocchi, E. Schiatti, R. Gandolfi and M. Burdisso, *ibidem* **86**, 783 (1990). (c) A. Rastelli and M. Cocchi, *ibidem* **87**, 249 (1991). (d) A. Rastelli and M. Bagatti, *ibidem* **88**, 2451 (1992). (e) A. Rastelli, M. Bagatti, A. Ori, R. Gandolfi and M. Burdisso, *ibidem* **89**, 29 (1993). (f) A. Rastelli, M. Bagatti and R. Gandolfi, *ibidem* **89**, 3913 (1993).
- 20) S.A. Pozzoli, A. Rastelli and M. Tedeschi, *J. Chem. Soc. Faraday Trans. 2* **69**, 256 (1973).
- 21) A. Rastelli, unpublished results.
- 22) (a) M. Tagliani, Thesys, University of Pavia, 1996. (b) M. Malagoli, Thesys, University of Modena 1997. (c) M. Freccero and R. Gandolfi, unpublished results.
- 23) (a) R. Greeé, F. Tonnard and R. Carrié, *Bull. Soc. Chim. Fr.*, 1325 (1975) and *Tetrahedron*, **32**, 675 (1976). (b) A. Padwa, L. Fisera, K.F. Koeler, A. Rodriguez and G.S.K. Wong, *J. Org. Chem.* **49**, 276 (1974). (c) T. Yakura, M. Nakazawa, T. Takino and M. Ikeda, *Chem. Pharm. Bull.* **40**, 2014 (1992). (d) K. Saito, H. Watanabe, M. Sakura and K. Takahashi, *Bull. Chem. Soc. Jpn.* **66**, 981 (1993). (e) T. Tejero, A. Dondoni, I. Rojo, F.L. Merchan and P. Merino, *Tetrahedron* **53**, 3301 (1997).
- 24) (a) M. Burdisso, A. Gamba, R. Gandolfi and R. Oberti, *Tetrahedron* **44**, 3735 (1988). (b) M. Burdisso, R. Gandolfi, P. Grunanger and A. Rastelli, *J. Org. Chem.* **55**, 3427 (1990).
- 25) K. Tada, T. Yamada and F. Toda, *Bull. Chem. Soc. Jpn.* **51**, 1839 (1978).
- 26) R.J. Loncharich, F.K. Brown and K.N. Houk, *J. Org. Chem.* **54**, 1129 (1989). M. Oliva, J. Bertran, J.J. Dannenberg, *J. Org. Chem.* **54**, 2488 (1989). D. Pitea, M. Gastaldi, F. Orsini, F. Pelizzoni, A. Mugnoli and E. Abbondanti, *J. Org. Chem.* **50**, 1853 (1985). K.N. Houk, R.J. Loncharich, J.F. Blake and W.L. Jorgensen, *J. Am. Chem. Soc.* **111**, 9172 (1989).
- 27) Y. Apeloig and E. Matzer, *J. Am. Chem. Soc.* **117**, 5375 (1995).
- 28) W.C. Herndon and L.H. Hall, *Tetrahedron Lett.* **1967**, 3095. J.E. Baldwin and V. Prakash Reddy, *J. Org. Chem.* **54**, 5264 (1989).
- 29) Calculations are in progress on the last interesting examples. We are also controlling the reported experimental results; our preliminary tests seems to confirm high endo selectivities, while excluding complete (100%) endo selectivity.

Solvent-mediated proton transfer reactions in cytosine: an ab initio study

Simone Morpurgo*, Mario Bossa, Giorgio O. Morpurgo

*Dipartimento di Chimica, Università degli Studi di Roma "La Sapienza"
P.le A. Moro 5, 00185 Roma, Italy*

Abstract

Solvent-mediated proton transfer reactions of mono- and dihydrated cytosine tautomers were investigated by ab initio quantum chemical calculations. MP2/6-31G** and MP2/D95** energy calculations were performed over geometries obtained at the HF/3-21G level. Corrections for the zero-point vibrational energy were included. It is shown that the coordination of one or two water molecules to cytosine tautomers produces a relative stabilization consistent with that obtained by continuum-based methods (PCM, SCRF). One or two water molecules are however insufficient to completely reproduce the order of stability. Coordination of even a single water molecule strongly activates the proton transfer process with respect to the gas phase. When corrections for ZPE are included in the calculations, water-promoted tautomerization reactions of cytosine have activation energies ranging from 10 to 16 kcal mol⁻¹ and are therefore expected to occur at room temperature.

1. Introduction

The relative stability of the tautomers of purine and pyrimidine bases is of fundamental importance to the structure and functioning of nucleic acids. The occurrence of rare tautomers was considered a factor responsible for the formation of mismatches leading to spontaneous mutations in the genetic code [1,2]. Cytosine, in particular, has been the subject of several studies, both experimental [3-5] and theoretical [5-15] which have provided a reliable picture of the relative stability of its tautomers, both in the gas phase and in solution. Tautomerization is generally the result of proton transfer (PT) reactions whose activation barriers may exert a kinetic control over the formation of some tautomers. As far as cytosine is concerned, a large majority of the studies available in the literature focus on the thermodynamic aspects of tautomerization and quite a few [16-19] are devoted to the elucidation of the kinetic aspects. The tautomerization of cytosine in the gas phase, with a special attention to the activation energy of the proton transfer reactions, has been afforded by this group in a previous paper [19]. By comparison with experimental data [4,5] it was

*corresponding author

shown that kinetic barriers in the gas phase are generally high (30-37 kcal mol⁻¹) and may affect the tautomers' population at $T \leq 500$ K. On the other hand, it is well known that the distribution of tautomeric forms, especially when it is proton transfer dependent, is modified under the influence of the environment. In this context, two factors are important the effect of the environment (i) on the relative stability of each tautomer and (ii) on the barrier height along the reaction coordinate separating two tautomeric forms.

The effect of the solvent is usually modelled either by the use of the Onsager's self consistent reaction field (SCRF) [20] or by the polarizable continuum method (PCM) [21]. With regard to the relative stability of cytosine tautomers in aqueous solution, these methods provided results [14,15] which, in spite of some discrepancies, are in reasonable agreement with experimental data [3]. However, continuum-based methods do not explicitly take into consideration the local solvent-solute interaction which is instead important in the description of the proton transfer mechanism in hydrogen-bonded systems. A reasonable approach to the problem was recently proposed [22,23] in which the molecule of interest and few solvent molecules are treated as a supermolecule acting as solute, while the bulk of the solvent is represented as a polarizable dielectric.

In the present paper the thermodynamic and kinetic aspects of the proton transfer reactions among cytosine tautomers assisted by specific solvent molecules was theoretically investigated. For the time being, bulk solvent effects were not considered and attention was only focused on the influence of hydrogen bonding on both (i) tautomers' relative stability and (ii) the catalytic process occurring between adjacent positions of cytosine. The computational results on point (i) are compared with those of PCM calculations [15]. The results on point (ii) are discussed with reference to the conclusions of other theoretical studies available in the literature [16,17].

2. Theoretical Methods

The Gaussian 94W [24] program package was employed for the *ab initio* calculations. The geometries of both minima and transition states were optimized at the HF/3-21G level using the Berny algorithm [25,26]. The transition states were localized by means of the STQN method [26,27]. All structures were vibrationally characterized, checking for the absence of imaginary frequencies in the minima and for the presence of only one imaginary frequency in the transition states. It was additionally verified through the graphical interface of HyperChem 4.5 [28] that the imaginary frequency of the transition states corresponds to the reaction coordinate of the proton transfer reaction. Zero-point vibrational energies (ZPE) were scaled by 0.91, which is a commonly accepted correction factor [5,9]. Single-point energy calculations were performed at the MP2/6-31G** and MP2/D95** level, the latter basis set being employed only for the monohydrated adducts (see next section). The frozen-core (FC) approximation was adopted for

all MP2 calculations with only few exceptions, where full MP2 correlation and D95** basis set were additionally used for the sake of comparison with literature data [17].

3. Results and discussion

3.1 Systems investigated: the five most stable tautomers of cytosine are shown in Fig. 1. The tautomeric equilibrium among these species is based on the $C1 \rightleftharpoons C2$, $C1 \rightleftharpoons C3$ and $C4 \rightleftharpoons C5$ interconversions. They may occur as direct proton transfer reactions in the gas phase, with activation energies ranging from 30 to about 37 kcal mol⁻¹, as suggested in a previous paper [19].

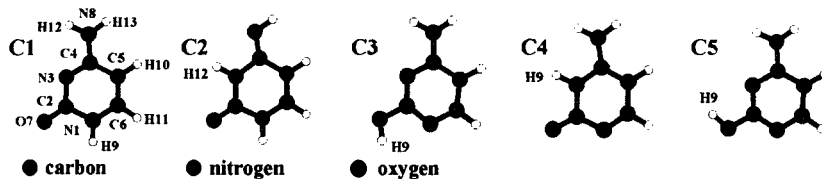


Figure 1. The five most stable tautomers of cytosine.

For mono- and dihydrated adducts of cytosine the N1, N3, O7 and N8 positions were considered for coordination, since these sites are the most suitable to hydrogen bond solvent molecules, as already shown both theoretically [16,29] and experimentally on molecules modelling cytosine and isocytosine [30-33]. H10 and H11 were expected to form comparatively weaker hydrogen bonds with solvent molecules and thus coordination to these sites was not considered. The water-assisted reactions investigated in the present study may be ideally divided into three groups (Fig. 2). The first one (reactions **a**, **b**, **c**) encloses the processes catalyzed by one hydrogen-bonded water molecule, which forms a bridge between the two adjacent sites involved in the proton transfer. The second group (**d**, **e**, **f**) deals with the same reactions, catalyzed by two bridging water molecules which give rise to a concerted triple proton transfer mechanism. The mechanisms considered in the third group (**g**, **h**, **i**, **l**) are the same as those in the first one, with a second water molecule coordinated to some other functional groups of cytosine not directly involved in the proton transfer. The $C3 \rightleftharpoons C5$ interconversion, which takes place in the gas phase by rotation of O7-H9 bond around the C2-O7 axis with an activation energy of about 8 kcal mol⁻¹ [19], in water solution is more likely to occur through a dissociative mechanism and therefore was not included in the present work.

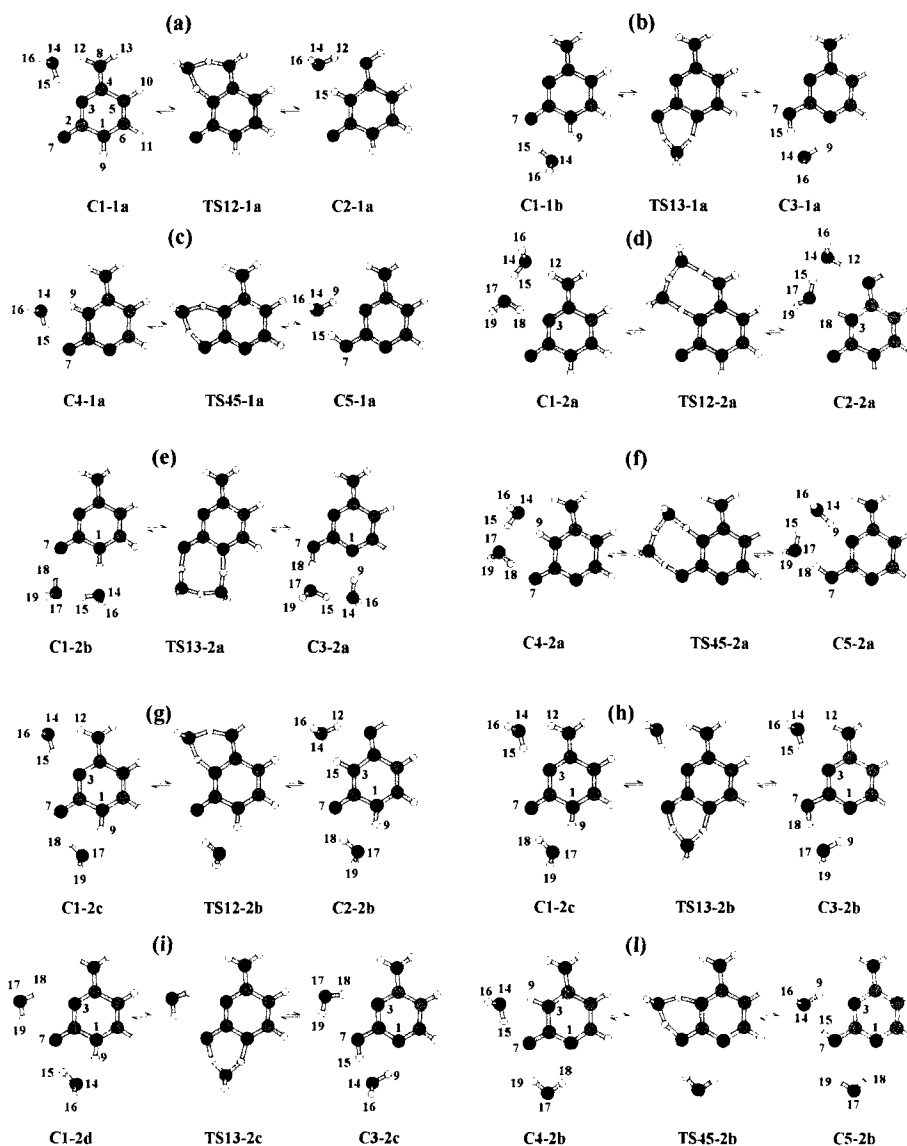


Figure 2. Scheme of the simulated proton transfer reactions occurring among mono- and dihydrated cytosine tautomers.

The structures reported in Fig. 3 are not directly involved in proton transfer reactions (some of them would eventually give rise to the rather unstable imino-hydroxy tautomeric forms [6,15]) but were included in the calculations in

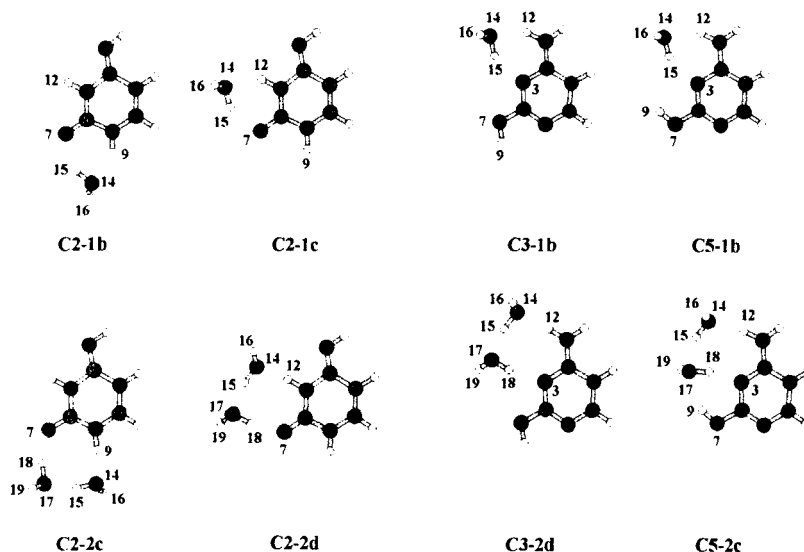


Figure 3. Mono- and dihydrated adducts of cytosine tautomers relevant for stability calculations.

order to investigate the relative stability of mono- and dihydrated cytosine tautomers. The computational results are presented and discussed in three separate sections which are respectively dedicated (3.2) to the effect of hydrogen bonding on the geometrical parameters of the solvated molecules, (3.3) to the influence of hydration on the thermodynamic stability of cytosine tautomers and (3.4) to the kinetics of solvent-assisted proton transfer reactions.

3.2 Geometrical parameters: the main HF/3-21G geometrical parameters of monohydrated cytosine tautomers and transition states are reported in Table 1. For the sake of comparison, the geometries of the C1-C4 tautomers calculated in vacuum at the same computational level are available in Ref. [6]. The structural changes induced in the solute by hydrogen bonding with one solvent molecule are generally consistent with those calculated at higher computational level for some related systems [22,23,34]. As an example, the hydrogen bond at N3 and H12 in

Table 1. Selected geometric parameters (distances in Å, angles in degrees) for monohydrated cytosine tautomers and transition states optimized at the HF/3-21G level.

	C1-1a	TS12-1a	C2-1a	C1-1b	TS13-1a	C3-1a	C4-1a	TS45-1a	C5-1a
r(2-1)	1.411	1.403	1.387	1.400	1.371	1.340	1.363	1.334	1.322
r(3-2)	1.366	1.359	1.363	1.358	1.332	1.322	1.407	1.378	1.342
r(4-3)	1.313	1.355	1.388	1.305	1.322	1.328	1.345	1.333	1.333
r(5-4)	1.443	1.445	1.459	1.436	1.419	1.409	1.377	1.394	1.400
r(6-5)	1.337	1.335	1.327	1.342	1.356	1.364	1.396	1.378	1.371
r(1-6)	1.355	1.359	1.371	1.348	1.337	1.339	1.306	1.325	1.333
r(7-2)	1.213	1.212	1.212	1.230	1.282	1.322	1.229	1.280	1.322
r(8-4)	1.331	1.298	1.269	1.342	1.341	1.344	1.346	1.346	1.349
r(9-1)	0.998	0.998	0.997	1.017	1.290	1.910			
r(9-3)							1.020	1.280	1.942
r(12-8)	1.014	1.231	1.875	0.998	0.997	0.997	0.997	0.996	0.996
r(13-8)	0.995	0.999	1.008	0.994	0.995	0.994	0.995	0.995	0.995
r(14-9)				1.791	1.199	0.982	1.763	1.207	0.979
r(14-12)	1.817	1.258	0.984						
r(15-3)	1.903	1.222	1.019						
r(15-7)				1.806	1.212	0.993	1.809	1.223	0.991
r(15-14)	0.983	1.270	1.796	0.982	1.210	1.647	0.983	1.199	1.657
r(16-14)	0.966	0.965	0.966	0.965	0.963	0.965	0.965	0.963	0.966
a(14-9-1)				146.75	147.79	138.66			
a(14-9-3)							148.84	148.78	138.95
a(14-12-8)	148.88	149.97	146.30						
a(14-15-3)	145.48	149.81	149.42						
a(14-15-7)				146.57	152.69	157.25	145.53	152.43	157.54
a(15-14-9)				82.99	87.29	86.75	83.07	86.79	86.06
a(15-14-12)	82.11	85.55	82.21						
a(16-14-15)	108.68	117.39	115.93	109.21	118.31	118.98	109.24	117.31	116.95
d(16-14-15-9)				122.94	122.47	111.49	-125.04	-122.43	-110.78
d(16-15-14-12)	-119.91	-120.13	-107.68						

the C1-1a adduct induces the following changes with respect to the geometry optimized in vacuum, (i) $r(\text{N8-H12})$ is increased by 0.017 Å, (ii) $r(\text{C4-N8})$ is shortened by 0.013 Å and (iii) $r(\text{N3-C4})$ increases by 0.017 Å. This implies that, as H12 tends to be moved away from N8, the double bond character of C4-N8 increases and, at the same time, the double bond character of N3-C4 decreases. As a further example, in the C1-1b adduct, hydrogen bonding (i) increases both $r(\text{N1-H9})$ and $r(\text{C2-O7})$ by 0.019 Å and (ii) decreases $r(\text{N1-C2})$ by 0.015 Å. The structural changes calculated for the adducts of the other tautomers are quantitatively similar. It should be stressed that geometry optimization at the HF/3-21G level tends to underestimate hydrogen bond distances with respect to the values obtained by using more extended basis sets with inclusion of polarization functions and treatment of electron correlation. However, it will be shown in the 3.3 section that, in the present case, such inaccuracies are not likely to affect appreciably the calculated values of the proton transfer activation energy.

Hydrogen bond interactions are also reflected in the calculated IR spectra of the monohydrated bases. Taking the C1-1a adduct as an example, the following

shifts are observed with respect to the frequencies of the isolated C1 tautomer [5,9] (all values are scaled by 0.91): (i) -40 cm^{-1} for the $-\text{NH}_2$ asymmetric stretching, (ii) -321 cm^{-1} for the O14-H15 stretching, (iii) -34 cm^{-1} for the O14-H16 stretching and (iv) $+67\text{ cm}^{-1}$ for the $-\text{NH}_2$ scissoring. Such frequency shift values are in reasonable agreement with those observed in Ar matrices and theoretically calculated for strictly related systems, such as monohydrated 4-aminopyrimidine [31] and 1-methylcytosine [32]. Furthermore, the shift of the $\text{C}=\text{O}$ stretching mode (-24 cm^{-1}) calculated for the C1-1b adduct is close to the value experimentally observed for either 1- and 3-methyluracile (ca. -20 cm^{-1}) [35].

3.3 Relative stability of tautomeric forms: it is widely accepted, on the grounds of both experimental [4,5] and theoretical [8-15] work, that the order of stability of cytosine tautomers in the gas phase is $\text{C3} > \text{C5} > \text{C1} > \text{C2} \gg \text{C4}$, the first four tautomers being enclosed in a range of about 3 kcal mol^{-1} and C4 being less stable than C3 by more than 7 kcal mol^{-1} . A rather different ordering exists in polar solvents, where C1 and C4 are the only experimentally observed species [3]. This finding was substantially confirmed by theoretical calculations. It was established, by either the SCRF and the PCM methods, that C1 is the most stable form in aqueous solution and it is preferred by about 5 kcal mol^{-1} over the other tautomers, which are enclosed in a range of 1.5 kcal mol^{-1} [14,15]. Notably, the C4 tautomer, which is energetically unfavoured in vacuum, becomes the second stable form in aqueous solution, being stabilized by its high dipole moment. Since continuum-based computational methods deal with a single component of the solvation process, namely the dipolar interaction, the present work was also aimed at elucidating how the formation of specific hydrogen bonds with solvent may affect the relative stability of the tautomeric forms of a selected species. Cytosine has several sites which are potentially capable of hydrogen bonding and, therefore, it appears as a particularly interesting case study.

The relative stability of cytosine tautomeric forms was estimated in the following way (i) the energy of all adducts was calculated with inclusion of ZPE, (ii) the most stable adduct with a given number of solvent molecules was identified among all tautomers, (iii) the energy of all other adducts was related to the energy of the most stable one. The results are listed in Table 2. At the MP2(FC)/6-31G**//HF/3-21G level, the most stable monohydrated adducts were found to be C1-1b, C2-1b, C3-1a, C4-1a and C5-1a, and the most stable dihydrated ones C1-2c, C2-2b ~ C2-2c, C3-2b, C4-2a and C5-2a respectively (Figs. 2-3). No appreciable differences were found when the ordering of monohydrated adducts was evaluated at the MP2(FC)/D95**//HF/3-21G level. The trend of the energy difference between the tautomeric forms when an increasing number of water molecules are coordinated to the bare cytosine is shown in Fig. 4. The mean energy of each mono- or dihydrated tautomeric species, \bar{E}_t , is calculated according to the Maxwell-Boltzmann distribution law

Table 2. Computational results obtained for the adducts of Figures 2-3. Energy (a.u), dipole moment (Debye), zero-point vibrational energy (ZPE/kcal mol⁻¹), ZPE-corrected relative energy of the adducts (ΔE_{rel} /kcal mol⁻¹) with stability order in brackets (a), activation energy uncorrected (ΔE^\ddagger /kcal mol⁻¹) and corrected ($\Delta E_{\text{corr}}^\ddagger$ /kcal mol⁻¹) for ZPE.

MP2(FC)/6-31G**//HF/3-21G results

monohydrated adducts

adduct	energy	dipole	ZPE (b)	ΔE_{rel}	ΔE^\ddagger	$\Delta E_{\text{corr}}^\ddagger$
formamide	-245.67403	3.32	44.07	0.00	23.65	20.33
TS	-245.63634	2.72	40.75			
formamidic ac.	-245.65512	2.30	43.89	11.69	11.78	8.64
formamidine	-225.81646	3.21	51.43		18.93	15.84
TS	-225.78629	4.19	48.34			
C1-1a	-470.04835	6.74	77.02	0.89	18.51	15.04
TS12-1a	-470.01886	6.89	73.55			
C2-1a	-470.04476	6.13	77.25	3.37	16.25	12.55
C1-1b	-470.04958	6.14	76.90	0.00 (1)	15.24	11.43
TS13-1a	-470.02530	5.46	73.09			
C3-1a	-470.04844	4.58	76.37	0.19 (2)	14.52	11.24
C4-1a	-470.03968	7.38	76.64	5.95 (5)	13.13	9.39
TS45-1a	-470.01875	7.06	72.90			
C5-1a	-470.04524	6.22	76.22	2.04 (3)	16.62	13.30
C2-1b	-470.04534	4.01	77.17	2.93 (4)		
C2-1c	-470.04163	5.41	76.98	5.07		
C3-1b	-470.04785	2.74	76.40	0.59		
C5-1b	-470.04374	3.76	76.29	3.05		
C1-1a (c)	-470.04631	5.81	76.51		20.90	17.29
TS12-1a (c)	-470.01300	6.15	72.90			
C2-1a (c)	-470.04198	5.20	76.65		18.19	14.44

dihydrated adducts

C1-2a	-546.28996	6.16	92.30	0.82	18.83	14.06
TS12-2a	-546.25995	6.34	87.53			
C2-2a	-546.28449	5.59	92.48	4.44	15.40	10.45
C1-2b	-546.29073	5.26	92.23	0.27	16.38	11.38
TS13-2a	-546.26463	3.88	87.23			
C3-2a	-546.28654	3.90	91.44	2.11	13.75	9.54
C4-2a	-546.28574	6.14	92.48	3.65 (5)	15.11	10.22
TS45-2a	-546.26166	5.30	87.59			
C5-2a	-546.28667	5.19	91.82	2.41 (3)	15.69	11.46
C1-2c	-546.29156	5.26	92.48	0.00 (1)	18.99	15.43
TS12-2b	-546.26129	5.25	88.92			
C2-2b	-546.28630	4.44	92.61	3.43	15.69	12.00

Table 2. (Continued).

C1-2c	-546.29156	5.26	92.48	0.00 (1)	15.66	11.81
TS13-2b	-546.26660	4.46	88.63			
C3-2b	-546.28888	3.60	91.87	1.07 (2)	13.98	10.74
C1-2d	-546.28468	8.66	91.50	3.34	15.84	12.04
TS13-2c	-546.25943	7.80	87.70			
C3-2c	-546.28134	6.65	90.86	4.79	13.75	10.59
C4-2b	-546.27484	10.84	91.26	9.27	13.64	9.93
TS45-2b	-546.25311	10.48	87.55			
C5-2b	-546.27817	9.51	90.70	6.62	15.73	12.58
C2-2c	-546.28628	3.20	92.57	3.40 (4)		
C2-2d	-546.28070	4.78	92.33	6.66		
C3-2d	-546.28790	1.86	91.67	1.49		
C5-2c	-546.28649	4.26	92.04	2.74		
MP2(FC)/D95**//HF/3-21G results						
<i>monohydrated adducts</i>						
formamide	-245.76834	3.46	44.07	0.00	22.48	19.16
TS	-245.73251	2.80	40.75			
formamidic ac.	-245.75031	2.33	43.89	11.13	11.17	8.03
formamidine	-225.90205	3.32	51.43		17.70	14.61
TS	-225.87384	4.28	48.34			
C1-1a	-470.12338	6.87	77.02	0.45	17.72	14.25
TS12-1a	-470.09514	6.98	73.55			
C2-1a	-470.11910	6.21	77.25	3.37	15.04	11.34
C1-1b	-470.12391	6.25	76.90	0.00 (1)	14.43	10.62
TS13-1a	-470.10092	5.56	73.09			
C3-1a	-470.12263	4.66	76.37	0.27 (2)	13.62	10.34
C4-1a	-470.11428	7.53	76.64	5.78 (5)	12.35	8.61
TS45-1a	-470.09460	7.19	72.90			
C5-1a	-470.11944	6.32	76.22	2.12 (3)	15.59	12.27
C2-1b	-470.11947	4.09	77.17	3.06 (4)		
C2-1c	-470.11554	5.50	76.98	5.33		
C3-1b	-470.12238	2.82	76.40	0.46		
C5-1b	-470.11797	3.87	76.29	3.12		
C1-1a (d)	-470.25632	6.87	77.02		17.81	14.34
TS12-1a (d)	-470.22793	6.98	73.55			
C2-1a (d)	-470.25204	6.21	77.25		15.13	11.43
C1-1a (e)	-470.05474	6.89	77.02		19.77	16.30
TS12-1a (e)	-470.02323	7.07	73.55			
C2-1a (e)	-470.05002	6.27	77.25		16.81	13.11
C1-1a (f)	-470.12257	5.88	76.51		19.99	16.38
TS12-1a (f)	-470.09072	6.22	72.90			
C2-1a (f)	-470.11761	5.24	76.65		16.87	13.12

Table 2. (Continued).

C1-1a	(g)	-470.25553	5.86	76.51	20.07	16.46
TS12-1a	(g)	-470.22355	6.21	72.90		
C2-1a	(g)	-470.25056	5.24	76.65	16.95	13.20
C1-1a	(h)	-470.05400	5.85	76.51	22.38	18.77
TS12-1a	(h)	-470.01834	6.25	72.90		
C2-1a	(h)	-470.04858	5.26	76.65	18.98	15.23

(a) the most stable adduct is considered for each tautomeric form;

(b) calculated at the HF/3-21G level and scaled by 0.91 [5,9];

(c) MP2(FC)/6-31G**//HF/3-21G, C_s constraint;

(d) MP2(full)/D95**//HF/3-21G;

(e) MP2(FC)/D95**//HF/3-21G;

(f) MP2(FC)/D95**//HF/3-21G, C_s constraint;

(g) MP2(full)/D95**//HF/3-21G, C_s constraint;

(h) MP2(FC)/D95**//HF/3-21G, C_s constraint.

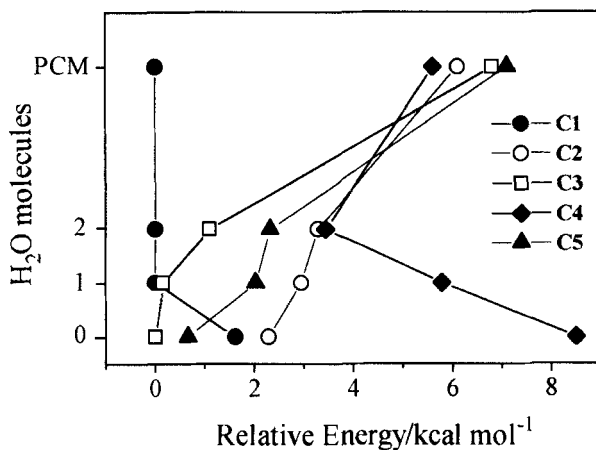


Figure 4. Relative stability of mono- and dihydrated cytosine tautomers compared with PCM [15] and *in vacuo* [19] relative stability.

$$E_t = \frac{\sum_i E_i \exp(-E_i / RT)}{\sum_i \exp(-E_i / RT)}$$

where the summation is over the adducts of a given tautomer and E_i is the relative

energy with respect to the most stable adduct of all tautomers considered [point (iii) above]. The values at the bottom of the figure are those calculated for unsolvated cytosine monomers [19]. The values at the top are those calculated by Colominas et al. [15] by means of the PCM method. It is apparent that two water molecules are insufficient to account for the final order of stability reported in [15], though some partial results are achieved: (i) C1, which is the third most stable form in vacuum ($+1.61 \text{ kcal mol}^{-1}$ with respect to C3) becomes the most stable form upon addition of one water molecule ($-0.16 \text{ kcal mol}^{-1}$ with respect to C3) and the stabilization is enhanced ($-1.09 \text{ kcal mol}^{-1}$) as a second water molecule is coordinated, (ii) the stabilization of C4 which, being less stable than C3 by about $8.5 \text{ kcal mol}^{-1}$ in vacuum, becomes less stable than C1 by about $3.3 \text{ kcal mol}^{-1}$ when the dihydrated adducts are considered.

3.4 Kinetics of water-assisted proton transfer: as anticipated in Section 3.2, HF/3-21G geometry optimizations tend to underestimate hydrogen bond distances with respect to the values obtained at higher computational level. As a consequence, MP2/6-31G** single-point calculations based on HF/3-21G geometries may yield, in principle, inaccurate values for the PT activation energies. For this reason, we have performed benchmark calculations on the water-assisted tautomerization equilibria of formamidine and formamide \rightleftharpoons formamidic acid. Such systems were chosen as a reference because the proton transfer occurs between the same functional groups as those involved in cytosine. The results of the computations at the MP2(FC)/6-31G**/HF/3-21G and MP2(FC)/D95**/HF/3-21G level are reported in Table 2. Comparison with MP2/6-31G**/MP2/6-31G** literature data [22,34] shows that the activation energies are computed with an error of about $\pm 1.5 \text{ kcal mol}^{-1}$. On the assumption that this approximation can be extended to proton transfer reactions of cytosine, we are led to conclude that HF/3-21G geometry optimizations are adequate for the scope of the present work.

The results obtained for the proton transfer reactions of cytosine illustrated in Fig. 2, are listed in Table 2. The activation energies are reported as a simple difference in electronic energy and with further correction for ZPE. As it is generally observed for PT reactions [22,34,36], the inclusion of ZPE lowers the activation barriers by 2-4 kcal mol^{-1} with respect to the values calculated on the basis of pure electronic energy changes. As ZPE was considered, it was found that the activation energies of $\text{C1} \rightleftharpoons \text{C3}$ and $\text{C4} \rightleftharpoons \text{C5}$ direct and reverse processes range from 10 to 12 kcal mol^{-1} , with small differences due to the relative energy of the minima. The $\text{C1} \rightarrow \text{C2}$ tautomerization has an activation energy of about 14-15 kcal mol^{-1} , while the reverse reaction, $\text{C2} \rightarrow \text{C1}$, has an activation energy of ca. 12 kcal mol^{-1} . For the processes labelled as a, b and c MP2(FC)/D95** single point energy calculations produced activation energies which are, on the average, 0.92 kcal mol^{-1} lower than those calculated at MP2(FC)/6-31G** level.

Remarkably, the inclusion of even a single bridging water molecule in the mechanism reduced the activation energy by 15-20 kcal mol^{-1} in comparison to

the direct tautomerization in the gas phase [19]. This result agrees with those of recent investigations on some related systems such as the tautomeric couples formamide/formamidic acid [22], 2-hydroxypyridine/2-pyridone [23], formamidine [34] and others [37,38], where a comparable lowering of the activation energy was found for the water-assisted reaction with respect to the gas-phase process. Notably, the major kinetic effect is produced by the first bridged solvent molecule (reactions **a**, **b**, **c**). Neither the inclusion of a second bridged water molecule (cases **d**, **e**, **f**) nor the coordination of a second water molecule to a site not involved in the proton transfer (cases **g**, **h**, **i**, **l**) did result in a further kinetic promotion.

The kinetics of the $C1 \rightleftharpoons C2$ interconversion mediated by a single water molecule was recently investigated in the ground state as well as in the lowest excited $\pi\pi^*$ and $n\pi^*$ singlet states [17]. In this work, as far as the ground state reaction is concerned, the 3-21G basis set was employed for geometry optimization at the HF level. The minima and the transition states of the cytosine \cdot H₂O adduct were optimized (i) without geometrical constraints and (ii) imposing C_s symmetry. In each case, MP2(full)/D95** single point energy calculations were performed along the reaction coordinate. For the $C1 \rightarrow C2$ reaction, the authors reported an activation energy of 1.0 eV under the C_s constraint which decreased by about 10% when geometry relaxation was allowed. On this basis, it was suggested that the $C1 \rightarrow C2$ proton transfer is extremely unlikely in the ground state, due to its high activation energy. Since our findings disagreed with this conclusion, we were prompted to analyze in deeper detail our computational results. Surprisingly, we were not able to reproduce the results of Ref. [17]. For $C1 \rightarrow C2$ we calculated, under the C_s constraint, an activation energy of 20.07 kcal mol⁻¹ [MP2(full)/D95**] and 19.99 kcal mol⁻¹ [MP2(FC)/D95**]. Upon geometry relaxation, these values decreased to 17.81 and 17.72 kcal mol⁻¹, respectively. We found a relative agreement only by MP2(FC)/D95* single-point calculations, which gave activation energies of 22.38 (C_s) and 19.77 (unconstrained optimization) kcal mol⁻¹. This result, however, is to be considered physically less reliable, due to the lack of p-type polarization functions on hydrogen atoms in the D95* basis set. Finally, HF/3-21G geometries and energies (-466.03406 a.u. for C1 \cdot H₂O and -466.03116 a.u. for C2 \cdot H₂O) of the unconstrained minima were found in agreement with those reported in Ref. [17]. A further agreement was found for the energy difference between unconstrained and C_s minima (350 and 480 cm⁻¹ for C1 \cdot H₂O and C2 \cdot H₂O, respectively). Unfortunately, the geometry of the transition states was not reported in Ref. [17]. The inclusion of the ZPE, not previously considered, further reduced the activation energy of the $C1 \rightarrow C2$ process by about 3.5 kcal mol⁻¹, to the final value of 14-15 kcal mol⁻¹. Our results are closer to those of Stepanian *et al.* [16], although the latter work was performed by the semiempirical MNDO/M [39,40] method and activation energies as low as 12 kcal mol⁻¹ could only be obtained for the concerted three-proton transfer mechanism.

On the basis of the present calculations on simplified hydrated models we can safely suggest that cytosine tautomerization reactions should take place at room temperature, and that the $C1 \rightarrow C2$ conversion is kinetically unfavoured by $2\text{--}4 \text{ kcal mol}^{-1}$ with respect to the $C1 \rightleftharpoons C3$ and $C4 \rightleftharpoons C5$ processes. Bulk solvent effects, which are not included in the present study, are expected to provide only a fine tuning of the activation energies, as variations of the dipole moment from minima to transition states are generally less than 1 Debye (Table 2).

4. Conclusions

The main computational results of the present work can be summarized as follows: (i) as far as HF/3-21G geometry optimizations are concerned, the structural changes induced in the solute by hydrogen bonding with one solvent molecule are consistent with those calculated at higher computational level for related systems such as monohydrated formamide, formamidic acid and formamidine, but hydrogen bond distances are generally underestimated; (ii) proton transfer activation energies calculated from these geometries through MP2/6-31G** and MP2/D95** single points differ by ca. $\pm 1.5 \text{ kcal mol}^{-1}$ from the values based on full MP2/6-31G** optimizations; (iii) coordination of a discrete number of solvent molecules produces a relative stabilization of cytosine tautomers which is close to that obtained by continuum-based methods (PCM, SCRF); (iv) one or two water molecules are however insufficient to reproduce the final order of stability given in [15]; (v) coordination of even a single water molecule strongly activates the proton transfer process with respect to the gas phase; (vi) coordination of more than one water molecule does not result in a further promotion of the proton transfer reactions; (vii) as ZPE correction is included in the calculations, water-promoted tautomerization reactions of cytosine have activation energies ranging from 10 to 15 kcal mol^{-1} ; (viii) the $C1 \rightarrow C2$ conversion ($\Delta E^\ddagger = 14\text{--}15 \text{ kcal mol}^{-1}$), though kinetically unfavoured with respect to the $C1 \rightleftharpoons C3$ and $C4 \rightleftharpoons C5$ processes, can take place at room temperature; (ix) as a general conclusion, kinetic factors do not seem to be important for the distribution of cytosine tautomers in water solution at room temperature. The most stable of the tautomers (C1) is expected to be much less kinetically protected by the solvent than it was suggested in ref. [17].

References

- [1] M. D. Topal, J. R. Fresco, *Nature (London)* **263**, 285 (1976).
- [2] M. D. Topal, J. R. Fresco, *Nature (London)* **263**, 289 (1976).
- [3] M. Dreyfus, O. Bensaude, G. Dodin and J. E. Dubois, *J. Am. Chem. Soc.* **98**, 6338 (1976).

- [4] R. D. Brown, P. D. Godfrey, D. McNaughton and A. P. Pierlot, *J. Am. Chem. Soc.* **111**, 2308 (1989).
- [5] M. Szczesniak, K. Szczepaniak, J. S. Kwiatkowski, K. KuBulat and W. B. Person, *J. Am. Chem. Soc.* **110**, 8319 (1988).
- [6] M. S. Scanlan and I. H. Hillier, *J. Am. Chem. Soc.* **106**, 3737 (1984).
- [7] P. Cieplak, P. Bash, U. Chandra Singh and P. A. Kollman, *J. Am. Chem. Soc.* **109**, 6283 (1987).
- [8] J. S. Kwiatkowski, R. J. Bartlett and W. B. Person, *J. Am. Chem. Soc.* **110**, 2353 (1988).
- [9] A. Les, L. Adamowicz and R. J. Bartlett, *J. Phys. Chem.* **93**, 4001 (1989).
- [10] E. L. Stewart, C. K. Foley, N. L. Allinger and J. P. Bowen, *J. Am. Chem. Soc.* **116**, 7282 (1994).
- [11] J. Šponer and P. Hobza, *J. Mol. Struct. (Theochem)* **304**, 35 (1994).
- [12] J. Šponer and P. Hobza, *J. Phys. Chem.* **98**, 3161 (1994).
- [13] I. R. Gould, N. A. Burton, R. J. Hall and I. H. Hillier, *J. Mol. Struct. (Theochem)* **331**, 147 (1995).
- [14] I. R. Gould, D. V. S. Green, P. Young and I. H. Hillier, *J. Org. Chem.* **57**, 4434 (1992).
- [15] C. Colominas, F. J. Luque and M. Orozco, *J. Am. Chem. Soc.* **118**, 6811 (1996).
- [16] S. G. Stepanian, G. G. Sheina, E. D. Radchenko and Yu. P. Blagoi, *J. Mol. Struct.* **270**, 459 (1992).
- [17] A. L. Sobolewski and L. Adamowicz, *J. Chem. Phys.* **102**, 5708 (1995).
- [18] A. L. Sobolewski and L. Adamowicz, *Chem. Phys. Lett.* **234**, 94 (1995).
- [19] S. Morpurgo, M. Bossa and G. O. Morpurgo, *Chem. Phys. Lett.* **280**, 233 (1997).
- [20] O. Tapia and O. Goscinski, *Mol. Phys.* **29**, 1653 (1975).
- [21] S. Miertus, E. Scrocco and J. Tomasi, *Chem. Phys.* **55**, 117 (1981).
- [22] C. Adamo, M. Cossi and V. Barone, *J. Comput. Chem.* **18**, 1993 (1997).
- [23] V. Barone, C. Adamo, *J. Phys. Chem.* **99**, 15062 (1995).
- [24] Gaussian 94, Revision B.2, M. J. Frisch, G. W. Trucks, H. B. Schlegel, P. M. W. Gill, B. G. Johnson, M. A. Robb, J. R. Cheeseman, T. A. Keith, G. A. Petersson, J. A. Montgomery, K. Raghavachari, M. A. Al-Laham, V. G. Zakrzewski, J. V. Ortiz, J. B. Foresman, C. Y. Peng, P. Y. Ayala, W. Chen, M. W. Wong, J. L. Andres, E. S. Replogle, R. Gomperts, R. L. Martin, D. J. Fox, J. S. Binkley, D. J. Defrees, J. Baker, J. P. Stewart, M. Head-Gordon, C. Gonzalez, and J. A. Pople, Gaussian, Inc., Pittsburgh PA, 1995.
- [25] H. B. Schlegel, *J. Comput. Chem.* **3**, 214 (1982).
- [26] C. Peng, P. Y. Ayala, H. B. Schlegel and M. J. Frisch, *J. Comput. Chem.* **16**, 49 (1995).
- [27] C. Peng and H. B. Schlegel, *Israel J. Chem.* **33**, 449 (1993).
- [28] HyperChem Computational Chemistry, Reference Manual, ed. Hypercube, Inc., Waterloo, Ontario, Canada, 1995.

- [29] K. Sagarik, G. Corongiu and E. Clementi, *J. Mol. Struct. (Theochem)* **235**, 355 (1991).
- [30] A. Destexhe, J. Smets, L. Adamowicz and G. Maes, *J. Phys. Chem.* **98**, 1506 (1994).
- [31] J. Smets, L. Adamowicz and G. Maes, *J. Phys. Chem.* **99**, 6387 (1995).
- [32] J. Smets, L. Adamowicz and G. Maes, *J. Phys. Chem.* **100**, 6434 (1996).
- [33] A. Destexhe, J. Smets, L. Adamowicz and G. Maes, *J. Phys. Chem.* **101**, 6583 (1997).
- [34] Q. Zhang, R. Bell and T. N. Truong, *J. Phys. Chem.* **99**, 592 (1995).
- [35] M. Graindourze, T. Grootaers, J. Smets, T. Zeegers-Huyskens and G. Maes, *J. Mol. Struct.* **243**, 37 (1991).
- [36] C.-C Wu and M.-H. Lien, *J. Phys. Chem.* **100**, 594 (1996).
- [37] D. Lee, C. K. Kim, B.-S. Lee, I. Lee and B. C. Lee, *J. Comput. Chem.* **18**, 56 (1997).
- [38] R. Minyaev, *Chem. Phys. Lett.* **262**, 194 (1996).
- [39] A. A. Voityuk and A. A. Bliznyuk, *Theor. Chim. Acta* **72**, 223 (1987).
- [40] A. A. Bliznyuk and A. A. Voityuk, *J. Mol. Struct. (Theochem)* **164**, 343 (1988).

Electron correlation at the dawn of the 21st century

Werner Kutzelnigg and Pasquale von Herigonte
Lehrstuhl für Theoretische Chemie
Ruhr-Universität Bochum, D-44780 Bochum, Germany

March 7, 1999

Abstract

The history and the present state of the treatment of electron correlation is reviewed. For very small atoms or molecules calculations of higher than spectroscopic accuracy are possible. A detailed account for many-electron methods in terms of one-electron basis sets is given with particular attention to the scaling of computer requirements with the size of the molecule. The problems related to the correlation cusp, especially the slow convergence of a basis expansion, as well as their solutions are discussed. The unphysical scaling with the particle number may be overcome by localized-correlation methods. Finally density functional methods as an alternative to traditional ab-initio methods are reviewed.

Contents

1	Introduction	2
2	Electron correlation in very small atoms and molecules	3
3	Many-electron methods in terms of one-electron basis sets	6
3.1	Full CI	6
3.2	The 2-particle density matrix and the n-representability problem	8
3.3	Many-body perturbation theory	9
3.4	Coupled-cluster and related methods	11
3.5	Multi-configuration-based methods	13

4	The convergence with the basis size and the R12 method	15
5	Localized correlation methods	18
6	Density functional methods	21
6.1	History	21
6.2	The Hohenberg-Kohn theorem as a Legendre transformation	23
6.3	Slater-Kohn-Sham type methods	26
7	Conclusions	28

1 Introduction

One of us [1] reviewed the situation of electron correlation a quarter of a century ago in a paper with the title '*electron correlation in the seventies*' [2]. At that time most quantum chemists did not care about electron correlation, and standard methods for the large scale treatment of electron correlation, like Møller-Plesset (MP) perturbation theory or coupled-cluster (CC) theory were not yet available. However precursors of these methods such as IEPA (independent electron pair approximation) and CEPA (coupled-electron-pair approximation) had already been developed and were being used, mainly in research groups in Germany [3, 4, 5, 6, 7, 8, 9, 10, 11, 12, 13].

A quite spectacular progress has been achieved since then, but electron correlation is still the severest bottleneck on the way to accurate quantum chemical results.

Electron correlation means everything that goes beyond the independent particle model for electrons, i.e. which is due to the correlation of the motion of the individual electrons [14]. There has been some controversy on whether or not *electron exchange* should be regarded as part of the correlation. (For a recent discussion of this aspect see ref. [15]). We adopt here the view that electron exchange is taken care of by the independent particle model and is not part of the electron correlation.

High accuracy of quantum chemical calculations not only requires a satisfactory treatment of electron correlation, but also relativistic and beyond-Born-Oppenheimer effects need to be considered [16, 17, 18]. These are not in the scope of the present review. We further concentrate on correlation effects on the energy (and on quantities directly derivable from potential energy surfaces) and we ignore correlation effects on properties, which is an important subject at present [19]. We further shall report more on the calculation than on the interpretation of correlation effects.

The correlation problem is more or less solved for systems with up to, say, four electrons. For these, calculations involving all interelectronic coordinates are possible such that one can satisfy all cusp conditions [20] and rapid convergence to *numerically exact* values is achieved. Sec. 2 of this review will deal with these systems. For medium-sized molecules one knows, in principle, what one should do. However, the computer resources for methods which are routinely available, scale so unfortunately with the size of the molecule and converge so slowly with extension of the orbital basis, that their application is rather limited. We shall review these classical methods of CI (configuration interaction) type in sec. 3. There seems to be a solution at least to the poor convergence with the size of the basis, namely to use explicitly correlated wave functions, either with linear terms in the electronic coordinates such as in the R12-methods, or by using so called *Gaussian geminals*. These methods and the related approximation schemes will be the topic of sec. 4. A possible way out of the scaling problem lies in the use of localized-correlation methods, to which we come in sec. 5. Finally sec. 6 is devoted to density functional methods which allow to account for correlation effects in an economic but rather uncontrolled way. An outlook to the future closes this review.

2 Electron correlation in very small atoms and molecules

A very compact and highly accurate wave function for the ground state of the He atom has already been constructed by Hylleraas long ago [21]. He expressed this in terms of the coordinates r_1, r_2 and r_{12} with r_1 and r_2 the distances of the first and second electron from the nucleus, and r_{12} the distance between the electrons. Thus the cusp conditions [20] could be satisfied. Essentially in the same philosophy Pekeris performed a calculation on the He-ground state [22], that remained an undisputed landmark for quite some time. A progress beyond this was possible when analytic properties of the exact wave function of a three-particle system (one nucleus and two electrons) were taken into account, which were ignored in earlier formulations. The keyword to this is *Fock expansion* and it requires terms that are logarithmic in the coordinates [23, 24, 25].

Including such terms Frankowski and Pekeris [26] needed only a 246 term wave function to be more accurate than Pekeris in his original work with more than 1000 terms. The performance was even superseded by Morgan and coworkers [27] who obtained the non-relativistic He ground state energy with 13-figure accuracy. One may celebrate this as an example where a careful study of properties of the exact wave function can inspire an improved

computational method, had there not been the more recent work by Drake [28, 29, 30, 31], who obtained an even higher accuracy with a rather simple-minded ansatz using a linear combination of two Hylleraas type wave functions with different orbital exponents,

$$\Psi = \sum_{i,j,k} r_1^i r_2^j r_{12}^k [c_{ijk}^{(1)} \exp(-\alpha_1 r_1 - \beta_1 r_2) + c_{ijk}^{(2)} \exp(-\alpha_2 r_1 - \beta_2 r_2)] \quad (1)$$

that was rather a result of a fortunate incident, and for which it is hard to give a justification in terms of physical principles. Meanwhile an 18-figure accuracy has been achieved [32, 33, 34] and this does not appear to be the end [35], where the ansatz by Goldman [35] which involves $r_<$ and $r_>$, looks particularly promising.

Recently Rychlewski and coworkers [36] have been able to achieve a similar accuracy as Pekeris even with a wave function of Gaussian geminal type

$$\Psi = \sum_i c_i \exp(-\alpha_{1i} |\vec{r}_1 - \vec{A}_i|^2 - \alpha_{2i} |\vec{r}_2 - \vec{B}_i|^2 - \beta_i (|\vec{r}_1 - \vec{r}_2|^2)). \quad (2)$$

For He 12-figure accuracy was reported [36, 16]. This is surprising since this ansatz neither fulfills the nuclear cusp nor the correlation cusp conditions. Although it is not yet fully understood why this works, some preliminary comments can be made.

It is well understood that expansions in orthogonal functions such as the famous Fourier expansion are extremely sensitive to singularities of the function to be expanded [37, 38]. The cusp singularities of electronic wave functions are at the origin of the slow convergence of CI-like expansions (see sec. 4). Alternatively to Fourier type expansions there are expansions that can best be rationalized as discretized integral transformations [39, 40]. For these the convergence behaviour is much different, in particular there is practically no sensitivity to singularities. The expansion in Gaussian geminals is obviously of this type.

We can mention only briefly, that hardly for He itself, but for the He isoelectronic series relativistic corrections and even QED (quantum electrodynamic) effects become important with increasing Z [41, 42, 43].

The first application of the Hylleraas method to the H_2 molecule by James and Coolidge appeared in the first volume of *J. Chem. Phys.* [44]. The accuracy was later pushed further by Kolos and Wolniewicz, with whose names the theory of the H_2 molecule is intimately linked [45, 46]. The first triumph of this group was a slight disagreement with the experimental dissociation energy of Herzberg et al. [47], which made Herzberg reconsider his analysis of the spectra, and confirm the theoretical prediction. The most recent calculations are really spectacular [48, 49]. However, also for H_2 , Rychlewski et al. [36]

using a Gaussian geminal expansion, were able to beat this accuracy. They thus invalidated the common belief, that H_2 is a special case insofar as one can use elliptical coordinates and an ansatz for the wave function that satisfies all cusp conditions, and that this is the reason for the much better performance for H_2 compared to all other molecules.

The H_3^+ ion is a two-electron system like He or H_2 , but it has resisted an accurate quantum chemical treatment much longer. On table 1 one can follow the history of the accuracy achieved for the energy of the H_3^+ ground at its (equilateral triangular) equilibrium geometry with $r_e = 1.65a_0$. For a while the conventional calculation (of CI type – see sec. 3 – and not including interelectronic coordinates) of Meyer, Botschwina and Burton [50] was a landmark, in particular as to a full potential surface of this system. Microhartree accuracy was only achieved in 1993 [51, 52]. Two years later the accuracy could even be pushed by two more decimal places [53]. At this level of accuracy, non-Born-Oppenheimer effects can no longer be neglected, especially if one wants to compare theoretical and experimental rovibronic spectra [54], but this is not the topic of the present review.

Table 1

Accuracy of the ground state energy of H_3^+ at the equilateral triangular equilibrium geometry ($r_e = 1.65a_0$) (after ref. [51])

Until 1970	-1.3.....	E_h
Until 1980	-1.34...	E_h
Until 1990	-1.343...	E_h
1991/92	-1.343 8	E_h
1993 (Bochum)	-1.343 835..	E_h
1995 (Poznan)	-1.343 835 624	E_h

In the context of H_3^+ one must mention the Monte-Carlo calculations by Anderson [55]. In fact, these authors were also able to achieve microhartree accuracy for H_3^+ at its equilibrium geometry. However, calculations of this type are extremely demanding as far as computer resources are concerned, and a potential energy surface for H_3^+ has not been computed by this method.

Interesting 3-electron systems are the Li atom and the H_3 ground state surface. H_3 is not a bound molecule, but essential for an understanding of the simplest chemical reaction $H+H_2 \rightarrow H_2+H$. For Li 10-figure accuracy was recently achieved with a generalization of the Hylleraas ansatz [56, 57]. The saddle point of H_3 has been evaluated with 7-figure accuracy (i.e. with an error of ~ 10 microhartree) with Monte-Carlo [58] and Gaussian geminals [59] methods, but for the whole surface only conventional calculations of CI-type

[60, 61, 62, 63, 64, 65] are available, for which the absolute error is of the order of ~ 1 millihartree. An extension of the MC calculation [58] to a full surface appears to be in progress [66].

As to 4-electron systems there has been special interest in the Be atom and the van-der-Waals interaction in He_2 . In a paper with 9 authors from 8 groups [67] the exact nonrelativistic energy of the Be ground state was estimated rather than computed. Meanwhile this energy could also be computed with microhartree accuracy [68, 69, 70]. A somewhat disappointing message has been that CCSDT (see sec. 3) is not sufficient and that linked quadruple excitations contribute as much ~ 90 microhartree to the ground state energy of Be [71].

The potential curve of He_2 , has been a big challenge to quantum chemistry, since the potential well of the van-der Waals interaction is only 11K, i.e. an extremely small fraction of the total energy. If one uses a method which accounts for the energy of an He atom with an error of, say, 1 millihartree (≈ 300 K) one can hardly expect a reliable result for the interaction energy, unless one can rely on a controlled error compensation.

Two highly accurate calculations are available, one by van Mourik et al. [72, 73] the other by Klopper and Noga [74]. Further recent calculations are those of ref. [75, 76]. These can be compared with a potential curve constructed from experimental and theoretical data by Aziz et al. [77]

3 Many-electron methods in terms of one-electron basis sets

3.1 Full CI

There is a method which allows one to solve – at least in principle – the Schrödinger equation of an n -electron system. The recipe is to choose a basis set of m orbitals or $2m$ spin orbitals and to construct all possible n -electron determinants from this basis. Their number is $\binom{2m}{n}$. One expands the Hamiltonian in this basis and diagonalizes it. This is called *full CI* (*CI* for configuration interaction). Next one increases the dimension of the orbital basis such that eventually it becomes complete (more precisely complete in the 1st Sobolev space [78]) and proceeds until convergence of the lowest eigenvalue(s). In the limit of a complete basis *full CI* becomes *complete CI* and virtually exact [79]. Unfortunately this method is completely intractable. For large m the number of Slater determinants increases as $\sim m^n/n!$, i.e. exponentially with the electron number n .

It is clear that *full CI* is only possible for relatively small basis sets. In view of this the progress in full CI calculations [83, 84, 85] is rather impressive. The main practical interest in full CI is to use it as benchmark to check the performance of approximations to full CI for the same basis, with the hope that good approximations to full CI can then be used successfully with larger basis sets.

The scaling of the computational effort with the number n of electrons (we shall henceforth simply say n -scaling) is particularly unfortunate for full CI, other current methods scale – as we shall see – as some power n^k of n . There is evidence that one does something basically wrong if one uses a method that scales unphysically with the particle number n , where it remains to be seen what is a *physical* n -scaling. If one compares calculations of related molecules with a different number N of similar atoms, the number n of electrons scales essentially with N such that n -scaling and N -scaling show the same pattern. One is also interested in the scaling with the number m of basis functions. This has a different meaning depending on whether one compares calculations on one system with constant n and varying m , or whether one consider different systems consistently with m essentially proportional to N .

The improvement of the n -scaling will definitely be one of the great challenges to quantum chemistry in the 21st century.

The n -electron wave function is a rather complicated quantity and it contains much more information than is usually needed. In order to evaluate the energy one has – in a modern Fock space notation [86, 87] –

$$H = h_q^p a_p^q + \frac{1}{2} g_{rs}^{pq} a_{pq}^{rs} \quad (3)$$

$$\begin{aligned} E &= \langle \Psi | H | \Psi \rangle = h_q^p \langle \Psi | a_p^q | \Psi \rangle + \frac{1}{2} g_{rs}^{pq} \langle \Psi | a_{pq}^{rs} | \Psi \rangle \\ &= h_q^p \gamma_p^q + \frac{1}{2} g_{rs}^{pq} \gamma_{pq}^{rs} \end{aligned} \quad (4)$$

Here a_p^q etc. are excitation operators with respect to an orthonormal spin-orbital basis $\{\psi_p\}$, while h_q^p and g_{rs}^{pq} are one- and two-particle matrix elements

$$a_q^p = a^p a_q = a_p^\dagger a_q; \quad a_{rs}^{pq} = a^p a^q a_s a_r \quad (5)$$

$$h_q^p = \langle \psi_q | h | \psi_p \rangle; \quad g_{rs}^{pq} = \langle \psi_r(1) \psi_s(2) | g(1,2) | \psi_p(1) \psi_q(2) \rangle \quad (6)$$

with h and g the one- and two-particle parts of the Hamiltonian respectively, and $\gamma_p^q, \gamma_{pq}^{rs}$ and the one- and two-particle density matrices respectively

$$\gamma_p^q = \langle \Psi | a_p^q | \Psi \rangle; \quad \gamma_{pq}^{rs} = \langle \Psi | a_{pq}^{rs} | \Psi \rangle \quad (7)$$

In the above expressions the Einstein summation convention is implied.

When the one electron basis $\{\psi_p\}$ on which our Fock space is built, is finite (of dimension $2m$), the Hamiltonian H given by (3) is exactly that of full CI [87]. The eigenfunctions and eigenvalues that one obtains in full CI, are the eigenfunctions and eigenvalues of this Hamiltonian.

3.2 The 2-particle density matrix and the n -representability problem

The number of density matrix elements γ_{ps}^{rs} scales with m^4 , i.e. it does not directly depend on n . However, since m should be chosen roughly proportional to n , there is a scaling $\sim n^4$. If it were possible to take the γ_{pq}^{rs} rather than the CI coefficients as variational parameters, we would have got rid of the scaling problem of full CI. Unfortunately the γ_{pq}^{rs} cannot be regarded as variational parameters, unless one can impose conditions which guarantee that a γ -matrix is derivable from an n -particle wave function. This n -representability problem has played a big role in the late sixties and has been most thoroughly formulated by Coleman [88, 89]. Unfortunately a simple solution of the n -representability problem which allows one to replace the n -electron wave function Φ by the two-particle density matrix γ_{pq}^{rs} in a variational approach has not been found. Note that γ_p^q is not independent of γ_{pq}^{rs} , but can be derived from this by partial contraction

$$(n-1)\gamma_p^q = \sum_r \gamma_{pr}^{qr} \quad (8)$$

Although the idea to formulate the n -electron problem in terms of density matrices has been more or less abandoned, it is likely that it will be revived in the future, especially in view of the success and the limitations of the much more simple-minded density functional approaches (see sec. 6). For interpretational purposes the density matrices have always been rather central quantities [90, 91, 92, 93, 94, 95].

The eigenfunctions and eigenvalues of $\{\gamma_q^p\}$ are known as natural spin-orbitals and their occupation numbers [80], those of $\{\gamma_{rs}^{pq}\}$ the natural geminals and their occupation numbers.

For typical closed shell atoms or molecules $\{\gamma_q^p\}$ is close to idempotent, i.e. its eigenvalues are either close to 1 or to 0. In this case a single determinant Φ built up from the n first natural spin orbitals (with occupation numbers close to 1) is a good first order approximation to the exact Ψ . Then Hartree-Fock theory, in which $\langle \Phi | H | \Phi \rangle$ is minimized with respect to variation of the orbitals contained in Φ , is a good first order approximation. In fact, everything not contained in Φ means electron correlation.

For Φ a single Slater determinant all information is contained in its one particle density matrix [96]. For this special case we use ϱ instead of γ .

$$\varrho_q^p = \langle \Phi | a_q^p | \Phi \rangle \quad (9)$$

$$\varrho_{rs}^{pq} = \langle \Phi | a_{rs}^{pq} | \Phi \rangle = \varrho_r^p \varrho_s^q - \varrho_s^p \varrho_r^q \text{ etc.} \quad (10)$$

If one defines a two-particle cumulant matrix

$$\lambda_{rs}^{pq} = \gamma_r^p \gamma_s^q - \gamma_r^p \gamma_s^q + \gamma_s^p \gamma_r^q \quad (11)$$

and analogously higher order cumulants [15, 97, 98], a simple Slater determinant wave function is characterized by vanishing of all cumulants. Obviously the two-particle cumulant describes two-particle correlations etc.. On the basis of cumulants [15] which are (at variance with the k -particle density matrices) extensive (additively separable quantities) a definition of the correlation energy is possible that does not require a single Slater-determinant reference state and the corresponding Hartree-Fock energy. We define

$$E_{nc} = h_q^p \gamma_p^q + \frac{1}{2} g_{rs}^{pq} (\gamma_p^r \gamma_q^s - \gamma_q^r \gamma_p^s) \quad (12)$$

$$E_{corr} = \frac{1}{2} g_{rs}^{pq} \lambda_{pq}^{rs} \quad (13)$$

Where the non-correlated energy E_{nc} is of the same form as the Hartree-Fock energy, but with $\{\gamma_q^p\}$ the exact one-particle density matrix, which is usually not idempotent. This concept has not yet been applied in practice.

3.3 Many-body perturbation theory

Noting that full CI is – in principle (when the basis limit is reached) – *exact* but unfeasible (except for very small basis set), and that Hartree-Fock is feasible, but a very crude approximation, some compromise between these two extrema has to be found.

One possibility is to use perturbation theory, truncated at some low order. There are various options for perturbation theory applied to an n -electron system. One of them consists in dividing the Hamiltonian H in the following way into an unperturbed Hamiltonian H_0 and a perturbation V

$$H = H_0 + \lambda V; \quad H_0 = h_q^p a_p^q; \quad V = \frac{1}{2} g_{rs}^{pq} a_{pq}^{rs} \quad (14)$$

On this partition many-body perturbation theory (MBPT) as developed by Brueckner, Goldstone and others is based [99, 100, 101, 102, 103, 104]. This

is also the basis of the Z -dependent perturbation theory of atoms of Layzer and others [105, 106, 107]. Strictly speaking one should distinguish between a perturbation theory in terms of the original Hamiltonian (not projected to a finite one-electron basis) and perturbation theory of the Fock space Hamiltonian in a *finite* basis, which is equivalent to perturbation theory of the matrix eigenvalue problem of full CI. When one refers to perturbation theory for electron correlation, almost exclusively the latter choice is implied, and we shall only consider this option.

The partition (14) corresponds to treating the bare nuclear Hamiltonian (BNH) as unperturbed and the entire electron interaction as perturbation. It is much better (i.e. leads to better results to low orders and gives a better overall convergence pattern), to include part of the electron interaction in H_0 . Again there are various possibilities, but the Møller-Plesset partition [108, 109, 110] has turned out to be most convenient. Here

$$H = E_0 + H'_0 + V' \quad (15)$$

$$H'_0 = f_q^p \tilde{a}_p^q; \quad V' = \frac{1}{2} g_{rs}^{pq} \tilde{a}_{pq}^{rs} \quad (16)$$

$$E_0 = h_q^p \varrho_p^q + \frac{1}{2} g_{rs}^{pq} \varrho_{pq}^{rs} \quad (17)$$

$$f_q^p = h_q^p + (g_{qs}^{pr} - g_{sq}^{pr}) \varrho_r^s \quad (18)$$

where ϱ_p^q are density matrices corresponding to a Hartree-Fock reference function Φ , and where \tilde{a}_q^p and \tilde{a}_{pq}^{rs} are excitation operators with respect to Φ as so-called *physical vacuum*. These have the property

$$\langle \Phi | \tilde{a}_p^q | \Phi \rangle = 0; \quad \langle \Phi | \tilde{a}_{qp}^{rs} | \Phi \rangle = 0 \quad (19)$$

and are related to the a_p^q and a_{qp}^{rs} with respect to the genuine vacuum as [111, 97]

$$\tilde{a}_p^q = a_p^q - \gamma_p^q \quad (20)$$

$$\tilde{a}_{qp}^{rs} = a_{qp}^{rs} - \gamma_q^r a_p^s + \dots \quad (21)$$

For the Møller-Plesset partition the first order perturbation vanishes

$$E_1 = \langle \Phi | V' | \Phi \rangle = 0 \quad (22)$$

If one chooses canonical orbitals, for which f_q^p is diagonal

$$H'_0 = \varepsilon_p^{(0)} \tilde{a}_p^p \quad (23)$$

the second order energy is simply

$$E_2 = \sum_{i,j,a,b} (\varepsilon_i^{(0)} + \varepsilon_j^{(0)} - \varepsilon_a^{(0)} - \varepsilon_b^{(0)})^{-1} | \langle \Phi | V' a_{ij}^{ab} | \Phi \rangle |^2 \quad (24)$$

with i, j counting spin-orbitals occupied in Φ , a, b *virtual* spin-orbitals.

Only doubly excited configurations

$$\Phi_{ij}^{ab} = a_{ij}^{ab} \Phi \quad (25)$$

contribute to E_2 . Also E_3 only requires double excitations, while for the evaluation of E_4 triple excitations are needed and so forth.

MP-perturbation theory is formally simple to low orders, but becomes increasingly complicated to higher orders. The most serious drawback is that convergence of MP-PT is by no means guaranteed. Depending on the choice of the basis, divergence can be enforced or avoided [112, 113], which indicates that much that one finds may be an artifact of the matrix representation, that has other singularities – which determine the radius of convergence – than the original Hamiltonian. Anyway even if the MP-PT series converges, convergence may be very slow [114] and one cannot break up the series, unless sophisticated extrapolation methods are used.

Actually only MP2 has become a kind of standard, MP3 is regarded as hardly superior to MP2, while MP4 is occasionally used, but it requires about as much computational effort as the usually much better CCSD(T) method.

Let us also mention that, independent of the partition of H that one chooses, always the Rayleigh-Schrödinger form of PT is used, because – at variance with the Brillouin-Wigner PT – it is extensive (connected). See later.

3.4 Coupled-cluster and related methods

Related to perturbation theory are methods that have been *inspired* by perturbation theory, but which are essentially non-perturbative. Early attempts on these lines were partial summations of certain classes of diagrams [115] (in a diagrammatic formulation of MBPT), where it was not always clear whether these diagrams were summed because this was formally easy or because these diagrams were regarded as particularly important. More simple-minded but rather effective has been selective CI based on arguments from MP-PT [116].

Noting that to the leading orders of MP-PT only *doubly excited* configurations Φ_{ij}^{ab} contribute, one can decide to do better than MP2 or MP3 by including all Φ_{ij}^{ab} in a CI (i.e. variational) calculation. The number of unknown coefficients scales then as $n^2 m^2$, i. e. essentially as n^4 , while the overall computational effort goes as $n^4 m^2$ i.e. essentially as n^6 . The scaling is much better than for full CI, but the quality of the result is, of course, much poorer.

One can so define a hierarchy of CI methods, called CI-SD, CI-SDT, CISDTQ etc. where S, D, T, Q stands for singly, doubly, triply, quadruply excited configurations. This hierarchy has the advantage over MP-PT that it does converge to full CI if one let the excitation rank go to the number of electrons. This is, however, just what one wants to avoid.

A serious disadvantage of these truncated CI schemes is that they are not extensive (size consistent). This means essentially that the energy of a supersystem consisting of two identical subsystems at large distances computed by CI is not twice the energy of the subsystem. For a system of N He atoms at mutually infinite distance the correlation energy goes for large N not as $\sim N$, but as $\sim \sqrt{N}$ [12, 117].

The size-consistency problem has been removed by using the coupled cluster (CC) ansatz [12, 118, 119, 120, 121, 122, 123, 124, 125]. While in CI one writes the wave function as (in intermediate normalization)

$$\Psi = (1 + X_a^i a_i^a + X_{ab}^{ij} a_{ij}^{ab} + X_{abc}^{ijk} a_{ijk}^{abc} + \dots) \Phi \quad (26)$$

in CC theory the formulation is

$$\Psi = \exp \left\{ S_a^i a_i^a + S_{ab}^{ij} a_{ij}^{ab} + \dots \right\} \Phi \quad (27)$$

If one truncates the CI expansion one gets a result which is variational, but not extensive, one can truncate the CC-expansion (in the exponential) without loosing extensivity. It is then, however, practically impossible to be variational as well [125]. Like for CI one can define CC-SD, CC-SDT, CC-SDTQ etc. The n -scaling of the computational demands is similar to that for the corresponding steps in the CI hierarchy. Like for the CI hierarchy the CC hierarchy also converges to full CI if the excitation rank goes to n , but the convergence is definitely faster.

While CCSD has become a kind of standard, full CCSDT calculations [126, 127, 128] are still too computer-resource demanding that their use is limited to rather small basis sets. Among the simplifications of CCSDT, the CCSD(T) method [129] has become very popular. There single and double substitutions are treated non-perturbatively, but triple substitutions by means of perturbation theory. An alternative to CCSD(T) is CCSD[T] – formerly called CCSD+T(CCSD) – that is probably better [131], although formal arguments are rather in favour of CCSD(T) [130]. While CCSDT scales with n^8 (and CCSDTQ with n^{10}), CCSD(T) and CCSD[T] scale *only* with n^7 , which matters a lot. CCSD(T) is these days regarded as the best that one can do for sufficiently small molecules. Nevertheless cases have been reported, where CCSD(T) is definitely not enough, e.g. if one wants to evaluate the harmonic vibration frequency of HF with an error of less than 1 cm^{-1} [131].

Closely related to CC theory (and also to MP-theory) are the IEPA [3, 10, 12] and CEPA [11, 12, 13, 132, 133, 134] methods, that were used in molecular calculations prior even to the large scale studies in terms of MP2. IEPA (independent electron pair approximation) has in common with MP2 that the various electron pairs are decoupled, and MP2 has, in fact, been a first step on the way to IEPA [3, 10, 12]. Unlike in MP2 the various decoupled pairs are treated exactly (in the limitations due to the use of a finite basis) in IEPA. In CEPA (coupled electron pair approximation) the coupling of the pairs is taken into account, but unlike in CCSD, to which CEPA is closely related, some (generally small) indirect couplings are ignored. Although CEPA can be formulated as an approximation to CCSD [11, 12], in practical applications it has turned out that CEPA performs even better than CCSD (although it is cheaper), because apparently effects of triple substitutions are, to some extent simulated in CEPA [135, 136]. IEPA and CEPA share with MP and CC that they are extensive and not variational.

It is often forgotten that the probably first large-scale ab-initio implementation of CCSD by Taylor et al. [120] was based on the CEPA code of Ahlrichs et al. [13]. As to a comparison of CEPA and CC methods see [137]. We come back to an interesting aspect of IEPA and CEPA in sec. 5.

Closely related to CEPA are the method of self-consistency electron pairs (SCEP) [138] and also the coupled-pair functional approach (CPF) [139].

3.5 Multi-configuration-based methods

Most of the effort in coupled-cluster theory has concentrated on systems which are essentially of closed shell type, where the wave function is dominated by a single Slater determinant Φ , such that the wave function can be expanded around this Φ and good convergence is expected.

The situation is much more complicated if to 1st order a single Slater determinant is not sufficient and rather a multiconfiguration reference Φ must be used. A completely satisfactory coupled-cluster theory for this case has not yet been formulated. This has both fundamental and practical reasons.

Among the fundamental reasons is the dilemma that the most straightforward formulation of an extensive theory leads inevitably to the appearance of the *intruder problem* and that it is hard to eliminate this problem without violating extensivity. In fact extensivity requires a Fock space formulation with a *multiplicatively separable* wave operator [12, 87]. This means that one formulates the wave operator and an effective Hamiltonian for the full valence space, for all possible particle numbers, i.e. that one uses a so-called *valence universal theory*. However then one can generally not avoid that *external orbitals* (i.e. which are not in the valence space) get energies close to those of valence

orbitals and dangerous energy denominators arise. These intruder problems are largely avoided in a *state-specific* theory limited to a single state, but this means to loose a formulation in Fock space and extensivity is no longer guaranteed. This dilemma has been analysed in detail by Mukherjee, [140, 141] who has also discussed possible solutions, which we can only mention without going into details. One possibility is the use of *intermediate Hamiltonians*, mainly proposed by Malrieu et al. [142], but see also refs. [143, 144]. Another possibility consists in the use of *incomplete model spaces* [145, 146, 148], a disadvantage of which is that they can usually not be applied to potential energy surfaces, since for different ranges of geometry different incomplete model spaces must be used. There are further methods in the framework of a *state universal theory* both for complete and incomplete model spaces [149, 150, 151], which are somewhat intermediate between valence universal and state specific, and which are to some extent based on the projection of a Fock space theory to a Hilbert space for finite particle number. Particularly promising appears the combination of extensivity and a state-specific theory using the recently developed concept of normal ordering (and the corresponding Wick theorem) with respect to a multiconfiguration wave function [15, 97, 98]. On this line there are certainly challenges for the next century.

From a practical point of view one has to decide whether one chooses a contracted [152, 153] or uncontracted excitation scheme. In the latter the number of excitations to include is tremendous, in the former one must find a way how to deal with the so-called *excitations with spectator-lines* (unless one neglects these, which appears to be justified to some extent). *Contracted* means that one considers formal single, double etc. excitations with respect to the full MC-SCF wave function Ψ , e.g. $a_q^p\Psi$, $a_{rs}^{pq}\Psi$, uncontracted means that one decomposes Ψ into a sum of Slater determinants and takes the excitations with respect to these.

As long as a satisfactory multireference coupled-cluster theory is missing, there are various options for states that need a zeroth-order multiconfiguration wave function. One possibility is to start from an MC-SCF calculation and to improve this by selected CI. Since the MC-SCF part is basically extensive, while the CI part is not, and since one can hardly go beyond external double excitations, one tends to include as many configurations in the MC-SCF part as possible. However, MC-SCF is usually of CAS (complete active space) [154] type, e.g. like full CI, which restricts the possible size of the active space. Such multireference CI scheme have been very popular for describing excited states, reaction barriers, dissociation processes etc.

Another possibility is to start from MC-SCF and to improve it by means of perturbation theory. The most popular approach on these lines is CASPT2 of Roos et al. [155]. This is *almost* extensive and one is not obliged to make

the active space as large as possible.

One can further try to formulate a generalization of CEPA or rather CPF to a multiconfiguration reference function. On these lines the *average coupled pair functional* (ACPF) has been derived by Gdanitz and Ahlrichs [157]. A straightforward MC-CEPA method has been proposed by Fink and Staemmler [158]. This is extensive, while ACPF is only approximatively so.

One can finally try to apply single reference CC, but to go to very high excitations, at least selectively [159]. It is hard to avoid a lack of balance in such treatments.

In this context one should also mention the rather old MRD-CI-method of Buenker and Peyerimhoff [160]. There one starts from a multideterminant reference function and improves it by CI with single and double substitution. This method has not been designed for single states, but rather for the computation of various states simultaneously.

4 The convergence with the basis size and the R12 method

All methods discussed in the previous chapter have two difficulties, one – on which we have commented already – is the convergence with respect to the sophistication of the level of the treatment of electron correlation (with the related n -scaling problem), the other is the convergence with the extension of the one-electron basis. We shall now concentrate on this aspect.

There are actually three types of expansions that one has to worry about

(a) The expansion in a Gaussian basis, which neither allows a correct description near the nuclei nor very far from them.

(b) The expansion of one-electron functions in a basis of eigenfunctions of angular momentum with respect to the atomic centers, i.e. essentially the LCAO expansion

(c) The expansion of the correlation cusp in a one-electron basis.

The expansion (a) is, contrary to what one might have expected, the least problematic. In fact, Gaussian basis sets were introduced, because they lead to simple two-electron integrals. On the other hand one knows that atomic orbitals are more like Slater type, i.e. exponential functions. Gaussians have the wrong behaviour both close to a nucleus and very far from it. The expansion of hydrogenic $1s$ function in an even-tempered Gaussian basis has been studied analytically [161] and the surprising result was found that the error ΔE of the energy depends on the number m of basis functions as

$$\Delta E = \pi(3m)^{3/2} \exp\left\{-\pi\sqrt{3m}[1 + O(m^{-1/2})]\right\} \quad (28)$$

This is not as good as exponential, but almost as good. For properties other than the energy one gets a similar behaviour but with a different m^k -factor in front and a different prefactor of \sqrt{m} in the exponential. Even the density at a nucleus has this convergence behaviour, although $\frac{\partial\psi}{\partial r}$ at $r = 0$ has an error independent of m and $\frac{\partial^2\psi}{\partial r^2}$ at $r = 0$ diverges with n .

The expansion (b) has not been studied in a formal way. A rather detailed unpublished investigation of R. Franke and one of the present authors on the H_2^+ ion has shown numerically [162] that the error of an expansion in atomic s, p, d etc. functions appears to converge exponentially. There is some evidence that this holds for all one-electron problems, especially for Hartree-Fock. It is, for not too large molecules, not too difficult to saturate a basis and to get sufficiently close to the Hartree-Fock limit at least for the energy.

Much more critical is the expansion (c). The simplest case is that of 2-electron atoms such as He ion their 1S ground states. Here it could be shown that for an expansion

$$\psi(1, 2) = \sum_{l, m} Y_l^m(\vartheta_1, \varphi_1) Y_l^{-m}(\vartheta_2, \varphi_2) \sum_{n, n'} f_n(r_1) f_{n'}(r_2) \quad (29)$$

the l -increments to the energy go as [163, 164]

$$\Delta E_l = A(l + \frac{1}{2})^{-4} + O\left\{[l + \frac{1}{2}]^{-5}\right\} \quad (30)$$

This is an extremely slow convergence and is related to the fact that the exact wave function has a correlation cusp [20], i.e. a discontinuous first derivative at $r_{12} \rightarrow 0$, such that

$$\lim_{r_{12} \rightarrow 0} \left(\frac{\partial \psi(1, 2)}{\partial r_{12}} \right)_{av} = \frac{1}{2} \psi(1, 2)_{r_{12}=0} \quad (31)$$

If one includes explicit linear r_{12} -dependent terms in the wave functions and expands only the remainder [165] as in (29), the l -increments of the remainder go essentially as $(l + \frac{1}{2})^{-8}$, at least at the level of 2^{nd} order perturbation theory, which is a substantial improvement.

It is difficult to derive the asymptotic behaviour of ΔE_l by purely numerical studies. One of the reasons for this is that for increasing l , the number of terms in the (n, n') -expansion necessary to reach convergence increases with l . In practical calculations one rather does the opposite, i.e. one uses smaller n -expansions for larger l , and one gets so the impression of a much faster convergence than that found analytically. Therefore empirical extrapolations [166, 167, 168, 169] to $l \rightarrow \infty$ are rather dangerous. Extrapolations based on exact properties are, however, a serious alternative to the use of R12 methods. An interesting approach on these lines is the CBS (complete basis set) extrapolation method of Petersson et al. [170].

One should also mention that the $(l + \frac{1}{2})^{-4}$ dependence of ΔE_l only holds for typical singlet states, for triplet states ΔE_l goes as $(l + \frac{1}{2})^{-6}$, and for non-natural-parity singlet states even as $(l + \frac{1}{2})^{-8}$ [164].

The slow convergence plagues all CI-type calculations. Since in view of the unfortunate scaling of the computational effort with the number of basis functions, one cannot choose very large basis sets, one cannot use CI-type methods if one strives at high accuracy. There are essentially three ways to overcome this problem.

(a) One uses wave functions with explicit linear r_{12} -terms to describe the correlation cusp correctly. The brute-force variant of this approach is known as Hylleraas-CI [171]. It leads to a large number of *difficult* integrals, even 3- and 4-electron integrals in addition to the 2-electron integrals needed in conventional SCF or CI calculations. Therefore it has so far only been applied to systems with 2 electrons, or slightly beyond this.

(b) It is however possible to use tricks to avoid the difficult integrals, without introducing unacceptable errors. This leads to the R12 methods [172, 173, 174, 175, 176, 177, 178, 179, 180, 181]. The variant MP2-R12 allows one to reach the MP2 basis limit with comparably little effort, and with an increase of the computer time with respect to a conventional MP2-calculation with the same basis by only a factor ~ 5 . In the case of CCSD-R12 vs. conventional CCSD the extra computer time for the same basis is only $\sim 30\%$ of that of the conventional calculation, but the gain in accuracy is spectacular. The best method available so far is CCSDT1-R12, but also the more approximate CCSD(T)R12 and CCSD[T]-R12 methods [181] can be used.

An essential ingredient of the R12 methods is the systematic introduction of completeness insertions in such a way that (i) 3- and 4-electron integrals don't arise explicitly, (ii) the results become exact in the limit of a complete one-electron basis, (iii) the basis truncation error decreases much faster with the size of the basis than in conventional calculations, such that much higher accuracy is achieved with less computational effort. The only disadvantage is that no strict upper-bond property holds, but this does not even hold for conventional coupled-cluster calculations. There is no stronger limitation of the size of the system to be computed than for conventional CC calculations. Typical examples of applications of R12-methods were to the Ar-benzene complex [176] or to $(\text{H}_2\text{O})_3$ [177].

In a systematic study of 10-electron molecules and ions [178] the total energies for CCSD[T]-R12 calculations turned out to agree within less than $1mE_h$ with the *experimental non-relativistic energies*.

For details on the R12-methods the reader is referred to recent reviews [179, 180] and original papers [172, 173, 174, 175, 176, 177, 178, 181]. The R12-method has been combined successfully with the ACPF approach by Gdanitz

[182].

(c) An alternative to the use of linear r_{ij} -terms as in the R12 method, is the method of Gaussian geminals. Here one introduces correlation factors of the form

$$\exp(-\gamma r_{12}^2) \quad (32)$$

With such functions it is not possible to satisfy the correlation cusp exactly, but all integrals that arise, including three and four-electron integrals, can be evaluated in closed form. The convergence of this kind of expansion is much faster than that of a CI. It is possibly similar to that of the expansion of 1s hydrogen wave function in a Gaussian basis. The Gaussian geminal method has been implemented e.g. for MP2 and CCSD [183, 184, 185, 186]. A rather difficult practical problem is that of the choice of the optimum non-linear parameters γ . This has so far been inhibited the application of the Gaussian geminal method beyond HF [185] or H₂O [186]. The technique of Rychlewski et. al. [36] to optimize non-linear parameters has to the authors' knowledge not yet been applied in this context.

For Hartree-Fock calculations alternatives to basis expansion methods, e.g. finite elements or finite differences have been used successfully. It does not appear straightforward to use such methods for the treatment of electron correlation, because for the lowest-level treatment of electron correlation, i.e. pair theory, one has a 6-dimensional problem, and this is hard to treat by finite-element or finite difference methods.

5 Localized correlation methods

The scaling with the number of particles is one of the most serious problems for all methods to treat electron correlation. Unfortunate scaling is, however, if one looks carefully, in most cases avoidable, and is a result of uneconomic computer codes.

For a long while it was believed that SCF calculations have to scale with N^4 , because the rate-determining step is the construction of the two-electron integrals ($pq|rs$) and their number is proportional to m^4 with m the number of basis functions, and m scales with the number N of atoms. Let us henceforth assume that we consider a molecule with N atoms and q basis functions per atom such that $m = N \cdot q$, with q constant.

One must be aware that the accuracy of a computation is limited by the number of significant figures with which numbers are stored in the computer. Since one cannot completely avoid small differences of large numbers, one loses a few figures anyway. It is convenient to impose a threshold defining the final accuracy that one wants to have. Quantities, say in a sum, which

are smaller than that threshold, don't contribute and can as well be ignored. It now turns out that the number of $(pq|rs)$ integrals above a given threshold scales – for sufficiently large N – only with m^2 (and hence N^2) rather than m^4 , so the majority of the m^4 integrals can safely be ignored. A particularly powerful screening of integrals has been proposed and coded by Häser and Ahlrichs [187].

If one goes one step further, one realizes that there are two types of integrals, namely Coulomb-like long range and exchange or hybrid-like short range integrals. One can take advantage of this and evaluate Coulomb type expressions by a multipole expansion. This has been exploited by Almlöf [188] in a formulation for large molecules.

Further progress with the multipole expansion has been achieved recently, which allows linear scaling for the electron interaction. [189, 190, 191].

It has almost been a dogma that post-Hartree-Fock methods (which treat correlation effects) require at least a N^5 scaling. The origin of this is that the time-determining step for MP2 (as the simplest post HF method) is an integral transformation from the integrals $(pq|rs)$ over basis functions to integrals over MOs. In fact a classification of MOs into occupied and virtual ones is at the basis of this formulation. The MOs used conventionally are delocalized and this means that all MO integrals have roughly the same order of magnitude, and no prescreening is possible. So although of $\sim m^4$ AO integrals only $\sim m^2$ are non-negligible, one has to take care of $\sim m^4$ MO integrals. The integral transformation, however, is a $\sim m^5$ step.

It is obvious that the problem is the delocalized nature of the MOs. Fortunately it has been known, based on the work of Lennard-Jones [192] and worked out mainly by Edmiston and Ruedenberg [193] and also by Foster and Boys [194], that it is possible to transform the (occupied) MOs to localized orbitals (LMOs) which span the same space, and which are orthogonal to each other, but which are mainly *localized* in rather restricted areas of space.

LMOs have been used in the IEPA- and CEPA-formulations by Ahlrichs et al. [3, 10, 12, 13], and the main difference in philosophy between the early work of Ahlrichs et al. and Meyer [11], is that the latter has preferred a delocalized formulation in terms of canonical MOs. Nevertheless the question of approximate invariance between a localized and a delocalized description has played an important role to justify the so-called CEPA-2 variant as slightly superior to CEPA-1 [11, 12].

In IEPA, like in MP2, one pair is treated at a time, in CEPA the coupling between the pairs is treated iteratively, with in each iteration cycle again one pair treated at a time. The number of pairs scales as n^2 for delocalized MOs, but only as $\sim n$ (for a large enough molecule). Take e.g. a linear chain molecule with one MO per atom, then the diagonal pairs k, k will denominate, followed

by pairs $k, k + 1$, then $k, k + 2$ etc. such that one can truncate at $k, k + \nu$ with ν fixed, and k variable. The number of pairs to be considered goes then roughly as $\nu \cdot n$. So using localized MO and screening the pairs according to their importance improves the scaling with respect to pairs of canonical MOs. The effort per pair then still goes as m^4 , which is the number of two-electron integrals that have to be processed. The scaling problem was actually solved in IEPA-PNO or CEPA-PNO, where one expanded the functions for one pair in pair natural orbitals (PNOs), a kind of optimized virtual orbitals for the various pairs. Their number was kept fixed, so the PNOs were a kind of localized virtual MOs, although they are not orthogonal [3, 12, 152]. An extension to infinite systems was recently proposed by Fink and Staemmler [195].

The N -scaling of CEPA was, in fact not bad, although not even the basic two-electron integrals were prescreened (since this was long before prescreening was discovered).

The methods which succeeded CEPA, i. e. essentially the hierarchy of CC methods, were formulated in terms of canonical MOs, hence very frustrating n -dependencies resulted. Only rather recently the advantage of the use of localized MOs were rediscovered and elaborated, mainly by Pulay [196] and Werner [197].

If one succeeds in transforming not only the occupied but also the virtual MOs to a set of well-localized MOs, such that one can associate q (occupied and virtual) MOs with each atom, then one can argue that for the description of intraatomic correlation only excitations in this q -dimensional (and hence n -independent) subspace need to be considered. For interatomic correlations between a pair of neighboring atoms excitations with the $2q$ dimensional space of the MOs of the two atoms are necessary, and so forth. Correlations beyond next-nearest neighbors may be regarded as unimportant. The number of pairs of atoms to be considered scales with n , so the overall computational demands should scale with n as well, provided that also takes advantage of fast multipole expansion [190, 191] for the Coulomb interaction.

To arrive at linear scaling with n should be possible, and is one of the big challenges of methodologic quantum chemistry. Werner et al. have at least arrived at a n^3 -scaling, which is a big progress [197]. Linear scaling has been possible in density functional theory (see sec. 6). An interesting new approach towards linear scaling even for MP2 theory has very recently been formulated by Ayala and Scuseria [198], taking advantage of an idea of Häser and Almlöf [199].

A generalization of the concept of localized MOs is that of extremal pair functions [200]. They may play a role in the future in the context of well-scaling methods. So far the main application of extremal pairs have been in

R12-theories in order to avoid near-linear dependencies [179].

Extremal pair functions are defined as linear combinations of a given set of (usually canonical) pair functions, such that they extremize some expectation value, e.g.

$$\langle w_\mu(1,2) | r_{12}^2 | w_\mu(1,2) \rangle = \text{extr.} \quad (33)$$

$$w_\mu = \sum c_\mu^{kl} [\varphi_k(1)\varphi_l(2) - \varphi_l(1)\varphi_k(2)] \quad (34)$$

$$\|w_\mu\| = 1 \quad (35)$$

With this criterion the extremal pair functions appear as a generalization of the LMOs attributed to Foster and Boys. Restricting the extremal pair functions to the form

$$w_{pq} = \frac{1}{\sqrt{2}} [\varphi_p(1)\varphi_q(2) - \varphi_q(1)\varphi_p(2)] \quad (36)$$

$$\varphi_p = \sum_k c_{pk} \varphi_k; \quad \|\varphi_p\| = 1 \quad (37)$$

one is led to LMOs.

6 Density functional methods

6.1 History

Density functional (DF) [201] methods (for reviews see [202, 203, 204, 205]) were very popular in solid state physics since about 1965, but were hardly applied in chemistry for quite a while (among the applications to structural chemistry see e.g. ref. [206]), before suddenly around 1988 they really conquered chemistry. Even before this the rather good performance in solid theory did not remain unobserved by quantum chemists, but the reluctance to consider density functional methods more seriously had various reasons.

(a) The justification of density functional methods in terms of the Hohenberg-Kohn theorem [207, 208, 209] appeared somewhat unorthodox and had a touch of mystery.

(b) DF methods performed surprisingly well at rather low cost. The results were usually superior to those of Hartree-Fock calculations, i. e. correlation effects were somehow taken care of, but not as accurately as in standard quantum chemical methods.

(c) There appeared to be no way to improve DF calculations systematically, when they were not good enough. The usual DF schemes did not appear to be steps in a hierarchy that eventually lead to an exact theory.

(d) A precursor of DF methods, the $X\alpha$ -scheme [210, 211] had been used in quantum chemistry before, but got a rather bad reputation, mainly due to overselling and the marriage with *muffin-tin* potentials [212].

(e) The existing DFT-codes of the first generation were numerically often rather inaccurate. Therefore calculations with one code could not be reproduced by another code, using, of course, the same functional. More serious was that the limited numerical accuracy made the calculation of potential curves rather problematic.

Things changed drastically when independently Becke [213] and Perdew [214] invented new gradient-corrected functionals, which performed much better than the previously used local density functionals and which turned out to be competitive with MP2 at a cost somewhat lower than that of SCF calculations. Various groups implemented DF calculations taking advantage of all the knowhow of traditional quantum chemistry, in particular using expansions in a Gaussian basis, and shortly afterwards DF codes became available in commercial program packages. Also the problems of accurately (and reproducibly) evaluating the exchange correlation functionals were solved [215, 216, 217]. Further the evaluation of energy derivatives became routine [218, 219]. For a black-box user it is now as easy to perform an SCF as a B3LYP calculation. 'B3LYP' stands for Becke-3-parameter for the exchange part and Lee-Yang-Parr for the correlation part. It is one of the most popular density functionals for use in chemistry and is implemented in the commercial GAUSSIAN program package.

The attitude of most users is pragmatic. One does not worry why DF methods work and uses them as one uses other methods implemented in the same black box. There are quite a few different functionals available and one can choose between them depending on the problem that one wants to solve, where the superiority of one functional over another is usually based on statistical comparison with experiment rather than on formal arguments. This pragmatic attitude is encouraged by the fact that some of the density functionals in current use, contain parameters that were adjusted to fit experimental data. This – in order not to say more – puts DF schemes in the neighborhood of semiempirical methods.

The density functionals which perform best at present, like B3LYP are *mixtures* of Kohn-Sham type functionals (see later) and Hartree-Fock functionals and exploit the fact that Kohn-Sham type functionals tend to overestimate binding, while Hartree-Fock underestimates it.

The acceptance of DFT by the ab-initio community necessarily implied some change of paradigm. In the ab-initio world it had always been regarded as problematic and even as a kind of cheating if one got good agreement with experiment due to a fortunate cancellation of errors (unless this cancellation was 'controlled'). In DFT one can judge the quality of a functional only from a comparison of the results with experiment or with some benchmark calculation. There is hence no criterion for the extent of error compensation on which the

performance of the functional is based. So the refutation of error cancellation can hardly be maintained. Nevertheless if one wants to get 'the right answer for the right reason' one should not rely on DFT.

6.2 The Hohenberg-Kohn theorem as a Legendre transformation

The essential problem with DF methods is to understand why they work, or rather which of their features is responsible for the good agreement with experiment in many cases. A systematic improvement but also a guide to scope and limitations rests on the answer to this question. Although some current studies concentrate on this aspect [220, 221, 222, 223], for the majority of people grown up with DF approaches even to ask this question is a kind of sacrilege. The argument often put forward is that *density functional theory is exact – in principle* – and that deviations from exact results are simply due to the approximations inherent in the used functionals. This argument, usually given with reference to the so-called Hohenberg-Kohn theorem, is rather meaningless and reveals a basic misunderstanding of the situation.

To appreciate what the Hohenberg-Kohn theorem [207] really implies it is useful to formulate it in a language that it is slightly different from that given in most papers in this field. The key reference is that to a study of E. H. Lieb [224, 225], who gave a mathematically rigorous analysis of density functional theory on the basis of the modern theory of convex functionals, in which the concept of a Legendre transformation plays a central role. This concept was, in a related context even been alluded to in a paper [208] contemporary with that of Hohenberg and Kohn. The main concern of Lieb was related to the appropriate definition of the domains of the important functionals $E(V)$ and $F(\rho)$. In fact Lieb criticized Hohenberg and Kohn for having been somewhat too careless with these domains. Nevertheless we can here only give a nonrigorous presentation of Lieb's approach, not worrying about the domains of $E(V)$ and $F(\rho)$ and other mathematical subtleties. Readers interested in the mathematical details are referred to Lieb's original paper [225] or to the excellent survey by Eschrig [205].

Let us consider a family of (exact) Hamiltonians for the same number n of electrons. These Hamiltonians can only differ in the external potential V , we hence have a V -dependent family of Hamiltonians. Let us further assume that V is a continuous set of local (multiplicative) potentials, and that for the whole family of potentials considered, the ground state is non-degenerate (the latter restriction is actually not necessary). The energy E of the ground state is then a *functional* of V , i.e. $E = E(V)$. It is also clear how one has to proceed to evaluate this functional: one constructs the Hamiltonians $H(V)$,

and solves the Schrödinger equations

$$H(V)\psi(V) = E(V)\psi(V) \quad (38)$$

for the respective ground states. $E(V)$ is even defined if there is no bound ground state, but this possibility causes some problems. For a potential $\tilde{V} = V + \delta V$, that only differs infinitesimally from a given potential V the change in E is given by 1st order perturbation theory as

$$\Delta E = E(V + \delta V) - E(V) = \langle \psi(V) | \delta V | \psi(V) \rangle = \int \delta V \varrho d\tau \quad (39)$$

where ϱ is the electron density corresponding to $\psi(V)$.

It can easily be shown that (for fixed particle number) the functional $E(V)$ is *concave* [205, 225], i. e. that

$$E(\alpha V_1 + [1 - \alpha]V_2) \geq \alpha E(V_1) + (1 - \alpha)E(V_2); \quad 0 \leq \alpha \leq 1 \quad (40)$$

The functional derivative of the ground state energy with respect to V is the density

$$\frac{\delta E}{\delta V} = \varrho \quad (41)$$

This relation between ϱ and V , together with (40) implies an invertibly unique mapping between V and ρ and suggests a change of variables (where the variables are functions) as is familiar from the Legendre transformation in thermodynamics (change from $U(V, T)$ to $H(p, T)$ with $p = -\frac{\partial U}{\partial V}$ or classical mechanics (change from $L(q, \dot{q})$ to $H(q, p)$ with $p = \frac{\partial L}{\partial \dot{q}}$). The corresponding change is now

$$E(V) \rightarrow F(\varrho) = E(V) - \int V \varrho d\tau \quad (42)$$

The functional $F(\varrho)$ is the *internal energy*, i. e. the total ground state energy minus the interaction of the ground state density with the external potential. It is equal to the sum of the kinetic energy and the electron interaction energy. The internal energy $F(\varrho)$ is independent of V and a functional of ϱ only. Hohenberg and Kohn have introduced the functional $F(\varrho)$ without seeing that (for appropriately chosen domains) it is just the Legendre transformation of $E(V)$ and have given $F(\varrho)$ the somewhat unfortunate name 'universal functional of the density'. Of course $F(\varrho)$ is a functional of ϱ in the same sense as $E(V)$ is a functional of V . There is no indication that there should be a simple and direct way to evaluate this functional.

In spite of the *universal* nature of $F(\varrho)$, a change of ϱ can (we always have the exact expressions in mind) only be caused by a change of V . Only those ϱ are admissible as arguments of F , which correspond to the considered V .

Although $F(\varrho)$ does not explicitly depend on V , it depends parametrically on V , and one finds that

$$\frac{\delta F}{\delta \varrho} = \frac{\delta E}{\delta \varrho} - V = -V \quad (43)$$

since the variation of E with respect to variations of ϱ vanishes, provided that ϱ is chosen such that it corresponds to the chosen V . Relation (43) actually allows one to *invert* the Legendre transformation and to arrive at $E(V)$ starting from $F(\varrho)$. This somewhat delicate nature of $F(\varrho)$ must be kept in mind if one really wants to appreciate density functional theory. The role of $F(\varrho)$ is somewhat obscured if one regards E as a functional of ϱ . Since E depends both on V and ϱ and since we are searching for the ϱ which *corresponds* to V the *double* dependence of E on ϱ and V is somewhat confusing. It can be shown that (for an appropriately chosen domain) $F(\varrho) + \int V \varrho d\tau$ is convex and hence attains its minimum for the exact ϱ , provided, of course, that $F(\varrho)$ is the exact (unknown) functional. This is known as the Hohenberg-Kohn variational principle. For a mathematically rigorous fomulation of the Hohenberg-Kohn theorem and especially of the Legendre transformation see [205, 225].

The main problem with $F(\varrho)$ is that it is entirely unknown, that it is at least as complicated as $E(V)$ which is unknown as well, and that there is no way how one should construct $F(\varrho)$. One can formally decompose $F(\varrho)$ into three parts

- (a) the kinetic energy T
- (b) the Coulomb contribution to the electron interaction energy

$$E_{Coul} = \frac{1}{2} \int \varrho(1) \frac{1}{r_{12}} \varrho(2) d\tau \quad (44)$$

(c) the remaining contributions to the electron interaction energy, i. e. the exchange and correlation energies.

Of these contributions only (b) happens to be known exactly, while for the other two one can at best best hope to approximate them somehow.

Density functional methods have been used even before the formulation of the Hohenberg-Kohn-theorem. The classical of these methods is the Thomas-Fermi model [226, 227, 228, 229]. It is based on an analysis of the homogeneous electron gas. This is characterized by a single parameter, namely the density ϱ (i. e. the number of electrons per unit volume), which is a constant, i.e. which is independent of the position \vec{r} . Other properties, like the density of the kinetic energy, must be expressible in terms of ϱ , the kinetic energy density is e. g. proportional to $\varrho^{2/3}$ and the exchange density to $\varrho^{1/3}$. These relations were applied to atomic theory, ignoring that the electron density in an atom is very far from homogeneous. Although various kinds of corrections were added to the simple Thomas-Fermi-model [228, 229], its success was very limited, it

could e.g. not account for the shell structure of atoms and not for chemical binding [230]. A careful analysis has shown that the most serious defect of the Thomas-Fermi model lies in the approximation of the *kinetic energy* as a functional of the density. Even till now no acceptable expression of the kinetic energy as functional of the density has been proposed.

6.3 Slater-Kohn-Sham type methods

Modern *density functional* methods, that can be traced back to a paper by Kohn and Sham [231], *avoid the evaluation of the kinetic energy as a functional of the density*. One rather introduces an artificial non-interacting system – in a modified external potential – with the same density as the considered system and one evaluates the kinetic energy of this system as the kinetic energy of a Slater determinant. So the *density functional methods* in current use, are strictly speaking not genuine density functional methods.

An ingredient of Kohn-Sham type DF methods is that the modified external potential for the artificial non-interacting system should be local (multiplicative).

Since in DF methods the unknown is the density, only basis sets to describe the density well are required. So much smaller basis sets are sufficient than for the genuine many-body methods described in sec. 6.

If one evaluates the kinetic energy (a) in the indicated way (plus an unknown correction, since the two systems – i. e. the real and the artificial one – only have approximatively the same kinetic energy), the two remaining parts (b) and (c) cause less problems. In fact (b) is a genuine and universal density functional, and (c) is regarded as relatively small, such that it does not matter too much how one approximates this term.

A curious aspect is that the dominant part of the exchange-correlation contribution is the removal of the unphysical self-interaction of the electrons contained in (b). Attempts to leave this out from the very beginning, were not too successful and have become popular only recently.

All essential ingredients of the Kohn-Sham approach were already contained in the much older $X\alpha$ method of Slater [210]. The main difference is that the $X\alpha$ method was designed as an approximation to Hartree Fock theory, replacing the (non-local) exact Hartree-Fock exchange by a local approximation, inspired by Thomas-Fermi theory. It was then somewhat surprising that the $X\alpha$ method performed often much better than the Hartree-Fock method that it was designed to approximate. The origin of this apparent superiority remained rather obscure for a long time. It has to do with the fact that in replacing the exact Hartree-Fock exchange by a local exchange one simulates to some extent the 'left-right-correlation', that is ignored in the Hartree-Fock

approximation. Now one tends to say that $X\alpha$ should rather be regarded as a density functional theory of Kohn-Sham type. Therefore it appears fair to refer to this class of functionals as of Slater-Kohn-Sham type, and to regard $X\alpha$ so to say as their 'zeroth generation'. That $X\alpha$ did not turn out too successful, had less to do with its shortcomings, e.g. that it did not treat exchange and correlation separately, but rather with its somewhat unlucky marriage with the 'muffin-tin approximation'.

Following the paper by Kohn and Sham various types of local exchange-correlation functionals were used successfully in solid state physics and with moderate success in chemistry. A big step in advance, especially as far as chemical applications were concerned, came with the generalized gradient-corrected functionals of Becke [213] and Perdew [214].

Meanwhile one counts three generations of density functional methods, (in addition to $X\alpha$ as zeroth order) namely

1. Local density (LD) functionals or local spin density (LSD) functionals
2. Generalized gradient-corrected (GGA) functionals
3. Optimized potential method (OPM).

While methods of the first generation were only of limited use for chemical applications, those of the second generation had a large impact on applied quantum chemistry. They were especially successful for transition metal compounds for which traditional quantum chemical methods has serious problems, due to the strong dependence of the correlation energy on the occupancy of the d -shell. Even systems with partially filled f -shells could be treated successfully by DFT [232].

Methods of the third generation have so far mainly been applied to atoms with rather good success, while for molecules they have not yet made the methods of the second generation obsolete. These involve to some extent *orbital functionals* [233, 234] rather than density functionals, and they are much closer in spirit to quantum chemical ab-initio methods than were the older DF methods. Like in older DF schemes one still insists on a local effective potential, but self-interaction is usually – unlike in the older schemes – eliminated, which makes the remaining exchange and correlation effects much smaller. In fact the bulk of the exchange contribution consists in eliminating the unphysical self interaction, that is characteristic for the older DF approaches.

In the OPM schemes one starts from a Hartree-Fock like exchange energy, but the energy is optimized under the restriction that the effective potential is local. So 'exchange only' OPM is as close to Hartree-Fock theory as a scheme with a local potential can be.

If one tries to forecast the future of density functional theory, the following statements can be safely made:

1. Density functional calculations with black-box programs will become

very popular, and this even for relatively large molecules, since one is now very close to linear scaling [235, 236] of the computational effort with the size of the molecule.

2. On the methodologic side there will be an increased pragmatic attitude, and functionals with adjustable parameters will continue to be proposed, so making the theory to a large extent semiempirical.

3. Simultaneously studies will be continued to understand the physical basis of DF theory better, in particular to understand which are the essential ingredients that make DFT work and whether it is possible to arrive at any desired accuracy. If one is very optimistic one will hope that a hierarchy of density functionals will be found, such that it is also possible to go to the next higher level, if the lower one was not good enough. At present one is very far from this situation. The history of DFT is rich in examples of *improvements* based on formal arguments which rather deteriorated the agreement with experiment.

4. There are indications that there may be some convergence between traditional attempts to solve the Schrödinger equation by ab-initio methods and the so far very different philosophy of DFT. The two approaches to many-electron systems have so far almost been orthogonal and there was hardly a communication between them. For DF methods of the third generation this has drastically changed.

If one compares the attempts reviewed in sec. 3.2 to base many-electron quantum mechanics on the two-particle density matrix, i.e. a *2-particle density matrix functional theory* with the current *density functional theory* one realizes that for the former the functional is exactly known, while the full n -representability condition is unknown. For DFT on the other hand, the functional is unknown, but the n representability does not cause problems. Why should one take incomplete information on n -representability as more serious as lack of information on the exact functional? Possibly there was just more reluctance in the two-particle-density matrix functional community to be satisfied with approximate n -representability conditions than in the density functional community to accept approximate density functionals, and that this different attitude was decisive for the historical development.

7 Conclusions

A quarter of a century ago electron correlation was a topic for a small group of specialists, now it is the main challenge on the way to accurate quantum mechanical calculations for atoms, molecules and solids. A corollary of this observation is that Hartree-Fock calculations no longer pose any serious prob-

lems, which was not the case some 25 years ago, when it did make sense to worry about the optimum implementation of Hartree-Fock theory.

The main difficulties with electron correlation, that are only partially solved are

- (a) the poor convergence with extension of the one-electron basis
- (b) the *unphysical* scaling of the computation effort with the number n of electrons or N of atoms
- (c) the lack of a fully satisfactory theory for those situations where a closed-shell Slater determinant has to be replaced by a multiconfiguration reference function.

As to problem (a) it is at least understood that the basic difficulty is caused by the correlation cusp and that much better convergence is obtained if one uses wave functions depending explicitly on the interelectronic coordinates. The problem of *difficult integrals* can be avoided in the R12-methods, or possibly by using Gaussian geminals. One may also think of improved extrapolation techniques based on the known behaviour of the wave function for $r_{ij} \rightarrow 0$.

The unphysical scaling (b) is one aspect of the fact that in standard quantum chemical computations one actually calculates more than is really needed. If one succeeds in ignoring everything that is irrelevant, one will have got rid of the scaling problem.

Even problem (c) is now being understood in principle, and satisfactory solutions will probably be found.

So far calculations of correlation effects are rather expensive, but hopefully this is going to change. As long as a rigorous improvement of ab-initio methods has not been achieved, it will be hard for these methods to compete with density functional approaches. These have the advantage of being relatively cheap. Even if they are often not exceedingly accurate, the price-performance ratio can hardly be beaten.

At the time of our first review [2] it would hardly have been possible to predict the progress obtained in a quarter of a century. This is a warning as to predictions for the next period of about the same lengths. One has to admit that the past progress was to a large part due to the improvement of computer hardware, and only to a smaller part the merit of theoretical chemists. In the next 25 years or so the progress in methodological development will probably become more important than that of computer technology.

The main challenge as to an improved theory of electron correlation as a basis of accurate numerical quantum chemistry have been mentioned in this review, namely (a) the explicit treatment of the correlation cusp, (b) the formulation of methods that scale with a low power of the number of particles, (c) the consistent combination of MC-SCF-theory for the nondynamic and coupled-cluster methods for the dynamic correlation.

Whether density functional methods will become dominating or whether eventually they will be replaced by genuine many-body methods is hard to predict. Possibly the two approaches will converge to a new simple and rigorous theory of the electronic structure of atoms and molecules.

Although electron correlation is still the main bottleneck toward a rigorous quantum chemistry, one should not forget that for molecules containing heavy elements relativistic effects are not less important [17], while for molecules with lighter atoms adiabatic and even non-adiabatic effects need to be considered [18]. The theory of both types of effects is, fortunately on a good way.

It has been the aim of the present review to concentrate on what we regard as the essential aspects. If we had cared to be complete as to methods that have been proposed to treat electron correlation, we would have had to add other methods, e.g.

(a) Valence bond (VB) approaches. There is a small, but rather convinced community that is in favour of VB [237, 238] as an alternative selection of configurations in a CI type formalism with a more complicated but also more compact structure with less variational parameters. The problems characteristic for CI, such as slow convergence with the basis size related to the correlation cusp are also shared by VB.

(b) So-called fully numerical methods [239, 240] of the type finite differences (FD) or finite elements (FE). Such methods perform very well for one-dimensional problems where they are among the most accurate ones. For multidimensional problems there are serious difficulties. Since correlation in an arbitrary molecule is at least a 6D problem much progress is needed for FD or FE to become competitive.

(c) Monte-Carlo (MC) type methods. We have mentioned such methods in the context of H_3^+ . Monte-Carlo calculations have also been performed for somewhat larger small molecules [241, 242]. For recent reviews see [243, 244, 245]. That the big breakthrough of such methods has not yet come, is due to two difficulties, the *node-problem* and the different time scales for core and valence-electrons. For multiboson systems where the node-problem does not arise and where there is no shell structure, MC methods perform very well. If these problems will be overcome, MC methods have a chance to become competitive with the many-body approaches presented here in more detail. MC methods actually have less difficulties concerning the scaling with the molecular size, and they are rather easily implemented on parallel computers. This may compensate that they are generally rather computer-time consuming.

(d) Pseudopotentials or effective-core potentials (ECP). These are not really methods to treat correlations effects, and are hence not the subject of the present review, but they can simplify ab-initio methods considerably without much loss in accuracy.

(e) Dimensionality scaling [246, 247]. Here one considers a space of dimension $n > 3$ and extrapolates finally to $n = 3$. This is intellectually very appealing. Whether it will gain a noticeable practical importance remains to be seen.

(f) Complementary to methods in which one cares for the energy of a single state, are approaches where energy differences between states are calculated *directly*. (For a review see [248], as to some fundamental work and more recent advances [249, 250, 251, 252, 253, 254, 255, 256]). From the point of view of electron correlation methods of this type (often based on propagator, Green's function or equation-of motion theory) exploit that the contributions to the correlation energy common to the two states don't enter. The gain is probably not as spectacular as thought originally, but methods of this type will probably continue to play some role, e.g. for the treatment of open-shell states based on a closed-shell reference [252, 253, 254, 255, 256]).

(g) Methods for the treatment of electron correlation which are more popular in solid state theory than for molecules are reviewed in [257].

(h) Other *unconventional* methods are mentioned in [247, 258].

Possibly methods will become important that have not even been conceived so far.

Acknowledgments The authors thank again the participants of the 1970 Ischia meeting on electron correlation. Their names, not mentioned earlier [2] are possibly more informative when given now. We remember the following participants

R. Ahlrichs, G. Berthier, W. A. Bingel, B. Cadioli, G. Del Re, P. Durand, M. Gelus, M. Jungen, B. Levy, J. P. Malrieu, R. McWeeny, W. Meyer, V. Staemmler

and apologize to all those whom we may have forgotten.

Some of the just-mentioned authors have collaborated with the present authors on electron correlation. In addition there has been collaboration in this field with many other scientists, especially F. Driessler, W. Klopper, S. Koch, H. Lischka, F. Maeder, J. D. Morgan III, D. Mukherjee, J. , H. Reitz, R. Röhse, V. H. Smith and Ch. van Wüllen. For comments on the manuscript the authors are grateful to V. Staemmler, D. Mukherjee, R. Jaquet, and Ch. van Wüllen.

References

- [1] As to the identity of P. v. H. and his curriculum see P. G. Mezey in WATOC Newsletters, June 1996, (http://www.ch.ic.ac.uk/watoc/watoc_newsletter_3.html)

- [2] P. v. Herigonte, *Structure and Bonding*, **12**, 1 (1972)
- [3] R. Ahlrichs, W. Kutzelnigg, *J. Chem. Phys.* **48**, 1819 (1968)
- [4] R. Ahlrichs and W. Kutzelnigg, *Theoret. Chim. Acta* **10**, 377 (1968)
- [5] R. Ahlrichs and W. Kutzelnigg, *Chem. Phys. Lett.* **1**, 651 (1968)
- [6] M. Gelus, R. Ahlrichs, V. Staemmler and W. Kutzelnigg, *Chem. Phys. Lett.* **7**, 503 (1970)
- [7] M. Gelus and W. Kutzelnigg, *Theoret. Chim. Acta* **28**, 103 (1973)
- [8] V. Dyczmons, V. Staemmler and W. Kutzelnigg, *Chem. Phys. Lett.* **5**, 361 (1970)
- [9] V. Staemmler and M. Jungen, *Theoret. Chim. Acta* **24**, 152 (1972); *Chem. Phys. Lett.* **16**, 187 (1972)
- [10] M. Jungen, R. Ahlrichs, *Theoret. Chim. Acta* **17**, 339 (1970)
- [11] W. Meyer, *Int. J. Quant. Chem.* **5**, 341 (1971); *J. Chem. Phys.* **58**, 1017 (1973)
- [12] W. Kutzelnigg, in *Modern Theoretical Chemistry*, Vol. 3 *Electronic structure theory*, H. F. Schaefer III ed., Plenum (NY) 1977
- [13] R. Ahlrichs, H. Lischka, V. Staemmler, and W. Kutzelnigg, *J. Chem. Phys.* **62**, 1225 (1975)
- [14] W. Kutzelnigg, G. Del Re, G. Berthier, *Phys. Rev.* **172**, 49 (1968)
- [15] W. Kutzelnigg, D. Mukherjee, submitted to *J. Chem. Phys.*
- [16] see e.g. W. Cencek, W. Kutzelnigg, *J. Chem. Phys.* **105**, 5878 (1996); *Chem. Phys. Lett.* **266**, 383 (1997)
- [17] A bibliography on relativistic quantum chemistry can be found in P. Pyykkö, *Lecture Notes in Chemistry*, Vol. 41 (1986) and Vol. 60 (1993), Springer, Berlin . This list is being updated on internet under <http://www.csc.fi/lul/rtam/>.
- [18] References on adiabatic and nonadiabatic theory can be traced back from W. Kutzelnigg, *Mol. Phys.* **90**, 909 (1997)
- [19] J. Gauss, J. F. Stanton, *J. Chem. Phys.* **103**, 3561 (1995)

- [20] T. Kato, Commun. Pure. Appl. Math. **19**, 151 (1957)
- [21] E. A. Hylleraas, Z. Phys. **54**, 347 (1929), **65**, 209 (1930)
- [22] C. L. Pekeris, Phys. Rev. **112**, 1649 (1958), **126**, 1470 (1962)
- [23] V. Fock, Kngl. Norsk. Vidinsk. Selsk. Forh. **31**, 138, 145 (1958)
- [24] P. C. Abbott and E. N. Maslen, J. Phys. A **20**, 2043 (1987)
- [25] J. D. Morgan III, Theoret. Chim. Acta **69**, 181 (1986)
- [26] K. Frankowski and C. L. Pekeris, Phys. Rev. **146**, 46 (1966)
- [27] D. E. Freund, B. D. Huxtable, J. D. Morgan III, Phys. Rev. **A29**, 980 (1984)
- [28] G. W. Drake, Phys. Rev. Lett. **59**, 1549 (1987)
- [29] G. W. F. Drake and Z.-C. Yan, Chem. Phys. Lett. **229**, 486 (1994)
- [30] G. W. Drake, Nucl. Instr. Math. Phys. Res. B **31**, 7 (1988)
- [31] A. Kleindienst, A. Lüchow, H. P. Merckens, Chem. Phys. Lett. **218**, 441 (1994)
- [32] A. J. Thakkar and T. Koga, Phys. Rev. A **50**, 854 (1994)
- [33] H. Kleindienst and R. Emrich, Int. J. Quant. Chem. **37**, 257 (1990)
- [34] F. T. Newman, Int. J. Quant. Chem. **63**, 1065 (1997)
- [35] S. P. Goldman, Phys. Rev. A **57**, 677 (1998)
- [36] J. Rychlewski, W. Cencek, and J. Komasa, Chem. Phys. Lett. **229**, 657 (1994)
- [37] J. D. Morgan III, in: *Numerical Determination of the Electronic Structure of Atoms, Diatomic and Polyatomic Molecules*, M. Defranceschi and J. Delhalle ed., Kluwer, Dordrecht, 1989, p. 49
- [38] R. N. Hill, J. Chem. Phys. **83**, 1173 (1985)
- [39] F. Stenger, *Numerical Methods based on Sinc and Analytical Functions*, Springer, New York, 1993
- [40] W. Kutzelnigg, Int. J. Quantum Chem. **51**, 447 (1994)

- [41] G. W. Drake, *Canad. J. Phys.* **66**, 586 (1988)
- [42] I. Lindgren, M. Persson, S. Salomonsen, and L. Labzowski, *Phys. Rev. A* **51**, 1167 (1995)
- [43] E. Ottschofski and W. Kutzelnigg, *J. Chem. Phys.* **106**, 6634 (1997)
- [44] H. M. James and A. S. Coolidge, *J. Chem. Phys.* **1**, 825 (1933)
- [45] W. Kolos, and C. C. J. Roothaan, *Rev. Mod. Phys.* **32**, 219 (1960)
- [46] W. Kolos, L. Wolniewicz, *J. Chem. Phys.* **41**, 3663, 3674 (1964); **49**, 404 (1968)
- [47] G. Herzberg and A. Monfils, *J. Mol. Spectr.* **5**, 482 (1960)
- [48] L. Wolniewicz, *J. Chem. Phys.* **99**, 1851 (1993)
- [49] W. Kolos, J. Rychlewski, *J. Chem. Phys.* **98**, 3960 (1993)
- [50] W. Meyer, P. Botschwina, P. G. Burton, *J. Chem. Phys.* **84**, 891 (1986)
- [51] R. Röhse, W. Klopper, W. Kutzelnigg, *J. Chem. Phys.* **99**, 8830 (1993)
- [52] R. Röhse, W. Kutzelnigg, R. Jaquet and W. Klopper, *J. Chem. Phys.* **101**, 2231 (1994)
- [53] W. Cencek, J. Komasa, J. Rychlewski, *Chem. Phys. Lett.* **246**, 417 (1995)
- [54] W. Cencek, J. Rychlewski, R. Jaquet, W. Kutzelnigg, *J. Chem. Phys.* **108**, 2831 (1998)
- [55] J. B. Anderson, *J. Chem. Phys.* **96**, 3702 (1992)
- [56] A. Lüchow, H. Kleindienst, *Int. J. Quantum Chem.* **51**, 211 (1994)
- [57] Z.-C. Yan and G. W. F. Drake, *Phys. Rev. A* **52**, 3711 (1995)
- [58] D. L. Diedrich and J. B. Anderson, *J. Chem. Phys.* **100**, 8089 (1994)
- [59] J. Komasa, W. Cencek and J. Rychlewski, in: *Computational Methods in Science and Technology*, Vol. 2, p. 87, Scientific Publishers OWN, Poznan, 1996
- [60] K. A. Peterson, D. E. Woon and T. H. Dunning, jr., *J. Chem. Phys.* **100**, 7410 (1994)
- [61] B. Liu, *J. Chem. Phys.* **58**, 1925 (1973), **80**, 581 (1987)

- [62] P. Siegbahn and B. Liu, *J. Chem. Phys.* **68**, 2457 (1978)
- [63] A. J. C. Varandas, F. B. Brown, C. A. Mead, D. G. Truhlar, and N. C. Blais, *J. Chem. Phys.* **86**, 6258 (1987)
- [64] A. I. Boothroyd, W. J. Keogh, P. G. Martin, and M. R. Peterson, *J. Chem. Phys.* **95**, 4343 (1991)
- [65] A. I. Boothroyd, W. J. Keogh, P. G. Martin, and M. R. Peterson, *J. Chem. Phys.* **104**, 7139 (1996)
- [66] A. Kupperman and J. B. Anderson, *Phys. Chem., Chem. Phys.* **1**, xxxx (1999)
- [67] A.-M. Mårtensson-Pendrill, S. A. Alexander, L. Adamowicz, N. Oliphant, J. Olsen, P. Öster, H. M. Quiney, S. Salomonson, D. Sundholm, *Phys. Rev.* **A43**, 3355 (1991)
- [68] J. Komasa, W. Cencek, and J. Rychlewski, *Phys. Rev.* **A52**, 4500 (1995)
- [69] G. Buesse and H. Kleindienst, *Phys. Rev.* **A51**, 5019 (1995)
- [70] G. Buesse, H. Kleindienst and A. Lüchow, *Int. J. Quant. Chem.* **86**, 241 (1998)
- [71] J. Noga, D. Tunega, W. Klopper and W. Kutzelnigg, *J. Chem. Phys.* **103**, 309 (1995)
- [72] T. van Mourik, R. J. Vos, J. H. van Lenthe and F. B. van Duijneveldt, *Int. J. Quant. Chem.* **63**, 805 (1997)
- [73] T. van Mourik, J. H. van Lenthe, *J. Chem. Phys.* **102**, 7479 (1995)
- [74] W. Klopper, and J. Noga, *J. Chem. Phys.* **103**, 6127 (1995)
- [75] H.L. Williams, T. Korona, R. Bukowski, B. Jeziorski, and K. Szalewicz, *Chem. Phys. Lett.* **262**, 4 31 (1996)
- [76] T. Korona, H.L. Williams, R. Bukowski, B. Jeziorski, and K. Szalewicz, *J. Chem. Phys.* **106**, 5109 (1997)
- [77] A. R. Janzen, R. A. Aziz, *J. Chem. Phys.* **103**, 9626 (1995)
- [78] B. Klahn, W. A. Bingel, *Theor. Chim. Acta* **44**, 9, 27 (1977)

- [79] This formulation of the many-electron problem has particularly been stressed by Löwdin [80], but it can be traced back to earlier textbooks [81, 82]
- [80] P. O. Löwdin, *Phys. Rev.* **97**, 1474, 1490, 1589 (1955)
- [81] J. I. Frenkel, *Wave mechanics, advanced general theory*, Oxford, Clarendon, 1934
- [82] H. A. Kramers, *Quantenmechanik* in: "Hand- und Jahrbuch der Chemischen Physik", Vol. 1 (1937)
- [83] P. J. Knowles, and N. C. Handy, *Chem. Phys. Lett.* **111**, 315 (1984)
- [84] C. W. Bauschlicher, S. R. Langhoff, P. R. Taylor, and H. Partridge, *Chem. Phys. Lett.* **126**, 4636 (1986)
- [85] S. Evangelisti, G.L. Bendazzoli, R. Ansaloni, E. Rossi, *Chem. Phys. Lett.* **233**, 353 (1995) ,**252**, 437 (1996)
- [86] W. Kutzelnigg, *Chem. Phys. Letters* **83**, 156 (1981)
- [87] W. Kutzelnigg, *J. Chem. Phys.* **77**, 3081 (1982)
- [88] A. J. Coleman, *Rev. Mod. Phys.* **35**, 668 (1963)
- [89] A. J. Coleman and I. Absat, *Int. J. Quant. Chem.* **18**, 1279 (1980)
- [90] R. McWeeny, *Rev. Mod. Phys.* **32**, 335 (1960)
- [91] V. Maslen, *Proc. Phys. Soc. (London)* **A69**, 734 (1956)
- [92] C. A. Coulson and A. H. Neilson, *Proc. Roy. Soc. (London)* **A78**, 831 (1961)
- [93] W. Kutzelnigg, *Theoret. Chim. Acta* **3**, 241 (1965)
- [94] V. Staemmler and W. Kutzelnigg, *Theoret. Chim. Acta* **9**, 67 (1967)
- [95] W. Kutzelnigg, *Topics Curr. Chem.* **41**, 31 (1973)
- [96] P. A. M. Dirac, *Proc. Camb. Phil. Soc.* **27**, 240 (1931)
- [97] W. Kutzelnigg and D. Mukherjee, *J. Chem. Phys.* **107**, 432 (1997)
- [98] D. Mukherjee, *Chem. Phys. Lett.* **274**, 561 (1997)
- [99] K. A. Brueckner, *Phys. Rev.* **97**, 1353, **100**, 36 (1955)

- [100] J. Goldstone, Proc. Roy. Soc. A **239**, 267 (1957)
- [101] N. M. Hugenholtz, Physica **23**, 481 (1957)
- [102] For a modern presentation of MBPT, see W. Kutzelnigg in: *Applied Many-Body Methods in Spectroscopy and Electronic Structure*, D. Mukherjee ed., Plenum, NY, 1992
- [103] W. Kutzelnigg, in: *Recent Progress in Many-Body Theories*, H. Kümmel and M. L. Ristig ed., Lecture Notes in Physics **198**, 361, Springer, Berlin 1984
- [104] I. Lindgren, J. Morrison, *Atomic Many-Body Theory*, Springer, Berlin, 1982
- [105] D. Layzer, Z. Horak, M. N. Lewis, and D. P. Thompson, Ann. Phys. **29**, 101 (1964)
- [106] C. W. Scherr and R. E. Knight, Rev. Mod. Phys. **35**, 436 (1963)
- [107] J. Midtal, Phys. Rev. **138A**, 1010 (1965)
- [108] L. Møller and M. S. Plesset, Phys. Rev. **46**, 618 (1934)
- [109] P. Claverie, S. Diner, and J. P. Malrieu, Int. J. Quant. Chem. **1**, 751 (1967)
- [110] J. S. Binkley and J. A. Pople, Int. J. Quant. Chem. **9**, 229 (1975)
- [111] W. Kutzelnigg, and S. Koch, J. Chem. Phys. **79**, 4315 (1983)
- [112] J. Olson, O. Christiansen, H. Koch and P. Jørgensen, J. Chem. Phys. **105**, 5082 (1996)
- [113] D. Cremer and Z. He, J. Chem. Phys. **100**, 6173 (1996)
- [114] N. C. Handy, P. J. Knowles, K. Somasundram, Theoret. Chim. Acta **68**, 87 (1985)
- [115] H. P. Kelly, Phys. Rev. **134A**, 1450 (1964), Adv. Chem. Phys. **14**, 129 (1969)
- [116] R. J. Buenker, S. D. Peyerimhoff, Theoret. Chim Acta **35**, 33 (1974), **39**, 217 (1975)
- [117] A. Meunier, B. Levy, G. Berthier, W. Kutzelnigg, Int. J. Quantum Chem. **12**, 777 (1977)

- [118] F. Coester and H. Kümmel, Nucl. Phys. **17**, 477 (1960)
- [119] J. Cizek, J. Chem. Phys. **45**, 4256 (1966)
- [120] P. R. Taylor, G. B. Bacslay, N. S. Hush, A. C. Hurley, Chem. Phys. Lett. **41**, 444 (1976); J. Chem. Phys. **69**, 4669 (1978)
- [121] R. J. Bartlett and G. D. Purvis, Int. J. Quant. Chem. **14**, 561 (1978)
- [122] J. A. Pople, R. Krishnen, H.-P. Schlegel, J. S. Binkley, Int. J. Quant. Chem. **14**, 545 (1978)
- [123] R. J. Bartlett, J. Phys. Chem. **93**, 1697 (1989)
- [124] W. Kutzelnigg, Theoret. Chim. Acta **80**, 349 (1991)
- [125] W. Kutzelnigg, Mol. Phys., **94**, 65 (1998)
- [126] M. Urban, J. Noga, S. J. Cole, and R. J. Bartlett, J. Chem. Phys. **83**, 404 (1985)
- [127] M. Urban, I. Černušák, V. Kellö, and J. Noga, in: *Methods in Computational Chemistry*, Vol. 1, S. Wilson ed., Plenum, NY, 1987
- [128] J. Noga, R. J. Bartlett, M. Urban, Chem. Phys. Lett. **134**, 128 (1987)
- [129] K. Raghavachari, J. A. Pople, and M. Head-Gordon, Chem. Phys. Lett. **157**, 479 (1989)
- [130] T. J. Lee and G. E. Scuseria, in: *Quantum Mechanical Electronic Structure Calculations with Chemical Accuracy*, S. R. Langhoff ed., Kluwer, Dordrecht, 1995
- [131] H. Müller, R. Franke, St. Vogtner, R. Jaquet, W. Kutzelnigg, Theoret. Chem. Acc., to be published
- [132] V. Staemmler and R. Jaquet, Theoret. Chim. Acta **59**, 48 (1981)
- [133] K. Schröder, V. Staemmler, R. Jaquet, M. D. Smith and D. Flower J. Phys. B: At. Mol. Opt. Phys., **24**, 2487 (1991)
- [134] R. Jaquet, V. Staemmler, M. D. Smith and D. R. Flower J. Phys. B: At. Mol. Opt. Phys., **25**, 285 (1992)
- [135] P. Botschwina, M. Oswald, J. Flügge, Ä. Heyl and R. Oswald, Chem. Phys. Lett. **209**, 117 (1993)

- [136] P. Botschwina, M. Horn, J. Flügge and S. Seeger, J. Chem. Soc. Farad. Trans. **89**, 2219 (1993)
- [137] S. Koch, and W. Kutzelnigg, Theoret. Chim. Acta **59**, 387 (1981)
- [138] W. Meyer, J. Chem. Phys. **64**, 2901 (1976)
- [139] R. Ahlrichs, P. Scharf, C. Ehrhard, J. Chem. Phys. **82**, 890 (1985)
- [140] D. Mukherjee, R. K. Moitra and A. Mukhopadhyay, Mol. Phys. **30**, 1861 (1975); **33**, 955 (1977)
- [141] U. S. Maha Patra, B. Datta, B. Bandyopadhyay and D. Mukherjee, Adv. Quantum Chem. **30**, 163 (1998)
- [142] J. P. Malrieu, Ph. Durand, and J. P. Daudey, J. Phys. A, **18**, 809 (1985)
- [143] U. S. Maha Patra, B. Datta, and D. Mukherjee, Mol. Phys. **94**, 157 (1998)
- [144] S. Koch, Theoret. Chim. Acta **81**, 169 (1991)
- [145] D. Mukherjee, Chem. Phys. Letters **125**, 207 (1986)
- [146] W. Kutzelnigg, D. Mukherjee, and S. Koch, J. Chem. Phys. **87**, 5902 (1987)
- [147] D. Mukherjee, W. Kutzelnigg, and S. Koch, J. Chem. Phys. **87**, 5911 (1987)
- [148] B. Datta and D. Mukherjee, Chem. Phys. Lett. **235**, 31 (1995)
- [149] B. Jeziorski and H. J. Monkhorst, Phys. Rev. **A24**, 1668 (1981)
- [150] D. Mukhopadhyay and D. Mukherjee, Chem. Phys. Lett. **163**, 171 (1989).
- [151] L. Meissner and R. J. Bartlett, J. Chem. Phys. **92**, 561 (1990)
- [152] W. Meyer, in: *Modern Theoretical Chemistry*, H. F. Schaefer III ed., Plenum, NY, 1977
- [153] H. J. Werner, and P. J. Knowles, J. Chem. Phys. **89**, 5803 (1988)
- [154] B. O. Roos, P. R. Taylor, P. Siegbahn, Chem. Phys. **48**, 157 (1980)
- [155] K. Anderson, P.-Å. Malquist, B. O. Roos, A. J. Sadlej and K. Wolinski, J. Chem. Phys. **94**, 548 (1990)

- [156] L. Serramp-Andrés, M. Merchán, I. Nebot-Gil, R. Lindh and B. O. Roos, *J. Chem. Phys.* **98**, 3151 (1993)
- [157] R. J. Gdanitz, R. Ahlrichs, *Chem. Phys. Letters* **143**, 413 (1988)
- [158] R. Fink and V. Staemmler, *Theoret. Chim. Acta* **87**, 129 (1993)
- [159] P. Piecuch, N. Oliphant and L. Adamowicz, *J. Chem. Phys.* **99**, 1875 (1993)
- [160] R. J. Buenker, S. D. Peyerimhoff, *Theoret. Chim. Acta* **12**, 183 (1968)
- [161] W. Kutzelnigg, *Int. J. Quant. Chem.* **52**, 447 (1994)
- [162] R. Franke, W. Kutzelnigg, unpublished
- [163] C. Schwarz, *Phys. Rev.* **126**, 1015 (1962)
- [164] W. Kutzelnigg, and J. D. Morgan III, *J. Chem. Phys.* **96**, 4484 (1992)
- [165] W. Kutzelnigg, *Theoret. Chim. Acta* **68**, 445 (1985)
- [166] T. H. Dunning, jr., *J. Chem. Phys.* **90**, 1007 (1989)
- [167] K. A. Peterson, A. K. Wilson, D. E. Woo, T. H. Dunning jr., *Theoret. Chim. Acta* **97**, 251 (1997)
- [168] A. K. Wilson, T. H. Dunning jr., *J. Chem. Phys.* **106**, 8718 (1997)
- [169] J. M. L. Martin, P. R. Taylor, *J. Chem. Phys.* **106**, 8818 (1997)
- [170] G. A. Petersson and M. Braunstein, *J. Chem. Phys.* **83**, 5129 (1985)
- [171] D. Frye, A. Preiskorn, G. C. Lie, and E. Clementi, *J. Chem. Phys.* **92**, 4948 (1990)
- [172] W. Klopper and W. Kutzelnigg, *Chem. Phys. Lett.* **134**, 17 (1987)
- [173] W. Kutzelnigg, W. Klopper, *J. Chem. Phys.* **94**, 1985 (1991)
- [174] W. Klopper, W. Kutzelnigg, *J. Chem. Phys.* **94**, 2020 (1991)
- [175] W. Klopper, *Chem. Phys. Lett.* **186**, 583 (1991)
- [176] W. Klopper, H. P. Lüthi, Th. Brupbacher, A. Bauder, *J. Chem. Phys.* **101**, 9747 (1994)

- [177] T. Bürgi, S. Graf, S. Leutwyler, and W. Klopper, *J. Chem. Phys.* **103**, 1077 (1995)
- [178] H. Müller, W. Kutzelnigg, J. Noga, *Mol. Phys.* **92**, 535 (1997)
- [179] J. Noga, W. Klopper, W. Kutzelnigg, in: *Recent Advances in Coupled-Cluster Methods*, R. J. Bartlett ed., World Scientific, Singapore, p.1 1998
- [180] W. Klopper, in: *Encyclopedia of Computational Chemistry*, P. v. R. Schleyer et al. ed. Wiley, Chichester, 1998
- [181] J. Noga, and W. Kutzelnigg, *J. Chem. Phys.* **101**, 7783 (1994)
- [182] R.J. Gdanitz, *Chem. Phys. Lett.* **283**, 253 (1998)
- [183] K. Szalewicz, B. Jeziorski, H. J. Monkhorst, and J. G. Zabolitzky, *J. Chem. Phys.* **78**, 1420 (1983), **79**, 5343 (1983)
- [184] S. A. Alexander, H. J. Monkhorst, and K. Szalewicz, *J. Chem. Phys.* **85**, 5821 (1986); **87**, 3976 (1987)
- [185] K. B. Wenzel, J. G. Zabolitzky, V. Szalewicz, B. Jeziorski, H. J. Monkhorst, *J. Chem. Phys.* **85**, 3964 (1986)
- [186] R. Bukowski, B. Jeziorski, S. Rybak, K. Szalewicz, *J. Chem. Phys.* **102**, 888 (1995)
- [187] M. Häser, R. Ahlrichs, *J. Comput. Chem.* **10**, 104 (1989)
- [188] I. Panas and J. E. Almlöf, *Int. J. Quant. Chem.* **42**, 1073 (1992)
- [189] L. Greengard, *Science*, **265**, 909 (1994)
- [190] C. A. White, B. G. Johnson, P. M. W. Gill, M. Head-Gordon, *Chem. Phys. Lett.* **230**, 8 (1994); **253**, 268 (1996)
- [191] J. P. Dombrowski, S. W. Taylor, and P. M. W. Gill, *J. Chem. Phys.* **100**, 6272 (1996)
- [192] J. E. Lennard-Jones, *Proc. Roy. Soc.* **A198**, 1, 14 (1949); **202**, 166 (1950)
- [193] C. Edmiston, and K. Ruedenberg, *Rev. Mod. Phys.* **33**, 457 (1963); *J. Chem. Phys.* **43**, 597 (1965)
- [194] J. M. Foster, and S. F. Boys, *Rev. Mod. Phys.* **32**, 296 (1960)
- [195] K. Fink and V. Staemmler, *J. Chem. Phys.* **103**, 2603 (1995)

- [196] S. Saebo, P. Pulay, Chem. Phys. Lett. **113**, 13 (1985); J. Chem. Phys. **88**, 1884 (1988); Ann. Rev. Phys. Chem. **44**, 213 (1993)
- [197] C. Hampel, H.-J. Werner, J. Chem. Phys. **104**, 6286 (1996)
- [198] P. Y. Ayala and G. E. Scuseria, J. Chem. Phys. **xxx**, xxxx (1998)
- [199] M. Häser and J. Almlöf, J. Chem. Phys. **96**, 489 (1992)
- [200] W. Kutzelnigg, and St. Vogtner, Int. J. Quant. Chem. **60**, 235 (1996)
- [201] We use the abbreviation DF for *density functional*. A confusion with Dirac-Fock, which is often abbreviated as DF as well, should not arise, since here we don't consider relativistic effects. The acronym DFT (with 'T' for theory) is rather common, but one may be reluctant to use the term *theory* in this context; *project* might be the more appropriate term.
- [202] R. M. Dreizler and E. K. U. Groß, *Density Functional Theory*, Springer, Berlin, 1990
- [203] R. G. Parr and W. Yang, *Density Functional Theory of Atoms and Molecules*, Oxford Univ. Press, 1989
- [204] E. S. Kryachko, E. V. Ludena, *Energy Density Functional Theory of Many-Electron Systems*, Kluwer, Dordrecht, 1990
- [205] H. Eschrig, *The Fundamentals of Density Functional Theory*, Teubner, Stuttgart 1996
- [206] R. O. Jones, D. Hohl, J. Chem. Phys. **92**, 6710 (1990)
- [207] P. Hohenberg, W. Kohn, Phys. Rev. **B136**, 846 (1964)
- [208] C. de Dominicis and P. C. Martin, J. Math. Phys. **5**, 14 (1964)
- [209] D. N. Mermin, Phys. Rev. **137**, A1441 (1965)
- [210] J. C. Slater, Phys. Rev. **81**, 385 (1951)
- [211] J. C. Slater, J. Chem. Phys. **43S**, 228 (1965)
- [212] K. H. Johnson, Adv. Quant. Chem. **7**, 143 (1973)
- [213] A. D. Becke, Phys. Rev. **A38**, 3098 (1988)
- [214] J. P. Perdew, Phys. Rev. **B33**, 8822 (1986)

- [215] B. G. Johnson, P. M. W. Gill, and J. A. Pople, *J. Chem. Phys.* **98**, 5612 (1993)
- [216] C. W. Murray, G. J. Laming, N. C. Handy, and R.D. Amos, *Chem. Phys. Lett.* **199**, 551 (1992)
- [217] Ch. van Wüllen, *Chem. Phys. Lett* **219**, 8 (1994)
- [218] J. Andzelm and E. Wimmer, *J. Chem. Phys.* **96**, 1280 (1992)
- [219] N. C. Handy, D. J. Tozer, G. J. Laming, C. W. Murray, and R.D. Amos, *Isr. J. Chem.* **33**, 331, (1993) (1986)
- [220] Q. Zhao, R. C. Morrison, and R. G. Parr, *Phys. Rev. A* **50**, 2138 (1994)
- [221] G. K. L. Chan, D. J. Tozer and N. C. Handy, *J. Chem. Phys.* **107**, 1 (1997)
- [222] A. Görling and M. Ernzerhof, *Phys. Rev. A* **31**, 4301 (1995)
- [223] A. Görling, M. Levy, *Phys. Rev.* **A50**, 196 (1994), **A53**, 3140 (1996)
- [224] E. H. Lieb, *Rev. Mod. Phys.*; **53**, 603 (1981), **54**, 311 (1982)
- [225] E. H. Lieb, *Int. J. Quantum. Chem.*; **24**, 243 (1983)
- [226] L. H. Thomas, *Proc. Cambr. Phil. Soc.* **23**, 542 (1927)
- [227] E. Fermi, *Rend. Accad. Linc.* **6**, 602 (1927)
- [228] P. A. M. Dirac, *Proc. Cambr. Phil. Soc.* **26**, 376 (1930)
- [229] C. F. v. Weizsäcker, *Z. Phys.* **96**, 431 (1935)
- [230] E. Teller, *Rev. Mod. Phys.* **34**, 627 (1962)
- [231] W. Kohn, L. S. Sham, *Phys. Rev.* **A140**, 133 (1965)
- [232] W. Liu, G. Hong, D. Dai, L. Li, and M. Dolg, *Theor. Chem. Acc.* **96**, 75 (1997)
- [233] J. B. Krieger, Y. Lie, G. J. Iafrate, *Phys. Rev.* **A46**, 5453 (1992); **47**, 165 (1993)
- [234] T. Grabo, T. Kreibich, S. Kurth, and E. K. U. Groß, in: *Strong Coulomb Correlations in Electronic Structure: Beyond the Local Density Approximation*, V. S. Anisimov ed., Gordon and Breach, Tokyo, 1998

- [235] M. C. Strain, G. E. Scuseria, and M. J. Frisch, *Science* **271**, 51 (1996)
- [236] R. E. Stratmann, G. E. Scuseria and M. J. Frisch, *Chem. Phys. Lett.* **257**, 213 (1996)
- [237] D. L. Cooper, J. Gerratt, and M. Raimondi, *Adv. Chem. Phys.* **69**, 319 (1987)
- [238] R. McWeeny in *Computational Molecular Physics*, S. Wilson, G. H. F. Diercksen ed., Plenum, NY, 1962
- [239] *Numerical Determination of the Electronic Structure of Atoms, Diatomic and Polyatomic Molecules*, M. Defranceschi and J. Delhalle ed., Kluwer, Dordrecht, 1989
- [240] L. Yang, D. Heinemann, and D. Kolb, *Phys. Rev. A*, 2700 (1993)
- [241] P. J. Reynolds, D. M Ceperley, B. J. Alder, and W. A. Lester jr., *J. Chem. Phys.* **77**, 5593 (1982)
- [242] A. Lüchow and J. B. Anderson, *J. Chem. Phys.* **105**, 4036 (1996)
- [243] B. L. Hammond, W. A. Lester jr, and P. J. Reynolds, 'Monte Carlo Methods in ab-initio Quantum Chemistry', World scientific, Singapore, 1994
- [244] D. M Ceperley and L. Mitas, *Adv. Chem. Phys.* **93**, 1(1996)
- [245] H.-J. Flad, M. Caffarel, A. Savin, in 'Recent Advances in Computational Chemistry' W. A. Lester jr,ed. , World scientific, Singapore, 1997
- [246] J. G. Loeser, and D. R. Herschbach, *J. Chem. Phys.* **86**, 2114 (1987)
- [247] *New Methods in Quantum Theory*, C. A. Tsipis et al. ed., Kluwer, Dordrecht, 1996
- [248] W. Kutzelnigg, H. Reitz, S. Durmaz and S. Koch, *Proc. Ind. Acad. Sci.* **96**, 177 (1986)
- [249] W. Kutzelnigg and D. Mukherjee, *J. Chem. Phys.* **99**, 5578 (1989)
- [250] J. Schirmer, *Phys. Rev. A* **26**, 2395 (1982); **A 43**, 4647 (1991)
- [251] D. Mukherjee and W. Kutzelnigg in 'Many-Body Methods in Quantum Chemistry', U. Kaldor ed., Lecture Notes in Chemistry 52, Springer, Berlin 1989

- [252] H. Nakatsuji and K. Hirao, Chem. Phys. Letters **59**, 362 (1978), J. Chem. Phys. **68**, 2053 (1988)
- [253] H. Monkhorst, Int. J. Quantum Chem. **S11**, 421 (1977)
- [254] D. Mukherjee and P. K. Mukherjee, Chem. Phys. **37**, 325 (1979)
- [255] J. Stanton and R. J. Bartlett, J. Chem. Phys. **98**, 7029 (1993)
- [256] M. Noojen and R. J. Bartlett, J. Chem. Phys. **102**, 3629 (1995)
- [257] P. Fulde, *Electron Correlation in Molecules and Solids*, Springer, Berlin, 1991
- [258] W. Kutzelnigg, J. Mol. Struct. (Theochem) **181**, 33 (1988)

Approximate Coupled Cluster Methods: Combined Reduced Multireference and Almost-Linear Coupled Cluster Methods with Singles and Doubles ¹

Xiangzhu Li^{a)}, Ireneusz Grabowski^{b)},
Karol Jankowski^{b)}, and Josef Paldus^{a),c)}

^{a)} Department of Applied Mathematics, University of Waterloo,
Waterloo, Ontario N2L 3G1, Canada

^{b)} Institute of Physics, Nicholas Copernicus University,
87-100 Toruń, Poland

^{c)} Max-Planck-Institut für Astrophysik, Karl-Schwarzschild-Str. 1,
87540 Garching bei München, Germany.

Abstract

The recently introduced version of the externally corrected coupled cluster method with singles and doubles (CCSD), exploiting a small active space multireference (MR) configuration interaction with singles and doubles (CISD) wave function as a source of the three and four body connected cluster amplitudes, which is referred to as the reduced MR (RMR) CCSD method, and the so-called almost-linear (AL) CCSD method based on the split-amplitude strategy, are combined to achieve a considerable saving of the computational effort, while yielding almost exact RMR CCSD results. The performance of the suggested approach is exemplified on several models involving four and eight hydrogen atoms in various geometric configurations that enable the quasidegeneracy effects to be varied from the completely degenerate limit to the nondegenerate case, as well as on the symmetrically stretched double zeta model of the water molecule and of the fluorine molecule. In all cases the suggested approach provides an excellent approximation to the full RMR CCSD energies, which in turn faithfully account for the nondynamical correlation effects involved.

¹This paper is dedicated to Professor Giuseppe Del Re at the occasion of his 65th anniversary.

Contents

1. Introduction
2. Externally Corrected CCSD
3. Almost-Linear (AL) CC Methods
4. Results and Discussion
 - 4.1 The H4 Model
 - 4.2 The H8 Model
 - 4.3 The S4 Model
 - 4.4 A DZ Model of H₂O
5. Conclusions
6. Acknowledgments
- References

1 Introduction

The usefulness of coupled cluster (CC) methodology (1,2) for the account of many-electron correlation effects is nowadays well recognized (for an overview and further references, see Ref. 3). The standard CC approach involving singly and doubly excited cluster amplitudes (CCSD method), particularly when supplemented with a perturbative account of triply excited connected clusters [CCSD(T) (4) or CCSD[T] (5) methods], represents a very efficient and reliable procedure that is routinely used to obtain highly correlated atomization or dissociation energies, molecular geometries, as well as numerous other molecular properties. These methods work extremely well (3,6,7) for nondegenerate closed shell states and reasonably well for those open shell systems that afford a reasonable zero order description via a UHF (of DODS type) wave function, although some properties (e.g., harmonic frequencies) may be very sensitive to the eventual spin contamination [or rather to the rate of change of the spin contamination with the geometry (8)].

Unfortunately, the CCSD approach, and in particular CCSD(T), will poorly perform, or even completely break down, in quasidegenerate or degenerate situations. Thus, while CCSD(T) will provide excellent dissociation energies for a vast number of closed and open shell systems, it will invariably fail for intermediate geometries, resulting in inferior or even nonphysical potential energy curves (PECs) or surfaces (PESs), unless the dissociation products are closed shell species. Clearly, the latter is not the case when breaking the standard single or multiple chemical bonds. The reason for a poor performance of standard CCSD at highly stretched molecular geometries is the non-negligible role of higher than pair clusters, in particular of connected three and four body clusters, obviating the usefulness of the single reference coupled cluster Ansatz. The situation is even worse for CCSD(T) in view of the complete breakdown

of the perturbative account of triples at large internuclear separations.

An obvious remedy in such cases is to employ one form or another of a multireference (MR) CC Ansatz that is capable of handling the general open shell situations. Unfortunately, the actual implementation and exploitation of such a formalism proved to be both methodologically problematic and computationally demanding. Indeed, there is no general purpose software that could be routinely exploited in such situations, and even various *ad hoc* implementations are often plagued with intruder state and multiple solution problems. It is thus highly desirable to develop approximate methods that can handle such systems, while being manageable computationally. Such approximations usually focus on one state at a time, resulting in the so-called state selective or state specific (SS) MRCC methods.

One of the SS MRCC methods that was recently introduced and showed considerable promise in preliminary testing relies on the idea of *externally corrected CCSD* (9–17), which achieves a more physical truncation of the full CC chain of equations at the pair cluster level by exploiting three and four body cluster amplitudes obtained by the cluster analysis of some relatively easily accessible wave function that is capable of describing nondynamical correlation effects brought about by the MR character of the state involved. Exploiting for this purpose MR CISD wave function of modest dimension leads to the so-called *reduced multireference* (RMR) CCSD procedure (15–17). The RMR CCSD method (15) may be regarded as a *de facto* MR approach in the sense that the method is unambiguously defined by the choice of a reference space and that the RMR CCSD Ansatz involves the same number of connected cluster components as the proper state universal (SU) (or Hilbert space) MR CCSD Ansatz (18) relying on the same reference space. We can thus also interpret RMR CCSD as an approximation to SU CCSD (15,16).

Another approximate procedure – that may or may not rely on the external information concerning the computed cluster amplitudes (including one and two body ones) – exploits the idea of the so-called *split-amplitude strategy* (19). The basic idea here is to represent the connected cluster amplitudes as a sum of an *a priori* fixed approximate value of the amplitude and of a small correction to be determined from CC equations. Using this ‘split-amplitude’ Ansatz in CC equations produces an analogous set of algebraic equations for the correction terms. However, assuming that the approximation employed for the *a priori* fixed part is good, one can neglect the higher order terms. In fact, it turns out that even the linear or almost linear (AL) approximation (20) can produce a very good estimate of the true amplitudes (20), and thus of the energy.

The objective of this study is to explore the possibilities offered by the AL version of RMR CCSD, since in the RMR-type approaches one obtains the three and four body clusters from the corresponding MR CISD wave function,

so that one also generates the one and two body amplitudes as byproducts. Usually, these amplitudes represent already a very good approximation to the true ones. We thus expect that the AL version of RMR CCSD should perform almost as good as its full version. After outlining the basic tenets of the methods involved and of their possible combination in Sections 2 and 3, we illustrate the performance of various versions of the AL-RMR CCSD approach in Section 4 on several model systems involving four and eight hydrogen atoms, the water molecule and the F_2 molecule. The conclusions are then drawn in Section 5.

2 Externally Corrected CCSD

The basic idea of the externally corrected CCSD methods relies on the fact that the electronic Hamiltonian, defining standard *ab initio* models, involves at most two body terms, so that the correlation energy is fully determined by one (T_1) and two (T_2) body cluster amplitudes, while the subset of CC equations determining these amplitudes involves at most three (T_3) and four (T_4) body connected clusters. In order to decouple this subset of singly and doubly projected CC equations from the rest of the CC chain, one simply neglects all higher than pair cluster amplitudes by setting

$$T_3 = T_4 = 0, \quad (1)$$

thus obtaining the ubiquitous CCSD equations.

The CCSD approximation was extensively tested and is widely employed to handle correlation effects, since it provides excellent correlation energies as long as the assumption of Eq. (1) is valid, i.e., as long as the three and four body connected cluster amplitudes are negligible. This is usually the case when considering nondegenerate closed shell ground states. However, surprisingly enough, CCSD often provides rather good results even in highly quasidegenerate situations. In cases when only three body clusters are non-negligible, yet small enough so that their effect can be accounted for perturbatively, the CCSD(T) method (4) proved to provide a superior performance (6).

Unfortunately, when generating the full potential energy surfaces, the regions of highly stretched geometries – corresponding to the breakup of one or more chemical bonds – often represent highly quasidegenerate open shell situations, which generally require multireference description. Using a single reference cluster Ansatz in such cases leads then to appreciable contributions of higher than pair cluster components, in particular of T_3 and T_4 , reflecting the importance of nondynamical correlation effects.

One possible avenue to overcome this problem, without resorting to a genuine multireference formalism, is to obtain the information concerning the

T_3 and T_4 cluster components from some independent, yet easily accessible, wave function, which at least qualitatively describes the dissociation channel at hand. The first attempts in this direction relied on the UHF wave function (of the DODS type), leading to the so-called ACPQ method (approximate coupled pair method with quadruples) (9), and its recent explicit version referred to as the CC(S)DQ' method (14). Unfortunately, for closed shell systems, the DODS-type wave function cannot provide any information about the T_3 clusters.

Recently, both valence bond (VB) and complete active space (CAS) SCF and CAS FCI wave functions were employed as a source of T_3 and T_4 cluster amplitudes (11,13) (see also Ref. 12). The most satisfactory approach, however, that was developed very recently, relies on the MR CISD wave function, based on a relatively small model space. This approach is referred to as the reduced MR (RMR) CCSD method (15–17).

The essence of the RMR CCSD approach is to select a suitable (usually incomplete) active or model space involving configurations that are essential for a proper account of nondynamical correlation effects, and to generate the corresponding MR CISD wave function $|\Psi^{\text{MR-CISD}}\rangle$. In order to make the method efficient, the dimension of the active space, and thus of the SD excited space, should be kept as small as possible. This is achieved by keeping the number of active orbitals as small as possible. Choosing then the leading configuration $|\Phi_0\rangle$ as a reference, one carries out the cluster analysis of the MR CISD wave function, obtaining

$$|\Psi^{\text{MR-CISD}}\rangle = \exp(T_1^{(0)} + T_2^{(0)} + T_3^{(0)} + T_4^{(0)} + \dots)|\Phi_0\rangle. \quad (2)$$

Using now $T_3^{(0)}$ and $T_4^{(0)}$ clusters in the SD projected CC equations,

$$\langle\Phi_i^{(1)}|H(1 + T_1 + T_2 + \frac{1}{2}T_1^2 + T_1T_2 + \frac{1}{6}T_1^3 + T_3^{(0)})|\Phi_0\rangle_C = 0, \quad (3a)$$

$$\begin{aligned} \langle\Phi_i^{(2)}|H(1 + T_1 + T_2 + \frac{1}{2}T_1^2 + T_1T_2 + \frac{1}{2}T_2^2 + \frac{1}{6}T_1^3 + \frac{1}{2}T_1^2T_2 + \frac{1}{24}T_1^4 \\ + T_3^{(0)} + T_4^{(0)} + T_1T_3^{(0)})|\Phi_0\rangle = 0, \end{aligned} \quad (3b)$$

rather than setting them equal to zero as in the standard CCSD [cf. Eq. (1)], we obtain CCSD-like equations for T_1 and T_2 amplitudes $\{t_i\}$,

$$a_i + b_{ij}t_j + c_{ijk}t_jt_k + \dots = 0, \quad (4)$$

where the summation over repeated indices is implied.

Clearly, the $T_3^{(0)}$ and $T_4^{(0)}$ terms contribute to the absolute terms a_i , while the $T_1T_3^{(0)}$ cross term modifies the linear b_{ij} coefficients involving monoexcited

t_i clusters. Thus, in principle, this term has to be evaluated in each iteration using the current values of t_i clusters. In such a case we speak of an iterative account of $T_1 T_3^{(0)}$ correction (13). However, it can be shown (13) that replacing the term $T_1 T_3^{(0)}$ by $T_1^{(0)} T_3^{(0)}$ represents an excellent approximation, usually changing the correlation energy by only a few microhartree. Since $T_1^{(0)}$ clusters are available to us as a byproduct of the cluster analysis of $|\Psi^{\text{MR-CISD}}\rangle$, this noniterative account of $T_1 T_3^{(0)}$ correction (13) is to be preferred. Even when one insists on using the iterative account, it is advantageous to correct the absolute term using $T_1^{(0)} T_3^{(0)}$, and consider explicitly only the correcting monoexcited cluster amplitudes $(t_i - t_i^{(0)}) = \tau_i$. In fact, such an approach corresponds precisely to the spirit of the split amplitude methodology.

The RMR CCSD procedure (15) has been tested on several systems involving dissociation of single, double or even triple bonds, as well as simultaneous breaking of two single bonds (15–17). In all cases very satisfactory results were obtained. Even in the case of triple bond breaking (in systems like N_2 or CN), RMR CCSD enables us to extend the validity of a CCSD-like description to highly stretched geometries, while using incomplete, rather small active spaces. Of course, the larger the active space and, correspondingly, the more precise the MR CI wave function that is used to generate $T_3^{(0)}$ and $T_4^{(0)}$ cluster components, the better the RMR CCSD result. Clearly, when full CI (FCI) T_3 and T_4 clusters are employed, externally corrected CCSD returns the exact FCI result.

3 Almost-Linear (AL) CC Methods

As we have already mentioned, all CC methods of practical interest are based on approximations imposed on the form of the cluster operators, which are very often followed by omitting some terms in CC equations. These two types of approximations have been referred to in the literature as *standard approximations* (21). The impact of any approximation procedure on the accuracy of the resulting CC method (assessed through the comparison with the FCI or, equivalently, FCC results) strongly depends on the structure of the cluster amplitudes for the state considered: If all the amplitudes have a small magnitude, these approximation schemes have little effect on the accuracy. If, however, some of the cluster amplitudes are relatively large, as is the case, e.g., for the T_3 and T_4 amplitudes when nondynamical correlation effects are significant, as mentioned in Section 2, the accuracy may deteriorate. This is due to the fact that the adopted approximation procedure discards some important terms in the original equations. This may be avoided if in the original equations we first replace those unknowns that are expected to be large by the unknowns that will take on smaller values, and only then impose the desired approximation(s).

A convenient formal framework for the discussion of various aspects of such an approach to the approximation process within the CC methodology was recently formulated as the so-called split-amplitude strategy (19), in which one represents the individual amplitudes in the form

$$t_i = t_i^{(0)} + \tau_i. \quad (5)$$

Here $t_i^{(0)}$ is an *a priori* known approximate value of t_i that is obtained from some independent source, while a small correcting term τ_i is subsequently obtained from the *modified CC equations*. Details concerning the form of these equations, as well as possible sources of $t_i^{(0)}$ -amplitudes, may be found in Ref. 19. Let us only mention that the split-amplitude strategy is primarily beneficial in those cases when the set of larger t_i -amplitudes represents a small subset of the entire set of cluster amplitudes, i.e., in cases when the effective splitting ($t_i^{(0)} \neq 0$) applies to only a small number of amplitudes. In addition of being helpful in designing new approximate CC schemes, the split-amplitude strategy has also been exploited in various algorithms that are used when solving CC equations, particularly when one employs iterative procedures based on a special choice of the starting approximation.

Inserting the split amplitudes, Eq. (5), into the FCC equations, we obtain modified CC equations for the τ_i -amplitudes that have the same structure as the standard CC equations, i.e.,

$$\tilde{a}_i + \tilde{b}_{ij}\tau_j + \tilde{c}_{ijk}\tau_j\tau_k + \cdots = 0, \quad (6)$$

where now

$$\tilde{a}_i = a_i + b_{ij}t_j^{(0)} + c_{ijk}t_j^{(0)}t_k^{(0)} + \cdots, \quad (7a)$$

$$\tilde{b}_{ij} = b_{ij} + 2c_{ijk}t_k^{(0)} + \cdots, \quad \text{etc.} \quad (7b)$$

Since the linear version of the standard CC methods, designated as L-CC, often provides an excellent approximation, this will likely be the case – to a much higher degree of accuracy – for the transformed system, Eq. (6), in view of the smallness of the correction terms τ_j . The approaches based on the linear equations

$$\tilde{a}_i + \tilde{b}_{ij}\tau_j = 0 \quad (8)$$

are referred to as ‘almost linear CC’ (AL-CC) methods. Notice that when setting the $t_j^{(0)}$ -amplitudes to zero, the AL-CC method reduces to the standard L-CC one. Moreover, the AL-CC equations can be viewed as the first Newton-Raphson iteration to the standard CC equations.

Various AL-CC approaches have been tested on a number of systems, including models that enable a continuous change in quasidegeneracy. For example, the so-called H8 model (20) was examined at the CCD, CCSD, CCSDT and even CCSDTQ levels, using $t_j^{(0)}$ -amplitudes resulting from the MP2, CID and various MR CISD wave functions. Moreover, the schemes in which only a subset of the latter amplitudes was employed, depending on the chosen cutoff, were also explored. A similar study was carried out for DZ or DZP models of H₂O, BH and HF at various geometries. These test calculations showed that the AL-CC approximation invariably provides the energy values that are very close to those given by the full solution of the corresponding nonlinear CC system. Needless to say that the singular behavior of the standard L-CC approaches, which is encountered in quasidegenerate situations, is avoided by the AL-CC ones.

In view of these results it is of interest to explore the performance of the AL version of the RMR CCSD method. Since the latter requires the solution of CCSD-like equations, one can expect a similar performance and savings as in the standard CCSD case. Moreover, in generating the $T_3^{(0)}$ and $T_4^{(0)}$ amplitudes, one obtains the $T_1^{(0)}$ and $T_2^{(0)}$ amplitudes as a byproduct. These can then be exploited using the split-amplitude strategy in obtaining AL-RMR CCSD.

Implementing this idea for RMR CCSD, we split the one- and two-body cluster amplitudes, employ the MR CISD method to calculate the one- and two-body $t_j^{(0)}$ -amplitudes, evaluate the coefficients \tilde{a}_i and \tilde{b}_{ij} , Eqs. (7a) and (7b), and finally, solve the resulting linear system, Eq. (8). Thus the absolute terms \tilde{a}_i involve the corrections for all the terms involving T_3 and T_4 cluster operators as well as for all nonlinear terms in T_1 and T_2 , all evaluated using $T_i^{(0)}$ MR CISD amplitudes, while the linear \tilde{b}_{ij} terms involve only corrections originating from the nonlinear CCSD terms. We shall refer to this version of the AL-RMR CCSD method as AL-RMR-CCSD-1.

Following the AL-CC approaches studied by Jankowski *et al.* (20), the T_1 and T_2 clusters are treated differently. Namely, only the T_2 amplitudes are effectively splitted, i.e., only two-body $t_j^{(0)}$ -amplitudes can take nonzero values. Except for this difference, one then proceeds in the same way as above, computing first the \tilde{a}_i and \tilde{b}_{ij} coefficients and then solving the linear system, Eq. (8). This method is referred to as AL-RMR-CCSD-2. When the amplitude splitting is carried out only for cluster amplitudes that are larger than a prescribed threshold, the approach is labeled by indicating the cut-off employed. We thus designate AL-RMR-CCSD-2 with a cut-off as AL-RMR-CCSD-2(η), with η being the threshold. Of course, AL-RMR-CCSD-2(0) \equiv AL-RMR-CCSD-2. In this paper only two cut-off values, namely $\eta = 0.02$ and 0.1, are considered.

To sum up, we examine here essentially three types of AL-CC approximation schemes. First, the AL-RMR-CCSD-1 approach representing a direct approximation of RMR CCSD in which the nonlinear terms in τ_j are neglected. Second, the AL-RMR-CCSD-2(η) methods, in which an additional approximation that ignores the nonlinear terms in T_1 is invoked. Finally, we examine the standard AL-CCSD approach that employs the same MR CISD $T_1^{(0)}$ and $T_2^{(0)}$ clusters as does AL-RMR CCSD. This last method can thus be regarded either as an approximation to the standard CCSD method or as an approximation to AL-RMR-CCSD-2 in which $T_3^{(0)}$ and $T_4^{(0)}$ corrections are ignored.

4 Results and Discussion

The above outlined almost-linear (AL) versions of the RMR CCSD method have been applied to several model systems involving four and eight hydrogen atoms, as well as to a double zeta (DZ) model of the water molecule at both the equilibrium and stretched geometries.

4.1 The H4 Model

We first examine the H4 model at a DZP level. This widely studied simple system (22–30), introduced by two of the co-authors (22), involves two slightly stretched hydrogen molecules in a trapezoidal conformation. Changing the \angle HHH angle ϕ from $\pi/2$ to π , one proceeds from the highly quasidegenerate square geometry ($\phi = \pi/2$) to the nondegenerate linear one ($\phi = \pi$), while keeping all nearest neighbor internuclear separations at 2 a.u. The geometry is thus fully specified by a single parameter α , $\alpha = \phi/\pi - 1/2$ (in radian). The attractiveness of this simple model is that it enables one to vary continuously the quasidegeneracy from the fully degenerate limit ($\alpha = 0$) to the nondegenerate one ($\alpha = \frac{1}{2}$).

The correlation energies for a series of geometries obtained with various AL-CCSD methods are compared with the standard CCSD and L-CCSD results, as well as with the (2,2)-RMR CCSD and the exact FCI values in Table 1. Here and in the following the symbol (2,2) designates a 2-electron/2-orbital reference space. Five AL-CCSD versions are considered: AL-CCSD relying on the (2,2)-MR CISD amplitudes, AL-RMR-CCSD-1, and AL-RMR-CCSD-2 with thresholds 0.0, 0.02 and 0.1. In all cases a (2,2) reference space is used. The well known CCSD and L-CCSD results (22) are included for the sake of comparison. We recall the singular behavior of the latter approach in the highly quasidegenerate regime and a rather satisfactory performance in the nondegenerate region of geometries.

We first note a very good performance of the RMR CCSD method, which

differs from FCI by less than a millihartree (mhartree) in the entire range of geometries. Indeed, the error in the correlation energy steadily decreases from 0.762 mhartree in the degenerate ($\alpha = 0$) limit to 0.229 mhartree in the nondegenerate ($\alpha = 0.5$) limit. This is a significant improvement over the standard CCSD, which differs significantly from the exact result in the degenerate limit (by 5.508 mhartree). The AL-CCSD method, which must be regarded as an approximation to CCSD, since in contrast to AL-RMR-CCSD-2 it does not correct for the $T_3^{(0)}$ and $T_4^{(0)}$ clusters, gives indeed the energies that

Table 1
Comparison of correlation energies (all signs reversed) for the ground state of the H4 DZP model (in mhartree), using a (2,2) model space. The AL-RMR-CCSD-*i* methods are simply designated as AL-RMR-*i*.

Method	α				
	0.0	0.01	0.05	0.1	0.15
FCI	131.362	117.956	98.646	91.006	87.121
L-CCSD	65.855	34.785	112.392	96.713	91.436
CCSD	125.854	114.354	97.384	90.095	86.310
AL-CCSD ^{a)}	126.097	114.403	97.370	90.085	86.301
RMR CCSD	130.600	117.300	98.240	90.700	86.854
AL-RMR-1	130.599	117.299	98.241	90.700	86.854
AL-RMR-2 (0)	130.525	117.252	98.225	90.689	86.845
(0.02) ^{b)}	130.582 ₁₉	117.353 ₂₃	98.465 ₂₀	90.869 ₂₃	87.030 ₂₂
(0.1) ^{b)}	130.829 ₇	117.523 ₇	98.719 ₇	92.727 ₁	88.639 ₁

	α			
	0.2	0.3	0.4	0.5
FCI	84.953	83.042	82.460	82.332
L-CCSD	88.760	86.509	85.844	85.702
CCSD	84.183	82.294	81.710	81.580
AL-CCSD ^{a)}	84.173	82.280	81.693	81.562
RMR CCSD	84.703	82.808	82.230	82.103
AL-RMR-1	84.704	82.808	82.230	82.103
AL-RMR-2 (0)	84.694	82.795	82.214	82.087
(0.02) ^{b)}	84.903 ₂₁	83.117 ₁₀	82.516 ₁₀	83.391 ₁₃
(0.1) ^{b)}	86.300 ₁	84.195 ₁	83.537 ₁	83.395 ₁

^{a)} $t_j^{(0)}$ -amplitudes from (2,2)-MR CISD.
^{b)} The subscripts indicate the number of nonzero $t_j^{(0)}$ -amplitudes.

are close to the CCSD ones, particularly in the nondegenerate region. Even more remarkably, the AL-RMR-CCSD-1 energies hardly differ from the full RMR CCSD ones, the differences being at the microhartree ($\mu\text{hartree}$) level. Likewise, the AL-RMR-CCSD-2 energies are very close to the RMR CCSD ones (the differences systematically decrease from 75 $\mu\text{hartree}$ to 16 $\mu\text{hartree}$). Naturally, larger discrepancies arise when only a truncated set of pair cluster amplitudes is employed.

The small differences between the standard CCSD and AL-CCSD, and between the full RMR CCSD and AL-RMR-CCSD indicate that the $T_1^{(0)}$ and $T_2^{(0)}$ amplitudes obtained from the (2,2)-MR CISD are very close to the final T_1 and T_2 amplitudes. Thus, a considerable saving in the computational effort can be achieved by using the “almost linear” strategy, with only a little loss in the accuracy.

The reduction in the computational effort is most pronounced when only a small subset of possible $t_j^{(0)}$ -amplitudes is employed. We consider two thresholds for the $t_j^{(0)}$ -amplitudes, *viz.*, 0.02 and 0.1, which means that only the amplitudes that are greater than 0.02 and 0.1, respectively, are taken into account. When applying these criteria to excitations producing multideterminantal configuration state functions, all the amplitudes associated with the excitations from the reference to these determinants are accounted for. The subscript at the energies presented in Tables 1–5 indicates the number of nonzero $t_j^{(0)}$ -amplitudes, e.g., in Table 1 for the H4 DZP model, we use 1 or 7 $t_j^{(0)}$ -amplitudes (threshold 0.1) instead of 540 amplitudes. As one can see in these tables, the AL-RMR-CCSD-2 results obtained with the reduced set of $t_j^{(0)}$ -amplitudes are still satisfactory despite a significant reduction in the computational effort. A very similar behavior is found for other systems considered in this paper.

Thus, on the whole, we observe that the simplifications arising from the AL-RMR CCSD versions afford significant savings in the computational effort, while causing only a relatively minor change in the RMR CCSD energies which, themselves, provide an excellent approximation to FCI.

4.2 The H8 Model

In order to render the original H4 model to represent more closely realistic systems involving a large number of quadruply excited cluster amplitudes, Jankowski *et al.* (31) introduced two ‘spectator’ H_2 molecules into the H4 [or rather P4 (22)] model. Thus, the H8 model involves four slightly stretched (2 a.u.) H_2 molecules, initially arranged in a regular octagonal configuration ($\alpha = 0$). The two opposing H_2 molecules then undergo a parallel shift (cf. Ref. 31) of magnitude α (in a.u.).

The results for this model considered at the minimum basis set (MBS) and double zeta (DZ) levels are given in Tables 2 and 3, respectively. In both cases, the (2,2) model space is used in multireference calculations. Again, both AL-RMR-CCSD-1 and AL-RMR-CCSD-2 represent a good approximation to the full RMR CCSD (both differing by only a few μ hartree at the MBS level and by 10–60 μ hartree at the DZ level). In turn, RMR CCSD represents a significant improvement over the standard CCSD (by more than 7 mhartree for $\alpha = 0$ for a DZ model).

Again, the closeness of the standard CCSD and AL-CCSD results, as well as RMR CCSD and AL-RMR CCSD ones, indicates the high quality of the $T_1^{(0)}$ and $T_2^{(0)}$ amplitudes that are extracted from the (2,2)-MR CISD wave function.

4.3 The S4 Model

The most demanding of the H_4 planar models is undoubtedly the S4 model (32), in which the H atoms are kept at all times in the square configuration, while the H—H separation α is continuously varied from the compressed geometry ($\alpha = 1$ a.u.) to a complete dissociation (in our case approximated by $\alpha = 6$ a.u.). In this way, we simulate a simultaneous breaking of four single bonds. Moreover, at all times we deal with the square geometry characterized by the degenerate ground state.

Table 2

Comparison of correlation energies (all signs reversed) for the ground state of the H8 MBS model (in mhartree). The multireference methods use a (2,2) model space. The acronym AL-RMR-CCSD-*i* is abbreviated to AL-RMR-*i*.

Method	α				
	0.0001	0.001	0.01	0.1	1.0
FCI	139.240	139.058	137.294	125.018	110.145
L-CCSD	90.275	90.011	88.292	−2.145	114.127
CCSD	134.206	134.057	132.625	122.904	109.599
AL-CCSD ^{a)}	134.366	134.212	132.737	122.876	109.609
RMR CCSD	138.380	138.200	136.455	124.418	109.795
AL-RMR-1	138.369	138.190	136.447	124.420	109.807
AL-RMR-2 (0)	138.361	138.181	136.439	124.414	109.806
(0.02) ^{b)}	138.327 ₅₇	138.146 ₅₇	136.386 ₅₇	124.421 ₇₈	109.811 ₇₆
(0.1) ^{b)}	138.363 ₁₃	138.183 ₁₃	136.445 ₁₃	124.525 ₁₃	114.345 ₀

^{a)} $t_j^{(0)}$ —amplitudes from (2,2)-MR CISD.

^{b)} The subscripts indicate the number of nonzero $t_j^{(0)}$ —amplitudes.

Two sets of results are presented in Table 4, employing two different model spaces for the RMR CCSD: One involves two electrons in two active orbitals, and the other one four electrons in four active orbitals. In each case we employ a DZP basis set and label these models as S4DZP (2,2) and (4,4), respectively. We note a complete breakdown of L-CCSD and a rather poor performance of CCSD [in fact, it is interesting to point out that the two-reference state universal CCSD also breaks down in this case (32), although good results can be obtained with the 2-reference version of the ACPQ method (33)].

Again, already the performance of (2,2)-RMR CCSD is remarkable in view of the complete breakdown of the standard 2-reference SU CCSD (32) just mentioned, the difference from FCI being almost constant (0.6 – 0.8 mhartree).

Table 3

Comparison of correlation energies (all signs reversed) for the ground state of the H8 DZ model (in mhartree). The multireference methods use a (2,2) model space. The acronym AL-RMR-CCSD-*i* is abbreviated to AL-RMR-*i*.

Method	α					
	0.0	0.0001	0.001	0.003	0.006	0.01
FCI	161.060	161.041	160.870	160.501	159.947	159.207
L-CCSD	124.025	124.012	123.893	123.624	123.206	122.621
CCSD	152.307	152.295	152.191	151.959	151.620	151.180
AL-CCSD ^{a)}	152.575	152.562	152.447	152.195	151.827	151.352
RMR CCSD	159.595	159.576	159.407	159.034	158.485	157.772
AL-RMR-1	159.587	159.568	159.399	159.027	158.479	157.768
AL-RMR-2(0)	159.527	159.508	159.340	158.968	158.422	157.712
(0.02) ^{b)}	159.630 ₇₇	159.611 ₇₇	159.441 ₇₇	159.068 ₇₇	158.491 ₇₁	157.778 ₇₁
(0.1) ^{b)}	159.672 ₁₃	159.653 ₁₃	159.486 ₁₃	159.119 ₁₃	158.578 ₁₃	157.876 ₁₃

	α				
	0.03	0.06	0.1	0.5	1.0
FCI	155.893	151.835	147.820	135.530	132.489
L-CCSD	119.100	110.660	79.523	142.544	137.424
CCSD	149.183	146.714	144.152	134.360	131.689
AL-CCSD ^{a)}	149.230	146.683	144.104	134.363	132.698
RMR CCSD	154.534	150.604	146.738	134.856	131.970
AL-RMR-1	154.537	150.613	146.752	134.874	131.992
AL-RMR-2(0)	154.489	150.574	146.722	134.864	131.982
(0.02) ^{b)}	154.638 ₈₅	150.775 ₈₇	146.956 ₇₆	135.103 ₈₀	132.241 ₇₆
(0.1) ^{b)}	154.699 ₁₃	150.924 ₁₃	147.380 ₁₃	140.661 ₁	143.131 ₀

^{a)} $t_j^{(0)}$ —amplitudes from (2,2)-MR CISD.

^{b)} The subscripts indicate the number of nonzero $t_j^{(0)}$ —amplitudes.

Table 4

Comparison of correlation energies (all signs reversed) for the ground state of the S4DZP model (in mhartree). Multireference approaches use (2,2) and (4,4) model spaces. The AL-RMR-CCSD-*i* methods are simply designated as AL-RMR-*i*.

Method	α							
	1.0	2.0	3.0	3.5	4.0	4.5	5.0	6.0
FCI	101.808	131.362	179.203	212.571	250.467	290.326	329.046	394.353
L-CCSD	57.718	65.855	164.056	295.049	536.341	989.607	1931.96	22874.7
CCSD	91.305	125.854	184.389	222.532	262.845	302.310	338.821	399.080
(2,2) model space								
AL-CCSD ^{a)}	92.495	126.097	183.779	220.741	258.984	297.089	334.010	396.668
RMR CCSD	101.044	130.600	178.425	211.998	249.815	289.644	328.419	393.554
AL-RMR-1	101.043	130.599	178.617	211.981	249.791	289.614	328.384	394.564
AL-RMR-2 (0)	101.030	130.525	178.449	211.791	249.594	289.401	328.144	392.721
(0.02) ^{b)}	101.143 ₃₀	130.852 ₁₉	178.399 ₁₈	211.734 ₂₄	249.531 ₂₄	289.343 ₂₄	328.089 ₂₄	392.682 ₂₄
(0.1) ^{b)}	102.869 ₁	130.829 ₇	178.398 ₈	211.668 ₈	249.445 ₈	289.268 ₈	328.038 ₈	392.729 ₈
(4,4) model space								
AL-CCSD ^{a)}	92.550	126.183	183.897	221.025	259.602	298.074	332.279	399.142
RMR CCSD	101.346	131.208	179.179	212.564	250.468	290.328	329.049	394.345
AL-RMR-1	101.346	131.208	179.179	212.564	250.468	290.328	329.049	394.345
AL-RMR-2 (0)	101.333	131.133	178.986	212.312	250.163	289.974	328.654	393.885
(0.02) ^{b)}	101.453 ₃₀	131.213 ₂₀	179.008 ₁₈	212.324 ₂₄	250.173 ₂₄	289.982 ₂₄	328.661 ₂₄	393.890 ₂₄
(0.1) ^{b)}	101.542 ₃	131.505 ₇	179.073 ₈	212.380 ₈	250.226 ₈	290.036 ₈	328.717 ₈	393.914 ₈

^{a)} $t_j^{(0)}$ —amplitudes from the corresponding MR CISD.

^{b)} The subscripts indicate the number of nonzero $t_j^{(0)}$ —amplitudes.

Consequently, the RMR CCSD potential is almost parallel to the FCI potential. The so-called non-parallelism error (NPE) (34), defined as the difference between the maximal and minimal deviations from the exact FCI potential, is only about 0.23 mhartree (see also Section 5). Although the absolute differences between the RMR CCSD and FCI energies are further decreased when enlarging the (2,2) model space to (4,4), (particularly for $\alpha \geq 3$ a.u.), this is not the case for the NPE. In all cases, however, we are within a 2 mhartree error, even for this very demanding model.

It is interesting to compare the RMR CCSD and AL-RMR CCSD results obtained with two different model spaces, namely (2,2) and (4,4) ones. For example, when using the (2,2) model space, the difference between the RMR CCSD and AL-RMR CCSD energies is very small, often less than 50 μ hartree. Nonetheless, the largest difference, amounting to 1 mhartree, is found for $\alpha = 6.0$ a.u. This indicates that in some cases, the $T_1^{(0)}$ and $T_2^{(0)}$ amplitudes from (2,2)-MR CISD are not very close to the final T_1 and T_2 , and the AL version may cause some errors. When the large (4,4) model space is used, the difference between RMR CCSD and AL-RMR CCSD in fact disappears. This is easily understood since the S4 model is a four-electron system and the $T_1^{(0)}$ and $T_2^{(0)}$ from (4,4)-MR CISD should be very close to the real T_1 and T_2 .

4.4 A DZ Model of H₂O

This often used benchmark model is represented by the symmetrically stretched H₂O molecule at the DZ level, for which the exact FCI results are available (35). In addition to the standard L-CCSD and CCSD correlation energies, we present the results obtained with RMR CCSD and four of its AL versions (Table 5). Similarly as for the S4 model, we employ two different reference spaces: the minimal (2,2) space, involving HOMO and LUMO, and the (4,4) space involving four electrons in four orbitals (2 occupied and 2 virtual ones). For an easier comparison, we also present the corresponding differences from the FCI result in parentheses.

We see again that a ‘better’ performance of L-CCSD than CCSD at the equilibrium geometry arises due to the fact that L-CCSD overestimates CCSD energies (cf., e.g., Ref. 36). This is clearly seen for distorted geometries, where this overestimate becomes extremely large in view of the increasing quasidegeneracy. In fact, the same holds for CCSD that again yields very respectable results, even far away from the equilibrium geometry. Nonetheless, this result is greatly improved when we account for the T_3 and T_4 clusters via RMR CCSD, particularly when using the (4,4) model space. Again, however, at $R = 2R_e$, we already see a slight tendency to overestimate the computed correlation energy, so that the trend for the differences between the FCI and RMR CCSD energies to increase is reversed.

Concerning AL approximations to RMR CCSD, we see that the best result is obtained with the AL-RMR-CCSD-1 version, although for $R = R_e$ or $1.5R_e$, it is hardly distinguishable from the AL-RMR-CCSD-2 result with zero cut-off. We see that the increase in the cut-off threshold seems to ‘improve’ the result for $R = R_e$. However, it is not difficult to realize that this is again the result of an overestimate, as becomes apparent at larger distortions.

On the whole, both AL versions of RMR CCSD give results that are reasonably close to the proper RMR CCSD ones, thus representing viable approximations, even though their performance deteriorates as the bonds are stretched and the quasidegeneracy sets in. In general, any AL version of RMR CCSD is closer to the full RMR CCSD when a larger model space is employed.

5 Conclusions

In this article we discuss the combined reduced multireference CCSD and

Table 5

Comparison of correlation energies (all signs reversed) for a double zeta model of the ground state of the H_2O molecule (in mhartree). The differences from FCI are enclosed in parentheses. The AL-RMR-CCSD- i methods are simply designated as AL-RMR- i .

Method	$1R_e$	$1.5R_e$	$2R_e$
L-CCSD	146.719 (1.309)	218.284 (−7.291)	353.922 (−43.855)
CCSD	146.238 (1.790)	205.402 (5.591)	300.735 (9.332)
(2,2) model space			
RMR CCSD	146.487 (1.541)	207.949 (3.044)	308.143 (1.924)
AL-RMR-1	146.487 (1.541)	207.988 (3.005)	309.641 (0.426)
AL-RMR-2(0)	146.502 (1.526)	208.135 (2.858)	312.702 (−2.635)
(0.02) ^a	146.880 ₅₀ (1.148)	208.721 ₆₁ (2.272)	316.713 ₆₀ (−6.646)
(0.1) ^a	146.867 ₀ (1.161)	213.775 ₂ (−2.787)	335.174 ₉ (−25.107)
(4,4) model space			
RMR CCSD	147.001 (1.027)	209.656 (1.337)	308.357 (1.710)
AL-RMR-1	147.000 (1.028)	209.665 (1.328)	308.356 (1.711)
AL-RMR-2(0)	147.013 (1.015)	209.784 (1.209)	312.078 (−2.011)
(0.02) ^a	147.341 ₅₂ (0.687)	210.276 ₆₁ (0.717)	313.597 ₆₀ (−3.530)
(0.1) ^a	147.380 ₀ (0.648)	211.570 ₈ (−0.577)	320.203 ₁₀ (−10.136)
FCI	148.028 (0)	210.993 (0)	310.067 (0)

^a) The subscripts indicate the number of nonzero $t_j^{(0)}$ -amplitudes.

almost-linear CC approaches relying on the split-amplitude strategy. There are many similarities between the externally corrected CCSD and the split amplitude strategy (19), the latter stemming from an earlier study of the VB corrected CCSD (11).

As already pointed out in Ref. 13, the externally corrected CCSD is equivalent to (truncated) CCSDTQ with zero-iteration on T_3 and T_4 amplitudes that are in turn obtained from some external sources. Depending on the source of these amplitudes, we usually deal with only a proper subset of all possible T_3 and T_4 amplitudes. This subset is fixed in the externally corrected CCSD calculations. The RMR CCSD is then a special case of the general externally corrected CCSD in which the MR CISD wave function is used as the external source. The RMR CCSD method represents in fact a multireference approach in the sense that it is uniquely defined by the choice of the reference space and the fact that the RMR CCSD wave function involves the same number of connected cluster amplitudes as the corresponding genuine MR CCSD, such as the state-universal CCSD employing the same reference space.

The split-amplitude strategy represents the total amplitudes as the sum of an *a priori* known approximate value, obtained from some external source, and an unknown correcting term. Assuming, further, that the known amplitudes represent a good approximation to the true ones, the unknown corrections can be obtained to a high degree of accuracy from a set of linear equations. The results of this article show that when a proper reference space is used, the connected clusters obtained from the MR CISD wave function represent indeed a very good approximation, and the almost linear versions of the RMR CCSD method performs very well.

As an overall measure of the quality of the shape of the computed potentials, two of the co-authors introduced the above mentioned non-parallelism error (NPE) (34), which is defined as the difference between the maximal and minimal deviations from the exact FCI potential. Clearly, $NPE=0$ when the computed potential differs from the FCI one by a constant shift. The NPE's of the computed potentials, given in Tables 1–5, are summarized in Table 6. We see that the CCSD and AL-CCSD NPE's, as well as the RMR CCSD and AL-RMR CCSD ones, are very similar, implying a similar quality of the resulting potentials. The RMR CCSD or AL-RMR CCSD NPE's are usually one order of magnitude smaller than the CCSD or AL-CCSD ones. For the H4 and H8 models, which are essentially two-reference cases, we indeed obtain similar results with either RMR CCSD or AL-RMR CCSD when using the (2,2) reference space. In the case of the S4 model and of the symmetric stretching of H_2O , the AL-RMR CCSD potentials are slightly inferior to those obtained with RMR CCSD. However, the quality of the AL-RMR CCSD potentials improves when we employ a (4,4) reference space.

Note that the present study also suggests a more economical computa-

tional approach to solving the full RMR CCSD equations (or in fact of any nonlinear CC equations) by repeatedly using the AL strategy, namely by alternately calculating the coefficients \tilde{a}_i and \tilde{b}_{ij} , Eqs. (7a) and (7b), and solving the linear equations, Eq. (8). In other words, starting from $T_1^{(0)}$ and $T_2^{(0)}$ amplitudes as obtained from the MR CISD wave function, one calculates \tilde{a}_i and \tilde{b}_{ij} , and solves the linear equations, Eq. (8). The resulting one- and two-body amplitudes are then used to recalculate \tilde{a}_i and \tilde{b}_{ij} , and new linear equations are solved. Clearly, once \tilde{a}_i vanish, the cluster amplitudes will satisfy the full RMR CCSD equations. In this way, we only solve linear equations at each stage, while the calculation of \tilde{a}_i and \tilde{b}_{ij} represents one iteration of the full RMR CCSD equations. The AL-RMR-CCSD-1 approach clearly represents a one-time application of such a strategy. The fact that the AL-RMR CCSD results are very close to the RMR CCSD ones then implies that only a few repetitions of the AL strategy will give us the full RMR CCSD solution.

As the final remark, let us emphasize that the AL approaches can be applied to much larger systems with many more electrons or can use more extensive basis sets. To illustrate this point, we present in Table 7 the potential for the ground state of the F_2 molecule using a 6-31G(d) basis set. In spite of dealing with a larger number of electrons, we can adequately describe the breaking of the F—F single bond using a (2,2) active space (or, in fact, a two-reference active space). Comparing the total energies, as well as the energy difference $E(3R_e) - E(R_e)$ (providing an estimate of the dissociation energy), we find that the RMR CCSD potential is very close to the highly accurate potential obtained with a large scale SR CISDTQ method. Moreover, the AL-RMR-CCSD-1 potential hardly differs from the RMR CCSD one. Both potentials are superior to that obtained with SR CCSD. We can thus conclude that with a suitable choice of the reference space we can safely employ

Table 6

Non-parallelism error (NPE, in mhartree) of resulting potentials for systems given in Tables 1–5.

System/Basis	Model Space	CCSD	AL-CCSD	RMR CCSD	AL-RMR CCSD-1	AL-RMR CCSD-2
H4/DZP	(2,2)	4.760	4.503	0.533	0.534	0.592
H8/MBS	(2,2)	4.488	4.338	0.310	0.533	0.540
H8/DZ	(2,2)	7.953	7.694	0.948	0.977	1.026
S4/DZP	(2,2)	22.881	17.830	0.226	0.976	0.878
	(4,4)	22.881	18.393	0.465	0.465	0.258
H ₂ O/DZ	(2,2)	7.542		1.503	2.579	5.493
	(4,4)	7.542		0.683	0.683	3.220

the AL approximation and obtain results of the same quality at a considerably reduced cost.

Table 7

Comparison of total energies (in a.u.) for the ground state of the F_2 molecule, obtained with a 6-31G(d) basis set. All multireference approaches use the same (2,2) model space. The total energies are reported as $-(E + 198)$, and $\Delta E = E(3R_e) - E(R_e)$.

Method	$1R_e$	$1.5R_e$	$2R_e$	$3R_e$	ΔE
SR CCSD	1.041576	0.975471	0.954995	0.951949	0.089627
RMR CCSD	1.048464	1.004269	0.993703	0.992708	0.055756
AL-RMR-CCSD-1	1.048474	1.004270	0.993698	0.992700	0.055774
SR CISDTQ	1.050969	1.004182	0.992775	0.991642	0.059327

6 Acknowledgments

The authors very much appreciate the invitation to contribute to this volume. The continued support by the Committee for Scientific Research (KBN) through the grants No. 3T09A 002 14 (I.G.) and 3T09A 025 13 (K.J.), and by the Natural Sciences and Engineering Research Council (NSERC) of Canada (J.P.) are hereby acknowledged. One of the senior authors (J.P.) also wishes to gratefully acknowledge an Alexander von Humboldt Research Award as well as the hospitality of Professor G. H. F. Dierksen and the Max Planck Institute for Astrophysics in Garching during his visit.

References

- (1) J. Čížek, J. Chem. Phys. **45**, 4256 (1966); Adv. Chem. Phys. **14**, 35 (1969).
- (2) J. Paldus, J. Čížek and I. Shavitt, Phys. Rev. A **5**, 50 (1972).
- (3) J. Paldus and X. Li, Adv. Chem. Phys. (in press).
- (4) K. Raghavachari, G. W. Trucks, J. A. Pople, and M. Head-Gordon, Chem. Phys. Lett. **157**, 479 (1989).
- (5) M. Urban, J. Noga, S. J. Cole, and R. J. Bartlett, J. Chem. Phys. **83**, 4041 (1985).

- (6) T. J. Lee and G. E. Scuseria, in *Quantum Mechanical Electronic Structure Calculations with Chemical Accuracy*, edited by S. R. Langhoff, (Kluwer Academic Publishers, Dordrecht, The Netherlands, 1995), pp. 47–108.
- (7) R. J. Bartlett, in *Modern Electronic Structure Theory*, Part I, edited by D. R. Yarkony (World Scientific, Singapore, 1995), pp. 1047–1131.
- (8) F. Jensen, Chem. Phys. Lett. **169**, 519 (1990).
- (9) J. Paldus, J. Čížek, and M. Takahashi, Phys. Rev. A **30**, 2193 (1984).
- (10) J. Paldus and J. Planelles, Theor. Chim. Acta **89**, 13 (1994).
- (11) J. Planelles, J. Paldus and X. Li, Theor. Chim. Acta **89**, 33, 59 (1994).
- (12) L. Z. Stolarczyk, Chem. Phys. Lett. **217**, 1 (1994).
- (13) X. Li, G. Peris, J. Planelles, F. Rajadell and J. Paldus, J. Chem. Phys. **107**, 90 (1997).
- (14) P. Piecuch, R. Toboła and J. Paldus, Phys. Rev. A **54**, 1210 (1996).
- (15) X. Li and J. Paldus, J. Chem. Phys. **107**, 6257 (1997).
- (16) X. Li and J. Paldus, J. Chem. Phys. **108**, 637 (1998).
- (17) X. Li and J. Paldus, Chem. Phys. Lett. **286**, 145 (1998).
- (18) B. Jeziorski and H. J. Monkhorst, Phys. Rev. A **24**, 1668 (1981).
- (19) K. Jankowski and K. Kowalski, Chem. Phys. Lett. **256**, 141 (1996).
- (20) K. Jankowski, I. Grabowski and K. Kowalski, J. Chem. Phys. (submitted).
- (21) S. A. Kucharski, A. Balková and R. J. Bartlett, Theor. Chim. Acta **80**, 321 (1991).
- (22) K. Jankowski and J. Paldus, Int. J. Quantum Chem. **18**, 1243 (1980); J. Paldus, P. E. S. Wormer, and M. Bénard, Coll. Czech. Chem. Commun **53**, 1919 (1988).
- (23) J. Paldus, P. Piecuch, B. Jeziorski and L. Pylypow, in *Recent Progress in Many-Body Theories*, Vol. 3, edited by T. L. Ainsworth, C. E. Campbell, B. E. Clements, and E. Krotscheck (Plenum Press, New York, 1992), pp. 287–303.

- (24) P. Piecuch and J. Paldus, *J. Chem. Phys.* **101**, 5875 (1994).
- (25) S. A. Kucharski, A. Balková, and R. J. Bartlett, *Theor. Chim. Acta* **80**, 321 (1991); A. Balková, S. A. Kucharski, L. Meissner, and R. J. Bartlett, *ibid.* **80**, 335 (1991).
- (26) S. Wilson, K. Jankowski, and J. Paldus, *Int. J. Quantum Chem.* **23**, 1781 (1983); U. Kaldor, *ibid.* **28**, 103 (1985); N. Iijima and A. Saika, *ibid.* **27**, 481 (1985); S. Zarrabian and J. Paldus, *ibid.* **38**, 761 (1990).
- (27) K. Jankowski, J. Paldus, and J. Wasilewski, *J. Chem. Phys.* **95**, 3549 (1991); K. Jankowski, J. Paldus, I. Grabowski, and K. Kowalski, *J. Chem. Phys.* **97**, 7600 (1991); *ibid.* **101**, 3085 (1994).
- (28) P. Piecuch and L. Adamowicz, *J. Chem. Phys.* **100**, 5792 (1994).
- (29) J. P. Finley, R. K. Chaudhuri, and K. F. Freed, *J. Chem. Phys.* **103**, 4990 (1995).
- (30) J. Mášik and I. Hubač, in *Quantum Systems in Chemistry and Physics*, edited by R. McWeeny (Kluwer Academic Publishers, The Netherlands, 1997), pp. 283–308.
- (31) K. Jankowski, L. Meissner, and J. Wasilewski, *Int. J. Quantum Chem.* **28**, 931 (1985); L. Meissner, K. Jankowski, and J. Wasilewski, *ibid.* **34**, 535 (1988).
- (32) J. Paldus, P. Piecuch, L. Pylypow, and B. Jeziorski, *Phys. Rev. A* **47**, 2738 (1993); P. Piecuch and J. Paldus, *ibid.* **49**, 3479 (1994).
- (33) P. Piecuch, R. Tobiła, and J. Paldus, *Chem. Phys. Lett.* **210**, 243 (1993).
- (34) X. Li and J. Paldus, *J. Chem. Phys.* **103**, 1024 (1995).
- (35) P. Saxe, H. F. Schaefer III, and N. C. Handy, *Chem. Phys. Lett.* **79**, 202 (1981); R. J. Harrison and N. C. Handy, *Chem. Phys. Lett.* **95**, 386 (1983).
- (36) J. Paldus, P. E. S. Wormer, F. Visser, and A. van der Avoird, *J. Chem. Phys.* **76**, 2458 (1982); J. Paldus, in *New Horizons of Quantum Chemistry*, edited by P.-O. Löwdin and B. Pullman (Reidel, Dordrecht, The Netherlands, 1983), pp. 31–60.

THE HALF PROJECTED HARTREE-FOCK MODEL FOR DETERMINING SINGLET EXCITED STATES.

Yves G. SMEYERS

Instituto de Estructura de la Materia, C.S.I.C.
Serrano, 113-bis, 28006-MADRID, Spain.

Keywords: DODS functions. Half-projected Hartree-Fock Model. Direct determination of singlet excited states. Core excitations calculations.

Abstract

The Half-Projected-Hartree-Fock model (HPHF) which introduces some electronic correlation effects into the a singlet ground state wave-function is briefly described. Two procedures for determining the HPHF orbitals are described and extended to the direct determination of singlet excited states. The procedure is applied to various examples of interest. The spectroscopic constants of the Li_2 molecule lowest singlet excited states are calculated. The optimal geometries of cyclobutanone and 3-cyclopenten-1-one in their singlet ($n \rightarrow \pi^*$) excited state are determined. Both molecules are found to exhibit, in their excited state, a pyramidal conformation with the carbonyl oxygen atom pointing outward with respect to the molecular plane. Finally, the HPHF procedure is applied to estimate core excitations in the SF_6 molecule.

Table of Contents

1. INTRODUCTION
2. THE HPHF FUNCTION FOR SINGLET GROUND STATE.
 - 2.1. The Brillouin Theorem.
 - 2.2. The Pairing Theorem.
 - 2.3. The HPHF Equations.
 - 2.4. Some Applications to Singlet Ground States.
3. THE HPHF EQUATIONS FOR SINGLET EXCITED STATES.
4. APPLICATIONS
 - 4.1. The Lithium Molecule Excited States.
 - 4.2. Cyclobutanone and 3-Cyclopenten-1-one in the first singlet excited states.
 - 4.3. Core Excitations.
5. DISCUSSIONS AND CONCLUSIONS

1. INTRODUCTION

As is well known, the restricted Hartree-Fock model (RHF) has the form of a single Slater determinant built up with doubly occupied orbitals which minimize the total energy [1]. This model may be used without any problem to determine the electronic energy and structure of closed shell molecular systems in their fundamental singlet state. It presents, however, the disadvantage of predicting incorrectly the molecular dissociation into ions instead of neutral atoms, because of the orbital double occupation. Thus, it should not be used for studying chemical reactions which involve bond breaking.

One way to overcome this difficulty is to use different orbitals for different spins (DODS model). This technique introduced, into the Hartree-Fock scheme, gave rise to the unrestricted Hartree-Fock model (UHF), the wavefunction being written as an open shell single Slater determinant[2]:

$$\Psi^{UHF} = \{ |a_1 \bar{b}_1 a_2 \bar{b}_2 \dots a_n \bar{b}_n \rangle \} \quad (1)$$

where the spinorbital of different spins, a_i and \bar{b}_i , may have different spatial functions:

$$\langle a_i | b_i \rangle \leq 1 \quad (2)$$

The procedure to obtain the UHF spinorbitals is exactly the same as that for the RHF ones, except that two pseudo-eigenvalue equations have to be solved simultaneously by successive iterations:

$$F_i^a a_i = [H_i^o + \sum_q^{n_a} (J_i^q - K_i^q) + \sum_q^{n_b} \bar{J}_i^q] a_i \quad (3)$$

and

$$F_i^b b_i = [H_i^o + \sum_q^{n_b} J_i^q + \sum_q^{n_a} (\bar{J}_i^q + \bar{K}_i^q)] b_i$$

where J_i^q and K_i^q are the usual Coulomb and Exchange operators, and the lack or presence of the upper bar means that the operators are constructed with α or β spinorbitals, respectively.

The UHF energy is expected to be lower than the RHF one, but in the case of closed shell systems close to the equilibrium geometry, the UHF energy usually coincides with the RHF one. This feature produces a sort of discontinuity in the potential energy curve the internuclear distance when increases.

In addition, the UHF function has the defect of not being an eigenstate of the total spin operator, \hat{S}^2 , so that it is not a pure spin function but, rather, a superimposition of states of different multiplicities:

$$\Psi^{UHF} = \Psi^1 + \Psi^3 + \Psi^5 + \Psi^7 + \Psi^9 \dots \quad (4)$$

As is well known also, this new inconvenient may be overcome by projecting the Slater determinant on the singlet space [3]. The projection can be performed before or after the minimization procedure. The latter (PUHF), however, does not avoid the problem of the discontinuity in the potential energy curve. In addition, it does not furnish a wave-function which corresponds to the energy minimum.

The determination of the spinorbitals after an orthogonal projection gave rise to the projected Hartree-Fock model (PHF), proposed by Lowdin in 1955 [3].

When an DODS Slater determinant of n electron pairs is projected on a spin space of spin quantum number S , its projection takes the form of a linear combination of $\binom{2n}{n}$ Slater determinants:

$$^S \hat{P} D_{\infty} = \sum_p C_p(n, S) \sum_k D_{pk} \quad (5)$$

where the C_p are the well known Sanibel coefficients which depend only on the S quantum number and on the number of electron pairs. The second sum runs over the k permutations corresponding to p transpositions, and the first sum runs over all the possible transpositions [4].

The determination of such a wave-function is very involved and has been studied by some authors [5-6]. Notice that the Sanibel coefficients are not variational parameters but constant, this feature is the defect of the model.

On the other hand, a linear combination of only two DODS Slater determinants in which all the α and β spins are interchanged, was shown to produce similar results [7].

$$\Psi^{HPHF} = \{|a_1 \bar{b}_1 \dots a_n \bar{b}_n| + |b_1 \bar{a}_1 \dots b_n \bar{a}_n|\} \quad (6)$$

Taking advantage of the symmetry properties of the Sanibel coefficients, this linear combination (6) was seen to contain only spin eigenstates with even S quantum number, i.e, singlets, quintuplets, etc.:

$$\Psi^{HPHF} = \Psi^1 + \Psi^5 + \Psi^9 + \dots \quad (7)$$

Because this new model is equivalent to a projection on half of the spin space, it is called the Half-Projected Hartree-Fock model (HPHF). The corresponding projection operator can be written easily in the following way [8]:

$$\hat{A}(S) = \frac{[1 + (-1)^S \hat{p}]}{2} \quad (8)$$

where \hat{p} is an operator which permutes all the a_i and b_i functions of a same electron pair.

It can be easily verified also that $\hat{A}(S)$ is a projection operator which depends only on the parity of the spin number S :

$$\begin{aligned} \hat{A}(S) &= [\hat{A}(S)]^2 \\ \hat{A}(0)\hat{A}(1) &= 0 \end{aligned} \quad (9)$$

where $\hat{A}(0)$ projects on the even spin space; and $\hat{A}(1)$ projects on the odd spin space.

Finally, it must be mentioned that the HPHF function is invariant under any unitary transformation applied to the orbitals because all permutations of the spin functions are performed [8].

The HPHF function is indeed not a pure spin function, but, in the ground state the wave function for singlets will not contain any triplet component which is usually the largest contaminant in the DODS function. Furthermore, it may be expected that, in the ground state, the quintuplet contamination will be very small because of its high energy. Different procedures have been developed and applied successfully to small molecular systems [8-11]. A review on this subject is given in Ref.[12].

In addition, the two-determinantal form of the HPHF function suggests the use of this model for the direct determination of the lowest singlet excited states. In this aim, a procedure similar to that for the ground state was developed and successfully applied to small molecular systems [13-16]. In these calculations, the HPHF model was shown to yield much better results than single excitation CI calculations [15].

2. THE HPHF FUNCTION FOR THE SINGLET GROUND STATE

2.1. The Brillouin Theorem

The first attempt to determine the HPHF orbitals was analogous to the procedure used initially for the PHF orbitals [5]. For this purpose, the Brillouin procedure was extended to the PHF scheme. Two sets of occupied orbitals, each of them associated with different spin functions, are written in terms of a limited basis:

$$\begin{aligned} a^1, a^2, \dots, a^p, \dots, a^{n/2} \\ b^1, b^2, \dots, b^p, \dots, b^{n/2} \end{aligned} \quad (10)$$

In the same way, the virtual orbitals corresponding to the complementary space can be expressed as:

$$\begin{aligned} a^{(n/2)+1}, \dots, a^t, \dots, a^m \\ b^{(n/2)+1}, \dots, b^t, \dots, b^m \end{aligned} \quad (11)$$

The trial occupied orbitals are then corrected in terms of the virtual ones:

$$\begin{aligned} a^p &= a_o^p + \sum_{t=(n/2)+1}^m c_{pt} a_o^t \\ b^p &= b_o^p + \sum_{t=(n/2)+1}^m c'_{pt} b_o^t \end{aligned} \quad (12)$$

and introduced in the PHF function which is developed in terms of single, double, triple, ..., excitations.

$$\Psi = \Psi_o + \sum_{pt} c_{pt} \Psi_o^{pt} + \sum_{pt} c'_{pt} P s i_o^{p't'} + \sum_{pt, qv} c_{pt} c'_{qv} \Psi_o^{pt, q'v'} + \dots \quad (13)$$

where Ψ_o^{pt} are the Slater determinants in which an occupied orbital, a^p , has been replaced by a virtual one, a^t , and so on. The corrections c_{pt} and c'_{pt} are then determined by minimizing the total energy.

The conditions which minimize the energy are obtained by setting the partial derivatives with respect to the corrections equal to zero:

$$\begin{aligned} 0 &= \langle \Psi_o^{pt} | H - E | \Psi_o \rangle + \sum_{qv} c_{qv} \langle \Psi_o^{pt, qv} | H - E | \Psi_o \rangle + \langle \Psi_o^{pt} | H - E | \Psi_o^{qv} \rangle \\ &+ \sum_{qv} c'_{qv} \langle \Psi_o^{pt, q'v'} | H - E | \Psi_o \rangle + \langle \Psi_o^{pt} | H - E | \Psi_o^{q'v'} \rangle \\ &+ \text{higher order terms} \end{aligned} \quad (14)$$

There are as many equations as corrections. These equations are not linear. Their solutions would yield the exact PHF orbitals in the functional space of dimension m , but they are unmanageable.

However, whenever the starting orbitals, a_0^p and b_0^p , are sufficiently close to the solutions, the terms of second and higher order in the corrections may be neglected in (14). As a result, the conditions (14) become linear and nonhomogeneous. The solution of this system will provide new improved orbitals, that may be used to start an iterative process. When selfconsistency is reached, the corrections are zero. The conditions (14) take the form:

$$0 = \langle \Psi^{p'} | H - E | \Psi \rangle \quad \text{and} \quad 0 = \langle \Psi^{p't'} | H - E | \Psi \rangle \quad (15)$$

These requirements on the matrix elements are precisely the generalized Brillouin conditions for the PHF functions [5]. They are very general and hold also for all the DODS type functions such as the HPHF function, as well as for the RHF function.

2.2. The Pairing Theorem

Since the HPHF function is invariant under an unitary transformation applied to the orbitals a_i or/and b_i , both sets may be conveniently transformed so that the orbitals belonging to different electron pairs are orthogonal:

$$\langle a_i | b_j \rangle = \lambda_i \delta_{ij} \quad (16)$$

Such orbitals are known as corresponding orbitals [4].

As a result, the overlap between the HPHF function with itself may be expressed as:

$$\langle \Psi^{HPHF} | \Psi^{HPHF} \rangle = 1 + D \quad (17)$$

where:

$$D = \prod_{i=1}^n \lambda_i^2 \quad (18)$$

2.3. The HPHF Equations

In order to deal with the HPHF equations, it is convenient to define a series of operators analogous to those of the UHF model:

$$\begin{aligned} \hat{F}^a &= \hat{h} + \hat{J}(\hat{R}^a + \hat{R}^b) - \hat{K}\hat{R}^a \\ \hat{F}^b &= \hat{h} + \hat{J}(\hat{R}^a + \hat{R}^b) - \hat{K}\hat{R}^b \end{aligned} \quad (19)$$

$$\hat{F}^{ab} = \hat{h} + 2\hat{J}(\hat{R}^{ab}) - \hat{K}\hat{R}^{ab}$$

In these expressions, \hat{h} , \hat{J} and \hat{K} are the usual monoelectronic coulombic, bielectronic coulombic and exchange operators, respectively. \hat{R}^a and \hat{R}^b are the one-particle density operators expressed in the a_i and b_i orbital basis:

$$\begin{aligned}\hat{R}^a &= \sum_{i=1}^n |a_i\rangle\langle a_i| \\ \hat{R}^b &= \sum_{i=1}^n |b_i\rangle\langle b_i|\end{aligned}\quad (20)$$

In the same way, \hat{R}^{ab} is a cross density operator between both basis sets:

$$\hat{R}^{ab} = \sum_{i=1}^n \frac{|a_i\rangle\langle b_i|}{\lambda_i} \quad (21)$$

With these definitions, the total HPHF electronic energy may be easily written down:

$$E_{HPHF} = \frac{E_{UHF} + E_{cross}}{1 + D} \quad (22)$$

where E_{UHF} should be the one-DODS-determinant energy and E_{cross} , the interaction energy between both determinants:

$$\begin{aligned}E_{UHF} &= \frac{1}{2}Tr[(\hat{R}^a + \hat{R}^b)\hat{h} + \hat{R}^a\hat{F}^a + \hat{R}^b\hat{F}^b] \\ E_{cross} &= DTr[\hat{R}^{ab}\hat{h} + \hat{R}^a\hat{F}^{ba}]\end{aligned}\quad (23)$$

From the energy expression for the HPHF function (23), the pseudoeigenvalue equations for the HPHF orbitals may be easily deduced resorting to the Generalized Brillouin Theorem expression [10]. This theorem has been shown to be valid for any MCSCF function [17] and, in particular, for a two determinant SCF function [7,8]:

$$\frac{\partial E}{\partial C_{it}} = \langle \Psi | H - E | \Psi^{it} \rangle = 0 \quad (24)$$

where Ψ is now the HPHF function for the singlet ground state and is Ψ^{it} a HPHF function in which an a_i occupied orbital has been replaced by a virtual one a_t .

This expression may be rewritten in terms of the two DODS functions and, taking into account the idempotency of the operator $\hat{A}(S)$ (9):

$$\frac{\partial E}{\partial C_{it}} = \langle \Psi_o | \hat{H} | (\Psi_o^{it} + \Psi_n^{it}) \rangle - \langle \Psi_o | (\Psi_o^{it} + \Psi_n^{it}) \rangle \quad (25)$$

Developing this last expression in terms of the corresponding orbitals, we have

$$\begin{aligned} & \langle a_i | \hat{F}^a | a_t \rangle + \frac{1}{\lambda_i} \langle b_i | a_t \rangle (E_{cross} - DE) + \\ & + \frac{D}{\lambda_i} \langle b_i | \hat{F}^a b | a_t \rangle - \frac{D}{\lambda_i} \sum_j^n \frac{1}{\lambda_j} \langle b_j | a_j \rangle \langle b_i | \hat{F}^{ba} | a_j \rangle = 0 \end{aligned} \quad (26)$$

We can now express this equation in compact form as:

$$\langle a_i | H^a | a_t \rangle = 0 \quad (27)$$

A similar equation may be written for the b_i orbitals.

Since Ψ^{HPHF} is invariant under an unitary transformation, two canonical sets of a_i and b_i which diagonalize the matrix representation of \hat{H}^a and \hat{H}^b operators, may be chosen:

$$\begin{aligned} \hat{H}^a | a_i \rangle &= \varepsilon_i^a | a_i \rangle \\ \hat{H}^b | b_i \rangle &= \varepsilon_i^b | b_i \rangle \end{aligned} \quad (28)$$

The expression (26) was developed in Ref. 10, and it is possible to show that it is equivalent to the diagonal of expression given by Smeyers et al. [11,18].

In matrix form, expression (26) may be rewritten as:

$$\begin{aligned} \mathbf{H}^a &= \mathbf{F}^a + \mathbf{S} (\mathbf{R}^{ab} + \mathbf{R}^{ba}) \mathbf{S} (E_{cross} - DE) + \\ &+ D \{ \mathbf{S} \mathbf{R}^{ab} \mathbf{F}^{ba} [\mathbf{I} - \mathbf{R}^{ab} \mathbf{S}] + [\mathbf{I} - \mathbf{S} \mathbf{R}^{ba}] \mathbf{F}^{ab} \mathbf{R}^{ba} \mathbf{S} \} \end{aligned} \quad (29)$$

where \mathbf{S} is the overlap matrix between the basis functions used for expanding the orbitals.

The procedure is carried out by diagonalizing the \mathbf{H}^a and \mathbf{H}^b matrices in an alternated way just as in the UHF procedure until the convergence is reached.

2.4. Some Applications to Singlet Ground States

Because of the complexity of the PHF function, only very small electronic systems were initially considered. As first example, the electronic energy of some four electron atomic systems was calculated using the Brillouin procedure [8]. For this purpose, a short double zeta STO basis set, $1s$, $1s'$, $2s$ and $2s'$, with optimized exponents was used. The energy values obtained are given in Table 1. In the same table, the RHF energy values calculated with the same basis are gathered for comparison. It is seen that the PHF model introduces some electronic correlation in the wave-function. Because of the nature of the basis set formed by only s -type orbitals, only radial correlation is included which account for about 30% of the electronic correlation energy.

Table 1. Electronic energy (in a.u.) for some four electron atomic systems calculated into the RHF, PHF and HPHF approximations.

	RHF	PHF	HPHF
Li^-	-7.42655	-7.44087	-7.44085
Be	-14.57213	-14.58556	-14.58560
B^+	-24.23644	-24.24959	-24.24946
C^{++}	-36.40718	-36.42013	-36.41955

In the same table, the HPHF energy for the same systems obtained with the same basis are also given. It is seen that the HPHF model furnishes energy values very close to the PHF ones with much less work and less computation time.

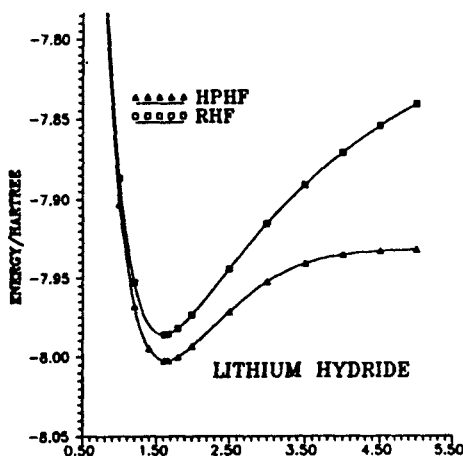


Fig.1. HPHF and RHF potential energy curves as a function of the nuclear separation for LiH .

The HPHF potential energy curve calculated as a function of the nuclear separation in lithium hydride is given in Figure 1. Six STO's as basis functions, $1s$, $1s'$, $2s$, $2p_\sigma$, on the Li atom, and $1s$ and $2p_\sigma$ on the H atom, with adjustable exponents, were used. In the same figure, the RHF potential energy curve obtained in the same conditions is also represented. It is seen that the HPHF curve dissociates correctly into neutral atoms, whereas the RHF one does it incorrectly into ions. The HPHF model is seen to introduce some alternant correlation effects in the wave-function.

It is interesting to point out that models such as the PHF and HPHF ones, which resort to orthogonal projection are able to open only one electronic shell, i.e., they are able to introduce either radial or alternant correlation [19]. This is the limitation of these models. To introduce simultaneously both effects non-orthogonal projection operators have to be used [20].

3. THE HPHF EQUATIONS FOR EXCITED STATES

The two-determinant form of the HPHF function suggests the use of this model to determine singlet excited states. There is indeed no simple method for the direct determination of the singlet excited states analogous to the UHF for the triplet with $M_S = 1$.

The HPHF wave-function for singlet excited states is constructed by simple substitution of an a_k or b_k occupied orbital by an a_t or b_t orbital of the virtual space in the two determinantal DODS function:

$$\Psi(b_k \rightarrow b_t) = \frac{1}{2} \{ |a_1 \bar{b}_1 \dots a_k \bar{b}_t| + |b_1 \bar{a}_1 \dots b_t \bar{a}_k| \} \quad (30)$$

The deduction of the HPHF equations for excited states gives rise to a new challenge, since the excited orbital b_t is usually orthogonal to the occupied one a_k . As a result, one of the overlap λ_i in equation (14) could be zero, (or close to zero) which will give rise to singularities.

In order to solve this problem, we adopted a procedure originally developed for biradicals [21]. New cross Fock and density operators are defined:

$$\begin{aligned} \hat{R}_o^{ab} &= \sum_{i \neq k}^n \frac{1}{\lambda_i} |a_i\rangle \langle b_i| \\ \hat{r}_k^{ab} &= |a_k\rangle \langle b_t| \\ \hat{F}_o^{ab} &= h + 2\hat{J}\hat{R}_o^{ab} - \hat{K}\hat{R}_o^{ab} \\ f_k &= h + 2\hat{J}\hat{r}_k^{ab} - \hat{K}\hat{r}_k^{ab} \end{aligned} \quad (31)$$

Finally we have:

$$D_o = \prod_{i \neq k}^n \lambda_i^2 \quad (32)$$

and for the energy:

$$E_{HPHF} = E_{UHF} + E_{cross}^o \quad (33)$$

where

$$E_{cross}^o = D_o Tr[\mathbf{R}_o^{ab} \mathbf{F}_o^{ba}]. \quad (34)$$

With these new definitions, the HPHF equations may be easily written in matrix form as:

$$\begin{aligned} \mathbf{H}_o^a = & \mathbf{F}^a + \mathbf{S}(\mathbf{R}_o^{ab} + \mathbf{R}_o^{ba})\mathbf{S} E_{cross}^o + \\ & + D_o \{ \mathbf{S} \mathbf{r}_k^{ab} \mathbf{f}_k^{ba} [\mathbf{I} - \mathbf{R}_o^{ab} \mathbf{S}] + [\mathbf{I} - \mathbf{S} \mathbf{R}_o^{ab}] \mathbf{f}_k^{ba} \mathbf{r}_k^{ab} \mathbf{S} + \\ & + \mathbf{S} [\mathbf{r}_k^{ab} \mathbf{F}_o^{ba} - \mathbf{R}_o^{ab} \mathbf{f}_k^{ba}] \mathbf{r}_k^{ab} \mathbf{S} + \mathbf{S} [\mathbf{r}_k^{ba} \mathbf{F}_o^{ab} - \mathbf{R}_o^{ba} \mathbf{f}_k^{ab}] \mathbf{r}_k^{ba} \mathbf{S} \} \end{aligned} \quad (35)$$

A similar expression for the \mathbf{H}_o^b matrix is obtained by interchanging the a and b indices in (35).

The HPHF program structure is similar to that of the standard UHF program except for the presence of additional cross Fock matrices, \mathbf{F}^{ab} and \mathbf{F}^{ba} . The corresponding orbitals have to be restored at each cycle of the iterative process.

The HPHF procedure was initially applied to excited states with symmetry different from that of the ground state. When the symmetry is the same, special care has to be taken in order to avoid the variational collapsing into the ground state [22].

There are different techniques for avoiding this problem. One way is to orthogonalize the excited orbital b_t to the occupied orbital a_p of the same shell, at each stage of the iterative procedure:

$$\langle a_p | b_t \rangle = 0 \quad (36)$$

The HPHF procedure for determining the orbitals of a singlet excited state is remarkably stable and converges very quickly. Usually, twenty iterations yield reasonable values of the total electronic energy.

4. APPLICATIONS

4.1. The Lithium Molecule excited states

In an attempt to check the performance of the HPHF model for determining singlet excited states, most of the excited states of the lithium molecule, Li_2 , were determined as a function of the nuclear separation, and their spectroscopic constants evaluated. In this aim, the standard 6-311G* basis set was used for all of them [15].

In Fig. 2, the corresponding potential curves are represented, including that of the $C^1\Sigma_g^+$ state with identical symmetry as that of the ground state.

Table 2. The equilibrium distances, R_e , (in Å), the force constants, ω_e , (in cm^{-1}) and the anharmonicity constants, $\omega_e x_e$, obtained by using the HPHF and other methods are given for some singlet states of the lithium molecule, together with the experimental values.

State	Methods	R_e	ω_e	$\omega_e x_e$
$X^1\Sigma_g^+$	RHF	2.784	343.17	2.96
	HPHF	2.931	259.71	1.66
	MCSCF	2.692	347.1	-
	Exp.	2.673	351.43	2.61
$A^1\Sigma_u^+$	HPHF	3.106	270.09	1.40
	MCSCF	3.13	254.	-
	Exp.	3.108	255.47	1.58
$B^1\Pi_u$	HPHF	2.884	325.76	1.46
	MCSCF	3.050	288.	-
	Exp.	2.936	270.12	2.67
$C^1\Sigma_g^+$	HPHF	3.182	256.30	0.138
	CCSD	3.56	137.	-
$D^1\Pi_g$	HPHF	3.183	258.19	1.80
	MCSCF	4.161	83.	-

In this table it is seen that the values obtained in the HPHF approach for the spectroscopic constants of Li_2 in its first singlet excited state are especially satisfactory when compared with the MCSCF and experimental values. The values for higher excited states are not so good, probably because of the contamination of higher spin states, as well as the use of a basis set built up essentially for the ground state. Finally, it is noticeable that the values found for the ground state are not satisfactory at all, this result is generally observed

when using DODS functions, which rise to a too flat potential energy curve.

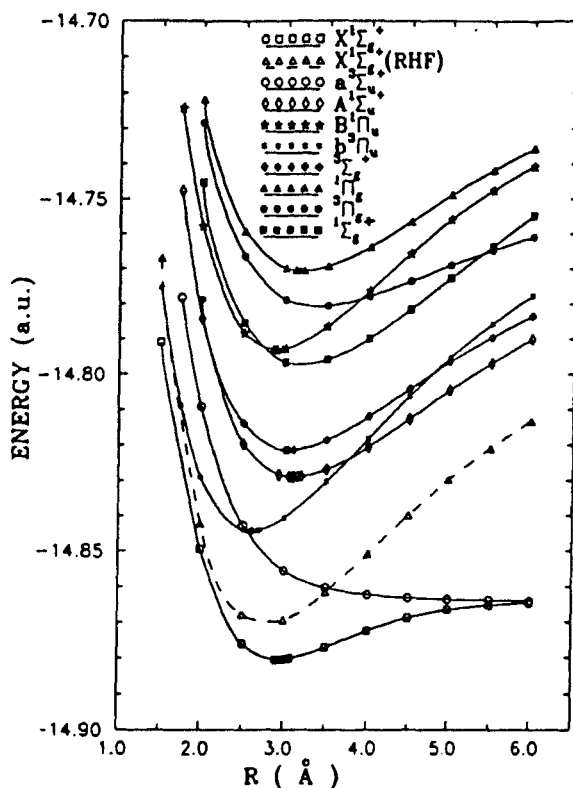


Fig. 2. Potential energy curves for some states of the lithium molecule calculated with the 6-311G* basis set.

4.2. Cyclobutanone and Cyclopentenone in their first singlet excited states

As a test for checking the effectiveness of the model, we have applied the procedure and determined the optimal geometries of two relatively large molecules: cyclobutanone and 3-cyclopenten-1-one [16], which are well known in their first ($n \rightarrow \pi^*$) excited state [23-26].

To optimize the geometry, we used the Simplex method recently implemented into the HPHF program [27].

4.2.1. Cyclobutanone

Cyclobutanone was considered in both the singlet fundamental and the first excited ($n \rightarrow \pi^*$) state [16]. The geometry was fully optimized, at the RHF and HPHF levels, respectively, using a dummy atom at the center of the molecule (X), and the minimal basis set [7s,3p/2s,1p] [28].

The following restrictions were imposed during the optimization: (i) the molecule was symmetric with respect to a plane perpendicular to the $C_2C_1C_4$ molecular plane; (ii) the hydrogen atoms, $H_{4'}$ and $H_{4''}$ were in this plane, $H_{2'}$ and $H_{4'}$ were in the XC_2H_2 and $H_{4''}C_4X$ planes, respectively; (iii) the bond length $C-H$ was the same for all hydrogens, as well as the HCH bond angle.

The optimal geometrical parameters of this molecule in its fundamental singlet and its first excited state are given in Ref. [16], where it is seen that the fundamental singlet state exhibits a planar conformation with the carbonyl oxygen atom lying very approximately in the $C_2C_1C_4$ plane. In contrast, the excited state ($n \rightarrow \pi^*$) shows a pyramidal conformation, with the $C_1 = O$ bond pointing outwards and forming a wagging angle of $\alpha = 38.66^\circ$ with its projection in the molecular plane $C_2C_1C_4$, in very good agreement with the experimental data 41° , 42° and 39° [23-26].

Table 3. Main geometry parameters (in \AA or degrees), barrier heights (in cm^{-1}), and S^2 mean values for cyclobutanone and 3-cyclopenten-1-one in their fundamental and lowest singlet excited states.

Molecules	Parameters *	Planar S_0 (RHF)	Pyramidal S_1 (HPHF)
Cyclo- butanone	α	0.0117	± 38.66
	$C_1=O$	1.2791	1.5410
	C_1-C_2	1.6311	1.5058
	$O-C_1-C_2$	134.48	118.55
	Barrier	-	1,362.2
	$\langle S^2 \rangle$	0.0	0.0885
3-Cyclo- penten-1-one	α	0.003	± 30.26
	$C_1=O$	1.2867	1.5233
	C_1-C_2	1.6169	1.5185
	$O-C_1-C_2$	126.03	118.265
	Barrier	-	895.6
	$\langle S^2 \rangle$	0.0	0.0803

* The UPAC atom numbering is used.

In order to evaluate the energy dependence on the wagging angle, the RHF and HPHF calculations were repeated in both states at some critical values: for the ground state at $\pm 40^\circ$, and for the excited state at 0° with the oxygen atom fixed in the molecular plane.

The most relevant results are given in Table 3, where it is seen that the ground state exhibits a single minimum, whereas the excited state presents a double minimum with an inversion barrier height of $1,362.2 \text{ cm}^{-1}$, in reasonable agreement with the experimental data: 1,940, 1,850, and $1,550 \text{ cm}^{-1}$ [23-25]. In the same table, the mean total spin momentum for $\langle S^2 \rangle$ is given. It is seen that the HPHF method yields practically a pure spin function for the singlet excited state.

4.2.2. 3-Cyclopenten-1-one

In the same way, 3-cyclopenten-1-one was considered in both the singlet fundamental and the first ($n \rightarrow \pi^*$) excited states. The geometries were also optimized at RHF and HPHF levels, respectively, using the same basis set [28].

The following restrictions were imposed during the optimization: (i) the molecule was symmetric with respect to a plane perpendicular to the molecular plane $C_2C_1C_5$. $H_{2'}$ and $H_{5'}$ were in the $XC_2H_{2'}$ and $H_{5'}C_5X$ planes, respectively; (ii) the $H_{3'}$ and $H_{4'}$ atoms were in the $C_3C_4X_1$ plane; (iii) finally, two values for the bond lengths $C-H$ were considered according to the hybridization.

The results are presented in Ref. [16]. As expected, the fundamental singlet state exhibits a planar conformation [23], with the carbonyl oxygen atom lying approximately in the molecular plane. In contrast, the singlet ($n \rightarrow \pi^*$) excited state shows a pyramidal conformation, with the $C_1=O$ bond forming an angle of $\alpha = 30.26^\circ$ with the molecular plane, $C_2C_1C_5$, in very good agreement with the experimental data: 26° and 33° [23,26].

In the same way the energy dependence on the wagging angle was evaluated by performing, RHF and HPHF calculations in both states at some critical values: for the ground state at $\pm 30^\circ$, and for the excited state at 0° with the oxygen atom fixed in the molecular plane.

The main results are given in Table 3, where it is seen that the ground state presents a single minimum, whereas the excited state exhibits a double minimum with an inversion barrier height of 895.6 cm^{-1} in very good agreement with the experimental data: 966 and 780 cm^{-1} [23,26].

In the same table 3, the mean total spin momentum is given. It is seen that the HPHF method furnishes practically a pure spin singlet function.

4.3. Core excitations

Finally, the applications of the Half-Projected-Hartree-Fock model have not to be limited to the excitations of the valence electron shell. This model can also be used to study core electron excitations. This aspect is especially interesting, since there are very few efficient methods for such calculations in molecular systems [29,30].

In order to illustrate this possibility, the SF₆ molecule, for which there exist experimental data has been tested [31]. For this purpose different basis sets for the different excitations have to be used. For 1s excitations in the central sulfur atom, the standard chlorine atom basis was employed for describing all the sulfur electrons. For the 2s or 2p excitations in the same atom, the chlorine atom basis was employed for describing the sulfur L and M shells. The corresponding excitation values are given in Table 4.

Table 4. HPHF excitation energies for different states of the SF₆ molecule, semi-empirical and experimental values(in a.u.), as well as the mean $\langle S^2 \rangle$ values.

Core Excitations	Semi-empical calculations	Flexible basis	Experimental	$\langle S^2 \rangle$
1s \rightarrow t _{1u}	91.678	91.524	91.358	0.170
2s \rightarrow t _{1u}	9.008	8.838	8.838	0.105
2p \rightarrow a _{1g}	6.467	6.253	6.331	0.091

It is seen that the HPHF model reproduces satisfactorily the core excitations in SF₆, even better than some semi-empirical procedures [32]. The mean total spin momentum values are seen also to be very small.

5. DISCUSSION AND CONCLUSIONS

Throughout this paper the HPHF model is described and applied to determine the optimal geometry of the first singlet excited state of some molecular systems. The procedure yields only one electronic state in each calculation but it is found to converge quickly. The results are in relatively good agreement with the available experimental data. The procedure permits also the use of different basis sets for the different states.

The model permits to determine spectroscopic constants, as well as to optimize the geometry in the lowest excited singlet state. The theoretical structures, inversion angles and barrier heights obtained for cyclobutanone and

tures, inversion angles and barrier heights obtained for cyclobutanone and 3-cyclopenten-1-one compare surprisingly well with the available experimental data.

Finally, the HPHF model permits also to determine core excitation in molecular systems.

It may thus concluded that this procedure can be advantageously used to determine the lowest singlet excited states of large molecules to which more sophisticated methods could not be easily applied.

ACKNOWLEDGEMENTS

The author gratefully acknowledges the Spanish DGICIT for the financial support by the Grant PB96-0882.

References

1. C.C.J. Roothaan, Rev. Mod. Phys., **23**, 69-89 (1951).
2. A.T. Amos and G.G. Hall, Proc. R. Soc. London, Ser. A **263**, 483-493 (1961).
3. P.O. Löwdin, Phys. Rev., **97**, 1509-1520 (1955).
4. R. Pauncz, "Alternant Molecular Orbital Method", Saunders, Philadelphia, 1967.
5. R. Lefebvre and Y.G. Smeyers, Int. J. Quantum Chem., **1**, 403 (1967).
6. I. Mayer, Int. J. Quantum Chem., **8**, 363-372, 893-899 (1974).
7. Y.G. Smeyers, An. Fis. (Madrid), **67**, 17 (1971).
8. Y.G. Smeyers and L. Doreste-Suárez, Int. J. Quantum Chem., **7**, 687 (1973).
9. Y.G. Smeyers and G. Delgado-Barrio, Int. J. Quantum Chem., **8**, 773 (1974).
10. P.A. Cox and M.H. Wood, Theor. Chim. Acta, **41**, 269 (1976); ib. **41**, 279 (1976).
11. Y.G. Smeyers and A.M. Bruceña, Int. J. Quantum Chem., **14**, 641 (1978).
12. Y.G. Smeyers, in "Self-Consistent Field, Theory and Applications", (R. Carbó et al. Eds.), Elsevier, Amsterdam, 1990, pp. 80-135.
13. M.B. Ruiz, P. Fernández-Serra and Y.G. Smeyers, Croat. Chem. Acta, **67**, 73 (1994).

14. P. Fernández-Serra, V. Botella, Y.G. Smeyers, A. Galano and G. Delgado-Barrio, *Int. J. Quantum Chem.*, **54**, 303 (1995).
15. Y.G. Smeyers, P. Fernández-Serra and M.B. Ruiz, in "*Strategies and Applications in Quantum Chemistry*", (Eds. Defranceschi et al.), Kluwers, Dordrecht, in press.
16. Y.G. Smeyers, M. B. Ruiz and P. Otto, *J. Mol. Struct. (Theochem)*, **390**, 91-99 (1997).
17. B. Levy and G. Berthier, *Int. J. Quant. Chem.*, **2**, 307 (1968).
18. B.H. Lengsfeld and D.H. Phillips, *J. Chem. Phys.*, **74**, 5174 (1981).
19. Y.G. Smeyers and G. Delgado-Barrio, *Int. J. Quantum Chem.*, **10**, 461 (1976).
20. Y.G. Smeyers, A. González-Guerra, J. Martin-González and P. Fernández-Serra, *Int. J. Quantum Chem.*, **60**, 493-504 (1996).
21. S. Olivella and J. Salvador, *Int. J. Quantum Chem.*, **37**, 713 (1990); *J. Comp. Chem.*, **12**, 792 (1991).
22. J. Laane in "Structure and Conformations of Non-Rigid Molecules", (Eds.
23. D. Firsh and R. McWeeny, *Mol. Phys.*, **32**, 1637 (1976). J. Laane et al.), Kluwer Ac., Dordrecht, NATO-ASI, Vol. 410. 1993, pp. 65-98.
24. M. Baba and I. Hanazaki, *J. Chem. Phys.*, **81**, 5426 (1984).
25. D.C. Moule, *Can. J. Phys.*, **47**, 1235 (1969); *J. Chem. Phys.*, **64**, 3161 (1976).
26. R.D. Gordon and D.R. Orr, *J. Mol. Spectrosc.*, **129**, 3161 (1988).
27. M.B. Ruiz, P.P. Otto and Y.G. Smeyers, *J. Mol. Struct. (Theochem)*, **365**, 151 (1996).
28. E. Clementi, F. Cavallone and R. Scordamaglia, *J. Am. Chem. Soc.*, **99**, 5531 (1977).
29. H. Hsu, E.R. Davison and R.M. Pitzer, *J. Chem. Phys.*, **65**, 609 (1976); A.R. Rossi and E.R. Davidson, *J. Chem. Phys.*, **96**, 10682 (1992).
30. H.J.A. Jensen, P. Jorgensen and H. Agren, *J. Chem. Phys.*, **87**, 451 (1987); A. Agren and H.J.A. Jensen, *Chem. Phys. Letters*, **172**, 45 (1993).
31. J. Maruani, M. Tronc and C. Dazarnaud, *J. Mol. Struct. (Theochem)*, **330**, 145 (1995).
32. J. Maruani, M. Tronc and C. Dazarnaud, *C.R. Acad. Sci. Paris*, **318**, 1191 (1994).

Complexation of transition metal cations (Sc^+ , Fe^+ , Cu^+) by one cyanide radical

by Celestino Angeli

Dipartimento di Chimica, Università di Ferrara, Via Borsari 46,
I 44100 FERRARA

Christian Rolando and Michèle Suard

Département de Chimie, Ecole Normale Supérieure, 24 rue Lhomond,
F 75231 PARIS cedex 05

Contents

- 1 . Monocoordinated complexes as molecular models and chemical species .
- 2 . Quantum-mechanical predictions
 - 2.1 Multireference second-order perturbation methods
 - 2.2 Cyanide and isocyanide structures
 - 2.3 Charge distributions
- 3 . Final remarks on the complexation by the CN ligand

Abstract : The structure of the MCN^+ and MNC^+ isomers cations are studied at the CAS level using extended Gaussian basis sets : all systems in question can be said to be linear and stable by geometry optimization . The MRPT2 method enables us to evaluate near Moller-Plesset and Epstein-Nesbet energies to less than 0.01 a.u. and to predict binding energies decreasing from scandium but remaining positive even for the copper compounds in spite of the closed-shell structure of the Cu^+ cation . The isocyanide isomers are found to be more stable than the cyanide ones for the scandium and copper products, whereas those of iron have quite close total energies .

dedicated to Professor Del Re

1 Monocoordinated complexes as molecular models and chemical species

Most of the transition-metal complexes known as chemically stable compounds include a rather high number of ligands, *i.e.*, as many as their usual coordination number allows (4, 5, 6) and possibly several metals ; this complicates the interpretation of their electronic structure in terms of classical σ , π , δ charge transfers of donation and back-donation types , because of their mutual interactions (see ref.[1]). During the last fifteen years , theoretical and experimental works have been devoted to the study of complexes of lower coordination involving neutral metals or ions and various ligands : diatomics and simple polyatomic molecules such as dinitrogen N_2 , dioxygen O_2 , carbon monoxide CO , water H_2O , ammoniac NH_3 , methane CH_4 and other alkanes etc... A typical example of this research line is the series of compounds $Fe(CO)_n$ derived from iron pentacarbonyl by successive abstraction of its CO groups, which has been investigated from $n = 5$ to 1 [2,3,4] .

Interestingly, among the ligands most often considered for cations, there are several closed-shell systems with ten electrons or ten valence electrons as CO [5]. More recently , the bonding of a transition metal with a ligand containing one electron more , as nitric oxide NO^\bullet [6,7,8] or one electron less , as the cyano radical CN^\bullet [9,10] has been also studied both from the experimental and theoretical points of view. Here , we will present a comprehensible account of our investigations concerning cyanide and isocyanide metal cations $M CN^+$, $M NC^+$, where scandium Sc^+ , iron Fe^+ and copper Cu^+ have been selected as representatives of early , medium and late transition metals M . The Cu^+ cation has a $3d^{10}$ entirely filled configuration , corresponding to a dominant 1S closed-shell ground state , Sc^+ an open-shell $3d^1 4s^1$ structure giving rise to two 3D and 1D low-lying states separated by about 0.3eV. , Fe^+ a $3d^6 4s^1$ structure in its 6D ground state and two different structures $3d^7$ and $3d^6 4s^1$ in its 4F and 4D first excited states for a total energy interval less than 1eV.

At first sight , the main interest of monocoordinated complexes for Quantum Chemistry lies in the simplicity of their energy-level diagrams , as given by the standard ligand field or molecular orbital theories [11] . It is then easy to identify various electronic energy components (*i.e.* , electrostatic , polarisation , exchange contributions and so on ...) in the theoretical results [12,13] , at least at the SCF level .

However , quantum-mechanical calculations on these systems are not merely theoretical exercises , for they may have direct or indirect laboratory counterparts . On the one hand , compounds with one ligand are observed in gas-phase experiments of mass spectroscopy either by fragmentation of parent molecules , or by reactions of bare transition-metal cations on simple molecules ; and this offers the opportunity of generating and studying species which are in fact reactive intermediates postulated for condensed-phase reactions (see[14,15])

Now, theoretical calculation methods of sufficient accuracy may fill the lack of quantitative information concerning so elusive species. On the other hand, the use of a monocoordinated complex as being the simplest molecular model to simulate a chemisorption phenomenon on a metallic surface, for instance the chemisorption of carbon monoxide on iron or nickel [16,17,18] enables to predict the shifts of the CO stretching vibration of the adsorbed species. Similar effects observed with cyanide anions CN^- on a cathode of platinum, silver or gold, using non-linear optics techniques can be rationalized by computing the CN vibration mode of the corresponding triatomic systems [19,20,21].

Finally, the monocoordinated complexes can be expected to be present in the interstellar space and detected in radioastronomy provided the elemental abundance of the metal is sufficient. This should be the case of iron ^{56}Fe , a very stable nucleus, the observation of which in molecules like FeCO [22] has failed up to now. Given the fact that cyano compounds formed by sodium and magnesium (*i.e.*, NaNC , MgNC and MgCN) have been already observed [23,24,25] calculations of iron complexes have some interest for Astrophysics.

2 Quantum-mechanical predictions

2.1 Multireference second-order perturbation methods

As experience gained in computing wave functions for monocoordinated complexes may be helpful for the treatment of more complicated systems, it is relevant to describe in this context the calculations made with only one ligand CN. Molecular orbital wave functions have been constructed from an appropriate set of atomic orbitals, using the MC-SCF formalism to generate a variational space of determinantal functions of not too large size, and the second-order perturbation technique to evaluate the contributions of the functions of the complementary space. This in principle includes all the singly and doubly excited determinants with respect to those already present in the variational space, that is to say a huge number of multiexcitations as soon as the generating space is itself large.

For all the systems considered in this work, the determination of the SCF molecular orbitals involved in the subsequent correlation treatment, and the optimization of molecular geometries have been achieved inside the C_{2v} symmetry subgroup for most cases, instead of the full $\text{C}_{\infty v}$ group valid for linear species, or of course inside the C_s group for possible bent forms. If the system in question contains non-completely filled electron systems, as in usual transition metals, the determination of a set of molecular orbitals adapted to the symmetry of the nuclear framework is often tedious, because the SCF algorithms do not automatically ensure the equivalence properties of the degenerate orbitals; for instance, the equivalence of the one-electron wave functions transforming as x and y or xy and x^2-y^2 with respect to the z internuclear axis. As done here, the problem is generally solved by using SCF treatments based on complete active spaces (CAS) with an appropriate number of active electrons distributed between

selected bonding and antibonding molecular orbitals . Accordingly , the so-called CAS natural orbitals issued from this treatment are taken as molecular orbitals .

The composition of the active spaces involved in the CAS-SCF calculations (numbers of active orbitals and active electrons, n and N respectively, numbers of generated determinants and numbers of configurations state functions) is given in Table 1 for the various complexes and their fragments . Concerning the latter, the orbitals of the Sc^+ and Fe^+ cations have been obtained by means of CAS-SCF calculations in C_1 symmetry made on the average of the configurations describing the ^3D and ^6D states respectively , and those of Cu^+ from its unique closed-shell configuration ; the orbitals of the CN^* ligand have been extracted from an active space formed by its 4σ , $1\pi_x$, $1\pi_y$, 5σ , $2\pi_x$, $2\pi_y$ energy levels . For the $(\text{M}^+ + \text{CN})$ systems themselves , the active space was built by the union of the active orbitals of the ligand and the $3d$, $4s$ orbitals of the metal .

The second-order perturbation calculations following the CAS-SCF treatments previously described are intended to supply the deficiency of correlation, if any, included in the latter. To compute the energy corrections to be added to the variational zero-order values obtained by diagonalizing the active-space Hamiltonian matrices (see tables 3a and 3b of section 2.2), we have performed two different kinds of multireference perturbation CI treatments, both of them being based on improvements of the general CIPSI algorithm [26] recently developed by the Ferrara-Pisa group[27, 28, 29,30] .

- Table 1 -

Characteristics of the CAS-SCF calculations

System	n	N	number of det.	CSF
ScCN^+	12	9	97894	46974
ScNC^+	12	9	97894	46974
FeCN^+	12	14	43608	35446
FeNC^+	12	14	43608	35446
CuCN^+	12	17	27327	14251
CuNC^+	12	17	27327	14251
CN	6	7		54
Sc^+	6	2		15
Fe^+	6	7		6
Cu^+	-	-	1	1

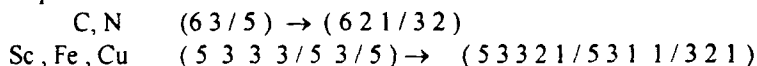
n = number of active orbitals ; N = number of active electrons , CSF = number of configuration state functions

In the first one, the zero-order variational space is just the active space of the CAS-SCF calculations; thus it can be depicted as a CASPT2 approach . In the second, a more refined variational space “ à la CIPSI ” is constructed ; it uses a specific selection procedure in order to ensure an “ aimed reference second-order perturbation ” MRPT2 treatment of the single and double excitations with

respect to the determinants included in the variational space, whatever the internuclear distances may be [30]. For each procedure, the two different partitions of the zero-order Hamiltonian, namely the barycentric Moller-Plesset and Epstein-Nesbet ones (see ref. [31]), have been implemented.

Concerning the use of second-order perturbation methods in connection with CAS calculations, the following point should be kept in mind: In a CAS-SCF calculation, even of moderate size, a large amount of determinants does not play a really important role as components of the active space, because their coefficients are vanishing in the expansion of the variational part of the total wave function. The MRPT2 method eliminates them from the active space and resorts to an extrapolation procedure in order to recover the full perturbation result. It yields better results than the CASPT2 method at a comparable cost of computer time, as shown first by the lowering of the zero-order energies and the reduction of the second-order corrections, second by the narrowing of the gap between the upper MP2 and lower EN2 results; In this respect, the norm of the first-order perturbative correction (*i.e.*, the sum of the off-diagonal elements of the interaction matrix divided by the corresponding excitation energies) gives an important piece of information, for an excessive value of this quantity suggests that the MP2 result should be discarded because of the presence of "intruder states" in the multireference space [32] (see below for an example: ScNC^+).

The atomic orbitals chosen for this work are derived from the MIDI Gaussian sets of Huzinaga preserving the $n \mid m$ shell structure of atoms. They are split valence bases whose last components are left free, increased by two p and one d diffuse functions for the transition atom whose exponents are the values recommended in ref. [32]. Writing the Gaussians in the $s/p/d$ descending order, they are expressed as follows:



2.2 Cyanide and isocyanide structures

In a preliminary series of calculations performed at the CAS level, it was found that the complexation of the transition metal cation M^+ by the cyano group CN^\bullet gives linear molecular structures preferentially, M^+ being located at the minimum of a rather flat potential energy surface along the CN axis. The geometry obtained at this step has been retained for the study of the stabilities of the various species MCN^+ , MNC^+ using, however, binding energies computed at the level of higher correlation (PT2). The corresponding ground-state configurations predicted by this treatment are $^2\Delta$, $^5\Delta$, $^2\Sigma$ for Sc^+ , Fe^+ , Cu^+ complexes respectively.

According to the geometry parameters collected in Table 2, the cyanide complexes MCN^+ have more lengthened structures than isocyanides MNC^+ , iron Fe^+ giving the most compact one in both cases. This simply reflects the variation

of the metal-ligand distances in each molecule , for the values of the CN bond lengths are not very different from the one evaluated at 1.2040 Å in the same theoretical conditions for the free radical CN^\bullet , and somewhat erratic (*i.e.*, exhibiting small changes not necessary concomitant with the metal distances) .

The computation of rotational constants B_e from the inertia moments I_e corresponding to the interatomic distances in both types of complexes illustrates the situation clearly : the cyanide and isocyanide isomers have rotational constants separated by about 0.6 GHz , and this shift upwards for the isocyanide species may be useful for their spectroscopic investigation , as already done for the pair of isomers MgNC and MgCN . Corresponding dipole moments are indicated in this connection . It should be added that the present values are consistent with the experimental parameter $B = 4.358596$ GHz assigned to a related complex FeCO [34] .

As explained in section 2.1 , the binding energies of the various systems with respect to their dissociation products ($\text{M}^+ + \text{CN}^\bullet$) have been evaluated by including second-order perturbation corrections to the CAS primitive treatment . For conveniences of calculation , the energies of the dissociation products have not been computed separately but as a whole , by locating the cation far enough from the ligand (*i.e.* , 90 a.u.) . Consequently , the energy differences obtained in this way have to be depicted as asymptotic dissociation energies D_e [35] . No correction for basis set superposition errors (BSSE) is taken into account by such a procedure; for related systems, standard SCF calculations have given an error of about 20 % on binding energies [36] .

The series of values presented in table 3a originate from CASPT2 calculations carried out in the frame of Moller-Plesset and Epstein-Nesbet second-order perturbation theories bracketing the total energy upwards and downwards by 0.02-0.05 a.u. .

- Table 2 -

Structural parameters for the cyanides and isocyanides at the CAS level

M ⁺	R (M-L)	r (C-N)	I	B _e	μ _e
cyanide					
Scandium	2.163	1.196	2.309	3.634	-13.11
Iron	1.978	1.199	2.184	3.843	-10.78
Copper	2.225	1.221	2.699	3.109	-2.47
isocyanide					
Scandium	2.015	1.212	1.971	4.258	-12.10
Iron	1.869	1.213	1.897	4.424	-10.62
Copper	2.073	1.197	2.259	3.715	-0.10

R and r are in angstroms ; L denotes C for cyanides and N for isocyanides; the moments of inertia are $1 \cdot 10^{-45}$ kg.m² , the rotational constants B_e are in GigaHertz ; the dipole moments μ_e , in Debye, are calculated with respect to the center of mass .

- Table 3 (a) -

CAS and CASPT2 energies of cyanides, isocyanides and fragments
(CAS equilibrium geometries)

Scandium

	Sc-CN ⁺	Sc-NC ⁺	Sc ⁺ ----- CN
CAS	-851.756917	-851.759404	-851.573566
CASMP2	-851.906993 (.043)	-851.914208 (.041)	-851.794318 (.069)
CASEN2	-851.915893 (.048)	-851.925339 (.047)	-851.838909 (.097)

Iron

	Fe-CN ⁺	Fe-NC ⁺	Fe ⁺ ----- CN
CAS	-1354.20981	-1354.19998	-1354.10982
CASMP2	-1354.40555 (.054)	-1354.40644 (.063)	-1354.32092 (.059)
CASEN2	-1354.42236 (.051)	-1354.42539 (.058)	-1354.34336 (.068)

Copper

	Cu-CN ⁺	Cu-NC ⁺	Cu ⁺ -----CN
CAS	-1730.54349	-1730.58086	-1730.49987
CASMP2	-1731.05296 (.124)	-1731.09213 (.123)	-1730.87325 (.076)
CASEN2	-1731.08326 (.136)	-1731.12767 (.138)	-1730.92887 (.098)

In brackets, norm of the first-order perturbation correction .

- Table 3 (b) -

MRPT2 energies of cyanides , isocyanides and fragments
(CAS equilibrium geometries)

Scandium

	Sc-CN ⁺	Sc-NC ⁺	Sc ⁺ -----CN
Variational	-851.906251	-851.911757	-851.781714
MP2	-851.932668 (.006)	-851.955259 (.006)	-851.805209 (.005)
EN2	-851.935777 (.006)	-851.941378 (.006)	-851.808953 (.006)

Iron

	Fe-CN ⁺	Fe-NC ⁺	Fe ⁺ -----CN
Variational	-1354.38503	-1354.38340	-1354.29395
MP2	-1354.41593 (.006)	-1354.41454 (.008)	-1354.32105 (.005)
EN2	-1354.41763 (.007)	-1354.41622 (.007)	-1354.32315 (.005)

Copper

	Cu-CN ⁺	Cu-NC ⁺	Cu ⁺ -----CN
Variational	-1730.79793	-1730.83448	-1730.76229
MP2	-1730.86785 (.012)	-1730.90286 (.011)	-1730.83718 (.012)
EN2	-1730.86921 (.012)	-1730.90450 (.012)	-1730.84348 (.013)

In brackets, norm of the first-order perturbation correction .

However all the cyanide and isocyanide systems in question can be said to be stable by some dozen kcal.mole⁻¹ with respect to their dissociation products , the binding energies decreasing from Sc⁺ but remaining positive even for the Cu⁺ cation in spite of its 3d¹⁰ closed-shell structure . The isocyanide forms are found to be more stable than the cyanide ones for the scandium and copper products , whereas those of iron FeCN⁺ and FeNC⁺ have quite close total energies .

The data of Table 3b have been computed by replacing the active space of the CASPT2 treatment by the CIPSI multireference space of the MRPT2 method documented in section 2.1 . The selection of the components of the reference space by this technique enables us to reduce the gap between the Moller-Plesset and Epstein-Nesbet total energies to less than 0.01 a.u. , and so to improve our evaluation of energy balances, disregarding a possible overestimation of the Moller-Plesset values due to intruder states, as it is the case in the ScNC⁺ system.

Table 4 give the dissociation energies of each complex in its fragments M⁺ and CN^{*}, evaluated in this way by the MRPT2 method . The error bar of the perturbational approach is reduced to a few kcal.mole⁻¹. However, the conclusions previously obtained at the CASPT2 level , namely a decreasing stability of the MNC⁺ and MCN⁺ complexes from early to late transition metals and a possible preference for the cyanide forms in the case of median cations , like iron Fe⁺, are still valid .

- Table 4 -

Dissociation Energies in kcal.mole⁻¹ (MRPT2 level)

cyanides		Scandium	Iron	Copper
D _e	MP2	79.98	59.54	19.25
	EN2	79.58	59.28	16.15
Isocyanides				
D _e	MP2	94.16	58.67	41.22
	EN2	83.10	58.40	38.29

2.3 Charge distributions

In spite of shortcomings due to its sensibility to basis set effects , the Mulliken population analysis gives useful information on intermolecular charge transfers because of the adequacy of its ingredients : It is based on molecular orbitals which may be conveniently calculated as natural orbitals at any level of the theory, including multireference perturbation treatments [37], and which do not require any preliminary kind of partitioning for the electron cloud , by virtue of the LCAO hypothesis [38] . The result of table 5 have been computed from the atomic populations of metal , carbon and nitrogen neglecting second-order perturbation .

The charges ΔQ , Δq_σ and Δq_π are the values obtained as differences between the total populations Q or their σ or π components q of the three atoms in each complex and the corresponding quantities in the fragments, the ion M^+ ($Q_{M^+} = Z_M - 1$) and the radical CN^\bullet (carbon : $q_\sigma = 3.9680$; $q_\pi = 0.8792$ and nitrogen : $q_\sigma = 5.0224$; $q_\pi = 1.1255$). The plus sign denotes a σ or π electron donation, the minus sign a back donation. Due to the lack of d polarisation orbitals in the C and N basis sets, no δ charge transfer appears.

In the case of the scandium and iron compounds, the metal-ligand electron transfer has an essentially σ character, π transfers being practically limited to the CN group; in the lump, it corresponds to an additional discharge of the metal cation notwithstanding its primitive positive charge. The situation is rather different for the copper systems which exhibit σ and π charge transfers of opposite directions depriving the Cu^+ cation of a part of its positive charge and reducing the electron density of the atom not directly linked to metal; it is reminiscent of the so-called "two-way charge transfer" in more familiar molecules [39].

Finally, we can be tempted to look for a possible parallelism between the dissociation energies of the monocoordinated complexes of transition metal cations and the magnitudes of the positive charges located on metals themselves, using the numerous theoretical data available for the three parent ligands CN, CO, NO. No clear-cut conclusion emerges from the data gathered in table 6: Obviously, the stability of the various systems is governed by a balance of electronic effects more complicated than in neutral complexes (see ref. [40]) or, equivalently, by a balance between the electrostatic, exchange and dispersion terms involved in ion-molecule interactions (see ref. [41]).

- Table 5 -

Charge transfers from Mulliken population analysis at the MR level

	Sc	C	N	Sc	N	C
ΔQ	-0.5117	+0.5315	-0.0195	-0.4842	-0.4280	+0.0565
Δq_σ	-0.5619	+0.3515	+0.2125	-0.6551	-0.0108	+0.6559
Δq_π^*	-0.0252	+0.0900	-0.1160	+0.0856	-0.2194	-0.2997
	Fe	C	N	Fe	N	C
ΔQ	-0.3352	+0.4196	-0.0846	-0.3910	-0.3323	+0.0578
Δq_σ	-0.3889	+0.1970	+0.1940	-0.5538	-0.1355	+0.6806
Δq_π^*	+0.0265	+0.1113	-0.1393	+0.0814	-0.2339	-0.3114
	Cu	C	N	Cu	N	C
ΔQ	+0.1041	+0.1599	-0.2639	+0.1195	-0.0800	-0.1990
Δq_σ	+0.1301	+0.2237	-0.3571	+0.1470	-0.0332	-0.1270
Δq_π^*	-0.0130	-0.0319	+0.0466	-0.0138	-0.0566	-0.0360

* Components π , only. ΔQ values include small Δq_δ contributions

- Table 6 -

Dissociation energies D_e and total positive charges Q_{M^+}

		Scandium		Iron		Copper	
		D_e	Q	D_e	Q	D_e	Q
MCN+	(a)	79.9	1.512	59.5	1.335	19.2	0.896
MNC+	(a)	94.2	1.484	58.7	1.390	41.2	0.880
MCO+	(b)	12.7	0.85	21.9	0.83	29.0	0.75
MNO+	(c)	62.8	1.197	50.1	0.913	30.0	0.728

(a) this work ; (b) ref 5 ; (c) ref. 7 (values including ZPVE corrections)

3 Final remarks on the complexation by the CN ligand

Our present knowledge on monocoordinated complexes brings out the remarkable properties of the cyano group as an efficient and versatile complexation agent with regard to transition metal cations . The CN radical is able to form a bounded compound even with a closed shell atom as $Cu^+(3d^{10})$ owing to its open-shell structure and to give cyanide and isocyanide isomers close in energy as with $Fe^+(3d^6 4s^1)$ owing to the similar electroaffinity of its two end atoms, carbon or nitrogen . The theoretical predictions are consistent with the experimental mass-spectroscopy data, which indicate the strong bonding power of early transition metals as $Sc^+(3d^1 4s^1)$ and do not exclude isomerism possibilities [9] . Since however, we have experiment information on the stability of the various complexes by comparison with the binding energy of the generating parent molecule, namely the bromine Br-CN or the iodine I-CN cyanides, further studies should include the reference molecules at the same theoretical level .

References

- [1] G. Del Re, G. Berthier, J. Serre, *Lect. Note Chem.*, n° **13**, Springer - Verlag, Berlin (1980)
- [2] G. Distefano, *J. Res. Natl. Bur. Stand.*, **A74**, 223 (1970)
- [3] A. Ricca, C.W. Bauschlicher Jr, *J. Phys. Chem.*, **98**, 12899 (1994)
- [4] C. Angeli, G. Berthier, C. Rolando, M. Sablier, C. Alcaraz, O. Dutuit. *J. Phys. Chem.*, **A101**, 7907 (1997)
- [5] L.A. Barnes, M. Rosi, C.W. Bauschlicher Jr, *J. Chem. Phys.*, **93**, 609 (1990)
- [6] J. Hrusak, W. Koch, H. Schwarz, *J. Chem. Phys.*, **101**, 3898 (1994)
- [7] A.T. Benjelloun, A. Daoudi, G. Berthier, C. Rolando, *J. Molec. Struct. (Theochem)*, **360**, 227 (1996)
- [8] J.L.C. Thomas, C.W. Bauschlicher Jr, M.B. Hall, *J. Phys. Chem.*, **A101**, 8530 (1997)
- [9] M. Sablier, L. Capron, H. Mestdagh, C. Rolando, *Tetrahedron Lett.*, **35**, 2895 (1994)
- [10] L. Bouslama, A. Daoudi, H. Mestdagh, C. Rolando, M. Suard, *J. Molec. Struct. (Theochem)*, **330**, 187 (1995)
- [11] R.L. DeKock, *Inorg. Chem.* **10**, 1205 (1971)
- [12] P.S. Bagus, C.J. Nelin, C.W. Bauschlicher Jr, *J. Vac. Sci. Technol.*, **A2**, 905 (1984)
- [13] K. Hirai, N. Kosugi, *Can. J. Chem.*, **70**, 301 (1992)
- [14] R.R. Squires, *Chim. Rev.*, **87**, 623 (1987)
- [15] K. Eller, H. Schwarz, *Chem. Rev.*, **91**, 1121 (1991)
- [16] G. Blyholder, *J. Chem. Phys.*, **36**, 2036 (1962) ; *ibid.*, **44**, 3134 (19966) ; *J. Phys. Chem.*, **79**, 756 (1975)
- [17] C. Barbier, G. Berthier, A. Daoudi, M. Suard, *Theor. Chim. Acta*, **73**, 494 (1988)
- [18] G. Berthier, A. Daoudi, M. Suard, *J. Molec. Struct. (Theochem)*, **179**, 407 (1988); *ibid.*, **210**, 139 (1990)
- [19] P. Guyot-Sionnest, A. Tadjeddine, *Chem. Phys. Lett.*, **172**, 341 (1990) ; *Electrochim. Acta*, **36**, 1849 (1991)
- [20] J.P. Flament, M. Tadjeddine, *Chem. Phys. Lett.*, **238**, 193 (1995) ; *ibid.*, *J. Molec. Struct. (Theochem)* **330**, 155 (1995)
- [21] A. Tadjeddine, A. Peremans in *Spectroscopy for Surface Science*, edited by R.J.H. Clark and R.E. Hester Chap. 4, Wiley, Chichester (1998)
- [22] E. Kagi, Y. Kasai, H. Ungerechts, K. Kawaguchi, *Astrophys. J.*, **488**, 776 (1997)
- [23] B.E. Turner, T.C. Steimle, L. Meerts, *Astrophys. J.*, **426**, 297 (1994)
- [24] L.M. Ziurys, A.J. Apponi, M. Guelin, J. Cernicharo, *Astrophys. J.*, **445**, 250 (1995)
- [25] M. Guelin, M. Foreshini, P. Valiron, L.M. Ziurys, M.A. Anderson, J. Cernicharo, C. Kahane, *Astron. Astrophys.*, **297**, 183 (1995)

- [26] B. Huron, J.P. Malrieu, P. Rancurel, *J. Chem. Phys.* , **58**, 5745 (1973)
- [27] R.Cimiraglia, M. Persico, *J. Comp. Chem.*, **8** , 39 (1987)
- [28] R. Cimiraglia, *Int. J. Quantum Chem.*, **60**, 167 (1996)
- [29] C.Angeli, R.Cimiraglia, M.Persico, A.Toniolo,
Theor.Chem. Acc. **98** , 57 (1997)
- [30] C.Angeli, M.Persico *Theor.Chem. Acc.* **98** ,117 (1997)
- [31] R. Cimiraglia, *J. Chem. Phys.*, **83**, 1746 (1985)
- [32] B.O. Roos, K. Andersson , *Chem. Phys. Lett.* , **245** , 215 (1995)
- [33] S.Huzinaga , *Gaussian Basis Sets for Molecular Calculations*, Physical Sciences Data 16 , Elsevier, Amsterdam, 1984
- [34] Y. Kasai, K.Obi, Y.Ohshima, Y.Endo, K.Kawaguchi,
J. Chem. Phys. **103**, 90 (1995)
- [35] P.E.M. Siegbahn, M.R.A. Blomberg *Chem. Phys.* **87**, 189 (1984)
- [36] L. Bouslama, H. Mestdagh, C. Rolando, M. Suard ,
Theor. Chim. Acta **85**, 121 (1993)
- [37] G.Berthier, A.Daoudi, G. Del Re , J.P. Flament,
J.Molec.Struct. (Theochem.) **210** , 133 (1990)
- [38] A. Julg , P. Julg , *Int. J. Quantum Chem.*, **13** , 483 (1978)
- [39] E. Clementi, H. Clementi , *J. Chem. Phys.*, **36** , 2824 (1962)
- [40] A.Douadi, M.Suard, G.Berthier,
J. Molec. Struct. (Theochem) **210** ,139(1990)
- [41] G.Berthier, R.Cimiraglia, A.Daoudi, H.Mestdagh, C.Rolando, M.Suard,
J. Molec. Struct. (Theochem) **254**, 4 (1992)

On the Photophysics of Molecules with Charge-Transfer Excitations between aromatic rings

Alessandro Ferretti, Alessandro Lami and Giovanni Villani

Istituto di Chimica Quantistica ed Energetica Molecolare del CNR,
via Risorgimento 35, I-56126 Pisa (Italy)

Abstract

We develop a naive but quite general model for interpreting the photophysical behavior of aromatic systems for which the ground state and the first excited state can be well described in terms of a limited number of configurations involving charge-transfer excitations between aromatic rings. Assuming that the charge transfer is controlled uniquely by an hopping term proportional to the cosine of the torsion angle (φ) between the two rings, one may build up and solve a complete vibronic model for the system under study. For the case of two interacting configurations (biaryl-like compounds) we allow dipole excitation from the vibronic ground state and study the time behavior of the total population of the excited electronic state (adiabatic). Adopting a purely quantum-mechanical approach we find that the radiationless decay is quite inefficient, since the rings move too rapidly when passing through the avoided crossing regions. The decay becomes much faster taking into account that the motion of the rings is damped by the solvent, as well as by the other internal modes. The computation is performed solving a Fokker-Planck equation for the distribution function in the φ space. If the torsional motion modulating the charge transfer is blocked by a σ bridge between the two rings the radiationless decay becomes again very inefficient (thus opening the way to the radiative channel, which will then become the dominant one).

Contents

1. Introduction
 2. Biaryls and related molecules
 3. A simple vibronic model
 4. The time evolution
 5. Conclusions
- ## References

1. Introduction

The behavior of molecules in excited electronic states is very different from that in the ground state, as witnessed by the existence of Photochemistry as a separate branch of Chemistry. The prediction of the route actually followed by a given species for its decay, after the absorption of a photon, remains a difficult challenge for Quantum Chemistry, being the result of the competition of different channels, either radiative (fluorescence and phosphorescence) or non-radiative (internal conversion, intersystem crossing, photochemical reaction). Some general rules merged already from the first systematic approaches, as the well known Kasha rule [1], stating that, independently of the excitation wavelength, the molecule undergoes a cascade of rapid radiationless decays till it ends in the first singlet or triplet (there is no rule concerning the last decay). A well studied exception to this rule is given by azulene. Only recently, however, the scientific community became aware that this general behavior has to be attributed to the occurrence of conical intersections between adiabatic energy surfaces [2-5], an event considered before as rare [6,7].

The study of the radiationless decay mechanism, i.e. of the way a molecule can transform its electronic energy into vibrational (and rotational) energy, has been recognized as a fundamental step towards the comprehension of the behavior of electronically excited molecules. As pointed out by Robinson [8] the problem was clearly stated already in 1929 by O. K. Rice [9-11], but only in the late sixties it became the subject of an huge theoretical and experimental effort, starting from the pioneering work of Kasha, Robinson, Siebrand, Jortner, Rhodes and others, documented for example in the reviews [1, 8, 12]. Some of the most important progresses realized are shortly resumed in the following few points.

- i) After some initial debate it became clear that the radiationless decay is the consequence of the optical preparation of a state which is not a true molecular eigenstate (i.e. an eigenstate of the full Hamiltonian). The excited state is an eigenstate of a suitable zero-order Hamiltonian, which does not contain the nuclear kinetic energy, responsible for internal conversion, and the spin-orbit coupling term which allows the intersystem crossing. It was also realized that, in general, preparation and decay are deeply related and can be considered as separate steps only in the case of short light pulses [13-15].
- ii) The necessity of solving the time-dependent Schrödinger equation was clearly stated, thus essentially opening a new field of research, although the Fermi-golden-rule (which can be derived by first-order time-dependent perturbation theory) was considered sufficient for large molecules.
- iii) The Fermi-golden-rule approach, in turn, led to put emphasis on Franck-Condon factors, in such a way that the role of high frequency modes (the C-H stretchings) in the decay of aromatic molecules comes into play naturally [16]. It also became clear the different role played by promoting and accepting modes [17]. In close parallelism with the many-phonon approach to the study

of lineshapes of impurities in solids, it was also derived an exponential gap law [16], a very useful theoretical instrument.

During the last thirty years the progresses in this field have been continuous, also due to the development of laser sources and of the techniques for doing spectroscopy in the time domain, with a resolution of a few femtoseconds. One may observe, however, that, in general, it remains still hard to extract from the large amount of experimental data, general rules capable of establishing a close correlation between structure and photophysical behavior. Apart from its intrinsic interest, the latter would be of great help for people involved in the material science, to whom is required the design of molecules for specific applications. In the intent of the authors, the present work, devoted to a specific class of molecules, is a modest contribution in that direction.

2. Biaryls and related molecules

Molecules made by (more or less) weakly interacting parts offer interesting possibilities for the study of both electron and excitation transfer processes. The most common situation is that of biaryl compounds, in which two aromatic systems (A and B) are directly linked to give A-B. In a certain range of interaction strength one can imagine that the ground state (as well as some excited states) of A-B can be well represented by mixing a small number of configurations describing the two separate subsystems. For example, the ground state may be well described by a linear combination of neutral states $|AB\rangle$, some charge-transfer states, either of the kind $|A^+B^- \rangle$ or $|A^-B^+ \rangle$ and some excitonic states, either $|A^*B \rangle$ or $|AB^* \rangle$. Depending on the nature of A and B one may have the predominance of contamination by excitonic or charge transfer configurations. Some general ideas on the origin of different contaminations can be derived assuming that only π electrons play a direct role and then making recourse to the popular PPP model Hamiltonian. The total Hamiltonian is easily partitioned into the sum of two Hamiltonians for the separated units A and B plus an interaction term:

$$H = H_A + H_B + V_{AB} \quad (1)$$

where:

$$H_A = \sum_{i \in A} \epsilon_i n_i + \sum_{i,j \in A} V_{ij} n_i n_j + \sum_{i \in A} U_i n_{i\uparrow} n_{i\downarrow} + \sum_{\substack{i,j=n,n \\ (i,j \in A), \sigma}} t_{ij} a_{i\sigma}^+ a_{j\sigma} \quad (2)$$

$$H_B = \sum_{i \in B} \epsilon_i n_i + \sum_{i,j \in B} V_{ij} n_i n_j + \sum_{i \in B} U_i n_{i\uparrow} n_{i\downarrow} + \sum_{\substack{i,j=n,n \\ (i,j \in B), \sigma}} t_{ij} a_{i\sigma}^+ a_{j\sigma} \quad (3)$$

$$V_{AB} = \sum_{\substack{i,j=n,n \\ (i \in A, j \in B), \sigma}} [(t_{ij} a_{i\sigma}^+ a_{j\sigma} + \text{h.c.}) + V_{ij} n_i n_j] \quad (4)$$

and

$$n_i = a_{i\uparrow}^+ a_{i\uparrow} + a_{i\downarrow}^+ a_{i\downarrow}, \text{ n.n. indicates nearest neighbours.}$$

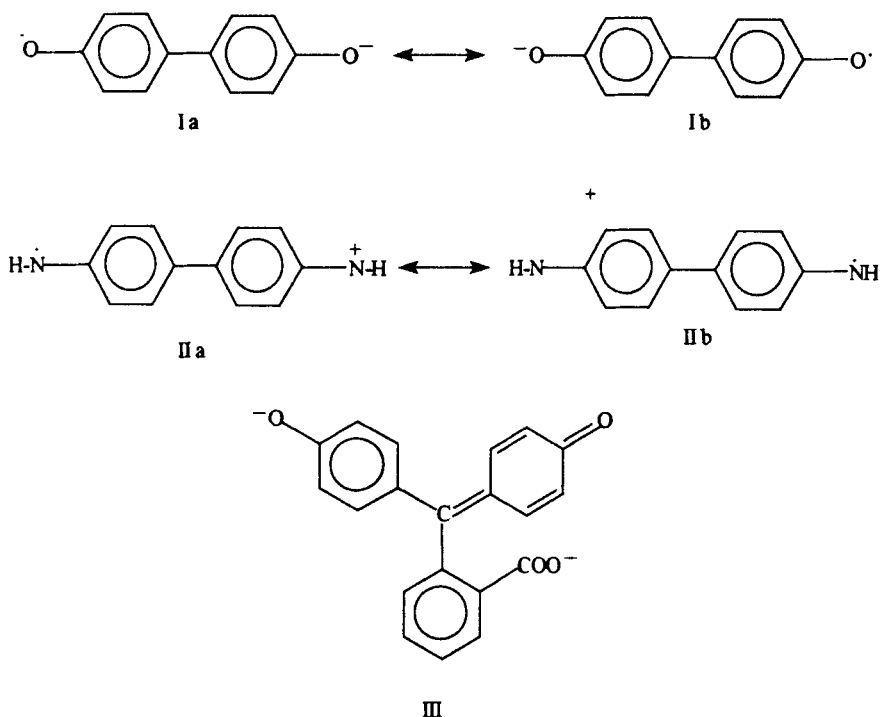
The multi-configurational eigenstates of $H_0 = H_A + H_B$ are then used as basis set for handling the full Hamiltonian, eq. (1). We notice that since only the total number of electrons is given, the above eigenstates can be partitioned in sets differing by the total charge on units A (q_A) and units B (q_B) (of course for neutral species $q_A = -q_B$). Looking at the structure of V_{AB} one can easily get convinced that the hopping terms give rise to charge-transfer (CT) interactions, whereas the repulsion terms are responsible for excitonic interactions. It is clear, in any case, that what happens is strictly dependent on the particular system under study as well as on the part of the energy spectrum considered; and no general conclusions can then be drawn, without facing the problem of determining the electronic structure through accurate quantum chemical computations. It is worthwhile to mention here that the application of standard computational packages to such problems is not straightforward, since the kind of analysis required here demand, in principle, localization of molecular orbitals. As should also result from the previous discussion, a valence bond approach may also reveal very useful for understanding this kind of processes [18].

Among the more recent studies on the behavior of biaryls upon optical excitation we recall here the experimental-theoretical investigation by Maus and Rettig [19] on the biphenil and its derivatives with a donor group (D) on one ring and an acceptor group (A) on the other. Their optical measures corroborated by CNDO computations are convincingly interpreted as an evidence that, while in the biphenil CT interactions do not play a role at low energy, in the DA compounds the first strong absorption band involves transition to a state which has a partial CT character. The dynamic of the excitation transfer in other biaryls, the 2-2'-binaphtil and in the 9-9'-bifluorene has been studied in various solvents, using femtosecond optical techniques, by the Hochstrasser group [20], with the aim of unraveling the role of the interaction with the solvent in promoting the dephasing of the intramolecular energy transfer.

A considerable amount of work has been also devoted to triphenil-methane dyes, which are known to give rise to fast internal conversion. They may exhibit oscillatory decay under pump and probe experiments [21], whose origin has been tentatively attributed to the fact that what is monitored in optical measurements is not the population of the excited adiabatic state, but that of the diabatic state, which is known to give rise to more persistent oscillations on the basis of computations on model systems with conical intersections [22]. We have not found in the literature, however, any clear interpretation of the electronic transition, especially concerning the degree of charge transfer involved, although some of these dyes are known to give rise to fast intermolecular ET in suitable solvents or when they are adsorbed onto surfaces [23,24].

The betaine-30 is another well studied molecule [25] exhibiting a $S_0 \rightarrow S_1$ transition with a marked charge transfer character, which enters in the class discussed here, being basically composed of two triphenyl-methane moieties linked together.

The above compounds are a subclass of a larger family, that of molecules undergoing charge transfer processes accompanied by large intramolecular rearrangements, upon optical excitation, which have been extensively studied for both their intrinsic interest [26,27], and as ideal systems for investigating the role of solvation in ET processes [28-31].



In some particular situations the chemical intuition strongly suggests that charge transfer interactions play a major role in determining the nature of the lowest energy states. This is the case, for example, of charged species derived from quinones, as the semiquinone radical anion (I) or from benzoquinone-di-imines, as in the cation radical (II), for which the presence of two dominating VB structures directly suggests a two state model. Even more rich is the situation for the derivatives of the tri-phenyl-methane, like the phenolphthalein dianion (III),

containing three different aromatic rings, communicating through the central carbon atom. Here one may simplify this complex case assuming (somewhat arbitrarily) that the central atom belongs to the low-lying aromatic system, in such a way that the charge may be in principle assigned to only three subsystems. In the following we introduce a basic model for these cases and show, on the basis of a simple prototypal calculation of the radiationless decay of the excited state for a two-ring system, that they might represent fascinating examples of molecules whose photophysical behavior can be modulated very efficiently through structural modification, which, at first sight, appear to be of minor importance.

3. A simple model

Let us proceed building up the basic model. The cases (I) and (II) can be modeled taking a basis set of two states $|A^-B^- \rangle$ and $|A B^- \rangle$, whereas for case (III) we need three states $|A^-B C^- \rangle$, $|A B^-C^- \rangle$ and $|AB C^- \rangle$. The interaction between the states is assumed to be given by an hopping term modulated by the torsion angle between the rings involved. Hence for (I) and (II) we can write down the electronic Hamiltonian in matrix form (φ is the torsion angle between the aromatic rings A and B and the two states are now labeled 1 and 2):

$$H = \begin{pmatrix} \varepsilon_1 & t\cos(\varphi) \\ t\cos(\varphi) & \varepsilon_2 \end{pmatrix}. \quad (5)$$

For the case (III), assuming that the rings A and C communicate only through B one has (φ_1 and φ_2 are the torsion angles between A and B and C and B):

$$H = \begin{pmatrix} \varepsilon_1 & t\cos(\varphi_1) & 0 \\ t\cos(\varphi_1) & \varepsilon_2 & t\cos(\varphi_2) \\ 0 & t\cos(\varphi_2) & \varepsilon_3 \end{pmatrix} \quad (6)$$

The above matrix representations utilized electronic states which are purely diabatic, being completely independent from the torsional coordinate(s). They are a very convenient starting point for the study of the full vibronic problem, which is required for investigating the photo-physical behavior of such molecules. The full vibronic Hamiltonian, in fact, is simply obtained adding to the electronic Hamiltonian, eq. (5) or (6), the proper nuclear kinetic energy operator (along the diagonal). The adiabatic electronic states and curves are obtained as eigenvectors and eigenvalues of the electronic matrix. The figure 1 shows a view of the potential energy curve for both the ground and the excited state (adiabatic) for the Hamiltonians (5) with the following choice of the parameters (in a.u.):

$$t = -0.0566, \varepsilon_1 = 0, \varepsilon_2 = 0.00167.$$

The figures 2 and 3 depict the ground and the excited state surface, respectively, for the Hamiltonian (6) with (a.u.):

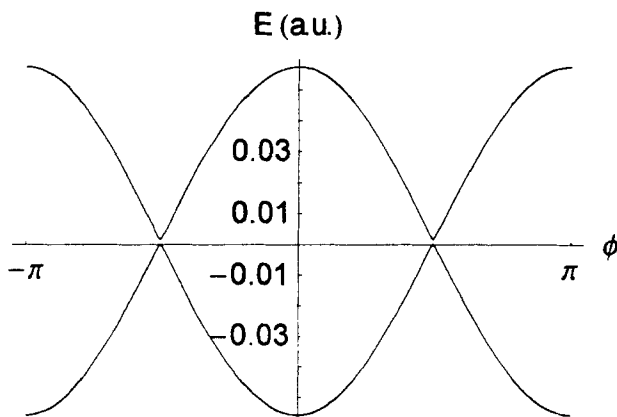


Figure 1

$$t = -0.0566, \varepsilon_1 = 0, \varepsilon_2 = 0, \varepsilon_3 = 0.00167.$$

It is clearly seen that the adiabatic surfaces exhibit avoided crossing at the angles for which the hopping terms vanish, i.e. $\phi = \pm\pi/2$ for the mono-dimensional case and at the four points $(\phi_1 = \pm\pi/2, \phi_2 = \pm\pi/2)$ for the bidimensional case.

In the following we will investigate on the simpler two-state case, which can be directly applied to species like (I) and (II). It is worthwhile to remind here that such a study may also serve to shed some light into the behavior of three-state systems for which $A=C$. In fact, in that case, one may recover a two-state situation by forcing the rings to move in a synchronous manner (i.e. maintaining $\phi_1 = \phi_2$), since, as one can easily realize, for that choice the antisymmetric combination of $|A^- B C\rangle$ and $|AB C^-\rangle$ is decoupled from the problem.

Since we are interested here in the study of the internal conversion from the excited to the ground adiabatic state, we need to tackle the full vibronic problem, whose Hamiltonian can be written as:

$$H = \begin{pmatrix} \varepsilon_1 + T_\phi & t\cos(\phi) \\ t\cos(\phi) & \varepsilon_2 + T_\phi \end{pmatrix} \quad (7)$$

Where ($\hbar=1$):

$$T = -\frac{1}{2I} \frac{\partial^2}{\partial \varphi^2} \quad (8)$$

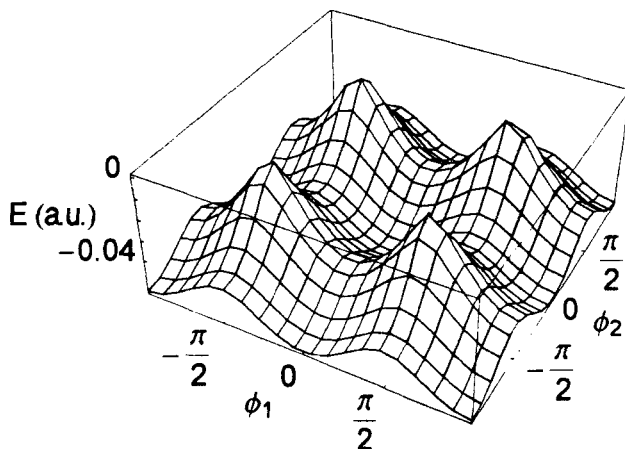


Figure 2

and I is the reduced momentum of inertia for the torsion of the two rings (in the following we take that of a benzene ring).

We notice here that the inclusion of a single nuclear degree of freedom is certainly an oversimplification of the problem. Recently Seidner and Domcke [32] performed some numerical studies on the dynamics of systems involving two diabatic electronic states and a large amplitude torsional angle φ . They assume that the potential energy curve along the torsional angle is different in the two diabatic states, as in many actual cases of photochemical interest, but they claim that the minimal model should include a further harmonic coordinate Q , responsible for the linear inter-electronic coupling (coupling mode). We want to notice here that, while the inclusion of additional modes may certainly result into a more realistic picture, in the present case this is unnecessary if we avoid considering two identical moieties (i.e. $\varepsilon_1 = \varepsilon_2$). In fact only in this latter case the adiabatic electronic states, i.e. the eigenstates of the matrix (5), becomes independent from φ by symmetry and, as such, perfectly stationary (the nuclear kinetic energy operator, responsible for non-adiabatic transitions, involves a second order derivative with respect to φ). It is then clear that only in such case is a further coupling mode absolutely needed.

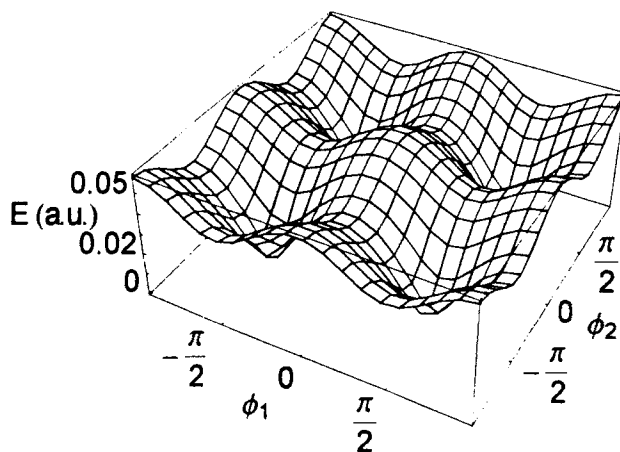


Figure 3

With the justification of pursuing the maximum simplicity we then remain here with a single mode (a torsion), leaving to a forthcoming paper a more complete study, including the exploration of the role of additional degrees of freedom. It is then clear that the present model calculation can be directly applied to molecules derived from I and II, with some symmetry-breaking substitution on the rings.

We then move to the next step, the study the dynamical behavior of a suitable excited state, generated by photon absorption from the ground state (both states are in the space spanned by the eigenstates of the full vibronic hamiltonian, eq. (7). In the present case the ground state can be numerically computed by direct diagonalization of a matrix representation of the Hamiltonian in a suitable basis set. For the multi-mode case this is no more possible, in general, due to the explosion of the dimensions and one can make use of Lanczos techniques which are very useful also for the time propagation and have been extensively used in the numerical exploration of systems exhibiting conical intersections or avoided crossings [33-35]. In the following we take the tensorial product of the diabatic electronic states and of the free rotor eigenstates, which are the complex exponential functions:

$$\chi_n(\varphi) = 1/\sqrt{2\pi} \exp[-in(\varphi)] \quad (n = 0, 1, \dots) \quad (9)$$

Since in practice we only need the matrix elements of $\cos[\varphi]$, it is convenient to work with real functions:

$$\chi_n(\varphi) = N_n \cos[n\varphi] \quad (n = 0, 1, \dots); \quad \psi_n(\varphi) = N_n' \sin[n\varphi] \quad (n = 1, 2, \dots) \quad (10)$$

where

$$N_0 = 1/\sqrt{2\pi}, N_n = N_n' = 1/\sqrt{\pi} \quad (n = 1, 2, \dots). \quad (11)$$

The matrix elements involving a cosine and a sine function vanish and so the Hamiltonian matrix has two blocks. We have verified that the ground state comes out from the cosine block for which the vibronic Hamiltonian of eq. (7) gives rise to the following matrix representation (each submatrix has dimension $N \times N$, where N is the number of free rotor eigenfunctions utilized:

$$\mathbf{H} = \begin{pmatrix} \mathbf{H}^{11} & \mathbf{H}^{12} \\ \mathbf{H}^{21} & \mathbf{H}^{22} \end{pmatrix}, \quad (12)$$

and $\mathbf{H}^{12} = \mathbf{H}^{21}$ are tridiagonal:

$$\mathbf{H}^{12} = t \begin{pmatrix} 0 & 1/2 & 0 & 0 \\ 1/2 & 0 & 1/\sqrt{2} & 0 \\ 0 & 1/\sqrt{2} & 0 & 1/\sqrt{2} \\ 0 & 0 & 1/\sqrt{2} & 0 \\ 0 & 0 & 0 & \ddots \end{pmatrix} \quad (13)$$

The diagonalization of the Hamiltonian matrix (12) gives two degenerate ground states, which can be linearly combined to give states localized around $\varphi = 0$ and $\varphi = \pi$, respectively. The above degeneration comes out because we have considered the two planar configurations, which are energetically identical in our model, as distinguishable. In the following we will take the state localized near $\varphi = 0$ as initial state. We will refer to it as $|g\rangle$, which adopting a spinor notation is written as:

$$|g\rangle = \begin{pmatrix} |g_1\rangle \\ |g_2\rangle \end{pmatrix}. \quad (14)$$

It is clear that exactly the same results would be obtained by taking the $\varphi = \pi$ configuration. It is interesting to notice that adopting a non localized ground state would instead give different results. This latter choice, however, while non violating the quantum mechanics for an isolated system, would contradict the common sense. In practice one can admit, without difficulty, that either the preparation of the system leads to a localized state or that the interaction with the external world operates a wave-packet reduction.

In order to discuss the decay of an optically excited state, we have to make some assumptions on the form of the dipole. As is well known, in fact, the whole time-dependent photo-physical behavior can be simply determined by propagating in time the doorway state, which is obtained by acting with the dipole operator on the ground state (and normalizing). Such excited state can be prepared by photon absorption from a light pulse whose profile in time is a δ , i.e. in practice, a pulse much shorter than the characteristic life-time of the doorway state itself (for

example, as we will verify in the following, a sub-picosecond pulse). The output from a time-resolved experiment with a coherent light pulse of arbitrary form and duration can be handled, in the weak-field limit, by simply convoluting the pulse shape with the output for δ excitation. This is however absolutely unnecessary for interpreting the photo-physical behavior upon optical excitation in ordinary conditions, since, even for laser sources, the molecule and the light interacts coherently only for very short times. In the following we will then assume that the basic physics of the problem can be understood simply looking at the time-dependent behavior of the doorway state.

Let us come to the dipole form. Since the two diabatic states depicts a situation in which charge are localized on the two rings, we will assume that they are also eigenstates of the dipole operator, which is directed along the line joining the centers of the rings. Hence, taking the above line as the z axis and assuming that the radiation is polarized along z we may take the dipole matrix as:

$$\mathbf{d} = d \begin{pmatrix} -1 & 0 \\ 0 & 1 \end{pmatrix} \quad (15)$$

and then the doorway state is (apart from the normalization factor):

$$|w\rangle = \mathbf{d}|g\rangle = \begin{pmatrix} -|g_1\rangle \\ |g_2\rangle \end{pmatrix}. \quad (16)$$

The density of probability in the φ space can be computed as a sum of contributions from the two diabatic states. In particular for the ground state:

$$P(\varphi) = P_1(\varphi) + P_2(\varphi), \quad (17)$$

where

$$P_j(\varphi) = \sum_{k=0}^N \langle g_j | j, k \rangle^2 \quad (j=1, 2). \quad (18)$$

Here j labels the diabatic electronic state, while k is the free rotor quantum numbers. As should be clear from eq. (16) the doorway state has exactly the same distribution. It is however much more interesting to look at the corresponding partition with respect to the adiabatic states. This may be easily derived in terms of the orthogonal matrix $U(\varphi)$ which diagonalizes the electronic Hamiltonian, eq. (5). For a generic state:

$$|a\rangle = \begin{pmatrix} |a_1\rangle \\ |a_2\rangle \end{pmatrix} \quad (19)$$

with

$$|a_j\rangle = \sum_k C_{jk} |j, k\rangle, \quad (j=1, 2) \quad (20)$$

one has:

$$P(\varphi) = P_1^{\text{ad}}(\varphi) + P_2^{\text{ad}}(\varphi), \quad (21)$$

$$P_{ad,j}(\varphi) = \sum_k \left| \langle j_{ad}, k | a_j \rangle \right|^2 = \sum_k \left| \sum_m \langle k | U_{ij}^* | m \rangle C_{1m} + \langle k | U_{2j}^* | m \rangle C_{2m} \right|^2. \quad (22)$$

Notice that in the final result the integration over electronic states has been explicitly performed and the bracket involves only integration over the torsional angle φ . The numerical analysis performed using eq. (22) reveals that, while the ground state for the full vibronic problem stays onto the potential energy curve for the adiabatic ground state, the doorway state belongs almost completely to the excited adiabatic state. Hence, according to our model, the excitation by a δ -pulse simply transfers the wave-packet to the excited adiabatic state, which is a reasonable result. We also notice that since the doorway state corresponds now to a φ distribution which is sharply peaked around a maximum of the potential energy curve, it would presumably give rise to a highly non-stationary behavior.

4. The time evolution

We then proceed propagating in time the doorway state and computing at any time the population of the excited adiabatic state, which can be evaluated performing a numerical integration of the distribution in eq. (22) over the torsional angle. The time dependent Schrödinger can be solved by matrix diagonalization and the results can be expressed in compact form, as discussed in ref. [36]. The results of the calculation (not reported here) are somewhat unexpected. In fact during the time evolution of the doorway state only a negligible fraction of the population is transferred to the adiabatic ground state, mimicking in this respect the behavior of a true stationary state. This behavior depends on the fact that the wave-packet travels through the avoided crossing regions near $\varphi = \pm \pi/2$, (see fig. 1), i.e. the regions where non-adiabatic coupling is expected to be more important, with high velocity. From a purely quantum point of view one may say that the time-dependent non-adiabatic matrix elements are small due to the high oscillatory character of the wave function in the φ -space. The semiclassical Landau-Zener formula [37-39] (which is the exact solution for the scattering problem for two electronic states, assuming a classical trajectory of the nuclei and a linear behavior of the diabatic potential curves near the crossing point) also predicts the same behavior if one evaluates the so called two-way probability [39], which takes into account that in one vibrational period the wave-packet travels two times across the intersection point between diabatic curves. In fact, according to this well known theoretical result, the adiabatic transition probability is given by the negative exponential of a term which is inversely proportional to the linear momentum of the nuclei at the time they pass through the intersection point (we are assuming that at $t=0$ the nuclei have zero momentum. Hence, in our situation, one has an high probability of adiabatic transition during the first passage which is however frustrated by an high

probability of the reverse transition during the second passage. It is however worthwhile to mention that, according to recent numerical investigations [33], the Landau-Zener formula becomes progressively less useful when going at high coupling strength.

In practice, we pay here the consequences of our basic assumption concerning the presence of a single mode (the torsion). In fact the initial wave-packet is placed in a region of high potential energy, which is then transformed totally into kinetic energy, since there is no way of transferring it to other degrees of freedom. One expects that this situation will change drastically introducing explicitly one or more other modes[22,32]. It is also possible to mimic the effect of additional internal modes as well as of collisions with solvent molecules moving towards a stochastic approach. The stochastic way of handling the problem has become very popular in the last few years as a powerful tool for investigating the static and dynamic role of the solvent in ET reactions involving large intramolecular rearrangements and the literature on this subject is very extensive (a comprehensive review is [40]). We touch here very marginally the problem just to show how the inclusion of dissipative processes for the torsional motion changes radically the time-dependent behavior of the system. This is accomplished by assuming that the initial distribution (i.e. that corresponding to the doorway state) undergoes a diffusional motion on the excited adiabatic surface described by a mono-dimensional Fokker-Planck differential equation:

$$\frac{\partial}{\partial t} P_e(\varphi, t) = \left\{ D_R \frac{\partial}{\partial \varphi} \left[\frac{1}{k_B T} \frac{\partial E_e}{\partial \varphi} + \frac{\partial}{\partial \varphi} \right] - k(\varphi) \right\} P_e(\varphi, t), \quad (23)$$

where D_R is diffusion coefficient for the torsional coordinate, k_B the Boltzmann constant, T the absolute temperature, $E_e(\varphi)$ the potential energy curve for the excited adiabatic state and $k(\varphi)$ the decay rate towards the ground state. It is worthwhile to recall here that equation (23) is often associated in the literature [30,31] to the name of Smoluchowsky, but we prefer to follow the Van Kampen notation [41]. The Fokker-Planck equation can be considered as the master equation associated with a continuous random walk of a particle in a potential. As discussed in ref. [30,31] a more correct approach would include diffusion along a further degree of freedom describing the solvent polarization, also important in determining the exact shape of the adiabatic surfaces for both ground and excited states, but the basic physics is caught by the present simplified model.

The rate $k(\varphi)$ for a given torsion angle φ has been determined solving numerically the time-dependent Schrödinger equation for a wave-packet sharply localized around φ on the upper adiabatic curve and computing the time-derivative (at $t=0$) of the probability of being on the excited surface. The computed function $k(\varphi)$ (not reported here) shows peaks at the angles where the curves exhibit avoided crossings, as expected. According to ref [30] the diffusion coefficient D has been taken as the inverse of the correlation time for the internal rotation

$D = \frac{1}{\tau_R}$, and the latter can be estimated from experimental data or taken as an adjustable parameter. We have assumed here $\tau_R = 150$ ps which seems a reasonable value for the torsion of an aromatic ring in water.

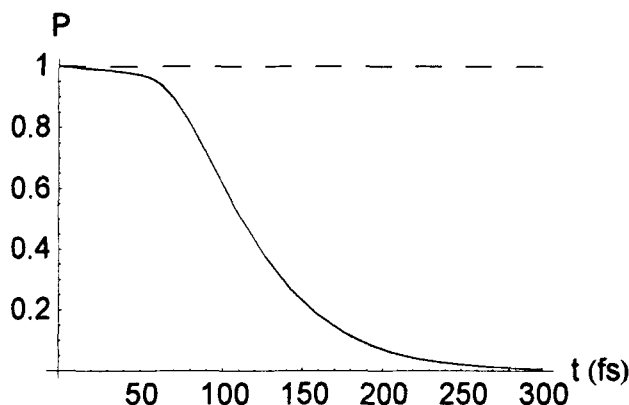


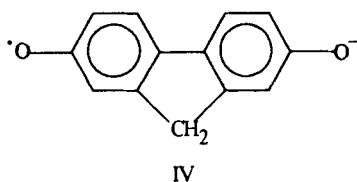
Figure 4

The above Fokker-Planck equation can be solved by linear algebraic methods, after making recourse to the matrix representation of the operator acting on the distribution function on the right hand side of eq. (23). For that purpose we made use of the same basis set as for solving the Schrödinger equation for the Hamiltonian in eq.(7). Due to the fact that all the operators (as well as the initial distribution) are even with respect to the inversion $\varphi \rightarrow -\varphi$ we may restrict our basis set to the normalized $\cos(n\varphi)$ functions with $n=0, 1, 2, \dots, N$. The proper dimension N is chosen following two criteria: i) the rate $k(\varphi)$ and the initial distribution $P_0(\varphi) = P(\varphi, t \approx 0)$ should be well represented and ii) the results of the computations should be stable with respect to the enlargement of the basis set. In our example we have taken $N=150$.

The continuous line in figure (4) shows the population of the excited adiabatic state as a function of time, at room temperature. It is now clear that now the possibility of dissipating the torsional kinetic energy gives rise to a true decay, which is very rapid with respect to the normal fluorescence lifetimes (from 0.1 to 1

nanosecond). We may then expect that molecules like (I) would prefer the radiationless route (internal conversion) for the decay.

As should be clear from the above example, the efficiency of internal conversion is related to the ability of the rings to give rise to large-amplitude librational motions, since according to our simple model, the initial excited wavepacket is placed far from the zone where non-adiabatic coupling is effective. One may then expect that structural modifications which tend to hinder the torsional motion might be also effective in altering the photo-physical behavior. Let us investigate, for example, the role of a bridge between the two aromatic rings created by σ bonds, like for example in IV:



We may maintain our simple two-state picture adding along the diagonal of the matrix (7) a potential energy term taking into account that when the torsion angle increases the σ bridge is stretched. For simplicity we treat this stretching as harmonic, with a force constant of 0.46 a.u. of energy (a.u. of length)⁻². The resulting adiabatic curves are reported in figure (5). It is evident that now the tendency to give an excited state with minimum at right angle is completely frustrated by the presence of the bridge joining the rings. The doorway state is now located in a region of minimum potential energy, and, during its time evolution, it is not able to reach the avoided crossing regions. As a consequence the population of the excited adiabatic state (dashed line in figure 4) remains essentially constant on the time scale studied here and one may expect that now the fluorescence will become the dominant decay channel. Hence, a change in the molecular structure which *a priori* could be judged of minor importance (especially due to the fact that we are discussing properties determined mainly by π electrons) results in a drastic variation of the photo-physical behavior.

The results presented here are only intended to draw the main lines of a general scenario concerning molecules in which the photon absorption leads to electron transfer between aromatic rings, which are essentially controlled by a torsional angle, like in biphenyl-like compounds. Another interesting class of systems which can be studied along the lines discussed here is that of pairs or even chains of mixed-valent transition metal ions bridged by an organic ligand like pyrazine or bipyridine [42-46], since the dependence of the intersite hopping term of the Hamiltonian on the orientation of the ring(s) introduces an important source of

electron-phonon coupling whose role is presently unknown. Of course reliable information on individual system can only be obtained through an accurate quantum chemical study, which should also include solvation effects, since one is dealing with charge transfer processes, to be confronted with experimental data. The present approach can be easily extended to include generic potential energy surfaces and coupling matrix elements. It appears highly suggestive, however, that a very simple basic model seems capable of explaining the behavior of a large class

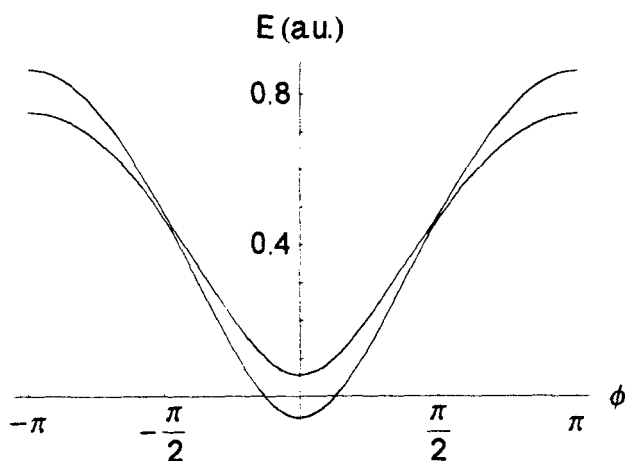


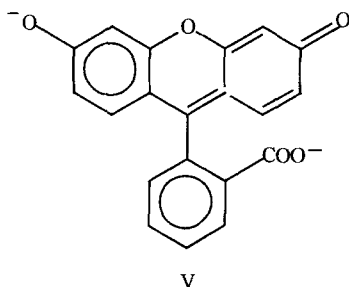
Figure 5

of compounds.

5. Concluding remarks

As a conclusion we mention an old problem for the solution of which one of us (A. L.) spent some time (with scarce success), when he was a young student, as a part of his work for obtaining the degree in Chemistry, under the guide of the person to whom this volume is dedicated. This concerns the striking different photophysical behavior of two similar species, which can be both considered as derivatives of the triphenyl-methane: the phenolphthalein (III) and the fluorescein dianions (V) [47]. As is well documented in the literature, the fluorescence quantum yield of the first excited singlet of the fluorescein ion is 1, while that of the phenolphthalein is essentially 0. We firmly believe that the very different efficiency of the radiationless decay channel of such molecules can be explained

along the lines sketched here, since, as is clear from a perusal of their structural formulas, the phenolphthalein is characterized by the possibility of large amplitude librational motions of the phenil rings that are not allowed in fluorescein. Of course this is only a working hypothesis that needs to be tested having at hands reliable computations of the electronic structure of the two molecules.



References

- [1] B. R. Henry and M. Kasha, *Ann. Rev. Phys. Chem.* 19, 161 (1968).
- [2] J. Michl and V. Bonačić-Koutecký, *Electronic Aspects of Organic PhotoChemistry* (John Wiley & Sons, New York, 1990).
- [3] M. Olivucci, I. N. Ragazos, F. Bernardi and M. A. Robb, *J. Am. Chem. Soc.* 115, 3710 (1993).
- [4] T. Patcher, L. S. Cederbaum and H. Köppel, in "*Advances in Chemical Physics*", vol. 84, 293 (Eds. I. Prigogine and S. A. Rice, John Wiley & Sons, New York, 1993).
- [5] W. Domcke and G. Stock, in "*Advances in Chemical Physics*", vol. 100, 1 (Eds. I. Prigogine and S. A. Rice, John Wiley & Sons, New York, 1997).
- [6] E. Teller, *J. Phys. Chem.* 41, 109 (1937).
- [7] G. Herzberg and H. C. Longuet-Higgins, *Discuss. Faraday Soc.* 35, 77 (1963).
- [8] G. W. Robinson, in "*Excited States*", vol. I, 1 (Ed. E. C. Lim, Academic Press, New York, 1974).
- [9] O. K. Rice, *Phys. Rev.* 33, 748 (1929).
- [10] O.K. Rice, *Proc. Nat. Acad. Sci. US.* 15, 459 (1929).
- [11] O. K. Rice, *Phys. Rev.* 34, 1451 (1929).
- [12] J. Jortner, S. A. Rice and R. M. Hochstrasser, *Advan. Photochem.*, 7, 149 (1969).
- [13] W. Rhodes, *J. Chem. Phys.* 50, 2885 (1969).
- [14] J. O. Berg, C. A. Langhoff and G. W. Robinson, *Chem. Phys. Letters* 29, 305 (1974).
- [15] P. Grigolini and A. Lami, *Chem. Phys.* 30, 61 (1978).

- [16] W. Siebrand, *J. Chem. Phys.* **44**, 4055 (1966).
- [17] S. H. Lin and R. Bersohn, *J. Chem. Phys.* **48**, 2732 (1968).
- [18] C. Amovilli and R. McWeeny, *Chem. Phys.* **198**, 71 (1995).
- [19] M. Maus and W. Rettig, *Chem. Phys.* **218**, 151 (1997).
- [20] F. Zhu, C. Galli and R. M. Hochstrasser, *J. Chem. Phys.* **98**, 1042 (1993).
- [21] F. W. Wise, M. J. Rosker and C. L. Tang, *J. Chem. Phys.* **86**, 2827 (1987).
- [22] W. Domcke and G. Stock in "*Advances in Chemical Physics*", vol. 100, 1 Eds. I. Prigogine and S. A. Rice, John Wiley, New York, 1997).
- [23] T. Kobayashi, Y. Takagi, H. Kandori, K. Kemnitz and K. Yoshihara, *Chem. Phys. Letters* **180**, 416 (1991).
- [24] K. Kemnitz, N. Nakashima and K. Yoshihara, *J. Phys. Chem.* **92**, 3915 (1988).
- [25] A. E. Johnson, N. E. Levinger, W. Jarzēba, R. E. Schlieff, D. A. V. Kliner and P. F. Barbara, *Chem. Phys.* **176**, 555 (1993).
- [26] P. J. Rossky, J. D. Simons, *Nature* **370**, 263 (1994).
- [27] H. Heitele, *Angew. Chem. Int. Ed. Engl.* **32**, 359 (1993).
- [28] Ch. Monte, A. Roggan, A. Subaris-Leitis, W. Rettig and P. Zimmermann, *J. Chem. Phys.* **98**, 2580 (1993).
- [29] A. Polimeno, A. Barbon, P. L. Nordio and W. Rettig, *J. Phys. Chem.* **98**, 12158 (1994).
- [30] D. Brown, P. M. Nordio, A. Polimeno and G. Saielli, *Chem. Phys.* **208**, 127 (1996).
- [31] G. Saielli, A. Polimeno, P. L. Nordio, P. Bartolini, M. Ricci and R. Righini, *Chem. Phys.* **223**, 51 (1997).
- [32] L. Seidner and W. Domcke, *Chem. Phys.* **186**, 27 (1994).
- [33] A. Ferretti, G. Granucci, A. Lami, M. Persico and G. Villani, *J. Chem. Phys.* **104**, 5617 (1996).
- [34] A. Ferretti, A. Lami and G. Villani, *J. Chem. Phys.* **106**, 934 (1997).
- [35] A. Ferretti, A. Lami and G. Villani, *J. Chem. Phys.* **107**, 3498 (1997).
- [36] G. Del Re, W. Förner, D. Hofman and J. Ladik, *Chem. Phys.* **139**, 265 (1989).
- [37] C. Zener, *Proc. Royal Soc. London*, **137 A**, 696 (1932).
- [38] L. D. Landau, *Phys. Z. Sov.* **2** (1932).
- [39] E. E. Nikitin and L. Zülicke, "*Theory of Chemical Elementary Processes*", (Springer-Verlag, Berlin 1978).
- [40] P. F. Barbara and W. Jarzēba, *Adv. Photochem.* **15**, 1 (1990).
- [41] N. G. van Kampen, "*Stochastic Processes in Chemistry and Physics*", (North-Holland, Amsterdam 1981).
- [42] A. Ferretti, A. Lami and G. Villani, *G. J. Phys. Chem.*, **101**, 9439 (1997).
- [43] A. Ferretti, and A. Lami, *Chem. Phys.* **186**, 143 (1994).
- [44] A. Ferretti, and A. Lami, *Chem. Phys. Lett.* **220**, 327 (1994).
- [45] A. Ferretti, A. Lami and G. Villani, *Inorg. Chem.* **37**, 2799 (1998).
- [46] A. Ferretti, A.; Lami, A.; M. J. Ondrechen, and G. Villani, *J. Phys. Chem.*, **99**, 10484 (1995); Erratum **100**, 20174 (1996).
- [47] A. Lami and G. Del Re, *La Chimica e L'Industria* **56** (5), 365 (1974).

Proton Assisted Electron Transfer

Mariangela Di Donato, Raffaele Borrelli, Amedeo Capobianco, Guglielmo Monaco, Roberto Improta, Meziane Brahimi,[†] and Andrea Peluso^{*‡}

Cattedra di Chimica Teorica, Università Federico II, via Mezzocannone 4, I-80134 Napoli, Italy.

Abstract

Likely mechanisms for long range electron transfer coupled to proton transfer are investigated. It is shown that, in model systems closely resembling realistic biochemical sequences, the injection of an electron on one end of the H-bonded chain can activate a sequential hopping of protons, which localizes the electronic charge on the opposite end of the chain. Once the additional electron is released to an outer electron acceptor species, then the initial situation is restored, but this time hydrogen atoms and not protons will move back to the original position, carrying the mobile electron from one side of the chain to the other. The dynamics of proton hopping in a model system where the two redox partners are *p*-monohydroquinone and xanthine, held together by H-bonds with a peptide bridge, shows that the process is fast, the transfer rate being of the order of a few picoseconds.

Introduction

About one decade ago, Del Re suggested that in certain biochemical systems long range electron transfer (ET) between two redox sites connected by a network of H-bonds may occur via a proton assisted mechanism.¹ Such a notion was probably ahead of its times, because, even though it was pointed out already in the sixties by Mitchell² and Onsager³ that proton translocation driven by ET could be a basic mechanism of energy conversion,⁴ experimental evidence available at that time was scarce to substantiate a microscopic mechanism. Nowadays, the notion that long range ET is coupled to proton transfer (PT) has acquired a wide popularity,^{5,6} especially after the determination of the X-ray crystal structures of bacterium photosynthetic reaction centers (RCs),⁷⁻⁹ and site directed mutagenesis experiments on RCs from *Rhodospseudomonas sphaeroides*.^{10,11} The discovery of water chains in the interior of protein backbone

[†] Permanent Address: Université des Sciences et de la technologie Houari Boumedienne BP 9, Dar-el-Beida, El-Alia, Algiers, Algeria.

[‡] Dipartimento di Chimica, Università di Salerno, I-84081 Baronissi, Salerno, Italy.

sphaeroides.^{10,11} The discovery of water chains in the interior of protein backbone of several biochemical energy transducers provides other evidence of the involvement of proton motion coupled to long range ET: a chain of 14 water molecules extending over 23 Å has been observed in the photosynthetic reaction center of *R. sphaeroides*,¹² in cytochrome *f*,¹³ and in the bacteriorhodopsin of *Halobacterium*.¹⁴ Remarkably, the determination of the changes accompanying the formation of charge separation in a photosynthetic reaction center has shown the presence, in the form crystallized under illumination, of a certain disorder which has been attributed to water movements concomitant to the formation of the charge separated state.¹⁵

Long chains of H-bonds can be characterized by a high proton mobility, as argued by Zundel, by IR spectroscopy,¹⁶ and confirmed by the evidence that in the channel of gramicidin A the dominant mechanism for proton transport is not the diffusion of the hydronium ion through the membrane channels, but probably proton hopping along H-bond chains which span the membrane.¹⁷ The high proton mobility of those polarizable H-bond chains is also expected to play an important role in the mechanism of long range ET in biochemical systems, but, actually, thirty years after the initial proposal, the mechanistic details of how PT can promote or assist long range ET are still unclear.

In this paper we will discuss a possible mechanism of proton assisted electron transfer (PA-ET). The essential idea is that the mobile electron, initially captured by or generated at site A, connected with its redox partner D by a H-bond chain, triggers a proton pump which gives rise to charge transfer (CT) from A, which takes a proton, to D, which releases a proton becoming negative. The CT process promoted by the proton pump activates D to release an electron to an external electron acceptor. Once D is again neutral, the initial situation has to be restored by switching the hydrogen atoms of the H-bond chain back to their initial positions. Since at that time a whole hydrogen atom (proton plus electron) is moving back an electron is physically transferred from A to D in this step.

The above PA-ET mechanism relies on the possibility of a temporary switching of the H-bond interface connecting the two redox sites and therefore one of the major problem is the proof that chemical events, such as oxidation or reduction at one site of the chain, can produce a driving force able to change the shape of the H-bond double well potential energy profile, inverting the most stable position of the H-bonded hydrogens (driving force). In this paper we will discuss the driving force problem on model systems, closely resembling realistic biochemical sequences. Several experimental studies attempting to clarify the role of PT in long range ET have been carried out on model systems, because of the high complexity of biological systems. Fitzmaurice *et al.* have designed and synthesized a few systems in which the electron-acceptor and donor groups are held together by a H-bond bridge, rigid enough that direct contact of the redox centers should be avoided. Injection of electrons by nano-electrodes, provokes

ET through the H-bond interface.¹⁸ Nocera *et al.* used salt bridges to create a H-bond interface between the acceptor and donor group. They found that ET proceeds through the proton interface, but with a significant attenuation of its rate with respect to that observed in systems with the same electron donor acceptor (EDA) pair, but connected by σ bonds.¹⁹ Hung *et al.* have synthesized a triad, consisting of an EDA pair and a proton donor group, in which ET is followed by rapid PT from the proton donor group to the electron acceptor group, which significantly stabilizes the charge separated state.²⁰ This is a particularly relevant result, because one of the most important problem in the artificial photosynthesis is the designing of supramolecular assemblies exhibiting long lived charge separated states. A few theoretical studies have been carried out on the possible involvement of PT in long range ET. Cukier has studied several model systems consisting of EDA pairs held together by a H-bond interface, such as those formed in carboxylic acid dimers.²¹ His results show that proton motion within the interface can influence the coupling between the two electronic states.²²

We will start by reviewing previous results of our group²³ which show that, in model systems consisting of supramolecular assemblies of H-bonded substructures, the arrival or departure of an extra electron can be sufficient perturbation to initiate the sequence of proton and/or hydrogen shifts, which give rise to charge transfer (CT) and then to ET from one end of the chain to the other. Then, we will discuss the dynamical features of PA-ET, by determining the time evolution of a certain distribution of vibrational states of the neutral system, after the injection of an extra electron has changed both the shape and the minimum energy position of the H-bond interface. Finally, we will briefly discuss preliminary results concerning the application of the PA-ET mechanism to a real system, *viz.* to photoinduced ET between primary and secondary quinone of the photosynthetic reaction center from *Rhodospseudomonas sphaeroides*.¹⁷

Proton assisted electron transfer

The general structure where PA-ET can take place in principle is a chain consisting of an *o*-electron acceptor A with n electrons, H-bonds, covalent bridges capable of tautomeric forms HP and PH, and an *o*-donor HD with m electrons. Here the prefix *o*, standing for "outer", indicates that A and D act as electron acceptor and donor with respect to some unspecified redox site, whereas they perform the opposite function with respect to one another.

The PA-ET mechanism involves the following succession of steps:

- 1) a negative charge is produced in the acceptor end A of the H-bond chain by the arrival of an electron from an outer electron donor (*o*ED) species;

- 2) A attracts an H-bond proton linked to the neighbouring site of the H-bond chain (P), so that its negative charge is transferred to that site, without change in the number of electrons of A;
- 3) a chain of proton shifts follows along the shortest hydrogen-bond peptide-bond chain connecting the acceptor A to the donor D, which becomes negative by losing the H-bond proton linked to it;
- 4) D yields an electron to an outer electron acceptor (oEA) to be reduced;
- 5) the reverse process (transfer of hydrogen by switching of the H-bonds) takes place, but this time hydrogen atoms and not protons move back to restore the original bond arrangement, carrying the mobile electron from A to D:

- 1) $oED^- + A \cdots H-P \cdots H-D \rightarrow oED + A^- \cdots H-P \cdots H-D$
- 2) $A^- \cdots H-P \cdots H-D \rightarrow A-H \cdots P^- \cdots H-D$
- 3) $A-H \cdots P^- \cdots H-D \rightarrow A-H \cdots P-H \cdots D$
- 4) $A-H \cdots P-H \cdots D + oEA \rightarrow A-H \cdots P-H \cdots D + oEA^-$
- 5) $A-H \cdots P-H \cdots D \rightarrow A \cdots H-P \cdots H-D$

Thus, the mobile electron initially captured by or generated at A can be transferred to D by H atoms after proton switching has made D negative and the latter has released an electron to an outer electron acceptor group.

As to the operation of the mechanism, the essential assumption is that under suitable conditions a hydrogen bridged system can behave as a bistable multivibrator, *i.e.* a system which, upon reception of a signal, will switch from its normal state *a*, *cf.* figure 1, to another stable state *b*, from which it will return to *a* upon reception of a second signal. The operation of the PA-ET mechanism is shown in figure 1: the input signal is the arrival of an extra electron at A, forming the unstable structure 1, the output signal is the release of an electron by D (structure 2). After an electron has been captured by A, which becomes negative, the double well profile sketched on the right of figure 1, which had the shape *r*, takes up the shape *l*, so that the right-hand minimum, where the proton is still localized, becomes higher in energy than the left hand one. Unless the free energy barrier is very high, after a time τ the proton will be found in the left-hand well and a negative charge will appear on D. As mentioned above, a completely similar process in the opposite direction and involving a whole hydrogen atom instead of a proton is expected as soon as D releases an electron to some external acceptor.

The PA-ET mechanism just described is formally plausible, since all the nuclear configurations involved in its steps obey to the formal rules of the valency. As mentioned above, a major problem is the proof that chemical events, such as oxidation or reduction, can produce the driving force for proton switching in a structure of the appropriate type. Such a problem is not easy to handle in a real system, especially because the electrostatic field of the protein backbone, which

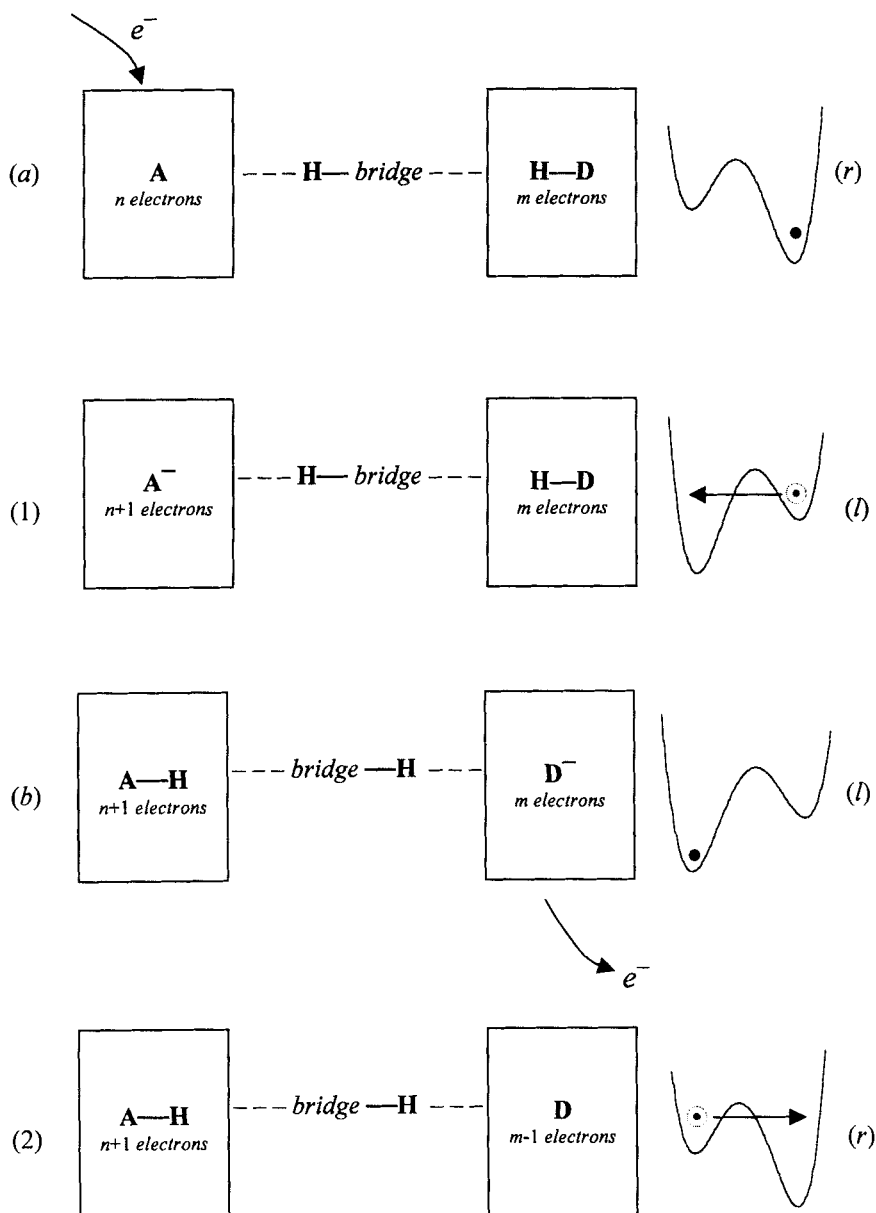


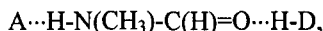
Fig1: The operation of PA-ET mechanism.

probably plays an important role, analogous to that of the solvent in outer sphere ET,²⁴ is difficult to model, due to the long range nature of the Coulomb interaction, and because of the large size of redox substructures involved in biochemical systems, often involving metal ions too. Therefore, the driving-force problem has been analyzed on model systems where the intermediate species are simple molecules not involving metal ions. The driving force problem can be recasted as follows: is it possible to find a molecular pair D and A, resembling simple biomolecules, such that a perturbation consisting of the arrival of an extra electron on one end of the chain will cause the H-bond protons to switch their positions, localizing the additional electronic charge on the opposite end?

Another important point concerns the effect of the H-bond chain connecting sites A and D. Of course, any molecule possessing two symmetric or degenerate tautomeric H-P and P-H forms is a suitable building block for it. However, structural considerations on multiheme cytochrome *c*₃ would suggest that a possible chain connecting the imidazole ligands of two iron-hemes should involve both peptide links and structural water molecules.^{1,25} The involvement of a peptide link is of particular interest, both because it is a very general bridge for biochemical systems and because it is a good model for strongly asymmetric proton interface, since its tautomeric form, *viz.* the hydroximine (imidol)²⁶ form, is a high energy intermediate, which, to our knowledge, has never been observed, either in the gas-phase or in solution. The latter observation does not rule out the possible involvement of a peptide link as appropriate unit of a PA-ET chain, because the hydroximine form is expected to be a transient structure with a short lifetime, so that the combination of short life and low concentration with respect to the normal amide form make its detection by standard techniques difficult. What really matters is the lifetime of the hydroximine intermediate. If the hydroximine form is a transient structure, it is sufficient that its lifetime is long enough to allow for the next proton shifts taking place. Recent inelastic neutron scattering (INS) study of polyglycine in the solid state would suggests that, in the crystalline state, where the amino protons form H-bonds with the C=O groups, the potential energy profile for proton motion between the N and O site is symmetric, so that the structure of the peptide unit is strictly intermediate between the keto form (HN-C=O) and the hydroximine form (N=C-OH).²⁶ That finding justifies the conjecture that a peptide link can be a possible H-bond bridge for PA-ET and legitimates further study on it.

The driving force for PA-ET

The problem of the driving force for PA-ET in EDA pairs connected by a chain of H-bonds has been recently studied by considering simple model systems of the type



which appears to embody all the critical features to be studied here.²³ For sake of completeness we will briefly review the results; details can be found in references 23.

As proton acceptor species we have considered the pyrimidinol (Pyr), the monohydroquinone (HQ) radicals and uracyl (Ur); a xanthine-like molecule (X) has been chosen as proton donor species. These systems have provided examples of small ($A = \text{Pyr}$), medium ($A = \text{Ur}$) and strong ($A = \text{HQ}$) driving force. Electron releasing and/or withdrawing substituents have then be introduced in order to determine to what extent the driving force for the CT steps can be chemically modulated, keeping the basic components of the chain fixed.²³

Let us start by considering the behaviour of a single H-bonded complex $A \cdots H-D$. In figure 2 are sketched the computed potential energy profiles for the neutral and negatively charged H-bond complexes formed by X with the three donor species mentioned above. If A is modelled (as in figure 2a) by a *p*-monohydroquinone radical, then the estimated energy difference between the ground states of $A \cdots H-D$ and $A-H \cdots D$ is $24.5 \text{ kcal mol}^{-1}$ in favour of the former at MNDO/PM3 level of theory. If an extra electron is injected on the *o*-acceptor group A, whose electronegativity is higher than that of D, the situation is reversed: the initial form $A^{\cdot-} \cdots H-D$ is less stable than the form $A-H \cdots D^{\cdot-}$ by $20.1 \text{ kcal mol}^{-1}$ at *ab initio* 6-31G** level with full geometry optimization ($19.5 \text{ kcal mol}^{-1}$ at PM3 level), and $21.5 \text{ kcal mol}^{-1}$ if the minimum energy geometry obtained by PM3 optimization is assumed in the *ab initio* computation.

The same behaviour is found if A is modelled by the pyrimidinol radical (figure 2b), uracyl (figure 2c), the latter being a closed shell system, and by several substituted pyrimidinol radicals.²³ As concerns the electronic distribution, the extra electron is localized on A before PT and on D after PT. The ionization potential of $D^{\cdot-}$ is significantly lower than that of D; the charge transfer process has roughly halved it, activating D to release an electron to an outer electron acceptor. Once that process has occurred, the system will be left in a high energy state, from which it relaxes to the lowest energy state by shifting the H-bond hydrogen (proton plus electron) back to its initial position. The latter step, which corresponds to ET from A to D, is expected to be very fast, because $A-H \cdots D$ is a high energy nuclear configuration for the neutral system, cf. figure 2.

Effect of a peptide bridge

The above energy analysis applies in its essential lines to all those cases where the A H-D pairs are connected by a H-bond interface whose building blocks are molecules capable of two nearly degenerate tautomeric forms. This is the case with chains formed by water molecules or hydroxyl groups, as discussed by Nagle

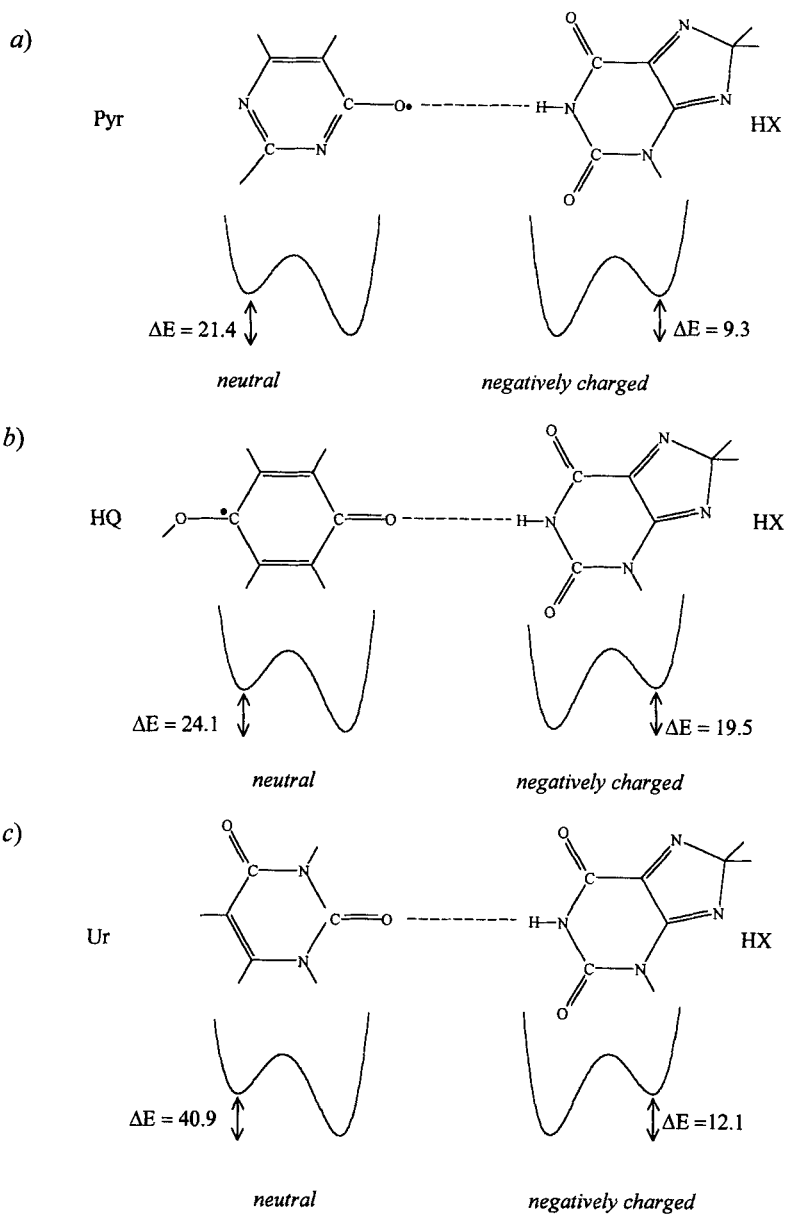


Figure 2. Changes of the potential energy profiles of selected H-bonded EDA pairs before (left) and after (right) injection of an electron on the “outer” electron acceptor species: (a) pyrimidinol-xanthine, (b) monohydroquinone-xanthine, and (c) uracil-xanthine.

and Morowitz,⁴ but also the case with polarizable H-bond chain, as discussed by Zundel.¹⁶

Let us now consider the same H-bonded complexes but with a peptide link, which will be modelled by N-methyl-formamide (NMF), connecting A to D. As mentioned above, the key point here is the effect of a nonsymmetrical covalent proton interface, whose tautomeric form P-H is significantly at higher energy than that of the normal form.

For the isomerization of NMF from the amide to the hydroximine form, *ab initio* computations with full geometry optimization give an energy difference of 13.3 kcal mol⁻¹ in favour of the amide form, whereas single point computations on the PM3 optimized structures yield an energy difference of 10.6 kcal mol⁻¹, always in favour of the amide form. Thus, if the driving force for PA-ET, *cf.* figure 2, is higher than 13 kcal mol⁻¹ there should be no problem concerning the lifetime of the imidol intermediate: the keto-enol isomerization will probably be the rate determining step of the whole ET process, but the hydroximine form will correspond to the lowest energy state of the charge relay system and therefore its lifetime will be long enough to allow D[•] to release an electron to its neighboring site in the redox chain. For a lower value of the driving force, or when several peptide links are involved in the H-bond chain connecting the two redox partners, the proton-shifted configuration will be a high energy intermediate, and then the question concerning its lifetime becomes of crucial importance.

The potential energy profiles for the negatively charged H-bonded A...H-D complexes of figure 2, but with an interposed peptide bridge are sketched in figure 3. As expected, the peptide bridge lowers the energy difference between the initial configurations and the proton shifted ones, but the latter ones are the most stable nuclear configuration for all the A species considered here.

The energy differences of figure 3 refer to MNDO PM3 computations, but *ab initio* computations on the system with A = *p*-monohydroquinone give very similar results: the energy of the CT state is now 12.1 kcal mol⁻¹ lower than that of the initial form with the negative charge localized on A. This result shows that the hydroximine form of the peptide link is stabilized in a H-bond environment with respect to the gas-phase, in line with the conjecture based on INS measurements.²⁶

Among the questions arising at this point one is particularly interesting and concerns the ability of a longer system of the type under discussion to behave efficiently as an electron wire. In order to answer to that question, the system of figure 4 has been considered.

The novelty is not only the greater length, but the presence of two structural water molecules in the H-bond interface. The energy variations accompanying each proton shift are shown in figure 4. The CT process is still exoergonic, the energy difference between the A[•]...H-bridge...H-D and the A-H...bridge-H...D[•] is 4.2 kcal mol⁻¹ in favour of the latter at PM3 level. Thus ET is

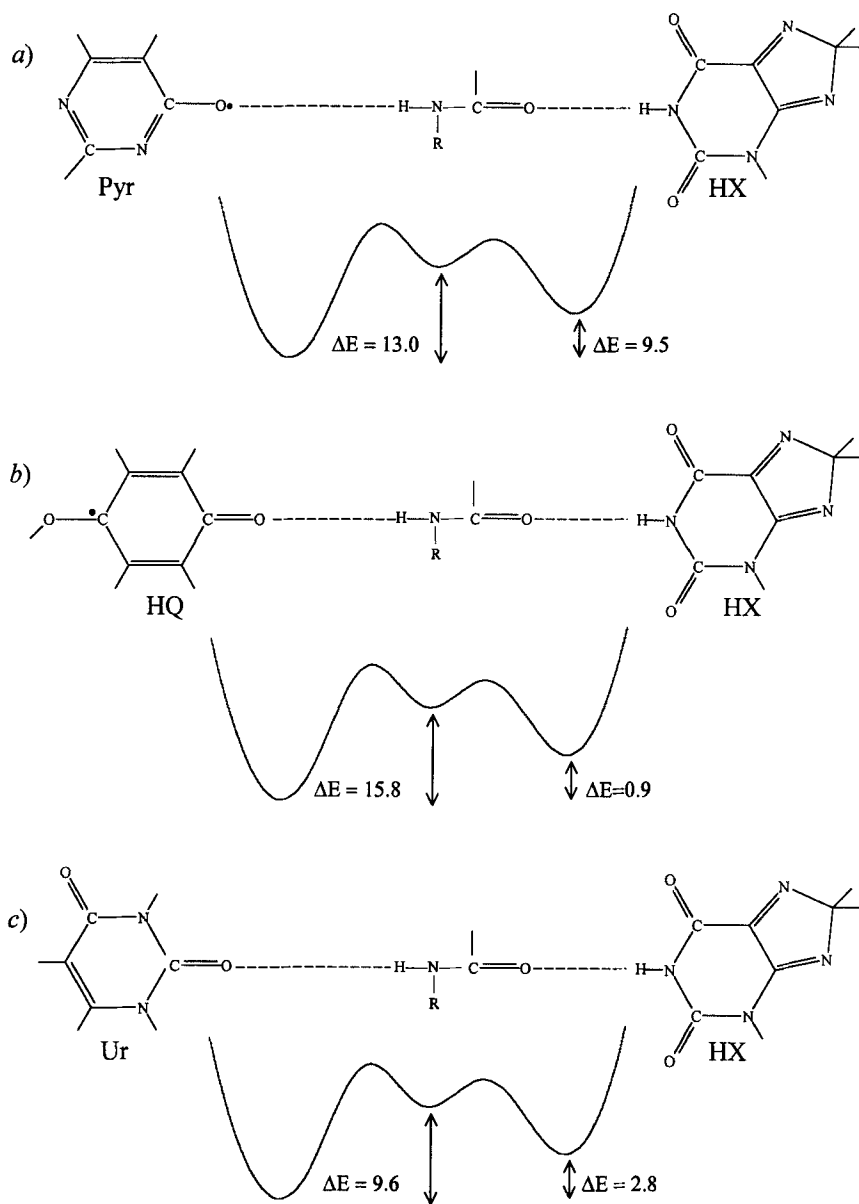


Figure 3. Schematic potential energy profiles of the same, negatively charged H-bonded EDA pairs but with an interspersed peptide link.

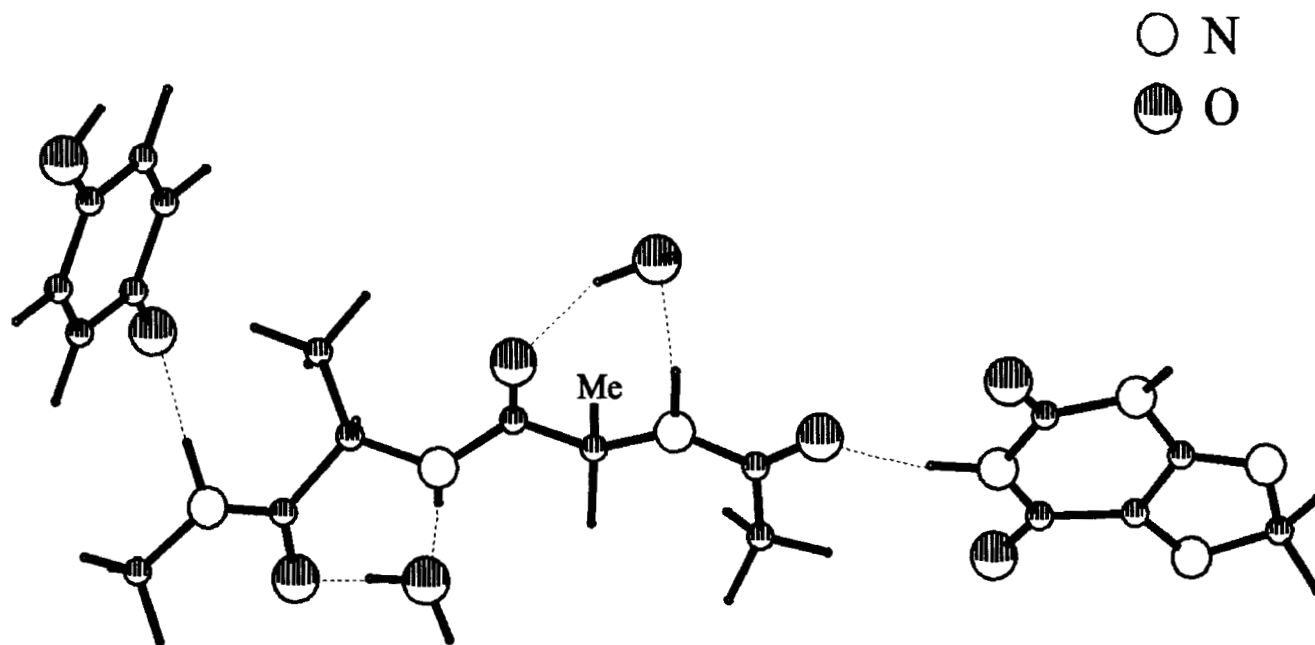


Figure 4. A chain consisting of five moieties: xanthine (on the right), a peptide bridge and two water molecules (in the center) and monohydroquinone (on the left). The energy variations accompanying each proton shift are: $+1.1 \text{ kcal mol}^{-1}$ ($A \cdots HP_1 \rightarrow AH \cdots P_1^-$), $+5.3 \text{ kcal mol}^{-1}$ ($P_1^- \cdots HP_2 \cdots HP_3 \rightarrow P_1H \cdots P_2H \cdots P_3^-$), $-0.8 \text{ kcal mol}^{-1}$ ($P_3^- \cdots HP_4 \cdots HP_5 \rightarrow P_3H \cdots P_4H \cdots P_5^-$), $-9.9 \text{ kcal mol}^{-1}$ ($P_5^- \cdots HD \rightarrow P_5H \cdots D^-$), where P_2 and P_4 are OH groups whose hydrogen atoms is not engaged in intra-chain bonding.

predicted to occur even in this rather unfavorable case, where the H-bond interface consists of three peptide units and therefore its tautomeric form is expected to be a very high energy intermediate.

Dynamical features of the PA-ET mechanism

The analysis of the potential energy surfaces of the systems of figure 3 has shown that CT takes place with a stepwise mechanism, in accordance with the observation that in the concerted mechanism the protons would pass simultaneously the corresponding energy barrier without any structural feature being stabilized at the same time. The first step is the shift of the nitrogen proton of the NMF, followed by the shift of the X one, which moves to the NMF oxygen. If the X proton moved first, it would yield the charge separated intermediate $\text{NMF-H}^+\cdots\text{D}^-$ and charge separation usually requires a lot of energy. The rate determining step of the whole process is the first PT. That is because it localizes the negative charge on the peptide bridge and the electron affinity of NMF is significantly lower than that of A and D, whose negative ions are both stabilized by resonance. As a consequence, in almost all the complexes, the first step is endoergonic, except for $\text{D} = \text{HQ}$, for which it is slightly exoergonic, whereas the second proton motion is always strongly exoergonic (*ca.* 12 kcal mol⁻¹), with usually a significantly lower barrier. Thus, in order to have a reasonable estimate of the kinetics of PA-ET, we will consider the first proton transfer with a higher accuracy, considering a two dimensional model for it, whereas we will use the results of the previous one-dimensional treatment^{23b} for the second PT, which does not affect significantly the transfer rates, being much faster. Computation have been carried out on the $\text{HQ}\cdots\text{NMF}\cdots\text{X}$ system.

The transfer of a light particle (H) between two heavy ones (X-Y) is a process which involves at least two large amplitude coordinates: the X-H or Y-H stretching coordinate and the X \cdots Y distance.²⁷⁻³³ In fact, the minimum energy path, the most important path for the thermally activated process, consists, in the transition state region, of the proton motion and approaches the region nearest to the two minima along the X-Y stretching coordinate.³⁴ The latter is important not only because it decreases the potential energy barrier for proton hopping, but because it modulates the distance between the two potential energy minima, and therefore the coupling between the vibrational wave functions associated with proton oscillations in the sites near X and Y. Thermal activation is not expected to play an important role in proton transfer reactions, since the potential energy barriers are usually high, at least of the order of tens of thermal quanta at room temperature.³⁵ Therefore, we will focus our attention on the Born transition probabilities for proton tunneling. We will adopt a two dimensional model taking as reaction coordinates the distance between the two heavy atoms (r_2) and the

rectilinear coordinate which straightly joins the two minima associated with the two bound sites of the moving proton (r_i). The contour plot of potential energy surface (PM3 computation) for the shift of the first proton from NMF to HQ as a function of the r_i and r_j coordinates is shown in figure 5.

The vibrational eigenstates have been computed variationally; the product of harmonic wavefunctions centered in both minima has been adopted as basis set. The Hamiltonian matrix has been computed by numerical integration using standard Hermite integration. The potential energy has been computed by PM3 method in each integration point. The kinetic couplings between the two modes have been neglected, on the grounds that the two coordinates are very similar to the Jacobi coordinates for a triatomic.³⁶

The computed eigenvalues and eigenvectors of the lowest vibrational states localized in either well have been reported in table 1.

Energy/eV	Eigenvectors
0.00000	$0.59 L_{0,0}\rangle - 0.47 L_{0,1}\rangle + 0.39 L_{0,2}\rangle + 0.29 L_{0,3}\rangle$
0.02282	$-0.54 L_{0,0}\rangle - 0.23 L_{0,2}\rangle - 0.34 L_{0,3}\rangle + 0.33 L_{0,4}\rangle$
0.04726	$-0.55 L_{0,1}\rangle - 0.24 L_{0,5}\rangle + 0.27 L_{0,6}\rangle - 0.26 L_{0,7}\rangle$
0.07322	$-0.41 L_{0,2}\rangle + 0.24 L_{0,3}\rangle - 0.21 L_{0,4}\rangle + 0.23 L_{0,8}\rangle$
0.09949	$-0.47 L_{0,2}\rangle - 0.20 L_{0,3}\rangle - 0.19 L_{0,4}\rangle - 0.28 L_{0,5}\rangle$
0.10534	$0.87 R_{0,0}\rangle + 0.30 R_{0,1}\rangle + 0.31 R_{0,2}\rangle + 0.16 R_{0,3}\rangle$
0.12814	$0.41 R_{0,0}\rangle - 0.56 R_{0,1}\rangle - 0.22 R_{0,2}\rangle - 0.36 R_{0,3}\rangle$
0.12836	$-0.19 R_{0,0}\rangle + 0.26 R_{0,1}\rangle + 0.10 R_{0,2}\rangle + 0.17 R_{0,3}\rangle$
0.14888	$0.63 R_{0,1}\rangle - 0.26 R_{0,2}\rangle - 0.34 R_{0,4}\rangle - 0.31 R_{0,6}\rangle$
0.15288	$0.49 L_{0,4}\rangle + 0.23 L_{0,7}\rangle - 0.19 L_{0,7}\rangle + 0.20 L_{0,9}\rangle$
0.16845	$-0.68 L_{0,2}\rangle - 0.23 L_{0,4}\rangle + 0.25 L_{0,7}\rangle + 0.21 L_{0,8}\rangle$
0.18821	$0.24 R_{0,3}\rangle - 0.45 R_{0,5}\rangle - 0.21 R_{0,8}\rangle - 0.14 R_{0,9}\rangle$
0.21567	$-0.53 R_{1,0}\rangle + 0.47 R_{1,1}\rangle - 0.35 R_{1,2}\rangle + 0.24 R_{1,3}\rangle$
0.30342	$0.81 L_{0,0}\rangle + 0.32 L_{1,1}\rangle + 0.31 L_{1,2}\rangle + 0.18 L_{1,3}\rangle$

Tab. 1: Selected vibrational eigenstates of the potential energy surface of figure 5. The first twelve are the lowest energy ones. $|L_{ij}\rangle$ and $|R_{kl}\rangle$ indicate Hermite basis functions localized on the left and right well, respectively; the subscripts refer to the quantum numbers on the r_i (i and k) and r_j (j and l) coordinates.

Then we have considered the time evolution of the vibrational wave packet prepared in the Boltzmann distribution with $T = 3000$ K, which roughly mimicks

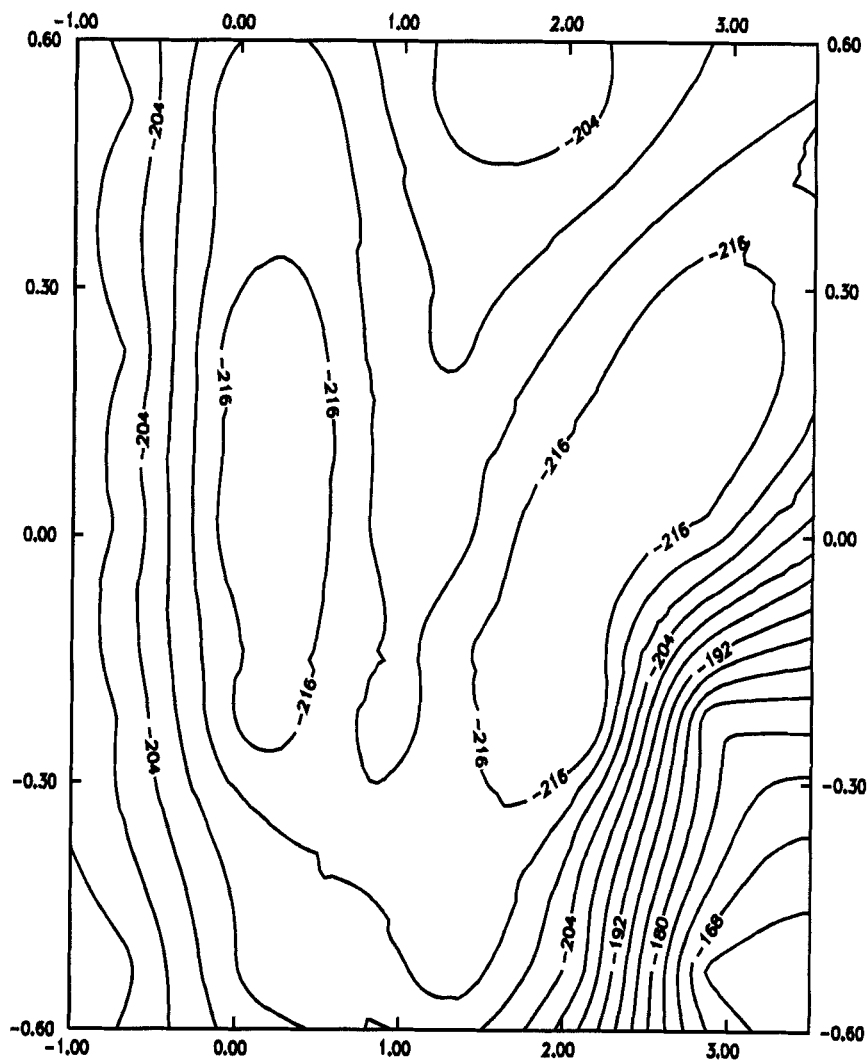


Figure 5. Contour levels of the potential energy of the NMF-monohydroquinone system as a function of r_1 ($-1.0 < r_1 < 3.5$) and r_2 ($-0.6 < r_2 < 0.6$) distances (bohr $\text{amu}^{1/2}$). For the definition of r_1 and r_2 see text.

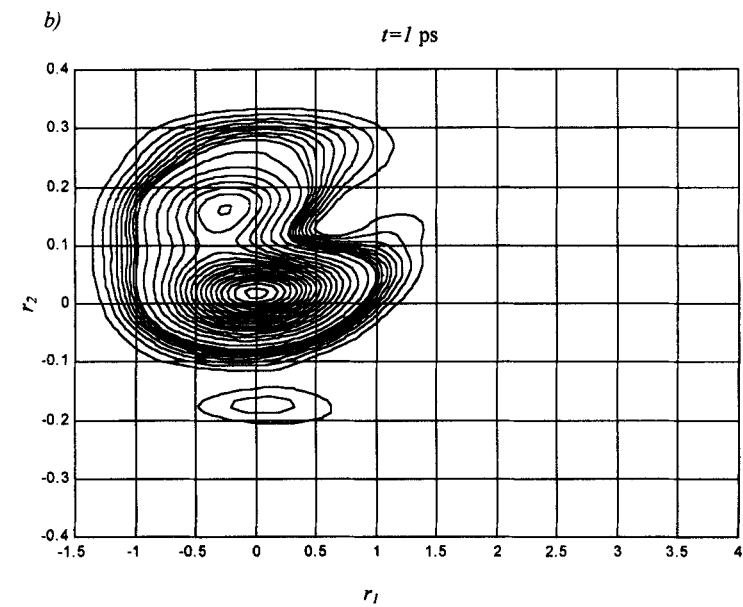
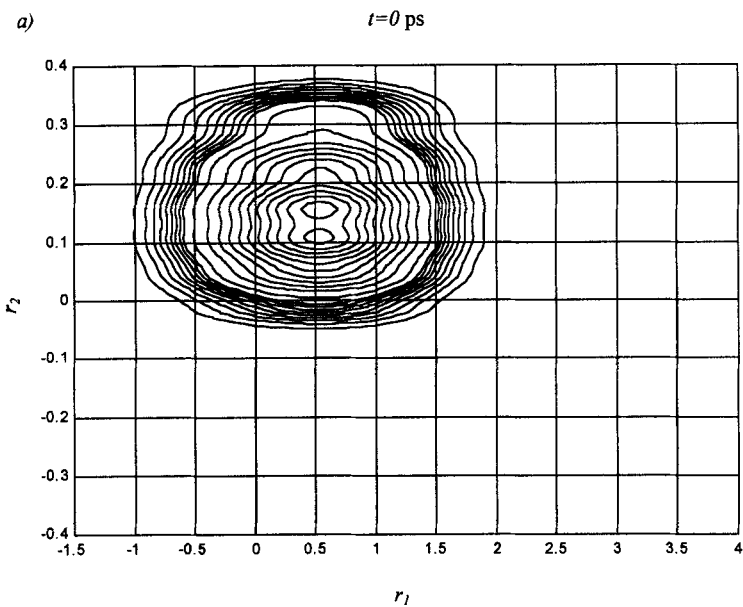
the vibrational wave packet which would be obtained by injecting an electron in the Boltzmann distribution with $T = 298$ K of the neutral HQ...NMF complex. The results are shown in figure 6. After *ca* 1 ps the initial wavepacket, *cf* fig. 7a, which is shifted with respect to the equilibrium position of the left-hand well of figure 6, is mainly localized in the minimum energy region of the left-hand well (7b), but with a non zero probability of finding the system at $r_2 = -0.5$ bohr amu^{1/2}. Until now the initial wavepacket has moved only on the low frequency coordinate r_2 , being localized in vibrational states corresponding to the left-hand well of figure 6 ($|L\rangle$) but for $r_2 = -0.5$ bohr amu^{1/2} the couplings with the vibrational states localized in the right-hand well of figure 6 ($|R\rangle$) becomes important and the $|R\rangle$ states begins to be populated ($t = 4$ ps). At $t = 10$ ps there is the maximum probability of finding the system in the other well (*cf* figure 7d).

The second proton transfer, from the xanthine ring to the NMF oxygen is faster. In that case, the motion over the r_2 coordinate is not important, because the two minima are much close each other and the energy barrier is significantly lower than that corresponding to the first proton transfer. The transition time evaluated with a simple one-dimensional model²³ is *ca.* 50 fs so that, after the first proton switches its position, the system will rapidly pass in a high excited vibrational state of the final state, from which it may either go back to the intermediate state and begin to oscillate between these two states, or decay to a lower vibrational state, redistributing the excess energy among the other vibrational degrees of freedom, being irreversibly trapped in the final state.

Application to a real system

As a first application to a real system, we will briefly discuss our preliminary results on electron transfer from the primary (Q_A) to secondary (Q_B) quinone in the photosynthetic reaction center of *Rhodopseudomonas Sphaeroides*. The crystallographic structure of the portion of system under consideration⁸ is shown in figure 7. Computations have been performed at PM3 level. In the optimization runs, the geometrical parameters governing the mutual orientations of each substructure with respect to the others have been kept fixed to their crystallographic values. The iron ion has been replaced by a zinc ion; it has been proven experimentally that this substitution slightly decreases the rate of ET.⁴⁰

The first step consists of the arrival of an extra electron on the right-hand quinone of figure 8 (Q_A). The presence of an extra electron on Q_A causes the shift of a proton from the histidine ligand which is H-bonded to the primary quinone to the oxygen of Q_A . This PT, which is significantly exoergonic (10.1 kcal mol⁻¹) and probably also very fast, localizes the negative charge on the imidazole ring H-bonded to the primary quinone. The next step is a rearrangement of the Zn-N interatomic distances, followed by a concerted motion of both hydrogen atoms (proton plus electron) engaged in the H-bonds connecting Q_A and Q_B to the



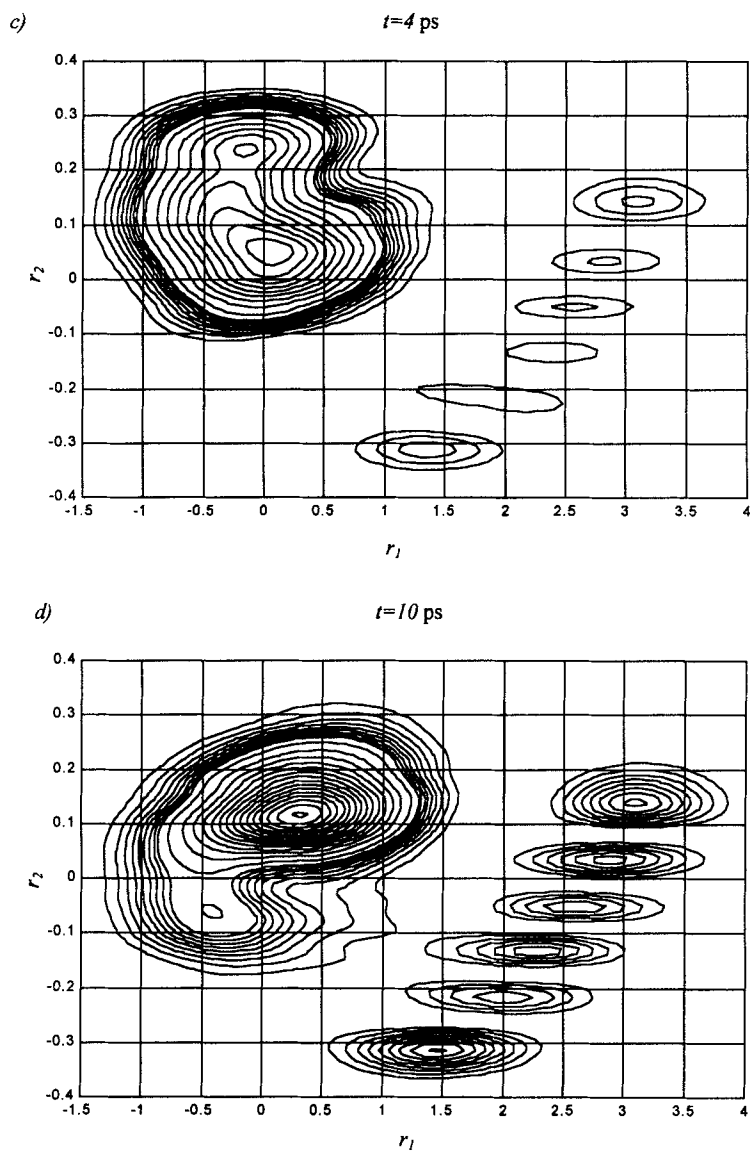


Fig. 6. Time evolution of the vibrational wave packet prepared in the Boltzmann distribution with $T=3000$ K

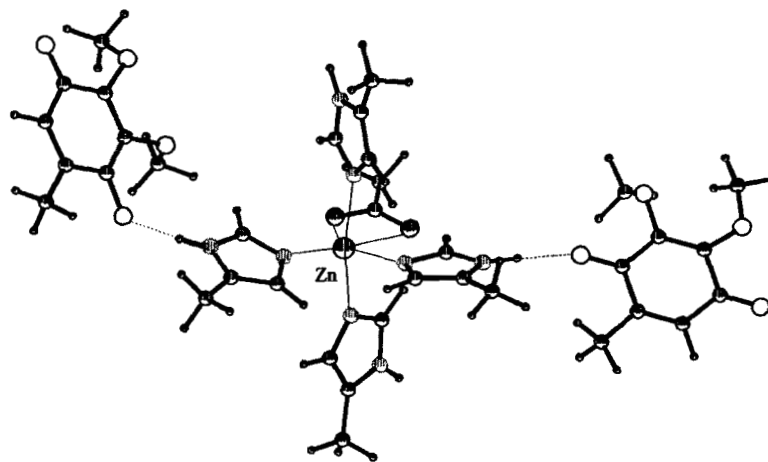


Figure 1. Portion of the photosynthetic reaction center of *Rhodospseudomonas Sphaeroides* including the primary (right) and secondary (left) quinones, with the histidine-Zn-histidine bridge (oxygen and nitrogen atoms in white and light gray, respectively) .

histidine ligands of the metal ion. That concerted motion bring the mobile electron from Q_A to Q_B . That step is slightly exoergonic (*ca.* 5.8 kcal mol⁻¹), due to the asymmetry around the metal center, and is also expected to be slow, in line with experimental results, which predict a ΔG of *ca.* 1.6 kcal mol⁻¹ for ET from Q_A^- to Q_B , with a transition time of the order of hundreds microseconds.⁴¹ Computations on the transfer of a second electron from from Q_A^- to Q_B are in progress; full details will be reported elsewhere.

Conclusions

We have discussed a microscopic mechanism for proton assisted electron transfer, which appears to be likely in systems closely resembling redox enzyme substructures. The mechanism applies well to the case of ET from primary to secondary quinone in photosynthetic reaction centers, but beyond that result, the existence of structures capable of sending an electron to one another *via* a H-bond-peptide link chain seems to be established, pending *ad hoc* experimental studies. The above results should be useful not only in attempts to understand selective long-range electron transfer in redox enzymes, but in the design of supramolecular assemblies exhibiting long lived charge separated states, a central problem in energy conversion.

Computational details

Energy estimates have been obtained both at *ab initio* and semiempirical MNDO PM3^{42,43}, using GAUSSIAN 94⁴⁴ and MOPAC⁴⁵ packages. UHF techniques have been employed for open shell systems. The standard 6-31G** basis set, which includes a set of *d* polarization functions and *p* diffuse functions on all the heavy atoms, and a set of *p* polarization functions on hydrogen atoms, has been adopted in the *ab initio* computations. Wherever not specified, the energy estimates refer to PM3 optimized structures. For the H-bridged complexes of figure 2 and 3 only the initial nuclear configuration has been fully optimized; for the other nuclear configurations both the valence and the dihedral angles which determine the mutual orientation of each block with respect to the others have been kept fixed to avoid large changes in the mutual orientations of the different subunits upon ET, which would be unrealistic in a real proteic system.

Acknowledgements

This paper is dedicated to Prof. G. Del Re on the occasion of his 65th birthday. We are thankful for his precious teaching, which has been of great importance to all of us.

The financial support of Italian CNR is gratefully acknowledged.

Bibliography

- [1] Del Re, G. *Spectroscopy of Biological Molecules*; Sandorfy, C.; Theophanides, T. ed.s Reidel, Dordrecht, 15; Del Re, G.; Peluso, A.; Minichino, C. *Can. J. Chem.* **1985**, 63, 1850.
- [2] Onsager, L. *Science* **1967**, 156, 541; *ibid* **1969**, 166, 1359-1364.
- [3] Mitchell, P. *Nature*, **1961**, 191, 144.
- [4] Nagle, J.F.; Morowitz, H.J. *Proc. Natl. Acad. Sci. USA* **1978**, 75, 298; Nagle J.F.; Mille, M.; Morowitz H.J. *J. Chem. Phys.*, **1980**, 72, 3959.
- [5] Cramer, W.A.; Knaff, D.B. In *Energy Transduction in Biological Membranes*; Springer-Verlag: New York, 1990.
- [6] Graig, M.S.; Paddock, M.L.; Bruce, J.M.; Feher, G.; Okamura, M.Y. *J. Am. Chem. Soc.* **1996**, 118, 9005-9016.
- [7] Deisenhofer, J.; Epp, O.; Miki, K.; Huer, R.; Michel, H. *J. Mol. Biol.* **1984**, 180, 385-398.
- [8] Allen, J.P.; Feher, G.; Yeates, T.O.; Rees, D.C.; Deisenhofer, J. *et al. Proc. Nat. Acad. Sci. USA* **1986**, 83, 8589-93.
- [9] Chang, C.H.; Tiede, D.; Tang, J.; Smith, U.; Norris, J.; Schiffer, M. *FEBS Lett.* **1986**, 205, 82-86.
- [10] Paddock, M.; Rongey, S.; Feher, G.; Okamura, M.Y. *Proc. Nat. Acad. Sci. USA* **1989**, 86, 6602-6.
- [11] Paddock, M.L.; McPherson, P.H.; Feher, G.; Okamura, M.Y. *Proc. Nat. Acad. Sci. USA* **1990**, 87, 6803-7; Takahasci, E.; Wright C.A. *Biochim. Biophys. Acta* **1990**, 1020, 107-11.
- [12] Baciou, L.; Michel, H. *Biochemistry* **1995**, 34, 7967.
- [13] Martinez, S.E.; Cramer, W.A.; Smit, J.L. Abstract published in: *Biophys. J.* **1995**, 68, A246.
- [14] Papadopoulos, G.; Dencher, N.; Zaccai, G.; Büldt, G. *J. Mol Biol.* **1990**, 214, 15.
- [15] Stowell, M.H.B.; McPhillips, T.M.; Rees, D.C.; Soltis, S.M.; Abresch, E.; Feher, G. *Science* **1996**, 276, 812.
- [16] Brzezinski B., Zundel G. *Faraday Discuss.* **1996**, 103, 363; Zundel G. In *Electron and proton transfert in Chemistry and Biology*; Muller, A.; Ratajaczaks, H., Ed.s; Elsevier: Amsterdam, 1990; pp 313-327.

- [17] Hille, B. *Ionic Channels of Excitable Membranes*; Sinauer Associates Inc.; Sunderland, MA, 1992.
- [18] Cusack, L.; Rizza, R.; Gorelov, A.; Fitzmaurice, D. *Angew. Chem. Int. Ed. Engl.* **1997**, *36*, 848; Cusack, L.; Nagaraja Rao, S.; Fitzmaurice, D.; *Chem. Eur. J.* **1997**, *202*; Marguerettaz, X.; Fitzmaurice, D.; *J. Am. Chem. Soc.*, **1994**, *116*, 5017.
- [19] Deng, Y.; Roberts, J.A.; Peng, S.; Chang, C.K.; Nocera, D.G.; *Angew. Chem. Int. Ed. Engl.* **1997**, *117*, 8051-2
- [20] Hung, S.C.; Alisdair, A.N.; Lin, S.; Liddell, P.A.; Seely, G.L.; Moore, A.L.; Moore, T.H.; Gust, D. *J. Am. Chem. Soc.* **1995**, *117*, 1657.
- [21] Zhao, X.G.; Cukier, R.I. *J. Phys. Chem.* **1995**, *99*, 945.
- [22] Cukier, R.I. *J. Phys. Chem.*, 1996, *100*, 15428.
- [23] Peluso, A.; Brahim, M.; Del Re, G. *J. Phys. Chem.* submitted; Del Re, G.; Brahim, M.; Peluso, A. *Chem. Phys. Lett.* submitted.
- [24] Marcus, R.A. *J. Chem. Phys.* **1956**, *24*, 966; Sumi, H.; Marcus, R.A. *J. Chem. Phys.* **1986**, *84*, 4894.
- [25] Pierrot, M.; Haser, R.; Frey, M.; Payan, F.; Astier, J.P. *J. Biol. Chem.* **1983**, *257*, 1431.
- [26] Kearley, G.J.; Fillaux, F.; Baron, M.H.; Bennington, S.; Tomkinson, J. *Science* **1994**, *264*, 1285.
- [27] Carrington, T., Miller, W.H. *J. Chem. Phys.* **1986**, *84*, 4364.
- [28] Shida, N.; Barbara, P.F.; Almlöf, J.A. *J. Chem. Phys.* **1989**, *91*, 4061.
- [29] Schnabel, U.; Gabriel, H. *Chem. Phys.* **1992**, *161*, 313.
- [30] Graf, F.; Meyer R.; Ha, T.K.; Ernst, R.R. *J. Chem. Phys.* **1981**, *75*, 2914; Meyer, R. Ernst, R.R. *J. Chem. Phys.* **1987**, *86*, 784; Stöckli A.; Meier B.H.; Kreis R.; Meier R.; Ernst R.R. *J. Chem. Phys.* **1990**, *93*, 1502.
- [31] Ruf, B.A.; Miller, W.H. *J. Chem. Soc. Faraday Trans. 2*, **1988**, *84*, 1523.
- [32] Sato N.; Iwata S. *J. Chem. Phys.* **1988**, *89*, 2932.
- [33] Sakun V.P.; Vener M.V.; Sokolov N.D. *J. Chem. Phys.* **1996**, *105*, 379.
- [34] Miller, W.H.; Ruf, B.A.; Chang, Y.T. *J. Chem. Phys.* **1988**, *89*, 6296.
- [35] Szczesniak, M.M.; Scheiner, S. *J. Chem. Phys.* **1982**, *77*, 4586; Scheiner, S.; Malgorzata, M.; Szczesniak, M.M.; Bigham, L.D. *Int. J. Quantum Chem.* **1983**, *23*, 739; Del Bene, J.E. *J. Phys. Chem.* **1988**, *92*, 2874.
- [36] Horn T.R.; Gerber R.B.; Ratner M.A. *J. Chem. Phys.* **1989**, *91*, 1813.
- [37] Nesbitt, D. J.; Field, R. W. *J. Phys. Chem.* **1996**, *100*, 12735.
- [38] Baskin, J. S.; Bañares, L.; Pedersen, S.; Zewail, A. H. *J. Phys. Chem.* **1996**, *100*, 12735.
- [39] Moore, J.W.; Pearson, R.G. *Kinetics and Mechanism*; J. Wiley & Sons: N.Y., 1981; Lewis, E.S.; Johnson, M.D. *J. Am. Chem. Soc.* **1960**, *82*, 5399.
- [40] Allen *et al.* *Proc. Nat. Acad. Sci. USA*, **1988**, *85*, 8491; Debus, R.J., Feher, G.; Okamura, M.Y. *Biochemistry* **1986**, *25*, 2276.

- [41] Moser, C.C.; Keske, J.M.; Warncke, K.; Dutton, P.L. In *Electron and proton transfert in Chemistry and Biology*; Muller, A.; Ratajaczaks, H., Ed.s; Elsevier: Amsterdam; pp 313-327.
- [42] Dewar, M.J.S.; Thiel, W. *J. Am. Chem. Soc.* **1977**, *99*, 4899.
- [43] Stewart, J.J.P. *J. Comp. Chem.* **1989**, *10*, 210.
- [44] GAUSSIAN 94, Revision C.2, Frisch, M.J.; Trucks, G.W.; Schlegel, H.B.; Gill, P.M.W.; Johnson, B.G.; Robb, M.A.; Cheeseman, J.R.; Keith, T.; Petersson, G.A.; Montgomery, J.A.; Raghavachari, K.; Al-Laham, M.A.; Zakrzewski, V.G.; Ortiz, J.V.; Foresman, J.B.; Cioslowski, J.; Stefanov, B.B.; Nanayakkara, A.; Challacombe, M.; Peng, C.Y.; Ayala, P.Y.; Chen, W.; Wong, M.W.; Andres, J.L.; Repogle, E.S.; Gomperts, R.; Martin, R.L.; Fox, D.J.; Binkley, J.S.; Defrees, D.J.; Baker, J.; Stewart, J.P.; Head-Gordon, M.; Gonzales, C.; Pople, J.A. Gaussian Inc., Pittsburgh PA, 1995.
- [45] Stewart, J.J.P. MOPAC95, *Quantum Chemistry Program Exchange*.

Lanczos calculation of the $\tilde{X}^2A_1/\tilde{A}^2B_2$ nonadiabatic Franck-Condon absorption spectrum of NO_2 ¹

Fabrizio Santoro and Carlo Petrongolo^a

*Dipartimento di Chimica, Università di Siena, Pian dei Mantellini 44,
I-53100, Siena, Italy.*

The nonadiabatic absorption spectrum of the $\tilde{X}^2A_1/\tilde{A}^2B_2$ conical intersection of NO_2 has been investigated by the Lanczos method. Within the Franck-Condon approximation, we have calculated both cold and hot intensities up to 22000 cm^{-1} , by using a nonorthogonal Hamiltonian and up to 14932 optimized molecular basis functions. We have checked the convergence of the spectrum with respect to the dimensions both of the molecular basis and of the Lanczos one, and we have compared the results of orthogonal and nonorthogonal Lanczos recursions between themselves and with those of conventional eigensolvers. We have employed the nonorthogonal Lanczos method for obtaining the levels and the intensities, and the orthogonal one for computing the expansion coefficients of the nonadiabatic states on the molecular basis. Therefore the advantages both of the nonorthogonal recursion and of the orthogonal one have been merged: we have calculated 1304 B_2 nonadiabatic levels and cold intensities up to 22000 cm^{-1} by the former, and we have assigned the \tilde{A}^2B_2 character of the vibronic bands up to 20300 cm^{-1} by the latter. The understanding of the conical-intersection effects in the NO_2 absorption spectrum has been improved by analyzing the individual nonadiabatic states, their Born-Oppenheimer main components, and the \tilde{A}^2B_2 Fermi polyads, by comparing cold and hot bands, and by finding the energy threshold for the beginning of the interactions between adjacent polyads. A statistical analysis of the spectrum confirms the irregular distribution of high-lying individual levels.

CONTENTS

I. Introduction

II. Method

A) Overview

B) Lanczos algorithm

III. Results

A) Convergence

B) Spectrum

IV. Conclusions

References

¹ Dedicated to Professor Giuseppe Del Re, on the occasion of his 65th birthday

^a Electronic mail: petro@carlo.icqem.pi.cnr.it

I. INTRODUCTION

The conical intersection between the \tilde{X}^2A_1 and \tilde{A}^2B_2 electronic states of NO_2 has a huge impact on its spectrum, from the \tilde{A}^2B_2 origin at 9734 cm^{-1} up to the first dissociation limit at 25129 cm^{-1} [1,2]: the number of bright B_2 cold bands is between one and two orders of magnitude larger than that expected by the Born-Oppenheimer (BO) approximation and the spectrum is much more irregular than that of the \tilde{A}^2B_2 vibrational progressions. Also the dynamical properties are strongly affected by this nonadiabatic interaction: the fluorescence lifetime increases by about a factor 100 and the \tilde{A}^2B_2 non radiative decay is very fast.

The recent and very accurate experiments of the Grenoble group [1] represent an exciting challenge for theorists involved in the development of quantitative models, which aim both at reproducing the frequencies and intensities of the NO_2 spectrum and at explaining the most important features of the \tilde{X}^2A_1 - \tilde{A}^2B_2 absorption system. We are engaged in this project since some years, and we have already investigated several aspects of the spectrum by employing an exact vibronic Hamiltonian, diabatic potentials, finite basis representations (FBR), and conventional eigensolvers, based on the Householder tridiagonalization [3-5].

Due to the strong anharmonicities of the potentials [3] and to the vibronic interactions, the convergence of the NO_2 levels is very slow and our previous spectrum [4] is therefore not fully converged above 17000 cm^{-1} . Moreover, the basis truncation errors of the states are larger and the strongest bands are above 17000 cm^{-1} [1,2]. By employing larger basis sets than that of Ref. 4, in this paper we check our previous results and extend the analysis of the high resolution spectrum towards its most dense and strong portion, up to 22000 cm^{-1} . The number of bands we are interested in is so large, that the dimensions of the molecular basis must be increased beyond the present limits of the Householder tridiagonalization [5]. We have therefore developed two versions of the Lanczos algorithm [5] which converge the levels up to 22000 cm^{-1} and allow to assign the nonadiabatic bands up to 20300 cm^{-1} .

II. METHOD

A. Overview

We have chosen a nonorthogonal bond lengths-bond angle vibronic Hamiltonian \hat{H} [6], which has a complicated kinetic term but gives the best convergence and assignment of the NO_2 spectrum. The nonadiabatic states $|n\rangle$ and levels E_n have been calculated by using diabatic electronic states $|e\rangle$ and two vibrational FBR,

$$|n\rangle = \sum_e \sum_s \sum_b |es_e b_e\rangle \langle es_e b_e | n\rangle \quad (1)$$

$$= \sum_e \sum_f |ef_e\rangle \langle ef_e | n\rangle, \quad (2)$$

$e = 1$ or 2 for \tilde{X}^2A_1 or \tilde{A}^2B_2 , respectively,

$$0 \leq s_e \leq NS_e, \quad 0 \leq b_e \leq NB_e, \quad 0 \leq f_e \leq (NS_e + 1)(NB_e + 1) - 1,$$

where $|s_e\rangle$ and $|b_e\rangle$ are optimized stretching and bending functions of $|e\rangle$, $|f_e\rangle$ are BO vibrational eigenstates of the effective Hamiltonian $\langle e | \hat{H} | e \rangle$, and the dimensions of the basis sets are equal [3].

The $|n\rangle \leftarrow |g\rangle$ absorption intensities have been calculated at some temperatures T for the lowest nonadiabatic states $|g\rangle$ of A_1 symmetry, namely the \tilde{X}^2A_1 (0,0,0), (0,1,0), (1,0,0), and (0,2,0) levels, which give rise to the cold and hot spectrum, respectively. The excited levels are at 760, 1331, and 1513 cm⁻¹ above the zero point energy value and the absorbing states are nearly unperturbed by the nonadiabatic couplings, which begin above 9500 cm⁻¹ [3]. They are thus very well described by their main BO components $|1g_1\rangle$, where $|1\rangle$ is the \tilde{X}^2A_1 electronic species and $|g_1\rangle$ are its BO vibrational functions. The spectral and dynamical properties depend on the electric-dipole matrix elements $\langle n | \mu | g \rangle$, and therefore on the doorway states $|d_g\rangle$

$$|d_g\rangle = \mu |g\rangle / \langle \mu g | \mu g \rangle^{1/2} = \mu |1g_1\rangle / \langle \mu 1g_1 | \mu 1g_1 \rangle^{1/2} = |2g_1\rangle, \quad (3)$$

where we have used the Franck-Condon (FC) approximation and $|2\rangle$ is the \tilde{A}^2B_2 electronic species. The states $|2g_1\rangle$ have been expanded in both the $|2s_2b_2\rangle$ and $|2f_2\rangle$ FBR of Eqs. (1) and (2), and are of B_2 symmetry. Only transitions to B_2 nonadiabatic states $|n\rangle$ are then allowed, in agreement with the ICLAS measurements [7] which have observed only B_2 bands above 11200 cm⁻¹. By labelling the A_1 or B_2 symmetries as $+$ or $-$, respectively, the nonadiabatic absorption intensities are then proportional to

$$I_{ng} = (E_n^- - E_g^+) |\langle n^- | d_g^- \rangle|^2 \exp(-E_g^+ / k_B T), \quad (4)$$

which are here reported in hartree.

B. Lanczos algorithm

The use of very large dimensions excludes the implementation of conventional eigensolvers, based on the Householder tridiagonalization, which requires the explicit calculation of the Hamiltonian matrix \mathbf{H} and its full storage in core memory. We have then self-developed FORTRAN codes which implement the Lanczos algorithm, with and without the full Householder reorthogonalization of the vectors [5]. By starting from a normalized state $|L_1\rangle$, this method generates recursively a basis $|\mathbf{L}\rangle$ of dimensions M and a tridiagonal matrix \mathbf{T}_M , which in exact arithmetics is the orthogonal projection of \mathbf{H} onto the subspace spanned by the vectors $|\mathbf{L}\rangle$. The matrix \mathbf{T}_M is then diagonalized by standard techniques and its eigenpairs are approximations of those of \mathbf{H} .

The state $|L_1\rangle$ is only sequentially coupled to the other ones and the main spectral and dynamical properties are thus well reproduced by Lanczos representations which are much smaller than the molecular one, though they approximate in a satisfactory manner only a very small fraction of the eigenvalues of \mathbf{H} . By employing large Lanczos expansions, the method becomes a powerful tool for obtaining a large number of eigenpairs of \mathbf{H} . Nevertheless, the generated vectors become nonorthogonal (sometimes even linearly dependent) after few iterations, owing to the computer finite precision, and one then obtains spurious eigenvalues and multiple copies of the correct ones. We have dealt with the orthogonality problem by following Lami and Villani (LV) [8] and Cullum and Willoughby (CW) [9], and the spectrum has been calculated according to Heller *et al.* (HKC) [10] and to Wyatt and Scott (WS) [11].

LV have reorthogonalized each new Lanczos vector with respect to all the previous ones with the Householder algorithm [5], which can be easily and safely employed for the calculation of the expansion coefficients of the eigenstates on the molecular basis. However, the orthogonal Lanczos algorithm may become very costly when a large number of converged eigenvalues is required and very large basis sets are then employed. In this case, we follow CW who do not reorthogonalize the vectors but have introduced some severe tests for identifying the good eigenvalues, based on the comparison of the eigenvalues of the \mathbf{T}_M and \mathbf{T}_{M-1} tridiagonal matrices, where the latter derives from the former by deleting the first row and column. By computing the last row $\langle L_M | n \rangle$ of the eigenvector matrix of \mathbf{T}_M , CW also estimate the convergence errors of the good single eigenvalues, the multiple ones being considered converged.

HKC have calculated the spectrum of Eq. (4) by simply starting the Lanczos recursion with the doorway state $|d_g\rangle$; therefore the scalar product $\langle n | d_g \rangle$ are just the components of the first row $\langle L_1 | n \rangle$ of the eigenvector matrix of \mathbf{T}_M . Finally, WS have diagonalized \mathbf{T}_M by a modified QL algorithm which computes only the first row of the eigenvector matrix, with a remarkable gain in CPU time and storage requirements. We have implemented this techniques in our codes both for the first and for the last eigenvector row, because we have employed the latter in

the CW estimate of the eigenvalue convergence errors, which have been further calculated by increasing the dimensions of the Lanczos basis. According to WS, the application of the CW tests can be avoided, realizing that spurious eigenvalues do not contribute to the spectrum and summing the contributions of the multiple copies of a good eigenvalue. We have followed their latter suggestion but we have retained the CW tests for a trustworthy identification of the spurious eigenvalues.

By using a large $|es_e b_e\rangle$ basis, we have obtained in this way a large number of levels, which are converged within 10^{-3} cm⁻¹ with respect to the number of Lanczos states. This direct calculation of the spectrum is very efficient but has a non-negligible cost: we do not know the eigenvectors on the molecular basis, because this calculation requires a huge amount of CPU and storage resources. The eigenvectors are however very useful for assigning the spectrum and for computing other state-dependent properties; therefore, they have been calculated by using a smaller $|ef_e\rangle$ basis and the orthogonal Lanczos eigensolver.

The rate limiting step of the Lanczos recursion is the matrix-vector product $|P_i\rangle = \hat{H}|L_i\rangle$ which must be carried out at each step i . By working with small basis sets, we have employed both the $|es_e b_e\rangle$ and $|ef_e\rangle$ representations of Eqs. (1) and (2), respectively. The latter diagonalizes the **H** blocks of the two electronic states, and the matrix-vector product is thus greatly simplified. Nevertheless, the calculation of all the BO states $|f_e\rangle$ becomes too costly by increasing the basis dimensions, and we have thus implemented a direct algorithm in the $|es_e b_e\rangle$ representation, without explicitly calculating and storing the matrix **H**, which is equal to

$$\begin{aligned} \langle e's'_e b'_e | \hat{H} | es_e b_e \rangle &= \delta_{e'e} \langle s'_e b'_e | \sum_{\alpha=1}^5 \hat{T}_{\alpha}^{str} \hat{T}_{\alpha}^{bnd} + V_{ee} | s_e b_e \rangle \\ &+ (1 - \delta_{e'e}) \langle s'_1 b'_1 | V_{12} | s_2 b_2 \rangle, \end{aligned} \quad (5)$$

where \hat{T}_{α}^{str} and \hat{T}_{α}^{bnd} are stretching and bending kinetic operators, respectively [6], labelled by α and $V_{e'e}$ are the diabatic potentials. The kinetic and the potential terms give respectively the product components

$$\langle s'b'|P_i\rangle^T = \sum_s \sum_{\alpha} \langle s' | \hat{T}_{\alpha}^{str} | s \rangle \left(\sum_b \langle b' | \hat{T}_{\alpha}^{bnd} | b \rangle \langle sb | L_i \rangle \right), \quad (6a)$$

$$\langle s'b'|P_i\rangle^V = \sum_k \sum_s \langle s'|V_k|s\rangle \left(\sum_b \langle k|b'\rangle \langle k|b\rangle \langle sb|L_i\rangle w_K \right), \quad (6b)$$

where we have omitted for simplicity the electronic labels, k runs on M_3 bending integration points, and w_k are the corresponding integration weights. By carrying out sequentially [12] the operations of Eqs. (6), the first requires about $10m^3$ flops and the latter about $2m^4$, where m is the average value of M_3 , NS_1 , NB_1 , NS_2 and NB_2 . This flop count is about one order of magnitude smaller than that corresponding to the explicit calculation of \mathbf{H} . We have used $M_3 = 110$ and thus the main cost is due to the calculation of the potential terms, and does not change by using orthogonal coordinates which simplify the kinetic operator. Moreover, some tests with the Radau Hamiltonian have shown that the level convergence with the basis dimensions is much slower than that of the present Hamiltonian.

III. RESULTS

A. Convergence

The absorption spectrum has been calculated with three molecular basis sets which are labelled as $N [(NS_1+1) \times (NB_1+1) + (NS_2+1) \times (NB_2+1)]$, where N is the number of basis functions and NS_e and NB_e are defined in Eqs. (1) and (2). We have used a small basis 6117 ($111 \times 36 + 101 \times 21$) for comparing the results of orthogonal and nonorthogonal Lanczos eigensolvers with those of the conventional ones, for computing the hot spectra, and for assigning the states. The convergence of the levels with respect to N has been checked with an intermediate basis 10682 ($161 \times 46 + 126 \times 26$). Finally the cold B_2 spectrum has been calculated with a large basis 14932 ($201 \times 51 + 151 \times 31$). The nonorthogonal Lanczos recursion has been stopped when about a 20% increase of the number M of the Lanczos vectors and the CW [9] estimate have shown that all the levels are stable within 10^{-3} cm^{-1} . The two checks are qualitatively different and usually give the same convergence. However, the former is more robust and the latter can be misleading. Sometimes, at a given M , some levels corresponding to states very poorly represented in the starting vector are completely missing in the energy range of CW fully converged eigenvalues, whereas they appear by pursuing the recursion (see also below). This finding has been already pointed out by CW who dealt with it by implementing further checks in their routines. Sporadically, the CW tests still assign a large convergence error to few eigenvalues, whereas all the levels are well stable with respect to M .

Table I and Fig.1 report some convergence results with respect to M and to the ratio M/N : NE_{LOW} and NE are the numbers of lowest and total stable levels, respectively, within 1 cm^{-1} , and NE_{TOT} is the total number of levels up to 22000 cm^{-1} . With $N = 6117$, 5000 orthogonal Lanczos vectors give 1272 levels E_n and states $|n\rangle$ which are identical to those obtained by the Householder

TABLE I. Convergence of the B_2 levels up to 22000 cm⁻¹.

M	6117, orthogonal		6117, nonorthogonal		14932, nonorthogonal	
	NE_{LOW}	NE	NE_{LOW}	NE	NE_{LOW}	NE
3000	651	830				
4000	985	1134				
5000	1272	1272	335	559		
10000			531	1017	219	681
20000			779	1271	845	1148
25000			1272	1272	1100	1263
30000					1304	1304
35000					1304	1304

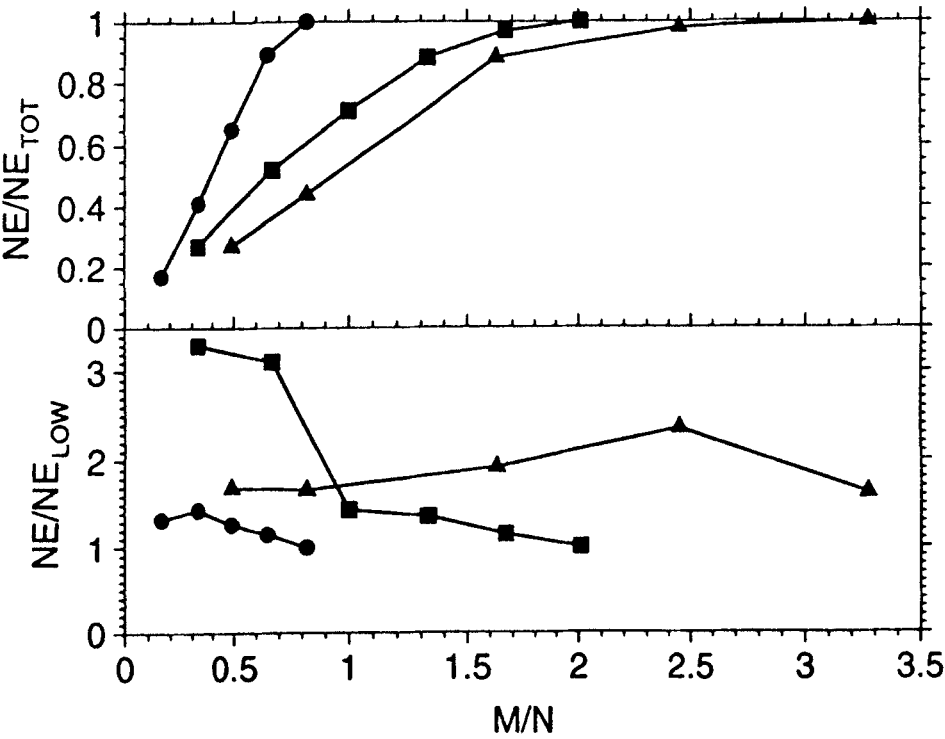


FIG. 1. Level convergence with respect to the ratio of the Lanczos dimensions M to the molecular ones N : NE_{LOW} and NE are the numbers of lowest and total stable levels, respectively, within 1 cm⁻¹, and NE_{TOT} is the total number of levels up to 22000 cm⁻¹. Basis 6117 orthogonal with circles, basis 6117 nonorthogonal with triangles, and basis 14932 nonorthogonal with squares.

tridiagonalization. As expected, the orthogonal recursion converges faster and more regularly than the nonorthogonal one. In the first case, the ratio NE/NE_{TOT} increases nearly linearly with M/N , and the ratio NE/NE_{LOW} is nearly equal to 1 during the recursion, showing a steady increase of the number of the lowest converged levels. The nonorthogonal method is slower, by requiring about 25000 or 31000 Lanczos states for converging 1272 or 1304 levels, within 10^{-3} cm^{-1} , with the bases 6117 or 14932, respectively. Nevertheless, the computation cost of the nonorthogonal recursion with the basis 6117 is just 35 % greater than that of the orthogonal one, owing to the smaller operation count per iteration. On the whole, the nonorthogonal algorithm is more depending on the initial state and on the local level density: NE/NE_{TOT} is not linear with respect to M/N , NE/NE_{LOW} may be remarkably larger than 1 and irregular, and it is very difficult to obtain levels E_n which correspond to very small components $|\langle L_1 | n \rangle|$ of the starting Lanczos vector. For example, the states 532 and 780 of the 6117 basis and the state 220 of the 14932 basis appear only for a very large number of Lanczos vectors because they have $|\langle L_1 | n \rangle| < 10^{-5}$.

Table II reports the maximum convergence errors of the levels with respect to the number N of the molecular basis functions.

TABLE II. Maximum convergence errors δ of the levels of the 6117 and 10682 bases with respect to the 14932 one. Energies in cm^{-1} .

basis	max δ up to						
	10000	12000	14000	16000	18000	20000	22000
6117	1.4	3.6	6.0	10.4	11.2	47.1	153.1
10682	0.4	0.8	1.1	1.8	1.8	4.3	19.8

As the maximum error, also the mean one increases with the energy, and is equal to 5.6 cm^{-1} between 20000 and 22000 cm^{-1} with the 10682 basis. By increasing N from 6117 to 10682, the largest error is reduced by about a factor 8, and we then estimate that the large 14932 basis should have converged even the highest levels at 22000 cm^{-1} within 3-4 cm^{-1} . Finally Fig. 2 shows the Gaussian convolutions of two stick spectra above 21000 cm^{-1} . The convolutions have been calculated with the nonorthogonal Lanczos method, with $N = 14932$ and $M = 35000$ or with $N = 6117$ and $M = 600$, and with half width at half maximum (HWHM) equal to 62.5 cm^{-1} . Note that the latter computation gives just 78 converged eigenvalues within 1 cm^{-1} .

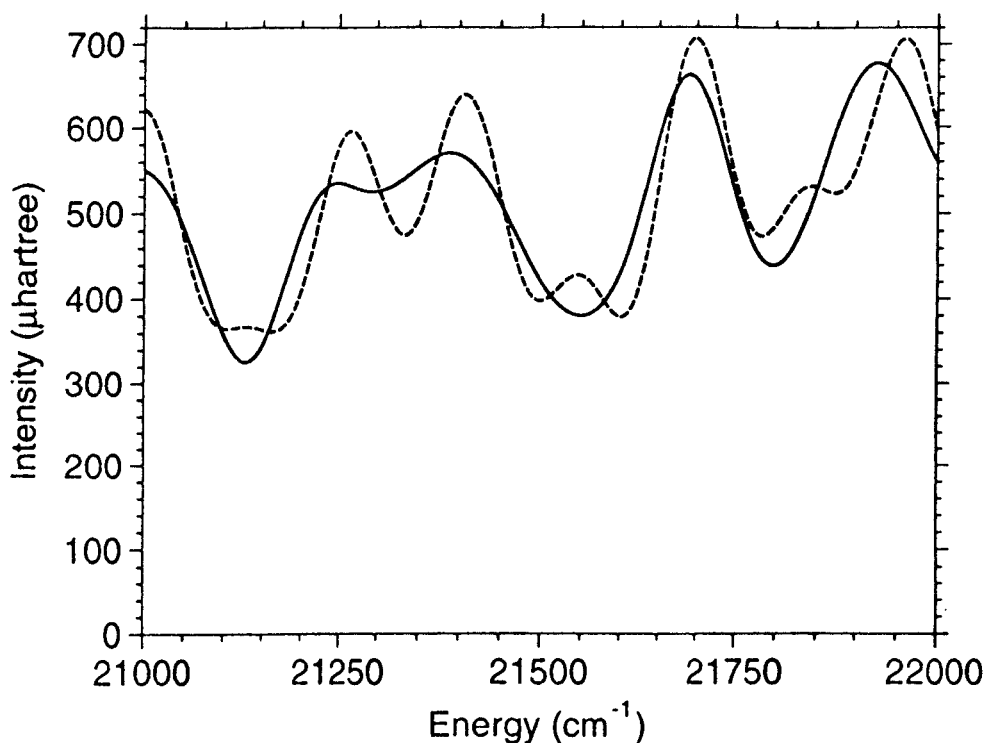


FIG. 2. Energy range 21000 - 22000 cm⁻¹. Gaussian convolution of the spectrum with HWHM = 62.5 cm⁻¹ and nonorthogonal Lanczos. Full line: $N = 14932$ and $M = 35000$; dashed line: $N = 6117$ and $M = 600$.

The two convolutions compare well enough, even in this high energy range (the agreement at lower energies is better), thus confirming that small molecular and Lanczos bases give acceptable low-resolution spectra. Of course, the orthogonal Lanczos results corresponding to $N = 6117$ and $M = 5000$ agree much better with those of the 14932 basis. These results show that the 6117 basis can be used to assign correctly strong nonadiabatic bands.

B. Spectrum

The absorption spectrum depends mainly on the different equilibrium geometries of the electronic states, which give rise to a very long \tilde{A}^2B_2 symmetric stretch-bending

TABLE III. Energy ranges, number of corresponding cold and hot bands stronger than I_{thr} , and \tilde{A}^2B_2 polyad features. Energy in cm^{-1} and intensity in $\mu\text{hartree}$.

Energy range	number of bands cold	hot	I_{thr}	ν	1st-last band	n_{max} ^a	E_{max}	I_{max}	\tilde{A}^2B_2
9500-13000	21	15	0.02	3	11727-11942	170*	11917	0.08	0,4,0*
13000-14500	6	1	0.8	4	12413-12693	170	12672	0.36	0,4,0
14500-15700	8		2.5	5	13394	207	13394	1.0	1,3,0
15700-17100	15		10	6	13924-14228	250	14105	3.5	1,4,0
17100-18100	14		15	7	14530-14818	298	14818	11	1,5,0
18100-19250	14		30	8	15350-15623	354	15550	11	1,6,0
19250-20250	15		50	9	15934-16284	407	16145	23	2,5,0
20250-22000	27		75	10	16637-17013	479	16871	19	2,6,0
				11	16890-17859	555	17563	62	2,7,0
				12	17581-18574	621	18090	124	3,6,0
				13	18557-19243	718	18812	276	3,7,0
				14	18292-19762	825 ^b	19516	305	3,8,0
				15	19667-	903	19972	292	4,7,0

^a A star labels a hot band from \tilde{X}^2A_1 (0,1,0) at 300 K.

^b Bands 825 and 826.

progression, and on the \tilde{A}^2B_2 (v_1, v_2, v_3) Fermi resonances, which cluster the bands in polyads corresponding to the quantum number $\nu = 2v_1 + v_2 + 2v_3$ [4]. We report in Table III a summary of the spectrum: the number of cold and hot bands stronger than some intensity thresholds I_{thr} in different energy ranges, the first and the last band of each polyad with $I_{ng} \geq I_{thr}$, and the corresponding intensity maxima with their \tilde{A}^2B_2 assignments. The spectrum up to 22000 cm⁻¹ is presented in Table IV, where the hot bands refers to the \tilde{X}^2A_1 (0,1,0) or (0,2,0) state at 300 K, are labelled as * or **, respectively, and are by far more intense than the hot ones due to other \tilde{X}^2A_1 species. Fig. 3 shows the stick bands, their \tilde{A}^2B_2 assignments and their convolution from 18000 to 22000 cm⁻¹.

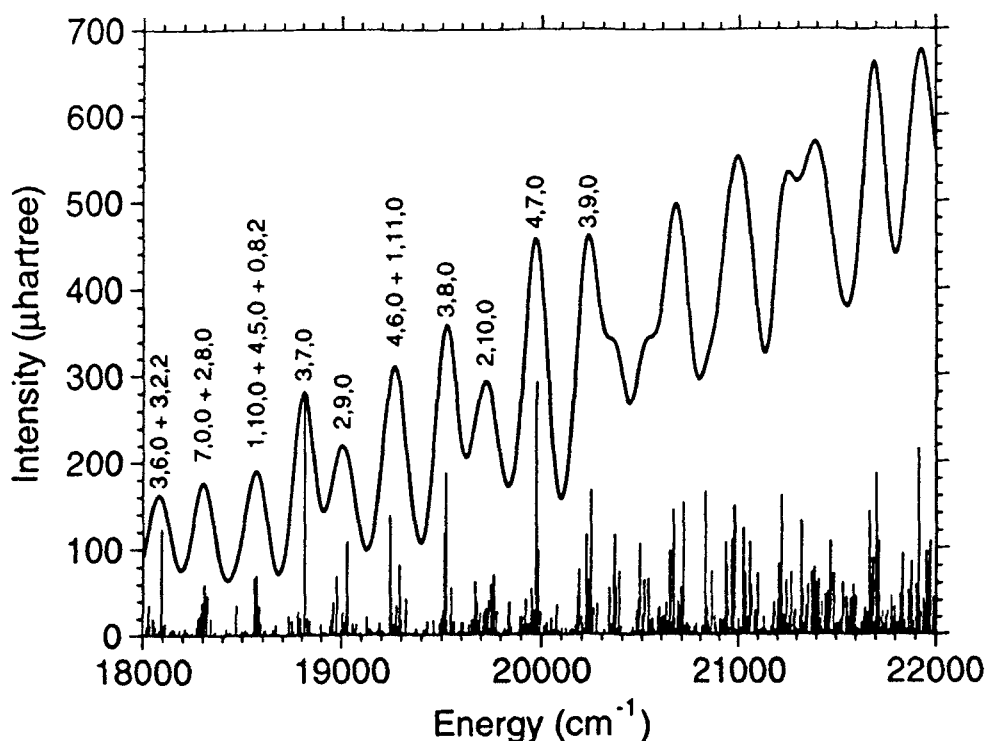


FIG. 3. Energy ranges 18000 - 22000 cm⁻¹. Nonadiabatic B_2 stick bands, Gaussian convolution with HWHM = 62.5 cm⁻¹, and \tilde{A}^2B_2 assignments. Basis 14932.

In our previous work [3,4] we have assigned the \tilde{A}^2B_2 character of the nonadiabatic B_2 bands up to 16200 cm^{-1} and of some of the strongest ones up to 18600 cm^{-1} . We here extend this analysis, by assigning the strong bands up to 20300 cm^{-1} ; above this energy value, both vibrational and vibronic mixings are so large that the assignment is impossible and the \tilde{A}^2B_2 polyads lose their physical meaning.

The nonadiabatic cold and hot bands are very weak near the \tilde{A}^2B_2 origin at about 9750 cm^{-1} : at 300 K, the intensity of both the transitions $\tilde{A}^2B_2(0,0,0) - \tilde{X}^2A_1(0,0,0)$ and $(0,1,0) - (0,1,0)$ is equal to about 1/50 of that of the first band of Table IV, whereas the hot diabatic band is about six times stronger than the cold one, in agreement with Ref. 13. The spectrum remains weak up to 13000 cm^{-1} , *i.e.* for the \tilde{A}^2B_2 polyads 0-4. Below 11700 cm^{-1} , the strongest cold bands have a dominant \tilde{X}^2A_1 character and their intensities are due to very small weights of excited and bright \tilde{A}^2B_2 BO states, whereas the first three \tilde{A}^2B_2 polyads and the hot bands do not contribute appreciably to the spectrum. Our coupling potential V_{12} therefore gives too large vibronic couplings in the region of the first three polyads, thus mixing vibrational species quite far in energy.

However, this shortcoming of V_{12} is less important for assigning the states and for the levels above 11700 cm^{-1} , where the polyad 3 begins: the hot band 170^* at 11917 cm^{-1} is the strongest one up to 12600 cm^{-1} and is due to an $\tilde{A}^2B_2(0,4,0) - \tilde{X}^2A_1(0,1,0)$ transition. The next polyad 4 contributes to the spectrum with several bands, from the hot one at 12413 cm^{-1} which corresponds to the absorption from $\tilde{X}^2A_1(0,2,0)$, up to a group of four states around 12650 cm^{-1} which give rise to three comparable intensity maxima: the first is due to the near degenerate species 167 and 205^* , and the next two correspond to the bands 207^* and 170 of type $\tilde{A}^2B_2(1,3,0)^*$ and $(0,4,0)$ respectively.

Above 13000 cm^{-1} , the hot bands are not longer important, except one at 14068 cm^{-1} , and the absorption structures are mainly due to \tilde{A}^2B_2 combination progressions $(\nu_1, \nu_2, 0)$: the weaker stretching $(\nu_1, 0, 0)$ and bending $(0, \nu_2, 0)$ overtones are respectively shifted to the red and to the blue of the strongest band of each polyad, and the $(0, 0, \nu_3)$ overtones borrow the intensity from vibrational resonances with strong \tilde{A}^2B_2 states. Up to 16000 cm^{-1} , the spectrum calculated with 14932 basis functions is not significantly different from those of the smaller 10682 and 6117 expansions: the maximum intensity change is about equal to 20%, save a splitting of the state 386 into two nearly degenerate bands and two permutations of the assignments of two pairs of adjacent levels.

TABLE IV. Cold and hot spectrum and \tilde{A}^2B_2 assignments up to 22000 cm⁻¹. E_{ng} in cm⁻¹ and I_{ng} in μ hartree.

n^a	E_{ng}	I_{ng}^b	$\tilde{A}^2B_2^c$	n^a	E_{ng}	I_{ng}^b	$\tilde{A}^2B_2^c$
99	10749	0.03		207	13394	1.0	1,3,0
121	11408	0.03		236	13924	0.8	2,2,0
122	11469	0.02		243	14038	0.8	0,2,2
129	11727	0.03	0,3,0	298*	14068	1.5	1,5,0
167*	11858	0.04	1,2,0	250	14105	3.5	1,4,0
207**	11886	0.02	1,3,0	257	14228	0.8	0,6,0
137	11910	0.04	0,3,0	276	14530	0.9	3,1,0
170*	11917	0.08	0,4,0	298	14818	11	1,5,0
139	11942	0.04	1,1,0	335	15341	3.5	
176*	12022	0.02		337	15350	6.9	2,4,0
141	12023	0.02		339	15378	8.8	2,4,0
147	12108	0.02		352	15524	3.0	0,4,2
151	12238	0.03		354	15550	11	1,6,0
153	12277	0.02		360	15623	2.7	
236**	12413	0.02	2,2,0	364	15663	3.5	
195*	12451	0.03		386	15934	17	3,3,0
196*	12456	0.02	2,1,0	403	16105	15	2,5,0
163	12516	0.02	0,0,2	407	16145	23	2,5,0
164	12527	0.02		410	16177	10	2,5,0
201*	12557	0.03	1,3,0	419	16284	12	1,7,0
202*	12558	0.04		454	16637	16	3,4,0
166	12592	0.05		457	16673	18	3,4,0
250**	12598	0.05	1,4,0	458	16689	10	3,4,0
167	12613	0.17	1,2,0	461	16711	12	2,2,2
205*	12615	0.12		462	16730	10	
207*	12639	0.24	1,3,0	472	16809	14	2,6,0
170	12672	0.36	0,4,0	475	16836	10	2,6,0
210*	12693	0.02	0,5,0	479	16871	19	2,6,0
171	12705	0.03		481	16890	10	5,1,0
175	12762	0.03		492	17013	17	1,8,0
176	12780	0.07		513	17170	22	4,3,0
216*	12786	0.06		531	17356	44	3,5,0
178	12792	0.06		543	17447	28	
217*	12802	0.03		549	17510	16	
180	12826	0.03		554	17551	26	
183	12922	0.04		555	17563	62	2,7,0

TABLE IV. (Continued).

n^a	E_{nr}	I_{nr}^b	$\tilde{A}^2B_2^c$	n^a	E_{nr}	I_{nr}^b	$\tilde{A}^2B_2^c$
556	17571	22	2,7,0	942	20183	76	
557	17581	16	5,2,0	947	20218	116	3,9,0
585	17806	22	4,4,0	948	20222	62	
589	17829	28	4,4,0	950	20233	64	
594	17859	26	0,11,0	952	20241	167	3,9,0
596	17875	39	4,4,0	969	20359	116	
613	18028	36		992	20485	106	
621	18090	124	3,6,0	1020	20638	98	
646	18292	39	7,0,0	1025	20655	145	
649	18306	60	2,8,0	1038	20706	153	
650	18319	47	2,8,0	1059	20820	166	
670	18466	36	1,10,0	1079	20930	107	
685	18557	67	4,5,0	1080	20936	80	
686	18567	70	4,5,0	1084	20964	110	
687	18574	33	0,8,2	1086	20977	149	
689	18581	34		1095	21023	123	
718	18812	276	3,7,0	1103	21055	107	
740	18956	39	5,4,0	1132	21204	82	
742	18975	69	5,4,0	1134	21217	161	
749	19025	108	2,9,0	1157	21319	131	
783	19242	139	4,6,0	1172	21388	78	
784	19243	77	1,11,0	1191	21469	108	
793	19290	82	4,6,0	1230	21666	143	
825	19513	117	3,8,0	1234	21684	89	
826	19518	188	3,8,0	1239	21702	186	
832	19545	56	3,8,0	1241	21713	108	
849	19667	63	5,5,0	1267	21834	94	
865	19749	59	2,10,0	1278	21879	85	
866	19762	70	2,10,0	1285	21914	216	
898	19949	55	4,7,0	1294	21951	97	
903	19972	292	4,7,0	1297	21963	81	
904	19981	99	4,7,0	1298	21970	109	

^a A star or a double star labels the hot bands from $\tilde{X}^2A_1(0,1,0)$ or $(0,2,0)$, respectively, at 300 K.

^b Larger than the intensity thresholds of Table III.

^c Up to 20300 cm⁻¹: main \tilde{A}^2B_2 configuration, with $|\langle \tilde{A}^2B_2(v_1, v_2, v_3) | n \rangle|^2 \geq 10\%$.

Each of the \tilde{A}^2B_2 polyads 5, 6, and 7 has one dominant bright level, at 13394, 14105, and 14818 cm⁻¹, respectively, whereas the polyads 8 and 9 are splitted into three and four bands, respectively, of comparable intensity. The strongest band up to 17350 cm⁻¹ is that relative to the transition to the state 407 at 16145 cm⁻¹, it belongs to the polyad 9 and is of \tilde{A}^2B_2 (2,5,0) type. In fact, the intensity of the following polyad 10 spreads on several weaker lines. This is the first signature of a gradual development of the spectral chaos above 16800 cm⁻¹, from $\nu = 10$ upwards, where the vibronic couplings begin to overlap next-neighbor polyads (see Table III). Indeed the bands 475 and 481 at 16836 and 16890 cm⁻¹, respectively, are vibrationally mixed between the polyads 10 (2,6,0) and 11 (5,1,0), and their relatively small intensities are due to an asymmetric-stretching character of their \tilde{A}^2B_2 third main configuration. The largest interactions involve polyads 12, 13, and 14, from about 18300 up to 19200 cm⁻¹: Table III and IV show that the first band of polyad 14 at 18292 cm⁻¹ is below the last band of polyad 12 at 18574 cm⁻¹, and that the polyad width increases from about 370 cm⁻¹ for $\nu = 10$ up to 1470 cm⁻¹ for $\nu = 14$. Fig. 3 shows these nonadiabatic effects on the intensity distribution, from the \tilde{A}^2B_2 (7,0,0) + (2,8,0) assignments of a group of bands at about 18300 cm⁻¹, up to the (4,6,0) + (1,11,0) characters of the absorption maximum near 19250 cm⁻¹. The strongest stick bands are at 18812 and 19972 cm⁻¹, nevertheless the convolution peaks increase nearly linearly up to 22000 cm⁻¹, at least. The nonadiabatic effects do not fully mask some residual regularities of the strongest bands: Fig. 3 shows that the convolution maxima are spaced by about 256 ± 17 cm⁻¹, a value which corresponds to a 8 % recurrence at 138 fs of the survival probability of the ground doorway state $|d_0\rangle$.

This qualitative analysis of the regular or chaotic behaviour of the spectrum has been confirmed by computing the next-neighbor spacing distribution (NNSD) of the levels. We have divided the spectrum in half-overlapping sets of 200 levels and we have best fitted in each set the Berry-Robnik q value [14] to the NNSD. The parameter q is 0 for regular systems and 1 for chaotic ones, and represents a quantitative index of the chaos of the set. Fig. 4 shows the variation of q with the energy, for the nonadiabatic B_2 bands (circles) and for the set of B_2 bands (triangles) obtained removing the vibronic coupling from the full nonadiabatic Hamiltonian. The chaos of the nonadiabatic levels increases up to about 18500 cm⁻¹ and then slightly decreases at higher energies. The comparison with the second curve (triangles) shows that the vibronic coupling strongly influences both the degree of chaos of the spectrum and its energy dependence, but it also shows that part of the nonadiabatic spectrum chaos is also due to the vibrational couplings within the single diabatic states. A detailed investigation on the causes of the spectrum chaos will be the subject of another paper.

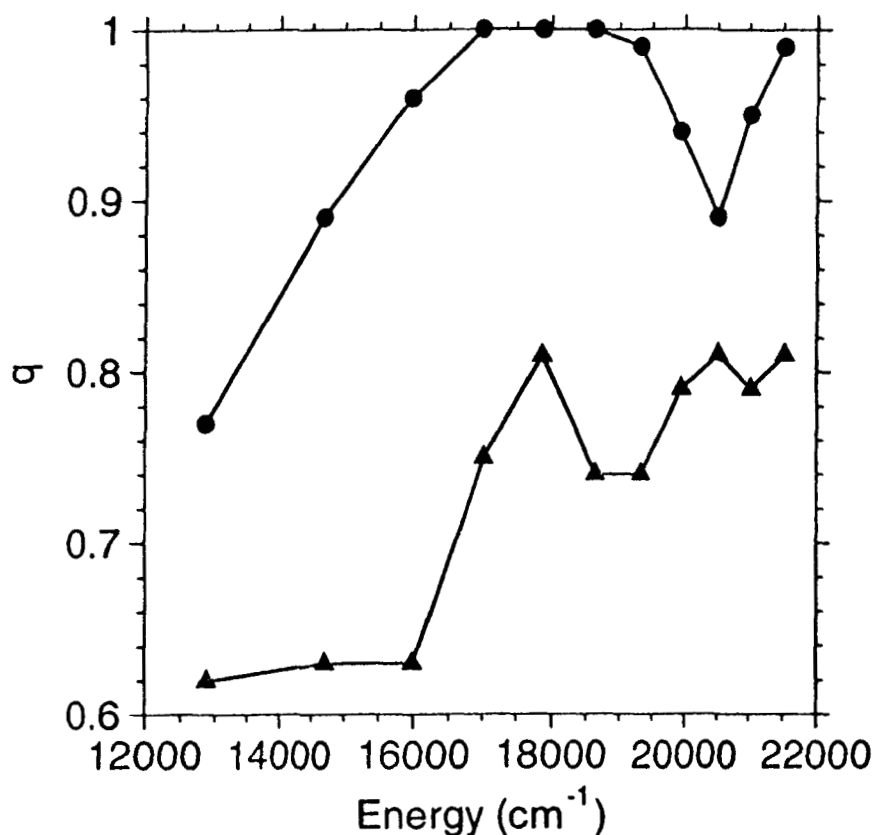


FIG. 4. Variation of the Berry-Robnik q parameter with the energy. Nonadiabatic B_2 lines with circles, and B_2 levels obtained removing the vibronic coupling from the full nonadiabatic Hamiltonian with triangles.

IV. CONCLUSIONS

We have implemented the Lanczos algorithm for the calculation of the $\tilde{X}^2A_1/\tilde{A}^2B_2$ nonadiabatic FC absorption spectrum of NO_2 up to 22000 cm^{-1} . We have employed a bond lengths-bond angle vibronic Hamiltonian, three realistic diabatic potentials, two FBR in optimized stretching and bending functions or in BO vibrational states of both electronic species, and both orthogonal and nonorthogonal recursions. By using up to 14932 optimized basis functions and

35000 Lanczos states and by analyzing the expansion coefficients on the molecular basis functions, we have removed the truncation errors of our previous works [3,4], we have discussed the convergence of the spectrum with respect to the dimensions of the molecular and Lanczos bases, we have calculated 1304 B_2 nonadiabatic bands and cold and hot intensities, and we have assigned the \tilde{A}^2B_2 character of the nonadiabatic states up to 20300 cm⁻¹.

We have compared the results of Lanczos orthogonal and nonorthogonal eigensolvers, by showing that to obtain the same accuracy one must utilize a nonorthogonal Lanczos basis which is about four-five times larger than the orthogonal one, and that however, this implies only a much smaller CPU time increase. The orthogonal recursion is preferable for assigning the nonadiabatic states and for high precision-small dimensions calculations. On the other hand, the hundreds of levels of the overall spectrum require large basis sets and nonorthogonal recursions, via Lanczos expansions which are about two-three times larger than the molecular ones. A final convergence check has shown that the computational effort can be reduced by more than two orders of magnitude, still obtaining a satisfactory low-resolution spectrum.

The main absorption features follow the \tilde{A}^2B_2 Fermi polyads, but the details of the intensity distribution in different spectral regions depend strongly on the $\tilde{X}^2A_1/\tilde{A}^2B_2$ electronic interactions and \tilde{A}^2B_2 vibrational resonances. We have therefore identified the following regions of the spectrum.

1. Up to 13000 cm⁻¹ (polyads 0-4). The cold and hot origins are very weak; \tilde{X}^2A_1 or hot bands are relatively important, and the spectrum is weak.
2. From 13000 to 16500 cm⁻¹ (polyads 5-9). The \tilde{A}^2B_2 symmetric stretch-bending bands are stronger than the bending overtones; the intensity increases quickly.
3. From 16500 to 17800 cm⁻¹ (polyads 10-11). The polyads begin to mix at 16800 cm⁻¹; beginning of the quantum chaos; the polyad 10 is weaker than the 9 one.
4. From 17800 to 19700 cm⁻¹ (polyads 12-14). Maximum polyad mixing and quantum chaos.
5. From 19700 to 22000 cm⁻¹. The polyads lose their identity and the bands cannot be assigned above 20300 cm⁻¹; residual regularity of the peaks of the gaussian convolution.

ACKNOWLEDGMENTS

We thank I. Cacelli for a copy of his plotting code, and A. Ferretti, A. Lami, R. Jost, and G. Villani for many helpful discussions and suggestions. This work has been supported by CNR and by MURST.

REFERENCES

- [1] A. Delon, R. Georges, and R. Jost, *J. Chem. Phys.* **103**, 7740 (1995), and references therein.
- [2] R. Jost, J. Nygård, A. Pasinski, and A. Delon, *J. Chem. Phys.* **105**, 1287 (1996).
- [3] E. Leonardi, C. Petrongolo, G. Hirsh and R. J. Buenker, *J. Chem. Phys.* **105**, 9051 (1996).
- [4] R. Brandi, F. Santoro, and C. Petrongolo, *Chem. Phys.* **225**, 55 (1997).
- [5] G. H. Golub and C. F. Van Loan, *Matrix Computations* (North Oxford Academic, London, 1986).
- [6] S. Carter and N. C. Handy, *Mol. Phys.* **57**, 175 (1986).
- [7] R. Georges, A. Delon, F. Bylicki, R. Jost, A. Campargue, A. Charvat, M. Chenevier, and F. Stoeckel, *Chem. Phys.* **190**, 207 (1995).
- [8] A. Lami and G. Villani, *Chem. Phys.* **172**, 285 (1993).
- [9] J. K. Cullum, R. A. Willoughby, *Lanczos Algorithms for Large Symmetric Eigenvalue Computations*, (Birkhäuser, Boston, 1985).
- [10] E. Haller, H. Köppel, and L. S. Cederbaum, *J. Mol. Spectrosc.* **111**, 377 (1985).
- [11] R. E. Wyatt and D. S. Scott, in *Mathematical Studies Series*, J. K. Cullum and R. A. Willoughby Eds. (North-Holland, Amsterdam, 1987), Vol. 127.
- [12] M. J. Bramley and T. Carrington Jr., *J. Chem. Phys.* **101**, 8494 (1994).
- [13] G. D. Gillespie and A. U. Khan, *J. Chem. Phys.* **65**, 1624 (1976).
- [14] M. V. Berry and M. Robnik, *J. Phys.* **A17**, 2413 (1984), Eq. (28). We have renamed q their \bar{p} .

Hyperspherical coordinates for chemical reaction dynamics

Vincenzo Aquilanti, Gabriella Capecchi and Simonetta Cavalli
Dipartimento di Chimica, Università di Perugia
I-06123 Perugia, Italy

Abstract

We present an introduction to various aspects of the hyperspherical approach to chemical reaction dynamics. The emphasis is on the choice of the coordinate systems for the study of the quantum mechanical problem of few interacting bodies. The treatment is appropriate when bonds break and form (as in chemical reactions) and also when large amplitude motions influence rovibrational spectra of polyatomic molecules and clusters. The development is kept at an elementary level and reference is made almost exclusively to the work carried out in our laboratory. Particular attention is devoted to point out the current research activity in this area as an extension of angular momentum theory, even for the purpose of developing efficient numerical codes.

1. Introduction
2. Separation of radial and angular variables. Orbital angular momentum.
3. Near separability. Adiabatic and diabatic representations.
4. Three-body problem. Orbital and rotational angular momentum.
5. Hyperspherical coordinates and harmonics. Hyperangular momentum.
6. Hyperspherical mapping of potential energy surfaces and alternative parametrizations of hyperangles.
7. Perspectives and concluding remarks.

References

1. Introduction

The modern theory of chemical reactions requires the treatment of the quantum mechanics of few bodies, an intrinsically multidimensional, non-separable problem. Accordingly, a proper choice of the coordinate system is of crucial importance for the theoretical approach to molecular dynamics. Introduction of alternative orthogonal coordinates allows the separation of the center of mass and thus the diagonalization of the kinetic energy tensor, leading to an essential simplification of the computational problems connected with the study of chemical reactivity and the mapping of potential energy surfaces [1, 2]. The basic geometric theory of the modern approach to the N-body problem is reviewed in ref. [3].

In the following, we emphasize aspects which illustrate the development of the theory as an extension of the elementary theory of angular momentum. As the latter is basically founded on the group theory of rotations in ordinary spaces, tremendous progress has been achieved by properly mapping multidimensional problems on hyperspheres. This article is kept at an elementary level and technicalities are to be found in the quoted references. There it is demonstrated that the theoretical methods based on hyperspherical coordinates have turned out to be essential tools in the quantum mechanical treatment of the interaction between few particles, involving studies both of bound states and of scattering problems.

The recent application of hyperspherical and related coordinates to treat the dynamics on a reactive potential energy surface offers, in fact, the possibility of exploring also those regions where reaction paths present sharp curvatures or bifurcations, taking into account of dynamical quantum effects like tunneling and resonances. Several reviews available [4–10] provide a useful introduction to various aspects of the hyperspherical approach.

In the next two sections of this article we face the problem of separability or “near” separability of variables related to the solution of Schrödinger equation, giving the definition of adiabatic and diabatic representations which applies to the present context. Then we focus our attention on orthogonal coordinate systems starting with the Jacobi vectors for the three body problem and stressing the implication of their choices on the proper handling of the involved angular momenta. In the fifth and sixth sections we give an overview of the hyperspherical coordinates in their different parametrizations and provide the connections with hyperspherical harmonics, which are the eigenfunctions of hyperangular momentum in a hyperspherical diabatic representation. In section 6 we also explore the mapping of potential energy surfaces from the perspective of hyperspherical coordinates, enlightening the characteristics of the regions most relevant for the reaction dynamics.

In the final section we briefly describe some recent developments of the hyperspherical approach, such as the hyperquantization algorithm as an important computational tool for the solution of dynamical problems and the extensions of the hyperspherical method to treat the dynamics of reactions involving polyatomic systems.

2. Separation of radial and angular variables. Orbital angular momentum.

In order to treat properly those atomic and molecular processes, which involve large amplitude motions and even breaking and formation of chemical bonds, one has to face the failure of the nearly harmonic separation on which molecular spectroscopy is rooted. In any case it is basic to try to solve the Schrödinger equation introducing some sort of "near" separability of variables, so to transform a partial differential equation in a set of ordinary coupled differential equations in a variable of the propagation type. In general, this would correspond to find operators which nearly commute with the hamiltonian, giving approximately "good" quantum numbers related with the external or internal angular momenta of the system.

To prepare for proper generalizations, we reconsider a familiar case where exact separability of radial and angular variables is possible: the interaction of two particles, of mass m_1 and m_2 , in a central field. Physically, this corresponds to the important example of elastic atom-atom scattering.

In three-dimensional space the positions of the two structureless atoms are specified by six coordinates which, after separating the motion of the center of mass, are reduced to three. Introducing the reduced mass μ of the system ($\mu = [m_1 m_2 / (m_1 + m_2)]^{1/2}$), we obtain a hamiltonian which is the sum of a kinetic part represented by the Laplacian operator acting in a three-dimensional space plus a potential energy $V(r)$, which is a function only of the distance, r , between the two particles:

$$\left[-\frac{\hbar^2}{2\mu} \Delta^{(3)} + V(r) - E \right] \Psi = 0 \quad (1)$$

The transformation of the Laplacian in polar coordinates introduces an effective simplification of the Schrödinger equation, here exploiting the separability of the radial coordinate from the angular ones. Here are the known formulas:

$$\Delta^{(3)} = \frac{\partial^2}{\partial x^2} + \frac{\partial^2}{\partial y^2} + \frac{\partial^2}{\partial z^2} = \frac{\partial^2}{\partial r^2} + \frac{2}{r} \frac{\partial}{\partial r} - \frac{1}{r^2} \Lambda_{\text{ang}}^{(3)} \quad (2)$$

where

$$x = r \sin\theta \cos\phi, \quad y = r \sin\theta \sin\phi, \quad z = r \cos\theta \quad (3)$$

$$r = (x^2 + y^2 + z^2)^{\frac{1}{2}}, \quad 0 \leq \theta \leq \pi, \quad 0 \leq \phi < 2\pi \quad (4)$$

Separate solutions of the angular and radial parts of the equation are to be found. The former can be done analytically, and leads to the spherical harmonics ($Y_{l,m}(\theta, \phi)$) as eigenfunctions of the angular Laplacian:

$$\Lambda_{\text{ang}}^{(3)} Y_{l,m}(\theta, \phi) = l(l+1) Y_{l,m}(\theta, \phi), \quad l = 0, 1, 2, \dots, \quad -l \leq m \leq l \quad (5)$$

where l and m represent the "orbital" angular momentum quantum number and its projection on an axis fixed in the center of mass.

The wave function is the product of a spherical harmonic and the radial factor $F_l(r)$ (a vectorial set):

$$\Psi = \frac{1}{r} Y_{l,m}(\theta, \phi) F_l(r) \quad (6)$$

For a general interaction, one has finally to solve the radial part of the Schrödinger equation

$$\left[-\frac{\hbar^2}{2\mu} \left(\frac{d^2}{dr^2} - \frac{l(l+1)}{r^2} \right) + V(r) - E \right] F_l(r) = 0 \quad (7)$$

If, e.g., $V(r)$ is a harmonic or Morse oscillator, or the Coulomb potential, as for the hydrogen atom, eq. (7) can be solved analytically, otherwise numerical solution is necessary, but involves only a one-dimensional integration and nowadays can be carried out routinely when needed, as for the analysis of elastic scattering experiments in atomic and nuclear physics.

3. Near separability. Adiabatic and diabatic representations.

The consideration that the velocity of electrons is much higher than that of the nuclei (a consequence of their much smaller masses) leads to the Born-Oppenheimer approximation, perhaps the better known example of the near separability of variables. We reconsider it in view of subsequent generalizations. Using the language of classical mechanics, we will speak of adiabatic separability, which can be shown to be related to a semiclassical expansion, i.e. to an asymptotic expansion in \hbar . See references [11–14] where we also discuss a "post-adiabatic" representation.

Let us consider again the atom-atom interaction, but permit now the atoms to have a structure. Namely, allow now for inelasticities, and indicate with R the internuclear distance and with \mathbf{r} the collection of vectors representing the electron-nucleus distances. We can write down the following Schrödinger equation:

$$\left[-\frac{\hbar^2}{2\mu}\Delta^{(3)} - \frac{\hbar^2}{2m_e}\Sigma_i\Delta_i^{(3)} + V(R, \mathbf{r}) - E \right] \Psi = 0 \quad (8)$$

where m_e is the mass of the electron.

Solving separately the electronic part of the equation for each fixed configuration of the nuclei, we obtain the spectrum of the electronic adiabatic eigenvalues ϵ_i^a , which depend parametrically on R , and have the meaning of potential energy curves

$$H_{el}\phi_i^a(R, \mathbf{r}) = \epsilon_i^a(R)\phi_i^a(R, \mathbf{r}) \quad (9)$$

In practice, one considers only a limited number of the lowest lying eigenvalues and eigenfunctions ϕ_i^a , corresponding to the energy range of interest. It is then possible to factorize the wave function in terms of electronic and nuclear eigenfunctions:

$$\Psi = \Sigma_i \phi_i^a(\mathbf{r}, R) F_i^a(R) \quad (10)$$

where $F_i^a(R)$ are now the solutions of a system of coupled second order ordinary differential equations:

$$\left[-\frac{\hbar^2}{2\mu} \left(1 \frac{d}{dR} + P(R) \right)^2 + \epsilon(R) - 1E \right] \mathbf{F}^a(R) = 0 \quad (11)$$

Such a system is in principle infinite, but, as we have seen, in practice a convenient truncation has to be introduced. According to the Hellmann-Feynman theorem, we can write the coupling terms as follows:

$$P_{ij}(R) = \langle \phi_i^a | \frac{d}{dR} \phi_j^a \rangle = \frac{1}{\epsilon_i - \epsilon_j} \langle \phi_i^a | \frac{dV}{dR} | \phi_j^a \rangle = -P_{ji}(R) \quad (12)$$

Solving eq. (11) including eq. (12) would amount to "exact" solution of the coupled-channel or close-coupling (CC) formulation in the *adiabatic* representation. The adiabatic approximation consists in neglecting the coupling terms, as it is done in the Born-Oppenheimer separation.

An alternative development leads to the *diabatic* representation, which requires the definition of an orthogonal matrix $T(R)$ to interconvert the eigenfunctions corresponding to the two different representations:

$$\mathbf{F}^a = \mathbf{T}\mathbf{F}^d \quad (13)$$

and

$$\mathbf{T}^{-1}\mathbf{T}' = \mathbf{P} \quad (14)$$

where the prime denotes differentiation with respect to R , so that, in spite of their innocent look, equations (13) and (14) correspond actually to an often formidable set of differential equations.

The final equation for the diabatic representation is

$$\left[-\frac{\hbar^2}{2\mu} \frac{d^2}{dR^2} + \mathbf{V}^d - \mathbf{1}E \right] \mathbf{F}^d(R) = 0 \quad (15)$$

where

$$\mathbf{V}^d = \mathbf{T}^{-1}\epsilon(R)\mathbf{T} \quad (16)$$

The main difference between (11) and (15) is that in the former case, the coupling acts in the kinetic energy, while in the latter it acts in the potential energy. This is often convenient for numerical solutions. However \mathbf{T} is not unique: solution to the equations (13) and (14) requires specification of boundary conditions and therefore the diabatic representation is not unique as well. This can be in practice a great advantage. A physically motivated diabatic expansion on a mathematically well-behaved orthonormal complete basis set, as the expansions in spherical and hyperspherical harmonics to be considered in the following, leads to analytical evaluation of matrix elements and to the possibility of exploiting powerful numerical techniques. This is the theme of the following sections, as far as chemical reaction theory is concerned.

See [15, 16] for the alternative diabatic representations which correspond to the alternative Hund's angular momentum coupling cases in the spectroscopy and dynamics of a diatomic system.

4. Three-body problem. Orbital and rotational angular momentum.

When molecules undergo large amplitude motions, or even bonds break and form as in a chemical reaction, one doesn't have any more a privileged interatomic distance and has to consider explicitly the interactions among the various bodies. To begin with, note that for the interaction among three particles it is certainly very difficult to identify a trivially separable variable. Nevertheless it is still possible to reduce the dimensionality of the problem eliminating those coordinates related with the motion of the center of mass.

There are several different representations of the six coordinates necessary to describe the positions of the three particles, but we will treat in detail the Jacobi scheme, not only because it came first chronologically but even because it is nowadays the one more widely employed. Alternatives are discussed elsewhere [1].

In the three body problem we can write down two Jacobi vectors: the first (\mathbf{r}) is simply the internuclear distance between two particles and the second (\mathbf{R}) connects their center of mass to the third particle.

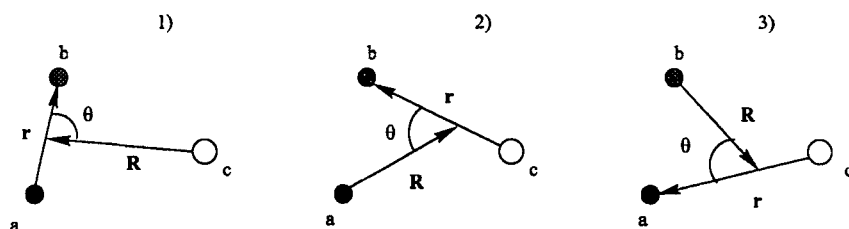


Figure 1: Jacobi vectors for three particles in space.

The resulting hamiltonian will contain as a kinetic term the sum of two three dimensional Laplacians acting on the coordinates of the Jacobi vectors plus a potential energy term describing the interaction between the three particles

$$\left[-\frac{\hbar^2}{2M} \Delta_{\mathbf{R}}^{(3)} - \frac{\hbar^2}{2m} \Delta_{\mathbf{r}}^{(3)} + V(\mathbf{R}, \mathbf{r}, \theta) - E \right] \Psi = 0 \quad (17)$$

where

$$m = \frac{m_1 m_2}{m_1 + m_2} \quad \text{and} \quad M = \frac{m_3(m_1 + m_2)}{m_1 + m_2 + m_3} \quad (18)$$

Expressing the vectors in polar coordinates $\mathbf{R} = (R, \theta_R, \phi_R)$ and $\mathbf{r} = (r, \theta_r, \phi_r)$, as before we have, as separate eigenfunctions of the angular part of the Laplacians, two spherical harmonics $Y_{lm_l}(\theta_R, \phi_R)$ and $Y_{jm_j}(\theta_r, \phi_r)$, where the quantum numbers of orbital (l and m_l) and rotational (j and m_j) angular momentum appear.

Because of the conservation of the total angular momentum ($\mathbf{J} = \mathbf{j} + \mathbf{l}$), we have to search for a proper combination of spherical harmonics. Introducing then the coupling coefficients of quantum mechanical angular momenta (the Clebsch-Gordan coefficients), we obtain a *bipolar* harmonic

$$Y_{jl}^{JM} = \sum_{m_l, m_j} \langle lm_l jm_j | JM \rangle Y_{lm_l}(\theta_R, \phi_R) Y_{jm_j}(\theta_r, \phi_r) \quad (19)$$

After the expansion of the wave function in terms of *bipolar* harmonics, we obtain:

$$\left[-\frac{\hbar^2}{2M} \frac{\partial^2}{\partial R^2} - \frac{\hbar^2}{2m} \frac{\partial^2}{\partial r^2} + \frac{\hbar^2}{2M} \frac{l(l+1)}{R^2} + \frac{\hbar^2}{2m} \frac{j(j+1)}{r^2} - E \right] F_{jl}^J = \sum_{j'l'} V_{jj'l'}^J F_{j'l'}^J \quad (20)$$

$$V_{jj'l'}^J(r, R) = \langle Y_{jl}^{JM} | V(r, R, \theta) | Y_{j'l'}^{JM} \rangle \quad (21)$$

where $\langle \dots \rangle$ implies the integration on the angle θ .

Also the potential energy $V(r, R, \theta)$ can be expanded as a function of Legendre polynomials. This expansion allows analytical evaluation of matrix elements according to the algebraic rules for the coupling of angular momenta [17]. Therefore, to solve an "inelastic" problem, where R and r remain appropriate throughout, we may solve first the Schrödinger equation in r, θ_r, ϕ_r , parametrically in R , obtaining the eigenvalues $\epsilon_{jv}^J(R)$ and the eigenfunctions $\phi_{jv}^J(R, \mathbf{r})$, where v is the vibrational quantum number, and then integrate a set of coupled equations in R . Computer programs are available to carry out such calculations of interest for the study of the exchange of rotational and vibrational energy in molecular collisions.

When treating reactions, the situation is obviously more complicated and we have to face the rearrangement problem. We have to take into account the Jacobi rearrangements related to the reactants and products respectively. The main question we should try to answer is whether it can be found a near separable coordinate for rearrangement scattering or in general for any many-body problem, even when one cannot use a manifest difference in masses, as in the Born-Oppenheimer separation. The solution to this problem requires an extension to spaces of mathematically higher dimensionality of the procedure we have been following so far. In such a hyperspace, we are going to introduce the radius of a hypersphere as our key variable.

For a prototypical three body problem, the Helium-like atom, the procedure is well known since the early days of quantum mechanics. More recently, Fano, Macek and Klar [18–23] identified a near separable variable $\rho = (r_1^2 + r_2^2)^{\frac{1}{2}}$, where r_1 and r_2 are the two Jacobi vectors of the system, named “hyperradius”, corresponding to the radius of a six-dimensional “hypersphere” parameterized by five “hyperangles”. However, note that the hyperradius is independent of the numbering of particles and is therefore very useful for rearrangement problems.

The hyperspherical coordinates, which will be discussed in detail in the present article, represent a generalization to any mass of the near separability for the hyperradius explored for Helium-like atom. Jacobi vectors, besides the reduction of the dimensionality of the problem eliminating the center of mass coordinates, allow us, after a proper mass-scaling, to express the kinetic energy of the system in a diagonal form which depends only on the reduced mass of the system.

If we multiply the vectors \mathbf{R}_k and \mathbf{r}_k , where k indicates one of the three possible arrangements of the particles (fig. 1), by the mass factor a_k

$$a_k = \left(\frac{\mu_{k,jl}}{\mu_{jl}} \right)^{\frac{1}{4}} \quad \mu_{k,jl} = \frac{m_k(m_j + m_l)}{m_k + m_j + m_l} \quad \mu_{jl} = \frac{m_j m_l}{m_j + m_l} \quad (22)$$

where we indicate with k the particle connected by the vector \mathbf{R} to the center of mass of particles j and i , we obtain the mass-scaled Jacobi vectors \mathbf{X}_k and \mathbf{x}_k

$$\mathbf{X}_k = a_k \mathbf{R}_k \quad \mathbf{x}_k = a_k^{-1} \mathbf{r}_k \quad (23)$$

Substituting the previous expressions in the kinetic energy operator in eq. (17), it will result a diagonal expression

$$T = -\frac{\hbar^2}{2\mu} (\Delta_{\mathbf{x}_k}^{(3)} + \Delta_{\mathbf{x}_k}^{(3)}) = -\frac{\hbar^2}{2\mu} \Delta^{(6)} \quad (24)$$

where we encounter the reduced mass for the three particles

$$\mu = \left(\frac{m_k m_j m_l}{m_k + m_j + m_l} \right)^{\frac{1}{2}} \quad (25)$$

The procedure can clearly be extended to treat more than three particles, and this is done, e.g. in ref. [24]. It has also to be pointed out the fact that the hyperradius is a measure of the total inertia of the n -body system, and this can be a physical motivation for its candidacy as a proper nearly separable variable, invariant with respect to the choice of the set of Jacobi vectors.

5. Hyperspherical coordinates and harmonics. Hyperangular momentum.

We are now ready to generalize to spaces of higher dimensionality the well known polar representation of the position vector of a particle in a three-dimensional space. A hyperspherical representation of the Jacobi vectors can be developed, corresponding to the projection on a d -dimensional hypersphere, with $d=(n-1)D$ for n particles in a D -dimensional space after the separation of the center of mass. The d hyperspherical coordinates consist of a hyperradius, which does not depend on the particular Jacobi set chosen, and $d-1$ hyperangles, dependent on the arrangement of the particles.

The case of three particles can be simply represented by the hyperradius ρ , related to the sum of the Jacobi vectors, plus five hyperangles, originating a kinetic energy operator [24, 25] consisting of a term depending exclusively on ρ plus a five dimensional Laplacian, $\Lambda(\Omega_5)$, corresponding to a "hyperangular" momentum [26]:

$$T = -\frac{\hbar^2}{2\mu}\Delta^{(6)}(\rho, \Omega_5) = -\frac{\hbar^2}{2\mu}\left[\rho^{-5}\frac{\partial}{\partial\rho}(\rho^5\frac{\partial}{\partial\rho}) - \rho^{-2}\Lambda(\Omega_5)\right] \quad (26)$$

There exist different parametrizations of the hyperangles, such as the commonly used asymmetric or Fock's parametrization and symmetric or Smith's, which will be discussed in the next section. The eigenfunctions of the hyperangular momentum are called hyperspherical harmonics and can be easily visualized by the tree method [4, 10, 24]. To a d -dimensional hypersphere, parameterized by d cartesian coordinates or one hyperradius and $d-1$ hyperangles, is graphically associated a tree which is composed of d leaves corresponding to the cartesian coordinates and each leaf is connected by a branch to one of the $d-1$ nodes representing the hyperangles and labeled with the proper quantum numbers.

Starting from a leaf and descending to the root of the tree, through the various nodes, we may find the relationship between coordinates and hyperangles, according to the convention which establishes that the branch converging to a node from the left-hand (right-hand) side corresponds to the cosine (sine) of the hyperangle.

If a hyperspherical parametrization can be represented by a tree, the coordinates can be shown to form an orthogonal set. This implies that the Laplacian on the hypersphere will contain no cross terms, the corresponding Laplace equations are separable and the hyperspherical harmonics can be constructed in closed form [24].

We start considering some examples in two and three-dimensional space and then generalize to spaces of higher dimensionality. On the plane it is possible

only one representation visualized by the tree in fig. 2.

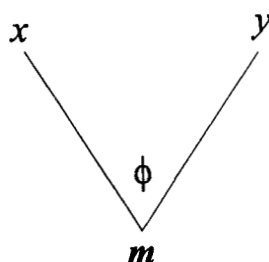


Figure 2: Illustration of eq.(27).

The tree represents the correspondence between cartesian and polar coordinates:

$$x = r \cos \phi \quad y = r \sin \phi \quad (27)$$

and the corresponding eigenfunction is given by $e^{im\phi}$ with $m = \dots, -1, 0, +1, \dots$

In three-dimensional space there are two possible symmetric trees (fig.3), the first corresponding to the usual polar representation related to the spherical harmonics $Y_{lm}(\theta, \phi)$.

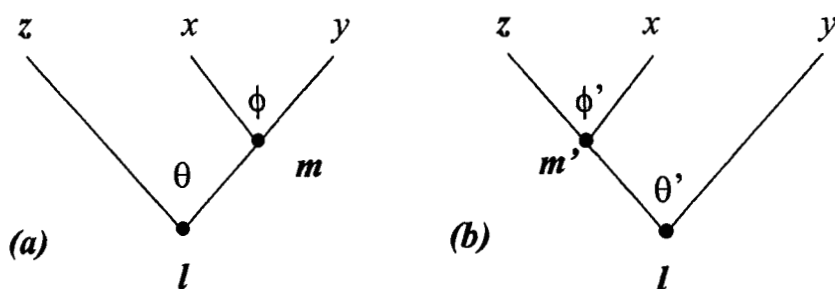


Figure 3: The trees a and b represent two alternative parametrizations of the three-dimensional sphere, S^2 .

In this case, the correspondence between polar and cartesian coordinates is:

$$\begin{array}{ll} x = r \sin \theta \cos \phi & x = r \cos \theta' \sin \phi' \\ y = r \sin \theta \sin \phi & y = r \sin \theta' \\ z = r \cos \theta & z = r \cos \theta' \cos \phi' \end{array} \quad (28)$$

The orthogonal transformation which allows the connection between $Y_{lm}(\theta, \phi)$ and $Y_{lm}(\theta', \phi')$ is in this case a Wigner's rotation matrix. For d greater than three the number of possible representations increases and we can have different hyperspherical harmonics. Transformations allowing the connection among them are orthogonal matrices, whose study is a current important topic of angular momentum theory.

In the four-dimensional case we have many possibilities. Of these, two are basically different. As an example, we show in fig. 4 the trees corresponding to such two different parametrizations (the others are obtained "anagramming" x, y, z and w).

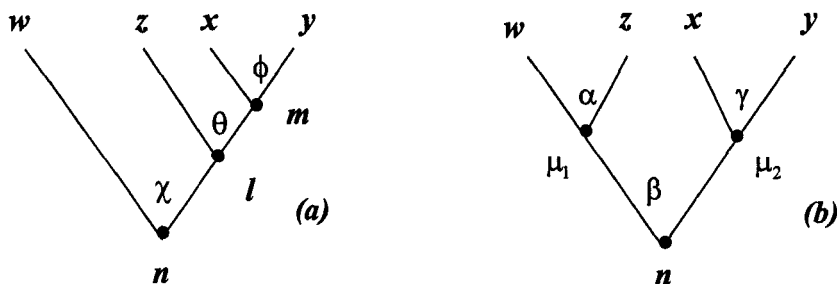


Figure 4: The trees a and b correspond to two alternative parametrizations for S^3 .

The related hyperspherical harmonics are:

$$Y_{nlm} = C_{nl}(\chi) Y_{lm}(\theta, \phi) \quad D_{\frac{n}{2}, \frac{\mu_1 + \mu_2}{2}, \frac{\mu_1 - \mu_2}{2}}^{\frac{n}{2}} = e^{i\mu_1 \alpha} d_{\mu_1 \mu_2}^n(\beta) e^{i\mu_2 \gamma} \quad (29)$$

where $\phi = \gamma$ and $m = \mu_2$.

To further illustrate the tree-method, consider the six-dimensional hypersphere which parameterizes the components of Jacobi vectors for the three-body problem: the symmetric tree, see fig. 5, corresponds to the hyperspherical harmonics

$$Y_{\lambda l_1 l_2 m_1 m_2}(\chi, \theta_1, \theta_2, \phi_1 \phi_2) = Y_{l_1 l_2}^\lambda(\chi) Y_{l_1 m_1} Y_{l_2 m_2} \quad (30)$$

The quantum number λ is the first example that we encounter of a kind of quantity that can be viewed as the generalization to hyperspace of ordinary angular momentum. They will be called hyperangular (or grandangular) momenta [10, 24, 26] and the connections among alternative harmonics are related to coupling and recoupling coefficients of hyperangular momentum.

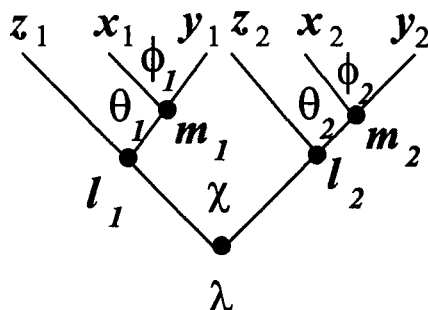


Figure 5: The tree represents the hyperspherical parametrization for the components of the Jacobi vectors describing three particles in space. l_1, m_1 and l_2, m_2 can be put into correspondence with j, m_j and l, m_l of section 4, and the upper part of the graph to the ordinary spherical harmonics.

The generalization of the hyperspherical treatment to n particles runs as follows. Considering that n particles in a three-dimensional space, after the separation of the center of mass, can be represented by $d=3(n-1)$ coordinates parameterized by a d -dimensional hypersphere with $d-1$ hyperangles and one hyperradius, we can write down explicitly the kinetic energy operator as follows:

$$-\frac{\hbar^2}{2\mu} \left[\rho^{-(d-1)} \frac{\partial}{\partial \rho} \rho^{d-1} \frac{\partial}{\partial \rho} - \rho^{-2} \Lambda(\Omega_{d-1}) \right] \quad (31)$$

where $\Lambda(\Omega_{d-1})$ (group-theoretically a quadratic Casimir operator) is the hyperangular Laplacian on the d -dimensional sphere of unit hyperradius.

The hyperspherical harmonics will then be the eigenfunctions of $\Lambda(\Omega_{d-1})$:

$$\hat{\Lambda} Y_{\lambda, \mu}(\Omega_{d-1}) = \lambda(\lambda + d - 2) Y_{\lambda, \mu}(\Omega_{d-1}) \quad (32)$$

λ being again the hyperangular or grandangular momentum quantum number and μ is here a set of $d-1$ quantum numbers.

The explicit form of the harmonics depends obviously on the particular parametrization chosen for the coordinates, giving rise to different possibilities, which are formally equivalent, but offer great flexibility to the method.

For the four-body problem in a system of symmetric hyperspherical coordinates the expression of the kinetic energy operator and the kinematic rotations connecting the different reactive channels have been explicitly derived in two

recent papers [27, 28]. Also, hyperspherical harmonics have recently attracted much attention because of their use as atomic and molecular orbitals in momentum space, allowing the treatment of the many body Coulomb problems via expansions of the Sturmian type over complete orthonormal basis sets, see [10, 29–35].

We consider now the consequences of extending the concept of near separability to the hyperspherical parametrization. The hyperradius can be identified as the near separable variable and it is then possible to expand the wave function as a product of a “hyperradial” term and hyperspherical functions [36, 37]:

$$\Psi(\rho, \Omega_{d-1}) = \rho^{-\frac{d-1}{2}} \sum_i F_i^a(\rho) \Phi_i^a(\rho, \Omega_{d-1}) \quad (33)$$

where Ω_{d-1} indicates the $d-1$ hyperangles of the d -dimensional problem, $\Phi_i(\rho, \Omega_{d-1})$ corresponds to the eigenfunctions of $d-1$ dimensional problem with eigenvalues $\epsilon_i(\rho)$ depending parametrically on ρ . We thus obtain a set of coupled differential equations

$$\left[-\frac{\hbar^2}{2\mu} \left(1 \frac{d}{d\rho} + \mathbf{P}(\rho) \right)^2 + \epsilon(\rho) - 1E \right] \mathbf{F}^a(\rho) = 0 \quad (34)$$

where $\epsilon(\rho)$ represents the matrix of adiabatic potential energy curves and $\mathbf{P}(\rho)$ is the matrix containing non-adiabatic coupling elements $P_{ij}(\rho)$, exhibiting maxima at avoided crossings, changes in coupling schemes, ridges between modes [38, 39]. An illustration will be provided in the next section, see fig. 7 below.

As in section 3, the diabatic representations are obtained finding the orthogonal matrix \mathbf{T} such that $\tilde{\mathbf{T}}\mathbf{T}' = \mathbf{P}$. Again, the diabatic representation is not unique because \mathbf{T} is defined within an overall ρ -independent orthogonal transformation. In actual calculations, one has to manipulate the potential energy matrix $\mathbf{V} = \mathbf{T}\epsilon(\rho)\tilde{\mathbf{T}}$, whose large dimensions are often the bottleneck in practice. Proper choice of \mathbf{T} is therefore crucial. The practical implementation (see the final section) of hyperspherical harmonics as the proper diabatic set is of great perspective power.

6. Hyperspherical mapping of potential energy surfaces. Alternative parametrization of hyperangles.

The hyperspherical approach leads to a change in perspective with respect to our views on reactive potential energy surfaces, not only with reference to their representation in terms of coordinates, but also regarding topological features. These are important both as a guide to the numerical implementation and as a tool to understand the qualitative features of the dynamics. The representation of potential energy surfaces in hyperspherical and related coordinates allows us to focus the attention on those regions which are relevant for the numerical implementation of the dynamics and therefore need to be known very accurately [2, 9]. If we start by limiting our consideration to a symmetric collinear three particle collision, the easiest to visualize, we may sketch the potential energy contour map as a function of skewed coordinates (fig. 6 a).

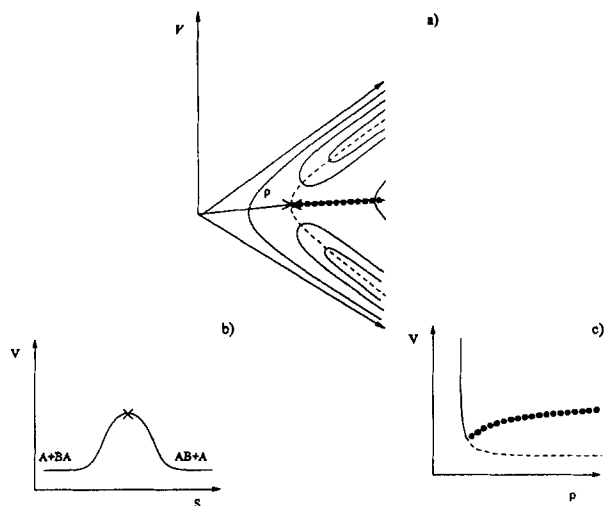


Figure 6: Schematic potential energy surface for a symmetric collinear triatomic system in skewed coordinates (panel a). The dashed and dotted lines correspond respectively to the valley bottoms and ridges, which are represented in panel c as a function of ρ . In panel b a conventional view of the minimum energy path is sketched as a function of a generic reaction coordinate s .

The idea of "skewing" the coordinates according to a mass-dependent an-

gle was put forward by the early pioneers of theoretical gas kinetics (Wigner, Polanyi, Eyring ...) in the thirties. Such a mass scaling is the first step towards the mass scalings employed in the hyperspherical approach (sect. 4). The dashed line represents the usual minimum energy path connecting the reagents and products channels (see fig. 6 b), the dots correspond to ridges of the potential energy surface and the continuous line follows the increase in hyperradius, starting from the coalescence of particles near the origin and to their alternative rearrangements far from it. It is possible to identify two main kinetic paths (fig. 6 c): the first, given by the evolution of energy minima or "valley bottoms" as a function of ρ , describes at large ρ values the rearrangement channels, while the second is the ridge line, corresponding to the evolution of saddles as a function of ρ .

Ridges play a crucial role in chemical reactions because of the coupling between rearrangement channels leading to non-adiabatic transitions. In correspondence of the "transition state" the valley bottom line undergoes an abrupt transition from single- to double-well situation, bifurcates and continue as a ridge line. Accordingly, the qualitative behaviour of adiabatic potential curves $\epsilon_v(\rho)$ drastically changes astride of the ridge (fig. 7 a) and non-adiabatic matrix elements $P_{vv'}(\rho)$ show a peak there, as we can see in fig. 7 b [39, 40].

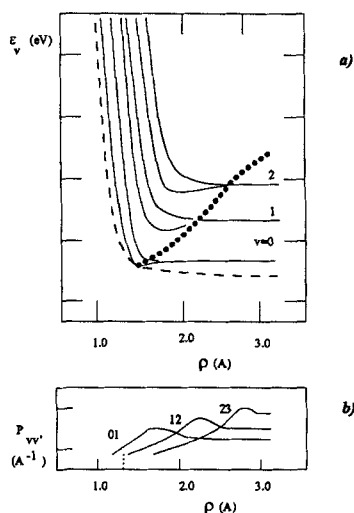


Figure 7: Adiabatic curves (panel a) and non-adiabatic matrix elements (panel b) as a function of ρ .

If we represent on a plane, which has been named "kinetic plane" [2], all the possible rearrangements of three particles constrained to lay on a line (fig. 8 a), we can identify the kinematic rotation angle Φ , which therefore is a proper generalization to continuous values of the skewing angle, which describes asymptotically the passage through the different rearrangement channels. In fig. 8 b are represented cuts through the potential energy surface at different ρ values which give a useful alternative view of the surface. Curves of fig. 7 are obtained by "quantizing" on these ρ -fixed cuts, obtaining eigenvalues and coupling matrix elements to be entered in eq. (34).

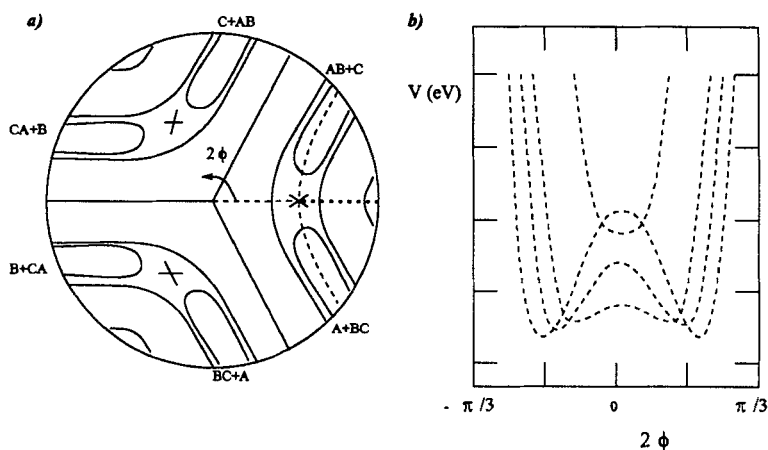


Figure 8: Schematic view of the various arrangements for a triatomic collinear reaction (a) and cuts through the potential at different ρ values (b) as a function of the kinematic angle.

In general, before any numerical calculation, and in order to explore potential energy surfaces of higher dimensionality, it emerges the crucial necessity to consider cuts as these, where some coordinate is held constant or is adjusted to minimize the potential energy [41].

We are now ready for the extension of the previous polar representation of the collinear case in terms of the radial variable ρ and the angle Φ . The case of three particles in three-dimensional space is described, as we have already shown, by a six-dimensional sphere corresponding to a hyperradius and five hyperangles. However, the potential energy surface requires only two angles and, in general, angular momentum conservation can be imposed to restrict the dynamics to a manifold of lower dimensionality. Among the

different possible parametrizations we will now consider the most commonly used, i.e. the asymmetric and the symmetric ones.

Asymmetric parametrization

The asymmetric parametrization [24, 42] can be expressed in terms of two coordinates referred to an internal reference system: the angle (ϑ) between the two Jacobi vectors and the angle (χ) related to their ratio plus the three Euler angles which specify the spatial orientation of the triangle formed by the three particles. Considering a system with zero angular momentum, we may consider only the three internal coordinates ρ , ϑ , χ :

$$\rho^2 = |\mathbf{X}|^2 + |\mathbf{x}|^2 \quad \vartheta = \frac{\arccos \mathbf{X} \cdot \mathbf{x}}{|\mathbf{X}||\mathbf{x}|} \quad \chi = \arctan \frac{|\mathbf{X}|}{|\mathbf{x}|} \quad (35)$$

and then

$$|\mathbf{x}| = \rho \cos \chi \quad |\mathbf{X}| = \rho \sin \chi \quad (36)$$

Symmetric parametrization

The symmetric parametrization, can be obtained taking as internal reference system the one which diagonalizes the inertia tensor and placing the principal axis in correspondence of the maximum inertia one [26, 43, 44]. In this way we obtain an angle (Θ) correlated with the area of the triangle made up by the three particles, invariant respect with their possible rearrangements (fig. 9), plus an angle (Φ) connected with the shape of the triangle and corresponding to the kinematic rotation angle whose value depends on the particular set of Jacobi vectors considered

$$\rho^2 = |\mathbf{X}|^2 + |\mathbf{x}|^2 \quad \sin 2\Theta = 2 \frac{|\mathbf{x} \wedge \mathbf{X}|}{\rho^2} = 4 \frac{|\boldsymbol{\eta}|}{\rho^2} \quad \tan 2\Phi = 2 \frac{(\mathbf{x} \cdot \mathbf{X})}{(|\mathbf{x}|^2 - |\mathbf{X}|^2)} \quad (37)$$

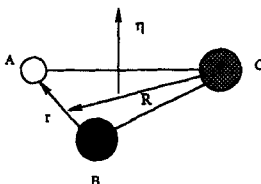


Figure 9: Illustration of the geometrical meaning of the Θ angle.

$\Theta = 0$ can be shown to correspond to the collinear case, while $\Theta = \frac{\pi}{4}$ to the equilateral triangle. The interconversion formulas between symmetric and asymmetric coordinates are [2]:

$$\sin 2\chi \cos \vartheta = \cos 2\Theta \sin 2\Phi \quad \sin 2\chi \sin \vartheta = \sin 2\Theta \quad \cos 2\chi = \cos 2\Theta \cos 2\Phi \quad (38)$$

All the relevant machinery for handling these coordinates and the explicit relationships with interatomic distances are given in ref. [2]. Symmetric and asymmetric representations for more than three particles are considered elsewhere [1]. For four particles see [27, 28, 45].

7. Perspectives and concluding remarks.

In this final section we will deal with current research problems. Although numerical implementations of the hyperspherical approach have been extensive, so that now they are considered the main route to full state-to-state information on the dynamics of elementary $A+BC$ type of reactions, they have not been discussed in this paper. However, note that the great power of this approach stems from the fact that, within the framework of the hyperspherical approach to reaction dynamics, it is possible to use angular momentum algebra (or its generalization, see below) to compute matrix elements of the Hamiltonian. The particularly advantageous aspects of the method is that the kinetic energy matrix is universal and sparse: salient features are the block tridiagonal structure and a number of symmetry properties.

Specifically, the technique developed in our group exploits the discrete analogues of orthonormal basis sets usually defined on continuous angular variables. These bases are orthonormal polynomial sets and our representation uses, as their discrete counterparts, polynomials orthogonal on lattice points, the so-called Hahn coefficients [31, 41, 46–48]. These can be identified, in particular cases, with the Clebsch-Gordan coefficients or vector coupling coefficients in the quantum theory of angular momentum. The algebraic work needed to develop this generalization is an important goal of current research.

Numerical aspects and performances of this "hyperquantization" algorithm have been demonstrated for a prototypical atom-diatom reaction ($F + H_2$) [49], including extensions for the treatment of the excited electronic surfaces. Calculations have been carried out on the reaction at total nuclear angular momentum equal to zero, the fine structure of the fluorine atom being explicitly taken into account. The technique presented is shown to be simple and effective for applications to reactive scattering problems, and the results are competitive with those obtained applying other current methods. The theory as well requires substantial effort to provide the ground to further develop-

ments. Expansions in alternative hyperspherical harmonics for three-body problems, corresponding to different couplings of particles and angular momenta, allow closed-form expressions for orthogonal transformations between coupling schemes. Similar transformations can also be found for alternative parametrizations of hyperangles [50].

Connections between harmonics are important for providing orthogonal transformations between basis set expansions pertaining to different Jacobi parametrizations. They were first introduced by Raynal and Revai. Their use, especially for nonorthogonal treatments where it may be convenient to expand over different basis sets for entrance and exit channels, is still to be exploited. The extension to more than three particles is the goal of current investigations.

Being the exact quantum mechanical treatment of the dynamics of systems containing more than four atoms presently computationally out of question, only particular cases or approximate methods are nowadays being developed in order to extend the hyperspherical method to complex reactions. Proper formulations of the coordinate systems and relevant hamiltonians have already been referred to [27, 28, 45], see also [51].

The reaction-volume Hamiltonian approach developed by Billing [52], in analogy with reaction path and surface Hamiltonian developed by Miller [53], consists in the reduction of the reactive process to a three- or four-center problem, focusing the attention on the dynamics of the subsystem constituted by the atoms directly involved in the reaction, while treating the remaining degrees of freedom within a harmonic decoupling scheme. Therefore the accurate hyperspherical method is used only for the reaction centers and the motion of the "spectator" atoms can be followed using the small amplitude approach. As a further example, the reaction $\text{OH} + \text{H}_2 \rightarrow \text{H}_2\text{O} + \text{H}$ has been studied [52, 54], considering that the initial O-H bond is not directly involved in the rearrangement.

Finally, time dependent methods are yielding interesting views on polyatomic reaction dynamics, although not actually leading to the full state-to-state information. Most promising for the future will be the blending of these methods with the hyperspherical approach under focus in the present paper.

References

- [1] V. Aquilanti and S. Cavalli. *J. Chem. Phys.*, **85**, 1355 (1986).
- [2] V. Aquilanti, S. Cavalli, G. Grossi, and R.W. Anderson. *J. Chem. Soc. Faraday Trans.*, **86**, 1681 (1990).
- [3] R. Littlejohn and M. Reinsch. *Rev. Mod. Phys.*, **69**, 213, (1997).

- [4] Yu.F. Smirnov and K.V. Shitikova. *Sov. J. Part. Nucl.*, **8**, 344 (1976).
- [5] L. Ballot and M. Fabre de la Ripelle. *Ann. Phys.*, **127**, 62 (1980).
- [6] H. Klar. *Physics of Electronic and Atomic Collisions*. S. Datz, North Holland, Amsterdam, 1982.
- [7] V. Aquilanti. in: *The Theory of Chemical Reaction Dynamics*. Ed. D.C. Clary, Reidel, Dordrecht, 1986.
- [8] V. Aquilanti and A. Laganà. in: *Nonequilibrium Vibrational Kinetics*. Ed. M. Capitelli, Springer, Berlin, 1986.
- [9] V. Aquilanti, S. Cavalli, and G. Grossi. in: *Advances in Molecular Vibrations and Collision Dynamics*, volume 2A. Ed. J.M. Bowman, JAI Press, Greenwich (Conn), 1993.
- [10] V. Aquilanti, S. Cavalli, C. Coletti, D. De Fazio, and G. Grossi. in: *New Methods in Quantum Theory*. Eds. C.A. Tsipis, V.S. Popov, D.R. Herschbach and J.S. Avery, Kluwer, 1996.
- [11] V. Aquilanti, S. Cavalli, and M.B. Sevryuk. *J. Phys. A.: Math. Gen.*, **24**, 4475, (1991).
- [12] V. Aquilanti, S. Cavalli, and M.B. Sevryuk. *J. Math. Phys.*, **34**, 3351, (1993).
- [13] V. Aquilanti, S. Cavalli, L. Yu. Rusin, and M.B. Sevryuk. *Theor. Chim. Acta*, **89**, 225, (1994).
- [14] V. Aquilanti, S. Cavalli, and M.B. Sevryuk. *J. Math. Phys.*, **35**, 556, (1994).
- [15] V. Aquilanti and G. Grossi. *J. Chem. Phys.*, **73**, 1165, (1980).
- [16] V. Aquilanti, S. Cavalli, and G. Grossi. *Z. Phys. D.*, **36**, 215, (1996).
- [17] U. Fano and G. Racah. *Irreducible Tensorial Sets*. Academic Press, New York, 1959.
- [18] H. Klar. *J. Phys. B: Atom. Molec. Phys.*, **7**, L436, (1974).
- [19] J. Maccek. *J. Phys. B*, **1**, 831, (1968).
- [20] U. Fano. *Phys. Rev. A*, **22**, 260, (1980).
- [21] J. Maccek. *Phys. Rev. A*, **33**, 2162, (1985).
- [22] U. Fano. *Phys. Rev. A*, **24**, 2402, (1981).
- [23] V. Aquilanti, G. Grossi, A. Laganà, E. Pelikan, and H. Klar. *Lett. Nuovo Cim.*, **41**, 541, (1984).
- [24] V. Aquilanti, S. Cavalli, and G. Grossi. *J. Chem. Phys.*, **85**, 1362, (1986).
- [25] B.R. Johnson. *J. Chem. Phys.*, **79**, 1906, (1983).

- [26] F.T. Smith. *Phys. Rev.*, **120**, 1058, (1960).
- [27] V. Aquilanti, L. Bonnet, and S. Cavalli. *Mol. Phys.*, **89**, 1, (1996).
- [28] V. Aquilanti and S. Cavalli. *J. Chem. Soc. Faraday Trans.*, **93**, 801, (1997).
- [29] J. Avery. *Hyperspherical Harmonics, Applications in Quantum Theory*. Kluwer Academic, Dordrecht, The Netherlands, 1989.
- [30] D.R. Hershbach, J. Avery, and O. Goscinski, editors. *Dimensional Scaling in Chemical Physics*. Kluwer Academic, Dordrecht, The Netherlands, 1993.
- [31] V. Aquilanti, S. Cavalli, and D. De Fazio. *J. Phys. Chem.*, **99**, 15694, (1995).
- [32] V. Aquilanti, S. Cavalli, C. Coletti, and G. Grossi. *Chem. Phys.*, **209**, 405, (1996).
- [33] V. Aquilanti, S. Cavalli, and C. Coletti. *Chem. Phys.*, **214**, 1, (1997).
- [34] V. Aquilanti and J. Avery. *Chem. Phys. Letters*, **267**, 1, (1997).
- [35] V. Aquilanti, S. Cavalli, and C. Coletti. *Phys. Rev. Lett.*, **80**, 3209, (1998).
- [36] V. Aquilanti, G. Grossi, and A. Laganà. *Chem. Phys. Lett.*, **93**, 174, (1982).
- [37] V. Aquilanti, S. Cavalli, and A. Laganà. *Chem. Phys. Lett.*, **93**, 179, (1982).
- [38] V. Aquilanti, S. Cavalli, and G. Grossi. *Chem. Phys. Lett.*, **110**, 43, (1984).
- [39] V. Aquilanti, S. Cavalli, and G. Grossi. *Chem. Phys. Letters*, **162**, 173, (1989).
- [40] V. Aquilanti and S. Cavalli. *Chem. Phys. Lett.*, **141**, 309, (1987).
- [41] V. Aquilanti, S. Cavalli, and D. De Fazio. *J. Chem. Phys.*, **109**, 3792, (1998).
- [42] V. Fock. *Kgl. Norske Videnskab. Selskabs Forh.*, **31**, 138, (1958).
- [43] F. T. Smith. *J. Math. Phys.*, **3**, 735, (1962).
- [44] R. Littlejohn, K. Mitchell, M. Reinsch, V. Aquilanti, and S. Cavalli. *Phys. Rev. A*, **a**, **58**, 3705, (1998).
- [45] R. Littlejohn, K. Mitchell, M. Reinsch, V. Aquilanti, and S. Cavalli. *Phys. Rev. A*, **b**, **58**, 3718, (1998).
- [46] V. Aquilanti and G. Grossi. *Lettere Nuovo Cim.*, **42**, 157, (1985).
- [47] V. Aquilanti and S. Cavalli. *Few-Body System Suppl.*, **6**, 573, (1992).
- [48] V. Aquilanti, S. Cavalli, and M. Monnerville. in: *Numerical Grid Methods and Their Applications to Schrodinger's Equation*. Ed. C. Cerjan, Kluwer, Dordrecht, 1993.
- [49] V. Aquilanti, S. Cavalli, D. De Fazio, A. Volpi, A. Aguilar, X. Gimenez, and J.M. Lucas. *J. Chem. Phys.*, **109**, 3805, (1998).

- [50] V. Aquilanti, G. Grossi, and A. Laganà. *J. Chem. Phys.*, **76**, 1587, (1982).
- [51] A. Kuppermann. *J. Phys. Chem.*, **101**, 6368, (1997).
- [52] G.D. Billing. *J. Chem. Soc., Faraday Trans.*, **93**, 833, (1997).
- [53] W.H. Miller, N.C. Handy, and J.E. Adams. *J. Chem. Phys.*, **72**, 99, (1980).
- [54] S.K. Pogrebnya, J. Echave, and D.C. Clary. *J. Chem. Phys.*, **107**, 8975, (1997).

On the Einstein-Podolsky-Rosen Paradox *

Roy McWeeny

Dipartimento di Chimica e Chimica Industriale
Università di Pisa, 56100 Pisa, Italy

Abstract

Central to the EPR paradox is a 'thought experiment' in which two spins are initially coupled to a state with $S = 0$ and are then separated to a large distance, at which they can be separately observed. Quantum mechanics apparently predicts that the two spins remain forever coupled, but this conflicts with Einstein's principle of 'locality' or 'separability', according to which spatially well separated systems must be independent, no matter how strongly they have interacted in the past. It is now widely held that Einstein was wrong and that 'non-locality' follows inevitably from quantum mechanics i.e. that even distant systems are never truly separable.

Here the question of separability is re-examined, within the framework of orthodox quantum mechanics but with a more realistic mathematical model than the one used in previous work, notably that by Bell.

The conclusion is that there is no conflict between Einstein's locality principle and the predictions of quantum mechanics: the discussions by Bell and others are based on an oversimplified model and on postulates that are untenable. Near the dissociation limit, states which differ only in spin coupling fall within an energy interval whose width tends to zero: representation of the system by a quantum mechanical ensemble then becomes mandatory, the coupling is broken, and the dissociation fragments become completely independent.

Contents

1. Introduction
2. The system density matrix
3. Reduced density matrices: the spin coupling density
4. An example: density functions for the hydrogen molecule
5. Dissociation of the hydrogen molecule
6. The general case
7. Conclusion

* Dedicated to my colleague and friend Giuseppe Del Re – for whom imagination and ideas have always been more precious than computations – on the occasion of his 65th birthday

1) Introduction

“Reality resists imitation through a model” (Schrödinger, 1935)¹

In the early days of quantum mechanics there was much discussion of the ‘reality’ of physical systems and of the ‘completeness’ of theories whose aim was to describe them mathematically. Much effort was expended in devising ‘thought experiments’ to test the validity of quantum mechanics: one such experiment was proposed by Einstein, Podolsky and Rosen [2], whose argument has since been extended and applied to many types of physical system. The EPR paper starts from the premise that “A sufficient condition for the reality of a physical quantity is the possibility of predicting it with certainty, without disturbing the system” and, after considering quantities whose associated operators do not commute, it is concluded that either (i) the description of reality given by quantum mechanics is incomplete; or (ii) that quantities whose operators do not commute can have no simultaneous reality. It is then a short step, by considering a system comprising two subsystems which interact for a short time and then separate, that if (i) is false then (ii) is also false. The final conclusion is that quantum mechanics (and in particular the wavefunction) cannot give a complete description of physical reality.

In 1951, Bohm [3] re-examined the EPR paradox and initiated the search for ‘hidden variables’, new ‘elements of physical reality’ not included among the variables of orthodox quantum mechanics, which might be used to formulate a more complete theory. Bohm took as his ‘model system’ a pair of electron spins, a model containing only six physically measurable quantities (the spin components of the two electrons) and thus amenable to straightforward analysis. His proposals were attacked by von Neumann and others and ultimately ruled out by the work of Bell[4,5], who proved formally that for such a system a hidden-variables interpretation was mathematically untenable. Bell’s work, however, was concerned purely with (i) the hypothetical system of two spins, initially interacting and then separating to a distance at which there was no further interaction; and (ii) with the question of whether or not the EPR paradox might be resolved by introducing hidden variables. Bell’s theorem [4] excludes that possibility; but it must be conceded that the model considered is so remote from the system it sets out to represent (namely *“a molecule containing two atoms in a state in which the total spin is zero”*) that the applicability of Bell’s analysis to any system encountered in ‘the real world’ is open to question.

Bell recognized very clearly, however, the fundamental problem, restating the views of Einstein [6]: it is the ‘common sense’ requirement that “the result of a measurement on one system be unaffected by operations on a distant system with which it has interacted in the past, that creates the essential difficulty” [4]. And in his second

¹ See Ref[1] for an English language version of Schrödinger’s famous 1935 paper and for a large collection of reprints of other papers on quantum mechanics and measurement.

paper [5] he pointed to the possibility of “replacing the arbitrary axioms [concerning hidden variables] by some condition of *locality*, or of *separability of distant systems*”, suggesting that “an interesting axiom would be that *mutually distant systems are independent of one another*. However, orthodox quantum mechanics apparently denies the possibility of such a separability: the two interacting spins in the EPR model, no matter how far they fly apart, must forever keep their original coupling to total spin zero. The same view has been expressed by d’Espagnat [7] and others, who claim that everything is connected to everything else in the universe. Such conclusions have given rise to the ‘many worlds’ and ‘many minds’ interpretations of quantum mechanics (well presented by, for example, Lockwood [8]), which continue to engage the minds of many philosophers. To the average physicist, however, such interpretations seem to border on science fiction; and one wonders whether such exotic deviations are really necessary (fascinating as they may be) in seeking an escape from the ‘separability/non-separability’ conflict.

The argument is real enough. The idea of non-separability, presented as an inevitable consequence of the axioms of quantum mechanics, appears to have been largely responsible for Einstein’s rejection of the Copenhagen interpretation. But sixty years later it is widely accepted [7] that “non-separability is now one of the most certain general concepts in physics”. One feels that the argument ought to be settled on the basis of orthodox quantum mechanics and that failure to do so may be connected not with the theory but rather with its application: could it not be that the alleged predictions of theory, on which the debate is centred, are simply artefacts arising from the use of drastically oversimplified models? For example, even a cursory inspection of the two-spin model reveals that it does not recognise some of the central features of quantum mechanics. How do we know where the two particles are, if the Hamiltonian contains no spatial variables, so how can we tell when they are ‘distant’? How can their *indistinguishability* be recognized if we use a wavefunction which does not conform to the Pauli (antisymmetry) principle? And if the (2-electron) model is indeed a non-separable system then at what point can independent observers make measurements on the *individual* electrons?

The aim of the present work is to reconsider the separability question, using the system referred to by Bohm and Bell but with a more realistic mathematical model: this should include the space and spin variables of all electrons, together with the nuclear coordinates which define the ‘geometry’ of the system. The simplest conceivable system of this type is the hydrogen molecule, to which orthodox quantum mechanics can be applied without difficulty – even with the recognition that the molecule may be in weak interaction with a ‘heat bath’ (i.e. with the rest of the world) and may thus be in an incompletely specified state, rather than a pure state (the isolated molecule singlet ground state). The question to be answered is: If the two hydrogen atoms move apart, at what point does an electron ‘forget’ that in the molecular ground state its spin was coupled to that of the other electron? And the aspects of the problem that seem to require special attention will be (i) the association of a statistical (or ‘density’) operator with the system; (ii) the in-

roduction of 'reduced' density operators and, in particular, a function to measure the *coupling* between the spins of two electrons at different points in space; and (iii) the importance of including electronic and nuclear coordinates in the Hamiltonian operator, which uniquely determines the evolution of the electronic wavefunction as a function of nuclear positions.

2) The system density matrix

First it is necessary to introduce appropriate notation and definitions and to recall some properties of the density operator introduced by von Neumann [10] and Dirac [11]. A general many-electron² wavefunction, for a system in stationary state K , will be written $\Psi_K(q)$, where q stands for all the required particle variables (space and spin coordinates). Such functions will be assumed orthonormal, so that the scalar product $\langle \Psi_K | \Psi_L \rangle = \delta_{KL}$, and being eigenfunctions of the Hamiltonian operator define a 'privileged' basis in the sense that their time evolution is unitary. For a system known to be in state K , the 'density matrix' may be represented symbolically by $\Psi_K \Psi_K^*$ (also written $|\Psi_K\rangle \langle \Psi_K|$) and in reality is an *operator*: thus, acting on an arbitrary state vector Φ , the result will be $\rho_K \Phi = \Psi_K (\Psi_K^* \Phi)$ or, in bra-ket notation

$$\rho_K |\Phi\rangle = |\Psi_K\rangle \langle \Psi_K | \Phi \rangle = c_K |\Psi_K\rangle \quad (c_K = \langle \Psi_K | \Phi \rangle).$$

The number c_K is clearly the 'component' of $|\Phi\rangle$ in the 'direction' $|\Psi_K\rangle$, when Φ is expanded in the form $\Phi = \sum_L c_L \Psi_L$; and the density operator is therefore a projection operator, with the characteristic property ($\rho_K^2 = \rho_K$). Thus,

$$\rho_K \rho_K = |\Psi_K\rangle \langle \Psi_K | \Psi_K \rangle \langle \Psi_K | = |\Psi_K\rangle \langle \Psi_K | = \rho_K.$$

When the particle variables q are introduced explicitly, ρ_K is represented as an integral operator, $\rho_K \rightarrow \rho_K(q; q') = \Psi_K(q) \Psi_K^*(q')$, whose effect on an arbitrary wavefunction $\Phi(q)$ is represented by

$$\rho_K \Phi(q) = \int \rho_K(q; q') \Phi(q') dq'. \quad (1)$$

Expectation values of all physical quantities A, B, \dots , with associated operators \hat{A}, \hat{B}, \dots may then be expressed typically as

$$\langle A \rangle = \langle \Psi_K | \hat{A} | \Psi_K \rangle = \int \Psi_K^*(q) \hat{A} \Psi_K(q) dq = \int [\hat{A} \rho_K(q; q')]_{q' \rightarrow q} dq, \quad (2)$$

where $q' \rightarrow q$ means the primed and unprimed variables are identified *after* the operation – so that the operator works only on the wavefunction and not on its

² It is sufficient to consider electronic variables alone and to employ the usual fixed-nuclei non-relativistic Hamiltonian

complex conjugate. The expectation value expression is thus expressed formally as a *trace*, with q, q' in the role of row and column indices.

Another important operator is the *transition* operator, $\rho_{KL} = \Psi_K \Psi_L^*$, connecting two states (Ψ_K, Ψ_L) , which is represented by the integral kernel $\Psi_K(q) \Psi_L^*(q')$. And an *off*-diagonal matrix element of any operator \hat{A} may then be expressed as

$$A_{LK} = \langle \Psi_L | \hat{A} | \Psi_K \rangle = \int \Psi_L^*(q) \hat{A} \Psi_K(q) dq = \int [\hat{A} \rho_{KL}(q; q')]_{q' \rightarrow q} dq. \quad (3)$$

Clearly $\rho_K = \rho_{KK}$ is the special case $L = K$ of ρ_{KL} - in which it is immaterial whether the single or double subscript is used.

If a discrete representation is adopted, by expressing all functions $\{\Psi_K\}$ in terms of a complete set $\{\Phi_K\}$ and collecting any set of expansion coefficients as a column vector c_K , all equations turn into matrix equations, in the usual way; for example, when $\hat{C} = \hat{A}\hat{B}$ there is a corresponding matrix equation $\mathbf{C} = \mathbf{A}\mathbf{B}$, where the elements of the (infinite) matrices are defined as above.

The density matrices play a special role in statistical mechanics; but also in any situation in which we possess incomplete information about some general system. In that case, the system will *not* be in a pure state and will thus *not be represented by a wavefunction*: instead, the 'mixed state' must be represented by a *density matrix*. The density matrix will then refer to an *ensemble* of identical systems of which a fractional number w_K are in the definite state Ψ_K ; and the ensemble density matrix will be

$$\rho = \sum_K w_K \Psi_K \Psi_K^*. \quad (4)$$

Since $\sum_K w_K = 1$, a system in which all the w_K are equal has $\rho = \rho_K$ - the density matrix for a single system, definitely known to be in state K ; but when more than one state is compatible with any given (often limited) knowledge of the system (e.g. that it be in a state with given energy E , without reference to other constants of the motion), the above sum does not reduce to a single term with $w_K = 1$. The criterion for the possibility of reduction to a pure state (irrespective of the particular representation chosen) is that the density operator be *idempotent*, $\rho^2 = \rho$. When this criterion is not satisfied (e.g. when there are many, equally accessible, states (K) of the same given energy, the *ensemble* expectation value of any quantity \hat{A} , with operator \hat{A} , will be

$$\bar{A} = \text{tr } \rho \hat{A} = \sum_K w_K (\text{tr } \rho_K \hat{A}) = \sum_K w_K \langle \Psi_K | \hat{A} | \Psi_K \rangle. \quad (5)$$

Evidently a 'double averaging' is involved, the quantum mechanical averaging implicit in the expectation value and the ensemble averaging associated with our inability to specify more completely the condition of an individual system. The time-honoured axiom of statistical mechanics (that of 'equal *a priori* probabilities and

random *a priori* phases'), whose validity is confirmed by innumerable applications in fields extending from biology to stellar structure, then asserts that the correct density matrix to use will be

$$\rho = \left(\frac{1}{g}\right) \sum_K \rho_K, \quad (6)$$

where g is the number of terms in the sum (e.g. the number of distinct terms of precisely specified energy).

3) Reduced density matrices; spin correlation

So far, no assumptions have been made about the precise form of the system of interest – it may be an electron or an arbitrary many-particle system. At this point we specialize to an N -electron molecule, introducing explicitly the variables (space and spin coordinates), collectively $\mathbf{x}_i = \mathbf{r}_i, s_i$ for electron i . With a small notational change, the wavefunction for state K of the system will be

$$\Psi_K = \Psi_K(\mathbf{x}_1, \mathbf{x}_2, \dots \mathbf{x}_N) = \Psi_K(\mathbf{x}), \quad (7)$$

the second form (with no subscripts) sometimes being used for brevity. The system density matrix, for pure state K , will then be (adding a superscript 'sys' to avoid confusion in what follows) $\rho_K^{\text{sys}}(q; q') = \Psi_K(q) \Psi_K^*(q')$ or more fully

$$\rho_K^{\text{sys}}(\mathbf{x}; \mathbf{x}') = \Psi_K(\mathbf{x}_1, \mathbf{x}_2, \dots \mathbf{x}_N) \Psi_K^*(\mathbf{x}'_1, \mathbf{x}'_2, \dots \mathbf{x}'_N) \quad (8)$$

– a function of both primed and unprimed variables. The so-called 'diagonal element' of the density matrix is obtained simply by removing the primes; and measures the probability density for finding electron 1 at point \mathbf{x}_1 , electron 2 simultaneously at point \mathbf{x}_2 , and so on. Since electrons are indistinguishable, the probability of finding volume elements $d\mathbf{x}_1, d\mathbf{x}_2, \dots \mathbf{x}_N$ simultaneously occupied by N particles *in any order* will be $N! \rho_K^{\text{sys}}(\mathbf{x}; \mathbf{x}) d\mathbf{x}$.

Reduced density matrices, introduced by Husimi [9], yield corresponding probability densities for the presence of n ($n < N$) particles simultaneously in selected volume elements $d\mathbf{x}_1, \dots \mathbf{x}_n$: thus, for $n = 1$, the probability/unit volume of finding an electron (no matter which) at \mathbf{x}_1 will be obtained by integrating $N! \rho_K^{\text{sys}}(\mathbf{x}; \mathbf{x})$ over the positions of all $N - 1$ volume elements $d\mathbf{x}_2, \dots d\mathbf{x}_N$ and dividing by $(N - 1)!$ (to avoid multiple counting). The quantity so defined is the 'one-particle reduced density matrix': more explicitly, it becomes

$$\rho(KK|\mathbf{x}_1; \mathbf{x}'_1) = N \int \Psi_K(\mathbf{x}_1, \mathbf{x}_2, \dots \mathbf{x}_N) \Psi_K^*(\mathbf{x}'_1, \mathbf{x}_2, \dots \mathbf{x}_N) d\mathbf{x}_2 d\mathbf{x}_3 \dots d\mathbf{x}_N. \quad (9)$$

The n -particle density matrices are widely used in molecular quantum mechanics (e.g.[10-12], where further references may be found. A well known property of the

one-particle density is that it relates matrix elements and expectation values of one-particle operators directly to the density: thus the kinetic energy (in state K) of all N electrons in any given system is expressible as

$$\langle K | \sum_i \hat{T}(i) | K \rangle = \int [\hat{T}(1) \rho(KK | \mathbf{x}_1; \mathbf{x}'_1)]_{\mathbf{x}'_1 \rightarrow \mathbf{x}_1} d\mathbf{x}_1, \quad (10)$$

where $\hat{T}(i)$ denotes the kinetic energy operator for the i th particle and the prime is removed after the operation.

The one-electron density matrix gives rise to others, for example $P(KK | \mathbf{r}_1; \mathbf{r}'_1)$, whose diagonal element gives the probable number of electrons per unit volume (without reference to spin) in the *spatial* volume element $d\mathbf{r}_1$ at point \mathbf{r}_1 ; and the spin density matrix $Q_z(KK | \mathbf{r}_1; \mathbf{r}'_1)$, whose diagonal element gives the contribution to the expectation value of the total spin z -component, $\langle \hat{S}_z \rangle$, associated with the same volume element. These functions are related to $\rho(KK | \mathbf{x}_1; \mathbf{x}'_1)$ as follows:

$$P(KK | \mathbf{r}_1; \mathbf{r}'_1) = \int [\rho(KK | \mathbf{x}_1; \mathbf{x}'_1)]_{s'_1=s_1} ds_1, \quad (11)$$

$$Q_z(KK | \mathbf{r}_1; \mathbf{r}'_1) = \int [\hat{S}_z(1) \rho(KK | \mathbf{x}_1; \mathbf{x}'_1)]_{s'_1=s_1} ds_1. \quad (12)$$

It is important to note that, while P is a scalar density, Q_z is one component of a *vector* density³, the components transverse to the quantization axis being defined in a similar way. Analogous *transition* densities, in which KK is replaced by KL , are required in discussing transitions between states K and L of the system, but are not needed in the present work.

It will be necessary to discuss also *spin correlation*: for if spins $\mathbf{S}(1), \mathbf{S}(2), \dots, \mathbf{S}(N)$ are coupled, to a resultant \mathbf{S} , then the expectation value of the squared total spin in state K will be

$$\langle K | \mathbf{S} \cdot \mathbf{S} | K \rangle = \langle K | \sum_i \mathbf{S}(i) \cdot \mathbf{S}(i) | K \rangle + \langle K | \sum_{i \neq j} \mathbf{S}(i) \cdot \mathbf{S}(j) | K \rangle \quad (13)$$

and, while the first term involves only a one-electron operator working on the variables \mathbf{x}_i , the second term contains the two-electron operator

$$\mathbf{S}(i) \cdot \mathbf{S}(j) = \hat{S}_x(i) \hat{S}_x(j) + \hat{S}_y(i) \hat{S}_y(j) + \hat{S}_z(i) \hat{S}_z(j). \quad (14)$$

Every 1-electron term in (13) reduces to $\frac{3}{4}$ (i.e. $s(s+1)$ with $s = \frac{1}{2}$), giving a total $\frac{3}{4}N$. It is the scalar product of the *different* spins in (13) that describes their coupling to a resultant, with quantum number S ; and discussion of the last term in

³ More correctly a *pseudovector* density, being an angular momentum per unit volume.

(13) requires knowledge of the *two*-electron density matrix, which will be denoted by $\pi(KK|\mathbf{x}_1, \mathbf{x}_2; \mathbf{x}'_1, \mathbf{x}'_2)$. This is defined (cf.(9)) by

$$\pi(KK|\mathbf{x}_1, \mathbf{x}_2; \mathbf{x}'_1, \mathbf{x}'_2) = N(N-1) \int \Psi_K(\mathbf{x}_1, \mathbf{x}_2, \dots, \mathbf{x}_N) \Psi_K^*(\mathbf{x}'_1, \mathbf{x}'_2, \dots, \mathbf{x}_N) d\mathbf{x}_3 \dots d\mathbf{x}_N. \quad (15)$$

As in the case of $\rho(KK|\mathbf{x}_1; \mathbf{x}'_1)$ a number of spatial densities may be derived by spin integration (the best known being the 'pair density' which gives the probability of volume elements $d\mathbf{r}_1, d\mathbf{r}_2$, at points $\mathbf{r}_1, \mathbf{r}_2$, simultaneously holding particles).

A contribution to the expectation value of a spin scalar product may be associated with every pair of volume elements in space through a 'coupling density', Q_c , defined by [11]

$$Q_c(KK|\mathbf{r}_1, \mathbf{r}_2; \mathbf{r}'_1, \mathbf{r}'_2) = \int [\mathbf{S}(1) \cdot \mathbf{S}(2) \pi(KK|\mathbf{r}_1, s_1, \mathbf{r}_2, s_2; \mathbf{r}'_1, s'_1, \mathbf{r}'_2, s'_2) s'_1, s'_2 \rightarrow s_1, s_2] ds_1 ds_2. \quad (16)$$

The key property of this function is that the diagonal element, denoted for brevity by $Q_c(KK|\mathbf{r}_1, \mathbf{r}_2)$, integrated over all positions of points \mathbf{r}_1 and \mathbf{r}_2 , will give a numerical measure of the spin coupling:

$$\langle \sum_{i \neq j} \mathbf{S}(i) \cdot \mathbf{S}(j) \rangle = \int Q_c(KK|(\mathbf{r}_1, \mathbf{r}_2) d\mathbf{r}_1 d\mathbf{r}_2. \quad (17)$$

This coupling density allows one to give a rather precise meaning to the probable degree of coupling between the spins of electrons occupying different volume elements in space.

The densities introduced in (12) and (16) may be interpreted in terms of the various 'spinless components' of the 1- and 2-body density matrices: the latter may be written, for brevity, in the forms

$$\rho = P_{\alpha;\alpha}(\alpha\alpha^*) + P_{\alpha;\beta}(\alpha\beta^*) + P_{\beta;\alpha}(\beta\alpha^*) + P_{\beta;\beta}(\beta\beta^*), \quad (18)$$

where, for example, the first term stands for $P_{\alpha;\alpha}(\mathbf{r}_1; \mathbf{r}'_1)\alpha(s_1)\alpha(s'_1)$; and

$$\pi = \Pi_{\alpha\alpha;\alpha\alpha}(\alpha\alpha^*\alpha^*) + \Pi_{\alpha\alpha;\alpha\beta}(\alpha\alpha^*\beta^*) + \dots + \Pi_{\beta\beta;\beta\beta}(\beta\beta^*\beta^*) \quad (19),$$

where $\Pi_{\alpha\alpha;\alpha\alpha}(\alpha\alpha^*\alpha^*)$ means $\Pi_{\alpha\alpha;\alpha\alpha}(\mathbf{r}_1, \mathbf{r}_2; \mathbf{r}'_1, \mathbf{r}'_2)(\alpha(s_1)\alpha(s_2)\alpha^*(s'_1)\alpha^*(s'_2))$, and so on. For states of definite total spin (quantum numbers S, M_S), only the first and last terms in (18) are non-zero; whereas only 6 of the 16 possible terms are present in (19). The diagonal elements of the spatial components in (18) have an immediate physical significance as probability densities: for example⁴,

$$P_{\alpha}(\mathbf{r}_1) = P_{\alpha;\alpha}(\mathbf{r}_1; \mathbf{r}_1)$$

⁴ In referring to diagonal elements it is convenient to suppress the redundant variables and labels that follow the semicolon

is the probability per unit volume of finding an up-spin electron at point \mathbf{r}_1 . Similarly, in (19),

$$\Pi_{\alpha\beta}(\mathbf{r}_1, \mathbf{r}_2) = \Pi_{\alpha\beta;\alpha\beta}(\mathbf{r}_1, \mathbf{r}_2; \mathbf{r}_1, \mathbf{r}_2)$$

is the probability density for finding an up-spin electron at point \mathbf{r}_1 and a down-spin electron simultaneously at point \mathbf{r}_2 .

It is essential to note that the labels on the variables *do not refer to the electrons*, but rather to *points in space*, which are chosen by an observer and are physically distinguishable. The Pauli principle has been respected from the start by insisting that $|\Psi|^2$ be invariant against any permutation of ‘electron labels’.

On removing the primes in equations (18) and (19) and integrating over spin, one obtains the spinless densities:

$$P(\mathbf{r}_1) = P_\alpha(\mathbf{r}_1) + P_\beta(\mathbf{r}_1), \quad (20)$$

which is the probability density for finding an electron at \mathbf{r}_1 , a sum of up-spin and down-spin contributions; while

$$\Pi(\mathbf{r}_1, \mathbf{r}_2) = \Pi_{\alpha\alpha}(\mathbf{r}_1, \mathbf{r}_2) + \Pi_{\alpha\beta}(\mathbf{r}_1, \mathbf{r}_2) + \Pi_{\beta\alpha}(\mathbf{r}_1, \mathbf{r}_2) + \Pi_{\beta\beta}(\mathbf{r}_1, \mathbf{r}_2), \quad (21)$$

showing that the pair density is also a sum of contributions from the various spin situations – both up, one up one down, or both down.

The spin density and the coupling density may be presented in a similar way, as follows from the definitions (12) and (16).

An example: density functions for the hydrogen molecule

In this section we derive the density functions for a prototype system in which, to quote Bohm [3] “we have a molecule containing two atoms in a state in which the total spin is zero ... and suppose that the system is disintegrated by some process that does not change the total [spin] angular momentum”. The simplest concrete realization of such a system is, of course, the hydrogen molecule. Instead of the usual two-spin Hamiltonian used by Bohm, Bell, and many others, let us start from the standard non-relativistic Born-Oppenheimer Hamiltonian, using a wavefunction which includes all electronic variables (both space and spin). This is the simplest possible Hamiltonian that can do full justice to the physics of the system: for example, even though it correctly⁵ contains no spin operators, the indistinguishability of the electrons dictates the form of the wavefunction through the Pauli requirement that Ψ be antisymmetric with respect to an exchange of space-spin variables

⁵ In the approximation normally used, the small magnetic interactions involving the spins are ignored: they belong to treatments based on the Dirac equation and lead only to the observed fine and hyperfine structure of the energy levels.

$\mathbf{x}_1, \mathbf{x}_2$; and it provides for an actual separation of the system into two parts as the nuclei (whose coordinates enter only as parameters) move apart – a process to be considered subsequently.

The possible wavefunctions for singlet or triplet coupling of the spins assume the well known forms [13]:

$$\begin{aligned}\Psi_s &= N_s(AB + BA)(\alpha\beta - \beta\alpha)/\sqrt{2} & (S = 0, M_S = 0) \\ \Psi_t^+ &= N_t(AB - BA)(\alpha\alpha) & (S = 1, M_S = 1) \\ \Psi_t^0 &= N_t(AB - BA)(\alpha\beta + \beta\alpha)/\sqrt{2} & (S = 0, M_S = 0) \\ \Psi_t^- &= N_t(AB - BA)(\beta\beta) & (S = 1, M_S = -1).\end{aligned}\quad (22)$$

Here A, B are hydrogen atomic orbitals centred on the two nuclei (a, b), while $N_s = (2 + 2S_{AB}^2)^{-\frac{1}{2}}$ and $N_t = (2 - 2S_{AB}^2)^{-\frac{1}{2}}$ are normalizing factors, $S_{AB} = \langle A|B \rangle$ being the ‘overlap integral’ for the two AOs. The space and spin variables (not shown) are assumed to be in natural order in all products: thus $\Psi_s(\mathbf{x}_1, \mathbf{x}_2)$ contains the spatial factor $(A(\mathbf{r}_1)B(\mathbf{r}_2) + B(\mathbf{r}_1)A(\mathbf{r}_2))$ and the spin factor $\alpha(s_1)\beta(s_2) - \beta(s_1)\alpha(s_2)$. These wavefunctions become ‘exact’ as the internuclear distance R tends to infinity and $S_{AB} \rightarrow 0$: for other values of R they can give a good account of the energy variation, as a function of R , provided the orbitals are optimized by standard methods. The important thing however is that they ‘dissociate correctly’, all giving the same energy $2E_H$ (that of two separate hydrogen atoms) for $R \rightarrow \infty$.

It is a simple matter to calculate, for each state, the expectation value of the total electronic energy E and to derive expressions for the required density functions. For the energy one obtains

$$E_s = \frac{(Q + K)}{(1 + S_{AB}^2)}, \quad E_t = \frac{(Q - K)}{(1 - S_{AB}^2)}, \quad (23)$$

where Q, K are the so-called ‘coulomb’ and ‘exchange’ integrals, which depend parametrically on the internuclear distance R .

The spin density Q_z and the spin coupling function Q_c follow from (12) and (16). On starting from the wavefunctions in (22) and finally taking the diagonal elements ($\mathbf{r}'_1, \mathbf{r}'_2 \rightarrow \mathbf{r}_1, \mathbf{r}_2$), it follows that in the singlet state the spin density is everywhere zero,

$$Q_z^s(\mathbf{r}_1) = 0, \quad (24)$$

while the spin-coupling function takes the form

$$Q_c^s(\mathbf{r}_1, \mathbf{r}_2) = -\frac{3}{2}F_s(\mathbf{r}_1, \mathbf{r}_2), \quad (25)$$

the function F_s being

$$F_s(\mathbf{r}_1, \mathbf{r}_2) = (2 + 2S_{AB}^2)^{-1} \times [ABAB + BABA + ABBA + BAAB], \quad (26)$$

(variables always in the order $\mathbf{r}_1, \mathbf{r}_2, \mathbf{r}_1, \mathbf{r}_2$). Corresponding densities for the three triplet states are

$$Q_z^{t+} = (1 - S_{AB}^2)^{-1} [A^2(\mathbf{r}_1) - 2S_{AB}A(\mathbf{r}_1)B(\mathbf{r}_1) + B^2(\mathbf{r}_1)] = -Q_z^{t-}(\mathbf{r}_1), \quad (27)$$

$Q_z^{t0}(\mathbf{r}_1)$ being everywhere zero, and,

$$Q_c^{t+}(\mathbf{r}_1, \mathbf{r}_2) = Q_c^{t0}(\mathbf{r}_1, \mathbf{r}_2) = Q_c^{t-}(\mathbf{r}_1, \mathbf{r}_2) = \frac{1}{2}F_t(\mathbf{r}_1, \mathbf{r}_2), \quad (28)$$

where

$$F_t(\mathbf{r}_1, \mathbf{r}_2) = (2 - 2S_{AB}^2)^{-1} \times [ABAB + BABA - ABBA - BAAB], \quad (29)$$

(variables again in the order $\mathbf{r}_1, \mathbf{r}_2, \mathbf{r}_1, \mathbf{r}_2$).

It remains only to ask what happens to the molecule, initially in its singlet ground state, as the two nuclei move apart.

5) Dissociation of the hydrogen molecule

The energy curves for the singlet ground state and the first excited triplet state of the hydrogen molecule have well known forms. The singlet curve shows a deep minimum at $R \sim 1.4a_0$ ⁶ and then rises to E_h (the energy of two isolated hydrogen atoms) as $R \rightarrow \infty$: the triplet curve shows no minimum, falling monotonically to the same asymptotic limit. In general the energies are only approximate (being those of Heitler and London [13]), but at $R \rightarrow \infty$ they become exact (for a non-relativistic Born-Oppenheimer Hamiltonian). The main concern here will be with this asymptotic region in which the system approaches dissociation into two subsystems: when, for example, $R = 20.0a_0$ the separation between the singlet and triplet curves is only $2.69 \times 10^{-7}E_h$ and the crucial question is then whether the electrons still retain the coupling to $S = 0$ appropriate to the equilibrium ground state. At this point the integral S_{AB} , which measures the overlap between the two subsystems is also small (0.962×10^{-6}); and as R increases both quantities diminish exponentially to zero. Nor is it reasonable any longer to regard the 'molecule' as an isolated system in a stationary eigenstate; for it is exposed to random fluctuations of the 'heat bath' (the rest of the universe!) in which it is embedded. Indeed, between the remote parts of the system there is room for eight more hydrogen atoms! In such a situation, as indicated already, the condition of the system is more correctly represented by means of a mixed-state density operator, not by a single energy eigenfunction.

The validity of using a statistical ensemble to represent an incompletely specified system is fundamental and is not in question. The important question is: which 'accessible states' are compatible with our limited information about the system?

⁶ Units of length, energy, and action are a_0 (the bohr radius), E_h (the 'hartree'), and \hbar (Planck's constant, $\hbar/2\pi$).

In the example under discussion there are four states that lie within an energy interval ΔE of the order $10^{-7} E_h$, among which there appears to be no possibility of distinguishing experimentally. The difficulty is clearly connected with the energy-time uncertainty relation, $\Delta E \Delta t \sim \hbar$, which has been extensively discussed, from many points of view (see [14] for a survey). For present purposes it is enough to recall only the simplest approach [15]. One considers the time evolution of a (non-stationary) wavefunction, represented as a sum of two states Ψ_1 and Ψ_2 with time factors $\exp -iE_1 t/\hbar$ and $\exp -iE_2 t/\hbar$, respectively: the square of the wavefunction then oscillates with period

$$\tau = \frac{\hbar}{|(E_1 - E_2)|}, \quad (30)$$

which is a 'characteristic time' for change of the physical properties of the system. To determine whether a system initially in State 1 is still in State 1 after a certain lapse of time, the energy measurement must be repeated within a time interval Δt , small compared with τ ; otherwise there is no guarantee that the same value will be found (i.e. that a transition has not occurred). In the hydrogen molecule example, with $R = 20a_0$, the characteristic time (which in essence measures the lifetime of the state) turns out to be 0.90×10^{-10} ; and the conclusion is that, when such stringent requirements on state preparation are not fulfilled, all states with energies in the small interval ΔE should be treated on an equal footing in setting up a density operator of the type (6).

First let us discuss the case in which singlet and triplet states are well separated in energy and are represented by eigenstates of the Hamiltonian and the total spin operators \hat{S}^2, \hat{S}_z . It is verified immediately (noting that the functions (26) and (29) are normalized to unity on integrating over both variables) that

$$\int Q_c(\mathbf{r}_1, \mathbf{r}_2) d\mathbf{r}_1 d\mathbf{r}_2 = S(S+1) - \frac{3}{4}N \quad (31)$$

for all states. It is also informative to consider the origin of the main contributions to the integrals: thus, when volume element $d\mathbf{r}_1$ is in the region of nucleus 'a' $A(\mathbf{r}_1)$ is large and $B(\mathbf{r}_1)$ is small; and the density of spin angular momentum (when non-zero) has the same form as the electron density $P(\mathbf{r}_1)$, but with up-spin character in state 't+', down-spin in state 't-'. The density of spin *coupling*, on the other hand, arises mainly when the electrons occupy volume elements $d\mathbf{r}_1$ and $d\mathbf{r}_2$ which are on different centres; this is true for both singlet and triplet coupling and is a crucial embarrassment because it suggests that coupled spins will stay coupled forever, no matter how far apart their parent atoms may move.

It is the non-zero value of the integral in (31), irrespective of the separation of A and B, that violates any principle of locality: it appears as a direct result of applying standard quantum mechanics and seems to imply some kind of 'action at a distance' that keeps the two spins coupled. It should be noted, however, that the postulate of Bohm and Bell – that the system is "disintegrated by some kind of process that

does not change the total angular momentum" – effectively *prescribes* this result at the outset. It is usually claimed that non-locality is a consequence of quantum mechanics; but, more precisely, it is a consequence of insisting that the system stays forever in its initial spin eigenstate. Let us now remove such restrictions.

On removing the atoms to a considerable distance, such that the singlet and triplet energies fall within a sufficiently small interval, the use of a representative ensemble becomes mandatory. The density matrix (6) then leads to ensemble averaged densities, \bar{Q}_z and \bar{Q}_c , as follows:

$$\bar{Q}_z(\mathbf{r}_1) = \frac{1}{4}Q_z^s(\mathbf{r}_1) + \frac{1}{4}Q_z^{t0}(\mathbf{r}_1) + \frac{1}{4}Q_z^{t,+1}(\mathbf{r}_1) + \frac{1}{4}Q_z^{t,-1}(\mathbf{r}_1) = 0 \quad (32)$$

and

$$\bar{Q}_c(\mathbf{r}_1, \mathbf{r}_2) = \frac{1}{4}Q_c^s(\mathbf{r}_1, \mathbf{r}_2) + \frac{1}{4}Q_c^{t0}(\mathbf{r}_1, \mathbf{r}_2) + \frac{1}{4}Q_c^{t,+1}(\mathbf{r}_1, \mathbf{r}_2) + \frac{1}{4}Q_c^{t,-1}(\mathbf{r}_1, \mathbf{r}_2) = 0 \quad (33)$$

In other words, as soon as the system breaks into two subsystems any initial spin density will fall to zero, along with any initial spin coupling between the subsystems. The subsystems are then truly independent in the sense that all expectation values for either may be calculated without reference to the other; and that the spin coupling density, which connected the two, is now everywhere zero.

This example clearly shows that the EPR conflict is not between locality and quantum mechanics but is simply between locality and non-locality – both alternatives following from orthodox quantum mechanics, provided the appropriate representative ensemble (pure or mixed) is employed.

6) The general case

A study of the hydrogen molecule hardly provides a sufficient basis for formulating general principles concerning the separation of a system into subsystems. In general one is concerned with the interaction of two subsystems, A and B, in spin states with quantum numbers (S_A, M_A) and (S_B, M_B) , whose total spin vectors $(\mathbf{S}^A, \mathbf{S}^B)$ are coupled to a resultant \mathbf{S} , yielding a set of states with quantum numbers S, M ($M = S, S - 1, \dots - S$). When A and B are close together and their interaction is appreciable, states that differ in S are usually well spaced in energy. The general question to be asked is again: What happens to the spin coupling between the different systems when they are pulled apart to a large distance? For the hydrogen molecule, there were only two spins and two possible couplings ($S = 0, 1$); exact wave functions for the separate subsystems were available; and the 2-electron wavefunction could be written as a product of space and spin factors, the Pauli principle being satisfied by choosing one factor symmetric and the other antisymmetric. In the general case no such simplifications apply.

Let us now study the general case, postulating the existence of exact eigenfunctions $\Phi_{S_A, M_A}, \Phi_{S_B, M_B}$ for two quite arbitrary subsystems (many-electron atoms or

molecules), with energy eigenvalues E_A, E_B ; and suppose all functions to be fully antisymmetric in electron indices. It is then possible to set up spin-coupled linear combinations of the $(2S_A + 1)(2S_B + 1)$ product functions arising from different choices of M_A, M_B : these will be

$$\Phi_{S,M}(\mathbf{x}_1, \mathbf{x}_2, \dots, \mathbf{x}_N) = (-1)^{(S_B - S_A - M)} (2S + 1)^{\frac{1}{2}} \sum_{M_A, M_B} \begin{pmatrix} S_A & S_B & S \\ M_A & M_B & -M \end{pmatrix} \times \Phi_{S_A, M_A}(\mathbf{x}_1, \mathbf{x}_2, \dots, \mathbf{x}_{N_A}) \Phi_{S_B, M_B}(\mathbf{x}_1, \mathbf{x}_2, \dots, \mathbf{x}_{N_B}), \quad (33)$$

where variables with labels 1, 2, ... N_A refer to electrons of subsystem A, while those with labels $\bar{1}, \bar{2}, \dots, \bar{N}_B$ (with $\bar{k} = N_A + k$) refer to subsystem B. The round-bracket quantity in (33) is a Wigner 3j symbol.

The vector-coupled function $\Phi_{S,M}$ is not properly antisymmetric against permutations which exchange electrons between the A and B subsystems. But this may be remedied by applying the 'antisymmetrizer'

$$\hat{A} = (N!)^{-1} \sum_{\hat{P}} \epsilon_{\hat{P}} \hat{P} = (N_A! N_B! / N!) \hat{A}' \hat{A}_A \hat{A}_B, \quad (34)$$

where \hat{A}_A, \hat{A}_B are subsystem antisymmetrizers (which will leave $\Phi_{S_A, M_A}, \Phi_{S_B, M_B}$ unchanged), while \hat{A}' denotes a coset sum of all (multiple) transpositions of variables *between* subsystem A and subsystem B. On applying the operator (34) to the vector-coupled function (33) we obtain a fully antisymmetric wavefunction

$$\Psi_{S,M} = K \hat{A} \Phi_{S,M} \quad (K = (N! / N_A! N_B!)^{\frac{1}{2}}), \quad (35)$$

where a convenient normalizing factor K has been added.

Expressions for the density functions $P(SS|\mathbf{r}_1; \mathbf{r}'_1)$ and $\Pi(SS|\mathbf{r}_1, \mathbf{r}_2; \mathbf{r}'_1, \mathbf{r}'_2)$, which (with the usual Hamiltonian) determine the total electronic energy of the system, are available elsewhere [16] and the derivations will not be repeated. Briefly, every function is a finite sum of terms arising from 0, 1, 2, ... N_{\min} (N_{\min} being the smaller of N_A, N_B) electron transpositions between the subsystems, and each term may be written as a functional containing densities for the separate subsystems. Such sums converge rapidly and in discussing molecular interactions it is seldom necessary to go beyond single interchanges. In the present context, where interest is focused on long range interactions, the effects of electron exchange are quite negligible and it is sufficient to consider zero-interchange contributions to all expectation values: this means that (33) in itself provides a satisfactory wavefunction for studying the spin coupling when A and B are remote.

To obtain the spin coupling function Q_c for any given vector-coupled state of the composite system AB, when A and B are remote, we use (33) to evaluate the expectation value of the total spin operator \mathbf{S}^2 . Thus,

$$\langle \Phi_{S,M} | \mathbf{S}^2 | \Phi_{S,M} \rangle = \langle \Phi_{S,M} | (\mathbf{S}_A^2 + \mathbf{S}_B^2 + 2\mathbf{S}_A \cdot \mathbf{S}_B) | \Phi_{S,M} \rangle. \quad (36)$$

The operator $\mathbf{S}_A^2 = \sum_{i=1, N_A} \mathbf{S}^2(i)$ represents a contribution from the electrons of subsystem A, the contribution from B assuming a similar form with A replaced by B and the summation index running from $\bar{j} = \bar{1}$ to \bar{N}_B . The first two terms in the expectation value (36) thus arise from the *internal* spin couplings in the separate subsystems and should reduce to $S_A(S_A + 1)$ and $S_B(S_B + 1)$, respectively. The third contribution arises from the spin coupling between the electrons of different subsystems: to evaluate it one may use the methods of Ref.[17]. Thus,

$$\begin{aligned} \langle \Phi_{S,M} | \mathbf{S}_A \cdot \mathbf{S}_B | \Phi_{S,M} \rangle &= \langle \Phi_{S,M} | \sum_{i=1}^{N_A} \sum_{\bar{j}=1}^{\bar{N}_B} \mathbf{S}(i) \cdot \mathbf{S}(\bar{j}) | \Phi_{S,M} \rangle \\ &= (-1)^{(S_A+S_B+S)} \left\{ \begin{matrix} S_A & S_B & S \\ S_B & S_A & 1 \end{matrix} \right\} \begin{pmatrix} S_A & 1 & S_A \\ -S_A & 0 & S_A \end{pmatrix}^{-1} \begin{pmatrix} S_B & 1 & S_B \\ -S_B & 0 & S_B \end{pmatrix}^{-1} \\ &\quad \times \langle \Phi_{S_A, S_A} \Phi_{S_B, S_B} | \sum_{i, \bar{j}} \hat{S}_z(i) \hat{S}_z(\bar{j}) | \Phi_{S_A, S_A} \Phi_{S_B, S_B} \rangle, \end{aligned} \quad (37)$$

where the scalar product $\mathbf{S}(i) \cdot \mathbf{S}(\bar{j})$ was written in terms of rank-1 spherical tensor operators ($\hat{S}_k, k = 0, \pm 1$) in order to exploit well known theorems [17]: the matrix element on the right now refers only to 'standard' states, with $M_A = S_A, M_B = S_B$, and is preceded by a Wigner 6j symbol and two 3j symbols.

The matrix element is easily related to the spin densities in subsystems A and B; thus

$$\begin{aligned} \langle \Phi_{S_A, S_A} | \sum_i \hat{S}_z(i) | \Phi_{S_A, S_A} \rangle &= \int \Phi_{S_A, S_A}^* N_A \hat{S}_z(1) \Phi_{S_A, S_A} d\mathbf{r}_1 ds_1 d\mathbf{x}_2 \dots d\mathbf{x}_{N_A} \\ &= \int Q_z(S_A | \mathbf{r}_1) d\mathbf{r}_1, \end{aligned} \quad (38)$$

with a similar expression for the B-factor.

The factor involving the Wigner coefficients may also be put into a simpler form: it is invariant against rotation of the axis of quantization and must therefore be expressible in terms of invariants formed from the total spin operators of the two subsystems. On denoting the numerical factor in (37) by $f_1(S_A, S_B, S)$, it follows easily [16] that

$$f_1(S_A, S_B, S) = \frac{\langle S, M | \mathbf{S}_A \cdot \mathbf{S}_B | S, M \rangle}{S_A S_B}. \quad (39)$$

The contribution to $\langle \mathbf{S} \cdot \mathbf{S} \rangle$ that arises from electrons belonging to the different subsystems is thus

$$\langle \Phi_{S,M} | \mathbf{S}_A \cdot \mathbf{S}_B | \Phi_{S,M} \rangle = \int Q_c^{AB}(\mathbf{r}_1, \mathbf{r}_2) d\mathbf{r}_1 d\mathbf{r}_2, \quad (40)$$

where

$$Q_c^{AB}(\mathbf{r}_1, \mathbf{r}_2) = \langle S, M | \mathbf{S}_A \cdot \mathbf{S}_B | S, M \rangle \frac{Q_z(S_A | \mathbf{r}_1)}{S_A} \frac{Q_z(S_B | \mathbf{r}_1)}{S_B} d\mathbf{r}_1 d\mathbf{r}_2. \quad (41)$$

The integrations in (40) obviously yield unity, since (41) contains two normalized spin density factors: in fact (40) is a precise analogue of (25) and (28) in the hydrogen molecule example. In any spin eigenstate the coupling density (41) will be non-zero; but the integrations over all space will evidently yield a simple scalar product coupling between the subsystems A and B, however complicated they may be. This result is quite independent of the distance between A and B.

The contributions to $\langle \mathbf{S} \cdot \mathbf{S} \rangle$ that arise from electrons belonging to the same subsystem follow immediately. Thus, for A, the expectation value of $\sum_{i \neq j} \mathbf{S}(i) \cdot \mathbf{S}(j)$ (i, j both belonging to the *same* subsystem) the expectation value becomes

$$N_A(N_A - 1) \int \Phi_{S_A, M_A}^*(\mathbf{x}_1, \mathbf{x}_2, \dots) \mathbf{S}(1) \cdot \mathbf{S}(2) \Phi_{S_A, M_A}(\mathbf{x}_1, \mathbf{x}_2, \dots) d\mathbf{x}_1 d\mathbf{x}_2 \dots d\mathbf{x}_{N_A}$$

and this is easily seen to be

$$\int Q_c^A(\mathbf{r}_1, \mathbf{r}_2) d\mathbf{r}_1 d\mathbf{r}_2.$$

There is a similar result for subsystem B and both are independent of M_A, M_B . The vector-coupled state $\Phi_{S, M}$ thus yields 'internal' contributions

$$\langle \Phi_{S, M} | \mathbf{S}_A \cdot \mathbf{S}_A | \Phi_{S, M} \rangle = \int Q_c^A(\mathbf{r}_1, \mathbf{r}_2) d\mathbf{r}_1 d\mathbf{r}_2 = S_A(S_A + 1), \quad (42a)$$

$$\langle \Phi_{S, M} | \mathbf{S}_B \cdot \mathbf{S}_B | \Phi_{S, M} \rangle = \int Q_c^B(\mathbf{r}_1, \mathbf{r}_2) d\mathbf{r}_1 d\mathbf{r}_2 = S_B(S_B + 1), \quad (42b)$$

which arise from strictly separate coupling functions, one localized in subsystem A and the other in B.

In the absence of any spin coupling between the remote fragments, A and B, the expectation value $\langle \mathbf{S}^2 \rangle$ would be simply $S_A(S_A + 1) + S_B(S_B + 1)$, as if neither subsystem 'knew' anything of the other. This would be the 'common sense' result. The fact that (40), on the contrary, takes a non-zero value in any state of definite total spin is the 'action at a distance' result that Einstein found totally unacceptable.

It is now easy to show that in the long range limit, where the energy curves for the $(2S_A + 1)(2S_B + 1)$ alternative spin couplings approach indefinitely closely, the ensemble-averaged coupling density derived from (41) becomes everywhere zero. The spatial density factors in (41) are in fact quite independent of coupling scheme and

the averaging thus concerns only the expectation value $\langle S, M | \mathbf{S}_A \cdot \mathbf{S}_B | S, M \rangle$ over all S, M : the average value of the latter is zero, by simple angular momentum theory, and this establishes that the ensemble-averaged values of the 'action at a distance term' (40) and its related spin-coupling density approach zero as A and B separate. It is also possible to estimate a good order of magnitude for the separation of A and B at which the transition from non-locality to locality will take place. The analogue of the squared overlap S_{AB}^2 in Section 5 is the quantity [16]

$$S_{AB}^{(1)} = \frac{1}{2} \int P_A(S_A S_A | \mathbf{r}_1, \mathbf{r}'_1) P_B(S_B S_B | \mathbf{r}'_1, \mathbf{r}_1) d\mathbf{r}_1 d\mathbf{r}'_1 \\ + 2f_1(S_A, S_B, S) \int Q_{z,A}(S_A S_A | \mathbf{r}_1, \mathbf{r}'_1) d\mathbf{r}_1 d\mathbf{r}'_1 Q_{z,B}(S_B S_B | \mathbf{r}'_1, \mathbf{r}_1) d\mathbf{r}_1 d\mathbf{r}'_1, \quad (43)$$

which contains electron and spin densities for the separate systems in their ground states. For the two hydrogen atoms in Section 5, this single interchange contribution to a generalized overlap correctly reduces to $2S_{AB}^2$ and at $R = 20.0a_0$ takes the value 2×10^{-12} . A similar discussion, applied in the general case, then suggests that the distance at which (43) assumes a value less than, say, 10^{-12} will provide a convenient measure of the 'forgetting distance' beyond which no spin coupling can persist.

7) Conclusion

The system considered in this paper is, again in the words of Bohm [3], "a molecule containing two atoms in a state in which the total spin is zero and the spin of each atom is $\frac{1}{2}$ ": but the restriction to a singlet state and to spin- $\frac{1}{2}$ atoms has now been removed. The molecule is dissociated by separating the nuclei to a large distance and the course of the reaction $AB \rightarrow A + B$ is followed using standard quantum mechanics. In the general case, the wavefunction Ψ for AB is taken to be a spin-coupled antisymmetrized product of two factors Ψ_A, Ψ_B , which are 'exact' many-electron wavefunctions for free atoms A and B in states of total spin S_A, S_B , respectively. In the dissociation limit Ψ yields the correct total energy $E = E_A + E_B$; but it may be any one of $(2S_A + 1)(2S_B + 1)$ accessible states, $\Psi_{S,M}$, obtained by coupling the spins S_A, S_B to a resultant with $S = S_A + S_B, S_A + S_B - 1, \dots |S_A - S_B|$ and $M = S, S - 1, \dots -S$, the energies of such states falling within an interval ΔE which tends to zero.

In this energy regime, the condition of the system is correctly represented not by any one state $\Psi_{S,M}$ but rather by a quantum statistical ensemble in which all the accessible states appear with equal *a priori* weights and random *a priori* phases. The appropriate density operator is then

$$\rho = \frac{\sum_{S,M} \Psi_{S,M} \Psi_{S,M}^*}{(2S_A + 1)(2S_B + 1)} \quad (44)$$

and its use implies the recognition of chaotic mixing of the states whose energies lie within ΔE , which arises from arbitrarily weak interaction with the environment (or

'heat bath'). In the case considered by Bohm, $S_A = S_B = \frac{1}{2}$ and there are 4 terms in ρ ; corresponding to $S = 0$ (1 term) and $S = 1$ (3 terms). But for two nitrogen atoms, say, $S_A = S_B = \frac{3}{2}$ and there would be 16 terms – coming from $S = 0$ (1 term), $S = 1$ (3 terms), $S = 2$ (5 terms) and $S = 3$ (7 terms).

It has been established in Sect.6 that whenever it becomes necessary to employ a mixed (rather than pure) ensemble, with density operator (44), the interatomic spin-coupling density $Q_c^{AB}(\mathbf{r}_1, \mathbf{r}_2)$ is everywhere zero and thus yields zero for the expectation value of the spin scalar product $\mathbf{S}_A \cdot \mathbf{S}_B$: *there can be no spin coupling between A and B*. Two regimes may thus be distinguished:

(i) Well below the dissociation limit the system is well represented by a pure state, the ensemble degenerates into a single term with the same spin (e.g. $S = 0$) as the initial state, other states being energetically distant and therefore inaccessible under weak ('heat bath') perturbations. Throughout this regime the generally accepted conclusion holds: the spin coupling remains that of the molecular ground state, as if each atom 'remembers' its coupling to the other – even when A and B are rather distant. Non-locality is thus apparently confirmed. It could hardly be otherwise of course! – because the coupling is *imposed* at the outset by Bohm's *postulate* that the molecule be "disintegrated by some process that does not change the total [spin] angular momentum".

(ii) In the ' ΔE ' regime, where use of the mixed ensemble is mandatory, the spin coupling *between* A and B falls to zero, only the *intraatomic* couplings (to S_A and S_B , within atoms A and B, respectively) remaining intact. At this point A and B become completely independent, neither having any 'recollection' of any previous coupling in the molecule. Throughout the rest of this regime, as A and B separate to infinity, experiments may be performed separately on the two subsystems and it is guaranteed that the expectation values of all observables will coincide with those for the free atoms.

To summarize: Below the dissociation limit, the system AB will display non-locality; but beyond that limit locality will re-emerge, each of the subsystems (A,B) being restored to its original (free-atom) condition, irrespective of any previous interactions. In other words, locality and non-locality are simply two faces of the same quantum coin.

At this point it seems appropriate to add a few words on the subject of 'physical reality' and 'mathematical models' – the touchstone for the EPR paper and the 60 years of discussion that followed it. EPR stress that "an element of physical reality cannot be determined by *a priori* philosophical considerations but must be found by an appeal to results of experiments and measurements": their approach is thus essentially pragmatic. Between this 'reality' and the 'mathematical models' we actually use stands the *physical theory*, in this case quantum mechanics, which operates with

the elements of reality and enables one to draw new, and experimentally verifiable, conclusions. When the conclusions are verified the theory is considered 'correct' – or at least satisfactory. In fact, however, the theory (in anything approaching a complete form) is almost always impossible to apply, owing to its mathematical complexity; and it is here that the 'mathematical model' intrudes. Such a model represents an attempt to simplify the theory, often drastically, by discarding all details not deemed *essential* for the purpose in hand (e.g. the prediction of some new observable property or the derivation of some relationship among the observables). To construct an adequate model, delicate and highly subjective choices have to be made and the various models proposed often lead to conflicting conclusions.

It has been argued that the mathematical model first put in concrete form by Bohm and then adopted by Bell and others (as a 'standard' formulation of the EPR experiment) does not do full justice to either quantum mechanics or physical reality. The system considered is said to be a *molecule* i.e. a many-electron system whose particles have masses, charges, positions, velocities and interactions: there is a Hamiltonian, whose associated operator governs the time evolution of the system and determines the energies of the stationary states and their dependence on molecular geometry as the system is dissociated into two fragments; and there are inviolable principles to be respected, notably the Pauli principle for fermions. These are all features of quantum mechanics that cannot be discarded (least of all in discussing a 'real physical system') except at the risk of tearing the whole fabric of the theory.

In the usual EPR model, the only variables considered are the six components of the two spins: all the rest has been thrown away. There are no masses, charges, positions, velocities, interactions, nor even particles! – only two disembodied spins. To use the imagery of 'Schrödinger's cat', this is a 'Lewis Carroll's Cheshire cat': the spin without the particle is like the grin without the cat.

References

- [1] J. A. Wheeler and W. H. Zurek (eds.): *Quantum Theory and Measurement*, Princeton University Press, Princeton N.J. (1984)
- [2] A. Einstein, B. Podolsky, and N. Rosen: *Phys. Rev.* **47**, 777 (1935)
- [3] D. Bohm: *Quantum Theory*, Prentice-Hall, Englewood Cliffs (1951)
- [4] J. S. Bell: *Physics* **1**, 195 (1964)
- [5] J. S. Bell: *Rev. Mod. Phys.* **38**, 447 (1966)
- [6] A. Einstein in *Albert Einstein, Philosopher, Scientist* (ed. P. A. Schilp), p.85, Library of Living Philosophers, Evanston Ill. (1949)
- [7] B. d'Espagnat in *The Physicist's Conception of Nature* (ed. J. Mehra), p.734,

Kluwer, Boston (1973)

[8] M. Lockwood: *Brit. J. Phil. Sci.* **47**, 159 (1996)

[9] K. Husimi: *Proc. Phys. Math. Soc. Japan* **22**, 264 (1940)

[10] R. McWeeny: *Rev. Mod. Phys.* **32**, 335 (1960)

[11] R. McWeeny and Y. Mizuno: *Proc. Roy. Soc. (Lond.)* **A259**, 554 (1961)

[12] R. McWeeny: *Methods of Molecular Quantum Mechanics 2nd ed.*, Academic Press, London (1993)

[13] W. Heitler and F. London: *Z. Phys.* **44**, 455 (1927)

[14] Y. Aharonov and D. Bohm: *Phys. Rev.* **122**, 1649 (1961)

[15] A. Messiah: *Quantum Mechanics*, North Holland, Amsterdam (1961)

[16] P. D. Dacre and R. McWeeny: *Proc. Roy. Soc. (Lond.)* **A317**, 435 (1970)

[17] A. R. Edmonds: *Angular Momentum in Quantum Mechanics*, Princeton University Press, Princeton (1957)

Index

A

- Ab initio* calculations, nitron reaction with acrylonitrile, 154
- Absorption spectroscopy
NO₂, Lanczos algorithm
 calculation specifics, 326–328
 convergence, 328–331
 nonadiabatic states, 324–325
 spectral details, 331–337
 solvent effects, 129–131
- Acidity, gas phase, calculations, 99, 109–111
- ACM, *see* Adiabatic connection methods
- Acrylonitrile, reaction
 with 5,5-dimethyl-1-pyrroline-1-oxide, 153
 with nitron
 solvent effects, 157–158
 theory vs. experiment, 158–159
 TS structures, 155
 with 1-pyrroline-1-oxide, 153
 with various nitrones, 153
- Activation barriers, nitron endo–exo selectivity, 162–165
- Adiabatic connection methods
 covalent interactions, 59–61
 electronic excitation energy, 70
 formulas, 57–59
 Kohn–Sham approach
 DF, 47–56
 generalized SCF model, 49–50
 molecular properties, 68–69
 noncovalent interactions, 62–64
 reactivity, 64–68
- Adiabatic representations, for reaction dynamics, 344–346
- Alanine
 GPA, 111
 PA and GPB, 107–108
- ALCC, *see* Almost linear coupled cluster methods
- Aliphatic amines, metal ion affinity, 113
- Almost linear coupled cluster methods, in RMR CCSD application
 to DZ model of H₂O, 245–246
 to H4 model, 239–241
 to H8 model, 241–242
 to S4 model, 242–245
 types, 236–239
- AM1 calculations, merocyanine M1 net atomic charges, 133–134
- Ammonium
 lone-pair functions, 15–16
 metal ion affinity, 113
- Angular variables, orbital angular momentum, 343–344
- Aniline
 neutral, Fukui index, 104–105
 protonation, 104
- Asymmetric parameterization, in mapping of potential energy surfaces, 358
- Atomic charges, net, merocyanine M1, 133–134
- Atomic natural orbital bases, in SDCl, 33
- Atomic orbitals
 algebraic manipulation, 2–3
 valence state theory, 3–4
- Atomic subunits, molecule partitioning, 28
- Atoms
 computational methods, 82
 neutral, exact and fitted exchange values, 83
 small, electron correlation, 187–190
- Attach sites, neutral molecules, DFT studies, 102–105

B

- Basicity, gas phase
 calculation, 99
 determination, 105–109

- Basis sets
 enlarged, extension, 16–17
 for NO₂ absorption spectrum, 328–331
 size, and R12 method, convergence,
 199–202
- Betaine-30, charge transfer processes, 287
- Biaryls, charge transfer processes, 285–288
- Born–Oppenheimer approximation
 in adiabatic and diabatic representations,
 344–346
 Hamiltonian, in DF for hydrogen, 373–
 374
- Brillouin theorem, HPHF function for
 singlet ground state, 257–258
- C**
- Carbon, SDCI computations, 33
- CCSD, *see* Coupled-cluster method with
 singles and doubles
- Charge
 electronic, core–valence separation,
 28–30
 net atomic, merocyanine M1, calculation,
 133–134
- Charge distribution, transition metal cation,
 278–279
- Charge transfer
 biaryls and related molecules, 285–288
 molecules with excitations
 models, 288–294
 time evolution, 294–298
- Chemical hardness
 matrix elements, 97
 for reactivity index, 96–98
- Chemical shifts, NMR, in ACM, 68–69
- Chemical species, Sc⁺, Fe⁺, and Cu⁺,
 272–273
- CI, *see* Configuration interaction
- Computational methods
 AM1, merocyanine M1 net atomic
 charges, 133–134
 for atomic systems, 82
 nitrene reaction with acrylonitrile, 154
- Computer programs
 CS INDO, 131–132
 FORTRAN codes for Lanczos algorithm,
 326
 Gaussian 94, 319
 DeMon, and DGauss, 99–100
 Gaussian 94W, 170–171
 for hybridization matrix, 12–13
 hybridization routines, 15
 MOPAC, 319
- Configuration interaction, full, in many-
 electron methods, 190–192
- Convergence
 with basis size and R12 method, 199–202
 in NO₂ absorption spectrum, 328–331
- Copper cation, as molecular model, 272–
 273
- Core excitations, in HPHF, 268
- Core–valence separation
 definitions, 42
 electronic charge, 28–30
 Poltzer's formula, 40
 theories, 41
- Coupled-cluster methods
 almost linear CC, 236–239
 in many-electron methods, 195–197
- Coupled-cluster method with singles and
 doubles
 ALCC, 234–236
 AL RMR CCSD, application
 to DZ model of H₂O, 245–246
 to H4 model, 239–241
 to H8 model, 241–242
 to S4 model, 242–245
 external correction, 234–236
- Covalent bridges, for PA-ET, 303–306
- Covalent interactions, in ACM, 59–61
- CS INDO model
 calculation details, 131–132
 Hamiltonian, 122
 merocyanine M1 test calculations,
 132–139
 merocyanine M2 and M3, 139–146
 merocyanines, 123–125
 SCF solvation model, 125–129
 for solvent, 123
 solvent effects on spectra, 129–131
- Cyanide, metal cations
 charge distribution, 278–279
 as molecular models, 272–273
 multireference second-order perturbation
 methods, 273–275
 structures, 275–278
- Cycloaddition, nitrenes, TS structures,
 159–160
- Cyclobutanone, singlet excited states,
 application of HPHF, 266–267

3-Cyclopenten-1-one, singlet excited states,
application of HPHF, 267

Cytosine

Li⁺ and Na⁺ ion affinity, 113

proton transfer

geometrical parameters, 173–175

tautomeric stabilities, 175–179

tautomers, 171–173

water-assisted transfer kinetics,
179–181

D

Deformation energy, nitrones, 162

Delocalization energy

analysis, 152

nitrones, 162

Del Re method

in delocalization energy analysis, 152

maximum overlap

basis set extension, 16–17

building procedure, 7–14

general methods, 6–7

lone-pair problem, 14–16

in PA-ET, 301

DeMon package, for DFT computations,
99–100

Density functional differential exchange
energy, for He dimers, 53

Density functionals

in core–valence separation, 41

covalent interactions, 59–61

for electron correlation

history, 205–207

Hohenberg–Kohn theorem, 207–210

Slater–Kohn–Sham-type methods,
210–212

electronic excitation energy, 70

GGA, 51–52

GGA corrections, 55–56

for hydrogen, 373–375

Kohn–Sham approach to adiabatic
connection methods, 47–49

LSD, 50–51

LYP correlation functional, 55–56

molecular properties, 68–69

MP2, 51–52

noncovalent interactions, 62–64

Padé summation approximation, 54

post-HF, molecules, 34–38

PW, 51–53

reactivity, 64–68

Vosko–Wilk–Nuisar parameterization, 55

Density functional theory

applications, 94

computer packages for calculations,
99–100

definition, 78–79

GPA calculations, 109–111

in GPB, 105–109

ion geometry, 100–102

molecule attach site studies, 102–105

in PA, 105–109

potential energy surfaces, 114–116

reactivity index, 96–98

theory, 94–96

thermochemical properties, 98–99

Density matrix, 2-particle, and *n*-

representability problem, 192–193

DF, *see* Density functionals

DFT, *see* Density functional theory

DGauss package, for DFT computations,
99–100

Diabatic representations, for reaction
dynamics, 344–346

Diels–Alder reaction, mechanism, 66–67

Different orbitals for different spins model,
in RHF, 254–255

3,4-Dihydro-isoquinoline-*N*-oxide, reaction
with acrylonitrile, 153

Dimethyl maleate, reaction with nitronic
esters. TS structures, 159–160

5,5-Dimethyl-1-pyrroline-1-oxide, reaction
with acrylonitrile, 153

DODS, *see* Different orbitals for different
spins model

o-Donor, for PA-ET, 303–306

Double zeta model, H₂O, application of AL
RMR CCSD, 245–246

Dunning's contracted GTO, molecules,
34–38

Dyes, triphenyl-methane dyes, charge
transfer, 286

DZ model, *see* Double zeta model

E

EDA, *see* Electron donor acceptor

Eigenstates, multiconfigurational, biaryl and
related molecules, 286

- Eigenvectors, hybrid orbitals, 10
- Einstein–Podolsky–Rosen paradox
 - DF for hydrogen, 373–375
 - in early quantum mechanics, 366
 - hidden variables, 366
 - hydrogen, 377–381
 - hydrogen dissociation, 375–377
 - non-separability, 367
 - reduced density matrix, 370–373
 - restatement, 366–367
 - spin correlation, 370–373
 - system density matrix, 368–370
- o*-Electron acceptor, for PA-ET, 303–306
- Electron correlation
 - convergence with basis size and R12 method, 199–202
- DF methods
 - history, 205–207
 - Hohenberg–Kohn theorem, 207–210
 - Slater–Kohn–Sham-type methods, 210–212
- localized methods, 202–205
- many-electron methods
 - coupled-cluster methods, 195–197
 - full CI, 190–192
 - MBPT, 193–195
 - multiconfiguration-based methods, 197–199
 - 2-particle density matrix, 192–193
 - in small atoms, 187–190
 - in small molecules, 187–190
- Electron density, in DFT, 94
- Electron donor acceptor
 - in ET, 303
 - PA-ET, driving force, 306–307
- Electronic charge, core–valence separation, 28–30
- Electronic excitation energy, in time-dependent DF, 70
- Electronic states, NO₂ absorption spectrum, 331–337
- Electron spin resonance, and hybridization, 17–20
- Electron transfer
 - electron donor acceptor, 303
 - proton-assisted, *see* Proton-assisted electron transfer
- Electrostatic solvent effects, in CS INDO scheme
 - calculation details, 131–132
 - SCF solvation model, 125–129
 - on spectra, 129–131
- Endo–exo selectivity
 - nitrones, activation barriers, 162–165
 - nitronic esters, TS structures, 159–160
- Energy
 - deformation, nitrones, 162
 - delocalization
 - analysis, 152
 - nitrones, 162
 - DF differential exchange, for He dimers, 53
 - excitation
 - core, in HPHF, 268
 - electronic, in time-dependent DF, 70
 - optical, biaryl and related molecules, 286
 - HF differential exchange, for He dimers, 53
 - valence-region, equations, 30–31
- EPR paradox, *see* Einstein–Podolsky–Rosen paradox
- ESR, *see* Electron spin resonance
- ET, *see* Electron transfer
- Evolution, time, molecules with charge transfer excitations, 294–298
- Exchange-energy density functional, theory, 79–82
- Exchange values, exact and fitted, for neutral atoms, 83
- Excitation energy
 - core, in HPHF, 268
 - electronic, in time-dependent DF, 70
 - optical, biaryl and related molecules, 286
- Excited states
 - HPHF equations, 262–263
 - Li, application of HPHF, 264–265

F

- Fermi resonance, in NO₂ absorption spectrum, 333
- Finite-difference approximation, in SDCl computations, 33
- Fokker–Planck equation, in time evolution calculations, 296
- Franck–Condon approximation
 - NO₂ absorption spectrum, Lanczos calculation
 - calculation specifics, 326–328
 - convergence, 328–331
 - nonadiabatic states, 324–325

- spectral details, 331–337
- in solvent effects on spectra, 129–131
- Fukui index
 - in DFT, 98
 - neutral aniline, 104–105
 - for sulfine, 104

G

- Gas phase acidity, calculation, 99, 109–111
- Gas phase basicity, calculation, 99, 105–109
- Gas phase proton affinity, in DFT, 98–99
- Gaussian 94
 - for DFT computations, 99–100
 - for PA-ET calculations, 319
- Gaussian 94W, for proton transfer in cytosine, 170–171
- GEA, *see* Gradient expansion approximation
- Generalized gradient approximation
 - in ACM, 58
 - covalent interactions, 59–60
 - as DF, 51, 55–56
 - in DFT, 78–79, 95–96
- Geometry
 - distortion, merocyanine M2 and M3, 139–146
 - hybrid orbitals, 5–6
 - proton transfer in cytosine, 173–175
- GGA, *see* Generalized gradient approximation
- Glycine
 - GPA, 111
 - Li⁺ and Na⁺ ion affinity, 113
 - PA and GPB, 107–108
- GPA, *see* Gas phase acidity
- GPB, *see* Gas phase basicity
- Gradient expansion approximation, in DFT, 78–79
- Gradient geometry optimization, nitron–acrylonitrile reactions, 154
- Ground-state ions, A⁺ and A[−], calculations, 31–33

H

- H4 model, application of AL RMR CCSD, 239–241
- H8 model, application of AL RMR CCSD, 241–242

- Half-projected Hartree–Fock model
 - application
 - core excitations, 268
 - to cyclobutanone singlet excited states, 266–267
 - to 3-cyclopenten-1-one singlet excited states, 267
 - definition, 256
 - equations for excited states, 262–263
 - Li excited states, 264–265
 - for singlet ground state
 - applications, 261–262
 - Brillouin theorem, 257–258
 - HPHF equations, 258–260
 - pairing theorem, 258
- Hamiltonian
 - Born–Oppenheimer, in DF for hydrogen, 373–374
 - for CS INDO model, 122
 - for Lanczos calculation of NO₂ absorption spectrum, 324–325
- Harmonics, hyperspherical coordinates for reaction dynamics, 350–354
- Hartree–Fock calculations, molecules, 34–38
- Hartree–Fock differential exchange energy, for He dimers, 53
- Helium, dimers, HF and DF differential exchange energy, 53
- HF, *see* Hartree–Fock calculations
- Hohenberg–Kohn–Sham density functional theory, electronic excitation energy, 70
- Hohenberg–Kohn theory
 - DF, 47
 - as Legendre transformation, 207–210
- Householder algorithm, for Lanczos
 - algorithm, 326
- HPHF, *see* Half-projected Hartree–Fock model
- Hybridization
 - geometrical constructions, 5–6
 - quantum-chemical flashback, 20–21
 - status, 4–5
 - structural applications, 17–20
- Hybridization matrix, hybrid orbitals, 11–12
- Hybrid orbitals
 - geometrical constructions, 5–6
 - maximum overlap
 - basis set extension, 16–17
 - building procedure, 7–14
 - lone-pair problem, 14–16
 - methods, 6–7

Hydrogen
 bonds
 long chains, characterization, 302
 for PA-ET, 303–306
 density functions, 373–375
 dissociation, in EPR paradox, 375–377
 EPR paradox, 377–381
 exact and fitted exchange values, 83
 valence-bond treatment, 2–3
 Hydroxyl groups, PA-ET, peptide bridge
 effect, 307–312
 Hyperangles, parameterization, in mapping
 of potential energy surfaces, 355–359
 Hyperangular momentum, hyperspherical
 coordinates for reaction dynamics,
 350–354
 Hyperspherical coordinates, for chemical
 reaction dynamics
 adiabatic and diabatic representations,
 344–346
 hyperangular momentum, 350–354
 orbital angular momentum, 343–344
 potential energy surface mapping,
 355–359
 three-body problem, 347–349

I

INDO calculations, merocyanine M1 net
 atomic charges, 133–134
 Ions, geometry, in DFT, 100–102
 Iron cation, as molecular model, 272–273
 Isocyanide, metal cations
 charge distribution, 278–279
 as molecular models, 272–273
 multireference second-order perturbation
 methods, 273–275
 structures, 275–278

J

Jacobi vectors, in three-body problem,
 347

K

Kinetics, water-assisted cytosine proton
 transfer, 179–181

Kohn–Sham one-electron equations, in
 DFT, 94–96
 Kohn–Sham orbital eigenvalues, in
 reactivity index, 97
 Kohn–Sham theory
 adiabatic connection methods
 DF, 47–49, 50–56
 generalized SCF model, 49–50
 in core–valence separation, 41
 KS theory, *see* Kohn–Sham theory

L

Lagrange multipliers, hybrid orbitals, 10
 Lanczos algorithm, NO₂ absorption
 spectrum
 calculation specifics, 326–328
 convergence, 328–331
 nonadiabatic states, 324–325
 spectral details, 331–337
 LDA, *see* Local density approximation
 Lee–Yang–Parr correlation functional
 in ACM, 58
 for covalent interactions, 59
 as DF, 55–56
 in DFT, 96
 reactivity, 65–68
 Legendre transformation, Hohenberg–Kohn
 theorem as, 207–210
 Levy condition, in GGA exchange
 functional, 52–53
 Lieb–Oxford bound, in GGA exchange
 functional, 52–53
 Lithium
 excited states, application of HPHF,
 264–265
 ion affinity for glycine and cytosine, 113
 Local density approximation, in DFT,
 78–79, 95
 Localized correlation methods, in electron
 correlation, 202–205
 Local spin density
 in ACM, 58
 as DF, 50–51
 in DFT, 95
 Lone-pair functions, NH₃, 15–16
 Lone-pair problem, for hybrid orbitals, 14–16
 LSD, *see* Local spin density
 LYP correlation functional, *see* Lee–Yang–
 Parr correlation functional

M

- Maleic anhydride, reaction with nitronic esters, 159–160
- Maleimides, reaction with nitronic esters, 159–160
- Many-body perturbation theory, in many-electron methods, 193–195
- Many-electron methods
- full CI, 190–192
 - one-electron basis sets
 - coupled-cluster methods, 195–197 - MBPT, 193–195
 - multiconfiguration-based methods, 197–199
 - 2-particle density matrix, 192–193
- Mapping, hyperspherical, potential energy surfaces, 355–359
- Matrices, chemical hardness, 97
- Maximum overlap, hybrid orbitals
- basis set extension, 16–17
 - building procedure, 7–14
 - lone-pair problem, 14–16
 - methods, 6–7
- MBPT, *see* Many-body perturbation theory
- Merocyanine M1, test calculations, 132–139
- Merocyanine M2, geometrical distortion and solvatochromism, 139–146
- Merocyanine M3, geometrical distortion and solvatochromism, 139–146
- Merocyanines, test systems, 123–125
- Metal ion affinity, organic bases, 111–114
- N*-Methylformamide, PA-ET, peptide bridge effect, 309
- Models
- application of AL RMR CCSD
 - to DZ model of H₂O, 245–246
 - to H4 model, 239–241
 - to H8 model, 241–242
 - to S4 model, 242–245 - CS INDO, *see* CS INDO model
 - DODS, 254–255
 - DZ, H₂O, application of AL RMR CCSD, 245–246
 - HPHF, *see* Half-projected Hartree–Fock model
 - hybridization, 4–5
 - molecules with charge transfer
 - excitations, 288–294 - PHF, spin orbitals, 255

RHF

- DODS, 254–255
 - single Slater determinant, 254
- S4, application of AL RMR CCSD, 242–245
- Sc⁺, Fe⁺, and Cu⁺, 272–273
- SCF, KS theory, 49–50
- solvent, 123
- CS INDO SCF, 125–129
 - UHF, spin orbitals, 254–255
- Molecules
- atomic subunit partitioning, 28
 - biaryl-related, charge transfer processes, 285–288
 - bonding, hybridization description, 4–5
 - with charge transfer excitations
 - models, 288–294
 - time evolution, 294–298 - Dunning's contracted GTO, 34–38
 - models, Sc⁺, Fe⁺, and Cu⁺, 272–273
 - neutral, application of DFT, 100–102
 - properties, ACM, 68–69
 - small, electron correlation, 187–190
- Momentum
- hyperangular, hyperspherical coordinates, 350–354
 - orbital angular, radial and angular variables, 343–344
 - rotational and orbital angular momentum, 347–349
- MOPAC, for PA-ET calculations, 319
- MP2, *see* Second-order many-body perturbation approaches
- Multiconfigurational eigenstates, biaryl and related molecules, 286
- Multiconfiguration-based methods, in many-electron methods, 197–199
- Multireference second-order perturbation methods, for transition metal cation complexation, 273–275

N

- Next-neighbor spacing distribution, in NO₂
- absorption spectrum, 337
- Nitrogen, SDCI computations, 33
- Nitrogen dioxide, absorption spectrum,
- Lanczos algorithm
 - calculation specifics, 326–328
 - convergence, 328–331

- Nitrogen dioxide, absorption spectrum,
 Lanczos algorithm (*continued*)
 nonadiabatic states, 324–325
 spectral details, 331–337
- N-H-Nitrone, reaction with acrylonitrile,
 153
- N-Me-Nitrone, reaction with acrylonitrile,
 153
- N-(t)-Bu-Nitrone, reaction with acrylonitrile,
 153
- Nitrones
 endo–exo selectivity, activation barriers,
 162–165
 functionality, 151–152
 reaction with acrylonitrile
 computational methods, 154
 solvent effects, 157–158
 theory vs. experiment, 158–159
 TS structures, 155
- Nitronic esters, endo–exo selectivity, TS
 structures, 159–160
- NMR, *see* Nuclear magnetic resonance
- Nonadiabatic state, NO₂ absorption
 spectrum, Lanczos calculation
 calculation specifics, 326–328
 convergence, 328–331
 Hamiltonian, 324–325
 spectral details, 331–337
- Nuclear magnetic resonance
 chemical shifts, in ACM, 68–69
 spin–spin, and hybridization, 17–20

O

- One-electron basis sets, in many-electron
 methods
 coupled-cluster methods, 195–197
 full CI, 190–192
 MBPT, 193–195
 multiconfiguration-based methods,
 197–199
 2-particle density matrix, 192–193
- Optical excitation, biaryl and related
 molecules, 286
- Orbital angular momentum
 hyperspherical coordinates for reaction
 dynamics, 347–349
 separation of radial and angular variables,
 343–344
- Organic bases, metal ion affinity, 111–114
- Overlap matrix, hybrid orbitals, 7–9
- Oxygen, SDCI computations, 33
- Ozone, PA, 108–109

P

- PA, *see* Proton affinity
- Padé summation approximation, DF, 54
- PA-ET, *see* Proton-assisted electron transfer
- Pairing theorem, HPHF function for singlet
 ground state, 258
- Pearson's principle, application, 97
- Peptide bridge, effect in PA-ET, 307–312
- Perdew–Wang correlation functional
 in ACM, 58
 as DF, 56
- Perdew–Wang exchange functional
 for covalent interactions, 59
 as density functional, 51–53
- Perturbation methods
 many-body perturbation, 193–195
 multireference second-order perturbation,
 273–275
 second-order many body perturbation,
 51–52
- Phenolphthalein dianion, charge transfer
 processes, 287–288
- C-Phenyl-*N*-methylnitrone, reaction with
 acrylonitrile, 153
- PHF, *see* Projected Hartree–Fock model
- Photosynthesis, RCs, PA-ET, 301–302,
 315–319
- Politzer's formula, core–valence separation,
 40
- Potential energy surface
 analysis, 312–315
 in DFT, 114–116
 hyperspherical mapping, 355–359
- Projected Hartree–Fock model, spin
 orbitals, 255
- Proton affinity
 determination, 105–109
 gas phase, in DFT, 98–99
- Proton-assisted electron transfer
 application of computational packages,
 319
 in EDA pairs, driving force, 306–307
 general structure, 303–306

mechanism, 302–303, 312–315
peptide bridge effect, 307–312
in photosynthetic RCs, 301–302, 315–319
Protonation, aniline, 104
Proton transfer, in cytosine
geometrical parameters, 173–175
tautomeric stabilities, 175–179
tautomers, 171–173
water-assisted transfer kinetics, 179–181
PW, *see* Perdew–Wang exchange functional
1-Pyrroline-1-oxide, reaction with
acrylonitrile, 153

Q

Quantum-chemical flashback, hybridization, 20–21
Quinone, PA-ET, in photosynthetic RCs, 315–319

R

R12 method, and basis size, convergence, 199–202
Radial variables, and angular variables, orbital angular momentum, 343–344
RC, *see* Reaction centers
Reaction centers, photosynthetic, PA-ET, 301–302, 315–319
Reaction dynamics, hyperspherical coordinates
adiabatic and diabatic representations, 344–346
hyperangular momentum, 350–354
orbital angular momentum, 343–344
potential energy surface mapping, 355–359
three-body problem, 347–349
Reactivity index, analysis with chemical hardness, 96–98
Reduced density matrix, in EPR paradox, 370–373
Reduced multireference methods, CCSD, ALCC, 234–236
n-Representability problem, 2-particle density matrix, 192–193

Restricted Hartree–Fock model
DODS, 254–255
single Slater determinant, 254
RHF, *see* Restricted Hartree–Fock model
Rhodopseudomonas sphaeroides, RCs, PA-ET, 301–302, 315–319
Root mean square deviation, in contracted GTO, 36
Rotational angular momentum, hyperspherical coordinates for reaction dynamics, 347–349

S

S4 model, application of AL RMR CCSD, 242–245
Scandium cation, as molecular model, 272–273
SCF, *see* Self-consistent field
Schrödinger equation, in full CI, 190–192
SDCI calculations, ground-state atoms and ions, 31–33
Second-order many-body perturbation approaches, as DF, 51–52
Self-consistent field
calculations, solute–solvent interaction, 132–139
KS theory, 49–50
solvation model, 125–129
Singlet excited states
cyclobutanone, application of HPHF, 266–267
3-cyclopenten-1-one, application of HPHF, 267
Singlet ground state, HPHF function applications, 261–262
Brillouin theorem, 257–258
HPHF equations, 258–260
pairing theorem, 258
Slater determinant, single, in RHF, 254
Slater–Kohn–Sham-type methods, for electron correlation, 210–212
Slater orbitals
ground-state atoms and ions, 31–33
valence state theory, 3–4
Sodium, ion affinity for glycine and cytosine, 113
Solute–solvent interaction, in SCF calculations, 132–139

- Solvatochromism, merocyanine M2 and M3, 139–146
- Solvent effects
models, 123
nitron reaction with acrylonitrile, 157–158
solute interaction, in SCF, 132–139
- Spin correlation, in EPR paradox, 370–373
- Spin density, in DF for hydrogen, 374–375
- Spinorbitals
in PHF, 255
UHF, 254–255
- Sulfine
attach sites, 103–104
Fukui index, 104
PA, 108–109
- Symmetric parameterization, in
hyperspherical mapping, 358–359
- System density matrix, in EPR paradox, 368–370
- T**
- Tautomers, cytosine
proton transfer, 171–173
stabilities, 175–179
- Thermochemistry, in DFT, 98–99
- Three-body problem, hyperspherical
coordinates for reaction dynamics, 347–349
- Time, evolution, molecules with charge
transfer excitations, 294–298
- Transformation, unitary, hybrid orbitals, 8
- Transition metal complexes
cyanide and isocyanide
charge distribution, 278–279
as molecular models, 272–273
multireference second-order
perturbation methods, 273–275
structure, 275–278
MCN⁺ MNC⁺, 272–273
- Transition operator, in EPR paradox, 369
- Transition-state structures
nitron reaction with acrylonitrile, 155
nitronic ester endo–exo selectivity, 159–160
- Triphenyl-methane dyes, charge transfer
processes, 286
- TS, *see* Transition-state structures
- U**
- UHF, *see* Unrestricted Hartree–Fock model
- Unrestricted Hartree–Fock model, spin
orbitals, 254–255
- V**
- Valence-bond treatment, H₂ molecule, 2–3
- Valence-region energy, equations, 30–31
- Valence state theory, atomic orbitals, 3–4
- Van der Waals interactions, in ACM, 62–64
- Vosko–Wilk–Nuisar parameterization
in ACM, 58
DF, 55
- VWN parameterization, *see* Vosko–Wilk–
Nuisar parameterization
- W**
- Water
DZ model, 245–246
PA-ET, peptide bridge effect, 307–312
role in cytosine proton transfer, 179–181
- Wigner's rotation matrix, in hyperangular
momentum, 352

ISBN 0-12-034836-5

